Conference Proceedings

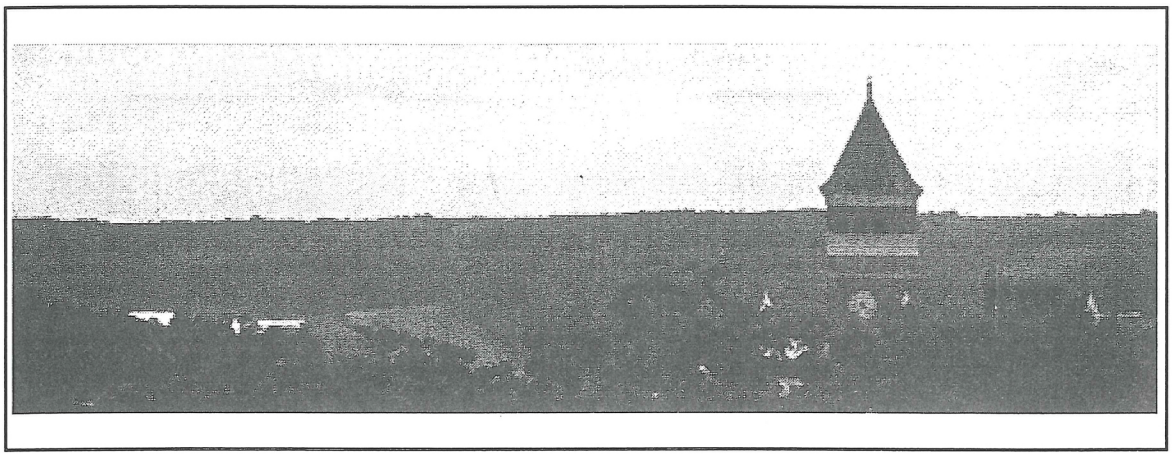

Twenty-First Annual Meeting of the American Society of Biomechanics

Clemson University
Clemson, South Carolina
September 24-27, 1997

The Bioengineering Alliance of South Carolina

Conference Proceedings

American Society of Biomechanics

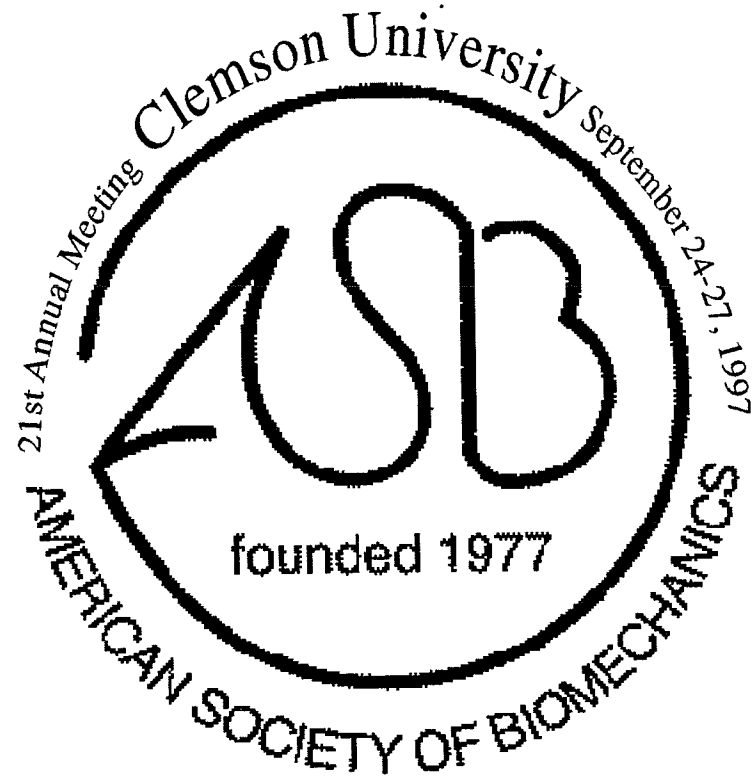

The organizers of the 21st Annual Meeting of the American Society of Biomechanics gratefully acknowledge the following organizations for their generous support of this Annual Meeting:

The Bioengineering Alliance of South Carolina
Clemson University
University of South Carolina
Medical University of South Carolina

The Greenville Hospital System
Greenville, SC

The Department of Bioengineering
Clemson University

SUPPORTING MEMBERS:

Peak Performance Technologies

American Society of Biomechanics

The American Society of Biomechanics was formed in 1977. The purpose of the Society is to provide a forum for interaction among the diverse disciplines in biomechanics research and applications. The term biomechanics in this context refers to the study of structure and function of biological systems using the methods of mechanics. The active membership of the Society includes scientists who conduct research in the biological sciences, engineering and applied sciences, ergonomics and human factors, exercise and sports sciences, and the health sciences.

The principle activity of the Society is an annual scientific meeting. The meeting is held over a three-day period, and consists of keynote addresses, tutorial sessions, podium and poster presentations and student member functions. In keeping with the objectives of the Society, the papers address a wide range of topics and broad interests.

The Executive Committee of the Society during the past year is represented by the following individuals:

President:	Robert J. Gregor, Georgia Institute of Technology
Past President:	Kai-Nan An, Mayo Clinic
President Elect:	Mark D. Grabiner, Cleveland Clinic Foundation
Secretary-Treasurer:	Joan E. Bechtold, Orthopaedic Biomaterials Lab
Meeting Chairperson:	Vasanti M. Gharpurary, Clemson University
Meeting Chairperson Elect:	M. Melissa Gross, University of Michigan
Program Chairperson:	Mary M. Rogers, University of Maryland
Membership Committee Chairperson:	J. Trey Crisco, Brown University
Education Committee Chairperson:	Suzanne D. Smith, Armstrong Laboratory
Newsletter Editor:	Joseph E. Hale, University of Virginia
Student Representative:	Sheila S. Stevens, Stanford University

Program Committee

Mary M. Rodgers, Ph.D.
University of Maryland

M. Melissa Gross
University of Michigan

Brian L. Davis
Cleveland Clinic Foundation

Rodger Kram
University of California

Richard E. Hughes
University of Washington

Exhibitors at the 1997 Meeting

AMTI
ATI Industrial Automation
Elsevier Science, Inc.
Instron Corporation
Kistler Instrument Corporation
MicroStrain, Inc.
Motion Analysis Corporation
MTS Systems Corporation
Noraxon USA, Inc.
Novel Electronics
Peak Performance Technologies
Qualisys, Inc.
Run Technologies

Conference Schedule

Wednesday, September 24, 1997

12:00 p.m.- 5:00 p.m.	Registration
1:00 p.m. - 4:30 p.m.	Lab Tours (Leave from the Madren Center)
5:30 p.m. - 8:30 p.m.	Opening Reception, Poster Session 1
6:30 p.m. -10:00 p.m.	Executive Board Meeting

Thursday, September 25, 1997

7:00 a.m. - 5:00 p.m.	Registration
8:00 a.m. - 5:00 p.m.	Exhibitor Display
7:45 a.m. - 8:00 a.m.	Welcome and Opening Remarks
8:00 a.m. - 9:00 a.m.	Keynote Lecture #1
9:30 a.m. - 11:00 a.m.	Award Finalists Session
11:15 a.m. -12:30 p.m.	Podium Sessions 1 and 2
12:45 p.m. - 2:00 p.m.	Awards Lunch
2:00 p.m. - 3:00 p.m.	Borelli Award Lecture
3:30 p.m. - 4:45 p.m.	Podium Sessions 3 and 4
5:00 p.m. - 8:00 p.m.	Wine and Cheese Poster Session 2

Friday, September 26, 1997

7:00 a.m. - 5:00 p.m.	Registration
8:00 a.m. - 5:00 p.m.	Exhibitor Display
8:00 a.m. - 9:00 a.m.	Keynote Lecture #2
9:30 a.m. - 10:45 a.m.	Podium Sessions 5 and 6
11:00 a.m. -12:15 p.m.	Podium Sessions 7 and 8
12:30 p.m. - 2:00 p.m.	Student Members Lunch Box Lunch provided for others
2:00 p.m. - 3:15 p.m.	Podium Sessions 9 and 10
3:45 p.m. - 4:45 p.m.	ASB Open Business Meeting
5:30 p.m. -10:00 p.m.	Banquet

Saturday, September 27, 1997

8:00 a.m. - 10:00 a.m.	Exhibitor Display
8:00 a.m. - 9:15 a.m.	Podium Sessions 11 and 12
9:45 a.m. - 11:00 a.m.	Podium Sessions 13 and 14
11:00 a.m. - 1:00 p.m.	Lunch on your own
1:30 p.m. - 3:00 p.m.	Tutorial #1
3:30 p.m. - 5:00 p.m.	Tutorial #2
6:30 p.m. - 10:00 p.m.	Executive Board Meeting

Invited Sessions

Keynote Lecture #1

Thursday, September 25, 1997, 8:00 a.m. - 9:00 a.m.

Keynote Lecture #2

Friday, September 26, 1997, 8:00 a.m. - 9:00 a.m.

Tutorial Lecture #1

Saturday, September 27, 1997, 1:30 p.m. - 3:00 p.m.

Molecular Biology Methods in Biomechanics
Richard L. Lieber
University of California - VA Medical Center, San Diego

Tutorial Lecture #2

Saturday, September 27, 1997, 3:30 p.m. - 5:00 p.m.

Biomechanical Experimentation: Avoiding Pitfalls When Manipulating Data
Brian L. Davis
Cleveland Clinic Foundation

Award Presentations

Borelli Award:

Nominees for the Clinical Biomechanics Award:

Pre-Doctoral Young Scientist Award:

Post-Doctoral Yount Scientist Award:

TABLE OF CONTENTS

WEDNESDAY, SEPTEMBER 24, 1997

5:30 p.m. – 8:30 p.m. Poster Session 1

METHODS

MODELLING

SPORT

ORTHOPEDICS

NEUROMUSCULAR

FUNCTION AND MOBILITY

THURSDAY, SEPTEMBER 25, 1997

8:00 a.m. – 9:00 a.m. Keynote Lecture 1

9:30 a.m. – 10:45 a.m. Award Finalist Session

11:00 a.m. – 12:15 p.m. Podium Session 1-Ergonomics

11:00 a.m. – 12:15 p.m. Podium Session 2-Orthopedics: Bone

12:30 p.m. – 2:00 p.m. Awards Lunch

2:00 p.m. – 3:00 p.m. Borelli Award Lecture

Manohar M. Panjabi, Ph.D.

3:30 p.m. – 4:45 p.m. Podium Session 3-Posture and Balance

3:30 p.m. – 4:45 p.m. Podium Session 4-Orthopedics: Lower Extremity

5:00 p.m. – 8:00 p.m. Poster Session 2

METHODS

MODELLING

SPORT

ORTHOPEDICS

NEUROMUSCULAR

FUNCTION AND MOBILITY

FRIDAY, SEPTEMBER 26

8:00 a.m. – 9:00 a.m. Keynote Lecture 2

9:30 a.m. – 10:45 a.m. Podium Session 5-Gait: Strategies

9:30 a.m. – 10:45 a.m. Podium Session 6-Orthopedics: Hand

11:00 a.m. – 12:15 p.m. Podium Session 7-Gait: Normal

11:00 a.m. – 12:15 p.m. Podium Session 8-Motor Control: Upper Extremity

2:00 p.m. – 3:15 p.m. Podium Session 9-Gait: Abnormal

2:00 p.m. – 3:15 p.m. Podium Session 10-Orthopedic: Models

3:45 p.m. – 4:55 p.m. ASB Open Business Meeting

5:30 p.m. – 8:35 p.m. Banquet

SATURDAY, SEPTEMBER 27

8:00 a.m. – 9:15 a.m. Podium Session 11-Sport

8:00 a.m. – 9:15 a.m. Podium Session 12-Joint Control

9:45 a.m. – 11:00 a.m. Podium Session 13-Muscle Mechanics

9:45 a.m. – 11:00 a.m. Podium Session 14-Orthopedics: Materials

1:30 p.m. – 3:00 p.m. Tutorial 1

Molecular Biology Methods in Biomechanics
Richard L. Lieber

3:30 p.m. – 5:00 p.m. Tutorial 2

Biomechanical Experimentation: Avoiding Pitfalls When Manipulating Data
Brian L. Davis

Invited Abstracts

BIOMECHANICS OF LOW BACK INJURY: THE CONTRIBUTION OF BIOMECHANICS FOR PREVENTION AND REHABILITATION

Stuart M. McGill

Occupational Biomechanics and Safety Laboratories, Department of Kinesiology,
Faculty of Applied Health Sciences, University of Waterloo, Waterloo, ON, Canada, N2L 3G1

OVERVIEW

How can a person hurt their back picking up a pencil from the floor after lifting safely all day? How does low back injury occur from sitting? Why do we pressurize the abdominal cavity upon exertion? Is it better to stoop or squat during lifting? Should the spine be in a flexed posture or in a neutral posture upon exertion? Is compression the most important loading variable when considering injury? What are the best training exercises for rehabilitation of the back injured? These are all important and fascinating questions related to mechanics of normal low back function and of injury. This lecture will review causes of low back injury considering anatomical, biomechanical and motor control perspectives. Applications of this science will be demonstrated with several examples relating to occupational injury risk reduction, and in designing better rehabilitation programs for specific types of back injury. **The purpose of this keynote lecture is to update delegates, who are experts in a variety of areas in biomechanics, on some of the issues associated with the biomechanics of low back injury.** While several issues will be discussed in the lecture only a few will be introduced here.

What really causes injury? Injury occurs when the magnitude of load applied to a tissue exceeds the failure tolerance. Despite the tendency for many people to cite a single event that caused their injury, in reality their injury was more likely the result of cumulative microtramma associated with repeated and prolonged loading. Furthermore, very specific loading scenarios result in very specific injuries. For example, overload in a compressive mode produces endplate fractures, overload in anterior shear and repeated flexion-extension strain reversals damages components of the neural arch, while overload with the spine in full flexion increases the risk of disc herniation (McGill, 1997). This information forms the basis for the development of powerful injury avoidance strategies and rehabilitation activities for the already injured.

The anatomical design of the various tissues of the low back contain many subtleties that both work to support loads in a safe way but may lead to tissue overload if the advantages in design go unrecognized. For example, some have implicated anterior-posterior shear forces as a potential injury mechanism (e.g., Troup, 1976). It is interesting that the major lumbar extensors create large posterior shear forces upon activation while the interspinous ligament causes anterior shear forces when stretched in fully flexed postures (Heylings, 1978). This is one example where spine posture determines the interplay between passive tissues and muscles which ultimately modulates the risk of several types of injury. This would suggest that it is important to consider the curvature of the spine which must be separated from hip rotation when discussing "trunk angle".

AN APPROACH TO INJURY ANALYSIS

Reasonable interpretation and assessment of injury mechanisms requires the acquisition of tissue load-time histories in vivo. The approach that I took with my colleague Bob Norman several years ago was to develop a model that incorporated sufficient anatomical detail and that used a biologically based strategy of obtaining tissue loads that was sensitive to the individual ways people support their spines (e.g., McGill et al., 1986; McGill, 1992). Measurement of 3D spine displacement is used to obtain passive tissue loads once the range of motion/passive resistance has been calibrated and multichannel EMG is used to assist in assigning muscle forces. In this way, full credit is given to muscle co-contraction during complex tasks together with enabling analysis of the subtle differences that lead to overload and injury of a particular tissue.

A major assumption with this approach has been to use surface electrodes to represent deep muscle activity. Recently we have attempted to justify this assumption and have concluded that deep muscles appear to have synergists that are myoelectrically accessible on the surface. This has enabled us to investigate some traditional rehabilitation exercises for the back injured with the objective of challenging muscles but minimizing the spine load penalty--several examples will be presented.

SOME INTERESTING PROBLEMS

Explaining injuries when forceful exertions are required have been attempted to varying degrees of success - but at least it follows intuition that high loads can cause injury. **Far more curious is the case where one "throws his back out" when picking up a pencil.** Recent work by my former graduate student and colleague Jacek Cholewicki, demonstrated that when the reaction moments are small, and muscle forces are correspondingly low, the risk of instability and short column buckling is much higher (Cholewicki et al. 1996). It would appear that it is much more likely that a motor control error, resulting in an inappropriate, but small and temporary change in muscle force could cause local buckling joint motion sufficient to create overload in a single tissue.

The spine has a memory. Its viscoelastic structures react to load in a way that depends on the previous loading history. For example, prolonged sitting in a flexed posture stretches the posterior passive tissues which require up to half an hour to restore normal joint stiffness (McGill et al., 1992), suggesting that focus on events prior to the demanding task is warranted. Several other biomechanically justifiable guidelines to minimize the risk of injury at work will be introduced in this lecture.

ISSUES FOR THE FUTURE

What are the major "hot" issues for the immediate future? Certainly the currently used, single values for occupational spine load exposure are woefully inadequate in the field of reducing the risk of injury. A load-time integral, that is sensitive to the direction and mode of loading, age, gender, load repetition, load duration, number and duration of rest breaks, etc. is needed. As well, the field of rehabilitation requires better mechanically based diagnoses of low back injury. Only then will clinicians be better able to optimize programs to heal and strengthen tissues without exacerbating the real injury or structural weakness.

The spine is a wonderfully complex structure that will continue to cause sufficient problems which in turn will motivate clever minds. This will enhance efforts to examine injury mechanisms in a wide variety of activities including materials handling, sitting, impact, etc. to determine how it works and how to minimize the risk of injury. Much remains to be done.

REFERENCES

Cholewicki, J. et al. *Mechanical stability of the in vivo lumbar spine: Implications for injury and chronic low back pain, Clin. Biomech.* **11**, 1-15, 1996.

Heylings, D. *Supraspinsous and interspinous ligaments of the human lumbar spine, J. Anat.* **123**, 127-131, 1978.

McGill, S.M. et al. *Partitioning of the L4/L5 dynamic moment into disc, ligamentous, and muscular components during lifting, Spine* **11**, 666-678, 1986.

McGill, S.M. et al. *Creep response of the lumbar spine to prolonged full flexion, Clin. Biomech.* **7**, 43-46, 1992.

McGill, S.M. *A myoelectrically based dynamic 3D model to predict loads on lumbar spine tissues during lateral bending, J. Biomech.* **25**, 395-414, 1992.

McGill, S.M. *The biomechanics of low back injury: Implications on current practice in industry and the clinic, J. Biomech.* **30**, 465-475, 1997.

Troup, J.D.G. *Mechanical factors in spondylolisthesis and spondylolysis, Clin. Orthop. Rel. Res.* **117**, 59-67, 1976.

Dynamics of Effortful Touch and Interlimb Coordination

M. T. Turvey
Center for the Ecological Study of Perception and Action
University of Connecticut, Storrs, CT. 06269-1020
and
Haskins Laboratories, New Haven, CT. 06510

Overview. The haptic perceptual system is the system by which one knows the body, and objects adjacent to or attached to the body, by means of the body. Its sensory basis is provided by mechanoreceptors and its loss severely limits a person to a few purposeful movements that can only be conducted with considerable concentration and intellectual effort (e.g., sneezing when standing, and note taking while sitting, result in a complete loss of balance). The intimate connection between this perceptual system and movement coordination defines the level of muscular-articular links or synergies, a functional level of the nervous system responsible for stable and reproducible spatio-temporal relations among body segments. Thorough information about muscle and joint states places this level in a unique position. Only it is able to control the large-scale movement patterns (e.g., running). Higher functional levels must rely on the level of muscular-articular links' ability when many muscles are involved. A person with peripheral neuropathy (loss of haptic perception) tends to limit visual control to one muscle at a time; when many are involved simultaneously, they are simply co-contracted, not orchestrated. The production of coordination patterns is no longer available to patients with peripheral neuropathy. Standing, walking, reaching and the manipulation of objects are challenging if not impossible tasks and the ability of these patients to perceive by eye proves to be a poor substitute for their inability to perceive by muscle. *The purpose of this keynote lecture is to summarize investigations into the rhythmic coordinations of contralateral limbs and the nonvisible perception of the properties of handheld wielded objects*, two *major achievements of the level of muscular-articular links. Understanding the bases for these achievements requires both classical dynamics and contemporary nonlinear, qualitative dynamics.*

Effortful or Dynamic Touch. Among the subsystems of haptic perception, that which is almost exclusively anchored in the mass action of the muscle and tendon mechanoreceptors—referred to as effortful or dynamic touch—is of largest significance to the level of muscular-articular links. In manual activity, this subsystem is functioning whenever one takes hold of something firmly and moves it (e.g., when one lifts a cup, turns a door handle, carries a briefcase, stacks a plate, hefts a ball, wields a stick, and so on) or uses one object to probe another, more distal object. Many spatial and other perceptual capabilities of effortful touch arise from the sensitivity of the body's tissues to the inertia tensor and attitude spinor, quantities of rotational dynamics about a fixed point that do not vary with variation in the rotational forces (torques) and motions. Specifically, research on the wielding of occluded handheld objects has shown that perceived length, width, and shape, and perceived heaviness, are functions of the magnitudes (eigenvalues) of the eigenvectors of the inertia tensor. Further, the research has shown that the perception of object-to-hand relations and hand-to-object relations, are functions of the directions of the tensor's eigenvectors and, additionally, of the object's attitude spinor when attention must be directed to one of two oppositely directed object segments. These lessons learned from wielding attachments to the body (handheld objects) apply to the body. The nested body segments can be interpreted as a nesting of inertia tensors. If the normal relation between an arm's spatial axes and the arm's inertial eigenvectors is broken by means of an attached splint, the positioning of the occluded arm is systematically altered relative to visual targets. People point with the arm's eigenvectors rather than the arm's longitudinal axis. When the position of one forearm is matched nonvisually with

that of the other, under conditions in which splints have rotated the eigenvectors relative to the limb segment's spatial axes, the matching is in terms of the respective forearm eigenvectors rather than elbow angles.

Rhythmic coordination. Oscillations of two or more body segments at the same frequency is a common feature of the movement patterns of most animals. Despite its elementary nature, each instance of 1:1 frequency locking involves a large number of components at very many levels. Despite the internal complexity of two limbs sharing a temporally repeating pattern, at their own level they seem to follow a relatively uncomplicated coordination law. Theory and experiments show that the collective dynamics can be modeled by a first order motion equation in relative phase. The equation successfully predicts interlimb coordination equilibria and their bifurcations as a function of movement speed and differences between limbs in natural frequency. The body's functional asymmetry shows up as a modification of the fundamental coupling function and attentional effects in bimanual coordination are revealed as parameterizations of the modified coupling function. For any rhythmic bimanual coordination, the collective variable at the pattern level is formed from the cooperative activity of a number of subsystems each expressible as a first-order, autonomous, ordinary differential equation identifying an active degree of freedom (DF). A reproducible, stable coordination pattern implies an attractor—a geometric object to which the (longer term) motions composing the pattern are confined. Because all variables are generically connected in a nonlinear process, measurement of a single scalar, such as the amplitude of one hand, can suffice to reconstruct the vector space of the attractor and to determine the number of active DFs governing motion on the attractor. Application of the phase-space reconstruction method reveals that the dynamics of single-joint rhythmic behavior contain more than the two active DFs expected from limit cycle dynamics. Observed positive Lyapunov exponents and fractal attractor dimensions suggests that the gross variability of rhythmic movement stems largely from low-dimensional chaotic motion on strange attractors.

References

Amazeen, P., Amazeen, E., & Turvey, M. T. (in press). Dynamics of human intersegmental coordination: Theory and research. In C. Collyer & D. Rosenbaum (Eds.), Sequencing and timing of movement: Neural, computational, and psychological perspectives. Cambridge, MA: MIT Press.

Bernstein, N. (1996). On dexterity and its development. In M. Latash & M. T. Turvey (Eds.), Dexterity and its development. Mahwah, NJ: Erlbaum Associates.

Gibson, J. J. (1966). The senses considered as perceptual systems. Boston: Houghton Mifflin.

Kelso, J. A. S. (1995). Dynamical patterns. Cambridge, MA: MIT press.

Mitra, S., Riley, M., & Turvey, M. T. (1997). Chaos in human rhythmic movement. Journal of Motor Behavior, 29, 195-198.

Pagano, C., & Turvey, M. T. (1995). The inertia tensor as a basis for the perception of limb orientation. Journal of Experimental Psychology: Human Perception and Performance, 21, 1070-1087.

Turvey, M. T. (1996). Dynamic touch. American Psychologist, 51, 1134-1152.

Abstract

NEW FINDINGS ABOUT THE MECHANISM OF WHIPLASH INJURY

Manohar M Panjabi, PhD, Dr. Tech.

Yale University School of Medicine

Whiplash injuries are on the rise as reported in several recent studies. Fifty percent of car to car traffic accidents in Japan result in neck injuries. Reports from several European countries indicate an alarming increase in the annual number of neck injuries in recent years due to the increased traffic density. The National Highway Traffic Safety Administration in the USA estimates that 84% of all neck injuries are classified as AIS1, i.e. soft tissue injuries. Whiplash injuries are soft tissue injuries.

Whiplash has been loosely defined as an acceleration injury and most commonly involves an unaware victim in a stationary vehicle being struck from behind. Resulting symptoms, including neck pain, dizziness, and headaches, are non-specific and are reported up to months or years after accidents. Whiplash investigations have ranged from reviews of clinical data to a number of different biomechanical laboratory approaches. The relatively recent Quebec Task Force on Whiplash-Associated Disorders found the need for further biomechanical studies.

Several attempts have been made to define the mechanism of whiplash injuries. A better understanding of injury mechanism will help in injury prevention, diagnosis and treatment. MacNab, realizing the difficulties of clinical studies, turned to experimental trauma of anesthetized monkeys. He found a predominance of anterior element injuries. He hypothesized that it is the hyper-extension of the cervical spine that caused the injuries. Based upon the MacNab theory of hyper-extension as the injury mechanism in whiplash, the head-restraint was designed to prevent neck injuries in rear-end collisions by blocking the hyper-extension of the neck. Although the head-restraint has decreased the injuries, it did not eliminate them. In a study from Sweden, Nygren and co-workers found only a 20% decrease in neck injuries after the introduction of the head-restraint. This would suggest that the hyper-extension injury mechanism, needs to be re-examined.

We hypothesized that there is another injury mechanism, different from the hyper-extension. The goals of our research were: to quantitatively document the intervertebral rotations during experimental whiplash trauma; to quantify the functional injuries to each intervertebral level after the trauma; to image the actual injuries that occurred; and, based upon the findings, to propose an injury mechanism for whiplash trauma.

Eight fresh cadaveric cervical spine specimens including the occiput were used. Functional radiographs and multidirectional flexibility studies documented and quantified mechanical properties of the specimens. Each specimen was provided with a metal head surrogate, and was subjected to simulated whiplash trauma, starting with sled acceleration of 2.5g and ending with 10.5g, in 2g increments. During the trauma the specimen was filmed at high speed. Head rotation and translations were recorded by attached potentionmeters. The entire experiment was conducted via a computer. The functional radiographs and multi-directional flexibility tests were repeated after each trauma to quantify the injury. Finally, the injury was visualized by CT-scan, MRI and cryomicrotomy.

Our findings did not support the hyper-extension hypothesis of whiplash injury mechanism. We found distinct bi-phasic kinematic response of the cervical spine to whiplash trauma. In the first phase (50-75ms after the impact), the spine formed an S-shaped curve with flexion at the upper levels and hyper-extension at the lower levels. In the second phase (starting at 100-125ms), all levels of the cervical spine were extended but within the physiological limits. The occurrence of anterior injuries in the lower levels in the first phase was confirmed by functional radiography, flexibility test and imaging modalities. Based upon the experimental findings, we propose a new hypothesis: the lower cervical spine is injured when the spine forms an S-shaped curve, significantly before the neck is fully extended; and the full extension of the neck does not cause cervical spine injuries.

Abstracts

GREYHOUND LOCOMOTION ANALYSIS VIA WAVELET TRANSFORM

Dan B. Marghitu[1], Prasad Nalluri[1], Paul F. Rumph[2], Janet E. Steiss [2]
[1]College of Engineering, Auburn University, Auburn, AL 36849
[2]College of Veterinary Medicine, Auburn University, Auburn, AL 36849

INTRODUCTION

In this paper we present a method of analyzing animal gait using wavelets. Time series data such as joint trajectories can be decomposed by the discrete wavelet transform to represent components of different frequency bandwidth. Differences between two similar trajectories were detected by comparing the components of the same bandwidth. Hind limb function of three clinically normal Greyhound dogs was evaluated prior to and 10 days after inducing Wallerian degeneration in the tibial nerve. A discrete wavelet transform was used to decompose each joint trajectory into components of different frequency bandwidth from which mean square maps and modified scalegrams were constructed. Alterations in the gait patterns during tibial nerve dysfunction were identified and described by comparing the mean square maps and modified scalegrams.

REVIEW AND THEORY

A common method to identify gait abnormalities was to compare profiles of joint rotations of normal and pathological individuals.[1] Although such techniques are simple to implement, they do not allow for an accurate quantitative measure of the discrepancies or deviations in the kinematic quantity when comparing profiles that are very similar in nature. Borrowing from the techniques of signal analysis, researchers in the biomechanics area have used the Fourier transform to break down the kinematic time series data into components of different frequency bandwidths. The coefficients associated with these components were then compared to detect discrepancies between normal and pathological subjects.[2,3] One significant disadvantage in using this method is that the frequency information cannot be correlated to time. This is a consequence of evaluating the Fourier transform integral from $-\infty$ to $+\infty$ and the frequency information obtained is an average over the entire length of the signal. This disadvantage is overcome by the wavelet analysis which provides an alternative method of analyzing the signal. The wavelet transform is an expansion of compactly supported functions (i.e, they equal zero everywhere except within a specific interval). These functions are referred to as wavelets and are used to decompose the signal into its constituent components.[4] The original signal may be regained by adding all the wavelet components together. The purpose of the study reported here was to utilize the discrete wavelet transform and the associated mean square maps to analyze two-dimensional kinematic data obtained from the hind limbs of three normal Greyhound dogs. The analysis was repeated on data collected from the dogs during an episode of tibial nerve dysfunction. We hypothesized that by comparing the energy distribution in different components of the transform, we could identify and specifically locate the discrepancies between the patterns of normal and abnormal gaits.

PROCEDURES

The opportunity to study kinematic data from dogs during an episode of tibial nerve damage arose as an adjunct to the development of a model of nerve regeneration. Three conditioned female Greyhound dogs, weighing between 22 and 35 kg were studied. A few days after acquiring the kinematic data from the dogs at the trot, they were clinically induced with Wallerian degeneration of the tibial nerve fibers on the left hind limb. On the tenth day following surgery, kinematic data were collected for the 3 dogs. Nerve regeneration typically resulted in functional recovery within 3 months.

RESULTS

Traditional graphs of flexion/extension movements for both conditions of gait were compared along with their corresponding mean square maps to distinguish abnormalities. From visual comparison of the flexion/extension angle graphs, we could not distinguish any dramatic pattern differences before and after surgery in the coxofemoral and

femorotibial angles. Several recognizable differences were noted in the tarsal joint angles.
The coefficients obtained after applying the discrete wavelet transform were arranged in eight levels (since the length of each dataset was 2^7 i.e. 128 points) with the index of each level indicating the wavelet scale. The energy distribution by components at different levels were computed by summing the squares of the wavelet coefficients at each level and expressed as a percentage of the total signal energy. When we compared the energy distribution patterns of two similar trajectories for each dog, the lower level components were very similar. Differences in the trajectories were distributed in the higher frequency components (higher levels). Therefore, trajectories of the same joints were assumed to be built on the same basic component, with differences in individual gait patterns being embedded in the higher frequency components. To magnify the discrepancies in the energy distribution at the higher levels, we excluded the components at levels -1 and 0 and computed the energy distribution for the remaining levels.
The most obvious differences were observed in the energy distribution patterns for the tarsal joint. For dog 1 after surgery, the energy distribution at level 1 was lesser by 20 percent and level 2 indicated an increase of 20 percent. Energy distribution levels for the tarsal joint angles of dog 2 exhibited a reduction of about 10 percent after surgery. The energy contribution for the tarsal joint angles of dog 3 had dropped by almost 40 percent at level 1 and at the same time, the energy contribution at level 2 had increased by 37 percent after surgery (Figure 1). The results of visual evaluation of the energy patterns shown in the levels of the mean square maps of the tarsal joints (Figure 2) were most dramatic, easily recognized and consistent among dogs. After surgery, the maps for each dog had a notable increase in energy at level 1 during the stance phase of the gait cycle. At the other two joints, the patterns were inconsistent.

REFERENCES

1. Vilensky J. A. et al. *Journal of Orthopedic Research* Serial Kinematic analysis of the unstable knee after transection of the anterior cruciate ligament: temporal and angular changes in a canine model of osteoarthritic, 12, 229-237, 1994.
2. Hottinger H. A. et al. *American Journal of Veterinary Research* Noninvasive kinematic analysis of the walk in healthy large-breed dogs, 57, 381-388, 1994.
3. DeCamp C. E. et al. *American Journal of Veterinary Research* Kinematic evaluation of gait in dogs with cranial cruciate ligament rupture, 57, 120-126, 1996.
4. Newland D. E. *An introduction to random vibrations, spectral & wavelet analysis*, Longman Scientific & Technical Cambridge, England, 1993.

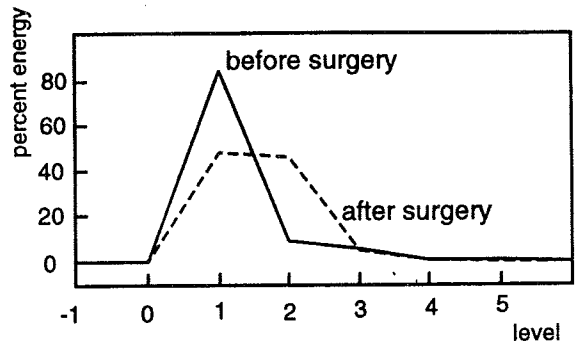

Figure 1: Energy distribution at different levels of discrete wavelet transform

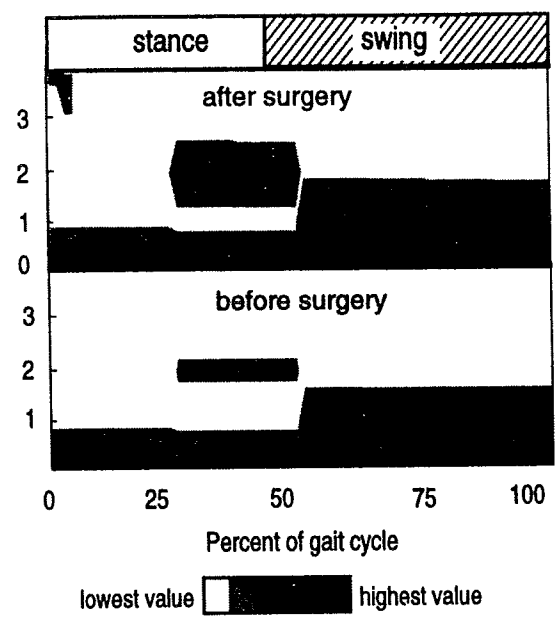

Figure 2: Mean square maps of tarsal joint

METHOD TO PREPARE CUSTOM IMPACTORS FOR *IV VIVO* IMPACTS TO RABBIT FEMORAL CARTILAGE

R.V. Baratta, M.S. Vrahas, D.M. Rosler, G.A. Smith
Bioengineering Laboratory, Louisiana State University Medical Center, Department of Orthopaedic Surgery, 2025 Gravier Street, New Orleans, LA 70112

INTRODUCTION

Post-traumatic arthritis (PTA) is a debilitating joint disease which occurs as a result of direct trauma to a joint. The pathological changes throughout the process have been well documented, but the initiating factors remain unknown. One theory suggests that upon impact, the cartilage is irreversibly damaged, initiating the cascade of destruction leading ultimately to PTA. It is conceivable that impact stresses over a given threshold initiate the PTA cascade. This possible etiology has not been studied extensively, partly because no adequate animal model exists.

REVIEW AND THEORY

One of the difficulties in applying an impact of given stress is that a fundamental assumption must be made: -the stress over the given area must be uniform. Given that joint surfaces are of complex shapes, it is necessary to apply impacts with a device which contours precisely to the shape of the area to be impacted. The purpose of this research was to develop a methodology to impact femoral condyles with blows of uniform, quantifiable stress. Furthermore, a method to estimate the impact area was developed and tested.

PROCEDURES

Impactors were developed using dead adult New Zealand White rabbits. The rabbit femur was mounted on an impaction jig, with exposing the medial femoral condyle. Polymethyl methacrylate (PMMA) bone cement was mixed and used to fill cups of 7 mm diameter and 5 mm depth when the PMMA achieved a doughy consistency. Then, the exposed medial femoral condyle was pressed into the impactor cup, leaving a contoured imprint on the curing PMMA. After the PMMA hardened, Fuji® pressure sensitive film was placed between the impactor and condyle. The impactor was pressed against the condyle with a 425 g weight, imprinting the pressure sensitive film. The uniformity of contact pressure between the impactor and condyle was assessed visually. The impact area was estimated by painting the impactor contour with a wax marker, then transferring the mark onto paper. The area imprinted on the paper was measured using a Digitizing tablet (GTCO, MD) with Research Metrics Software. The validity of this area measurement technique was validated by making 10 impressions of a 12 mm marble on impactor cups in the same manner that the femoral condyles were imprinted. The 10 imprints were made at different depths, to give a range of areas. These areas were measured in the same manner as the femoral condyles. The depth and diameter of the imprints was measured by micrometer, and these measurements plugged into the analytical expression for the surface area of a spherical base.

RESULTS

Figure 1 shows the comparison between the indentation area as estimated through the marker and calculated through the above equation. The mean difference between estimated and calculated areas was 0.007 cm^2, which amounted to 2% deviation. The maximum difference was 0.04 cm^2, which was 12% of that specific area. The excellent fit between these shows that the marker technique gives accurate determinations of the imprint area, despite the small distortions caused by representing a three-dimensional area on a two dimensional surface. Similarly, the pressure sensitive film shows that relatively uniform pressure is found throughout the impact area, as all of the film is uniformly developed, with no saturation within the imprinted area.

DISCUSSION

The technique developed to produce this custom impactor produces a contour which closely matches the condyle surface. Impacts are delivered after the PMMA hardens fully, which ensures that the impactor surface does not change during the course of the impact. The bone cement is also sterile, which makes it particularly well suited for survival experiments. Following the surgical procedure, the impactor can be removed, imprinted with a wax marker, and its area measured post-operatively. The excellent relationship given by comparing imprints of

a known area with that measured by the digitizing tablet enables us to accurately measure the area impacted in the surgical procedure. Given this technique, and an impactor cup holder instrumented with force sensing strain gages, it is possible to deliver blows of quantifiable stress to ther femoral condyles of live rabbits. Consequently, a live animal model of the development of post-traumatic arthritis can be developed.

REFERENCES

Moskowitz, st al., "Osteoarthritis Diagnosis and Management," W.B. Sanders, Philadelphia, 1984.
Repo, R.U., Finley, J.B. JBJS, 59A:1068-1076, 1975.

ACKNOWLEDGEMENTS

Supported by a Grant from the AO Foundation

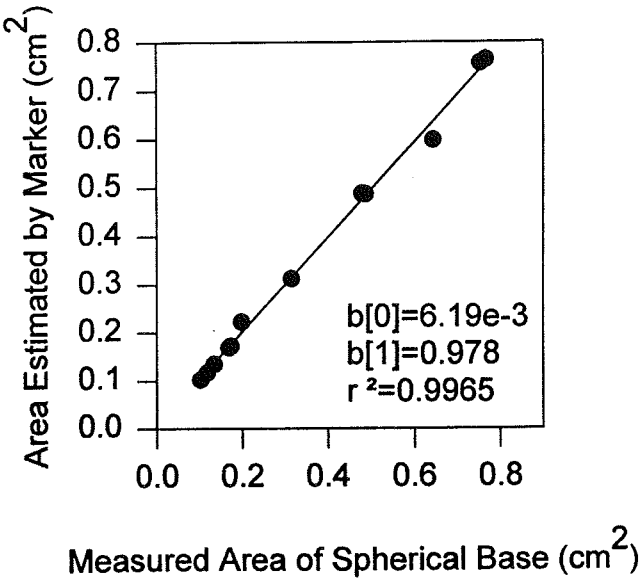

Figure 1

METHODS FOR ACCURATE EMG POWER SPECTRUM ASSESSMENT FOR BIOMECHANICAL APPLICATIONS

M. Solomonow and R. Baratta
Bioengineering Laboratory, Department of Orthopaedic Surgery
Louisiana State University Medical Center, New Orleans, Louisiana 70112

INTRODUCTION

The Power Density Spectrum (PDS) of the EMG was shown to provide important information on various muscle properties such as fatigue, force production process (motor unit recruitment), fiber composition and changes with skill acquisition. While the PDS is based on statistical analysis which has its inherent variability, other factors such as power line, environmental and system noises were responsible for introduction of additional variability which prevents scientists from developing logical conclusions as to the muscles mechanical properties. For example, during low level contractions, typically in the 0 - 30% maximal voluntary contraction (MVC) force, the signal to noise ratio is very low, and the noises PDS is dominant, introducing significant artifacts into the conclusion.

Furthermore, the production of MVC can not be taken at its face value since most subjects generate only 70 - 80% MVC without training. Calculations of PDS when considering the "untrained" MVC as true MVC, further creates an environment for additional artifactual conclusions which are not correct or logical.

The objectives of this report is to describe three methods that can significantly increase the reliability of PDS data, and restore the confidence in this analytical tool.

METHODS

The first methods consists of recording a short segment of the EMG at rest (e.g. 0% MVC), calculating the PDS of this segment which mostly includes noises of various sources. The PDS of the rest period is then subtracted from the PDS of each EMG epoch during active contraction, such that the resulting PDS excludes any components due to noise of any sources.

The second method consists of estimating the amplitude and phase of a noisy periodic waveform that may contaminate the EMG baseline during rest (e.g. 0% MVC). The periodic waveform, e.g. a sinusoid, could be than subtracted from the active EMG to obtain a clean signal from analysis.

Training subjects to obtain their true MVC consists of first asking a subject to produce his maximal force contraction while displaying it on the monitor as a moving line on a scale. The experimenter than sets a new line, 10% higher than the last obtained by the subject, than asking him to exceed it. The procedure is repeated until the subject can not exceed the new goal, and his last (highest obtained) force level is set as MVC.

RESULTS

Figure 1 shows the Median Frequency (MF) of the PDS of a subject performing linearly increasing isometric force contraction from 0 to 100% MVC over 3 seconds. The curve consisting of the circle data points is from calculations of the MF of the PDS without eliminating the noise, whereas the curve consisting of the square data points is from calculations in which the noises PDS was subtracted from each epoch of the EMG's PDS. Clearly, one can see that the "clean" MF trace has a near linear increase up to about 80% MVC whereas the unclean MF curve is erratic, showing decrease in the low force range of 0 -25% MVC, and then an increase.

Figure 2 shows the EMG, PDS and MF of the EMG obtained in a mild isometric elbow

flexion immediately after a rest (0% MVC). The left column shows a low level cyclic noise prior to the contraction, and the associated MF of the PDS at 57 Hz. The right column shows the EMG after subtracting the power line noise according to Method 2, and the associated MF of the PDS at 52 Hz. Clearly, the noise resulted in an erroneous increase of 5 Hz in the estimation of the MF.

The MF of the PDS as a function of force before and after training a subject to generate his true MVC shows that nearly 37% additional force was obtained with a completely different curve of MF progression during the force increase.

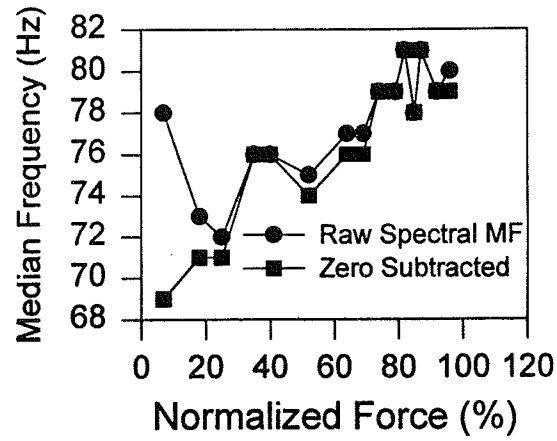

Figure 1

DISCUSSION

Three Methods were described, with an example for each, that could significantly reduce the variability and components of the PDS of the EMG during force production of a muscle. The Methods allow scientist to use the PDS as an analytical tool to provide precise insights into the force production mechanism of a skeletal muscle free of artifactual inputs from environmental noise and subject/experimenter error. It is conceived that the described techniques will restore lost confidence in the PDS as a tool to assess muscle properties.

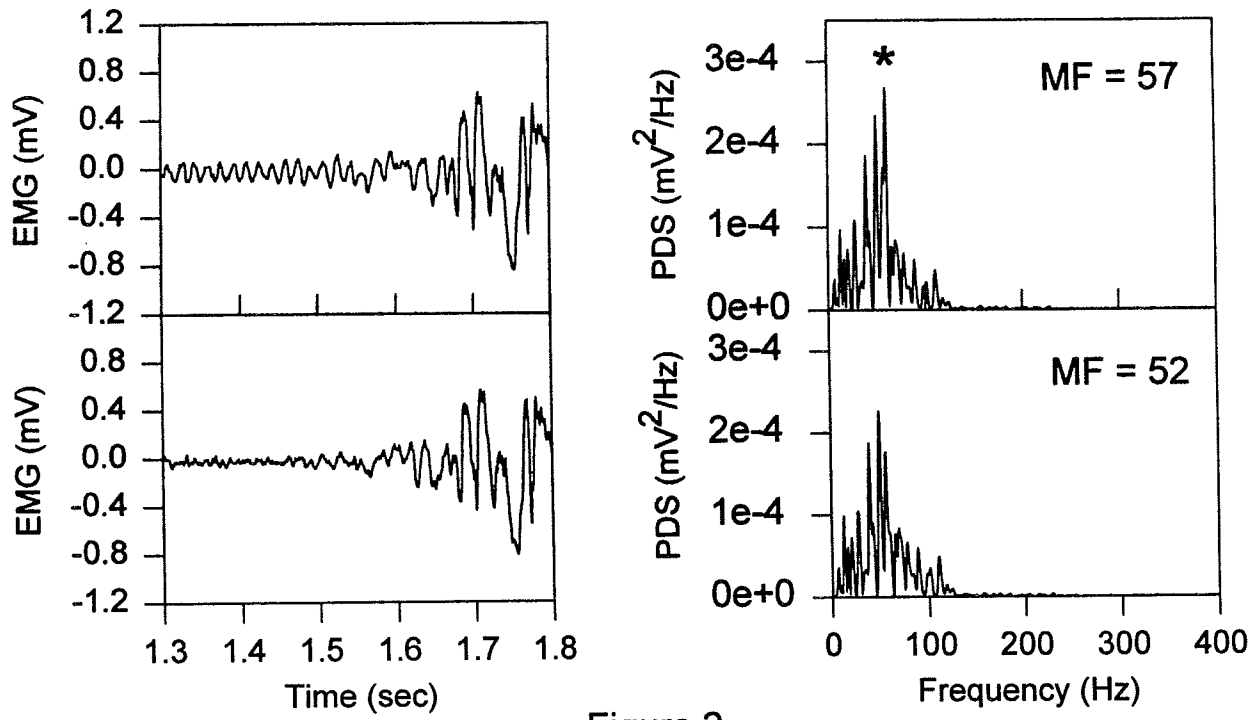

Figure 2

VALIDATION OF EMG SPECTRAL INDEX CHANGES DURING ISOINERTIAL BACK ENDURANCE TEST

M.Kankaanpää[1,2], S.Taimela[3], C.L. Webber Jr[4], O.Airaksinen[1], and O.Hänninen[2].

[1]Kuopio University Hospital, [2]Kuopio University, Kuopio, Finland
[3]DBC International,Vantaa, Finland
[4]Loyola University Chicago, Chicago, USA

INTRODUCTION

Our group has recently developed an isoinertial back endurance test utilizing EMG spectral index calculations as an objective measure of paraspinal muscle fatigue. The validity of spectral index calculations in isoinertial loading has been questioned.This study examined the validity of EMG spectral changes in isoinertial back endurance test by comparing them to EMG spectral changes obtained with validated isometric contractions performed before and immediately after the isoinertial loading.

REVIEW AND THEORY

Reduced endurance capacity of lumbar paraspinal muscles is related to chronic low back pain. Isometric endurance tests based on measurements of maximal endurance (time) are often used to assess paraspinal muscle fatigability and monitoring functional restoration. However, isometric conditions with high levels of loading are seldom related to everyday function of the back muscles, since the trunk loading is mostly dynamic and isoinertial. In addition, measurement of endurance time is dependent of subject qualities, e.g. motivation. We have recently developed an submaximal (90 sec) isoinertial back endurance test simulating the daily use of the back muscles (Kankaanpää et al. 1997). In the test, paraspinal EMG spectral indices are used as an objective estimate of fatigue. In the study the short term stationarity and therefore acceptability for Fourier transform calculation was confirmed by novel Recurrence Plot Analysis (Webber et al., 1995). Still the validity of EMG spectrum results obtained from isoinertial endurance run has been questioned. The aim of the present study was to assess the validity of EMG spectral decreases in isoinertial back endurance test by comparing them to EMG spectral indices obtained during validated isometric contractions performed before and immediately after the isoinertial loading.

PROCEDURES

31 middle aged females participated the study.

Age (y)	45.0 ± 5.6
Height (cm)	164.4 ± 5.4
Weight (kg)	70.1 ± 11.2

Table 1: Subject characteristics

Subjects performed submaximal 90 sec isoinertial upper trunk extensions (30 repetitions / min) in a specially designed testing unit where vertebral columns below L3 were guided not to move. The movement amplitude was adjusted between 25 degrees flexion and 5 degrees extension and the load level was calculated on the basis of upper body weight, sex and age. 10 sec isometric contractions were performed before and immediately after the isoinertial endurance test with the target load that was related to the isoinertial test load. Continuous surface EMG recordings were made bilaterally over the paraspinal muscles at L5-S1 level during the entire protocol. The guided movement procedures minimize the movement of paraspinal muscles in relation to the measuring electrodes and minimize artefact nonstationarities.
Mean power frequency (MPF) was calculated by using Fast Fourier Transformation.
Isometric contractions: The mean MPF was calculated for the first 5 sec of the contractions obtained before ($\mathbf{MPF}_{pre}$) and after ($\mathbf{MPF}_{post}$) the isoinertial endurance test. Relative decrease ($\mathbf{MPF}_{test}$, %/min) from $\mathbf{MPF}_{pre}$ to $\mathbf{MPF}_{post}$ was calculated.
Isoinertial endurance test: Relative slope (%/min) of MPF ($\mathbf{MPF}_{slope}$) was calculated by using the linear fitting. In addition, mean of MPF values were calculated for the first ($\mathbf{MPF}_{init}$) and last ($\mathbf{MPF}_{late}$) 5 sec of the MPF_{slope}. For statistical analysis t-test and Pearson correlation procedures were used. The statistical significance was set at $p<0.05$. All values are expressed as mean ± SD.

RESULTS

Isometric contraction MPF (MPF_{pre}) (obtained before endurance test) and isoinertial endurance test initial MPF (MPF_{init}) were similar ($p>0.05$), and correlated highly (Table 2).

	Left	Right
MPF_{pre} (Hz)	81.3 ± 14.5	80.0 ± 15.0
MPF_{Init} (Hz)	82.0 ± 16.3	81.9 ± 16.3
Correlation	0.84 p<0.001	0.85 p<0.001

Table 2: Comparison of MPF in test contraction (before isoinertial test) and in initial 5 sec of isoinertial test, and their correlation coefficients.

MPF_{post} was higher than MPF_{late}, however, they correlated very highly (Table 3).

	Left	Right
MPF_{post} (Hz)	65.8 ± 13.4	64.7 ± 12.3
MPF_{late} (Hz)	61.8 ± 14.7	61.2 ± 14.5
Correlation	0.92 p<0.001	0.92 p<0.001

Table 3. Comparison of MPF in isometric contraction (after isoinertial test) and in last 5 sec of isoinertial test, and their correlation coefficients.

Similar lumbar paraspinal muscle MPF decreases were observed between isometric contractions (MPF_{test}) and during isoinertial endurance test (MPF_{slope}), indicating similar results in both testing procedures. Correlation coefficients between MPF_{test} and MPF_{slope} were high (Table 4).

	Left	Right
MPF_{test}	-13.2 ± 7.3	-13.3 ± 8.0
MPF_{slope}	-19.6 ± 10.8	-20.1 ± 11.5
Correlation	0.79 p<0.001	0.76 p<0.001

Table 4. Comparison of MPF slopes in test contractions (MPF_{test}) and in isoinertial test (MPF_{slope}), and their correlation coefficients.

DISCUSSION

Since the MPF values and their decrease over time were similar in both isometric contractions and during the isoinertial endurance test, it is concluded that EMG spectral index calculations can be used for signal analysis obtained during the isoinertial back endurance test. The use of EMG frequency alteration measurements in isometric contractions as an assessment tool for muscle fatigue has been validated in earlier studies (Hägg et al., 1991). In the present study MPF_{post} was higher than MPF_{late}. This could be explained by the fact that there was approximately 5 sec time period between the end of repetitive endurance test and test contraction allowing sufficient time for the partial recovery.

REFERENCES

Hägg G. Zero crossing rate as an index of electromyographic spectral alterations and its applications to ergonomics., 10-11, Chalmers University of Technology, Göteborg, Sweden, 1991.

Kankaanpää M., Webber C.L. Jr., Taimela S., Airaksinen O., Hänninen O. Eur. J. Appl. Physiol., in press, 1997.

Webber CL Jr, Schmidt MA, Walsh JM. J Appl Physiol 78, 814-822, 1995.

ACKNOWLEDGMENTS

This study was supported by Finnish Academy and Ministry of Education (TULES Graduate School), Finnish Work Environmental Fund, Emil Aaltonen Foundation, Instrumentarium Science Foundation and Yrjö Jahnsson Foundation.

Validation of An Algorithm for Calculating Gravity Line Displacement while Standing

D.L. King and V.M. Zatsiorsky

Department of Kinesiology, The Pennsylvania State University, University Park, PA 16802

INTRODUCTION

Over the past few years several algorithms have been proposed to estimate gravity line displacement (GLP) directly from force platform data during quiet standing tasks (Shimba, 1984; Benda, et al., 1994; King and Zatsiorsky, 1997). Few of these methods, however, have been validated against standard methods of determining gravity line displacement such as videography. In this study a validation of one algorithm, zero-crossing algorithm, was performed using optical techniques.

REVIEW AND THEORY

Gravity line displacement provides a direct measure of body sway, but due to difficulties in measuring gravity line displacement during standing tasks, center of pressure (COP) migration is often used as an indirect measure of body sway.

The horizontal displacement of the gravity line can be determined from the double integration of the horizontal acceleration of the center of gravity. Algorithms proposed by Shimba (1984) and King and Zatsiorsky (1997) utilized different techniques for estimating the two unknown constants of integration which appear during the double integration. An algorithm, introduced by Benda, et al. (1994), involved filtering center of pressure displacement data to estimate gravity line displacement. This method does not require the knowledge of integration constants and is based on the presumption that the COP fluctuates about the GLP.

During quiet standing it is not apparent that videography is an acceptable technique for determining gravity line location. The magnitude of gravity line migration is typically of the same order as errors in estimating segment masses and center of mass locations. However, during one legged standing the gravity line displacements are on the order of magnitude of centimeters. The purpose of this study was to validate the zero-crossing algorithm proposed by King and Zatsiorsky (1997) for determining gravity line location from force platform data using optical techniques during one legged standing.

PROCEDURES

Five subjects gave their informed consent to participate in this study. The subjects were instructed to stand on their preferred leg for 45 seconds with their eyes closed. The subjects stood with their hands on their hip with no specific instructions given as to the position of the non-supporting leg

A force platform operating at 30 samples per second was used to record the ground reaction forces (GRF). The horizontal accelerations along the medial lateral axis of the subjects were calculated form the medial lateral GRF force. These accelerations were then integrated twice using the zero-crossing algorithm proposed by King and Zatsiorsky (1997).

Step 1. Determine the locations of the COP migration at the instances when the horizontal ground reaction force is zero, $F_x(t) = 0$. A threshold range, $\pm\delta$, around zero was used to determine the zero crossing, $-\delta < F_x(t) < \delta$.

Step 2. Calculate the second integral of $\ddot{x}_x(t) = F_x(t)/m$ starting at $t_0 | -\delta < F_x(t) < \delta$ and ending at $t_1 | -\delta < F_x(t) < \delta$. Use $x_{cop}(t_0) | -\delta < F_x(t) < \delta$ as the first initial constant of integration, initial position, and $\dot{x}(t_0) = 0$ as a temporary value for the second constant of integration, initial velocity.

Step 3. Compare the experimentally recorded value of center of pressure, $x_{cop}(t_1)$, and the calculated value, $x(t_1) | -\delta < F_x(t) < \delta$. The

difference divided by $\Delta t = t_1 - t_0$ is equal to the actual initial velocity, $\dot{x}(t_0)$.

Step 4. Repeat Step 2 with the actual initial velocity integration constant, $\dot{x}(t_0)$ calculated in *Step 3*.

Step 5. Continue Steps 2 through 4, integrating from $t_n | -\delta < F_x(t) < \delta$ to $t_{n+1} | -\delta < F_x(t) < \delta$ for the entire curve, $\ddot{x}_x(t) = F_x(t)/m$.

A video recorder was used to record the frontal plane of the subjects during the one legged standing task. Retro-reflective markers were used to define an 11 segment model of the human body. Segment mass characteristics (Zatsiorsky and Seluyanov, 1983) were used to calculate whole body center of mass displacements with a Peak5 motion analysis system.

Summary statistics of the gravity line displacement as calculated with the zero-crossing algorithm (GLPz) were compared with the horizontal displacement as determined from the video recordings (GLPv). Additionally a cross correlation analysis was performed between these two parameters.

RESULTS AND DISCUSSION

The Figure contains representative data of the GLPz and GLPv results from one subject. Notice that the GLPz and GLPv are of similar magnitude and phase. The observed GLP magnitudes indicate that one legged standing is appropriate for using optical methods to validate the GLPz algorithm.

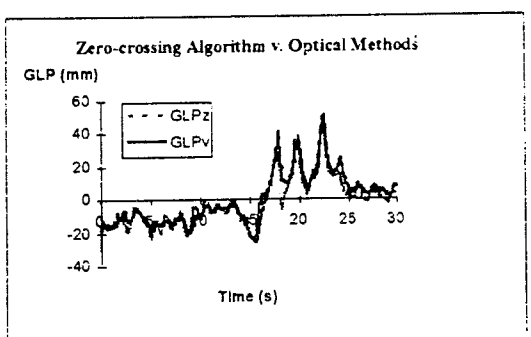

Figure. GLPz and GLPv curves for 1 subject. Cross correlation is 0.94.

The average RMS and range values for GLPz and GLPv over all subjects are presented in Table 1. The results indicate that the zero crossing algorithm is a valid technique for determining GLP during standing tasks.

Table 1. Average ranges and RMS values.

	GLPz (mm)	GLPv (mm)
Range*	46.8 ± 17.7	41.8 ± 21.7
RMS	9.28 ± 2.97	9.04 ± 4.22

* all values are mean ± SD

Table 2 presents the cross correlation results between GLPz and GLPv. These cross correlations further substantiate the use of the zero crossing algorithm for determining GLP during standing tasks.

Table 2. Cross correlations for GLPz and GLPv.

Subject	correlation
1	0.94
2	0.83
3	0.88
4	0.96
5	0.79

Due to small gravity line displacements during quiet standing tasks, optical methods may not be acceptable for determining GLP. During the more dynamic one legged standing tasks where GLP migration is several times greater than in quiet standing the optical method was appropriate for validating the zero-crossing algorithm. The high cross correlation values indicate the validity of the zero-crossing algorithm. Thus for quiet standing tasks where optical methods are inappropriate the zero-crossing algorithm is a valid alternative for determining gravity line migration.

REFERENCES

Benda BJ, et al. IEEE Trans Rehab Engng, 2, 3-10, 1994.

King DL and Zatsiorsky VM. Gait & Posture. In press, 1997

Shimba T. J Biomech, 17, 53-60, 1984.

Zatsiorsky VM and Seluyanov VN. In: Biomechanics VIII-B, 1152-1159. 1983.

WAVELET ANALYSIS OF EMG SIGNALS

W.M. Sloboda, V.M. Zatsiorsky

Department of Kinesiology, Pennsylvania State University, University Park, PA 16802

INTRODUCTION

The correlation of spectral changes in electromyographic (EMG) recordings with corresponding force production has shown promise in recent years (2,3). Previous studies have used calculations based on Fast Fourier Transforms (FFT) to accomplish this work. This research alternatively applies wavelet transforms to surface EMG's recorded during isometric ramped force production. This mathematical technique is shown to have promise in unraveling the physiologic phenomena underlying the EMG spectral changes.

REVIEW AND THEORY

Basmajian and De Luca (1) have shown how the affects of superposition and tissue filtering join to produce a single Motor Unit Action Potential (MUAP) detected by electrodes. In additional work both De Luca (3) and Solomonow (2) have reported overall spectral shifts in the surface EMG. These shifts are attributed to the type of muscle fibers activated and may therefore be used for characterization of motor unit recruitment and muscle composition. Investigation of these shifts have been limited to changes in the median frequency of the power spectrum derived using windowed FFT. These methods, however, try to capture time varying spectral shifts, that are due to changes in the underlying irregular discrete waveforms, using continuous regular sine waves. Wavelet analysis allows investigation of these changes using irregular discrete "little waves". These are functions whose shape and duration are much more similar to an actual MUAP. By scaling and translating these "little waves" the resulting decomposition may produce information about the recruitment of the motor units of different type.

PROCEDURES

Subjects were asked to produce ramped isometric elbow flexion. A maximal force value was obtained by averaging three attempts. Using the max force value several ramps were constructed of one, three, and five second duration that ended in 25%, 50%, 75%, and 100% of maximal force. The subject was then asked to match his force output with that of the prescribed ramp. Force and EMG signals were collected at 1000 Hz. Surface EMG was collected using Delsys Inc. Differential Electrode DE-02.3H. Typical results are shown in figure 1. Wavelet Analysis was performed using the 'db3' Daubechies wavelet shown in figure 2.

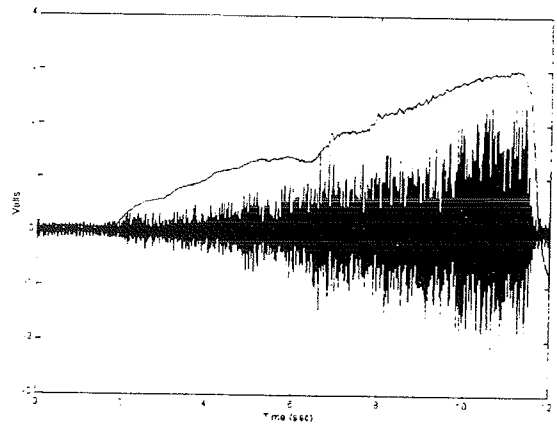

Figure 1: Ramp Force and EMG vs Time

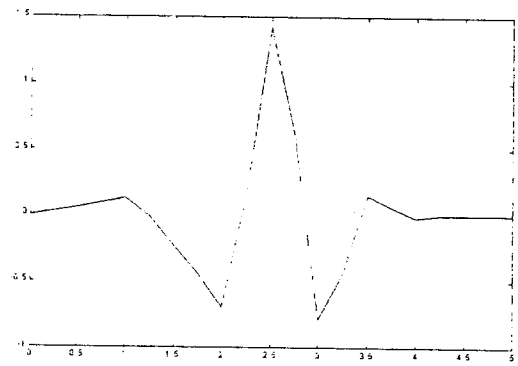

Figure 2: The Daubechies 'db3' Wavelet

The analysis is based on a decomposition of the EMG signal using the following scaled and translated function :

$$C(a,b) = \int EMG(t)\frac{1}{\sqrt{a}}\,'db3'\left(\frac{x-b}{a}\right)dt$$

The scales a were chosen in conjunction with the sampling rate to give wavelets with a period in the 3-20 ms range. This range is reported for single human muscle action potentials. The 'db3' wavelet was chosen because of it's similarity to the MUAP, described by Basmajian and De Luca (1). The magnitude of C(a,b) is a measure of the matching of the original with the 'db3' scaled and translated wavelet. Results of the decomposition are shown in figure 3. Analysis was performed using the Matlab 5 (The Math Works, Inc.) Wavelet Toolbox. This is a gray scale plot with greater blackness reflecting increases in the coefficients absolute value. A force tracing is also provided as a reference.

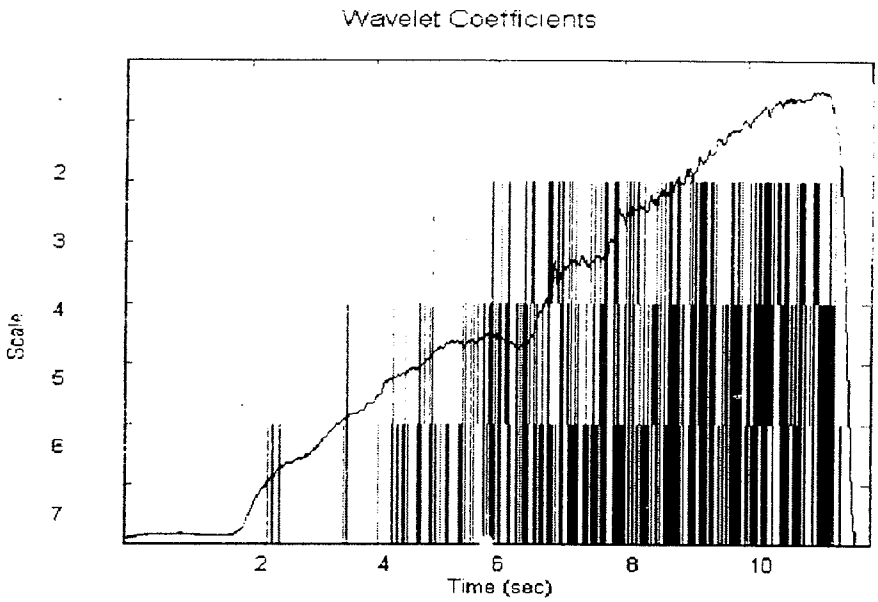

Figure 3: Wavelet decomposition of EMG.

RESULTS

As the force increases nearly linearly with time, scales containing higher bands of frequency become activated. Near 50% of the maximum force all bands that will be activated have been. This is consistent with the findings of both Solomonow(2) and De Luca(3) who found that between 50 to 75% of MVC the spectral shifts they observed also reached an upper limit.

DISCUSSION

The spectral shifts that take place during changes in force production have generally been explained by the changes in types of motor units recruited. Fast motor units have larger propagation velocities and also appear to posses different membrane qualities that lead to the changes in spectral characteristics. While similar changes are noted using a windowed FFT approach they are more clearly and realistically documented using the wavelet approach. This is due to the wavelets ability to mimic a MUAP, the underlying building block of EMG, as opposed to the continuous sine waves utilized by FFT's. The wavelet analysis promises to be a useful tool in explaining the underlying muscle recruitment strategies that make up the EMG signal.

REFERENCES

1. Basmajian, J.V. and De Luca, C.V. *Muscles Alive*. Baltimore, MD: Williams & Wilkins, 1985.
2. Solomonow, M., Baten, C., Smit, J., Baratta, R., Hermens, H., D'Ambrosia, and Shoji, H. Electromyogram power spectra frequencies associated with motor unit recruitment strategies. J. Appl. Physiol. 68(3): 1177-1185, 1990.
3. Kupa, E.J., Roy, S.H., Kandarian, S.C., and De Luca, C.V. Effects of muscle fiber type and size on EMG median frequency and conduction velocity. J. Appl. Physiol. 79(1): 23-32, 1995.

WAVELET TRANSFORMS FOR SMOOTHING KINESIOLOGICAL DATA

M. Wachowiak[x], G. Rash[¥], A. Desoky[x], P. Quesada[§]
[x]Department of Computer Science, University of Louisville, Louisville, KY
[¥]Gait and Biomechanics Lab, Frazier Rehab Center, Louisville, KY
[§]Department of Mechanical Engineering, University of Louisville, Louisville, KY

INTRODUCTION

An important problem in the analysis of biomedical data is the filtering (smoothing) of signals which have sharp spikes and/or discontinuities. This problem is particularly evident in biomechanical and kinesiological data, where recorded measurements corresponding to impacts (for example, foot strikes) appear as spikes in graphical representations. These spikes are short-duration high frequency components, which are normally treated as noise in traditional filtering methodologies. Thus, standard filters, such as Butterworth and spline filters, perform well in smoothing the noise from the data, but have the unwanted effect of attenuating the impact signals. Additionally, smoothing kinesiological data with standard techniques underscore the problem of edge effects, or errors in filtered data which occur at the beginning and end of measurements, and between areas of abrupt frequency changes. It is proposed that wavelet transforms may be useful in smoothing noise from kinesiological data, while at the same time leaving the impact signals intact, and avoiding undesirable side effects.

REVIEW AND THEORY

Wavelet theory is a relatively new branch of applied mathematics which has applications in such areas as numerical analysis, mathematical modeling, and especially in image and signal processing. Wavelet transforms have been successfully used to analyze a wide variety of biomedical data. The most attractive feature of wavelets transforms is their good localization in both the frequency and time/spatial domains. Because wavelet decompositions produce signal representations with good time resolution at high frequencies and good frequency resolution at low frequencies, different window sizes can be used to analyze the signals

The two constraints on wavelet functions are: (1) It must decay with respect to time/space (providing time localization), and (2) its integral must vanish over all values of time/space (providing oscillation). Additionally, unlike the Fourier transform, which is based on sine and cosine functions, there are an infinite number of wavelets. Thus, a great number of wavelet functions exist which can be used to analyze signals with differing characteristics. The existence of fast transform algorithms add to the attractiveness of applying wavelet techniques to biomedical data. However, very little work has been done to specifically use wavelet transforms for analyzing and filtering biomechanical and kinesiological data.

For the present study, the Haar wavelet was used. This simple wavelet function is based on the square wave. The Haar wavelet, although useful for analyzing piecewise continuous functions, is not ideal for smooth or differentiable functions. However, it was used as a first step in determining the validity of applying wavelet techniques to data with sharp spikes.

METHODS

A simple "ball drop" experiment was performed to study the validity of applying wavelet techniques to kinesiological signals with impact components. A sturdy metal wire was tightly drawn over a metal frame. This served as a vertical guide for freefall of a metal cylinder. Half of a rubber ball was attached to the base of the frame to allow the cylinder to bounce. The cylinder, which was designed so that an accelerometer could be attached, was wrapped with reflective tape to allow the collection of positional (video) data. Accelerometer data (1200 Hz) and positional measurements (120 Hz) were recorded from ten ball drop trials. A MotionAnalysis™ EVA Hi-Res, Version 3.65 system, running on a Sun SparcStation, was used for the collections. The accelerometer data, although not analyzed in the present abstract, will be used in comparisons with positional data to which the wavelet transform is applied.

Four seconds of positional data, or 480 frames, were collected, and padded with zeros to 512 elements. The acceleration for a representative trial was derived from the z-component of the position data using the central difference formula. A personal computer C-language program was written to apply the Haar wavelet transform and its inverse to the z-component, using a user-defined cutoff frequency value which was applied to the entire transform.

DEVELOPMENT OF A THREE-DIMENSIONAL ARM STRENGTH PREDICTION MODEL

Richard E. Hughes, Andrew Westreich, Michael G. Rock, and Kai-Nan An
Mayo Clinic/Mayo Foundation, Rochester, MN 55905

INTRODUCTION

Sometimes muscles are resected during oncologic reconstructions of the shoulder, which can have profound affects on arm strength. The purpose of this study was to develop a three-dimensional biomechanical model for predicting arm strength (e.g. push, pull, lift, etc.) from musculoskeletal geometry and muscle physiology. Such a model could be used to pre-operatively evaluate effects of tissue resection.

REVIEW AND THEORY

Three-dimensional biomechanical models of the upper extremity have been developed (van der Helm, 1994; Högfors *et al.*, 1987; Karlsson and Peterson, 1992, Nieminen *et al.*, 1995). These models have used optimization methods to compute muscle forces. Nieminen *et al.* (1995) used a 3D model to predict maximal arm strength.

All of these models used an idealized representation of musculoskeletal geometry to determine the moments produced by individual muscles. Specifically, it was assumed that each muscle took the shortest distance between origin and insertion subject to the constraint that the path did not pass through a bone. Hughes *et al.* (1996) found that this method produces moment arm estimates that can be substantially different from moment arms determined by using the relationship between tendon excursion and joint angle measured in *in vitro* experiments.

PROCEDURES

A 3D static biomechanical model of the upper extremity (glenohumeral joint, elbow, and wrist) was formulated. The glenohumeral, ulnohumeral, and radiohumeral joints were modeled as ball-and-socket, revolute, and revolute joints, respectively. The wrist was modeled as a universal joint. Coordinate systems on the hand, ulna, humerus, scapula, and torso were used to specify upper extremity posture. Body segment masses and center of gravity locations were taken from the literature (Chaffin and Andersson, 1984) and scaled to stature and weight. Muscle moment arms were taken from studies that used the tendon excursion-joint angle method: glenohumeral joint (Kuechle, 1994), elbow (Murray *et al.*, 1995; Schuind *et al.*, 1994), and wrist (Horii *et al.*, 1993). Maximum muscle force was modeled as the product of specific tension (Ikai and Fukunaga, 1968) and physiological cross sectional area (An *et al.*, 1981; Veeger *et al.*, 1991; Karlsson and Peterson, 1992). Two external forces were allowed in the model (radial and ulnar side of palm), and the directions were specified. The model was formulated as a linear program, were the objective to be maximized was the sum of the reaction forces acting on the palm of the hand.

Isometric arm strength measurements were made on ten subjects (5 male; 5 female) ages 23 to 66 (median 34) in order to evaluate model predictions. Strength measurements were made using a cylindrical grip attached to 500 lb load cell via a nylon cord. Three repetitions of each test condition were performed, and subjects were given rest between exertions. Each test consisted of a three second exertion, and the middle two seconds were averaged and stored. Three upper arm postures (neutral, flexed 45°, abducted 45°) were tested, and an 85° elbow angle was used in each condition. Maximal lift up and push down forces were measured with the upper arm in neutral (posture 1). Lift up, push down, pull medially, and pull laterally were measured in the flexed posture (posture 2). Lift up, push down, push and pull forces were measured in the abducted posture (posture 3). The order of postures tested were randomized, and the order of exertion directions was randomized within each posture. Anthropometric

measurements were taken and used as input for the biomechanical model.

Inter-subject variability was reduced by normalizing strength test data by maximal forces measured in the opposite direction (e.g. ratio of push to pull forces). Wilcoxon signed rank tests were used to test for differences between predicted and measured strength ratios.

RESULTS

The model predicted the ratio of pull up to push down strength when the humerus was in a neutral posture. Statistically significant differences between measured values and model predictions were found in all other test conditions (Figure 1). The largest difference was found in the push/pull forces with the arm abducted 45 degrees.

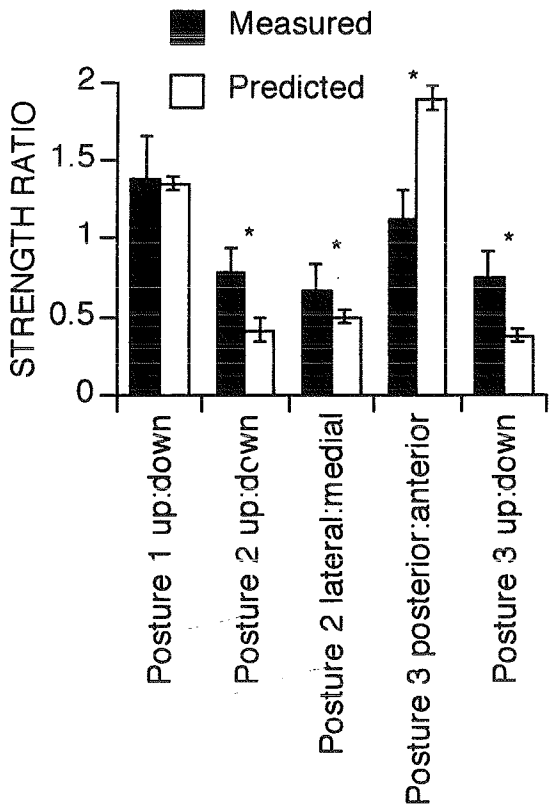

Figure 1. Measured and predicted hand force exertion ratios. * denotes statistically significant difference ($P<0.05$) between measured and predicted values.

DISCUSSION

The biomechanical model predicted the ratio of lift up to push down forces when the upper arm was in a neutral posture. However, the model did not predict forces well when the arm was flexed or abducted. The discrepancies between predictions and measurements may be due to not including the length-tension property of muscle, because the largest differences occurred in flexed or abducted postures. The inability of model to predict push and pull forces in an abducted arm posture may be caused by the representation of the glenohumeral joint, which did not include shear forces and the need for active stabilization by the muscles.

REFERENCES

An, K-N et al. *J. Biomech.*, 14, 659-669, 1984.

Chaffin, D.B. and Andersson, G.B.J. *Occupational Biomechanics*, NY: Wiley, 1984

Högfors, C. et al. *J. Biomech.*, 699-709, 1991.

Horii, E. et al. *J. Hand Surg.*, 18A, 83-90, 1993

Hughes, R.E. et al. *ASB Proceedings*, pp. 245, 1996.

Ikai, M. and Fukunaga, T. *Int. A. agnew. Physiol. einschl. Arbeitsphysiol*, 26, 26-32, 1968.

Karlsson, D. and Peterson, B. *J. Biomech.*, 25, 189-199, 1992.

Kuechle. D.K. MS Thesis, Mayo Graduate School, Rochester, MN, 1994.

Murray, W.M. et al. *J. Biomech.*, 5, 513-525, 1995.

Nieminen, H. et al. *J. Biomech.*, 28, 555-566, 1995.

Schuind, F. et al., 1994 *J. Shoulder Elbow Surg.*, 3, 191-199.

van der Helm, F.C.T. *J. Biomech.*, 27, 551-569, 1994.

Veeger, H.E.J. et al. *J. Biomech.*, 24, 615-629, 1991.

ACKNOWLEDGEMENTS

This study was supported by NIH grants AR41171 and HD07447 and the Musculoskeletal Transplant Foundation.

AN OPTIMIZATION-BASED DIFFERENTIAL INVERSE KINEMATICS APPROACH FOR MODELING THREE-DIMENSIONAL DYNAMIC SEATED REACHING POSTURES

Xudong Zhang and Don B. Chaffin
Center for Ergonomics, The University of Michigan, Ann Arbor, MI 48109

INTRODUCTION

Although optimization techniques have been extensively utilized to model human postures and movements, the implementation of three-dimensional (3D) dynamic models with a desirable level of sophistication remains a challenge. Existing optimization-based models for posture prediction or motion simulation are either static, or dynamic but restricted in the scale or dimension of the biomechanical systems. Static models, 2D or 3D, usually rely on static optimization to resolve the postural indeterminacy for only one stance. Such models can be used in a sequential fashion to emulate movements (Ryan, 1970; Kilpatrick, 1970) but incur laborious computation, as every time instant corresponds to a fairly sizable and often non-linear optimization problem. For dynamic movement modeling, many have resorted to and advocated dynamic programming (Ayoub et al., 1974; Hsiang, 1992; Yamaguchi, 1990). Because the use of dynamic programming places a stringent limit on the number of model variables, either the dimension of or the number of body segments included in a model has to be compromised.

This paper describes a new optimization-based differential inverse kinematics approach for modeling three-dimensional dynamic postures. It has the potential of being computationally very efficient, and can accommodate a reasonable number of degrees of freedom (DOF). Specifically, this approach was applied to the modeling of right-handed seated reaching movements, wherein both torso and right arm motions were involved.

METHODS

Differential kinematics (Whitney, 1969) has been primarily used in the robotics field for trajectory planning. It considers the differential relationships between the end-effector motions and joint motions. In the context of human posture modeling, such a relationship can be described as:

$$\dot{\mathbf{P}} = \dot{f}(\Theta) = \mathbf{J}(\Theta)\dot{\Theta} \qquad (1)$$

where $\dot{\mathbf{P}}$ is the hand velocity ($\mathbf{P}$ as hand position), $\dot{\Theta}$ is the angular velocity, and $\mathbf{J}$ is the Jacobian matrix. Establishment of the above relationship is based on a biomechanical linkage representation of the human body. In the present modeling effort, a 4-segment 7-DOF linkage is employed to describe the kinematics of the torso and right arm in 3D (Figure 1). Thus, $\dot{\mathbf{P}} = [\dot{x} \quad \dot{y} \quad \dot{z}]^T$, $\dot{\Theta} = [\dot{\theta}_1 \quad \dot{\theta}_2 \quad \dots \quad \dot{\theta}_7]^T$, and $\mathbf{J}$ is a 3×7 matrix. The seven joint angles $\theta_{1\text{-}7}$ represent torso flexion, torso lateral bending, torso twisting (clavicle rotation), shoulder extension, shoulder abduction, humeral rotation, and elbow extension.

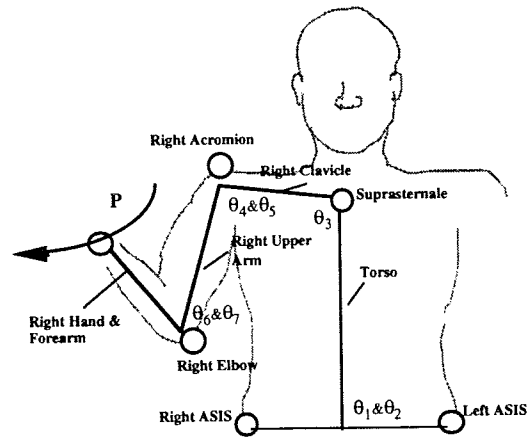

Figure 1. A 4-segment 7-DOF linkage in reference to surface markers to represents the torso and right arm.

By taking a weighted pseudoinverse of (1), the joint angular velocity can be derived as

$$\dot{\Theta} = \mathbf{W}[\mathbf{J}\mathbf{W}^{-1}]^{\#}\dot{\mathbf{P}} \qquad (2)$$

where # symbolizes the pseudoinverse, and $\mathbf{W}$ is a weighting matrix as $\mathbf{W} = \mathbf{I}_7 \bullet [w_1 \quad w_2 \quad \cdots \quad w_7]^T$ ($\mathbf{I}_7$: a 7×7 identity matrix). The solution by (2) minimizes the instantaneous weighted system kinetic energy $\frac{1}{2}\dot{\Theta}^T\mathbf{W}^T\mathbf{W}\dot{\Theta}$. Given the initial angle set and hand path, the weights $w_{1\text{-}7}$ are the only variables that influence the movement profiles.

We proposed a four-weight $\mathbf{W}$ configuration as $\mathbf{W} = \mathbf{I}_7 \bullet [w_1 \quad w_1 \quad w_2 \quad w_3 \quad w_3 \quad w_4 \quad w_4]^T$ where w_1 is designated to θ_1 & θ_2, w_2 to θ_3, w_3 to θ_4 & θ_5, and w_4 for θ_6 & θ_7. We further postulated that the weights remain time-invariant for a movement. Therefore, $\mathbf{W}$ quantifies an inter-segment allocation strategy for postural control during a movement—a smaller weight value indicates the corresponding segment is relatively more involved in the movement.

With the above hypothesized setting, the modeling approach was applied to a real data set to assess the best fitting accuracy achievable, and to identify the weight values resulting in the best emulation of the

measured profiles (i.e., $|\Theta - \Theta^*|$ minimized). This fitting process was accomplished by optimization procedures based on simulated annealing.

The data set contained three-types of seated reaching movements performed by six subjects. The movements were distinguished by the direction of hand motions: anterior-posterior (AP), medial-lateral (ML), and up-down (UD). Each type was performed at four hand path locations formed by varying height, distance to the body, and asymmetry of the torso.

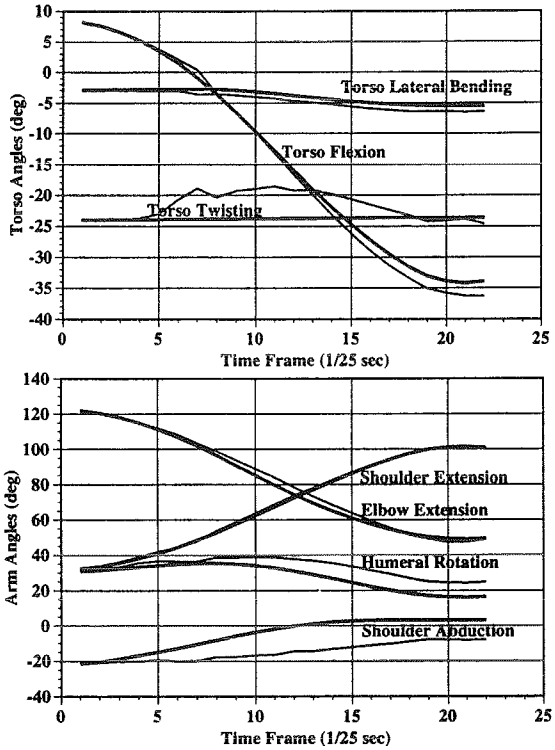

Figure 2. Predicted (thick) vs. measured (thin) profiles for one particular trial with a 3.3-degree modeling error (averaged across the movements).

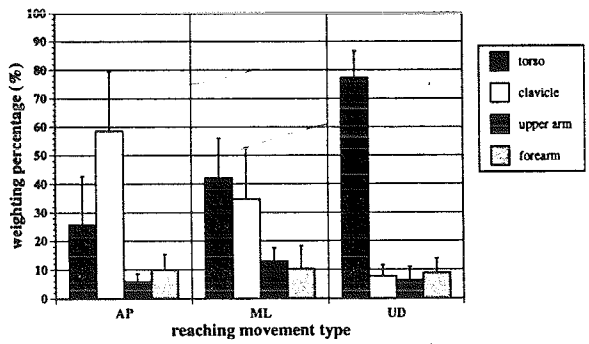

Figure 3. Weight values are normalized as percentages and averaged with respect to three types of reaching movements. Whiskers represent SD values.

RESULTS

The average error in modeling a total of 504 measured angle profiles (7 angles×12 movements×6 subjects) was 3.3 degrees (SD: 2.7; median: 2.4). Figure 2 illustrates the predicted vs. measured profiles for one particular trial with which a modeling error close to the overall average was achieved. Weight values, as statistically summarized and presented in Figure 3, demonstrate a distinctive difference between but some congruence within types of movements.

DISCUSSION

The proposed approach offers a potential means for modeling 3D dynamic complex postures without extreme computational demand. Once the weight values are specified, the movement profiles can be delivered via simple integrations. Our current effort is focused on empirical test of the approach against a population database containing a large variety of movements. The intention is to be able to estimate the weight values a priori for most common seated reaches so that we can fully enjoy the computational advantage for real time motion simulation, and achieve a robust predictive model.

The general success of this modeling approach with the specific parameter setting also leads to several important interpretations. First, the fact that the weights are time-invariant suggests the movements are being pre-organized. Second, the success of the four-weight scheme which represents an inter-segment allocation strategy indicates a segmental level coordination for specific motions considered. Third, the advantages (e.g., computational efficiency) offered by this velocity-domain approach may support the notion that rate control mechanism plays a primary role in organizing human movements.

REFERENCES

Ayoub, M.A. et al. Human Factors, 16, 585-594, 1974.

Ryan, P.W. JANAIR Report (#700201), 1970.

Kilpatrick, K.E. Ph.D. Thesis, Univ. of Michigan, 1970.

Yamaguchi, G.T. In Multiple Muscle Systems: Biomechanics and Movement Organization, Woo, S.L-Y. and Winter, J.M. (Eds.), 1990.

Hsiang, M.S. Ph.D. Thesis, Texas Tech Univ., 1992.

Whitney, D.E. IEEE Transactions on MMS, 10, 47-53, 1969.

ACKNOWLEDGMENT

This work was supported by Chrysler Corporation Challenge Fund.

A MUI TIPLE DEGREE-OF-FREEDOM VISUAL SIMULATION FOR THE UPPER EXTREMITY

J. M. Pickard, W. L. Buford, Jr., K. W. Elder, R. M. Patterson

Biomechanics Lab. Department of Orthopaedic Surgery and Rehabilitation
University of Texas Medical Branch, Galveston, TX, 77555-0892

INTRODUCTION

Kinematic modeling workstations and/or software are enduring continuous development. This project defines an interactive, three-dimensional, computer graphical, hierarchical simulation of the upper extremity that provides for the study of hypothetical models of joint motion (by providing for the adjustment of up to three arbitrary axes of motion at each joint).

REVIEW AND THEORY

Buford, et al., developed an interactive kinematic simulation on Evans and Sutherland systems which are no longer available. Lin., et al, developed a three dimensional kinematic simulation using PHIGS (Programmer's Hierarchical Interactive Graphics System 1988 ISO Graphics Standard) programming software. Since PHIGS is no longer the accepted standard for graphics software, this simulation is no longer portable.

Other biomechanics simulation packages are currently under development. The works of Delp, et al., and Chao, et al., are commercial systems which provide certain kinematic animation and anatomic visualization capability. The simulation described here is a research tool with multi-degree of freedom joint axis adjustment capability written within a flexible programming environment.

PROCEDURES

Upon acquisition of a fresh (unembalmed) adult cadaver, the upper extremity was imaged using a G.E. Model 9800 Computerized Tomography scanner. Using 1mm thick slices for the wrist, elbow, and shoulder joints, and 5mm thick slices for remaining sections of the arm, 490 consecutive slices were produced. From these images, UTMB-developed software was used to construct the three-dimensional bone structures, consisting of over 160,000 triangular polygons.

To begin software development, these three-dimensional polygonal images were transferred to a Sun UltraSparc 170 workstation with an Evans and Sutherland Freedom™ 3200 graphics accelerator. With the capability of processing 600,000 polygons per second, the Evans and Sutherland graphics accelerator allows for a real-time interactive simulation of the upper extremity. The program was written using C++, OpenGl, and Motif software within the UNIX X (Solaris) Window environment.

RESULTS

The present simulation provides for the interactive control and visualization of the upper extremity bony structures, the three-dimensional adjustment of each axis of rotation for each joint, and the rotation of each segment about the defined axes. The defined axes are:

- A hinge axis for each of the distal and proximal interphalangeal joints of the fingers.
- Two axes for each of the metacarpophalangeal joints of the fingers.
- Three axes for the carpometacarpal joint of the thumb.
- Three axes for the wrist and forearm.
- One axis for the elbow joint.
- Three axes for the shoulder joint.

This kinematic model allows for the arbitrary (6 degrees of freedom) adjustment of multiple axes of motion for each joint using keyboard or other peripheral input. The user interface (keyboard, mouse, and spaceball) provide scaling, translation, and rotation of the model in any perspective.

With respect to skeletal landmarks, the rotational axes of motion for each joint are placed in their appropriate locations. Each axis can be transformed to any position and orientation in space to show theoretical or effective joint motion articulations. **Figure 1** shows extension of the elbow around the effective flexion-extension axis of the elbow joint. The effective flexion-extension axis passes transversely through the middle of the trochlea of the humerus (Youm, et al., 1979). **Figure 2** shows pronation and supination of the forearm around the effective pronation-supination axis of the elbow joint. This axis passes from the distal end of the ulna, through the radius, to the center of the capitulum in the humerus (Youm, et. al., 1979).

While this kinematic model is based upon the structure of a single cadaver specimen, variables are included in the simulation to allow for geometrical changes. Scaling of each bone segment, limits in joint range of motion, and other variables provide for the ability to model a given person based on radiographic or other clinical measurements. Specifically, by changing geometric data files, this system can be used to model different cases.

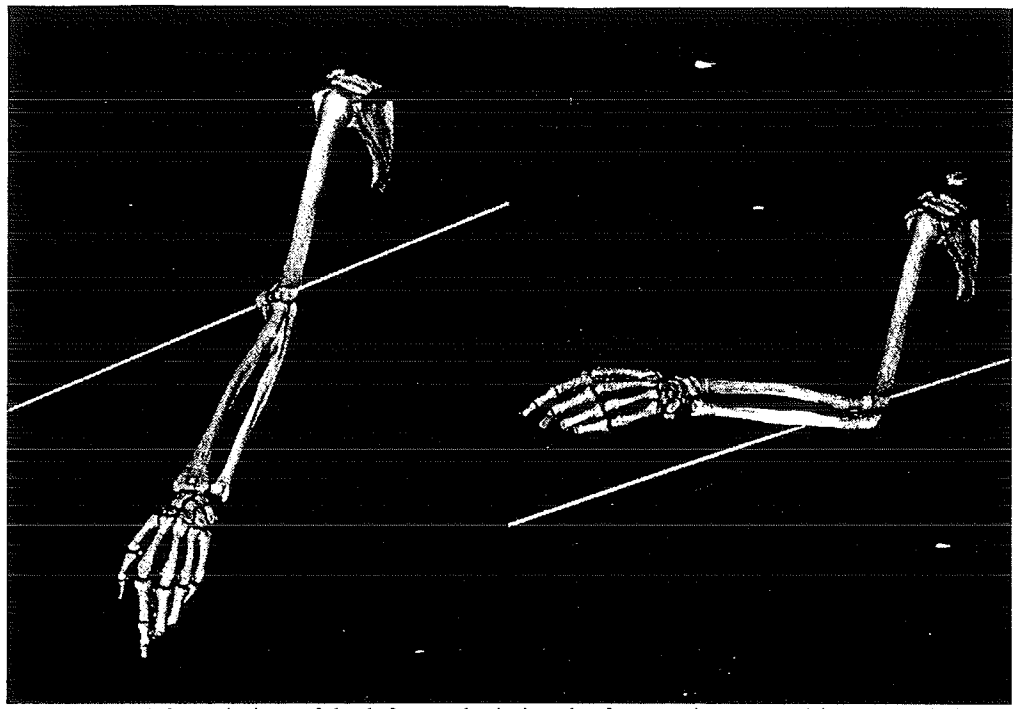

Fig. 1 A lateral view of the left arm depicting the forearm in two positions near full extension (left) and mid-flexion (right) about the elbow flexion-extension axis as defined in the kinematic model.

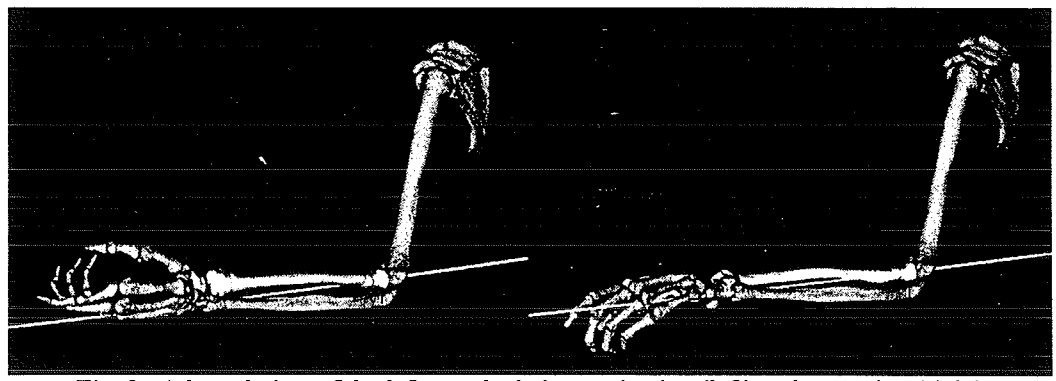

Fig. 2 A lateral view of the left arm depicting supination (left) and pronation (right) about the pronation-supination axis of the forearm.

DISCUSSION

The flexibility required in UTMB Orthopaedic Biomechanics research dictates the development of a portable three-dimensional, computer graphic, kinematic simulation of the upper extremity. While this kinematic model is based upon the structure of a single cadaver specimen, variables are included in the simulation to allow for changes in geometry. By changing geometric transformations or data files, this system can be used to model different cases. Scaling of each bone segment, limits in joint range of motion, muscle size, muscle constraints, and other variables provide for the ability to model a given person based on radiographic or other clinical measurements.

REFERENCES

Buford, Jr.,W.L. and Thompson, D.E., *IEEE Trans. on Biomed. Eng.*, 34:6, 444-453, June 1987.

Delp, S.L., et al., *IEEE Trans. on Biomed. Eng.*, 37:8, 757-767, 1990.

Chao, E.Y.S.,et al., *Trans. of the ASME*, 115, 562-568, November 1993.

Lin, Horng-Haur, et al., Proc., *XV Int. Soc. Biomech. Congress*, 84-85, June 1995.

Youm, Y.,et al., *J. Biomechanics*, 12, 245-255, 1979.

ACKNOWLEDGMENT

This research is funded by the Texas Higher Education Coordinating Board/Advanced Research Program.

BIOMECHANICAL MODEL OF THE HUMAN SPINE AS AN ARCH

D.C.Xiao[1], K.Case[1], B.S.Acar[2], J.M.Porter[3]
[1] Dept. of Manufacturing Engineering, [2] Dept. of Computer Studies, [3] Dept of Design and Technology,
Loughborough University, Loughborough, Leicestershire LE11 3TU, UK

INTRODUCTION

The human spine is the main structure to support human body weight and external loads, to allow the torso to reach a variety of positions and to protect the spinal nervous system. Lumbar back pain and disorders might be related to spine curvature and disc pressure, and it is an objective of this work to include consideration of these issues in the SAMMIE computer aided ergonomics design system. Such a design system would then be used in evaluating a wide range of situations including manual handling, car seat design, etc. The human spine is a statically indeterminate structure. The work reported here generates a criterion for the failure of the human spine, and describes the method used to determine a better or even the best fitting thrust line using optimisation techniques. This is considered to be a better predictor, when compared to the previously published arch model under the same load conditions[1].

REVIEW AND THEORY

Many attempts have been made to represent the spine using elastic analysis applied to structural models including levers, simple beams and cantilever beams. Some work is reported in the literature that models the spine as a single arch[1]. Stability of the spine under a variety of loading conditions can then be determined using plastic analysis methods, in compliance with the criterion that stability requires that the thrust line should be located within all cross sections of the arch. Lever models typically describe the spine as rigid levers with balancing reaction forces at the sacrum with no proper consideration of spinal curvature. This form of analysis is unable to explain how vertebral disc pressure increases with increasing intra–abdominal pressure and can produce results that are not proper. For example, the holding of a 90kg weight in a stooped posture leads to a predicted reaction force of 6.6 kN[3] which is sufficient to fracture the end–plates of the vertebral body (whose bearing strength is about 6 kN). Clearly this situation, although well outside normal working practices, is sustainable without damage as shown in the extreme by weightlifters. This discrepancy is considered to arise from the way in which lever models ignor spinal curvature. In contrast this paper describes the spine as an arch under assumptions that compressive forces can be transmitted in the spine only, the spine has enough compressive strength and sliding failure cannot occur in the spine. This provides a good explanation of disc and intra–abdominal pressure, and produces a calculated reaction force of 1.3–1.5 kN for the situation described above. The body weight, external loads and/or supporting forces from the seat back in a sitting posture were treated as forces applied at appropriate points on the arch spine. Muscle and ligament forces were treated as internal reaction forces applied to both ends of the spine. As an arch spine model[1], a criterion of the failure of the spine need to be generated and the best fitting thrust line need to be found using optimisation techniques.

PROCEDURES

In this developed single arch spine model, the loads applied to the arch spine are in general directions rather than being limited to a single (vertical) direction as in previous studies[2], which was developed based on the established use of vertical direction loads applied to an arch to provide a more realistic set of loads for the spine in typical working postures. A criterion for the failure of the arch spine is established. An infinite number of thrust lines for a single arch can be obtained as it is a statically indeterminate structure. There is one thrust line, however, which is the best fitting for the arch or spine. Hence there is an optimisation problem. A definition of the "best fitting" thrust line is that the resultant thrust line is the closest one to the central line or reference line of the arch or spine. It is not difficult to reach a criterion for the failure of the spine, if the best fitting thrust line among of all thrust lines in an arch spine can be found but it is not located within the "core"[2] of the spine, then hinges form[2] and spinal failure or disorders can occur. The principles and methods of optimisation for a better, or even the best

fitting thrust line in the arch spine are presented. The methods used to calculate a better or best fitting thrust line of the arch spine from force polygons, are described as an optimization, whose objective function is that the thrust line is as close as possible to the central line or reference line of the arch spine. Four objective functions are described as follows:

a) f_1=Minimise[max d_i], i=1, n;
b) f_2=Minimise[$\Sigma\, d_i^2$], i=1, n;
c) f_3=Minimise[$\Sigma\, w_i \times d_i$], i=1, n;
d) f_4=Minimise[$w_1 \times d_n + w_2 \times \max d_i$], i=1, n–1

where d is the distance between current calculated thrust line and the spine reference (or centre) line and w is a weighting factor for the optimization calculation. The best result of several locally optimised values of the above four objective functions was chosen as the final optimisation result.

RESULTS AND DISCUSSION

Examples are given for optimisation of thrust lines from the corresponding force polygon in Fig.1. A comparison between optimised thrust line in this paper and the one of previously published arch model under the same conditions[1] is shown in Fig.2. It should be noticed that the optimised thrust line is closer than the one in reference[1] to the central line or reference line of the arch spine. The reaction force calculated is about 1.3–1.5 kN. The developed arch model with optimisation is shown to be a better predictor of spinal loading. Spine disorders may occur in both situations and the one in reference[1] may be even more serious than as given in this paper, according to the criterion of the failure of the spine developed in this paper. It might due to posterior extrusion of fibrocartilage from disc, stretch of ligament and cause of back pain in these situations. If a lordosis can be introduced and the "core" can contain a thrust line, the spine disorders may be avoided. This means lordosis and abdominal pressure work together to strengthen the spine. Further work is concerned with the extension of a single arch spine into a S shaped multi–arch spine, extension of the 2D model into 3D and integration with the SAMMIE computer aided ergonomics design system.

REFERENCES

[1] Aspden R.M., The Spine as an Arch: A New Mathematical Model, Spine, 1989, 14, pp266–274

[2] Heyman, J., The Masonry Arch, Ellis Horwood Ltd, Publishers, Chichester, New York, Brisbane, 1982

[3] Morris J.M. etc,Role of the Trunk in Stability of the Spine, The Journal of Bone and Join Surgery, April 1961, 43–A, pp327–351

ACKNOWLEDGMENTS

The research is funded by EPSRC (Engineering and Physical Sciences Research Council) of the UK under Grant No. GR/K58241, 'Spine Modelling: A Tool for Safe to Use Equipment Design'.

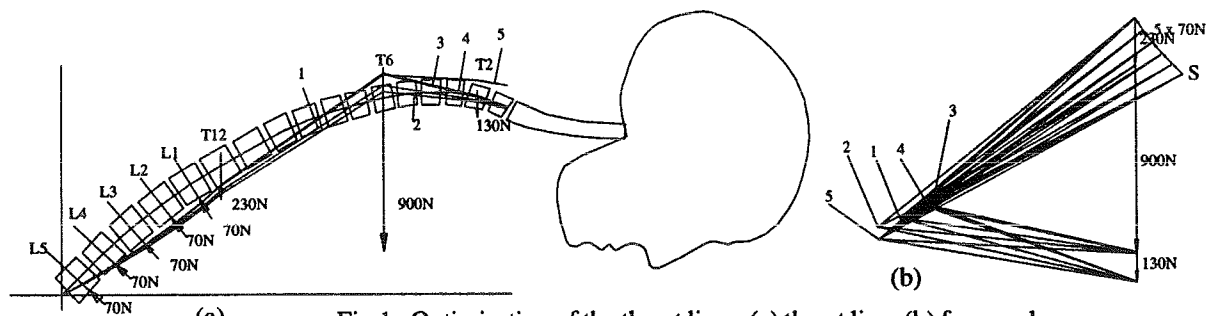

Fig.1: Optimisation of the thrust lines, (a) thrust line; (b) force polygon

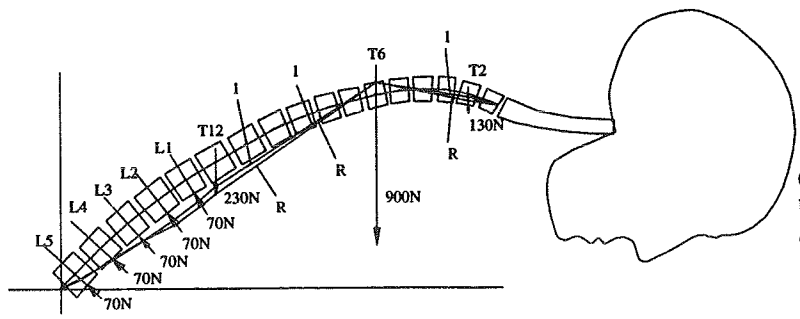

Fig.2:
Comparison of two thrust lines between the one in reference [4] (line R) and the optimised one (line 1)

A NOVEL METHOD FOR QUANTIFYING KNEE JOINT KINEMATICS: THE COMPOUND PINNED HINGE MODEL

D.L. Churchill, S.J. Incavo, C.C. Johnson, B.D. Beynnon

McClure Musculoskeletal Research Center, Department of Orthopaedics & Rehabilitation, University of Vermont, Burlington, VT 05405-0084

INTRODUCTION

The kinematics of the knee have historically been difficult to quantify. Anatomic rotations and translations are subject to axis alignment difficulties which inhibit comparisons between subjects. Helical axes, while mathematically concise, are difficult to interpret.

Previous authors (Hollister *et al.*, 1993) have demonstrated that it may be possible to describe knee kinematics simply as two simultaneous rotations occurring about fixed axes: a flexion/extension (*FE*) axis fixed to the femur, and a longitudinal rotation (*LR*) axis fixed to the tibia. Such a system could be described as a "compound pinned hinge" (CPH) model of knee motion. The objective of this study was to develop the mathematical basis for such a model, including provisions for error measurement, and then to evaluate its effectiveness in describing the kinematics of knees undergoing a realistic loadbearing activity.

REVIEW AND THEORY

Any 3-D motion can be resolved into six components (three rotations and three translations). In the CPH model this is written,

$$\boldsymbol{K} = \Theta_{FE} + \Theta_{LR} + \boldsymbol{R}_{\theta} + \boldsymbol{R}_{dX} + \boldsymbol{R}_{dY} + \boldsymbol{R}_{dZ}$$

Where: $\boldsymbol{K}$ = Complete kinematic motion
Θ_{FE} = Rotation about the femoral *FE* axis
Θ_{LR} = Rotation about the tibial *LR* axis
$\boldsymbol{R}_{\theta}$ = Residual rotation component (Abduction/Adduction)
$\boldsymbol{R}_{dX}$, $\boldsymbol{R}_{dY}$, $\boldsymbol{R}_{dZ}$ = Residual displacements

The central postulate of the CPH model is that, with proper location of the *FE* and *LR* axes, the residual terms will all drop to zero. Knee kinematics can then be described simply by the rotations, Θ_{FE} and Θ_{LR}. In actual use, the residuals are likely to have small, but non-zero values. The ability to evaluate the deviation from true CPH motion through these residual terms is an important feature of the CPH model.

Hollister's work suggests that the *FE* axis passes close to the centers of the femoral condyles, an orientation which is approximately 7°-10° offset from the sagittal plane normal. In addition, the *LR* axis was found to lie nearly parallel to the tibia's mechanical axis, but displaced from it. Based on these results, two assumptions were made in this initial study (eliminating them is conceptually straightforward, and is the subject of ongoing work):

1) The *FE* axis passes exactly through the centers of the femoral condyles,
2) The *LR* axis is exactly parallel to the tibia's mechanical axis.

The location of the *LR* axis within the tibia is the remaining unknown. Given the kinematic behavior of the knee, $\boldsymbol{K}$, the "optimal" *LR* axis location for any knee is the one which minimizes the magnitudes of the residuals.

PROCEDURES

The tibio-femoral kinematics of ten cadaveric knees were recorded while executing a simulated squatting activity in an "Oxford" style loading jig. Afterwards, each joint was exposed, and the articular surfaces of the posterior femoral condyles digitized. Additional landmarks were digitized to find the tibia's mechanical axis.

An *FE* axis was constructed such that, when viewing along it, the digitized condyle surfaces appeared circular in profile, with the axis passing through their centers. An *LR* axis was constructed in the tibia with its direction parallel to the mechanical axis, but with its location left as an unknown variable.

An optimization routine was then used to search for the optimal *LR* axis location. The configuration of the knee was evaluated at two degree flexion angle increments from 0° through 100°. The objective function was the pathlength of the medial/lateral and anterior/posterior residual displacements, $\boldsymbol{R}_{dX}$ and $\boldsymbol{R}_{dY}$. Abduction/adduction, and proximal/distal residuals were not considered. The optimizations were carried out a second time considering only 0°- 40° flexion.

RESULTS

FE axes were successfully fit to the digitized articular surfaces of each specimen (Fig 1). All

specimens exhibited the typical screw-home mechanism consisting of 10°-15° of external tibial rotation during terminal extension (Fig 2).

There was substantial variability among specimens, but in all cases the optimal *LR* axis was found to be medial and posterior to the center of the joint (Fig 3, Table 1). It lay outside of the bone boundary in one case. The residual displacements were less than 6mm for seven of ten specimens.

When considering only the 0°-40° flexion range the optimal *LR* axis locations were identical to those found when the full flexion range was used. The residual displacements, however, were considerably smaller, averaging less than 1mm (Table 1).

DISCUSSION

The small residual displacements found for most of the specimens indicates that the CPH model is indeed effective in describing knee kinematics. It is exceptionally accurate in the 0°-40° flexion range where the majority of tibial rotation occurs. The differences between individual knees are made readily apparent. It is possible that the existence of large non-zero residuals, such as those seen in specimen 5, could be correlated with specific knee pathologies.

The CPH model represents a subtle, but important change in the understanding of knee kinematics. The key feature is that, in contrast with previous models, the *FE* and *LR* axes are *fixed* to their respective bones. This should prove advantageous to basic researchers as well as to prosthetic device designers.

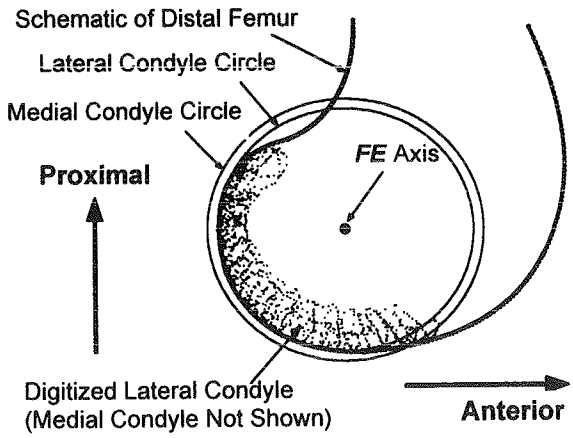

Figure 1 Illustration showing construction of *FE* axis through centers of femoral condyles.

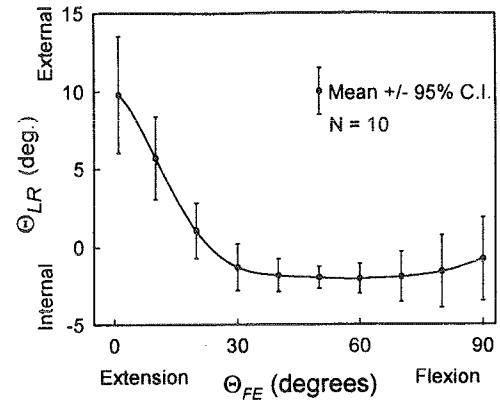

Figure 2 Θ_{LR} (rotation about logitudinal axis of tibia) vs. Θ_{FE} (rotation about femoral flexion axis)

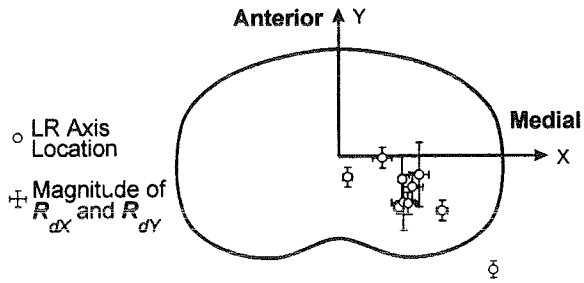

Figure 3 Schematic of Tibial plateau showing *LR* axis location for each specimen, and corresponding R_{dX} and R_{dY} magnitudes.

Spec.	*LR* Axis Location X (mm)	Y (mm)	0-40° Flexion R_{dX} (mm)	R_{dY} (mm)	0-100° Flexion R_{dX} (mm)	R_{dY}(mm)
1	15	-12	0.5	0.4	2.3	3.2
2	2	-5	0.5	0.4	2.5	4.7
3	27	-13	0.3	0.6	2.6	4.9
4	10	-1	0.4	0.4	2.6	4.9
5	29	-5	0.9	1.3	4.7	15.5
6	35	-27	1.2	1.8	1.4	4.2
7	15	-6	0.6	1.0	2.0	11.3
8	15	-11	0.3	1.9	5.7	13.6
9	17	-7	0.5	0.4	5.2	5.9
10	16	-12	0.4	0.5	4.2	5.4
Avg.	18	-10	0.6	0.9	3.3	6.7
S.D.	9.6	7.2	0.3	0.6	1.5	4.0

Table 1. *LR* axis location, and maximum R_{dX} and R_{dY} residual displacements for each specimen. Residuals calculated both for full range of flexion, and for first 40° of flexion.

REFERENCES

Hollister AM, *et al.*, *Clin Orthop* **290**:259-268, 1993

ACKNOWLEGEMENTS

Supported by NIH #AR07568 & Osteonics Corp.

FINITE ELEMENT SIMULATION OF PULSATILE REGURGITANT JETS: QUANTIFICATION BY CONSERVATION OF MOMENTUM TRANSFER

S.F.C. Stewart

Center for Devices & Radiological Health, Food & Drug Administration, Rockville, MD 20852

INTRODUCTION

Color Doppler ultrasound (CDU) is used clinically for assessing regurgitation in natural and prosthetic heart valves, but an accurate quantitative method remains elusive. Conservation of momentum transfer is one promising approach to quantifying regurgitation from the CDU image.

REVIEW AND THEORY

Regurgitant jet flows (Q) can be quantified by dividing the momentum transfer (computed from the CDU jet velocities u) by the orifice velocity U_0 (measured separately by continuous wave Doppler) (Thomas et al., 1990):

$$Q = \frac{2\pi \int_0^\infty u^2(x,r)\, r\, dr}{U_0} \qquad (1)$$

where x = axial distance from the orifice and r = radial distance from the jet axis. All velocities u must be included in the integration, but aliasing (where high velocities masquerade as lower ones) can cause errors in the measured Q. To overcome aliasing, a model based on boundary layer theory of turbulent jet flow (Schlichting, 1979) is first fit to the jet:

$$u = \frac{U_0 C}{(x+C)} \left[1 + B \left(\frac{r}{x+C} \right)^2 \right]^{-2} \qquad (2)$$

where B describes the jet width and C is the position of a virtual orifice behind the actual one. Aliased velocities are excluded by iterating the curve fit: those velocities above the aliasing velocity (as calculated by eq. 2 using parameters from the previous curve fit) are rejected in the current curve fit. This iterative rejection of aliased velocities continues until no more aliased velocities are found. U_0 scales Eq. 2 so that omitting higher velocities does not bias the curve fit. Substituting Eq. 2 into Eq. 1 yields an expression for Q (Stewart, 1995):

$$Q = \frac{\pi U_0 C^2}{3B} \qquad (3)$$

This method has been extensively verified in steady flows (Stewart, 1997), and is now being extended to pulsatile flows.

PROCEDURES

Steady and pulsatile flow turbulent jets were modeled using the FIDAP finite element program running on an IBM RISC workstation. An axisymmetric dual chambered tank with a 0.357 cm radius orifice was modeled using a paved mesh, to produce tiny elements near the orifice and larger elements elsewhere. Pulsatile jets were driven by a mitral flow regurgitation waveform derived from a published Doppler spectrum (Hatle et al., 1985) at 60 beats/min. Resulting velocity fields were converted to pseudo-CDU images by interpolation. Aliasing was introduced artificially by subtracting 220 cm/s from each velocity over 220 cm/s. Eq. 2 was fit to the steady flow and peak pulsatile velocities using a Levenberg-Marquardt non-linear curve fitter (Press et al., 1986), and the resulting B and C were used to calculate Q using Eq. 3.

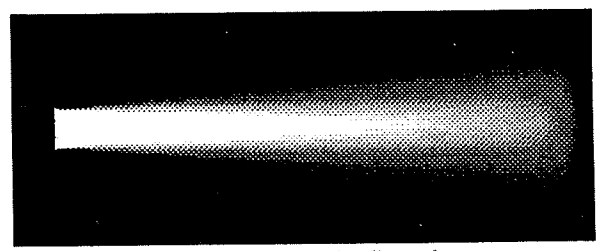

Figure 1: Simulated steady flow jet.

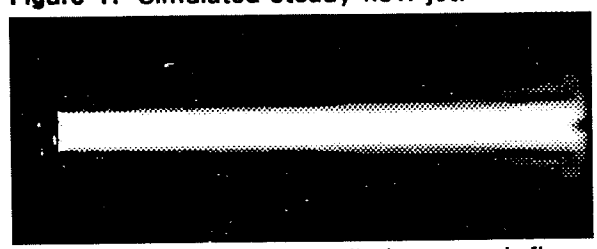

Figure 2: Simulated pulsatile jet at peak flow.

RESULTS

Steady flow jets (figure 1) were observed to be qualitatively different from the pulsatile jets (figure 2). Examination of the flow profiles shows that the pulsatile jets did not spread out like the steady flow jets. Models fitted to non-aliased jets are shown in figure 3 (steady) and figure 4 (pulsatile). In the steady flow jets, good agreement was found between the calculated (Q_c) and measured (Q_m) steady flow (Table 1), even when aliasing was present. Good agreement was also found between the calculated and measured peak flow in the non-aliased pulsatile jet, but the agreement was much worse in the aliased pulsatile jet.

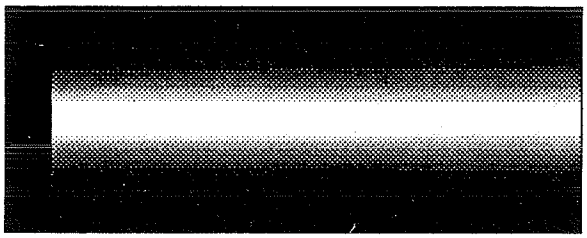

Figure 3: Curve fitted steady flow jet.

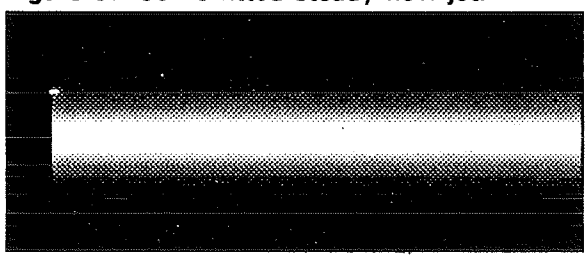

Figure 4: Curve fitted pulsatile jet.

DISCUSSION

The parameters B and C determine the fitted jet shape, the virtual orifice position, and the calculated flow, Q. The original boundary layer solution includes a singularity at the orifice: u is proportional to $1/x$, so that at $x = 0$, u is undefined. Eq. 2 eliminates this problem, giving a virtual orifice C cm behind the real one. In steady flow jets, the jet spreads as it flows away from the orifice. The fitted virtual orifice is a reasonable length behind the true orifice (C = 60 cm for the nonaliased jet and 16.5 cm for the aliased jet), and the calculated Qs are fairly accurate (Table 1). In contrast, the pulsatile jet remains narrow far from the orifice, possibly because there was insufficient time for the

Flow	S*	S*	P†	P†
Alias	No	Yes	No	Yes
Q_m	80.0	80.0	80.0‡	80.0‡
Q_c	87.0	71.4	72.8‡	15.2‡
B	9177	851	3.9e5	191
C, cm	60	16.5	358	3.63

Table 1 Calculated vs. measured flow rate. *Steady flow. †Pulsatile flow. ‡Peak flow.

turbulent mixing to develop. The fitted virtual orifice was far away from the true one (C = 358 cm), one possibe cause of the low Q_c (= 72.8 ml/s) in the non-aliased jet. The virtual orifice was at a more reasonable distance behind the aliased pulsatile jet, but Q_c was much less accurate (= 15.2 ml/s). The lack of turbulent mixing and jet spreading caused a much smaller locus of non-aliased velocities, so that the iterative curve fit had fewer data points to work with. It is concluded that more sophisticated models will have to be built for this conservation of momentum transfer method to work accurately with aliased pulsatile flows.

REFERENCES

Hatle, L. et al. Doppler Ultrasound in Cardiology, 180, Lea & Febiger, 1985.

Press, W.H. et al. Numerical Recipes: The Art of Scientific Computing, 523-538, Cambridge University Press, 1986.

Schlichting, H. Boundary-Layer Theory, 747-750, McGraw-Hill, 1979.

Stewart, S.F.C. Finite element tests of a conservation of momentum transfer method to quantify valvular regurgitation [Abstract]. J. Amer. Soc. Echocard., 8, 377, 1995.

Stewart, S.F.C. Aliasing-tolerant color Doppler quantification of regurgitant jets. Submitted to Ultrasound Med. Biol., 1997.

Thomas, J.D. et al. Quantification of jet flow by momentum analysis: an in vitro color Doppler flow study. Circulation, 81, 247-259, 1990.

Relationships Between Selected parameters For The Evaluation of Hardwood Sports Surfaces

Dr. Paul W. Elliott
Robbins, Inc.
4777 Eastern Avenue
Cincinnati, OH 45226

Prof. Kamyar Haghighi Prof. Gary W. Krutz
Department of Agricultural and Biological Engineering
Purdue University
West Lafayette, IN 47907

Mike Niese
Robbins, Inc.
4777 Eastern Avenue
Cincinnati, OH 45226

Jay Seals
Robbins, Inc.
4777 Eastern Avenue
Cincinnati, OH 45226

Introduction

Six floors were tested to determine the ball reflection, shock absorption, standard vertical deflection (StVv). And area indentation, according to the DIN standard 18032 part II (1991) for the evaluation of sports surfaces. The relationships between these four parameters were examined. It was hoped that strong relationships could be found between several of the parameters, and that these relationships could ultimately be used to simplify the current testing procedures. The significant relationships which exist between floor performance and safety characteristics, will help to guide future floor designs. These relationships will also provide a starting point for re-evaluating the test procedures currently used on hardwood sports surfaces.

Review and Theory

Little, if any, scientific or engineering principles have been applied to developing new basketball floors to improve safety, or performance. Such scientific principles were applied to the design of indoor running tracks by McMahon and Green (1978). They developed a simple model of human muscles and reflexes, and used this model to tune the stiffness of the track to improve the times of the athletes performing on the track. Design of basketball floors is more complicated. While improving the safety is of course a major concern, the floor must maintain certain ball rebound characteristics. The characteristics of hardwood athletic floors are commonly obtained using the DIN standard 18032 (1991). If scientific and engineering principles are to be used to improve current floor design, then the relationships between the most important characteristics must be examined. This study does not fully endorse any current materials test, as materials tests have been found to be poorly correlated to subject tests (Nigg and Yeadon, 1987). The significant relationships determined in this study, can also be used as a starting point to improve current materials testing methods, and hopefully improve the correlation between the subject and materials tests along the way.

Procedures

Data collection was performed using current data acquisition technologies. Data was stored on an NEC DX-4 75 MHz notebook computer. The NEC computer was connected to an Hewlett Packard 75000 B-sized VXI mainframe. The HP 75000 contained the multimeter and multiplexer used to perform the analog to digital conversion of signals from respective transducers. Control of the HP-VEE, (Hewlett Packard's Visual Engineering Environment software). Ball Rebound height was measured using a Massa 411/40 ultrasonic distance sensor. Impact forces were recorded using model 53 Sensotec load-cells. The deflections of the playing surface were measured using Sensotec model MLV7A Linear-Velocity-Displacement-Transducers (LVDTs).

The characteristics analyzed in this study include: ball reflection, shock absorption, standard vertical deflection, and area indentation. Tests and analysis were performed according to the DIN standard 18032 part II (1991), only slight modifications to the procedures were made. These modification were only to ease the analysis of the data, and the accuracy of the measurement. Ball reflection is determined by using the rebound height obtained on concrete, and on the playing surface in the following equation:

$$\text{Ball Reflection} = \frac{Height\ (floor)}{Height\ (concrete)} x\ 100$$

Impact test equipment was developed for the shock absorption test according to the DIN standard 18032 part II, (1991). Shock absorption was obtained by using the maximum force generated on the floor system to the maximum force generated on a rigid surface (DIN standard 18032 part II, 1991). In both tests where the impact force is recorded, the impact is generated by dropping a known mass onto a spring of know stiffness.

$$\text{Shock Abs.} = \left(1 - \frac{F_{\max,\ floor}}{F_{\max,\ rigid\ concrete}}\right) x\ 100$$

Six floors of various resiliency were tested over a three month period, and the aforementioned parameters were obtained. Testing was performed at 9 points spaced over one half of the playing surface. Testing for each parameter was carried out according to the DIN standard. Linear regression was then used to determine if the average characteristics of each floor parameter were related to each other.

Results

Two significant relationships were found to exist between the average characteristics of the playing surface. The equations illustrating the relationships and respective correlation coefficients are presented in Table 1 (B.R. is ball reflection, STV is standard vertical deflection, and S.A. is shock Absorption. Ball reflection and standard vertical deflection were found to be significantly related to the shock absorption characteristic. Ball reflection and shock absorption were found to be negatively related. In other words increasing the shock absorption properties of a floor system, will tend to reduce the rebound height obtained on the same system which is not desirable. Standard vertical deflection was found to be positively related to shock absorption. Increasing shock absorption of a playing surface will increase the StVv, and this is desirable according to the current DIN standard.

Table 1: Significantly Related DIN Standard 18032 Parameters

Parameters (X-Y)	Regression Equation	R
SA-BR	SA = -4.1 BR + 448	0.84
SA-STV	SA = 18.0 STV + 24	0.81

Discussion

This study has found that significant relationships do exist between current DIN standards. It shows that changing one of the floors characteristics will have an effect on other characteristics. These studies suggest that one floor which produces high shock absorption, ball reflection, and standard vertical deflection, will be difficult to develop. While this is true, new floor designs can be developed which keep the requirements in mind. Floors intended for the weekend athlete or children can be designed with high shock absorbing characteristics, but at the expense of lower ball rebound heights, and larger area indentations. Floors with high caliber athletes as the main end-user, can be designed with optimal ball rebound characteristics but shock absorbing properties will have to be sacrificed. The fact that significant relationships exist between several of the current DIN standard characteristics can be used to develop a new simpler test procedure. If new tests are to be developed, they should be based on fundamental biomechanical knowledge, in hopes that they will be more closely related to subject tests.

References

1) DIN Standard 18032 part II (1991). Sports halls, halls for gymnastics and games sports floors requirements, testing.
2) McMahon, T.A. and P.R. Greene. Fast Running Tracks. Scientific American 1978, December.
3) Nigg, B.M., and M.R. Yeadon. 1987. Biomechanical Aspects of Sport Surfaces. Sport Surfaces, August.

Acknowledgments

The authors would like to thank the schools in this study for allowing them to include their floors in this study.

ELECTROMYOGRAPHIC AND KINEMATIC ANALYSIS OF CUTTING MANEUVERS: IMPLICATIONS FOR ANTERIOR CRUCIATE LIGAMENT INJURY

S Colby ME, A Francisco BS, M Finch BS, A Beutler BA, W Garrett Jr. MD, PhD
Coach Krzyzewski Human Performance Laboratory
Department of Orthopaedics and Sports Medicine, Durham, NC 27710

INTRODUCTION

Acute anterior cruciate ligament disruption is a common and potentially devastating injury. It is estimated that in any given year, one in 3,000 people in the general population will suffer an anterior cruciate ligament (ACL) tear (Smith et al, 1993). An estimated 70% of ACL injuries are sports related. Unfortunately, other than in skiing, research concerning ACL injury has tended to focus on surgical repair and rehabilitation rather than actual mechanisms of injury. The goal of this study was to analyze the biomechanical effects of various athletic maneuvers commonly associated with ACL injury.

REVIEW AND THEORY

The majority of the non-skiing mechanisms of ACL injuries are non-contact situations where the injured player was not hit or touched by another player (Boden et al, 1996). In addition, these non-contact situations occur near foot strike when the quadriceps are eccentrically contracting to resist flexion. They are also characterized by the following: deceleration, change of direction as in cutting or landing, and a varus/valgus moment about the knee or an internal/external rotation of the leg (Boden et al, 1996). In the analysis of human movement, only inertia, which is an object's resistance to any change in motion, and muscle, which can exert a tensile (pulling) force could contribute to these non-contact injuries (Enoka, 1994). Given the non-contact situation of cutting or landing from a jump, inertial forces would cause an anterior force on the femur and a posterior force on the tibia which would stress the posterior cruciate ligament (PCL). Therefore, it seems reasonable to assume that the mechanism of non-contact injury to the ACL involves internal forces that are generated by the leg muscles of the athlete.

The quadriceps have been implicated for their role in pulling the tibia in the anterior direction and stressing the ACL at low knee flexion angles. In contrast, the role of the hamstrings in stabilizing the ACL is similarly well documented (Ciccotti et al, 1994). Research documenting quadriceps and hamstring activity during cutting, stopping, and landing, however, has been minimal. Previous works studying cutting have primarily dealt with the strategies and kinematics of the movement (Andrews et al, 1977, Cross et al, 1989).

Therefore, while it is known that full activation of quadriceps muscles can potentially generate sufficient anterior shear force to rupture the ACL at low angles of knee flexion, the balance of quadriceps and hamstring muscle activity during common athletic motions is unknown. The purpose of this study was to qualitatively characterize the muscle activation of the quadriceps and hamstrings, as well as knee flexion angle during the eccentric motion of athletic maneuvers most involved with ACL injury: sidestep cutting, cross-cutting, stopping, and landing.

METHODOLOGY

Fifteen healthy collegiate and recreational athletes were tested. The subjects average age was 22.2 (± 1.70) years. Surface electrodes were placed over the following muscles on the subject's dominant side: vastus lateralis, vastus medialis oblique, rectus femoris, biceps femoris and medial hamstrings. Retro-reflective markers were placed on the hip (greater trochanter of the femur), knee (lateral condyle of the femur) and ankle (lateral malleolus). During the testing session, the subject first performed a series of isometric maximum voluntary contractions (MVCs). EMG (600 Hz) and two-dimensional kinematic data (60 Hz) were collected while the subjects performed four athletic maneuvers: sidestep cutting, cross-cutting, stopping, and landing. Sidestep cutting and cross-cutting involved running along an eight meter runway, planting with the test limb and cutting to the contralateral and ipsilateral sides, respectively. Stopping was performed with the subject running along an eight meter runway and decelerating with the test limb. Landing was performed with the subjects jumping down from a height of 0.5 meters, landing on both legs, and then pivoting to the contralateral side.

The rectified EMG signals recorded during the four maneuvers were integrated to match the frame speed of the camera. For the MVCs, the rectified EMG signals were integrated every second, and the highest second of muscle activation (representing 100% EMG activity) was used to normalize the dynamic contractions recorded during the four maneuvers. Knee angles were analyzed using a Peak Performance motion measurement system. Maneuvers were analyzed during eccentric motion (five frames before heel strike until the subject moved outside of the 2D reference frame).

RESULTS

Representative examples of EMG and the corresponding knee flexion angle during the eccentric phase for the sidestep cut and cross-cut are presented in Figure 1. Qualitatively, all maneuvers demonstrated increasing activity in the quadriceps at heel strike. Meanwhile, all maneuvers except landing were characterized by increasing hamstring activity at and following heel strike. To help explain the eccentric part of the motion, three points of interest were examined: peak quadriceps activation, minimum hamstrings activation, and the maximum activation difference between the two muscle groups. The quadriceps activation peaked at mid eccentric motion while the minimum hamstrings activation occurred just after heel strike. The maximum difference between quadriceps and hamstring muscle activation occurred after the minimum hamstring activation, but prior to the peak quadriceps activation. Heel strike occurred at an average of 22° of knee flexion for all maneuvers.

DISCUSSION

The results of this study indicate quadriceps activation begins just before heel strike and peaks in mid eccentric motion for these movements. This may be related to non-contact injuries. In these maneuvers, the level of quadriceps activation frequently exceeded that seen in a maximum isometric contraction. Furthermore, there was submaximal activity in the hamstrings at and following heel strike. Coupled with this partial hamstring relaxation, forces generated by the quadriceps muscles at the knee could produce significant anterior force to tear the ACL. While the forces which athletes encounter are usually well controlled, unexpected conditions or uncoordinated action such as a slip or fall may result in an ACL injury.

There have been several studies which have shown that the quadriceps pull the tibia in the anterior direction and significantly stress the ACL at low knee flexion angles (Markolf et al, 1990, Smidt, 1973). Moreover, in a study examining the mechanisms of non-contact ACL injuries, Boden reported that the average angle of knee flexion at the time of injury was 21° (Boden et al, 1996). In this study, the average knee flexion angle at heel strike was 22° for each of the four maneuvers suggesting that the quadriceps may be exerting a force strong enough to pull the tibia in the anterior direction, straining the ACL. The hamstrings provide dynamic stability to the knee by resisting both mediolateral and anterior translational forces on the tibia (Norkin and Levangie, 1983). In these four dynamic events, the level of quadriceps activation during the eccentric phase frequently exceeded that seen in a maximum isometric contraction. Furthermore, there was submaximal activity in the hamstrings at and following heel strike. This muscle imbalance is more clearly illustrated when looking at the maximum difference between quadriceps and hamstring activity which ranged from 64 - 87% MVC in the four maneuvers. The results of the study suggest that the levels of hamstring activity might not be sufficient enough to prevent anterior tibial displacement. A preventive strategy involving strength programs may reduce the number of injuries in contact sports. Strengthening programs and different techniques of performing these maneuvers may be developed to help reduce the incidence of ACL injuries.

REFERENCES

1. Andrews JR, et al, *Am J Sports Med*, 5(3), 111-121, 1977
2. Boden BP, et al, *Med Sci Sports*, 28(5), 526, 1996
3. Ciccotti MG, et al, *Am J Sports Med*, 22(5), 645-650, 1994
4. Cross MJ, et al, *Am J Sports Med*, 17(3), 363-366, 1989
5. Enoka RM, Neuromechanical Basis of Kinesiology, Chapter 2, Human Kinetics, 1994
6 Markolf KL, et al, J Bone Joint Surg, 72A(4), 557-567, 1990
7. Norkin C and Levangie P, Joint structure and function: A comprehensive analysis, 1983
8. Smith BA, et al, *Clinics Sports Med*, 4(12), 637-670, 1993
9. Smidt JG, J Biomech, 6:79-92, 1973

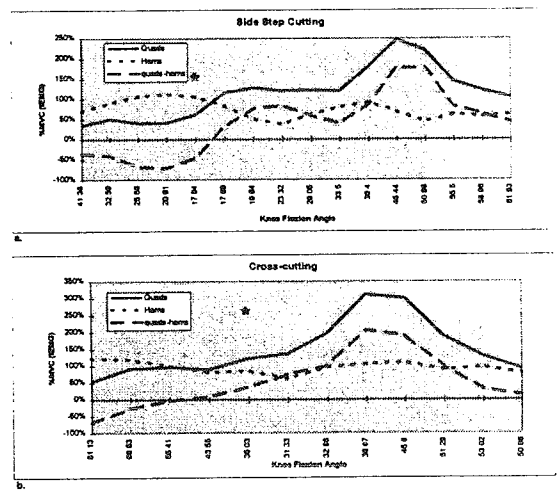

Figure 1. Representative example of EMG (%MVC) and the corresponding knee flexion angle at a given time frame for one subject for a) side step cut and b) cross-cut. * represents heel strike

BASEBALL PITCHING BIOMECHANICS AT VARIOUS LEVELS OF DEVELOPMENT

G.S. Fleisig, S.W. Barrentine, N. Zheng, R.F. Escamilla, J.R. Andrews
American Sports Medicine Institute, Birmingham, AL 35205

INTRODUCTION

The biomechanics of baseball pitchers from youth league to professional league were analyzed. Results may show unique aspects for different developmental levels, and an evolution in mechanics as athletes progress. Understanding proper mechanics at each level can help the coaches improve their pitchers' performance and minimize their risk of injury.

REVIEW AND THEORY

Published kinematic and kinetic data of baseball pitching have been limited to small samples ($n<30$) of elite adult pitchers (Dillman et al., 1993; Elliott et al., 1986; Feltner et al., 1986; Fleisig et al., 1995, 1996; Pappas et al., 1985, 1995; Sakurai et al., 1993; Vaughn, 1985; Werner et al., 1993). Although only adult pitchers were studied, results from these publications have been used as a basis for teaching mechanics to pitchers of all ages. The purpose of this study was to quantify pitching biomechanics for various levels. It was hypothesized that younger pitchers produce less force and torque than adult pitchers, reduced approximately by the difference in bodyweight and height. It was also hypothesized that several kinematic differences exist between mature pitchers and young, developing pitchers.

PROCEDURES

From 1989-1996, 227 healthy male baseball pitchers were analyzed. Included were 21 youth (age range: 10-15 yrs, height: 1.68±0.09 m, mass: 56±10 kg), 31 high school (15-20 yrs, 1.83±0.07 m, 76±10 kg), 115 college (17-23 yrs, 1.84±0.05 m, 82±9 kg), and 60 professional (20-29 yrs, 1.87±0.08 m, 90±9 kg) level athletes. After providing informed consent, history, and physical information, each pitcher was tested in an indoor laboratory. Reflective markers were attached bilaterally to the distal end of the mid-toe, lateral malleolus, lateral femoral epicondyle, greater trochanter, lateral tip of the acromion, and lateral humeral epicondyle. A reflective band was wrapped around the wrist on the throwing arm and a reflective marker was attached to the ulnar styloid of the non-throwing arm. After stretching and warming up, the subject threw ten fastball pitches from a portable pitching mound toward a strike zone ribbon located over a home plate. For the distance from the pitching rubber to home plate, the pitcher's league regulation was used. Velocity of the ball as it left the pitcher's hand was measured with a radar gun (Jugs Pitching Machine Company, Tualatin, OR).

Three-dimensional coordinates were determined with a four-camera 200 Hz automatic digitizing system (Motion Analysis Corporation, Santa Rosa, CA) for the three fastest pitches that hit within the strike zone ribbon. Root mean-square error in calculating the three-dimensional location of markers randomly placed within the calibrated space was 1.0 cm. Using the digitized data and published anthropometric data, seven kinetic and sixteen kinematic parameters were calculated as previously described (Dillman et al., 1993; Fleisig et al., 1995, 1996). To compensate for differences in body size, forces were normalized by percent bodyweight and torques were normalized by percent bodyweight-times-height. A one-way Analysis of Variance was performed for each parameter to identify differences among the four levels.

RESULTS

Even when normalized by bodyweight and height, all seven kinetic parameters increased with competition level (Table 1). Of the sixteen kinematic parameters analyzed, all five velocity parameters and only one of eleven position parameters showed significant differences (Table 2). The position parameters without significant differences were stride length, shoulder external rotation, shoulder horizontal adduction, elbow flexion, knee flexion, and trunk tilt at various times during the pitch.

DISCUSSION

The greater shoulder and elbow angular

Table 1: Kinetic differences between levels. Forces expressed as percent bodyweight, and torques expressed as percent bodyweight*height.

	Youth (n=21)	High School (n=31)	College (n=115)	Pro (n=60)
Arm cocking phase				
Elbow varus torque**	3.1±.6	3.5±.7	3.7±.7	3.9±.7
Shoulder internal rotation torque**	3.4±.6	3.7±.7	3.9±.7	4.1±.7
Shoulder anterior force*	41±9	39±7	43±8	45±10
Arm acceleration phase				
Elbow flexion torque*	3.2±.6	3.3±.5	3.5±.6	3.5±.7
Arm deceleration phase				
Elbow compressive force**	74±14	84±13	97±11	103±13
Shoulder compressive force**	90±17	99±15	114±12	122±17
Shoulder posterior force*	31±8	36±11	44±19	44±25

*p<0.05 **p<0.01

Table 2: Kinematic differences between levels.

	Youth (n=21)	High School (n=31)	College (n=115)	Pro (n=60)
Instant of foot contact				
Elbow flexion (°)*	74±17	82±15	85±18	87±15
Arm cocking phase				
Pelvis velocity (°/s)**	650±110	640±90	670±90	620±80
Upper torso velocity (°/s)*	1180 ±110	1130 ±110	1190 ±100	1200 ±80
Arm acceleration phase				
Elbow extension velocity (°/s)**	2220 ±310	2190 ±330	2380 ±300	2320 ±300
Shoulder internal rotation velocity (°/s)*	6850 ±1060	6840 ±1390	7430 ±1270	7240 ±1090
Instant of ball release				
Ball speed (mph)**	63±3	74±4	79±4	83±4

*p<0.05 **p<0.01

velocities produced by adult pitchers were most likely due to their greater forces and torques during the arm cocking and acceleration phases. The combination of more arm angular velocity and a longer arm resulted in greater linear ball velocity for the adult pitcher.

While many features of the game (e.g., field dimensions, bat weight) are scaled down for younger players, standard adult baseballs are used at all levels. Use of a lighter baseball might allow youth league pitchers to generate arm velocities more similar to those produced by adult pitchers, even though youth pitchers produce significantly less force and torque. Also, a ball with a smaller diameter might allow the young pitcher to learn proper grips. Research with smaller baseballs would be helpful.

Ten of the eleven position parameters showed no significant differences. Thus, results from this study did not support the hypothesis that pitching mechanics change significantly with level; rather, the results seem to support the common coaching philosophy that a child should be taught "proper" pitching mechanics that can be used throughout a career.

REFERENCES

Dillman C.J. et al. JOSPT, 18, 402-408, 1993.
Elliott B. et al. Int J Sport Biomech, 2, 20-28, 1986.
Feltner M. et al. Int J Sport Biomech, 2, 235-259, 1986.
Fleisig G.S. et al. Am J Sports Med, 23, 233-239, 1995.
Fleisig G.S. et al. J Appl Biomech, 12, 207-224, 1996.
McLeod W.D. et al. Phys Ther, 66, 1901-1904, 1986.
Pappas A.M. et al. Am J Sports Med, 23, 312-315, 1995.
Pappas A.M. et al. Am J Sports Med, 13, 216-222, 1985.
Sakurai S. et al J Appl Biomech, 9, 47-65, 1993
Werner S.L. et al. JOSPT, 17, 274-278, 1993.

ACKNOWLEDGEMENTS

The authors would like to thank Heather Conn, Andy DeMonia, David Downs, Gene Jameson, and David Stodden for their assistance.

ERRORS IN HAMSTRING MUSCLE FIBER LENGTH ESTIMATES DURING SPRINTING USING A TWO-DIMENSIONAL VERSUS THREE-DIMENSIONAL ANALYSIS

B.J.C. van Don

Department of Exercise Science, University of Iowa, Iowa City, IA 52242

INTRODUCTION

The purpose of the present study was to evaluate the error obtained in estimations of hamstring muscle fiber lengths during sprinting with the use of a two-dimensional (2D) versus three-dimensional (3D) analysis. This was accomplished using a computer simulation of the leg motion and hamstring muscles during sprinting. It was concluded that a 2D analysis is sufficient for determination of hamstring muscle fiber lengths during sprinting.

REVIEW AND THEORY

The kinematics and kinetics of walking with the use of 2D and 3D analysis have been well documented in the literature. For sprinting the kinematics and kinetics are also well documented but are usually obtained with a 2D analysis, with the exception of Novacheck's (1995) study in which a 3D approach was used. The appropriateness of a 2D instead of a 3D analysis for the sprinting motion has not been studied and is of importance for future research in sprinting.

Presently the attention of many biomechanists is focused on the roles of individual muscles during the execution of a motion. Knowledge of individual muscle forces has many applications. For example, it is of interest to predict the maximum force or individual muscle force versus time relationships of the hamstring muscles during sprinting with regard to training, injury prevention and rehabilitation. With the use of a model the force-length-velocity-activation relationship for each muscle of the hamstring group can be estimated. However, to obtain an accurate estimation of the muscle force , the muscle fiber length must be determined as accurately as possible with the use of the current technology. A question that arises is, what is the magnitude of error in hamstring muscle fiber length estimates obtained by neglecting hip adduction (AD) and abduction (AB) and internal (IntR) and external (ExtR) rotations during sprinting when a 2D analysis is used instead of a 3D analysis ? The purpose of this study was to evaluate the influence of these motions during sprinting on the estimation of the muscle fiber lengths of the bi-articular muscles of the hamstring group; the semitendinosus (ST), semimembranosus (SM) and the biceps femoris long head (BFL).

PROCEDURES

A computer simulation of the leg motion of an individual (1.70m, 70 kg) during sprinting was developed. The hip angle versus time and the knee angle versus time relationships reported by Mann et al. (1986) for a skilled sprinter were used to determine the hip, knee and ankle joint centers during one sprint cycle for the 2D condition. The ranges of hip AD/AB and IntR/ExtR superimposed on the 2D motion to obtain a 3D sprinting motion were as follows:

	Angle(deg)	step(deg)
Adduction (AD)	5 - 30	5
Abduction (AB)	5 - 40	5
Internal Rotation (IntR)	5 - 45	5
External Rotation (ExtR)	5 - 45	5

The definitions for the embedded coordinate systems and the geometrical muscle data reported by Pierrynowski (1995) were used to determine the muscle-tendon lengths for the ST, SM and BFL. Lines of action of the SM and BFL were modeled as straight lines joining origin and insertion. The muscle-tendon length of the ST was modeled as the sum of two line segments to simulate the wrapping of the tendon around the femoral condyle. The muscle fiber lengths were determined according to the formula's given by Herzog (1985) for pennate muscles. It was assumed that the tendon length and the muscle thickness (perpendicular distance between the tendons) were constant during contraction. The % error in estimation of the muscle fiber length obtained due to the use of a 2D analysis (L_F^{2D}) versus a 3D analysis (L_F^{3D}) relative to the muscle fiber length in anatomical position (L_F^{A}) was determined with the following equation:

$$\% \text{ Error} = [(L_F^{3D} - L_F^{2D}) / L_F^{A}] * 100$$

The maximum % errors were determined with the use of the % error versus % sprint cycle relationships of each muscle for all the simulated conditions. If the maximum error obtained for a simulation was less than 5% it was concluded that a 2D analysis is sufficient.

RESULTS AND DISCUSSION

From the %error versus % sprint cycle relationships for AD/AB and the IntR/ExtR conditions for each muscle (e.g. Fig. 1) the maximum error was determined.

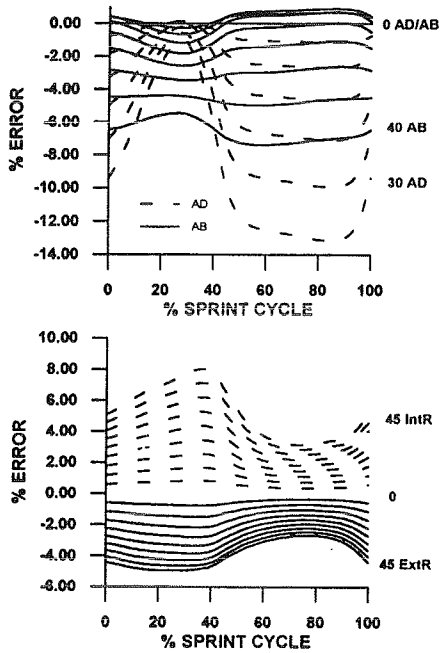

Figure 1: The % error for BFL by adding AD/AB and IntR/ExtR during the sprint cycle.

An increase in AD and AB angle (no IntR/ExtR) caused an increase in error for all muscles. The maximum AD/AB angles for each muscle for which an error of < 5 % was obtained during the simulated sprint cycle are summarized in Table 1. These data show that the maximum errors were < 5% of L_F^A if the motion was simulated with AD <15° and AB <35°.

	ST	SM	BFL
AD	20°	30°	15°
AB	40°	40°	35°

Table 1 : Error < 5 % for AD/AB.

An increase in IntR and ExtR (no AD/AB) also caused an increase in error for all the muscles. The maximum IntR/ExtR for each muscle for which an error of < 5 % was obtained during the simulated sprinting cycle are summarized in Table 2. These data show that the maximum errors were < 5% of L_F^A if the motion was simulated with IntR <25° and ExtR <45°.

	ST	SM	BFL
IntR	45°	45°	25°
ExtR	45°	45°	45°

Table 2 : Error < 5 % for IntR/ExtR

Novacheck (1995) reported values < 10° for AD and AB, < 15° IntR and 0° ExtR. These values were obtained for children (5-18 years). Smaller values would be expected for skilled sprinters due to training and improvement in coordination. If, due to the use of a 2D instead of a 3D analysis, the AD/AB and IntR/ExtR motions as reported by Novacheck are ignored the maximum errors shown in Table 3 may develop. These data show that the use of a 2D rather than a 3D analysis for sprinting will produce a maximum error in hamstring muscle fiber length estimates of < 2.2% of L_F^A.

	ST	SM	BFL
15° IntR + 10° AD	-1.58	-2.13	1.67
15° IntR + 10° AB	0.78	0.31	1.70

Table 3: Maximum %error expected using 2D.

Conclusion

The errors obtained in the estimates of the muscle fiber lengths of the bi-articular muscles of the hamstring group using a 2D rather than a 3D analysis are very small. Therefore, a 2D analysis of sprinting is sufficient to obtain estimates of hamstring muscle fiber lengths.

REFERENCES

Herzog, W. Dissertation, University of Iowa, 1985.

Mann, R.A. et al. Am. J. Sports Med., 14, 501-510,1986.

Novacheck, T.F. Instr. Course Lect.,44,497-506, 1995.

Pierrynowski, M.R. Three dimensional analysis of human movement. 215-256, Human Kinetics, 1995.

ACKNOWLEDGMENTS

I thank Dr. W.G. Darling for his assistance in discussion of the data and preparation of this manuscript.

INITIAL AND LANDING IMPACT ACCELERATION WITH MOUNTAIN BIKE SUSPENSION FORKS

M.S. Orendurff and G.A. Smith,

Biomechanics Laboratory, Oregon State University, Corvallis, OR 97331

INTRODUCTION

In mountain biking, cyclists are frequently subjected to substantial impact forces while riding. In an effort to reduce these impacts, suspension forks have been developed. When a bump is struck while mountain biking, two acceleration peaks are observed: the first at initial contact (P_1) and following a brief airborne period another peak occurs at landing (P_2).

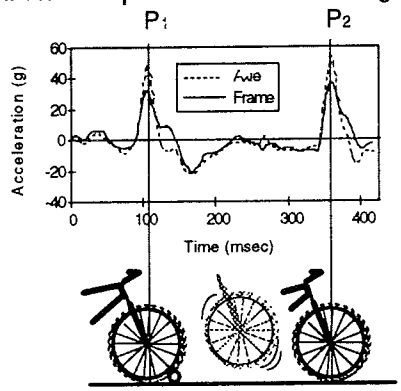

Figure 1. Initial contact and landing peak acceleration.

REVIEW AND THEORY

Published scientific data regarding the effectiveness of suspension forks is sparse. Previous investigations (Orendurff, et al., 1994) suggest that acceleration at the frame increased as fork stiffness increased. However, rigid forks were not included, and the single subject design makes generalization to the population somewhat tenuous. The purpose of this investigation was to determine the effect of rigid fork and suspension fork stiffness (resistance to axial compression) on impact acceleration at the axle and frame during initial contact, and upon landing over three bump sizes.

PROCEDURES

A bicycle (20" Klein Pinnacle) was fitted with two small accelerometers (PCB 302A), one mounted at the axle and another on the frame at the head tube. Accelerometer output was telemetered to a microcomputer, sampled at 1000 Hz and stored for later analysis. Seven experienced mountain bike riders gave their informed consent to participate in the study. Subjects rode the bicycle down a ramp (1.4 m high by 5 m long) to consistently produce a 5.2 m/s speed. A bump was placed 2.3 m from the base of the ramp. The bicycle was fitted with a rigid fork (F_R) or a suspension fork (Rock Shox Mag 20) set on soft (F_1), medium (F_3) or firm (F_6) stiffness for a total of 4 different fork conditions. Three bumps were selected to mimic obstacles typically encountered during mountain biking: A rod 4 cm in diameter (B_1); a 45 cm ramp with 15 cm drop-away (B_2); and a 12 cm rounded timber (B_3). Bumps and suspension fork settings were fully randomized across subjects. Rigid fork data were collected subsequently, and bumps were randomly assigned. Raw accelerometer output was smoothed with a Butterworth filter at 120 Hz cutoff and peak acceleration values determined for the initial peak (P_1), and landing peak (P_2). Statistical analysis utilized a 3 way, 2x3x4 repeated measures ANOVA for each dependent measure, with linear contrasts post hoc. The $p < .01$ level of significance was chosen. Axle and frame values were compared between and within forks to determine if impact to bike wheel and impact at frame remained constant across fork conditions and bump types.

RESULTS

For the initial contact peak (P_1) on large bumps (B_2 and B_3), all suspension forks allowed significantly greater axle acceleration than the rigid fork ($p<.0001$). No significant differences in acceleration at the axle were seen between forks for the small bump (B_1). P_1 data at the frame show that F_1 and F_3 provide significant reductions in acceleration for large bumps (B_2 and B_3) compared to all other forks ($p<.0001$). On the small bump (B_1), F_R and F_3 showed

P1 (g) Axle	F_1	F_3	F_6	F_R	*p* value	Between Forks
B_1	14.0 ± 3.0	13.3 ± 2.2	13.6 ± 1.7	12.2 ± 1.7	0.520	NS
B_2	31.0 ± 2.4	28.4 ± 1.9	28.7 ± 1.8	22.8 ± 2.6	< 0.000	$F_R < F_1, F_3, F_6$
B_3	45.3 ± 6.6	45.8 ± 3.5	40.5 ± 3.5	35.2 ± 3.4	< 0.000	$F_R < F_6 < F_1, F_3$
Frame						
B_1	14.7 ± 2.3	11.1 ± 1.0	15.7 ± 2.0	12.0 ± 1.7	0.001	$F_R, F_3 < F_6$; $F_3 < F_1$
B_2	25.3 ± 1.6	21.9 ± 2.1	27.2 ± 2.1	25.7 ± 3.0	< 0.000	$F_3 < F_1, F_6, F_R$
B_3	35.1 ± 1.9	28.3 ± 3.9	36.8 ± 3.4	36.8 ± 3.0	< 0.000	$F_3 < F_1, F_6, F_R$
Within Forks	$B_2A > B_2F$ $B_3A > B_3F$	$B_2A > B_2F$ $B_3A > B_3F$	NS	NS		

P2 (g) Axle	F_1	F_3	F_6	F_R	*p* value	Between Forks
B_1	22.5 ± 5.0	26.9 ± 3.2	22.2 ± 5.0	18.7 ± 3.2	0.041	NS
B_2	25.0 ± 7.9	33.1 ± 5.8	30.4 ± 6.2	31.4 ± 8.6	0.021	NS
B_3	45.6 ± 9.6	48.3 ± 14.7	48.0 ± 9.2	44.2 ± 14.8	0.861	NS
Frame						
B_1	25.5 ± 8.6	20.4 ± 2.5	23.5 ± 5.7	18.2 ± 5.0	0.124	NS
B_2	28.0 ± 4.8	29.5 ± 2.4	30.2 ± 6.6	30.9 ± 9.1	0.451	NS
B_3	43.5 ± 7.3	34.8 ± 11.5	45.5 ± 8.8	45.5 ± 15.2	0.065	NS
Within Forks	NS	$B_3A > B_3F$	NS	NS		

Table 1. Axle and frame acceleration for 4 fork conditions and 3 bump types (Mean ± SD).

similar acceleration at the frame and were significantly lower than F_6 ($p<.001$). Despite the fact that F_3 had greater resistance to axial compression, acceleration values at the frame were still significantly less than F_1 on the small bump ($p<.001$). Unexpectedly, no significant differences in acceleration were detected between fork conditions at the axle or frame for the landing impact (P_2). Only for F_3, the fork with moderate stiffness, was frame acceleration significantly reduced compared to axle acceleration on the landing impact ($p<.0013$).

DISCUSSION

Suspension forks clearly reduced large impacts transmitted to the rider through the front wheel during initial contact with an obstacle. The increased acceleration at the axle on large bumps suggest that the suspension forks allow the front wheel to move more rapidly. It may be that with suspension forks the tire will more closely follow the surface than with rigid forks. The subsequent landing impact (P_2) showed no differences between the suspension forks and the rigid fork. Although this was unexpected, there are many possible reasons why this result was obtained. Since a rider's mass would be accelerated upward on the initial contact, and then descend on the landing contact this may reduce the effectiveness of the suspension forks. The riders may also have been somewhat off balance upon landing, and this may account for the increased variability seen in the P_2 acceleration. The characteristics of the obstacle at initial contact and landing contact are not identical. The force vector of the landing impact may be more vertical than on the initial impact, resulting in a bending moment at the fork rather than long-axis compression. Also, impact attenuation may be reduced on successive bumps. Since no reduction in peak acceleration was seen during landing impacts (P_2), this is a possible area of focus for future developments in suspension fork performance.

REFERENCES

Orendurff, MS. et al., *Med Sci Sports Exer*, 26, p. S176, 1994.

PUNCTURE MECHANICS FOR THE INSERTION OF AN EPIDURAL NEEDLE

L. Hiemenz[1], A. Litsky[1], P. Schmalbrock[2]

[1] Biomedical Engineering Center, Ohio State University, Columbus, OH
[2] Department of Radiology, Ohio State University Medical Center, Columbus, OH

INTRODUCTION

Although needle puncture is a common technique in medical practice, little research has been done to understand how much force is required to puncture biological materials. Needle puncture force was measured for gelatin analogues developed to model the consistency of the tissues in the lumbar region of the back. MRI parameters, T1 and T2 relaxation times, were calculated for the samples and correlated to the puncture resistance. This study was the first step in developing quantitative models for epidural needle puncture which will be used to drive the force feedback device for an epidural needle insertion simulator [Hiemenz, et.al, 1996].

REVIEW AND THEORY

A review of the literature and calls to needle manufacturers revealed only one study that measured puncture force. In that study, puncture forces were measured for segments of dissected cadaveric ligamentum flavum [Baumgarten, 1995]. A comprehensive understanding of needle puncture for biological materials is needed to create accurate analogues for simulating needle insertion techniques.

There is also limited research investigating the relationship between MRI imaging parameters and material properties. Chu and Rutt [1997] show that by changing the mechanical properties of a polyvinyl alcohol cryogel the T1 and T2 relaxation times are changed. A proportional relationship has also been found between viscosity and T1 relaxation times for a variety of liquids. [Abragam, 1966]

This study tested two hypotheses:

- Hypothesis 1: Over the range of insertion velocities typical for epidural needle placement the force at the tip of the needle is independent of the insertion speed.
- Hypothesis 2: For each type of test sample, the puncture resistance is related to MRI imaging parameters, T1 and T2 relaxation times. These parameters describe proton longitudinal relaxation time and transverse relaxation time respectively in response to a magnetic field.

PROCEDURES

Five solid samples were made using Knox™ unflavored gelatin mixed with distilled water in the following concentrations: 70.9%, 47.3%, 36% 15.8% and 5.3% gelatin by weight. The recipe for gelatin of edible consistency calls for 3.5% gelatin by weight. Two gelatin analogues of the tissue layers in the lumbar region of the back were also created. These analogues were made by layering [47.3% 5.3% 70.9% 5.3%] and [36% 5.3% 70.9% 15.8%] gelatin concentrations.

A materials testing system [Bionix 858, MTS Corporation, Eden Prairie, MN] was used to measure force vs. displacement curves for the tip of an 18 gauge Tuohy needle as it was inserted into the samples under displacement control.

Twenty epidural procedures had previously been videotaped and analyzed; needle insertion speeds were found to range from 0.4 to 10 mm/s. Therefore, forces were recorded for each sample at three penetration rates: 0.1 mm/s, 1 mm/s, and 10 mm/s. The modulus of compression was also obtained using a 1 inch diameter solid steel compression fixture. A 7 point equally weighted moving average filter was used to remove noise from the data. Linear regression was performed using Minitab.

High-resolution Magnetic Resonance images were obtained for each of the samples tested using a General Electric 1.5 Tesla MRI system. An inversion recovery sequence was used to measure the T1 relaxation times. T2 relaxation times were determined using a spin echo sequence.

RESULTS

No statistically significant differences were found in the force displacement curves across the three

insertion speeds. The data for the highest speed of insertion were noisy due to the load cell used. Future studies will be done using a more accurate load cell. All data presented in this paper are for the 1mm/sec rate of insertion. The puncture resistance (PR) and the modulus of compression (CM) were found to be linearly related. Results are summarized in the following table:

%gel (g/g)	PR (N/mm)	CM (N/mm^2)	T1 (msec)	T2 (msec)
70.9	0.167	9.306	266.8	35.7
47.3	0.067	5.308	434.2	115.5
15.8	0.021	1.136	751.1	240.9
5.3	0.003	0.192	1153.4	737.2

Table 1: Data Summary

The penetration force was found to be a linear function of the water content as shown below:

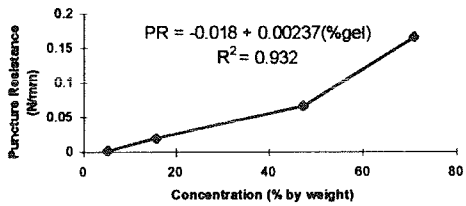

Figure 1: Puncture resistance vs. concentration.

The difference in needle penetration force required to puncture each layer of the layered samples was clearly identifiable. The following diagram shows the 1mm/sec load-displacement curve for Mix 2 [36% 5.3% 70.9% 15.8%]:

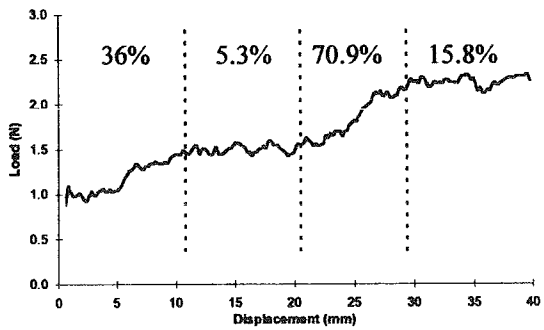

Figure 2: Load-displacement curve for Mix 2.

An exponential relationship was found between the puncture resistance and both the T1 and T2 relaxation times from the MRI study. Stiffer gelatin mixtures have larger resistance to puncture and shorter T1 and T2 times than more compliant mixtures. This relationship is illustrated in the following diagram:

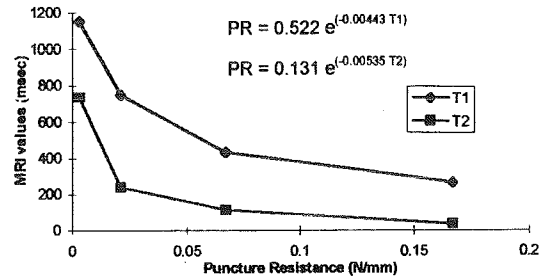

Figure 3: Relationship between puncture resistance and T1, T2 relaxation times.

DISCUSSION

These experiments with gelatin analogues for tissue are the first step in creating a quantitative model of the forces at the tip of the epidural needle with respect to insertion depth as the needle penetrates the layers of the human back. Gelatin was chosen because the samples were homogeneous and layered analogues were easy to create. The next step in this project will be to refine the haptic model using the procedures defined above with more complex materials such as ex vivo tissue samples.

The exponential relationship found between MRI values and both the puncture resistance and the compressive modulus allows us to base the force models for the gelatin samples on their MRI values. Further experimentation is required to determine if this empirical relationship exists across the types of tissues transversed by epidural needles.

REFERENCES

Abragam, Principles of Nuclear Magnetism, 264-353 (1961).
Chu, K., Rutt, B., MRM 37:314-319 (1997).
Hiemenz, L.,et.al. , P 15th S Biomedical Eng Conf, 170-173 (1996).

ACKNOWLEDGMENTS

This study has been funded through the Link Foundation Fellowship for Simulation and Training.

A NEW TECHNIQUE FOR QUANTIFYING SPINAL COUPLING ANGLES: THE TILT / TWIST METHOD

N.R. Crawford[1], G.T. Yamaguchi[2], C.A. Dickman[1]
[1]Spinal Biomechanics Research Laboratory, Barrow Neurological Institute, Phoenix, AZ 85013
[2]Department of Chemical, Bio, and Materials Engineering, Arizona State University, Tempe, AZ 85287-6006

INTRODUCTION

Although helical angles are the method of choice for representing rigid body angular orientation in a research setting, they are nonintuitive for representing spinal angles, especially in a clinical setting. Clinicians communicate about spinal motion using the well-established anatomical plane angles: flexion/ extension, lateral bending, and axial rotation. These angles are based on the projections seen in x-ray and computed tomography images. A scientifically sound method is needed to convey three-dimensional coupled spinal motion in terms of these familiar planar angular components; for example, "*X* degrees of flexion/extension was coupled with *Y* degrees of lateral bending and *Z* degrees of axial rotation."

The two most common techniques for extracting planar angles from three-dimensional rigid body motion are the Euler method and the projection method. The validity of both techniques can be questioned because both techniques give significantly varying results depending on the rotation sequence or vectors used in their application to spinal motion. In addition, both methods have been shown to be unstable at some angles approaching 90°. A new method of computing spinal rotation angles based on a cylindrical representation of vertebral geometry is presented that overcomes the problems of the Euler and projection techniques. This method gives values of flexion/extension, lateral bending, and axial rotation that are consistent with intuitive expectations over ranges of both small and large angles and are stable approaching 180°. This alternative technique, the method of "tilt and twist", is easily understood in geometrical terms using an analogy of two stacked, overlappable cylinders to represent a lower fixed vertebra and an upper moving vertebra, but may also be implemented as a classical, non-Cardanic Euler rotation sequence (Ry, Rx, Ry'). This method is proposed as a standard in three-dimensional spinal motion studies.

REVIEW AND THEORY

Currently, two techniques are chiefly used for determining spinal coupling angles from marker coordinate data: the Euler method and the projection method. In the Euler method, an equivalent sequence of three rotations (one about each coordinate axis) is calculated that would rotate the vertebra from its initial orientation to the orientation observed. In the projection method, vectors associated with a vertebra are projected in each plane and the angles between the vector projections in the vertebra's initial and final orientation are measured.

Both the Euler and projection techniques are ambiguous in their application to the spine: there are six possible rotation sequences when using the Euler method (Smith and Fernie, 1991) and there are two possible angles in each plane when using the projection method (Crawford *et al.*, 1996). Although resolution of ambiguities is possible for angles less than about 30° (Crawford *et al.*, 1996), it is unclear which Euler sequence or projection angle set best applies when studying larger spinal motion.

In addition to their ambiguity, a major difficulty with both the Euler and projection methods is that a singularity is approached in cases where a vector for projection nears orthogonality to the projection plane and in cases where the second Euler angle approaches 90° (gimbal lock—Woltring, 1991). At the singularity, the angles are undefined. Near the singularity, small changes in orientation result in large changes in the angles calculated (Woltring, 1991).

Because a representation of spinal angles capable of passing 90° is desirable in some cases (*e.g.*, measuring head-neck motion) and because it is unclear which, if any, of the current methods provides intuitively correct spinal coupling angles over a large range, a new technique for determining spinal angles was developed: the method of *tilt and twist*.

PROCEDURES

In the tilt/twist method, the vertebrae of a motion segment are represented by two stacked, overlappable cylinders, as shown in Figure 1. Three angles are measured geometrically from vectors associated with the cylinders in their initial and final orientations: the tilt magnitude (ϕ), tilt azimuth (θ), and twist (τ) angles.

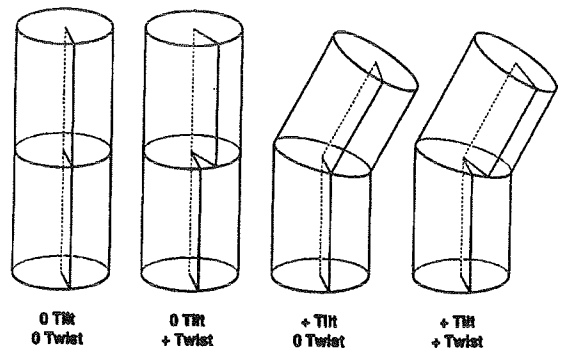

Figure 1: Stacked cylinder analogy showing tilt and twist.

The angle ϕ is the magnitude of bending of the upper cylinder with respect to the lower cylinder. The angle θ is the direction in the transverse plane in which this bending occurs. The angle τ is the twisting of the upper cylinder on the lower cylinder.

Twist corresponds to the axial rotation spinal angle. Flexion/extension (F) and lateral bending (L) are the anteroposterior and lateral components (respectively) of tilt, derived from tilt azimuth and tilt magnitude using the following relations:

$$F = \phi \cos \theta$$
$$L = \phi \sin \theta$$

Although described above as angles measured geometrically from spinal vectors (similar to the projection method), the tilt magnitude, tilt direction, and twist angles may instead be obtained from a sequence of three rotations (similar to the Euler method). This sequence is non-Cardanic, i.e., rotation occurs about the same axis twice. The motion is represented as first a rotation θ about the y-axis, then a rotation ϕ about the new x-axis, then a rotation ξ about the new y-axis. The angle τ is the sum of θ and ξ. Representation as a non-Cardanic Euler sequence is advantageous because matrix techniques may then be used to invoke the resulting rotations (Paul, 1982).

To compare the stability of the tilt/twist angles, the tilt/twist-derived spinal angles, projection angles and Euler angles, a stability test was devised where a one-degree conical test movement was applied to a mathematical model of a vertebra in a specified starting angular orientation, and the range of resulting angles reported as determined by each method. This stability test was performed for rotations about each coordinate axis.

RESULTS AND DISCUSSION

For small movements (<30°), the tilt/twist-derived spinal angles behave similarly in flexion/extension and lateral bending to the projection angles derived from the inferosuperior vector (the preferred projection angles for describing spinal motion—Crawford et al., 1996). In axial rotation, they approximate the *average* of the projection angles derived from the anteroposterior and lateral vectors. In terms of Euler angles, the tilt/twist-derived spinal angles behave similarly in flexion/extension and lateral bending (<30°) to R_x and R_z from the $R_y \rightarrow R_z \rightarrow R_x$ Euler sequence (the preferred Euler sequence for spinal motion—Crawford *et al.*, 1996). In axial rotation, they behave approximately the same as the *average* of R_y determined from all six Euler sequence permutations. For larger rotations, the tilt/twist-derived spinal angles do not follow any of the Euler or projection angles.

As expected, the Euler and projection methods showed instabilities as they approached 90° rotation about certain axes. Although the tilt azimuth angle showed instability near 0° and 180°, the tilt magnitude, twist, and tilt/twist-derived flexion/extension and lateral bending angles were stable from 0° to nearly 180°, twice the range of spinal angles derived from the Euler or projection methods.

Because they are based on an intuitively straightforward geometrical representation and are stable over twice the range of Euler and projection angles, the tilt/twist-derived spinal angles are recommended as the standard for representation of spinal coupling.

REFERENCES

Crawford, N.R. et al. Hum. Mvmt. Sci., 15, 55-78, 1996.

Paul, R.P. Robot Manipulators: Mathematics, Programming, and Control. (pp.45-71), MIT Press, 1982.

Smith, T.J., Fernie, G.R. Spine, 16, 1197-1203, 1991.

Woltring, H.J. Hum. Mvmt. Sci., 10, 603-16, 1991.

ACKNOWLEDGMENTS

This work was funded in part by a grant from the National Science Foundation (grant #BCS 9257395-01)

QUANTIFICATION AND VISUALIZATION OF *IN VIVO* 3D CARPAL BONE KINEMATICS

J. J. Crisco[1,2], R. D. McGovern[1], L. D. Katz[3], S. W. Wolfe[4]

[1]Department of Orthopaedics, Rhode Island Hospital, Providence, RI;
[2]Division of Engineering, Brown University, Providence, RI;
[3]Department of Diagnostic Imaging, [4]Department of Orthopaedics,
Yale University School of Medicine, New Haven, CT.

INTRODUCTION

An algorithm for quantifying and visualizing the three dimensional (3D) kinematics of the carpal bones of the wrist *in vivo* was developed.

REVIEW AND THEORY

It is well appreciated that the carpal bones exhibit complex 3D kinematics during normal wrist motion. However, quantification of carpal kinematics has been limited in the past to cadaveric studies because of the small size of the carpal bones and the need for invasive markers. Cadaveric studies are limited in their ability to simulate physiological loading patterns, healing effects, and rehabilitation. Several studies have examined the relative 3D posture and orientation of the carpal bones [1,2,4], but a quantitative analysis of 3D carpal kinematics *in vivo* has not yet been accomplished. It is also well appreciated that the motions of the carpal bones are coupled in 3D. Coupled motions are motions that are not separable and distinct from the main motion. Such motions are extremely difficult to fully appreciate from graphs. The purpose of this work was to describe an algorithm and to demonstrate its application for *in vivo* 3D kinematic analysis.

PROCEDURES

The algorithm consists of image acquisition, segmentation of bone surfaces, kinematics, and visualization.

Image Acquisition. Multiple positions of the wrist were imaged using CT (HiSpeed Advantage, GE Medical Systems, Milwaukee, WI). The subject's (n = 1) wrists were positioned within the gantry in a custom positioning jig. Volume images were collected in axial format with typical voxel dimensions of 0.2x0.2x1 mm^3. All image processing was performed on a Silicon Graphics workstation (Indigo^2 XZ, SGI, Mountain View, CA) using the 3D biomedical imaging software system Analyze (Biomedical Imaging Resource, Rochester, MN).

Segmentation of Bone Surfaces. CT volumes were thresholded to emphasize the outer cortical shell. Contours were extracted after each bone cross-section was closed and filled. Automated matching of the contours to each bone is not presently attainable because of the number of bones, the complexity of the contours, and the potential for branching and holes. Interactive software (Open Inventor, C++, SGI; MATLAB, Mathworks, Natick, MA) was developed that allows visualization and manipulation of these contours in 3D to allow the user to define the correct contour-bone associations.

Kinematics. Each bone was assumed to move independently as a rigid body. Kinematic values were calculated using an existing method that minimizes the mean squared distance between two bone surfaces [3]. Bone kinematics were described using the helical axes of motion (HAM) parameters of rotation and translation about the helical axis. Additionally, kinematic error was studied using a cadaveric wrist specimen at four calibrated positions, allowing six kinematic comparisons (n = 6).

Visualization. Visualizing bone position and orientation is helpful to ensure algorithm success and can also provide diagnostic assistance [1]. Specifically written code in C++ and Open Inventor was utilized for visualization and animation.

RESULTS

Kinematic error was influenced by the particular carpal bone and the varied with the direction of motion (Table 1).

Table 1. Average 3D kinematic error.

	Trans. (mm)	Rot. (deg)
Scaphoid	1.7 ± 1.4	1.0 ± 0.9
Lunate	2.7 ± 2.0	1.7 ± 1.7

The 3D *in vivo* motions were complex and coupled as the capitate moved with wrist position and the scaphoid moved in an almost orthogonal direction (Table 2 and Figure 1).

Table 2. HAM rotations and translations (n = 1). The orientations and positions of helical axes are rendered in Figure 1.

	Radial Deviation	Ulnar Deviation
Capitate	34°, 0.7 mm	26°, 2.6 mm
Scaphoid	18°, 0.6 mm	25°, 2.6 mm

Figure 1. Palmer view of the left wrist of a healthy subject in neutral 1A and white), radial deviation (light gray), and ulnar deviation (dark gray). The motions of capitate (C) and scaphoid (S) are rendered (1B and 1C) with their respective helical axes for each wrist position. The radius (R) and ulna (U) are also rendered.

DISCUSSION

These data demonstrate the ability to accurately and noninvasively measure 3D joint kinematics *in vivo*. While we have shown that it is possible to precisely measure 3D carpal motion from CT volume images, the level of accuracy necessary to detect pathologic aberrations in kinematics is unknown.

The accuracy and visualization capabilities of the algorithm described herein will enable intricate analysis and deeper understanding of normal and abnormal carpal kinematics, carpal nonunions, malunited distal radius fractures, and metacarpophalangeal implants.

REFERENCES

[1] Belsole RJ et al. (1991) J Hand Surg., 16A(1): 82 - 90. [2] Patterson RM et al. (1995) J Hand Surg, 20A(6):923-929. [3] Pelizzari CA et al. (1989) J Comput Assist Tomogr. 13:20-26. [4] Viegas SF et al., (1993) J Hand Surg., 18A(2): 341- 349.

ACKNOWLEDGMENTS

Supported in part by NIH AR44005.

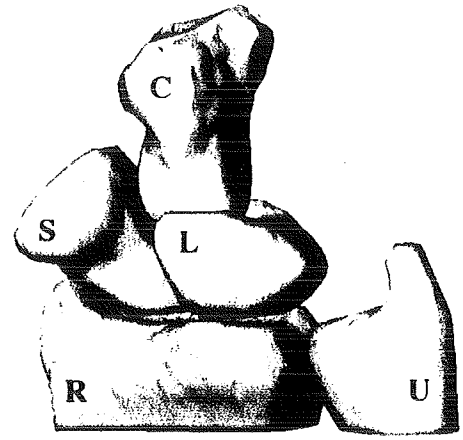

Figure 1A. Neutral position.

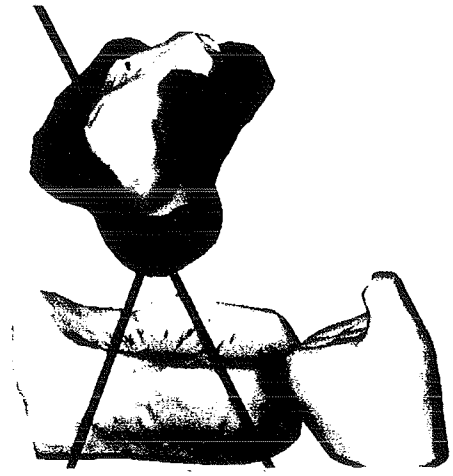

Figure 1B. Capitate motion.

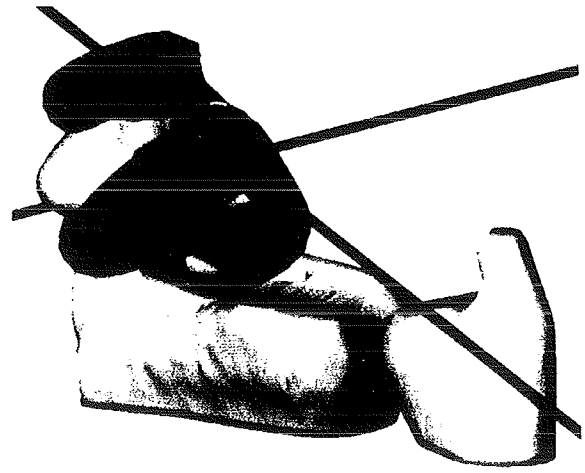

Figure 1C. Scaphoid motion.

A BIOMECHANICAL EVALUATION OF RS-KETOPROFEN AND PGE_2 TREATMENT IN REDUCING BONE LOSS IN OVARIECTOMIZED RATS

S. Saha[1], W. J. Wechter[2] and L. W. Bridges[2]

[1]Dept. of Bioengineering, Clemson Univeristy, Clemson, SC 29634-0905
[2]Department of Medicine, Loma Linda University, Loma Linda, CA

INTRODUCTION

Several newly developed drugs have been proposed as effective treatments for osteoporosis. Ovariectomized rats is an accepted model of osteoporosis due to estrogen deficiency. The objective of this study was to determine if a combination of an arylpropionic acid (ketoprofen) and prostaglandin E_2 (PGE_2) could reduce the adverse effect on ovariectomy on the load carrying capacities of long bones in rats.

METHODS

Two month old Sprague-Dawly female rats were divided into eleven groups, group 1 being the sham-operated control. The other ten groups were ovariectomized (OVX) and groups 3 to 10 received treatment with PGE_2 and/or RS-ketoprofen daily and group 11 received similar treatment with an experimental drug ED-5090 (Table 1). Each group consisted of 12 animals and half of each group was sacrificed at 10 and 60 days after initiating the treatment. The femur and tibia were removed and tested mechanically in 3-point bending using an Instron mechanical testing machine (Model 1011).

Table 1. Treatment Groups

GROUP		Dosage (mg/kg/d) PGE_2	KTP
1		Control (Sham-Operated)	
2	OVX	0	0
3	OVX	0	5.0
4	OVX	0	0.1
5	OVX	0.3	0
6	OVX	1.0	0
7	OVX	0.3	5.0
8	OVX	1.0	5.0
9	OVX	0.3	0.1
10	OVX	0.1	0.1
11	OVX	100	ED 5090

RESULTS

The failure loads and the energy absorption capacities for the femurs of each group is shown in Figures 1 and 2 respectively. It is evident that although the 60 day animals showed an increased strength compared to 10 day animals for all the groups, this increase was much larger for the treatment groups compared to sham-operated controls. This increase was statistically significant for several groups ($P<0.05$). The failure load of 10 day animals for groups 4 and 8 was significantly higher ($P<0.05$) than the ovariectomized controls (group 2). The failure loads of the other groups as well as the energy absorption capacities were not statistically different from those for the ovariectomized controls. Similar results were also obtained for the tibia.

DISCUSSION

This study shows that treatment with PGE_2 and KTP could be effective in reducing the bone loss due to estrogen deficiency. However, the exact combination of drug dosages for optimum effectiveness has yet to be determined. We are also investigating the effectiveness of various biomaterials as a drug delivery system for influencing bone growth and metabolism.

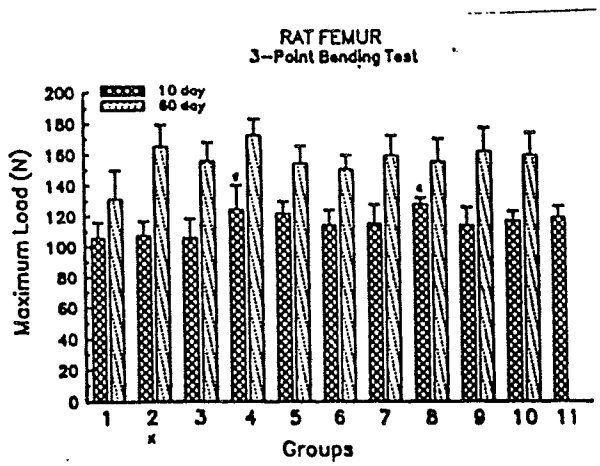

Figure 1

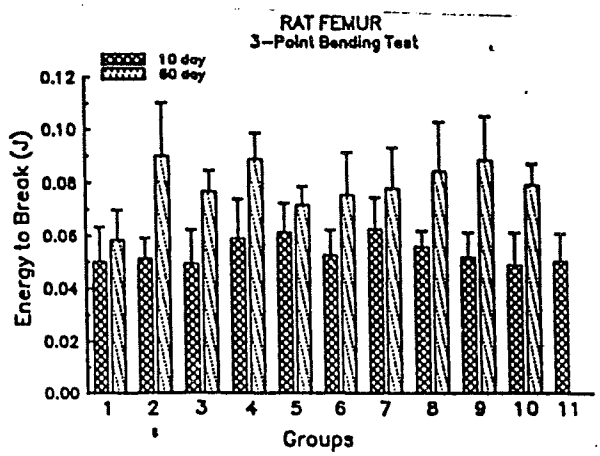

Figure 2

DOES SPINAL FUSION WITH INSTRUMENTATION AFFECT RANGE OF MOTION AT ADJACENT LEVELS?

S. Zyblewski[1], D.L. Powers[1], S.P. Massia[1], B.G. Cuddy[2], W.C. Hutton[3], V.M. Gharpuray[1]

[1]Department of Bioengineering, Clemson University, Clemson, SC 29634
[2]Department of Neurosurgery, Medical University of South Carolina, Charleston SC, 29425
[3]Emory Spine Center, Emory University, Atlanta GA, 30303

INTRODUCTION

Spinal fusion is often indicated to correct instabilities associated with deformity, traumatic injury, degenerative disc disease, and prolapse. Several researchers have suggested that such a procedure significantly changes the mechanics of the spine (Lee et al. 1984, Yang et al. 1986). Clinically, these changes have been implicated as the cause of numerous pathological conditions that arise post-operatively, including degeneration of adjacent discs and facet joints, bone resorption in the fused region, and stenosis of the spinal canal (Whitecloud et al. 1994, Rothman et al. 1985, Hutter 1985). In the present study, range of motion (ROM) was selected as a non-invasive means of quantifying *in vivo* changes in the mechanical behavior of the juxta-fused segments of the cervical spine.

REVIEW AND THEORY

Historically, it has been difficult to define the role of fusion in the development of pathological conditions that arise post-operatively; clinically, no differentiation can be made between iatrogenic effects and those that arise as a result of the patient's pre-existing condition(s). However, it may be possible to design an animal model which isolates the effect of fusion on the mechanical behavior of previously-healthy components of the spine.

Since mechanical factors play a dominant role in causing degenerative changes, the animal model should be carefully selected if results are to be extrapolated to the human case. In the past, numerous experiments have used dog, calf, rat, and rabbit models to study fusion in the lumbar spine.

The caprine model for cervical fusion was introduced by Zdeblick and co-workers (1992, 1993), who believed that vertebral structure and loading were similar to the human. Fusion rates obtained with autogenous bone grafts in this model were similar to those reported clinically. Further, the mechanical properties of caprine intervertebral discs have been shown to be similar to those of human discs (Janeway, 1995).

PROCEDURES

Six age and weight-matched castrated male Nubian goats were used in this study. Pre-operative roentenographs of the cervical spine were obtained for all animals to ensure the absence of gross pathological conditions. An anterior approach was used to expose the cervical spine, and discectomies were performed at the C3-4 and C4-5 levels. Autogeneous bone grafts from the iliac crest were impacted into disc spaces, and commercially available anterior human cervical instrumentation (Ti-6Al-4V) was used to stabilize the spine and promote a solid arthrodesis (Figure 1).

While under general anesthesia, lateral radiographs were obtained with the neck passively flexed and extended as shown in Figure 2 (Dvorak et al., 1988). The range of motion at each level was determined by measuring the angles between lines drawn parallel to the anterior aspect of the spinal canal on adjacent vertebral bodies (modified from Buette-Bäuml, 1954).This procedure was performed pre-operatively, immediately post-operatively, and six months after surgery.

RESULTS AND DISCUSSION

No complications were experienced during surgery, and all animals withstood the procedure well. The range of motion data is summarized in Figure 3. The figure shows that the ROM at the fused levels (C3-4, C4-5), decreased significantly post-operatively, and increased slightly six months after surgery. At the level cephalad to the fusion mass (C2-3), no changes in mobility were observed post-operatively. At the caudal level (C5-6), however, a significant increase in ROM was observed six months post-operatively.

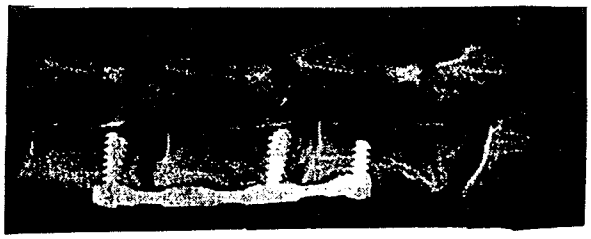

Figure 1: Lateral view of fused (C2-3 and C3-4) cervical spine with anterior instrumentation.

Figure 2: Flexion angle measured from lateral radiograph. This was repeated in extension to obtain the total ROM for each joint

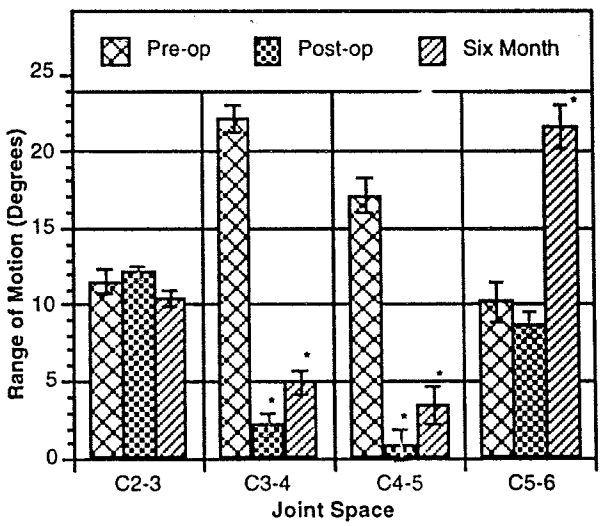

Figure 3: Range of motion at the fused and juxta-fused segments (* indicates significant difference ($p<0.05$) from pre-operative value at the same level).

In the literature, a controversy exists as to the relationship between spinal pathology and the motion it effects. While a few studies have found no correlation (Rolander, 1966; Hirsch et al., 1968; Nachemson et al., 1979), others have demonstrated that mobility increases in the presence of disc degeneration (Hagelstam, 1949; Panjabi et al., 1982; Knuttson, 1944). The results obtained here could support the latter conclusion. Clinically, it is not uncommon for evidence of focal degenerative changes to arise below the fusion mass (Hunter et al., 1980), but as yet, that result has not been correlated with changes in range of motion

Histopathological and biochemical analyses are currently being performed to quantify compositional and morphological degenerative changes in the fusion and juxta-fused regions.

REFERENCES

Buette-Bäuml C. Ergänzungsband, 70, 1954.
Dvorak J. et al. Spine, 13(7), 748-755, 1988.
Hagelstam L. Acta Chir. Scand., 143(Suppl.), 1949.
Hirsch C. et al. Acta Orthop. Scand., 39, 303, 1968.
Hunter L. et al. Spine, 5(5), 399-401, 1980.
Hutter C. et al. Clin. Orthop. and Rel. Res., 193, 103-114, 1985.
Janeway T. J. Invest. Surg, 8(4), 300, 1995.
Knuttson F. Acta Radiol., 24, 593-609, 1944.
Panjabi M. et al. Trans. Int. Soc. for Study of Lumbar Spine, Toronto, 1982.
Nachemson A. et al. Spine, 4(1), 1, 1979.
Rolander S. Acta Orthop. Scand., 99, 1966.
Rothman S. et al. Clin. Orthop. and Rel. Res., 193, 47-56, 1985.
Whitecloud T. et al. Spine, 19, 531-536, 1994.

ACKNOWLEDGMENTS

The Clemson University / Greenville Hospital System Research Cooperative is gratefully acknowledged for funding. Internal fixation devices were provided by Johnson & Johnson, Professional, Inc..

PATHWAY OF INSTANT AXES OF ROTATION OF THE ANKLE JOINT - IMPLICATIONS FOR THE APPLICATION OF ARTICULATED EXTERNAL FIXATION

M. Bottlang[2], J. L. Marsh[1], T. D. Brown[1,2]

Departments of [1]Orthopaedic Surgery and [2]Biomedical Engineering,
University of Iowa, Iowa City, IA 52242

INTRODUCTION

In a cadaveric ankle study we determined the instant axes of rotation of the talocrural joint via an electromagnetic motion tracking system. The pathway of these axes was accessed in detail and the implication of articulated external fixation for the ankle joint was investigated.

REVIEW AND THEORY

Articulated external fixation of the ankle joint has been used with encouraging results for the treatment of tibial plafond fractures (Bonar et al., 1993). Hinged external fixators restrict the motion of the talocrural joint to be rotation around a fixed hinge, which can cause distortion to the ankle kinematics (Fitzpatrick et al., 1995). Alignment of the external hinge with the axis of the ankle joint is essential to preserve physiologic joint kinematics over a wide range of motion. Therefore quantitative assessment of the pathway of instant axes of the ankle joint is fundamental to enable a correct hinge alignment.

PROCEDURES

Four fresh frozen cadaveric below-knee specimens were mounted into a specially designed ankle motion applicator. The tibia was fixed rigidly while the foot was passively flexed / extended at a constant angular velocity of 10°/s via a DC motor. The tibia was rigidly connected with the calcaneus via an external bar to simulate conditions imposed by most unilateral articulated ankle fixators as well as to extract the kinetics of the talocrural joint by eliminating motion in the subtalar joint. An electromagnetic motion tracking system ("Flock of Birds"®, Ascension Technology Corp., Burlington, VT) was used to record the 3-D-motion of the talus with respect to the tibia. These motion data were used to determine the pathway of instant axes of rotation of the talocrural joint, which were described as screw displacement axes (SDA) (Figure 1). First, the SDA for neutral ankle position (0° dorsiflexion) was calculated. Then, the change of this SDA during plantar-flexion (PF) and dorsiflexion (DF) was determined. The change of the SDA was expressed in translation (anterior / posterior , proximal / distal) and angulation (eversion / inversion, int. / ext. rotation). The translation was accessed in a mid-talar sagittal plane as well as in a parallel plane located 60 mm medial (i.e. the estimated locus of the fixator hinge).

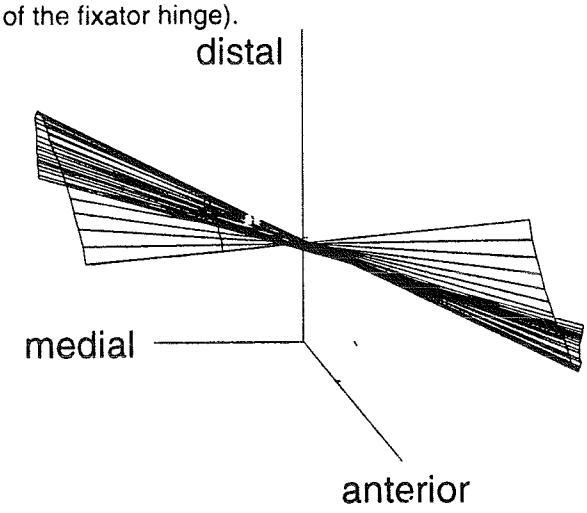

Figure 1: 3-D Pathway of instant axes of rotation of the ankle joint, described as screw displacement axes.

RESULTS

The reproducibility of SDA pathway detection of a given specimen was within 1 mm and 1°. During PF, the instant axes of rotation of the ankle joint translated in a mid-talar plane posterior and distal (Figure 2), and angulated into eversion and external rotation (Figure 3). During DF, the instant axes of the ankle joint translated in a mid-talar plane anterior and

proximal, and angulated into inversion, while continuing to rotate externally. For a 15° range of motion, from 5° PF to 20° PF, an average SDA translation of 1.5 mm (anterior / posterior) and 0.6 mm (proximal / distal), and an average change in SDA angulation of 9.6° (eversion / inversion) and 2.3° (int. / ext. rotation) was detected among the four specimens. If the 15° range of motion was chosen between 5° DF to 10° PF, the average translation increased more than five fold and the average change in SDA angulation more than doubled. The pathway of the SDA in a mid-talar plane as well as 60 mm medial to that plane is shown in Figure 4.

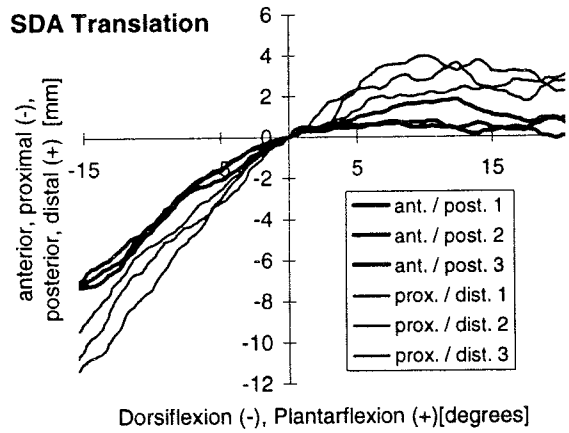

Figure 2: Translation of the instant axis of rotation in the mid-talar sagittal plane.

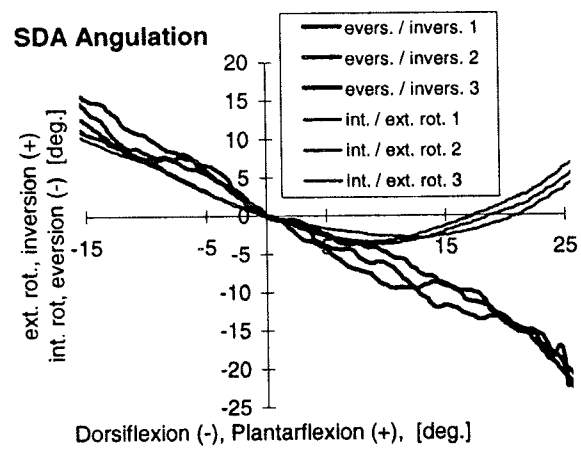

Figure 3: Angulation of the instant axis of rotation (specimen # 4)

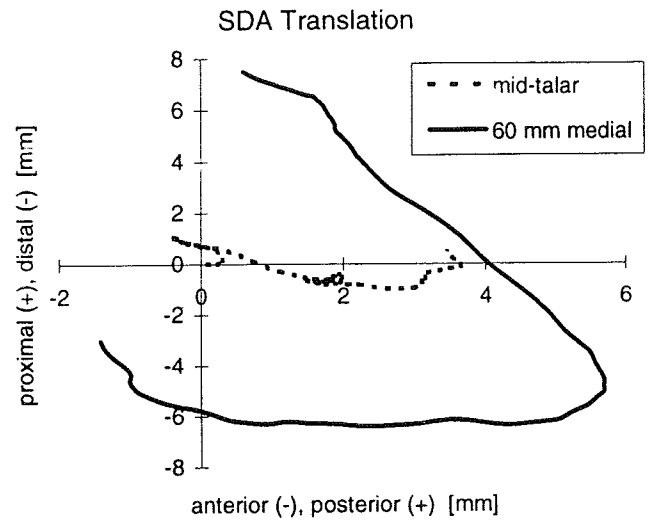

Figure 4: Translation of the ankle axis in the mid-talar sagittal plane and in a parallel plane located 60 mm medial (approx. fixator location).

DISCUSSION

This study described the translation and angulation of the instant axes of rotation of the ankle joint in relation to the range of motion. The amount of translation and angulation for a given incremental ankle rotation (i.e. 15°) varied significantly within the total range of motion. The most severe changes of the instant axis were observed towards the extremes of range of motion. This finding can be especially important for early post-operative mobilization as well as to determine an optimized axis position of the articulated fixator hinge in respect to the ankle joint. This research emphasizes the importance of a correct placement of the fixator hinge. While a mechanical axis finder (Hollister et al., 1992) can be used in the clinical setting to estimate a joint axis, there is still a need for an advanced inter-operative "axis-finding" technique.

ACKNOWLEDGEMENTS

Financial support provided by EBI Inc.

REFERENCES

Bonar SK *et al.*, Foot & Ankle 14:57-64, 1993
Fitzpatrick DC *et al.*, J Orthop Trauma 9:1, '95
Hollister A et al., J Orthop Res 10:454-469, '92

THE EFFECT OF COMBINED FACETECTOMY AND DENUCLEATION ON THE FLEXIBILITY OF THE LUMBAR SPINE MOTION SEGMENT

J. Millar*, A.G. Patwardhan**, R. Havey**, R.N. Natarajan, S.A. Lavender and G.B.J. Andersson
Dept. Orthop. Surg.; Rush Pres. St.Luke's Med. Ctr, Chicago, IL
* University of Illinois at Chicago, Chicago, IL
** Dept. Orthop. Surg.; Loyola Univ. Med. Ctr, Maywood, IL

INTRODUCTION

It has been documented in the literature that a complete unilateral facetectomy in a lumbar motion segment causes an increase in flexibility at the level the surgery was performed. However, the results of combined facetectomy and denucleation on the flexibility of the motion segment has not been studied. Using human cadaveric specimens of the lumbar spine, the following hypotheses were tested: (i) The flexibility of the lumbar motion segment, subjected to both complete unilateral facetectomy and full disc denucleation, increases with respect to graded facetectomies. (ii) The increase in flexibility of the lumbar motion segment, subjected to both complete unilateral facetectomy and full disc denucleation, is affected by the loading mode.

METHODS

Four human cadaveric two motion segment specimens of the lumbar spine (L1 to L3 and L4 to S1) were used in this study. The end vertebral bodies were mounted in cups using bone cement and pins. The cup containing the inferior vertebral body was then rigidly attached to the testing frame through a six component load cell.

In order to compensate for the weight of the torso and the role of active musculature, a "follower" axial load was applied. Cables were securely fixed to the top cup and passed through guides attached to a screw through the middle vertebral body. The cables passed over pulleys connected to the cup containing the inferior vertebral body, and were loaded to 400 N.

A loading bar, mounted to the top cup, was used to generate moments up to 8 Nm for flexion, extension, right and left lateral bending, and right and left torsion. The six component load cell placed under the specimen was used to measure the ground reaction forces and moments. The motion of the lumbar segments was measured using an optoelectronic motion measurement system and infrared light emitting diodes that were attached to the center of the moving vertebral bodies. The diodes representing the non-moving vertebral body were rigidly attached to the testing frame. In order to ensure that each test began from the same position, angle sensors were mounted on the top cup.

A continuous loading scheme was used in order to obtain the desired moments for each loading condition. After the desired moment was achieved, there was a 30 second delay, to account for creep response, before the data were collected.

The graded facetectomies were done on the right side of the motion segment and included a partial laminectomy and resection of the intraspinous ligament and the ligamentum flavum ligament. The full disc denucleation, with a 6 mm square annular incision, was also performed at this level. All loading modes were applied in a random order for each of the surgeries.

RESULTS

Overall, surgical interventions affected the range of motion for all loading modes ($p<0.01$). A 50% unilateral facetectomy produced less increase in motion than complete unilateral facetectomy or complete unilateral facetectomy and complete denucleation ($p<0.01$). In the case of combined facetectomy and denucleation, removal of the nucleus with the complete unilateral facetectomy resulted in

greater increase in motion than in the complete unilateral facetectomy case ($p<0.001$).

Figure 1 shows the percent change in range of motion with a 7Nm applied moment for each of the surgical conditions with respect to the intact motion segment. In flexion, there is a 15.5% (SD=11.5%) increase in range of motion due to a 50% unilateral facetectomy, which increases to 18.7% (SD=10.4%) upon full excision of the facet. When the disc nucleus is removed, a 63.2% (SD=23.9%) increase in flexibility is seen with respect to the intact. In extension, there is a 11.6% (SD=2.2%) increase due to a 50% unilateral facetectomy, which increases to 18.7% (SD=8.9%) after a 100% unilateral facetectomy. This value decreases to 8.4% (SD=13%) upon removal of the nucleus. In left torsion (placing the surgically altered facet under compression), a 50% unilateral facetectomy caused an increase of 23.7% (SD=31.9%) in the range of motion, while a complete unilateral facetectomy and a combined complete facetectomy and full denucleation produced increases of 96.7% (SD=60%) and 107.8% (SD=64.7%), respectively. In right torsion, the increases in the range of motion due to the 50% and 100% unilateral facetectomies were very similar (13.4% (SD=26.5%) and 11.3% (SD=14%)), while the combined facetectomy and denucleation increased the motion by 61.9% (SD=20.6%).

DISCUSSION

A large increase in flexibility was observed for all loading modes, except extension moment loading, when the nucleus was completely removed after complete unilateral facetectomy. This increase was much larger than those observed after graded facetectomy. For the loading moments shown in Figure 1, as well as the lateral bending moment loading, the flexibilty of the lumbar motion segment progressively increased, with respect to the intact segment, for each subsequent surgery. During some of the extension moment loading cases with the complete facetectomy and full denucleation procedure, it was noted that the posterior aspect of the superior vertebral body in the motion segment impinged upon the posterior aspect of the inferior vertebral body, thus resulting in less motion. Right rotation was not affected significantly by the graded facetectomies since the facetectomy was performed on the right facet, however, it increased due to nucleus removal.

Under flexion loading or right rotational moment loading, the range of motion due to complete unilateral facetectomy combined with full denucleation increased nearly three times that observed in the complete unilateral facetectomy alone. Although increases in flexibility existed for extension, lateral bending, and right rotation loading moments, the magnitudes of these increases were not as large. These lead to the conclusion that the loading mode does have an effect on the change in flexibility of lumbar motion segments due to facetectomy and denucleation. The study suggests that surgeries which involve complete unilateral facetectomy and denucleation may require rigid fixation to prevent instability.

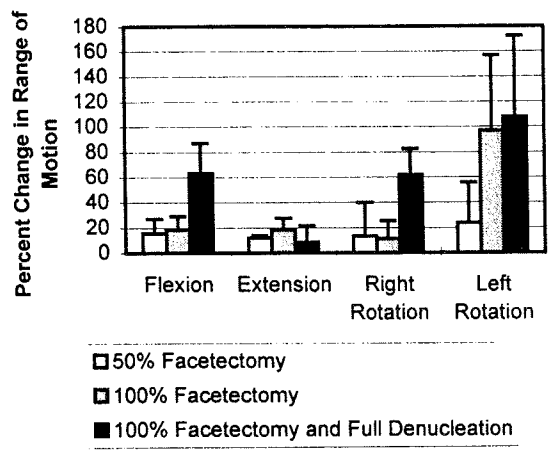

Figure 1: Percent Change in Range of Motion with respect to Intact

ACKNOWLEDGEMENT

VA Grant: A 830-RA

STRESSES IN BONE NEAR TRANSCORTICAL IMPLANTS

Xin Zhang [1], Lonny L. Thompson [2], Vasanti M. Gharpuray [1]

[1] Department of Bioengineering, Clemson University, Clemson, SC 29634 -0905

[2] Department of Mechanical Engineering, Clemson University, Clemson, SC 29634

INTRODUCTION

Osseocompatibility tests usually involve the implantation of cylindrical "plugs" transcortically into the long bones of test animals. After a specified period of implantation, the implants are retrieved and the bone/implant interface is assessed either histologically or mechanically. However, using this test method, different studies have obtained contradictory results when evaluating essentially the same material. One factor that influences the results of the test is bone remodeling around the implant, which in turn is influenced by the strain state in bone surrounding the implant [1]. Therefore, the objective of this study was to develop a finite element (FE) model to predict the stress and strain states in bone around a transcortical implant.

REVIEW AND THEORY

Adaptive bone remodeling occurs when bone is strained differently from its natural state. Thus, any variable that affects the strain state will affect remodeling around the implant and may also affect the results of a transcortical test. A previous study using a simplified mathematical analysis suggested that the strains around transcortical implants may vary with position around the implant, location of the implant along long axis of the bone, implant stiffness and bone/implant interface conditions [2]. A later experiment showed that the results evaluated using the push out tests vary with location of the implant [3]. However a FE model of the intact caprine femur predicted that strains in bone do not vary with location in the region in which implants are normally placed [4]. Relatively few studies have measured strains *in vivo* near a transcortical implant [5,6]. However, due to large animal to animal variations these studies have not been able to show statistically significant differences with implant location and modulus.

These previous studies have given us a good insight into the problem. However the previous models used several idealizations and the *in vivo* measurements were limited to a few locations and orientations. Therefore, to overcome some of these limitations we decided to use the FE method to predict the stress (or strain) state in bone surrounding implants of different moduli and different bone/implant interface conditions.

PROCEDURES

Since the lateral side of a goat femur is consistently under uniaxial tension [4] and the region of implantation is relatively flat, bone was considered as orthotropic square plate under uniaxial tensile loading and implant was inserted into the center of the plate. Due to symmetry, only one quarter of the model was built (Figure1). Two different implant materials (UHMWPE and Ti6Al4V, Table 1) and three interface cases were investigated: Case 1 was based on the most ideal case in which the transcortical implant was assumed to be perfectly bonded to the surrounding bone; Case 2 accounted for the partial debonding that inevitably occurs between the implant and the bone if complete adhesion has not been achieved; Case 3 determined the effect that a press fit implant has on the magnitude of the stresses at the bone/implant interface. In this case, the radius of implant was assumed to be 4% larger than the radius of the hole.

RESULTS AND DISCUSSION

Figures 2, 3 and 4 depict the radial stresses at the bone/ implant interface at different positions around implant in the three cases. θ denotes the angle to the long axis of the bone and β

denotes the debonding angle. As expected, radial stresses are highest when $\theta=0$ and decrease as θ increase. Further the larger the modulus of the implant, the higher the radial stress at interface. In the perfect bond case, the interface is consistently under radial tension at any orientation around implant though this tension decreases with θ. In the partial debonding case, stresses are singular at $\theta=\beta$ (i.e., at the debonding crack tip), but then decrease sharply with θ. The oversized implant induces high compressive interfacial stresses, which increase dramatically with modulus of the implant.

Our model has predicted the initial stresses in bone near transcortical implants for different interfacial conditions. The results illustrate that the dynamic nature of the interface between implant and bone will cause a large variation in stresses over time. Further, the modulus of the implant and the amount of press fit also play a role in stress perturbations. This suggests that these factors may play an important role in the influencing the results of a trancortical implant test.

	E1 (GPa)	E2 (GPa)	n12	G12 (GPa)
Bone	20.0	10.0	0.200	5.50
UHMWPE	1.40	----	0.300	0.54
Ti6Ai4V	100.7	----	0.361	37.0

Table 1. Material Properties. (The "1" direction is along the long axis of the bone)

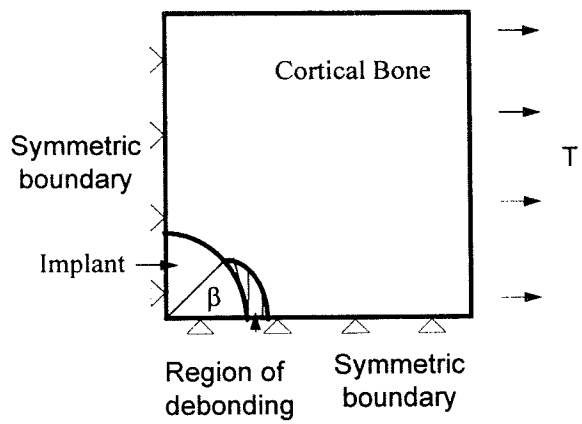

Figure 1. Schematic Diagram of the FE Model. (The FE mesh has been omitted for clarity

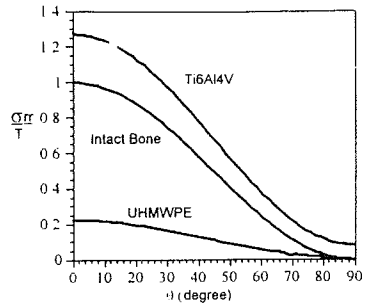

Figure 2. Radial Stresses at the Interface of a Perfectly Bonded Implant

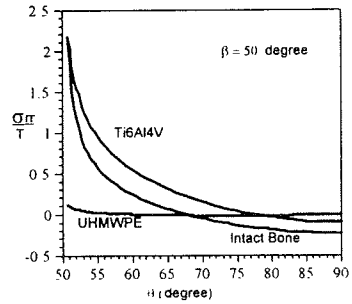

Figure 3. Radial Stresses at the Interface of a Partially Debonded Implant

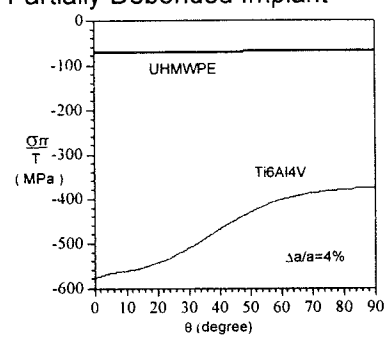

Figure 4. Radial Stresses at the Interface of a Press Fit Implant

REFERENCES

1. J. Wolff. *Law of bone remodeling*, Berlin (1892)
2. V.M.Gharpuray *et al, J.Biomed. Mater. Res.*
3. J.E.Dalton and S.D.Cook, *J. Biomed. Mater. Res.*, 29, 133-6 (1995)
4. S.Zyblewski, Thesis, Clemson Univ. (1995)
5. M. J. Hiatt, Thesis, Clemson Univ. (1996)
6. Yi-Xian Qin *et al, J. Orthop. Res.*, 14: 862-70 (1996)

ACKNOWLEDGMENTS

NIH GRANT 1-R15-AR-42726

"*In Vivo*" Pose Estimation of Artifical Knee Implants in Fluoroscopy Images Using a Model Fitting Technique

S.A. WALKER[1,2], R.D. KOMISTEK[1,2], W.A. HOFF[2], D.A. DENNIS[1,2]
[1]ROSE MUSCULOSKELETAL RESEARCH LABORATORY, DENVER, CO, 80222
[2]DIVISION OF ENGINEERING, COLORADO SCHOOL OF MINES, GOLDEN, CO

INTRODUCTION

Premature polyethylene wear is a major concern in total knee arthroplasty (TKA) and total hip arthroplasty (THA). Previous research has shown that the kinematics of implanted knees differ from those seen in normal knees [1,2]. Kinematics of artificial knee joints have been measured "in vivo", through various approaches that have limitations [1,2,3]. The goal of this research project is to develop a model fitting approach that accurately measures knee kinematics, without the limitations that hinder the previously developed methods.

REVIEW AND THEORY

Previous work with fluoroscopy images has primarily concentrated on measuring the rotation and translation of components within the plane of the image. Stiehl et al., [1] analyzed still photographs of the fluoroscopic video to measure rotations and translations of the knee joint members. His work was limited to the in-plane rotations and translations of the implant components. Some limitations of this approach is that out of plane rotations and translations can not be determined, the process is time consuming, and the accuracy is low.

One approach for pose estimation is to use a template matching technique. If the complete silhouette of the object is visible, an algorithm can match the entire silhouette of the object with a pre-computed template. Other researchers have used this approach to measure the full six degree of freedom motion of knee prostheses by matching the projected silhouette contour of the prosthesis against a library of shapes representing the contour of the object over a range of possible orientations[2,3]. Library matching requires a large amount of time to create the libraries, and the libraries are created for only certain vantage points The time required for analysis is large since the algorithm must step through each image in the library. And the out-of-plane translational error is large.

Model fitting techniques produce the full 6 degree of freedom pose using an accurate 3-D cad model and an accurate computer generated scene of the fluoroscopy unit. It is not limited to a set vantage point. The speed of the model fitting process is makes use of accelerated graphics hardware to make the process faster.

PROCEDURES

The central idea in our process is that we can determine the relative pose of two objects (i.e. knee implant components) from a single perspective image by manipulating a cad model in 3-D space. In order for this to maintain the accuracy required, a 3-D scene of the fluoroscopy unit is created inside the computer. This scene consists of a light source (X-ray), an image plane to project the fluoroscopic image (image intensifier), an area to manipulate a 3-D model (subject area) and a camera to view the entire scene. Figure 1 shows the layout of the computer generated scene with cad models in place.

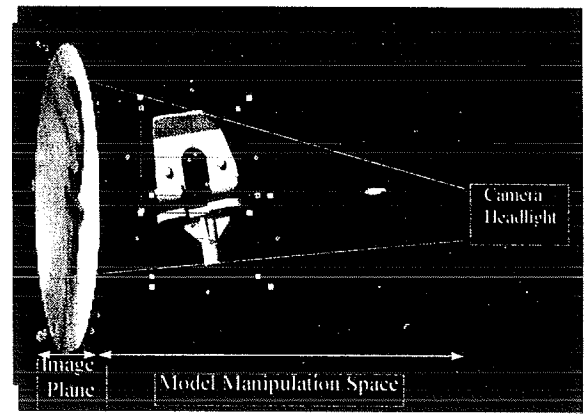

Figure 1: Computer Generated Scene

The process is used to determine pose estimates from fluoroscopy videos at 5° increments of knee flexion. These images are projected on to the image plane and the corresponding implant models are added to the scene. The operator manipulates the models to create accurate femoral and tibial component fit. [Figure 2] The correct fit is established when the silhouette of the

implant components match the fluoroscopic image. Pose estimation of each component is recorded and the measurements of interest are extracted using a cad modeling program.

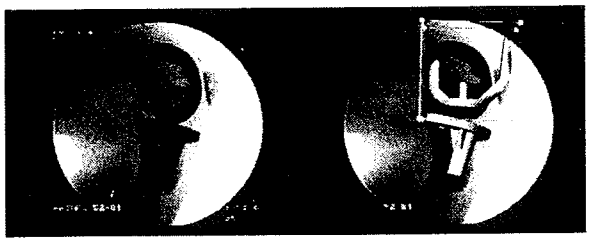

Figure 2: The Captured Images and 3-D Models

The model fitting approach and the template matching were used to analyze subjects having a TKA. Images were captured at heel strike, toe off and two equally spaced increments of stance phase.

RESULTS

The average time required to analyize a single image and a full sequence of images was significantly better for the model fitting technique [Table 1]. Using the model fitting approach to estimate femoral tibial pose a simular accuracy was recorded for both methods, in-plane. However, the out-of-plane translational accuracy was significantly better than for the library matching technique [Table 2]. The correct fit and an incorrect fit that forces the femoral and tibial components to the inverted option [Figures 3]. The frontal images in figure 3 are shown in figure 4. The incorrect fit shows one condyle digging into the polyethlene and the other condyle with an extreme amount of liftoff. The incorrect fit also shows a large amount of internal/external rotation. The combination of a poor fit, extreme liftoff that often translates into a condyle indenting into the metal tibial tray, and abnormally large internal/external rotation help to eliminate incorrect pose estimations.

	Time for Single Image	Time per Subject
Library Matching	45 minutes	4 hours
Model Fitting	15 minutes	1 hour

Table 1: Average Times for Techniques

	Library Matching	Model Fitting
In-Plane Rotational	< 0.3°	< 0.3°
Out-of-Plane Rotational	< 0.5°	< 0.5°
In-Plane Translational	< 0.4 mm	< 0.4 mm
Out-of-Plane Translational	< 2.5 mm	< 1.5 mm

Table 2: Error Results

Figure 3: Correct and Incorrect Fit of Components

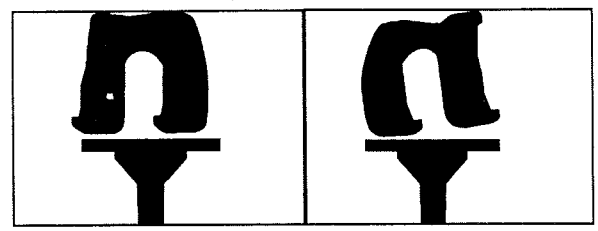

Figure 4: Frontal Views of Correct and Incorrect Fit

DISCUSSION

Pose estimation has been critially reviewed as an estabolished technique to determine "In Vivo" joint kinematics. Our model fitting approach has proven to be a valid approach that eliminates the limitations seen with template matching.

REFERENCES

[1] Stiehl et al. "Biomechanical Aspects of Posterior Cruciate Retaining Total Knee Arthroplasty,", Contemporary Orthopaedics, Vol. 1995.

[2] D.A. Dennis et al., "An In Vivo Determination of Condylar Lift-Off Using an Inverse Perspective Technique that Utilizes Fluoroscopy," Orthopaedic Transactions, Vol. 1996.

[3] S.A. Banks et al., "Direct measurement of 3D knee prosthesis kinematics using single plane fluoroscopy," Proc. of Orthopedic Research Society, pp. 428, 1993.

COMPARISON OF THREE-DIMENSIONAL PHOTOELASTIC STRESS MEASUREMENT TO STRAIN GAGE ANALYSIS IN A HUMAN CADAVER FEMUR

T. Loebig, D. Anderson

Biomechanics Research Laboratory, Allegheny-Singer Research Institute, Pittsburgh, Pennsylvania 15212

INTRODUCTION

CT-scans from a human cadaver femur were used as the template for generating a plastic model for three-dimensional photoelastic stress analysis. The plastic model was constructed using a laser stereolithography (SLA) apparatus. It was loaded to simulate single-leg stance and the strain in the calcar region was measured using the frozen-stress techniques. To evaluate the accuracy of this methodology, the calcar of the original femur was strain-gaged, and subjected to a similar loading. Stresses from the photoelastic model were compared to similar-location stresses from the strain-gaged femur (considered the "gold-standard").

Photoelastic testing of SLA models has the potential to provide internal stress data that cannot be obtained by other experimental methods. This method could be applied to the analysis of trabecular mechanics, joint contact, and implant mechanics, among others.

REVIEW AND THEORY

SLA is one of several methods of "rapid prototyping" in which a physical model is generated one layer at a time using a laser to solidify a liquid photopolymer. SLA produces very accurate plastic models of complex geometries, including internal features. The epoxy used for SLA models has properties suitable for frozen stress three-dimensional photoelastic analysis.

In frozen-stress analysis, the model is heated above a critical temperature, loaded, and cooled while maintaining load to permanently "freeze" residual stresses into the model. The stressed model can then be sectioned to view the stresses using two-dimensional photoelastic analysis techniques.

This project was intended to assess whether stress data obtained from SLA photoelastic testing is equivalent to data obtained from strain gage testing of a cadaver bone. Detailed procedures for testing, calibrating, and analyzing photoelastic specimens are given by Measurements Group, Inc., Raleigh, North Carolina, USA (Measurements Group, 1989 and 1982).

MATERIAL AND METHODS

CT scans of a human cadaver hip joint (52 y.o. male) were obtained at a 2 mm slice spacing. The region scanned included the proximal fifth of the left femur. MATERIALISE software (Materialise N.V., Belgium) was used to convert the CT data for input to an SLA machine (SLA-250, 3D Systems, Inc., Valencia, California). For the purposes of this study, much of the cancellous structure of the femoral head and femoral neck was modeled as a solid. Bi-linear interpolation was used to smooth the boundaries of each CT image and cubic interpolation was used to smooth the surfaces between slices. The reconstructed surface geometry was converted into contours (SLI contour format) necessary to drive the SLA machine. The femur model and a calibration beam were then built on the SLA-250 with Ciba-Geigy 5170 epoxy resin.

The model was mounted in single leg stance position without muscle loading. The inferior 24 mm of the femur model was potted in PMMA at an orientation of neutral flexion, 15° adduction, and neutral version. A cylindrical loading block was created to simulate the acetabulum.

Testing of the SLA model was conducted at Measurements Group, Inc. A dead-weight loading fixture delivered a nearly vertical compressive load of 53 N to the acetabular block. The calibration beam was tested concurrently with the specimen. A programmable oven was used to precisely control the temperature during the test.

The anterior and posterior thirds of the model were cut away to expose the central coronal third, yielding a slice that was 13 mm thick. A Measurements Group Model 500 polariscope was used for analysis. The directions of the maximum principal stresses were determined, followed by evaluation of the fringe magnitudes. Model stress magnitudes were calculated using a stress-optic coefficient determined from the calibration beam. The first coronal slice was sliced in half again to produce two 6 mm thick slices.

Four strain gage rosettes (WA-13-060WR-120, Measurements Group, Raleigh, NC.) were applied to the coronal midline of the calcar region of the same cadaver femur that was used to construct the photo-

elastic model. An MTS servohydraulic testing machine (Bionix 858.20, MTS Systems Corp., Minneapolis, MN.) applied compressive ramp loading from a preload of -15 N to a maximum load of -1500 N.

The rosette strain data were continuously recorded and later reduced to principal and strain magnitudes and directions. The bone stress was calculated using a value for Young's Modulus of 15.0 GPa (Cowin, 1989). Stress-to-load ratios were computed for each test, allowing direct comparison of the data.

RESULTS

Figure 1 shows a coronal slice of the SLA model. The fringe patterns indicated that the location of maximum stress was in the calcar region. This stress pattern is similar to published stress analyses (Walker P.S. et al., 1988, Wuh H.C.K. et al., 1987). Increases in stress were observed after the initial slice was cut into the thinner slices.

The calculated stress distributions (figure 2) in both the SLA and cadaver models followed similar trends. The stress values obtained from the thin SLA section were larger than those from the thick section, which is typical due to the averaging effect in thick sections.

Regions of elevated stress that were not specifically analyzed appeared in the superior region of the femoral neck, at the interior of the greater trochanter, and at areas of contact with the acetabular loading block. The entire lateral cortex of the femoral shaft was relatively unstressed, indicating the majority of the load was carried by the calcar region, for the conditions of this test.

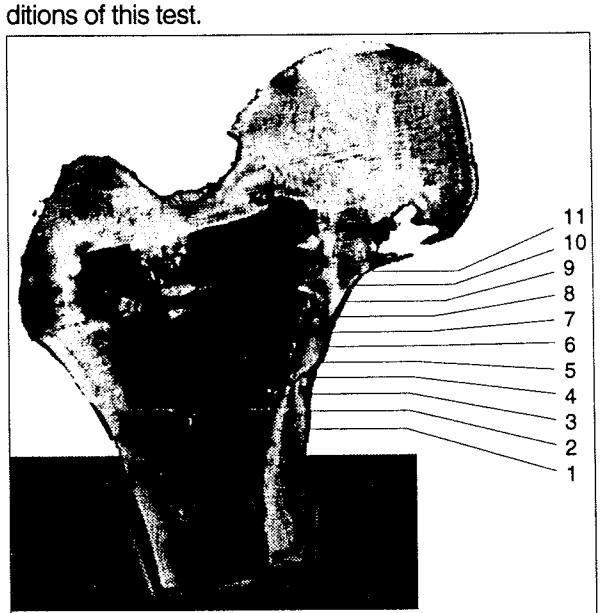

Figure 1. Central slice of femur model and locations on surface where the stresses were analyzed.

DISCUSSION

Stresses in the calcar region of a human femur model, computed from three-dimensional photoelastic testing of an SLA model, compared favorable with strain-gage testing of a cadaver femur. As section thickness of the SLA model slice was decreased, the measured stress approached 70% of the stress calculated from the strain-gage test.

These methods are being evaluated in our laboratory for future analysis of contact stresses in joints and for detailed analysis of trabecular bone architecture. They offer an additional experimental tool for integrated computational and experimental investigations in the field of orthopaedics. Further refinement and validation are necessary, however, before the full potential of this type of analysis can be realized.

REFERENCES

Cowin S.C., Bone Mechanics, 97-127, CRC Press, 1989
Measurements Group, TN-702-1, 1989.
Measurements Group, TN-707, 1982.
Walker PS, et al, CORR, 235, 25-34, 1988.
Wuh HCK, et al ASTM STP 953, 249-263, 1987.

ACKNOWLEDGEMENT

The authors would like to thank the Albert B. Ferguson, Jr., M.D. Foundation for funding this project, and M. James Rudert for technical and editorial assistance.

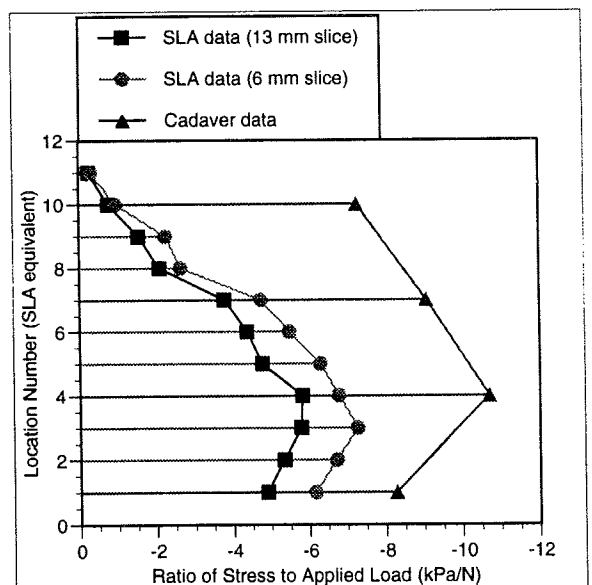

Figure 2. Surface stress normalized to applied load versus location number.

FRICTION COEFFICIENTS OF POROUS TANTALUM AND CANCELLOUS & CORTICAL BONE

D. Fitzpatrick[1], P. Ahn[1], T. Brown[1], R. Poggie[2]
[1]Orthopaedic Biomechanics Laboratory, 2432 Stiendler Bldg, University of Iowa, Iowa City, IA 52242
[2]Department of Applied Research, Implex Corp., 80 Commerce Drive, Allendale, NJ 07401

INTRODUCTION

The use of structural autografts for fracture stabilization, deformity reconstruction, and arthroplasty is well accepted in orthopaedic practice. However, for natural bone grafts, the associated donor site morbidity (including motor weakness, sensory defects, and pain) is often a concern [1]. As such, porous ceramics and metals provide an attractive alternative to naturally derived autografts. Typically, porous metals are a thin (about 0.5 to 1.0 mm) coating of sintered titanium or Co-Cr-Mo alloy wire or beads onto a like solid substrate, resulting in a 20-35% porous surface. A new porous tantalum material characterized by 75 to 85% porosity, pore size between 500 and 600 μm, 3-D interconnecting pores, and fabricated in bulk form (not a coating) is an attractive alternative to traditional porous metals, and in substitution for autograft and allograft bone. A primary function of any porous bone substitute material is to provide for initial stabilization of the bone-implant interface to permit bone ingrowth and long term fixation. The purpose of this study was to measure the friction of porous tantalum in contact with periosteum intact and denuded cortical bone and cancellous bone using an established model for bone-on-bone friction, and to compare these values to those for bone-on-bone, and sintered bead porous coating on bone. The primary utility of this information the defining of boundary and interface conditions for FEA computer modeling of devices and loaded fabricated from porous metals and in comparison to bone.

MATERIALS AND METHODS

An inclined plane apparatus based on ASTM Specification D4518-91 was used to determine the coefficients of friction. The apparatus consisted of a horizontal stationary plate which was rigidly mounted to an MTS Bionix® machine, with a second hinged plate attached to the MTS actuator. Movement of the actuator arm permitted adjustable inclined planes of up to 90°. The substrate block (either cancellous bone or porous tantalum) was secured to the inclined plane with a smaller slider block (either porous tantalum or cortical bone) placed on top. By gradually raising the incline from 0°, the angle of slippage (ϕ), and thus the coefficient of friction ($\tan \phi$), was determined.

Ten fresh bovine radii were obtained from a local abattoir. Cortical bone squares measuring 2 x 2 x 0.6 cm were machined from the anterior radial diaphysis. The overlying soft tissue was carefully dissected until only periosteum remained. Two mutually perpendicular holes, 3 mm in diameter, were drilled through each specimen parallel to the periosteal surfaces. A metal rod was placed through the hole and weights attached to each end. A normal force of 4.4 N was applied to the slider specimens, and even at steep angles near 90°, sample tilting did not occur. Cancellous bone specimens 4 x 4 x 2 cm were obtained from the proximal epiphyses, subsequently potted in a circular mold with PMMA, and milled flat.

Testing of the cancellous-porous tantalum interface was accomplished using 2 x 2 cm sliders placed on 4 x 4 cm cancellous bone substrates. The two surfaces were copiously wetted with normal saline prior to testing. The angle of inclination was increased from 0° at a rate of 1.5° s^{-1} until the point of slippage. The tangent of the slip angle provides for calculation of the coefficient of friction. Five trials were performed for each of the four possible "downhill" orientations of the cancellous substrate. It was not possible to obtain flat cortical blocks measuring greater than 2 x 2 cm, therefore, testing of cortical specimens was done

with the porous tantalum as the substrate and the cortical bone as the slider. With this exception, the same testing protocol was used for both periosteum intact and denuded specimens.

RESULTS

The average friction coefficient of porous tantalum against cancellous bone was 0.88 (n=100 trials, s.d.=0.09). There was no visually perceptible bone residue on the porous tantalum surfaces after testing. The determination of friction between the periosteum-intact cortical bone and the porous metal proved complex because the periosteum was extremely adherent to the porous metal. For three of the five cortical blocks, the periosteum was more that 50% defaced from the underlying bone before testing was completed. The friction coefficient calculated from the two specimens for which periosteum-intact testing was performed was 1.75 (n=40 trials, s.d.=0.33), indicating an adhesive character between the porous tantalum and periosteum. There was visually perceptible periosteal residue on the porous tantalum after testing. For periosteum-free cortical bone against the porous metal, the average coefficient of friction was 0.74 (n=100 trials, s.d.=0.07).

DISCUSSION

The friction coefficients for this novel porous tantalum material were higher than those previously reported for cortical bone against cancellous bone (0.608) [2] and for traditional porous coated materials on cancellous bone (0.50 - 0.66) [3]. Table 1 below summarizes the coefficient of friction (COF) data from this and previous studies.

Friction Couple	COF
Porous Ta - cortical bone+periosteum	1.75
Porous tantalum - cancellous bone	0.88
Porous tantalum - cortical bone	0.74
Cortical bone - cancellous bone	0.61
Sintered beads - cancellous bone	0.5-0.66

Table 1: Summary of coefficient of friction data

The supra-unity friction coefficient for periosteum against porous tantalum was an interesting finding in that soft tissue fibers have a tendency to be "snagged" by the small spicules at the surface of the porous tantalum, resulting in what appeared to be an adhesive effect. The coefficient of friction for the porous tantalum material was higher than that exhibited by bone-on-bone and sintered beads-on-bone. The results of this study will be applied to future FEA modeling, and specifically for prediction of the implant-bone stability based on the parameters of design, loading, and interface friction.

REFERENCES

[1] Parker and Urbaniak, JBJS, 78A:2, 1996.
[2] Ahn et al., Trans. 42nd ORS:603, 1996.
[3] Shirazi-Adl et al., J Bio Mat Res, 27, 1993.

ACKNOWLEDGEMENTS

Financial support (grant) and porous tantalum samples provided by Implex Corp.

SYNAPTIC CONNECTIONS FROM WRIST FLEXOR AND EXTENSOR MUSCLE LARGE AFFERENTS TO SYNERGISTIC MOTONEURONES IN MAN

G.R. Chalmers[1], P. Bawa
School of Kinesiology, Simon Fraser University, Burnaby, B.C., Canada V5A 1S6
[1] Current address: Dept. of PEHR, Western Washington University, Bellingham, WA, 98225

INTRODUCTION

Short latency excitatory Ia reflex connections were determined between pairs of human wrist muscles. Spindle Ia afferents were stimulated by either tendon tap or electrical stimulation. The activity of voluntarily activated single motor units was recorded intramuscularly. Cross-correlation between stimuli and the discharge of the motor units provided a measure of the homonymous or heteronymous excitatory input to a motoneurone.

REVIEW AND THEORY

For the cat ankle, it has been demonstrated that the primary spindle afferents in the ankle flexor and extensor muscles form heteronymous connections upon the motor nuclei innervating functional synergists (Eccles et al., 1957; Hultborn, 1976). This simple pattern of synergist excitation is not, however, found in the cat forelimb (Fritz et al., 1989) or the human ankle (Meunier et al., 1993; Mao et al., 1984). There are only fragmentary comparable data in humans on monosynaptic excitatory reflex connections in the wrist. The goal of the present study was to determine the excitatory projections of large muscle afferents from the major wrist flexor and extensor muscles in humans to determine monosynaptic connections linking these muscles.

PROCEDURES

Muscle spindle afferent excitation was elicited by tendon tap for the flexor carpi ulnaris (FCU), flexor carpi radialis (FCR), extensor carpi ulnaris (ECU), extensor carpi radialis (ECR) and extensor digitorum communis (EDC) muscles, or by electrical stimulation of the median nerve for the FCR. Single motor unit (SMU) activity was recorded in 6 subjects from pairs of forearm muscles (FCU & FCR; ECR & ECU; ECR & EDC; ECU & EDC) using bipolar intramuscular electrodes (Calancie et al., 1985). Subjects was asked to contract the muscles slightly to simultaneously recruit a motor unit in each of the two muscles recorded. Input to a single motoneurone was assessed from short latency changes (20-30 ms post stimulus time) in the motoneurone response probability (P_r), determined from the peristimulus time histogram constructed between the stimulus and the respective motor unit spike train (Bawa et al., 1993). Data for all motor units from all subjects for a single muscle are summarized by the average response probability of all units examined under that condition (i.e., tendon tapped homonymous muscle response versus simultaneous heteronymous muscle response).

RESULTS

A basic assumption in the data collection and analysis was that a homonymous motor unit should respond to the spindle input at a latency shorter than 30 msec after the stimulus. Results are summarized in Table 1.

DISCUSSION

Almost all homonymous motoneurones examined responded to Ia afferent input. Bidirectional facilitation was observed between the two primary flexor muscles and between almost all of the extensor muscle pairs examined. The effectiveness of the afferent Ia volley was usually greater on homonymous than on heteronymous motoneurones, similar to that observed in the cat wrist (Fritz et al., 1989) and the human (Cody et al., 1989). One reflex Ia excitatory connection between forearm muscles was observed routinely which is seldom present in the cat forearm. A weak ECU short latency facilitation by EDC Ia afferents was observed in humans, while in the cat it is not present (Fritz et al., 1989).

The latency of the heteronymous ECR response when the ECU tendon was tapped, was later than the homonymous ECU response, and later than the homonymous ECR response. It was included in the analysis because it was the first excitatory response observed and it falls within the period of time defined as the M1 spinal response to muscle stretch. It is possible that ECU Ia reflex connections to the ECR are only through an oligosynaptic pathway which delays the increase in

firing probability. Whatever the cause, it is apparent that while there is a Ia excitatory reflex connection from the ECU to the ECR, it does not have as short of a latency as observed between other forearm muscles. This observation is particularly interesting when combined with the fact that a reflex connection was not observed from the ECR to the ECU. It is clear that in humans the two principal wrist extensors are not connected through a monosynaptic excitatory reflex pathway

Stimulation	Muscle studied	Number of motor units#	Time of peak onset (ms)*	Peak width (ms)*	P_r*
Median nerve	FCR	13/13	17	1.7	0.55
Median nerve	FCU	17/17	18	1.6	0.27
FCR Tendon	FCR	6/6	22	4.3	0.63
FCR Tendon	FCU	6/5	24	6.5	0.30
FCU Tendon	FCU	18/18	25	5.3	0.31
FCU Tendon	FCR	17/13	28	6.2	0.15
ECR Tendon	ECR	12/12	25	4.2	0.38
ECR Tendon	ECU	14/0	NA	NA	0
ECU Tendon	ECU	8/7	23	3.4	0.17
ECU Tendon	ECR	8/8	31	6.4	0.22
ECR Tendon	ECR	13/13	22	5.9	0.48
ECR Tendon	EDC	13/7	23	6.6	0.16
EDC Tendon	EDC	13/13	23	4.0	0.30
EDC Tendon	ECR	12/11	23	5.2	0.25
ECU Tendon	ECU	8/8	24	3.6	0.23
ECU Tendon	EDC	8/4	21	4.6	0.09
EDC Tendon	EDC	10/10	23	5.3	0.26
EDC Tendon	ECU	9/7	26	3.2	0.08

Table 1: Excitatory short latency connections between wrist muscles.

Number of units studied / number of responding units

* Mean

P_r = response probability

NA = Not applicable, no heteronymous motor units responded.

It has been demonstrated that muscles which have a very similar mechanical action on a common joint tend to have Ia connections between them which are bidirectional and balanced, i.e. of approximately equal strength in both directions (Eccles et al., 1957, Fritz et al., 1989). In the cat wrist, where there are many degrees of freedom and even adjacent muscles do not have exactly the same mechanical action, bidirectional and balanced Ia connections do not exist among all the flexors and extensors (Fritz et al., 1989).

It is apparent that in the human wrist, as in the cat wrist, the primary wrist extensors, ECU and ECR which have very different mechanical actions, are not strongly interconnected through the reflexes tested. As a result, they can be more free to operate independently to serve the multiple degrees of freedom at the wrist than if they were bilaterally connected through strong Ia reflexes. In contrast, the FCU and the FCR wrist flexors in humans, are connected through a balanced, bidirectional short latency Ia pathway despite their very different mechanical actions. It may be that the great importance of the hand grasping action, usually requiring a combined effort of both the FCU and the FCR as well as the finger flexors, has demanded that tight reflex Ia connections exist between the FCR and the FCU, despite the different actions these muscles have during other wrist movements.

REFERENCES

Bawa P et al. J Physiol (Lond) 47: 445-464 1993

Calancie B et al. J Neurophysiol 53:1179-1193 1985

Cody FWJ et al. J Physiol 411:379-392 1989

Eccles JC et al. J Physiol 137:22-50 1957

Fritz N et al. J Physiol 419:321-351 1989

Hultborn H Prog Brain Res 44:235-255 1976

Mao CC et al. Exp Brain Res 56:341-50 1984

Meunier S et al. Exp Brain Res 96:534-44 1993

ACKNOWLEDGMENTS.

Supported by the Natural Research and Engineering Council of Canada and the Medical Research Council of Canada.

MUSCLE BALANCE AT THE KNEE DURING INTERNAL AND EXTERNAL KNEE ROTATION

W.L. Buford, Jr., F.M. Ivey, A.A. Stewart,
R.M. Patterson, D. Nguyen

Department of Orthopaedic Surgery
The University of Texas Medical Branch, Galveston, TX 77555-0892

INTRODUCTION

The human leg functions as it does partially because of an inherent muscle balance at the knee that provides adequate range of motion and strength. Disturbing this muscle balance can alter the functionality of the leg. Mechanical systems, such as the human knee, cannot be completely described without knowledge of the forces and moments associated with them.

The human knee joint acts like a pulley where muscle-tendon units apply forces to bones to cause or prevent movement about an axis or axes of rotation. Hence, each muscle that crosses the knee has a moment arm associated with it that extends perpendicularly from that muscle's line of action to the axis of rotation of the knee joint. The axes we use to measure the muscle moment arms from are those described by Hollister, et. al. **Figure 1** shows both the flexion/extension and internal/external rotation axes.

REVIEW AND THEORY

Many earlier studies have focused on muscle moment arms of the knee during flexion/extension motion, but none have been located that study internal/external knee rotation. The studies that deal with flexion/extension motion have been limited or incomplete due to use of preserved specimens, knees isolated from ankle and hip, small sample size, static positioning, and exclusion of certain muscles. In this study we seek to identify the normal excursion and moment arm values throughout the range of motion for 13 muscles and the patellar tendon at the knee. We have established an excursion/moment arm database for the normal knee for flexion/extension knee motion. Analysis of the internal/external rotation data is the subject of this report. This experiment has been repeated in 13 fresh cadaveric specimens.

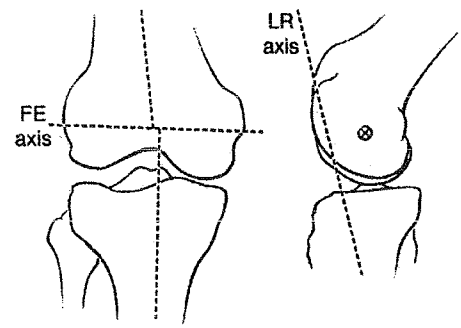

Figure 1: Flexion/extension axis and internal/external (longitudinal rotation) axis as described by Hollister, et. al.

PROCEDURES

Thirteen fresh, hemi-pelvis specimens were skinned and the muscle-tendon units

instrumented to measure the excursions and joint angular motion during dynamic rotation of the knee. Excursions were measured for thirteen muscles that cross the knee (plus the patellar tendon). Potentiometers measured motion about the flexion/extension and internal/external axes. The instantaneous moment arm was calculated as the derivative of the tendon travel with respect to the joint angular motion (using a fifth order smoothed derivative (moment arm: $dr/d\theta$). Legs were mounted into a test apparatus (each muscle tensioned with 2 lb. weights) and passively rotated through the full range of flexion/extension motion for at least 10 cycles of motion during data acquisition. The experiment was then repeated with the anterior cruciate ligament resected, then with a posterior cruciate ligament (PCL) sparing total knee prosthesis implanted, and finally, with a PCL sacrificing total knee prosthesis implanted.

RESULTS AND DISCUSSION

Results for the normal knee shows that each muscle has a unique moment arm that changes throughout the range of motion for flexion/extension motion. Prostheses have a wide and variable effect upon the moment arm balance. The range of motion for internal/external rotation is 25 to 30 degrees. Furthermore, the results identify 6 muscles as primary contributors to internal/external rotation motion. The biceps femoris long and the biceps femoris short have significant moment arms for external rotation of the knee while the sartorius, gracilis, semimembranosus, and semitendinosus are responsible for internal rotation of the knee. **Figure 2** depicts a typical average moment arm for these six muscles in a normal knee.

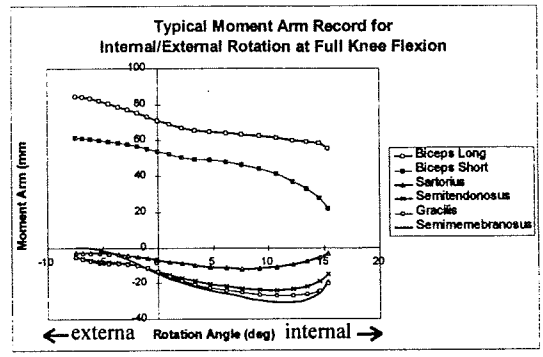

Figure 2: Typical moment arm values throughout the internal/external range of motion for 1 specimen. 6 muscles have been identified as the major contributors to internal/external rotation knee motion. By arbitrary choice, moment arms for internal rotation are negative.

REFERENCES

Hollister, A.M., Jatana, S., Singh, A.K., Sullivan, W.W. and Lupichuk, A.G. The Axes of Rotation of the Knee. *Clin Orthopaedics and Rel Res*, 290:259-268, 1993.

ACKNOWLEDGEMENTS

Primary Funding - **Sulzer Orthopedics of Austin, TX.**
Prostheses donated by: Sulzer Orthopedics of Austin, TX, Zimmer, Biomet, Richards, Depuy, and Howmedica.

ARTIFICIAL MUSCLES ACROSS THE HUMAN ELBOW: A PERFORMANCE STUDY OF POLYACRYLONITRILE FIBERS

R. Gonzalez, H. Bock, G. Collison, C. Lee, C. Smokowicz, J. Thielman

Division of Engineering, LeTourneau University, P.O. Box 7001, Longview, TX 75607

INTRODUCTION

Computer models on coordination of elbow movements have been developed on a detailed musculoskeletal level (Gonzalez, et al., 1996). Nonetheless, physical models of the human elbow joint using artificial actuators are rare to nonexistent. Using a skeletal replica of a human arm for elbow joint motion, polyacrylonitrile (PAN) fibers could potentially be used as an artificial muscle actuator to perform various elbow movements. To accurately represent the muscles across the elbow, the PAN fibers should have similar active mechanical properties as human muscle. These properties include the characteristics of force-length (F-L) and force-velocity (F-V). PAN fibers were chosen because of their potential use as artificial muscle (Shahinpoor et al., 1994). In addition to the properties above, the relationship of force-molarity (F-M), force-time (F-T), and length-molarity (L-M) were developed. The results of this performance study were compared to human muscle properties and were used to obtain the necessary lengths and size of the PAN fibers for a microcontroller to execute the movement of the physical model of an elbow.

REVIEW AND THEORY

PAN fibers could potentially be used as artificial human actuators but an investigation of their mechanical properties is needed. PAN fibers contract and expand when submerged in acidic and basic solutions, respectively, and while it has a potential application as artificial skeletal muscle, no extensive tests have been performed on this material to compare it to A.V. Hill's classical muscle experiments (Hill, 1970). It is hypothesized that as the molarity of the acid increases the force generated by the PAN fibers increases and the time constant of the contraction decreases. To investigate these relationships as well as the F-L, F-T, F-M, and L-M properties, two experimental apparatuses were constructed and an array of experiments were performed.

PROCEDURES

Six bundles of PAN fibers of various lengths and number of fibers were obtained from Dr. Shahin-poor of the University of New Mexico. PAN fibers contract to their minimum length when placed in 2 molar (M) Hydrochloric acid (HCl), while the maximum length can be obtained by placing the PAN fibers in 2M Sodium-Hydroxide (NaOH) (Shahinpoor et al., 1994). One apparatus was used for the F-L, F-T, and F-M experiments. This apparatus consisted of a trough, in which the PAN fibers were positioned, and a lever that was pulled by the PAN fibers on one end and pushed against a force gauge (Omega DFG51-50) on the other. The force gauge was connected to a data acquisition board (Keithley DAS-8/EXP16) on a PC. The software used was LABTECH Notebook (v 8.1) and Unkelscope (Release 3.08c). The sampling rate varied between 1 Hz and 500 Hz depending on the experimental needs. For the F-L, F-T, and F-M experiments, the PAN fibers were expanded in 2M NaOH first, then in water to obtain the "resting" length. They were then placed in the trough, where acidic solutions were poured and data acquisition was initiated. Depending on the experiment, the PAN fibers were left in the solution for three to five minutes. The solutions used were 0.5, 1, 1.5, 2, 4, 6, and 8 molar HCl. In each of these experiments the overall lengths of the PAN fibers were kept constant and therefore considered isometric.

A second apparatus was constructed to investigate the F-V characteristic of PAN fibers. This apparatus was similar to the one used by A.V. Hill in his experiments done on frog muscles (Hill, 1970). PAN fibers were expanded in 2M NaOH, then in water, and placed in a vertical cylinder. One end of the fibers was fixed while the other end was connected to a lever. The pivot of the lever was attached to a potentiometer and was connected to a power source. The output was sampled using a data acquisition board. Various weights, ranged from 40g to 578g, were hung on the opposite end of the lever. Acid was poured into the cylinder and after 30 seconds the lever was suddenly released. The voltage change given by the potentiometer was used to find the maximum average velocity of the PAN fibers. This velocity was obtained by finding the steepest slope on the curve of voltage, which represented angular position versus time of the lever. The maximum velocity typically took place between 0.4 to 0.6 seconds after the release of the lever.

RESULTS

Through the L-M experiment, the relationship between fiber length and molarity was developed. PAN fibers reached their longest length (i.e. defined as resting length

for the PAN fibers) after they had been saturated with 2M NaOH and then in water. They reached their minimum length by using HCl as weak as 2M. The F-T experimental data (not shown) indicated that the higher the molarity of HCl, the faster the fibers reached their maximum force output. The force output of the PAN fibers increased as the molarity of the HCl increased, as shown in Figure 1. The increase in force output was not substantially larger for solutions stronger than 2M HCl. PAN sample 5 produced the largest force beyond 1M HCl; it was the longest (6.4 inches at rest) and had the largest number of fibers (250). Figure 1 also indicates that the larger fibers generated smaller forces when placed in HCl solutions under 1.5M HCl. This was most likely due to the excess NaOH and water absorbed by the larger fibers diluted the weaker acids as they were poured into the trough. Figure 2 shows the relationship between force exerted by sample 3 and sample 5 and the length of the samples; the samples were placed in 4M and 8M HCl solutions. The maximum force outputs were obtained at or close to the resting lengths of the samples. A linear force-length relationship was found for the passive-elastic properties of the fibers (not shown). Figure 3 shows that velocity was inversely proportional to the force. Lengthening velocities (negative) were obtained when the force was larger than what the PAN fibers could generate.

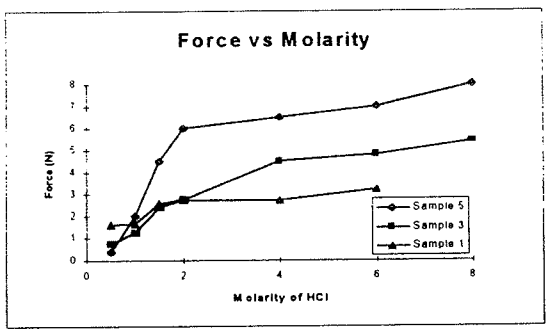

Figure 1: Force output increased as molarity increased, leveling out after 2M.

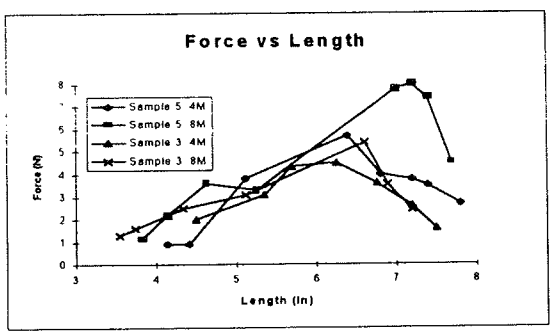

Figure 2: Force vs. Length of PAN samples 3&5, placed in 4M & 8M HCl. Force outputs increased until the resting lengths were reached.

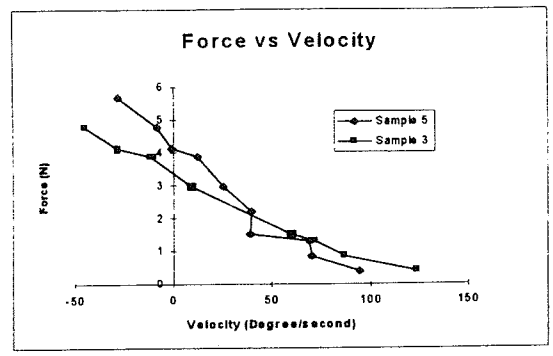

Figure 3: PAN samples 3&5 were placed in 2M HCl for 30 seconds. Force varied inversely with velocity.

DISCUSSION

Comparing the results with data on skeletal muscle, it was concluded that PAN fibers have somewhat similar F-L and F-V properties. The F-M, F-T, and F-L data confirmed the hypothesis that the fibers exert a larger force more quickly when using a higher molarity HCl solution and the maximum force possible is obtained when the fibers are at the "resting" length. The 4M HCl solution was determined to be the highest molarity solution that will be used in future work on PAN fibers. The reasons are the insignificant increase in force generated and the insignificant decrease in time constants for higher levels of HCl molarity.

The data collected was sufficient for the purpose of determining the feasibility of using PAN fibers to model elbow movement. It is concluded that PAN fiber is a valid substitute of human muscle in this particular model. Additional tests are recommended if PAN fibers are to be used in other applications.

REFERENCES

Gonzalez, R. V. et al. *J Biomch Engr*, 118: 32-40, 1996.
Hill, A.V. *First and Last Exp. in Muscle Mech.*, 6-7, 1970.
Shahinpoor, M. et al. *Proceeding ICIM*, 1079-1084, 1994.

ACKNOWLEDGMENTS

This work is supported, in part, by PSC Scanning Inc. and Omega Engineering Inc. We would like to thank Dr. Mohsen Shahinpoor and Karim Salehpoor of the University of New Mexico for providing us the PAN fibers.

MODIFICATIONS IN REACTION FORCE AND JOINT KINETICS AS A RESULT OF RECEIVING REAL TIME KINETIC FEEDBACK

J. L. McNitt-Gray+, P.S. Requejo+, J. Eagle+, B. A. Munkasy+, and S. Smith*
+Biomechanics Research Laboratory
University of Southern California
Los Angeles, CA 90089-0652
*US Olympic Training Center
Colorado Springs, CO

INTRODUCTION

Multijoint control strategies used by humans to negotiate reaction forces experienced during high velocity impact are poorly understood. The long jump event presents a particularly challenging problem because the athlete must effectively anticipate a high velocity impact, coordinate muscle power generation across multiple joints, and distribute load within the lower extremity without sustaining musculoskeletal injury. Success in the long jump, defined by a maximum horizontal displacement of the body from the take-off board, is largely dependent on the ability of the athlete to generate horizontal velocity during the approach while precisely positioning the body in preparation for the take-off phase of the jump (Hay, 1993).

One method used to maximize the horizontal velocity of the total body center of mass (TBCM) at departure from the take-off board (TD) is to reduce the braking impulse created by the horizontal reaction force applied to the foot during the take-off phase. This study tests the hypothesis that elite athletes have the ability to reduce the horizontal reaction force during take-off and increase horizontal velocity at board departure when provided with real time kinetic feedback. In addition, multijoint control and mechanical loading consequences associated with a reduction in horizontal force are assessed by comparing joint kinetics between conditions.

PROCEDURES

Members of the USA Men's Decathlon Team (n=12) performed a series of long jumps into a sand pit as part of a training session at the USOTC in Chula Vista, CA. Each athlete performed a series of long jumps under the direction of their coach. During the performance of each jump, kinetic information regarding reaction forces experienced during the take-off (last foot contact) were recorded in real time onto the video images using the Real Time Kinetic Feedback (RTKF) System developed by the USC Biomechanics Lab. Between jumps, coaches reviewed the RTKF tape frame by frame with the athletes and encouraged them to reduce the magnitude of the horizontal reaction force opposing the forward momentum of the athlete. Reaction forces during take-off were quantified using a force plate mounted in the runway in the region near the take-off board (800 Hz, Kistler, 0.6x0.9m force plate). Sagittal plane kinematics were recorded simultaneously using video tape(60 fps). Each coordinate of the body landmarks (Deleva, 1996; Zatsiorsky et al., 1987) were digitized (Motus, Peak Performance, Inc.), filtered using a fourth order Butterworth Filter (Saito & Yokoi, 1982) with cut-off frequencies determined using a method based on Jackson (1979). Kinematic and reaction force data were synchronized at force plate contact and net joint forces and moments (NJM) for the ankle, knee, and hip of the take-off leg were determined using Newtonian mechanics. Comparisons between trials before and after reductions in horizontal reaction forces were made within subject.

RESULTS AND DISCUSSION

In general, all athletes were able to modify their horizontal reaction forces (maximum reduction in horizontal impulse of 30%). The greater horizontal velocities of the TBCM at board departure (TD) observed after reductions in horizontal force were due to reductions in braking impulse rather than increases in horizontal velocity generated during the run-up (TC). A delay in time to peak vertical force and significant increases in knee and hip NJM were also observed during trials after reducing horizontal reaction forces (B) as compared to earlier trials (A) (Figure 1). These modifications in multijoint control appear to be more dependent on the force-time characteristics of the resultant reaction forces and initial kinematics at contact rather than substantial

changes in knee and hip joint angle relationships during contact (e.g. similar angle-angle diagrams were observed for A and B trials). These results emphasize the need to be aware of significant changes in multijoint kinetics and mechanical loading despite minimal changes in joint kinematics.

REFERENCES

ISEK Standards, 1985.

Jackson, K, IEEE Trans Biomed. Eng, 26, 122-4, 1979.

Hay, 1993. J of Biomech., 26, 7-21.

McNitt-Gray, J., J of Biomech., 26, 1037-46, 1993.

McNitt-Gray, J. ASB Proceedings, 1996.

Prilutsky, B.I. & Zatsiorsky, V. M., J. Biomech, 27(1), 25-34, 1994.

Ramey & Williams, 1985. IJSport Sci, 1, 233-239.

Saito, S., & Yokoi, T. Bull. of Hlth & Sport Sci, U of Tsukuba, 5, 201-206, 1982.

Zatsiorsky, V. & Seluyanov, V. (1983). Biomechanics VIII-B, 1152-1159.

ACKNOWLEDGMENTS

This project was funded in part by USOC. The authors would like to thank members of the USA Decathlon Program, VISA, members of the Sports Science Division of the USOTC, Jen Simpson, Kelly Mirabella, Jacki Heino, Stephanie Elkins and the undergraduate research assistants in the USC Biomechanics lab for their assistance with this project.

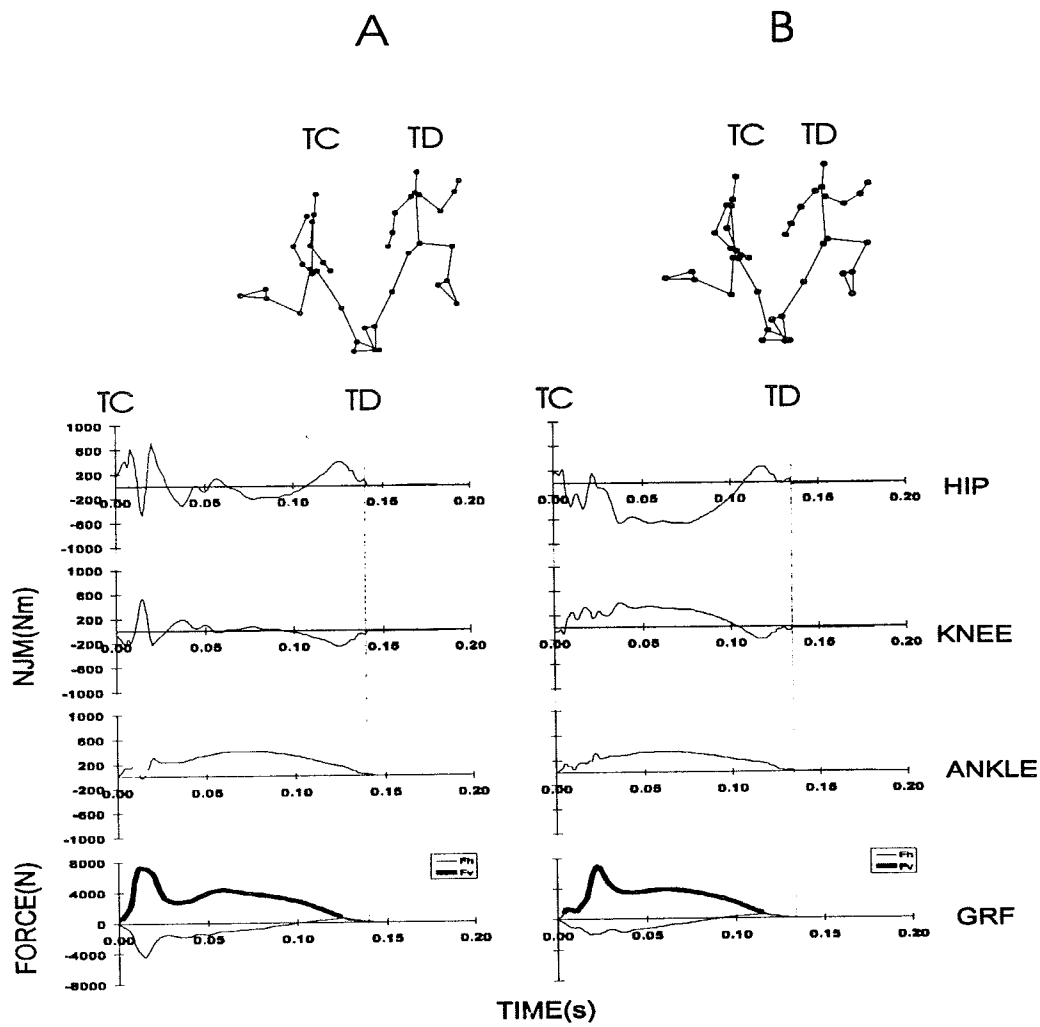

FIGURE 1: Representative vertical and horizontal reaction forces and ankle, knee, and hip net joint moments of one subject during trials before(A) and after(B) reducing horizontal reaction forces.

SEAT INTERFACE PRESSURES OF PARAPLEGICS: INFLUENCE OF DYNAMIC WHEELING COMPARED TO STATIC SEATED MEASUREMENTS

T.W. Kernozek[1], J.E.K. Lewin[2]
[1]Physical Therapy Department, University of Wisconsin-LaCrosse, LaCrosse, WI 54601
[2]Division of Kinesiology, University of Minnesota, Minneapolis, MN 55455

INTRODUCTION

Seat interface pressure assessment is of interest to both researchers and clinicians since 25-85% of all spinal cord injured (SCI) develop pressure sores accounting for over 2.3 million Medicare hospital days in 1987 resulting in 1.1 billion dollars in direct insurance costs (Dinsdale, 1974; Staas & Cioschi, 1991). While both intrinsic and extrinsic factors are associated with the etiology of pressures sores, pressure is thought to be one of the key extrinsic factors in sore development (Reswick & Rogers, 1976). Currently, seat interface pressure distributions are measured statically in a clinical environment with the patient in a fixed position if measured at all. It is likely that the seat interface is loaded differently throughout the day with different activities of daily living (ADL's). One of the most common ADL skill utilized by paraplegics to move from one place to another is wheeling.

REVIEW AND THEORY

There is a general paucity of literature on the dynamic assessment of seat interface pressures. Few studies examined reaching tasks (Park, 1992; Swarts et al., 1988), the average pressures over time (Fisher & Patterson, 1983; Patterson & Fisher, 1986), and the average pressure with various cushions (Bar, 1991). The last three papers addressing the average pressures collapsed the discrete pressure values over a fixed time period causing the time dependent fluctuations in the pressure values to be lost. Currently, the only published study on assessing the dynamic pressures examined two able bodied participants on a specially designed wheelchair seat while wheeling (Eckrich & Patterson, 1991). The study was notable since it was the first to demonstrate the difference between static and dynamic seat interface pressures but lacks the external validity due to the participants selected for study and that no seat cushion was used as an interface. Eckrich & Patterson (1991) even claimed that " the effect of these dynamic pressure changes may act in a manner similar to a 'wheelchair pushup' supporting the vascular and lymphatic pumping mechanisms" (p. 121) based on their results. Due to this claim, indeed a further investigation of the dynamic assessment of seat interface pressures is warranted. Therefore, the purpose of the study was to investigate the peak pressure and pressure time integral during static seating in comparison to the ADL skill of wheeling of a group of SCI participants.

PROCEDURES

A convenient sample of fifteen patients which propelled a manual wheelchair for at least 5 hours per week over the past 6 months and functioned at a neurological level of T1 or below were used in this study. The Novel Pliance System™ which consisted of a flexible, 32 X 32 capacitive sensor mat (each sensor 1.5 cm^2) interfaced with a PC was sampled at 10 Hz was used to measure seat interface pressures. The mat was calibrated by homogenous air pressure throughout the measurement range prior to collection. The participants were measured in their own wheelchair with a new Jay Active seat cushion prescribed for each participant. The order of measurement was randomized (static vs. dynamic) and the pressure sensitive mat was placed between the patient and the cushion . To identify a wheeling cycle from the data, a hand switch interfaced with an LED on the chair was placed in the participant's right hand. When the participant made contact with the push rim, the switch would close illuminating the LED. From the Pliance System™ a synch pulse was discharged from the analyzer illuminated a second LED on the chair. These LED's were captured on videotape with a camcorder (30 Hz) to determine the onset (right hand on push rim) and termination (right hand on push rim for the second time) of a wheeling cycle. The dependent measures were peak pressure (PP) in N/cm^2, pressure time integrals (PTI) in $N/cm^2 \cdot s$. The PP was the peak pressure value that occurred from any single sensor during the static and dynamic trials. This PP value occurred in the region of one of the ischial tuberosities in all trials. The PTI was calculated by integrating the peak pressure time curve for each trial enabling a cumulative effect of the peak pressure to be calculated over a specific time period. Three consecutive wheeling cycles from four wheeling trials at a speed of 1.2m/sec (±10%) were averaged and compared to the mean from two static trials. Use of a photoelectric timing system monitored wheeling speed. Figure 1 depicts the mean and 95% confidence interval from a single trial of three consecutive cycles. Note, that PP varies by 40% from the peak to the minimum throughout the cycle. The

minimum PP value even drops below the PP during static loading. Measurement time for the static trials were truncated to the length of time required to complete an average dynamic wheeling cycle for that participant. To determine differences between static and dynamic variables a single factor repeated measures multivariate analysis of variance (RM MANOVA) was used. Follow up dependent t-tests using the Bonferoni alpha was used in the event that a significant multivariate effect was found.

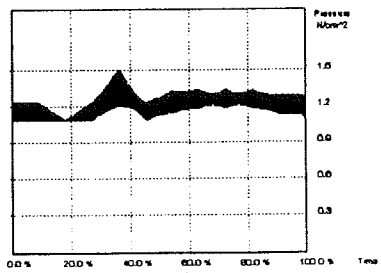

Figure 1 - Mean and 95% confidence interval for peak pressure of three consecutive cycles from a single wheeling trial.

RESULTS AND DISCUSSION

The results of the RM MANOVA showed a significant difference in the PP and PTI between the static and dynamic measurements (Wilk's = 0.00, $p < .05$). Follow up dependent t-tests yielded a difference in PP between the static and dynamic trials ($t=5.40$, $p < 0.025$) and no difference in the PTI between static and dynamic trials ($t= 1.45$ $p > 0.025$). Table 1 depicts the mean and standard deviation for static and dynamic trials for the two dependent variables.

Variable	Static	Dynamic
PP (N/cm^2)	1.62 (0.50)	2.03 (0.66)**
PTI ($N/cm^2 \bullet s$)	3.01 (0.93)	3.62 (1.81)

n=15, **p<0.025

Table 1 - Means and standard deviations for peak pressure (PP) and pressure time integral (PTI) for static and dynamic trials.

The PP during static seating was less than during dynamic seat interface pressures during wheeling. However, the PP varied throughout the wheeling cycle by 42% to a PP below the static loading condition. The differences between static and dynamic loading were results were similar to the results found by Eckrich and Patterson (1991). As is often the case in pressure measurement research, the pressure values cannot be directly compared to this study due to the instrumentation utilizing differing sensor sizes. Since PP changes throughout the wheeling cycle, is this as damaging to tissue as the static loading? To answer, this we must recognize Brand's (1980) warning that we do not know enough about the etiology of pressure sores to speculate as to the direct causes of tissue breakdown. On the other hand, does this fluctuation in PP facilitate a sort of "pumping mechanism" as suggested by Eckrich & Patterson (1991)? Since there are other therapeutic techniques utilize external manipulation of the skin to stimulate blood and lymphatic activity, it seems logical that this fluctuation in PP throughout the cycle could promote this activity. The PTI was calculated to determine the impulsive load of the PP. Between the static and dynamic conditions the impulsive loading was similar. Thus the cumulative effect of the loading was similar while the rate and range were quite different. Further research will address how these loading variables are influenced by the use of various seat cushions as a medium for altering pressures at the seat interface.

REFERENCES

Bar, C.A. Pros Ortho Inter, 15, 232-240, 1991.
Brand, P.W. Bull of Pros Res, 10, 3-4.
Dinsdale, S.M., Arch Phys Med Rehab, 55, 147-152, 1974.
Eckrich, K.M. et al. Inter Journ Indus Ergo, 8, 115-123, 1991.
Fisher, S.V. et al. Paraplegia, 21, 99-106, 1983.
Patterson, RP et al. Arch Phys Med Rehab, 67, 812-814, 1986.
Park, C.A. Am Journ Occ Ther, 46, 904-909, 1992.
Reswick, J.B. et al. Bedsore Biomechanics, 301-310, Macmillan, 1976.
Staas, W.E. et al. W Journ of Med, 154, 539-544, 1991.
Swarts, A.E. et al. Arch Phys Med Rehab, 69, 97-100, 1988.

THE EFFECT OF TOE-OBSTACLE DISTANCE ON TOE-OBSTACLE CLEARANCE OF THE TRAILING FOOT

Li-Shan Chou and Louis F. Draganich

Section of Orthopaedic Surgery and Rehabilitation Medicine, Department of Surgery
The University of Chicago, Chicago, Illinois

INTRODUCTION

Changes in the proximity of the trailing foot with an obstacle during stance of the crossing stride (i.e., during stance just prior to stepping over the obstacle) would be expected to change the geometrical configuration of the lower extremities and affect elevation of the swing foot. The purpose of this study was to test the hypothesis that reducing the distance between the obstacle and the toe of the trailing foot would decrease toe-obstacle clearance.

REVIEW AND THEORY

Tripping over obstacles is the most frequently mentioned cause of falls in the elderly (Blake et al., 1988; Campbell et al., 1990; Overstall et al., 1977; Tinetti et al., 1989). Tripping over obstacles with the trailing foot might be expected to occur more frequently than tripping over obstacles with the leading foot given the closer proximity between the obstacle and the trailing foot during stance just prior to stepping over the obstacle and given the lack of visual feedback. It was found that when stepping over obstacles of various heights in a self-selected manner the subjects consistently placed their trailing feet at the same distance from the obstacle (Chen et al., 1991; Chou et al., 1996). This indicates that the toe-obstacle distance of the trailing limb is well controlled by our central neural system to ensure a safe crossing. Any changes in the proximity of the trailing foot with the obstacle from the self-selected proximity would be expected to alter the geometrical configuration of the lower extremities and, therefore, the path of the trailing foot over the obstacle. Thus, we hypothesized that decreasing the distance between the obstacle and the trailing foot during stance just prior to stepping over the obstacle would decrease the toe-obstacle clearance.

PROCEDURES

Gait analysis was performed on fourteen healthy young adults (7 males, 7 females) having a mean age of 23 years (range, 19 to 32 years). Subjects were instructed to walk with their own low-heel shoes along a 9.5m walkway. Three sets of experiments were performed. For each experiment subjects walked along a 9.5 m walkway at their comfortable, self-selected speeds. In the first experiment, each subject's average step length over several strides was measured. In the second experiment, the subject was instructed to walk along the walkway and step over an obstacle (white elastic band 1 mm thick and 6 mm wide) of 51, 102, 153, or 204 mm height in his/her usual self-selected manner. To do this, the subject's beginning position and obstacle location were adjusted until with practice the subject had established a comfortable gait and the toe of the trailing foot landed within ±5 cm of a marker on the force plate before lifting the trailing foot to step over the obstacle. This beginning position was used in the third experiment. For the third experiment the average step length for the subject found in the first experiment was used to compute lengths of 10, 20, 30, and 40% of step length. The obstacle of each height was randomly selected and placed at these distances from the marker on the force plate. The subject was instructed to maintain the stride attained in the second experiment until heel-strike of the trailing foot just prior to stepping over the obstacle. Thus, the distance from the toe of the trailing foot (during stance just prior to stepping over the obstacle) to the obstacle was controlled. Trials were accepted only if the toe of the trailing foot was within ±5 cm of the marker on the force plate. Three trials were collected for each test condition.

Motion data were collected with a two camera Watsmart 3-D digitizing system at a rate of 100 Hz. The average RMS accuracy of the system was better than 5 mm for a volume 2 m long, 1.5 m high, and 0.7 m wide. Motion data for the trailing limb were analyzed for the crossing stride, which is the period from heel-contact just before crossing the obstacle to the next heel-contact just after crossing the obstacle.

When stepping over obstacle of different heights the effects of obstacle location on toe-obstacle clearance, swing time of the trailing limb from toe-off to when the toe was over the obstacle, and 3-D joint angles of

the trailing limb when the toe was over the obstacle were tested using two-way ANOVA with repeated measures. A polynomial test was performed to determine the trend (linear, quadratic, or cubic).

RESULTS

Compared to toe-obstacle clearances found for self-selected toe-obstacle distances, stepping over obstacles with shorter toe-obstacle distances resulted in significant reductions in toe-obstacle clearances (Fig. 1). Clearance decreased linearly ($p \leq 0.041$) as distance decreased when stepping over obstacles of 51 and 102 mm heights. Quadratic relationships ($p \leq 0.015$) were detected between clearance and distance when stepping over obstacles of 153 and 204 mm heights. The reduction in toe-obstacle clearance led to contact of the trailing foot with the obstacle. Contact occurred when stepping over the obstacle of 153 mm height for locations of 10, 20, and 30 percent of step length and when stepping over the obstacle of 204 mm height for locations of 10, 20, 30, and 40 percent of step length.

The swing time of the trailing limb from toe-off to when the toe was over the obstacle decreased linearly ($p<0.000001$) as distance decreased (Fig. 2). When the toe of the trailing limb was over the obstacle knee flexion decreased linearly ($p=0.000004$) as distance decreased. Hip flexion decreased linearly ($p<0.000001$) as distance decreased. Abduction and external rotation of the hip increased linearly ($p=0.002$) as toe-obstacle distance decreased. Ankle flexion changed linearly ($p=0.00003$) from dorsi- to plantar-flexion as distance decreased. A significant height by distance interaction effect ($p=0.0004$) was also found.

DISCUSSION

We found that reducing the toe-obstacle distance significantly decreased the toe-obstacle clearance and led to foot-obstacle contact for obstacle heights of 153 mm and 204 mm. Therefore, these results support our hypothesis. Furthermore, these data suggest the closer the toe of the trailing foot is to the obstacle during stance of the crossing stride, the greater the risk of contact with the obstacle.

Reductions in flexion of hip, knee, and ankle are at least in part responsible for the reduction in toe-obstacle clearance. One explanation for this is that the reduction in flexion occurring with a shorter toe-obstacle distance is the result of having less time for the joints to flex after toe-off. It was reported that reductions in available reaction time significantly decreased the rate of success when crossing an obstacle in both young and elder adults (Chen et al., 1994). Thus, stepping over an obstacle with a shorter toe-obstacle distance may not allow enough time to elevate the foot to clear the obstacle and increase the risk of tripping.

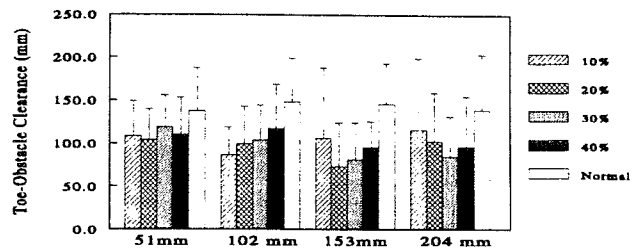

Figure 1. Average toe-obstacle clearances of the trailing limb when stepping over the obstacle of 51, 102, 153, or 204 mm heights for toe-obstacle distances of 10, 20, 30, or 40 % of the step length and for self-selected (normal) toe-obstacle distance.

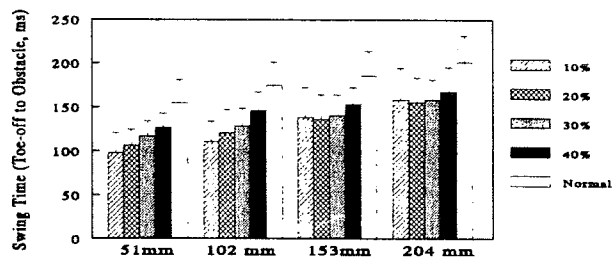

Figure 2. Average swing time of the trailing limb from toe-off to when the toe was over the obstacle when stepping over the obstacle of 51, 102, 153, or 204 mm heights for toe-obstacle distances of 10, 20, 30, or 40 % of the step length and for self-selected (normal) toe-obstacle distance.

REFERENCES

Blake et al., *Age Ageing* 17: 365-372, 1988.
Campbell et al.: *Age Ageing* 19: 136-141, 1990.
Chen et al.: *J. Gerontol* 46: M196-203, 1991.
Chen et al.: *J. Gerontol* 49: M227-233, 1994.
Chou et al.: *Proc. of 20th ASB meeting*: 137-138, 1996.
Overstall et al.: *British Med J.* 1: 261-264, 1977.
Tinetti et al.: *N Engl J Med* 320: 1055-1059, 1989.

TEMPORTAL AND GEL VOLUME EFFECTS ON PLANTAR PRESSURE RELIEF WITH USE OF SILICONE GEL-FILLED SHOE INSOLES

INTRODUCTION

In this investigation, we assessed efficacy of silicone gel-filled shoe insoles for relieving elevated plantar pressures, and examined whether factors such as walking speed and gel volume affect the pressure relieving abilities of the insoles. Our assessment of the insoles was conducted in a manner consistent with the mechanism by which these gel insoles can relieve plantar pressure (i.e. maintaining nearly uniform pressure within the fluid and transmitting such pressure across the upper surface).

Of particular interest, in this study, was the computation and identification of peak plantar pressure gradients in the heel and forefoot regions. High pressure gradients are anticipated to be precursors to customary indications of ineffective orthotic insoles, such as high peak pressures.

REVIEW AND THEORY

Orthotic shoe insoles, which reduce elevated local pressures at the plantar foot/shoe interface, can be of substantial preventative and/or therapeutic value to a variety of patients. Successful reduction of plantar pressure by means of orthotic shoe insoles dictates that insole materials have properties that are useful for redistributing load away from sites of localized elevated plantar pressure.

Investigators reporting on potential use of various materials and designs for orthotic pressure management generally have used parameters such as peak pressures and pressure-time-integrals, at plantar surface regions of interest, to assess efficacy of such materials and designs.[1-5] Such evaluative measures generally have been appropriate with regard to the mechanisms by which most orthotic insoles relieve elevated plantar pressure.

The mechanism by which the gel-filled insoles, used in this study (Fig. 1), can relieve plantar pressure differs substantially from those of other insole materials and designs. These gel insoles can maintain nearly uniform pressure within the fluid and transmit such pressure across the upper surface. Thus, if without such an insole, elevated pressures exist adjacent to regions of low pressure, then a gel insole can reduce elevated pressures by distributing load equally across the contacting plantar surface. Pressure reduction, using gel-filled insoles, however, would seem most effective while fluid is present beneath the entire contacting plantar surface. When no fluid exists beneath a portion of the contacting surface (Fig. 2), then that portion of the plantar surface is essentially in direct shoe sole contact, and substantial disparities in plantar pressure can persist.

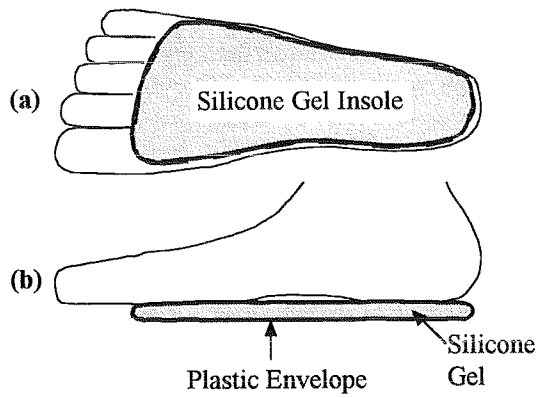

Fig. 1 Sketch of foot with silicone gel insole: (a) dorsal view, (b) medial view

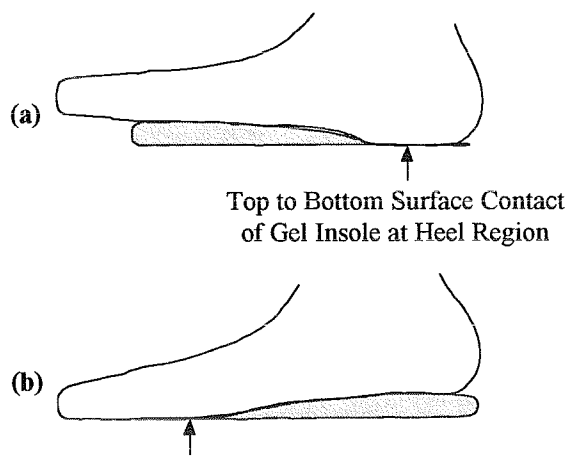

Fig. 2 Loss of gel between top and bottom surfaces at (a) heel and (b) forefoot

PROCEDURES

Fifteen healthy adults (7 males, 8 females, mean age = 37 years, mean weight = 698 N) participated in this study. We selected, for each subject, three pairs of silicone gel-filled insoles (PGB Medical,

Inc.), a pair of pressure sensing inserts (PEDAR, Novel, Inc.), and a pair of standard shoes (from a supply of shoes of similar type, but of different sizes). One of the insole pairs ("base" insole pair), for each subject, contained a volume of silicone gel determined by an existing, standard protocol. The other pairs contained either two fluid levels less gel or two levels more gel. The difference in fluid volume between fluid levels was proportionally similar for all insole sizes. For each subject, we obtained pressure data for multiple steps under the following conditions: (1) slow walking (nominally 50% slower than self-selected), (2) self-selected walking and (3) fast walking (nominally 25% faster than self-selected) while wearing shoes only, and while wearing each of the three insole pairs.

Raw pressure data for each step of every subject was processed using software provided by the equipment manufacturer to obtain center of pressure (COP) trajectories. For every subject, representative steps were determined, for each velocity/insole condition, as the trials with minimum planar area between trial COP trajectory and mean COP trajectory. The representative steps were then the trials for which all further processing and analyses were performed. For each of these trials, we computed pressure gradients across the plantar surface for each frame of pressure data using "in-house" software. Peak gradients at the heel and forefoot regions were identified at each frame; and these data were interpolated to 2% stance time intervals between 0% and 100%. Overall heel and forefoot peak gradients then were determined for each velocity/insole combination. Also, the percentage of stance at which forefoot gradients exceeded 100 kPa/cm was determined, along with the percentage of stance at which heel gradients dropped below 100 kPa/cm.

RESULTS

Results for peak pressure gradients at the heel and forefoot are shown in Table 1. Reductions in peak pressure gradients with insole use were generally more apparent at the heel than at the forefoot. A general trend toward increasing pressure gradients at both heel and forefoot was noted with increasing velocity for all conditions. Results for times (in %Stance) when heel pressure gradient drops below 100 kPa/cm and forefoot gradient exceeds 100 kPa/cm are summarized in Table 2. These results demonstrated that insole use tended to foster earlier subsidence of heel gradients below 100 kPa/cm as well as delayed increase of heel pressure gradients above 100 kPa/cm. These effects appeared to be accentuated at higher walking speeds.

Table 1. Heel and Forefoot Peak Pressure Gradients

Insole Condition		Slow kPa/cm	Self-sel. kPa/cm	Fast kPa/cm
No Insole	Heel	211 (47)	258 (65)	331 (92)
mean (sd)	Fore.	324 (103)	355 (133)	372 (145)
Low Fill	Heel	165 (47)	186 (63)	263 (83)
mean (sd)	Fore.	329 (78)	369 (97)	381 (71)
Middle Fill	Heel	155 (54)	182 (56)	241 (82)
mean (sd)	Fore.	315 (66)	352 (72)	369 (81)
High Fill	Heel	163 (59)	190 (58)	258 (80)
mean (sd)	Fore.	316 (111)	357 (79)	388 (132)

Table 2. Time of Heel Gradient Below 100 kPa/cm and Forefoot Gradient Above 100 kPa/cm

Insole Condition		Slow %Stance	Self-sel. %Stance	Fast %Stance
No Insole	Heel	52 (9)	43 (8)	43 (6)
mean (sd)	Fore.	44 (14)	40 (14)	45 (16)
Low Fill	Heel	40 (10)	34 (5)	38 (5)
mean (sd)	Fore.	45 (16)	46 (17)	47 (16)
Middle Fill	Heel	42 (14)	34 (7)	37 (6)
mean (sd)	Fore.	56 (11)	52 (11)	54 (12)
High Fill	Heel	37 (14)	35 (9)	37 (7)
mean (sd)	Fore.	53 (11)	55 (9)	53 (16)

DISCUSSION

The results of this investigation suggest that these silicone gel insoles may have some potentially beneficial effects for managing elevated plantar pressure. Lower peak pressure gradients at the heel suggest an ability to relieve locally elevated plantar pressure in this region. The heel region appears to enjoy an additional benefit in that the heel pressure gradients subsides more quickly with insole use. Consequently, the time during which the heel is subjected to elevated pressure is also lessened. The peak pressure gradients at the forefoot were not notably reduced with insole use; however, the onset of pressure gradients above 100 kPa/cm was delayed. Thus the benefit of reduced elevated pressure duration appears to extend to both regions.

REFERENCES

1. Holmes GB, and Timmerman L. Foot and Ankle. 11(3):141-145, 1990.
2. Murray HJ, et al. Diabetic Care. 16(8):1190-1192, 1993.
3. Novick A, et al. J Amer Pod Med Assoc. 83(3):115-122, 1993.
4. Pratt DJ. Pros & Orth Inter.;14(2):59-62, 1990.
5. Sanfillipo PB, et al. . J Amer Pod Med Assoc. 82(10):507-513, 1992.

REPETITIVE IMPULSIVE LOADING: CORRELATION OF FORCE PLATE AND OBSERVATIONAL ASSESSMENT

C Riegger-Krugh

Physical Therapy Program, University of Colorado Health Sciences Center, Denver, CO 80262

INTRODUCTION

A functional mobility battery was designed and used to distinguish movement performance between people with hip or knee osteoarthrosis and controls. During part of the battery, subjects walked across a camouflaged force plate at self-selected speed. This report involves the ability to accurately assess by observational criteria the level of repetitive impulsive loading as defined by force plate data.

REVIEW AND THEORY

Repetitive impulsive loading (RIL) is hard and fast joint loading with inadequate shock absorption. RIL has been shown to cause knee joint degeneration or osteoarthrosis in an animal model (1) and has been implicated in knee joint osteoarthrosis (OA) in humans (2). RIL has been identified during the initial contact period of the gait cycle by using the force plate variable of the loading rate of the vertical component of the ground reaction force expressed in multiples of body weight(BW)/second (2).

Few clinical practice settings have access to a force plate. If access were available, few clinicians have the time to determine whether this RIL risk factor and potential cause of knee joint OA is present in their patients or in people for whom prevention of future pathology might be addressed. If RIL could be determined by observational assessment with confidence, clinicians could recommend intervention to alter RIL or its effects. This assessment skill could be taught as a standardized part of gait assessment for students of physical therapy and other professions involved in movement performance assessment.

Purpose: Determine the correlation of repetitive impulsive loading as defined by force plate data with observational assessment based on specific criteria.

Hypothesis: With specific criteria defined, a positive correlation will exist between RIL as defined by force plate data and RIL as determined by observational assessment.

PROCEDURES

Subjects were asked to walk barefoot at self-selected speed across a force plate camouflaged in a walkway. Subjects included 11 control subjects and 25 subjects with either hip or knee OA or both, all 65 years of age or older. Individual starting positions on the walkway were altered without explanation to allow subjects to step squarely on the force plate. Three gait trials were recorded with a Kistler force plate, saved to a MacIntosh computer, and analyzed by a Biopac software program.

The force plate variable which defined RIL in this study was the peak value of the slope (loading rate, speed of rise) of the vertical component of the ground reaction force during the initial contact period (2), defined as the initial 1.5% of the gait cycle. The peak value was the maximum slope in any 2 msec interval within the initial contact period. The Biopac program allowed a minimum interval of a 2 msec sampling rate. Peak loading rate, normalized as multiples of BW/sec, was calculated by dividing the peak value (volts/sec) by volts/BW, measured when a

subject stood quietly on the center of the force plate.

Observational assessment of RIL occurred during individually scheduled visits to subjects' homes at dates following testing for the full functional mobility battery. Subjects were assessed walking barefoot on non-carpeted floor for a minimum of 30 steps. RIL was assessed on a 1 to 3 scale in .5 increments, with 1 considered little evidence of RIL. Specific criteria which were used to indicate observational evidence of RIL at initial contact included: loudness of the heel striking the floor and visual presence of a shock wave on the calf, indicating limited absorption of the ground reaction force (3).

Peak loading rate in multiples of BW/sec for a subject was correlated to the observational assessment of RIL on a 1 to 3 scale using a Pearson's Product Moment Correlation Coefficient test.

RESULTS

Correlation coefficients with all subjects analyzed together was 0.57, for control subjects was 0.51, and for OA subjects was 0.65.

DISCUSSION

With specific criteria defined, a positive correlation did exist between RIL as defined by force plate data and all RIL values as determined by observational assessment. Correlation was better for OA subjects alone than for control subjects alone or control and OA subjects together. This may be partly explained by the restricted range of scores in the control group (4), (5.32 to 71.74 x BW/sec), as compared to OA subjects (2.91 to 84.29 x BW/sec).

Future research to improve the correlation between the two variables for RIL include:

1. making an observational assessment based on a single criterion
2. making an observational assessment based on a combination of criteria
3. using different force plate variables to define RIL
4. distinguishing scores for the right and left sides

REFERENCES

1. Radin E.L. Clin Orthop, 131, 288-293, 1978.
2. Radin E.L. et al. J Orthop Res, 9, 398-405, 1991.
3. Voloshin A. et al. Trans ASME, 103, 48-50, 1981.
4. Dumholdt E. Physical Therapy Research Principles and Application, WB Saunders Co., 1993.

ACKNOWLEDGMENT

This project was supported by a Geriatrics Training Grant from the Department of Health and Human Services CFDA 93.191. Thanks is given to Hsiu-Hui Chung MS, PT for assistance in data collection.

CUMULATIVE TRAUMA DISORDER: IMPLICATIONS OF WORK HEIGHT AND CUTTING TASK ON MUSCULAR PERFORMANCE

R. J. Gregor, PhD, M.M. Ryan[1], PhD, A. Albrecht, D. Ortiz[1] and M. Burrow[1]

Department of Health and Performance Sciences, Georgia Tech Research Institute[1]
The Georgia Institute of Technology, Atlanta, GA 30332-0110

INTRODUCTION

Work related chronic musculoskeletal disorders or cumulative trauma disorders (CTD) are recognized as significant occupational health problems as the effect of monotonous, highly repetitive, and strenuous jobs on the musculoskeletal system, particularly the upper extremity, becomes more clear. Disorders, such as carpal tunnel syndrome, tendonitis, tenosynovitis, and chronic muscle strain have become linked to jobs that are repetitive, that require high forces, and require continuous or repeated extreme or awkward postures (Armstrong et al., 1982). Recent publications have demonstrated relationships between dose and response related to force, repetition, and musculoskeletal disorders (Silverstein et al.,1987). Specific to the poultry industry, repetitive tasks in the processing of poultry, which require workers to perform the same cut over extended periods of time lead to a number of chronic disorders. Knowledge of repetition rates, environmental forces acting on the hand and wrist, and activity patterns of involved musculature in the upper extremity are important in the evaluation of these repetitive tasks and in the ultimate modification intended to prevent cumulative disorders. In light of the significance of this problem, an ergonomic work assessment system was developed to monitor upper extremity function while workers performed their tasks on the poultry processing line.

METHODS

The Ergonomic Work Assessment System (EWAS) is comprised of a bi-directional goniometer (Penny and Giles), two pair of bipolar electrodes sampling from flexor and extensor muscle compartments, and a six component sensor adapted to a standard cutting knife to monitor loads (forces and torques) on the knife. In the knife blade system (right hand rule) Fx represents vertical forces, Fy the medial/lateral forces and Fz the axial tension and compression forces acting on the knife blade. Fifteen workers from 3 separate plants in the state of Georgia were monitored while performing 2 separate tasks, a wing cut and a tender cut. Twenty trials of each cut from each worker were collected while the workers performed these tasks "off-line." The ten channels of data were recorded for a period of fifteen seconds during which time each worker made the requested cuts on both the left and right sides of the chicken. Recent modifications to data acquisition hardware and software (LabView) and upgrades in sensor technology have provided a system whereby workers in the plant can be monitored on-line. In addition to making 40 separate measurements on each subject, video records were taken during each trial to monitor posture while the subjects performed each task.
In addition, a group of five workers were asked to perform the same two tasks but at 7 different work heights (elbow height and 2,4,and 8" above and 2, 4 and 8" below elbow height). Loads on the knife were recorded according to the procedures described above and two EMG channels were added to the flexor and extensor activity to include the activity of the medial deltoid and the upper trapezius muscles.

RESULTS

In the group of thirty workers, peak forces recorded during the wing cut were significantly higher than forces recorded during the tender cut. Exemplar records of Fx and both flexor and extensor EMG from a 71" female (see Fig. 1), highlight some of the differences between the two tasks. These differences include 1) peak Fx

(Fig 1) and Fy forces were up to three times larger while peak Fz components (also not shown) were twice as large in the wing cut as opposed to the tender cut, 2) flexor and extensor compartments were co-active during each cut with very similar mean EMG magnitudes within cut and within subject, 3) mean EMG was greater during the wing cut than during the tender cut, and 4) both flexors and extensors remained on after the termination of the tender cut with greater activity observed when the workers were required to pull the chicken tenders down with their hands than when they were using the knife to cut the chicken. In the group of five subjects in the work height group the following observations were made: 1) work height, subject and cut type all produced significant effects on the measured variables, 2) the wing cut produced higher forces and EMG than the tender cut and 3) EMG, in general, decreased as work height decreased with flexor compartment and deltoid EMG significantly affected by both task and work height.

In summary, recording information in the workplace related to the repetitive loads experienced by workers performing job related tasks is requisite to the understanding of cumulative trauma disorders. Information on environmental loads, EMG and limb position during the performance of repetitive tasks in the poultry processing industry has provided useful insight to modifications designed to attenuated repetitive loads and reduce injury in the workplace.

REFERENCES

Armstrong, T. et al. Am. Ind. Hygiene Assoc. J. 43,103-115, 1982.

Silverstein, B. et al. Am. J. Ind. Med. 11,343-358, 1987.

Fig. 1 Fx force components for a wing and tender cut synchronized with EMG from the flexor and extensor compartments in a single exemplar subject.

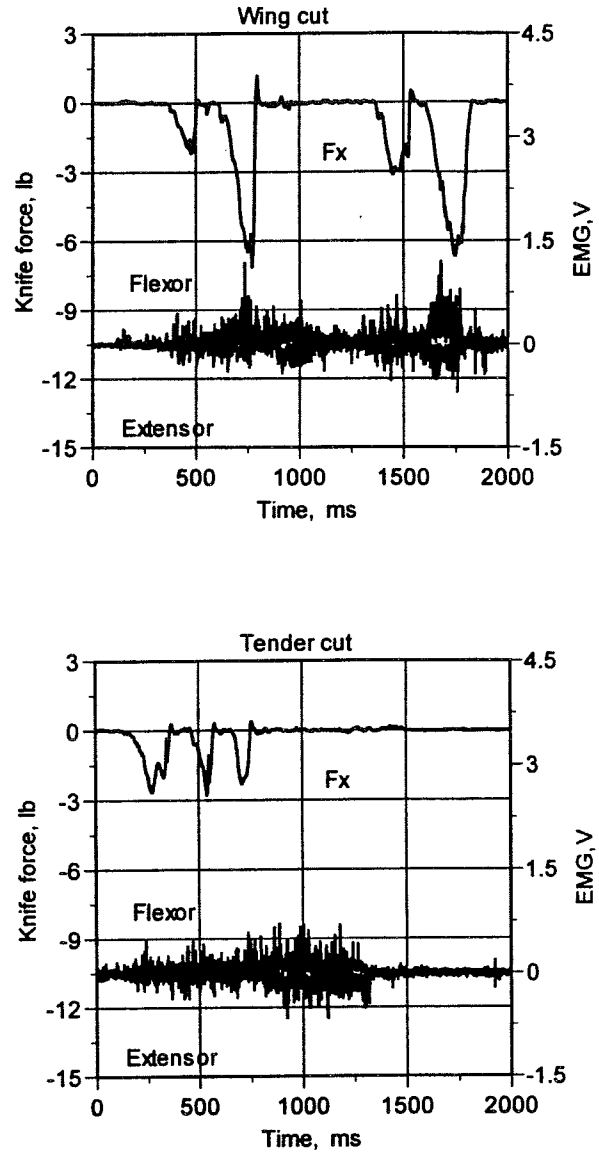

Effect of a Synch Offset on Joint Moments in ACL/PCL Deficient Patients

Gregory Rash[¥], Craig Roberts[§], Mark Wachowiak[Ж]

[¥]Gait and Biomechanics Lab, Frazier Rehab Center, Louisville, KY
[§]Department of Orthopeadic Surgery, University of Louisville, Louisville, KY
[Ж]Department of Computer Science, University of Louisville, Louisville, KY

Introduction

It is typical in modern gait labs to use video based motion analysis and forceplate data to calculate the kinematics & kinetics of the gait cycle via the inverse dynamic approach. There are a number of estimations regarding anthropometrics, estimations of joint centers, inertial properties, etc which introduce error into the calculations. One area which has the potential for creating error is the synchronization of the motion and analog data. Alexander et. al. showed in normal subjects that synchronization errors as small as 1/120th of a second had significant effects on the lower limb moment calculations, with the knee and hip moments showing the most sensitivity. Based upon Alexander's findings, we wished to investigate the effect of asynchronization of the motion and analog data on pathological gait, specifically ACL & PCL deficient individuals.

Methods

The joint kinetics of 12 ACL deficient and 5 PCL deficient patients were studied. All ACL/PCL tears were isolated and clinical evaluations were all performed by the same Orthopaedic surgeon. The subjects walked down a 25 ft walkway stepping on a Kistler forceplate at a self selected speed while a 5 camera Qualisys video based motion analysis system and Biopac analog collection system gathered data at 60 Hz and 600 Hz respectively. Three trial of data were collected and analyzed per subject. A device was made such that a voltage simultaneously illuminated an infrared diode and registered on an analog channel when a button was pushed. The diode was placed in view of one of the cameras and the synchronization of the system verified prior to data collection. A computer program was written to allow for addition or subtraction of data from the 3D coordinate data to create a synch offset between the motion and force data. The coordinate data were made to be -3, -2, -1, 1, 2 & 3 fields (1/60th of second per field) off from the force data. Joint kinetics were then determined via the AutoGait3D software program which uses the inverse dynamic approach for the synchronized trials and each of the additional 6 asynchronous trials. All data were graphically displayed and specific data (i.e. maximum moment at foot strike, midstance, etc.) were determined for each trial and averaged within and between subjects.

Results

Similar results to Alexander et. al. were found as there were numerous changes in the parameters studied, most of which were at the knee and hip and probably not clinically significant. However, in four of the ACL deficient patients there was clinically significant findings. The shape of the knee moment graphs remained somewhat similar with the exception of a "DC" shift. The shift was great enough that the subjects no longer displayed an internal extension moment in the early to mid stance phases. (A typical knee moment pattern to a "Quad-Advoidance" pattern). This is clinically significant and occurred when the analog data lagged behind the motion data. Nothing clinically significant

was changed in the PCL deficient patients nor the one ACL deficient patient who displayed an absence of a knee extension moment pattern in the properly synchronized data. Average values for selected parameters across the four subjects are shown in table 1. Figure 1 shows the properly synched hip, knee and ankle moments for one of the subjects whose pattern switched. Figure 2 shows the same moment graphs when the analog data lagged behind the motion data by three fields (0.05 sec)

Table 1. Selected Average Parameters of 4 Individuals Who's Patterns Changed

	Synched	.05 lag
Max ankle mom	138.0	135.0
Max knee mom @≈ FS	34.0	95.0
Max knee mom @≈ 2nd B	4.0	29.0
Max knee mom @≈ OFS	25.0	55.0
Max hip mom @≈ FS	78.0	175.0
Max hip mom @≈ 2nd B	54.0	106.0
Max hip mom @≈ OFS	-22.0	38.0

FS = Initial foot strike, 2nd B = 2nd bump which typically occurred around opposite toe off, OFS = Opposite foot strike.

Discussion

Results of this study indicate that synchronization errors can have significant effects on the moment calculations in pathological gait. Each lab must keep this in mind and should evaluate the synchronization of their systems prior to conducting clinical or research evaluations

References

Alexander, E.J., Hurwitz, D.E. & Andriacchi, T.P., (1997). "Effect of Synchronization Error Between Force & Position Data in Moment Calculations". Gait & Posture, 5(2).

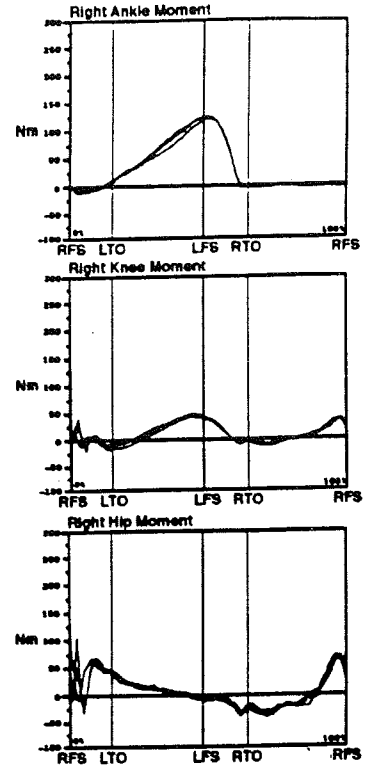

Figure 1. Moments from Synchronized Data

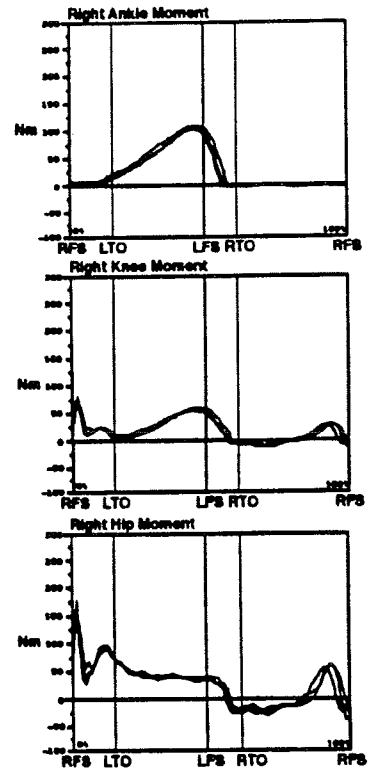

Figure 2. Moments from Unsynchronized Data (.05 lag in analog data)

Static Assessment of Pedar and F-Scan Inshoe Pressure Sensors; Revisited

Gregory S. Rash[¥]; Peter M. Quesada[§], Nathan Jarboe[¥]
[¥]Gait and Biomechanics Lab, Frazier Rehab Center, Louisville, KY
[§]Department of Mechanical Engineering, University of Louisville, Louisville, KY

Introduction

The respective merits of the PEDAR (Novel Electronics, Inc.) and F-Scan (Tekscan, Inc.) systems have been a topic of debate among engineering, biomechanists, and clinicians for some time now. Proponents of the PEDAR system (which employs capacitive sensors) have claimed higher repeatability, greater durability, and more software processing options. Advocates of the F-Scan system (Which employs resistive ink sensors) have noted the system's higher spatial resolution, and lower cost. Previous experimental results by Cavanagh, et. al. (1992) and McPoil et. al. (1995) have suggested that the PEDAR system for plantar pressure measurement was able to measure known static pressures more accurately than the F-Scan system. McPoil et. al. suggests that the reliability of the F-Scan system was so poor that it would be debatable as to whether the F-Scan system could be used as a clinical or research tool. These measurements, however, were made prior to two recent developments of the F-Scan system (the release of new resistive ink sensor insoles and software allowing for calibration via an air pressure bladder). We sought to address the following questions: (a) Which system measures known pressure more accurately? (b) Which system is more repeatable? (c) Which system has lower measurement variance across a uniform distribution? (d) Is F-Scan repeatability improved with re-calibration?

Methods

Pressure measurements were made using a single PEDAR and new ink F-Scan insole. All measurements were made in a Novel air bladder, which provided generated known, uniform pressure distributions and allowed for both sensors to fit in the bladder at the same time without overlapping the sensors. The PEDAR insoles were calibrated using the standard protocol involving the air bladder. This calibration was used for all PEDAR measurements. F-Scan insoles were calibrated on each of three testing days using the new bladder calibration technique. The second testing day was one day after the first; while the third testing day occurred four days following the first. Each set of measurements involved placing both insoles in the bladder side by side and loading the bladder, at 100kPa intervals (100 up to 500kPa and 500 down to 100kPa). Data were recorded at each interval and the bladder was emptied between each recording. One set of data was collected on the first testing day. On each of the remaining test days, one data set was collected with the F-Scan system using the calibration from the first day, and another set was collected using a calibration obtained that day. For each recording we computed the average and standard deviation of pressure values across sensors in a 4cm x 20cm area. For statistical purposes, we subtracted the known pressure from the obtained measures of the respective systems and analyzed the average absolute differences and their

standard deviations as well as the percent absolute difference from the known pressure.

Results

There were no significant differences in the average absolute pressure difference between the two systems. Across all data sets and all conditions, the mean absolute differences between the area average pressure and the bladder pressure gauge value were 7.5 and 8.8kPa for the PEDAR and F-Scan systems, respectively. The mean absolute differences for the five sessions were 2.6, 6.7, 10.5, 8.6, & 7.4kPa for the PEDAR insoles. For the F-Scan insoles the means were 6.2, 7.4, & 7.0kPa with the first day calibration, and 8.3 & 11.2kPa with same day calibrations. The mean standard deviations across the indicated region were significantly different with means of 2.8 and 9.7kPa, respectively. When breaking the data down to a percent absolute difference there was a statistically significant difference between the systems. The mean percent absolute difference was 2.0 & 3.1% respectively, and the mean percent difference of the standard deviations was 1.1 and 3.6% respectively.

Discussion

The results obtained suggest that there is no difference in the Pedar and F-Scan (with new ink & calibration via a bladder) systems ability to measure uniform absolute pressures. The PEDAR insole system had a slightly smaller absolute differences (although not significant) and demonstrated significantly lower variance across sensors. Variance differences suggests that sensor to sensor random errors were lower in the PEDAR system. It was noted that the higher standard deviations for the F-Scan sensors were noted primarily for the third test session where the standard deviations were twice that for the previous two test sessions. It was not know at the time of writing this abstract if re-equilibrating the sensors in addition to re-calibrating the sensors would alleviate this phenomenon.

The mean percent absolute difference between systems was statistically significant. However, the 1.1% difference in systems would probably not be considered clinically significant. This finding may indicate that applications requiring the greatest accuracy and/or repeatability may be best performed with a PEDAR system. Regardless, the results of this study do not reflect the poor accuracy and repeatability of the F-Scan system as indicated by Cavanagh, et. al. (1992) or McPoil et al (1995).

Lastly, one finding from this study (although not statistically significant) which has beneficial implications for F-Scan users in clinical settings was the improved reliability when a calibration from a single day was used across days. This suggest that trends over time could be better detected if the insoles & calibrations initially used by the patient are used again on the second or third visit.

References

Cavanagh, P.R., Bewitt, F.G., Perry J.E. (1992). "In-Shoe Plantar Pressure Measurement: A Review". Foot, 2:185-194.

McPoil, T.G., Cornwall, M.W., Yamada, W. (1995). "A Comparison of Two In-Shoe Plantar Pressure Measurement Systems". The Lower Extremity, 2(2): 95-103.

Scapulothoracic muscle fatigue associated with alterations scapulohumeral rhythm kinematics during maximum resistive shoulder elevation.

Kevin J. McQuade *,
*New York Medical College Physical Therapy, Valhalla, NY,10570

INTRODUCTION

Twenty-five adult males were required to elevate their arm overhead against maximum resistance at a controlled velocity as many times as possible. Three-dimensional humeral and scapular kinematics were determined and bipolar surface electromyographic (EMG) activity was recorded from selected muscles. The study suggests that shoulder fatigue affects the way in which the scapula moves concomitantly with the humerus. Fatigue tends to result in hypermobility of the scapular. The clinical implications and importance of the recognition of proper scapular function are discussed.

REVIEW AND THEORY

Of particular importance to normal function of the shoulder complex, is the kinematic relationship between the scapula and the humerus commonly referred to as the scapulohumeral rhythm. It is generally accepted that a properly synchronized scapulohumeral rhythm is necessary for normal shoulder function. Since fatigue is a process that affects the force generating capacity of a muscle, one approach to studying the relationship between kinematics and clinical pathology at the shoulder is by inducing a state of local muscle fatigue at the shoulder and assessing the effect on kinematic coupling. There has been limited discussion of the role of muscle fatigue to the development of various shoulder pathologies (Bradley and Tibone,1991, Jobe, Tibone,1990). For example, Bradley and Tibone reported that dysfunction of scapular rotation was a result of fatigue in athletes, and suggested that this may induce added stress on anterior shoulder stabilizers. McQuade and Wei reported results from a pilot study on four subjects looking at the effect of fatigue on the Scapulohumeral rhythm (McQuade, Wei,1995). In two of the four subjects, there seemed to be an increase in the scapulohumeral ratio following fatigue with little change in the other two subjects. The study was limited by the small sample size, relied on static measurement techniques, and used only one ratio to represent the scapulohumeral rhythm for the full range of motion. We have now advanced the methodology to the present study using dynamic measurements, a larger sample size, and have considered the non-linearity of the scapulohumeral rhythm.

The purpose of this investigation was first to determine if the scapulohumeral rhythm is altered as a result of fatigue-inducing overhead elevations of the arm in the plane of the scapula. It was hypothesized that as fatigue occurs, stabilizing muscular forces would be compromised, thus scapular motion would become more erratic and generally increase relative to the motion of the humerus during simple arm elevation. Furthermore, it was hypothesized that this decrease in slope value would be significantly associated with electromyographic evidence of scapular muscle fatigue.

PROCEDURES

Joint angular and linear displacements were monitored by an electromagnetic tracking System (FasTrak™ Polhemus Navigation's, Colchester, VT.). Sensors were attached to the anterior trunk at the level of the sternum, the arm via a thermoplastic arm cuff, and directly to the broad superficial flat portion of the acromion process of the scapula. Electromyographic (EMG) recordings (Therapeutics Unlimited, Model 67,Iowa City IA) were obtained from the upper trapezius, lower trapezius, serratus anterior, and the middle deltoid muscles.

Subjects were required to perform repetitive overhead elevations of their right arm against maximal isokinetic resistance until they were no longer able to continue.
The median power frequencies and average root mean square amplitudes were determined for each repetition. These values were normalized for between subject comparisons.

To determine the ratio of scapulothoracic rotation to humeral elevation, piecewise linear regressions were done on the smoothed data for five phases of elevation (20% intervals). Repeated measures analysis of variance and regression analysis were used to determine the association between the changes in the slopes (scapulohumeral rhythm),

median power frequencies ,and root mean square amplitudes as a function of fatigue time. All tests of significance used an overall significance level of less than or equal to 0.05.

RESULTS AND DISCUSSION

The results of this study can be summarized as follows: First, the phasewise slopes for phases 3-5, as well as the median of all the phasewise scapulohumeral rhythm decreased significantly as a consequence of fatiguing repetitive overhead elevations of the arm. Second, the upper trapezius, lower trapezius, serratus anterior, and middle deltoid showed myoelectric signs of fatigue. Third, the decrease in the median scapulohumeral rhythm was most highly associated with fatigue (as indicated by decreases in the median power frequency) of the upper trapezius and the serratus anterior, but this association was dependent on the amplitude of the signal for the upper trapezius. Taken collectively, the results of this study suggest that shoulder fatigue directly affects the way in which the scapula moves concomitantly with the humerus. Fatigue tends to result in a destabilization of the scapula or compensatory increased rotation primarily in the mid range of arm elevation. Further, that the scapular muscles are susceptible to fatigue and are associated with alterations of the scapulohumeral rhythm.

The median power frequencies and amplitudes decreased somewhat in parallel across all muscles. In other words, there was no obvious shifting between muscles that one might expect given the force coupling function of the scapular muscles. That is, if the upper trapezius was fatiguing more than the serratus anterior, the activity of the serratus might be expected to increase as the trapezius activity decreased to maintain the same resultant kinetic effect.

Direct cause and effect inferences of the results must be made with caution, because the kinematic changes seen may also be related to other muscular dynamics. For example, if the rotator cuff was fatigued this might have resulted in a reduced ability of the rotator cuff muscles to prevent the deltoid from pulling the head of the humerus superiority into an impingement position under the subacromial arch. Increased scapular rotation may be a compensatory response to rotate the acromion upward and backward out of the way to decrease the possibility of subacromial impingement. The increased scapular motion may also represent an attempt to increase the length of the deltoid or supraspinatus to maintain a efficient length-tension relationship, or to increase the moment arm of the deltoid to compensate for reduced deltoid muscle force generating potential.

Current clinical beliefs regarding scapular function underscore the importance of understanding scapulohumeral coupling. For example, the belief that when weakness is present in the scapular musculature, this will affect normal scapular positioning (Paine and Voight,1993). It has also been suggested that, if excess motion (hypermobility) of the scapula occurs, this might place increased stress on the glenohumeral capsular structures and lead to increased glenohumeral instability. (Abrams,1991). Finally, patients may present with normal gross shoulder motion, but still have an abnormal scapulohumeral rhythm (Eto,1991). Thus, gross motion assessment may not always be sensitive enough to pick up imbalances that may be associated with progressive shoulder dysfunction, implying detailed assessment of the scapulohumeral rhythm as part of a through diagnostic examination.

REFERENCES

Abrams J. (1991) Special shoulder problems in the throwing athlete: Pathology, Diagnosis, and nonoperative management. *Clinics in Sports Med.*10(4),839-850.

Bradley JP, Tibone JE. (1991) Electromyographic analysis of muscle action about the shoulder. *Clinics in Sports Medicine*10(4),789-795.

Eto M. (1991) Analysis of the Scapulo-humeral rhythm for periarthritis scapulohumeralis. *J Japan Orthop Assoc.*65,693-707.

Jobe FW, Tibone JE, Jobe CM, Kvitne RS. The shoulder in Sports. New York.: eds. WB Saunders Co., 1990. (Rockwood CA, Matsen FA, eds. The shoulder; vol 1).

McQuade K, Wei S, Smidt G. (1995) Effects of Local Muscle fatigue on three-dimensional scapulohumeral rhythm. *Clinical Biomechanics*10(3),144-148.

Paine RM, Voight M. (1993) The role of the scapula. *J. Orthop and sports Phys Ther*20(2),128-134.

BIOMECHANICAL EVALUATION OF METHODS OF SCAPULOTHORACIC FUSION FOR THE TREATMENT OF FSH MUSCULAR DYSTROPHY

C.V. Bensen[1], R.A. Draughn[2], and J.D. Thompson[1]
[1]Department of Orthopaedic Surgery, [2]Department of Materials Science
Medical University of South Carolina, Charleston, SC 29425

INTRODUCTION

To determine the optimal treatment of patients with facioscapulohumeral muscular dystrophy, three different techniques of scapulothoracic fusion were compared using a novel cadaveric model. Ribs were removed from cadavers and mounted in dental stone in anatomic position. Scapulae were then fused to the ribs using single wire fixation, double wire fixation or tension band wiring as previously described. Constructs were loaded to failure and biomechanical properties of the three techniques were compared.

REVIEW AND THEORY

Facioscapulohumeral (FSH) Dystrophy is an uncommon form of muscular dystrophy primarily involving the muscles of the face and shoulder stabilizers. First described by Duchenne in 1862[1],this disease has an autosomal dominant inheritance and is usually diagnosed in the third decade of life. Although longevity is rarely affected, patients are severely limited in forward flexion and abduction of the arm. In the subset of patients whose deltoid and supraspinatus function is spared, surgical fixation of the scapula to the rib cage has been shown to restore useful range of motion, enhance physical appearance, improve exercise tolerance and activities of daily living. A variety of methods of scapulothoracic fusion have been described including single wire fixation and double wire fixation[2], tension band wiring[3], fascial tethering[4], plate and screw fixation[5], and tibial strut bone grafting[6]. However, to date there has been no direct comparison of the biomechanical properties of these methods of scapulothoracic fusion. The purpose of the present study was to compare the biomechanical properties of three described techniques of wire fixation in a cadaver model.

PROCEDURES

Both scapulae and the fourth, fifth, and sixth pairs ribs were harvested from ten adult cadavers. The specimens were debrided free of soft tissue, cleaned, and mounted in dental stone in anatomic position. Scapulae were then fused to the ribs using single wire fixation (n=5), double wire fixation (n=8), or tension band wiring (n=6) with 18 gauge stainless steel wire. The samples previously had been randomly assigned to one of the three groups. Following the fixation procedures, samples were carefully inspected for fractures of either the ribs or scapulae and to ensure no laxity existed at the stone-rib interface. Constructs were then mounted on an Instron materials testing system using c-arm clamps such that the piston of the MTS would contact the base of the glenoid process and exert a downward or inferiorly directed force upon the scapula. The constructs were subsequently loaded in distraction to failure. Load-deformation curves were generated using a chart recorder linked to the load cell of the system. The following three parameters were examined: maximum load to failure (kg), stiffness (kg/mm), and displacement to failure (mm). Maximum load to failure values were determined by measuring the highest force in kilograms tolerated by the construct prior to failure. Failure was arbitrarily defined as the first major fracture sustained by the construct. Stiffness was calculated using the slope of the initial portion of the load-deformation curve. Finally, displacement to failure was defined as the distance in millimeters traveled by the MTS piston prior to failure. The mean values of the three groups were compared using a t-test with $p<0.05$ required for statistical significance.

RESULTS

There were no significant differences in fracture pattern among the three methods

of fixation. A summary of the three study parameter results is given in Figure 1.

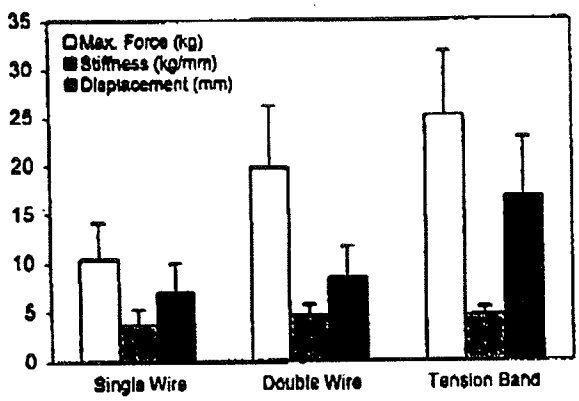

Figure 1. Results

The double wire fixation group had a significantly higher maximum force (19.8kg) than the single wire fixation group (10.4kg, $p<0.01$). The tension band group had a significantly higher maximum force (25.1kg) than both the single wire group ($p<0.001$) and the double wire group ($p<0.05$). There were no significant differences among the three groups with respect to the stiffness parameter measured. The tension band group (16.8mm) had a significantly higher displacement to failure than both the single wire group (8.5mm, $p<0.05$) and the double wire group (7.1mm, $p<0.01$).

DISCUSSION

Failure of fixation and rib and scapula fractures have been reported as complications following scapulothoracic fusion often requiring revision surgery. In the present experiment, fractures occurred at significantly higher forces using the tension band technique. This suggests that mechanical failure would be less likely using this method of fixation *in vivo*. Constructs can be loaded to failure in only one direction; an inferior distraction force was chosen since the weight of the patient's arm would represent the most significant force acting on the construct. Immobilization of the ribs reduces compliance of the chest, thus functionally decreasing the vital capacity of the lung. Consequently, pulmonary complications such as atelectasis and pleural effusions have been reported[5]. The higher displacement to failure in the tension band wiring technique suggests the ribs are somewhat less immobilized compared to the other groups. This would be desirable and should reduce the incidence of postoperative pulmonary complications in these patients.

REFERENCES

[1]Duchenne, G-B. Paris:J-B Balliere, 1862.
[2]Bunch et al. *JBJS*, **75A**:372-76, 1993.
[3]Thompson, J.D. Manuscript submitted.
[4]Ketenjian, A. *JBJS*, **60A**:476-80, 1978.
[5]Letournel et al. *JBJS*, **72A**:78-84, 1990.
[6]Copeland et al. *JBJS*, **60B**:547-51, 1978.

ACKNOWLEDGEMENTS

The authors would like to thank Troy Marlow, M.D. for his help with cadaver bone procurement. We would also like to acknowledge the assistance of Mr. Mark Fielding of the Department of Cell Biology and Anatomy; without his help, this project would not have been possible.

BILATERAL WITHIN-SUBJECT Q ANGLE ASYMMETRY IN ASYMPTOMATIC CONTROLS VERSUS ANTERIOR KNEE PAIN SUFFERERS

L.A. Livingston[1], J.L Mandigo[2]

[1]Department of Physical Education, Wilfrid Laurier University, Waterloo, ON N2L 3C5

[2]Faculty of Physical Education and Recreation, University of Alberta, Edmonton, AB T6G 2H9

INTRODUCTION

Investigators have traditionally adopted between-group analysis-of-variance (ANOVA) designs to test for differences in quadriceps (or Q) angle magnitude between those asymptomatic versus symptomatic for anterior knee pain (AKPS). Few (Hvid et al., 1982; Messier et al., 1991), in contrast, have tested for bilateral (ie, right versus left) within-subject lower limb differences. In this study, goniometric measurements of right and left Q angles were compared between-groups (ie, asymptomatic, unilateral symptomatic, bilateral symptomatic) and within-groups (ie, right versus left lower limb).

REVIEW AND THEORY

An excessive Q angle (ie, >15-20°) is commonly viewed as anatomic risk factor in the etiology of overuse injuries of the knee (Cowan et al., 1996). However, it is now considered to be a less reliable clinical measure than was previously believed (Woodall et al., 1990). The inability of researchers to consistently link excessive Q angles with the occurrence of AKPS is to blame. Methodological differences (eg, measurements drawn in supine versus weight-bearing positions) may account for some of the observed discrepancies in reported Q angle values, but so too may the tendency for investigators (Cowan et al., 1989; Woodland et al., 1992) to derive Q angle measures from only one lower limb. In one study, right and left Q angle values were combined into one sample for the purposes of subsequent analysis (Caylor et al., 1993). These approaches are problematic for they imply that Q angles are bilaterally symmetric, an assumption that does not appear to have been thoroughly examined.

A review of the literature revealed only two investigations (Hvid et al., 1982; Messier et al., 1991) in which Q angles were measured and reported bilaterally. While no significant right to left limb differences were reported, the generalizability of the results are limited by the small sample sizes that were utilized.

The purpose of this investigation, therefore, was to compare measured values of the left and right Q angles to examine whether bilateral similarities or differences existed between a group of asymptomatic controls and those symptomatic for anterior knee pain syndromes. The null hypotheses were that there would be no significant between-group (ie, asymptomatic, unilateral AKPS, bilateral AKPS) or within-subject (ie, right vs left limb) differences, or interaction effects.

PROCEDURES

Seventy-five young-adult males (n=36) and females (n=39), ranging in age from 15 to 48 years (M=26.1, SD=7.2), volunteered to participate in this study. After completing a general information and an AKPS screening questionnaire, they were assigned to one of three groups: asymptomatic control (n=50), unilateral knee pain sufferers (n=11), or bilateral knee pain sufferers (n=14).

Goniometric measurements were taken with the subjects in a standing position and the knees in full extension. Q angles were measured bilaterally using the standard clinical method of measurement (Horton et al., 1989). A universal goniometer was used to measure the Q angle with the anterior superior iliac spine, midpoint of the patella, and the center of the tibial tubercle as landmarks. All measurements for a given subject were taken by the same investigator. Intertester reliability was established in a preliminary study by measuring the right Q angle in a group of 14 subjects. An r=0.67 (ICC (2,1)) (Shrout et al., 1979) determined that

intertester reliability was good (Fleiss, 1986).

The data were analyzed using a mixed between-within multi-way ANOVA procedure. The dependent variable was Q angle magnitude while the independent variables included group, gender, and lower limb. The data were also reviewed on a case-by-case basis.

RESULTS

Descriptive statistics for the Q angle by group and by limb are presented in Table 1. A significant difference in Q angle magnitude between groups ($F(2,138)=3.34$, $p=0.04$) was observed, as was a significant group by limb interaction effect ($F(2,138)=2.99$, $p=0.05$). Significant differences in Q angle by gender ($p=0.62$) and limb ($p=0.33$) were not observed. Forty-seven percent of all the subjects studied demonstrated a minimum 4° difference in Q angle values between the right and left lower limb, while 17% displayed bilateral differences of 8° or more.

Group	Left Q Angle (degrees)	Right Q Angle (degrees)
Control (n=50)		
M (SD)	11.3 (5.5)	10.0 (4.4)
Maximum	23.0	21.0
Minimum	0.7	1.0
Unilateral (n=11)		
M (SD)	12.5 (6.6)	12.8 (6.0)
Maximum	21.7	19.0
Minimum	3.3	0.3
Bilateral (n=14)		
M (SD)	11.4 (5.3)	15.7 (7.2)
Maximum	23.7	30.0
Minimum	0.7	3.3

Table 1. Mean Q angle values by group and limb.

DISCUSSION

A lack of comparable investigations (ie, in terms of the subject groups studied and the measurement methodologies utilized) prevents comparisons between the results reported herein and those of previous investigations. The findings do suggest, however, that the assumption of bilateral symmetry in Q angle values may be erroneous. While mean left lower limb Q angle values varied little more than 1° between the control and symptomatic groups, the mean right Q angle values differed by up to 5.7° between the asymptomatic and bilateral AKPS sufferers. Moderate (ie, 4°) to substantial (ie, 8°) amounts of bilateral asymmetry in Q angle values were also observed when cases were viewed on an individual basis.

The presence of an interaction effect provides some evidence that the magnitude of the left and right Q angles, as well as the degree of asymmetry between them, needs to be considered when attempting to link the occurrence of AKPS to the Q angle measure. In order to validate this speculation, more research utilizing large sample sizes (ie, larger than even that utilized in this investigation) and the bilateral measurement approach is required.

REFERENCES

Caylor et al. JOSPT, **17**, 11-16, 1993.
Cowan et al. Med Sci Sports Exerc, **28**, 945-952, 1996.
Fleiss, J.L. Reliability of Measurement, 1-12, Wiley, 1986.
Horton et al. Phys Ther, **69**, 897-901, 1989.
Hvid et al. Acta Orthop Scand, **53**, 577-579, 1982.
Hvid et al. Acta Orthop Scand, **52**, 661-666, 1981.
Messier et al. Med Sci Sports Exerc, **23**, 1008-1015, 1991.
Shrout et al. Psych Bull, **86**, 420-428, 1979.
Woodall et al. J Orthop Sports Phys Ther, **11**, 535-542, 1990.
Woodland et al. Am J Sports Med, **20**, 208-211, 1992.

ACKNOWLEDGMENTS

The authors gratefully acknowledge that financial support for this research was received from a grant provided by WLU Operating funds.

EFFECTS OF SPACEFLIGHT ON POSTURAL RESPONSE TO ALTERED SENSORY CONDITIONS

R. Speers[1], W. Paloski[2], A. Kuo[3]

[1] Dept. of Biomedical Engineering, The University of Michigan, Ann Arbor, MI 48109
[2] Space Biomedical Research Institute, NASA Johnson Space Center, Houston, TX 77058
[3] Dept. of Mech. Engr. and Applied Mechanics, The University of Michigan, Ann Arbor, MI 48109

INTRODUCTION

Postural and gait instabilities in astronauts returning from spaceflight are thought to result from in-flight adaptive changes in central nervous system processing of sensory inputs from the vestibular, proprioceptive, and visual systems (Paloski et al., 1992). Such postflight instabilities may present operational hazards if emergency egress is required soon after landing, or if visual inputs are distorted by darkness or smoke. We investigated changes in postural control following spaceflight by examining the multivariate characteristics of postural response and comparing the motor control gain used for maintenance of upright stance during altered sensory conditions.

REVIEW AND THEORY

Astronauts display a variety of postural difficulties upon returning to earth, including inability to maintain a stable posture with eyes closed, using a wide stance to stand and walk, feeling sensations of lateral acceleration while walking, and inability to detect small changes in head position. During the period of readaptation, the CNS must adjust weightings on sensory inputs from the visual, vestibular, and proprioceptive systems and simultaneously re-establish preflight postural movement control programs.

In the absence of appropriate otolith organ signals in weightlessness, information from other receptors, including the eyes, semicircular canals, and neck position receptors, may be used by astronauts to maintain spatial orientation and movement control. Alternatively, signals from the otolith organs may be reinterpreted by the brain. Young, et al, (1984) have proposed that during adaptation to weightlessness, the nervous system reinterprets signals from the otoliths to represent linear acceleration rather than pitch or roll of the head with respect to vertical. Maintenance of such reinterpretation following spaceflight would result in postural instability with eyes closed and increased reliance on visual information for orientation.

PROCEDURES

In the Sensory Organization Test (SOT) (EquiTest, Neurcom International) subjects are asked to stand quietly for 20 sec on a computer-controlled movable platform under six sensory conditions which alter the available visual and proprioceptive information. The six conditions of the SOT are:

1 *eyes open, quiet stance (control condition)*
2 *eyes closed, quiet stance*
3 *sway-referenced visual surround*
4 *sway-referenced support surface*
5 *sway-referenced support with eyes closed*
6 *sway-referenced support and visual surround*

By incorporating sagittal plane hip, shank and neck kinematics during the test conditions with standard center of force measurements, several descriptive measures of the postural response can be derived (Peterka and Black, 1990). Sway about the ankles and hips was plotted in a two-dimensional coordinate system. Covariance of these joint angles described the extent of sway by acting as a multivariate generalization of the univariate variance. Joint torques were calculated using a least squares estimation approach to inverse dynamics in order to reduce noise in the measurements (Kuo, 1996). Postural response gains were then computed using rms-values of either ankle or hip joint torque as output, and hip, shank, or neck angle as input.

Of the available data from astronauts who completed the SOT at NASA Johnson Space Center, ten "rookies" (mean age = 38.4 yrs) were selected. All were undergoing their first spaceflight mission of 7 to 16 days duration and seen for preflight balance testing at 10 days before liftoff, as well as postflight analysis within a few hours after egress. All results were normalized to those for preflight SOT Condition 1 (quiet stance with eyes open). The postural response gains were compared using paired t-tests for significant differences between pre- and postflight means across any of the 6 SOT conditions.

RESULTS

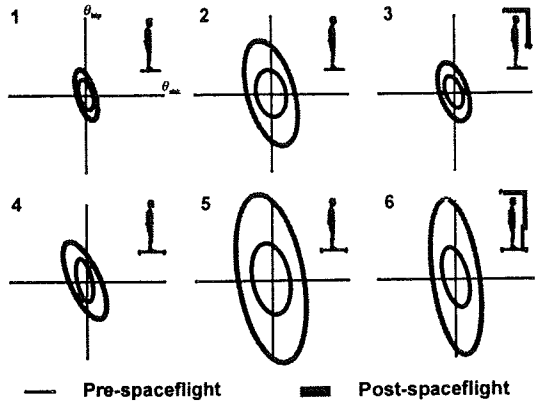

Figure 1. Covariances of hip and shank kinematics exhibit an increase following spaceflight.

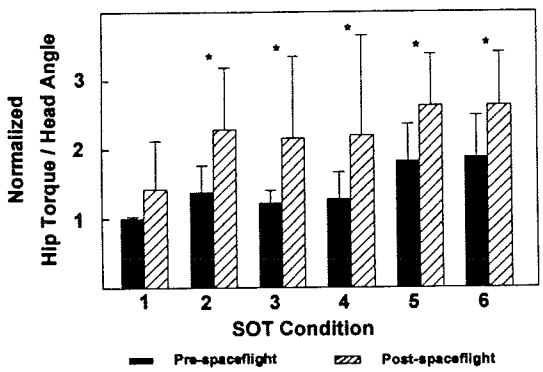

Figure 2. Postural response gain T_{hip}/θ_{pitch}. Following spaceflight, hip joint response to head pitch angle was increased for conditions 2 - 6.

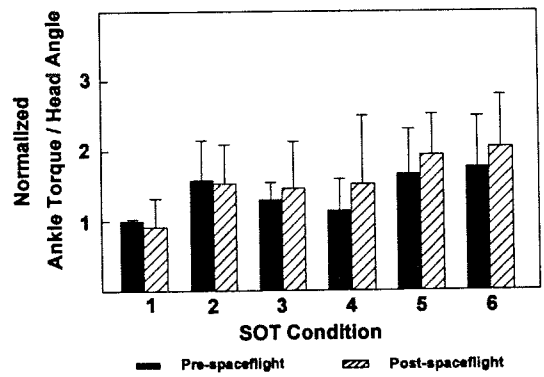

Figure 3. Postural response gain T_{ank}/θ_{pitch} Following spaceflight, the average ankle joint response to head pitch angle was unchanged.

SOT	1	2	3	4	5	6
Pre	.08	.11	.08	.12	.18	.13
Post	.14*	.17	.13*	.18	.25	.27*

Table 1. Average rms-values of head pitch angle for pre- and post-spaceflight (n = 10).

DISCUSSION

Changes in postural response due to spaceflight are multivariate in nature, as shown by the covariance ellipses having increases along different dimensions (Fig. 1). This indicates not only a change in the amount of sway, but a change in postural coordination as well. Following spaceflight, the astronauts exhibited an increase in neck motion (head pitch angle) during altered vision conditions (3 and 6), but not for the altered proprioceptive conditions (4 and 5), suggesting that they are dependent on vision in order to stabilize the head following spaceflight (Table 1).

There was greater motion in both ankle and hip joints after spaceflight, but the *gains* (ankle and hip torque in response to ankle, hip, and head motion) showed largest differences for hip torque. For example, hip torque response to head motion was significantly greater for SOT conditions 2 - 6 (Fig. 2), while there was no noticeable change in ankle torque response to head motion (Fig. 3). In a separate comparison, hip joint gain to ankle and hip motion also exhibited postflight changes while ankle joint gain to these joint angles did not. These results suggest that postural changes were due primarily to altered control of hip torque. This may be due to adaptive locomotion strategies used in weightlessness or to lingering increased sensitivity to otolith signals which were diminished during spaceflight.

REFERENCES

Kuo, A.D. *J Biomech Eng*, (in press) 1996
Paloski et al. *Ann NY Acad Sci*,747-754,1992
Peterka and Black *J Vestib Res*,1, 73-85,1990
Young, et al, *Science*, 225, 205-208, 1984

ACKNOWLEDGMENTS

NASA Graduate Student Researchers Program, NIH grant 1R29DC02312, and the NASA/NIH Center for Vestibular Research grant P60-DC02072.

THE EFFECT OF BOUNDARY CONDITIONS ON EXPERIMENTALLY MEASURED TRABECULAR STRAIN IN THE THORACIC SPINE

S. Yerby, B. Bay, E. Toh, R. McLain, M. Drews
Orthopaedic Research Laboratories, University of California, Davis, Sacramento, CA 95817

INTRODUCTION

Although a vast amount of experimental and analytical work is ongoing in order to better understand the loading behavior of trabecular bone in the spine, little direct information regarding the effects of boundary conditions has been gathered. This study addresses the differences in strain distribution of vertebral trabecular bone as a function of the loading conditions at the vertebral endplates. Vertebral specimens were elastically loaded using three different boundary conditions: 1) intact superior and inferior discs, 2) ½ of the superior and inferior discs, and 3) no discs. Minimum principal strains within the trabecular bone were measured at high spatial resolution using a texture correlation technique.

REVIEW AND THEORY

Previous studies of vertebral loading, strain, and fracture patterns have incorporated vertebral specimens either cut through the intervertebral discs or embedded in PMMA at the endplates in order to provide "parallel loading surfaces" (Guo, *et al.*, 1995; Hansson, *et al.*, 1980; Silva, *et al.*, 1996; Smith, *et al.*, 1996). However, these controlled loading configurations may not closely represent the loading of the discs on the body and may alter the loading pattern, creating erroneous results. We hypothesized that the minimum principal strain pattern will become more uniform and the statistical distribution will become more normal as the disc is removed and replaced with PMMA. The aims of this study were to measure the minimum principal strain as a function of the loading boundary conditions and compare the strain patterns and distributions between boundary conditions.

PROCEDURES

Four vertebral specimens (T10-T12) were harvested from fresh cadavers and stripped of all muscle and adipose tissues. The mean age of the specimens was 55 years. After harvesting, the specimens were sectioned on the medial and lateral sides of either the right or left pedicles, creating a 10 mm thick specimen through one of the pedicular planes. The 10 mm sections were then ground to 6.35 mm thick specimens using a customized cryo-vise and a 120 grit conical grinder affixed to a mill.

Each specimen was then placed in a custom loading frame housed in a contact radiography unit. The specimens were loaded in each of three configurations: 1) intact, 2) ½ discs, and 3) no discs. The "intact" configuration consisted of polymethlymethacrylate (PMMA) molded between the exposed endplates of T10 and T12 and the respective loading platens. The T11 vertebrae was loaded through the adjacent vertebrae and discs of T10 and T12. The "½ disc" configuration was achieved by sectioning through the mid-portion of the discs between T10 and T11, and T11 and T12. The T11 vertebrae was loaded through the remaining ½ discs. The "no disc" configuration was created by removing the remaining superior and inferior discs of T11 and placing PMMA between the endplates and the loading platens. Specimens were loaded from 0 to 150 N and contact radiographs were exposed at the 0 and 150 N load levels.

The radiographic images were captured using a 16 bit, 1024 x 1024 digital camera (Photometrics, Tucson, AZ). A 41 x 51 mesh of 2091 points was generated using Patran (Patran 3.0, Costa Mesa, CA) and minimum principal strains were measured at each point using a custom texture correlation routine (Bay, 1995). Strain patterns were compared qualitatively using contour plots spatially averaged on a point-by-point basis. Histograms of the averaged strain distributions were prepared and checked for normality (Stata 4.0, College Station, TX). Also, the mean minimum principal strains were compared between the three specimen configurations using a single factor ANOVA.

RESULTS

The minimum principal strains were concentrated near the anterior cortex and "mottled" throughout the rest of the body for the "intact" boundary condition (Figure 1). The ½ disc boundary condition showed less strain concentration at the anterior cortex and a more uniform strain distribution throughout the body. The no disc condition showed a relatively uniform strain distribution throughout the body with no distinct areas of strain concentration. The histograms

(Figure 1) show that as the boundary conditions change from "intact" to no discs, the strain distributions change from a skewed, log-normal distribution to a relatively normal distribution with strain concentrated around a central value. This is also described by the skewness values of the "intact", ½ disc, and no disc distributions: -1.87, -0.91, and -0.08 respectively. The mean minimum principal strains show that the "intact" configuration has a lower mean strain and a larger distribution than either the ½ disc or no disc configurations (Figure 2).

DISCUSSION

We have shown dramatic differences in the minimum principal strain distributions between the same specimens loaded "intact", ½ disc, and with no disc. In these lower thoracic samples, the discs seem to distribute a portion of the load, and thus strain, anteriorly. This has clinical relevance since the majority of thoracic fractures occur anteriorly (De Smet, *et al.*, 1988). Although we were unable to show a statistical difference between the results from the different boundary conditions due to the small sample size, the skewness values from the distributions show that as the disc is removed, the statistical distribution becomes more normal. There is little difference, however, between the mean strain values for the ½ disc and no disc conditions, yet a large difference between the previous two and the intact condition (Figure 2). By sectioning the discs or replacing the existing intervertebral discs with PMMA to provide "parallel loading surfaces", the load is more uniformly distributed throughout the body at a higher mean strain than the intact condition. This is represented in the histograms, contour plots, and bar graph. This uniform distribution may introduce erroneous results when comparisons to the physiologic case are made or when attempting to validate the trabecular loading response of an analytical model with intervertebral discs included.

REFERENCES

Bay BK, J Orthop Res, 13, 258-267, 1995.
De Smet AA, *et al.*, Radiol, 166, 497-500, 1988.
Hansson T, *et al.*, Spine, 5, 46-55, 1980.
Guo XE, *et al.*, Proc ORS, 41, 532, 1995.
Silva MJ, *et al.*, Proc ORS, 42, 273, 1996.
Smith EA, *et al.*, Proc ORS, 42, 604, 1996.

ACKNOWLEDGMENTS

This work was supported by grants from the Hibbard E. Williams Fund and the Whitaker Foundation.

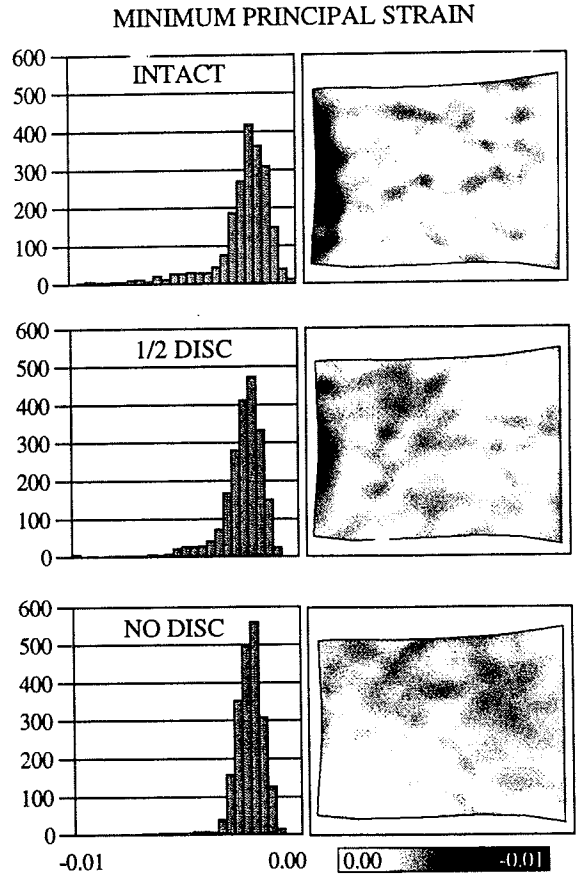

Figure 1. Histograms and contour plots of the mean population of strain values for the given boundary conditions.

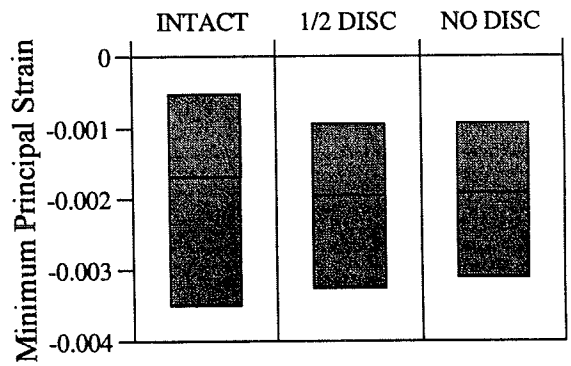

Figure 2. The mean minimum principal strains as a function of the boundary condition. The mean is bounded by one standard deviation. Note the non-normal (log-normal) distribution about the mean, particularly for the intact case.

SPINAL LOADING ON L3-4 and L4-5 DURING FREE DYNAMIC ASYMMETRIC LIFTING TASKS

K. Bolte, M. Pope

Iowa Spine Research Center, The University of Iowa, Iowa City, IA 52242

INTRODUCTION

This study measured the compressive, lateral shear and anterior-posterior (A/P) shear forces on the planes L3-4 and L4-5 during unconstrained lifting tasks.

REVIEW AND THEORY

Researchers have found that when a worker's lifting capacity is exceeded, low back pain is more likely to occur. Many biomechanical models have been developed to predict the spinal loading for different postures and activities but often, these models either constrain the motion of the lifter or simplify the musculature of the trunk.(McGill, 1992, Granata et al., 1995) The main hypotheses for this study were that spinal loading changed as the load lifted increased, as the side of the lift varied from dominant to recessive and also between disc levels. The purpose of this study was to understand spinal loading on subjects performing free dynamic, asymmetric lifting tasks using a detailed muscle model.

PROCEDURES

In order to test the hypotheses, five subjects with no history of low back pain were asked to perform seven lifts. One lift was symmetric at a load of 20 lb. Three of the lifts were from the subject's dominant side while the remaining three were from the recessive side. Each subject lifted three loads. These loads were 10 lb., 20 lb. and a final weight between 20 lb. and 35 lb. which was determined from the subject's body mass index (weight/height^2). The BackTracker™, a three-axis electrical goniometer, was implemented to measure the dynamic motion of the spine. Four Selspot cameras were used to track the motion of infrared LEDs placed on plates located on the back of the subject's calves and thighs. Another plate was mounted on the base of the BackTracker™ to identify its location in space. A force platform measured the reaction forces at the subject's feet. The BackTracker™ output also served to rotate the two cutting planes of interest: L3-4 and L4-5. The kinematics and kinetics of the lower body were used to calculate the external forces and moments acting on L3-4 and L4-5.

Eight channels of EMG were measured. These muscles were the left and right erector spinae, latissimus dorsi, abdominals and external obliques. These eight EMG measurements were then assumed to represent the activity of internal musculature for modeling purposes. (McGill et al., 1996) The additional muscle groups modeled were the internal obliques, psoas, iliocostalis lumborum, longissimus thoracis, and pars lumborum. The origin and insertion points for the muscles were adopted from McGill and then scaled based on each subject's height, depth of trunk, and width of trunk. The insertion points were rotated through space using the BackTracker™ output to determine their direction of action and their instantaneous length. The force in each muscle group was first predicted as shown in the following equation.

$$\text{Force}_i = G \cdot \frac{EMG_i}{EMG_{MVC_i}} \cdot P_o \cdot \delta + F_{pec}$$

where G is the error term, P_o is the maximum force producing potential in a given muscle, δ is the modulating term for length changes and F_{pec} is an additive term accounting for the passive elasticity of the muscle.

These forces were then optimized using Cholewicki's EMG-assisted optimization algorithm to minimize their change from the originally predicted force while balancing the external moments in three planes. (Cholewicki et al., 1994) The forces in each of the muscle groups along with the external forces were summed to determine the compressive, lateral shear and A/P shear forces on the lumbar spine at the planes L3-4 and L4-5.

RESULTS

Five points during the lift were identified. These points were: 1) halfway between the first motion of the subject and the point where the load was lifted, 2) at load lift, 3) halfway between load lift and load placement, 4) at load placement, and 5) halfway between load placement and end of motion. An analysis of variance was performed on the data to test the hypotheses stated at the beginning of this abstract. Significant differences were found between disc levels for the compressive and A/P shear forces ($p < 0.05$). A trend was found for the effect of weight lifted on the A/P shear forces ($p = 0.079$). Significant differences were also found between the different points during the lifting sequence ($p < 0.0001$).

The mean compressive, lateral shear, and posterior shear forces varied from 5345.2 N to 8346.9 N, -1205.2 N to 562.7 N, and 1860.0 N to 3004.3 N, respectively depending on the weight of the load lifted and the side on which the subject lifted. The variation in compressive, lateral shear and A/P shear forces can be viewed in Figure 1.

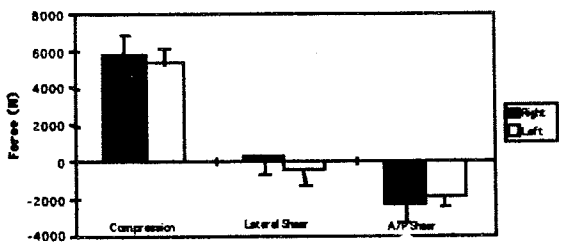

Figure 1: Mean compressive, lateral shear and A/P shear forces for a 20 lb. lift from both the right and left sides.

A sample of the forces acting on the level, L3-4, for a subject lifting 20 lb. from the dominant side is shown in Figure 2.

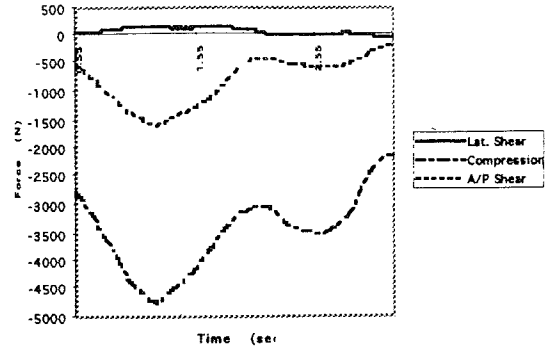

Figure 2: Forces acting through L3-4.

DISCUSSION

This model calculated the forces acting through two cutting planes while allowing co-contraction of the trunk muscles and balancing the external moments for a free dynamic asymmetric lifting task.

The ranges of spinal forces appear to be similar to those found by Cholewicki et al. (Cholewicki et al., 1995) and also by Granata and Marras (Granata et al., 1995). Although significant differences were not found for the load lifted and the variation in the side of the lift, the authors believe this may be the result of a limited subject population. Further testing may reveal these differences.

The authors conclude that spinal compressive and A/P shear forces differ from level L3-4 to L4-5. In addition, the spinal compressive forces are extremely different depending on the point during the lift, with maximum forces occurring at load lift. Further investigations aim to show significant variations with the weight of the load lifted and also as the side of the lift changes.

REFERENCES

Cholewicki J. et al. J Biomech, 27, 1287-1289, 1994.
Cholewicki J. et al. J Biomech, 28, 321-331, 1995.
Granata K.P. et al. J Biomech., 28, 1309-1317, 1995.
McGill S.M. J Biomech, 25, 395-414, 1992.
McGill S.M. et al. J. Biomech, 29, 1503-1507, 1996.

LEG MUSCLE STRENGTH AS A LIMITING FACTOR IN LIFTING TASKS

T. A. Buhr and D. B. Chaffin

Department of Biomedical Engineering, University of Michigan, Ann Arbor, MI 48109

INTRODUCTION

In a survey of 9805 currently or formerly employed individuals ages 55-74, up to 41% reported having difficulty stooping, crouching, kneeling, or lifting or carrying 25 pounds. (Kovar et al., 1987) Difficulty or inability increased with increasing age, and was much greater for women than for men.

To examine how declines in functional abilities may lead to the inability to perform such tasks, the specified areas of difficulty were combined for a pilot study into a 15 kg low lifting task which required some form of a stoop or crouch to lift a small box. Since functional declines were confounded in the older subjects, a forward dynamic model was developed to further explore the effects of specific leg strength declines on lifting tasks.

REVIEW AND THEORY

Age-related declines in functional abilities, such as strength, balance, and joint range of motion, has been well-documented. (Schultz, 1992) In addition, many studies have examined the relationship between these functional declines and various activities of daily living in elderly adults, such as the sit-to-stand task. (Hughes *et al.* ,1996; Schultz *et al.*, 1992; Pai *et al.*, 1994)

Not as well studied have been employment-related tasks in older workers. Most studies of manual materials handling tasks have focused on the abilities of younger people. For example, Schipplein *et al.* (1990) found that healthy young subjects would change lifting techniques as their quadriceps muscles were pushed to their strength limits. Such results indicate a need to extend the studies to the older working population and their functional abilities.

Results from our initial pilot study of the heavy low-lifting task indicated that strength declines affected the lifting motions and abilities more than balance abilities or joint ranges of motion. One of the older subjects was in fact unable to perform the lifting task, apparently limited by her weak muscles. It remained unclear just how the weakness at each joint contributed to her overall inability. Therefore, the purpose for this study was to model how typical age-associated declines in leg muscle strength could affect the capability of performing a heavy low-lifting task.

PROCEDURES

Subjects

Twelve healthy, active, highly-motivated women ages 25-69 participated in the pilot study data collection phase. To control for anthropometric differences, only women within the height range of 160-170 cm were selected to participate.

Data Collection and Tasks

A Biodex™ dynamometer was used to collect isometric and isokinetic strength measurements at the hips, knees, and ankles of all subjects.

For the lifting task, subjects were asked to squat down and vertically lift a small (16cm x 21cm x 20cm) 15kg box from the ground to waist height. Reflective markers placed at the major body joints were tracked with MotionAnalysis™ software. A dynamic biomechanical program calculated joint angles and torques used.

Model

A planar, three-link rigid body inverted pendulum model was developed, similar to that used by Kuo *et al.*, (1995) Model links included the shank, thigh, and combined head, trunk, upper extremities and box, and were connected with ideal hinge joints.

The dynamic equations of motion were derived through Kane's equations, and were of the form:

$$\ddot{\Theta} = M(\Theta)^{-1}[T(\Theta,\dot{\Theta}) - C(\Theta)\dot{\Theta}^2 - G(\Theta)]$$

Where: M is the mass matrix, T is the matrix of applied external torques, C is the matrix of coriolis and centrifugal effects, G is the matrix of gravitational effects, Θ is the vector of joint angles, $\dot{\Theta}$ is the vector of joint angular velocities, and $\ddot{\Theta}$ is the vector of joint angular accelerations.

Muscle forces were modeled as applied external torques acting on the links, with the basic torque polynomials derived from the joint torque-muscle length relationships of the actual pilot study lifting tasks. In the simulations, joint torque polynomials were decreased by fixed percentages to approximate strength declines. The initial starting posture was based on postures used by the strongest subjects during the pilot study. Analysis was completed with a differential equations solving computer program.

RESULTS

Each strength limitation had its own effects. With small hip strength declines, the initial lifting postures with less forward flexion at the hip and more flexion at the knee still resulted in the weak model figure successfully lifting. Decreasing applied hip extension torques up to 60% (as measured in the one subject unable to lift the box), confirmed that the individual would not be able to lift her torso and the box.

The more squat-like initial starting posture was most limited by weak knee extension strength, with declines of only 20% in strength resulting in predicted inability to complete the lifting task. Two different strategies could be used to compensate for weak knee extension strength. Alteration of the initial posture to one with greater flexion at the hips and less flexion at the knees resulted in lower torques about the knees and a successful lifting simulation. (See Figure 1.) Also successful was the strategy of altering the extension torques used at neighboring joints. In this case, a successful lifting simulation resulted from the more flexed starting position if smaller muscle torques were used at the hip and ankle.

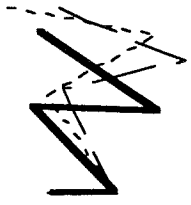

Figure 1. Postures at initiation of successful lifts.
——— Strong subject, or weak hip extension.
— — Weak knee extension strength.
- - - - Weak ankle plantarflexion strength.

The model demonstrated that both types of strategies could also be used to overcome weak ankle plantarflexion strength. In those cases, the model predicted that either an initial lifting posture with less flexion at the ankle or a strategy of using greater hip extension torque would be required to accomplish the task.

DISCUSSION

From this work, it was concluded that muscle strengths at all leg joints make important contributions to the kinematics of the lifting task. This supports studies such as the earlier cited work of Schipplein *et al.* (1990) In some cases, strength deficits can be overcome by the redundancy of the linkage system, compensating for a deficit in one area by increasing extension torques in another area. In other cases, strength deficits can be overcome by changing the initial lifting posture to one which decreases torques about the affected joint. Since the subjects of the pilot experiment had strength deficits at multiple joints, exact confirmation of a specific strategy was impossible, although subjects appeared to use both types of strategies.

Severe limitations at one joint or combined limitations at multiple joints can lead to an inability to perform a lifting task. This has important ramifications for employment-related tasks as well as for activities of daily living.

REFERENCES

Hughes, M.A. et al. J Biomech, 29,1509-1513,1996.
Kovar, M.G. et al. Adv Data,136,1-11, 1987.
Kuo, A.D. et al. J Biomech,26(S),137-150,1993.
Pai,Y-C. et al. Arth Rheum,37,1297-1304, 1994.
Schipplein, O.D. et al. J Biomech, 23,907-912, 1990.
Schultz, A.B. J Biomech, 25,519-528, 1992.
Schultz, A.B. et al. J Biomech, 25,1383-1391,1992.

ACKNOWLEDGMENTS

The authors would like to acknowledge the Whitaker Foundation for their support of a graduate fellowship for Ms. Buhr.

CHANGES IN MUSCLE RECRUITMENT PATTERNS DURING FATIGUING DYNAMIC TRUNK EXTENSION EXERTIONS

PJ Sparto[1], M Parnianpour[2]

[1]Biomedical Engineering Center, The Ohio State University, Columbus, OH 43210
[2]Dept. Industrial, Welding & Systems Engineering, The Ohio State University, Columbus, OH 43210

INTRODUCTION

Low back pain continues to be a major source for Workers' Compensation payments and leading cause for time lost at work. Reduced trunk extensor muscle endurance and the performance of repetitive lifting appear to be strongly implicated as a risk factors for acquisition of low back pain (Biering-Sorensen, 1984, Andersson, 1981). However, the role that fatigue plays in the development of low back injury is unclear. The purpose of this study was to quantify the trunk muscle recruitment patterns during repetitive dynamic extension exertions. It was hypothesized that fatigue would result in greater activation of all the trunk extensor muscles.

PROCEDURES

Trunk muscle electromyography (EMG) and torque output were measured in 16 healthy men [mean (s.d.) 23 (3) yrs, 178 (5) cm, 79 (9) kg] as they performed repetitive trunk extension exertions. A factorial design consisting of two load levels (35% and 70% of the maximum dynamic trunk extension torque) and two repetition rates (5 and 10 reps per minute) was implemented in order to cause different rates of fatigue. Each of the four load/rep combinations was tested during a single session, with at least one week in between. After the subjects stretched, bi-polar surface electrodes were applied to the skin. Three bilateral trunk extensor muscles were sampled - latissimus dorsi (LAT), erector spinae (ERS), and posterior internal obliques (PINO) (Mirka, 1991) - as well as three trunk flexors - rectus abdomini (RAB), external obliques (EOB) (Mirka, 1991), and anterior internal obliques (AINO) (McGill and Norman, 1986).

The pelvis and lower extremities of the subjects were restrained within a trunk dynamometer. Maximal voluntary isometric exertions in each of the six cardinal directions were performed at 17.5 degrees of forward flexion, to measure the maximum electromyographic activity of each muscle. The average of 3 dynamic maximal voluntary contractions (MVC) in trunk extension was obtained, in order to measure the initial maximum torque generating capability. During the dynamic exertions, subjects extended their trunks from a forward flexion posture of 35 degrees to upright standing, at a constant velocity of 15 degrees per second. The torque was measured using a load cell and knowing the distance from the point of force application to the center of rotation of the trunk. Two minutes of rest was provided between all maximum exertions.

During the repetitive endurance test, trunk extension was performed at 15 deg/sec while subjects controlled their torque output at 35% or 70% of the initial dynamic MVC, by using visual feedback displayed on a computer monitor. The exertion rate, 5 or 10 reps per minute, was regulated by an audible tone. Once per minute, a dynamic MVC was performed, to quantify the reduction in the maximal torque generating capability (fatigue). The exertions continued until a 35% reduction in the MVC occurred, the subject could no longer continue, or 30 minutes elapsed.

The raw EMG from each exertion was sampled at 1536 Hz, rectified, and low pass filtered at 3 Hz (McGill). After normalizing with the maximum EMG obtained from the isometric MVCs, the root-mean-square (rms) value of the EMG between the trunk angles of 25 and 10 degrees of flexion was computed. From the exertions whose rms torque was within 5% of the designated load level, the change in EMG with time, or SLOPE, was quantified using linear regression. In order to obtain an estimate of the slope for each muscle group, the slopes were averaged for the right and left muscle pairs. The effect of the load magnitude and repetition rate on the slope was tested using repeated measures multiple analysis of variance (MANOVA).

RESULTS AND DISCUSSION

The effect of the repetitive endurance test on the decline in maximum torque generating capability and change in muscle recruitment is readily apparent in Figure 1. For this test, the maximum torque declined by 35% in about 4 minutes, during which the EMG of the left latissimus dorsi muscle increased by 10%.

The endurance time (point at which the predicted maximum torque declined by 35%) for each of the load/reps combinations is shown in Table 1. The effect of load, repetition rate, and their interaction on the endurance time were all highly significant ($p<.001$), indicating the study design was effective at eliciting different rates of fatigue. It can be seen that doubling the repetition rate from 5 to 10 reps/min had a greater effect in causing fatigue than doubling the load magnitude.

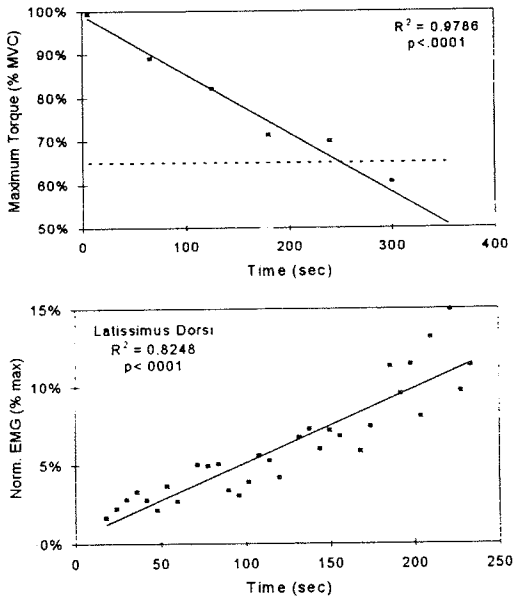

Figure 1: Top: Decline in maximum dynamic torque generating capability during an endurance test performed at 35% MVC, 10 reps/minute. A 35% decline in torque is indicated by the dashed line. Bottom: The normalized EMG of the left latissimus dorsi during the same test.

	35% MVC	70% MVC
5 reps/min	24.1 (8.1)	9.8 (3.8)
10 reps/min	5.7 (3.9)	2.4 (0.9)

Table 1: Mean (s.d.) endurance time, in minutes, for the 4 load/reps endurance tests.

The results of the MANOVA indicated that as a group, the slopes of all muscles were significantly affected by the effects of load, repetition rate and their interaction ($p<.005$). Furthermore, Table 2 demonstrates that significant differences in slope were found in each of the trunk extensor muscles (LAT, ERS, PINO). Figure 2 shows the mean slope as a result of the interaction between load and repetition rate for the latissimus dorsi. The other extensor muscles display a common pattern.

SLOPE	Load (L)	Reps (R)	L * R
LAT	.0001	.0001	.0011
ERS	.0001	.0001	.0001
PINO	.0001	.0001	.0007
RAB	.0209	.0094	.2441
EXO	.0636	.0836	.2947
AINO	.4040	.1338	.3949

Table 2: P-values from the univariate ANOVA, testing the effect of load, repetition rate, and interaction on the slope.

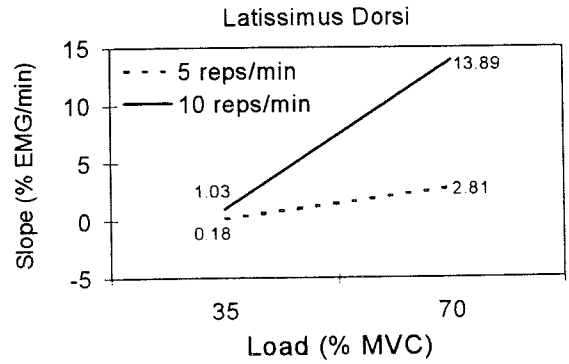

Figure 2: Increase in slope of the regression between the normalized EMG of the latissimus dorsi and time, due to the interaction between the load and repetition rate.

Because of the ambiguity in relating the amplitude of the time-domain EMG to muscle tension, we cannot speculate if the increase in activation resulted in greater muscle force, or represented a decreased efficiency in EMG/force production due to fatigue. Furthermore, it is not known if the function of the increased activation of the secondary trunk extensors (LAT and PINO), is to provide greater stability, or augment the torque generation. The increased and altered trunk extensor muscle activation due to fatigue requires further investigation to determine its effect on the spinal loading.

REFERENCES

Andersson G.B.J. Spine, 6, 53-60, 1981.
Biering-Sorensen F. Spine, 9, 106-119, 1984.
McGill and Norman, Spine, 11, 666-678, 1986.
Mirka G.A. Ergonomics, 34, 343-352, 1991.

ACKNOWLEDGMENTS

We are grateful for the support from the NIDRR, RERC grant #H133E30009, the Presidential Fellowship from the Ohio State University, and Profs. WS Marras and SR Simon.

VARIABILITY IN TRUNK AND SPINAL LOADS DURING REPEATED LIFTING EXERTIONS

K.P. Granata, W.S. Marras
Biodynamics Laboratory
The Ohio State University

INTRODUCTION

Risk of chronic low-back injury is typically associated with spinal loads incurred during lifting tasks. Mirka and Marras (1993) suggest that biomechanical variability also influences the risk of injury. Although a particular exertion may generate spinal loads safely below injury tolerance thresholds, variability in the biomechanical performance during repeated exertions may result in a significant number of the exertions exceeding injury tolerances. Considering biomechanical performance variability can influence the risk of low-back pain (LBP), it is necessary to 1) quantify the magnitude of the variability and 2) identify the factors that influence it.

METHODS

Twelve healthy males including 7 college students and 5 experienced manual materials handling employees volunteered to participate. The average height and weight of the subject population was 179.2 ±4.5 cm. and 74.7 ±7.0 kg. respectively. Subjects were required to lift 13.6 kg. and 27.3 kg. boxes from a knee height platform to an upright posture. Lifts were performed at two levels of task asymmetry (sagittally symmetric, 60^0 right), and two subjective lifting velocities (preferred lifting velocity, faster than preferred). Asymmetric tasks were achieved by requiring the subject to lift the weighted box from a knee height platform located 60^0 to the subject's right.

Lifting exertions were performed one at a time, with one minute of rest between exertions to minimize the possibility of fatigue. Each condition was repeated ten times. Trials were randomized with respect to weight, asymmetry, lifting velocity and repetition number.

Three-dimensional trunk motion data were recorded from a Lumbar Motion Monitor (Marras et al 1992), and dynamic external trunk loads were determined from a force plate and electromechanical tracking goniometers (Fathallah 1995, Granata 1996).

EMG data from the right and left erector spinae, rectus abdomini, latissimus dorsi, external abdominal obliques, and internal abdominal obliques were collected and processed as described in Marras and Mirka (1993). EMG data were normalized by maximum values collected during maximum static flexion, extension, right twist, left twist, right lateral, and left lateral exertions.

A biomechanical model employed the EMG, kinetic, and kinematic data as input to compute the dynamic loads on the spine (Granata and Marras 1995, Marras and Granata 1995).

RESULTS

Inter-class correlations were examined to describe the relative variability associated with each independent factor. As expected, the weight of the box accounted for a significant amount of the variability associated with dynamic sagittal trunk moment and spinal compression, whereas task asymmetry strongly influenced the lateral and twisting moments and spinal AP and lateral shear loads (Table 1). However, trial-to-trial variations describe nearly one quarter of the sagittal trunk extension moment variability and 35% of the lateral moment variability. Trial-to-trial variability in spinal load ranged from almost 20% in compression to nearly 50% in lateral shear load. Thus, spinal load changes from one exertion to the next despite identical task designs.

	Trunk Moment (% Var)		
	Sagittal	Lateral	Twist
Wt	4.68	0.00	0.00
Vel	18.66	0.61	5.24
Asym	32.37	93.37	80.92
Trial	44.28	6.02	13.82

	Spinal Load (% Var)		
	Lat Shear	AP Shear	Compress
Wt	8.22	21.85	59.39
Vel	5.49	5.18	1.44
Asym	38.72	42.79	20.58
Trial	47.56	30.18	18.59

Table 1. Inter-Class Correlation results.

Recognizing that trunk dynamics significantly influence trunk moments and help to explain spinal loads, it was not be surprising that the kinematic and kinetic inter-class correlation distributions look similar. None-the-less, it is important to note that trial-to-trial variability explained 42% to 77% of the task acceleration variability. Hence, performance of identical

lifting tasks does not necessarily produce similar lifting kinetics or kinematics.

Box weight and task asymmetry dramatically influenced the width of the spinal load variability distributions. ANOVA and post-hoc results (Table 2) demonstrated variability in the AP shear and compressive loads on the lumbo-sacral spine increased 43% and 20% respectively as the box weight increased from 13.6 to 27.3 kg. Task asymmetry significantly increased AP shear load variability, lifting experience was associated with a 38% increase in spinal compression variability. Coefficients of variation, i.e. STD/Mean, illustrated that increases in spinal load variability was more than can be attributed to a proportional increase in the mean values.

		Lat Shear (N.)	AP Shear (N.)	Compress (N.)
Exper	Inexp	**86.0**	**174.0**	**502.6**
	Exp	**155.1**	**290.8**	**692.0**
Wt (kg)	13.6	113.6	**191.5**	**543.3**
	27.3	127.5	**273.2**	**651.3**
Vel	Prefer	115.5	249.2	617.1
	Fast	125.6	215.5	577.6
Asym	0^0	120.1	**176.2**	556.3
	60^0	121.0	**288.6**	638.4

Table 6. Post-hoc analyses of spinal load variability. Bold numbers note significance differences at $\alpha<.05$

DISCUSSION

These analyses have demonstrated that identical lifting tasks in terms weight, origin, and destination will generated a wide range spinal loads. The exertions performed here generated mean dynamic spinal compressions of 5790 ±1480 N. Although the mean compressive load on the spine was below the NIOSH (1981) limit of 6400 N, over 20% of the lifts exceeded the recommended injury threshold. Therefore, it is necessary to recognize biomechanical variability associated with a lifting task and the factors that influence that variability.

Our analyses have demonstrated that parameters such as box weight and task asymmetry can increase the variability in trunk motion and force. Previous research efforts demonstrated that muscle co-contraction similarly increases with task asymmetry and box weight, but were unable to explain the reason behind this increased activity (Marras and Mirka, 1993). We agree with others (Zetterberg et al. 1987) who have hypothesize that the increased co-contraction is recruited to stabilize the trunk against injury associated with the increased variability in trunk motion and force.

The risk of occupationally-related LBD has been linked to asymmetric postures in the workplace (Kelsey 1984, Marras et al 1993). Our results demonstrate that both spinal load and spinal load variability increase significantly with task asymmetry. Increased spinal load variability with task asymmetry will increase the relative number of exertions that exceed biomechanical tolerances. Furthermore, the capacity to control increased lateral and twisting moment variability may be challenged during asymmetric exertions due to reduced lateral and transverse plane trunk strength (Parnianpour et al 1991, Marras and Granata 1995). Variability in spinal loading patterns associated with asymmetric lifting tasks may help explain the relation between LBD and asymmetric lifting tasks in industry.

When interpreting these results, one must consider the limitations associated with the study design. First, subjective lifting velocities were selected to avoid artificially influencing the motion variability. However, the resulting motions failed to generate significantly different trunk velocities between the two conditions. Therefore, it was not possible to examine the influence of velocity upon the variability of spinal loading. Future research may attempt to examine the repeatable lifting variability as a function of trunk velocity. Second, the length of time to complete all of the repeated exertions and experimental conditions was less than two hours. Future research might examine how daily fatigue may affect the kinetic and kinematic variability associated with a task.

REFERENCES

Fathallah FA. Ph.D. Dissertation, Ohio State Univ, 1995

Granata KP, Marras WS. *J. Biomechanics* 28, 1309-1317, 1995

Granata KP et al. *J Biomechanics* 29, 1219-1222, 1995

Kelsey KL. Et al. *J. Ortho. Res.* 1984; 2 (1): 61-66

Marras WS. et al. *Int. J Ind. Ergon* 1992; 9: 75-87

Marras WS, Granata KP. *Spine* 20, 1440-1451, 1995

Marras WS et al. *Spine* 18, 617-628, 1993

Mirka GA, Marras WS. *Spine* 18, 1396-1409, 1993;

NIOSH (1981) Tech. Report No.81-122, U.S.

Parnianpour M. et al. *Intl. J. Ind. Ergon.* 8, 279-287, 1991

Zetterberg C. et al. *Spine* 12, 1035-1040, 1987

ESTIMATION OF 3D MOMENTS AT L5/S1 USING A DYNAMOMETRIC BOX : A COMPARATIVE VALIDATION STUDY

G. Drouin [1] & D. Gagnon [2], & A. Ghorbal [2]

[1] Groupe de recherche en réadaptation physique, IRDPQ, Québec, Canada, G1M 2S8

[2] Laboratoire de biomécanique occupationnelle, Université de Sherbrooke, Canada, J1K 2R1

INTRODUCTION

Low back pain (LBP) is a widespread problem in modern society. In the workplace, it affects mainly manual material handling (MMH) workers. Studies of the back using biomechanical modeling provide insight into the stresses exerted on body structures. They also provide a non-invasive tool to better understand LBP phenomenon. The present study attempted to validate a new biomechanical approach that could be more adapted to assess real workplace situations.

REVIEW AND THEORY

Real MMH tasks are difficult to study mainly because of limitations imposed by the instrumentation. In general, studies use two dimensional (2D) motion analysis restricting upper and lower limb movements to one plane. However, the presence of three dimensional (3D) asymmetric loading is recognized for MMH (Gagnon & Gagnon, 1992) and for gait (Eng & Winter, 1995). The results regarding MMH are in accordance with epidemiological observations (Baril-Gingras & Lortie, 1995; Kuorinka, 1992). In many 2D studies, upper body modeling (DOWNWARD) was used to better represent MMH but most 3D studies used lower body modeling (UPWARD) (de Looze et al., 1992; Kromodihardjo & Mital, 1986, Plamondon et al., 1996). We propose a new 3D approach using a dynamometric box. The interest in this approach comes from its potential for adaptation and applicability to real workplace situations without affecting the accuracy of low back loading estimation at lumbosacral joint (L5/S1).

PROCEDURES

Eight male subjects executed four tasks involving the handling of a 12-kg box : (1) free lifting with lower limb displacement (LLD), (2) free lowering with LLD, (3) free lifting without LLD and (4) fast lifting without LLD. A five-camera video system, two force plateforms and a custom designed dynamometric box were synchronized to collect 3D kinematics and external forces applied on the feet and hands. Two dynamic 3D multisegmental models were used (Larivière & Gagnon, in press). An UPWARD model included 7 body segments of lower limbs and the pelvis and was used as the gold standard. A DOWNWARD model included 8 body segments of upper limbs and trunk. Net moments at the common joint for both models (L5/S1) were compared through : (1)cross-correlation of moment-time curves, (2) model random-error sensitivity and (3) absolute differences in moment amplitude. The L5/S1 moment was resolved in three orthogonal components of a local reference system fixed on the pelvis : longitudinal (L), sagittal (S) and transverse (T) axes.

RESULTS

	Resultant (R) and components of moment			
	L	S	T	R
TASKS	Coefficient of correlation mean ± standard deviation			
TASK 1	0.653 ±0.115	0.826 ±0.187	0.994 ±0.002	0.995 ±0.001
TASK 2	0.862 ±0.100	0.913 ±0.080	0.997 ±0.001	0.997 ±0.001
TASK 3	0.762 ±0.197	0.987 ±0.009	0.996 ±0.002	0.995 ±0.002
TASK 4	0.627 ±0.109	0.964 ±0.014	0.990 ±0.005	0.989 ± 0.006
TOTAL	0.723 ±0.158	0.919 ±0.120	0.994 ±0.004	0.994 ±0.004

note : critical coefficient value was 0.895.

Table 1 : Cross-correlation coefficient between curve forms of moment at L5/S1 estimated by both models.

As shown in Table 1, the longitudinal component curve of net moment seems to be problematic in all tasks. The test of sensitivity (Table 2) also reveals an important random-error on the same component in both models that mainly results from joint center location variability. This fact decreases the precision and accuracy of estimated L5/S1 loading for both models.

MODELS	L	S	T
	CASE 1 mean ± standard deviation (maximum) in Nm		
UPWARD	5 ± 3 (21)	7 ± 5 (28)	7 ± 5 (26)
DOWNWARD	4 ± 3 (17)	5 ± 4 (22)	6 ± 4 (21)
	CASE 2		
UPWARD	13 ± 10 (64)	12 ± 9 (46)	7 ± 5 (32)
DOWNWARD	11 ± 8 (47)	11 ± 8 (46)	6 ± 5 (24)

note : Case 1 : sequence of free lifting withoout LLD
Case 2 : sequence of LLD without lifting

Table 2 : Random-error sensitivity at L5/S1 for both models.

The absolute differences in moment amplitude shows a significant gap between models on the transverse component (Figure 1). It may be partly attributed to trunk segment parameters calculated by equation of regression.

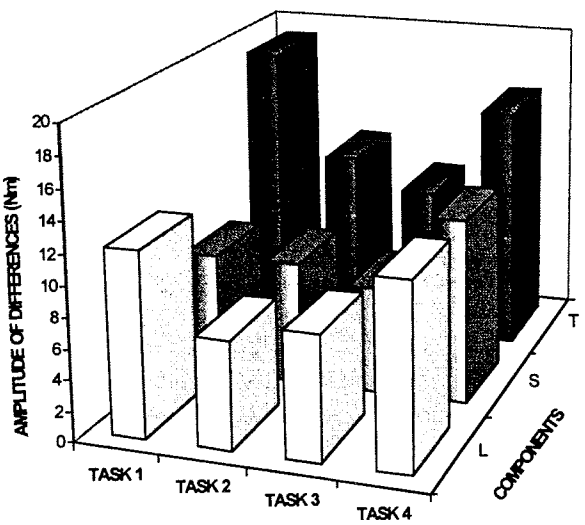

Figure 1 : Absolute differences in L5/S1 moment amplitude between both models.

DISCUSSION

Results show a partial validity of the new approach using a dynamometric box. At this point, it would seem important to improve modeling through a better adjustement of the individual body segment parameters for the subsections of the trunk. The precision and accuracy of the location of some joint centers should be improved to reduce errors on the moment at L5/S1. However, because workers are often involved in locomotion when handling a load, the approach using a dynamometric box has potential for the future since it allows the biomechanical analysis of MMH including weight transportation. Techniques and strategies used in the workplace that were never assessed biomechanically before could then be successfully investigated. However, additional developments in instrumentation and 3D modeling are necessary to take the approach out of the laboratory and to use as a diagnostic tool.

REFERENCES

Baril-Gingras, G. & Lortie, M. *Ergonomics*, **38**, 905-925, 1995

de Looze, M. P. et al. *Clinic. Biomech.*, **7**, 161-169, 1992.

Eng, J.J. & Winter, D.A. *J. of Biomech.*, **28**, 753-758, 1995.

Gagnon, D. & Gagnon, M. *J. of Biomech.*, **25**, 891-901, 1992.

Kromodihardjo, S. & Mital, A. *Int. Journ. of Industrial Ergonomics*, **1**, 77-90, 1986.

Kuorinka, I. et al. *Ergonomics*, **37**, 655-661, 1994.

Larivière, C. & Gagnon, D., *Clin. Biomech.*, (in press).

Plamondon, A. et al. *Clinic. Biomech.*, **11**, 101-110, 1996.

ACKNOWLEGMENTS

This work received the financial support of Natural Sciences and Engineering Research Council of Canada and Institut de Recherche en Santé et Sécurité au Travail du Québec. We thank Christian Larivière, Brad McFadyen, Karine Ainsley and Sophie Dancause for their technical assistance.

THE EFFECTS OF TRANSVERSE, ANTERIOR COLUMN, AND POSTERIOR COLUMN ACETABULAR FRACTURES ON THE STABILITY OF THE HIP JOINT

Kevin A. Thomas, Kirstin K. Widding, Mark S. Vrahas
Department of Orthopaedic Surgery, Louisiana State University Medical Center
New Orleans, LA 70112

PURPOSE

Posttraumatic arthrosis may result from unreduced acetabular fractures. This is particularly true if the fracture crosses a portion of the acetabulum necessary for weight bearing. However, the exact portion of the acetabulum necessary for normal weight bearing is not known. At the very least, normal weight bearing requires a stable hip joint. Thus, an acetabular fracture that affects hip joint stability can be assumed to invlove an important weight bearing area. Such a fracture, if left unreduced, most likely would lead to arthrosis. The purpose of this study was to assess how various transverse, anterior column, and posterior column acetabular fractures affect hip joint stability.

METHODS

A total of 24 fresh-frozen cadaveric hip joints were used in this investigation. All soft tissues were removed. Each specimen was mounted in a mechanical testing machine so that compressive forces of various magnitudes could be applied. The femur was mounted vertically on a freely moving instrumented x-y displacement table. Stability of the hip joint depended upon only the intrinsic stability of the articulation between the femur and the acetabulum. The acetabulum was mounted in a fixture that allowed simulation of the various fractures and allowed positioning of the joint so that the magnitude and direction of the peak forces seen during normal gait could be applied. For each of the fracture types, the specimens were loaded in compression four times at each of three loads (800 N, 1200 N, and 1600 N). Each specimen was first tested intact, and again following each of the various simulated fractures. Simultaneous recordings were made of the load, actuator displacement, and translation of the femur. A hip was considered stable if no dislocations occurred over the four loading cycles.

Transverse acetabular fractures were evaluated in 12 specimens. Each specimen was tested with successive transverse fractures having roof-arc angles of 60°, 50°, 40°, 30°, and 20°. The roof-arc angles were determined radiographically. Anterior column fractures were evaluated in an additional 6 specimens. For each specimen, very low, low, intermediate, and high fractures were tested successively. Posterior column fractures also were evaluated in 6 additional specimens; very low (at the level of the ischial spine) and low (just superior to the ischial spine) posterior column fractures were tested.

RESULTS

All 24 intact hips were stable when loaded to 800 N, 1200 N and 1600 N. For the transverse fractures, for each of the applied loads, the number of stable specimens decreased with each successive fracture (Figure 1). For these fractures, stability was significantly affected by both the location of the fracture (roof-arc angle) and the magnitude of the applied load. For the anterior column fractures, all specimens with very low, low, and intermediate fractures remained stable throughout all tests (Figure 2). With high anterior column fractures, 66% of specimens were stable when loaded to 800 N, only 33% were stable when loaded to 1200 N, and none were stable when loaded to 1600 N. Overall, the posterior column fractures were the least stable (Figure 3). All six specimens were unstable with the simulated low fracture (exiting the posterior column just superior to the ischial spine).

DISCUSSION

The simulated fractures produced in this investigation do not exactly imitate fractures that occur *in vivo*. However, this study does provide new information concerning what portions of the acetabulum may be critical for

weight bearing. This study suggests that the radiographic roof-arc angle is a useful technique for evaluating transverse acetabular fractures. It is generally accepted clinically that transverse fractures with roof-arc angles of 40° or less affect an important weight bearing portion of the acetabulum. The present results support this belief. Nearly 100% of the specimens (11 of 12) were unstable with transverse fractures at the 40° roof-arc angle. No specimen was stable with a fracture having a roof-arc angle of 30° or 20°. However, a substantial number of specimens were unstable with transverse fractures at the 50° and 60° roof-arc angles, with instability directly proportional to the magnitude of the applied load.

Anterior column fractures were more stable than expected. No specimen was unstable unless the fracture was of the high type. Fractures at the base of the pubic rami did not affect stability. This suggests that fractures at the base of the pubic ramus may be less important then previously thought. Only those fractures that exited through the iliac crest caused instability.

Posterior column fractures were much less stable than expected. Even low fractures, that is fractures just superior to the ischial spine, rendered the hip unstable in all six specimens, even at the lowest applied load.

CONCLUSIONS

The results of this study have direct implications in the treatment of anterior column and T-type fractures. Based on these results, currently only anterior column fractures that exit through the iliac crest are treated surgically. For T-type fractures, the posterior column is the greater concern, and requires reduction and fixation even if the fracture is very low. The anterior column portion of the fracture is of concern only if it is the high type.

ACKNOWLEDGMENTS

This investigation was supported in part by a research grant from the Orthopaedic Trauma Association.

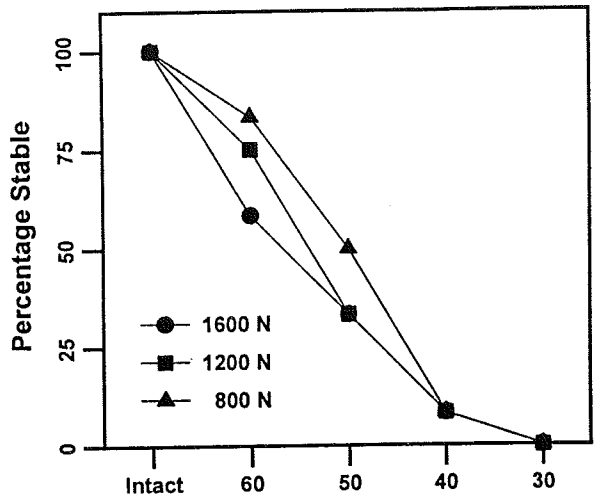

Figure 1: Transverse Fracture Roof-Arc Angle, *degrees*

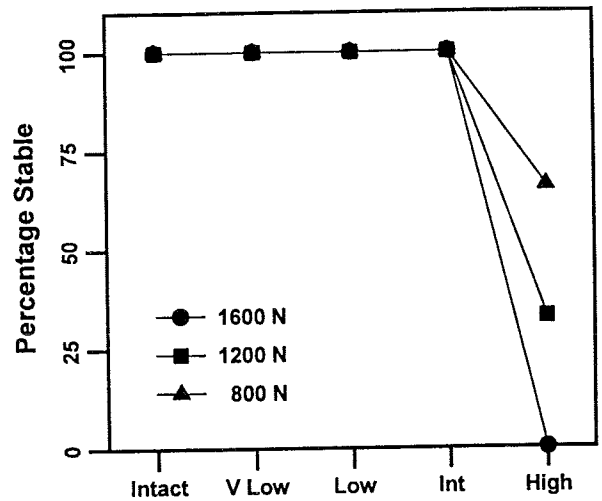

Figure 2: Anterior Column Fractures

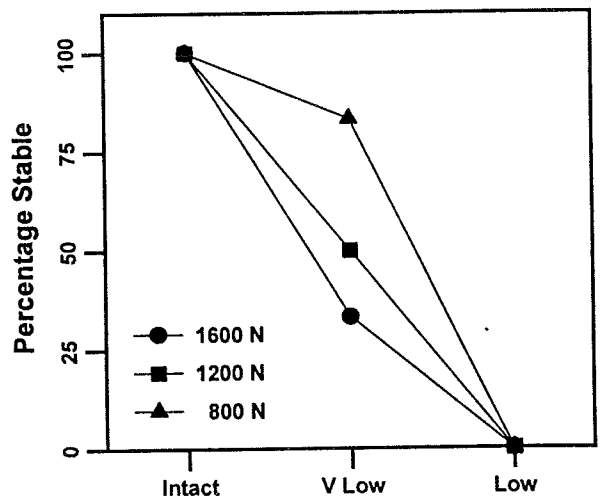

Figure 3: Posterior Column Fractures

EFFECT OF FIXATION AND STORAGE CONDITIONS ON THE TORSIONAL PROPERTIES OF TIBIAE FROM SHAM-OPERATED AND OVARIECTOMIZED EWES

C. Beardsley[1], A.S. Turner[2], D. Barlow[1], H. Aberman[1]
[1] Howmedica R&D, Rutherford, NJ 07070
[2] Department of Clinical Sciences, Colorado State University, Fort Collins, CO 80523

INTRODUCTION

A study was performed to examine the effects of fixation and storage conditions on the torsional properties of ovine tibiae. Formalin-fixed tibiae stored in 70% ethanol (ETOH) were compared to fresh-frozen contralateral controls for both sham-operated sheep and ovariectomized (OVX) sheep.

REVIEW AND THEORY

Fixation of tissue is necessary for a variety of reasons; fresh tissue carries potential risk of infection, and specimens can rarely be analyzed immediately after harvesting. There are many effective methods of fixation, but some options may not always be feasible due to logistical constraints (i.e., shipping time, chemical hazard, etc.). From this, the need arises to examine the effect of fixation and storage on the mechanical properties of tissue.

Osteoporosis is the leading cause of bone fractures in postmenopausal women (Marcus et al., 1996). It is characterized by lower bone density and micro-architectural deterioration of the bone tissue, which leads to increased bone fragility. Some researchers have hypothesized that there are differences between non-osteoporotic and osteoporotic bone that extend beyond the readily-apparent difference of lower density in the latter (Hodgkinson et al., 1993). Osteoporotic bone may experience fixation and storage effects that differ from those exhibited in non-osteoporotic bone. It has been established that ovariectomy in a ewe causes bone loss after a year. This large animal model has been used to predict performance of osteoporotic bone.

PROCEDURES

Tibial specimens originated from sixteen healthy, skeletally-mature ewes of the same breed and age. Eight sheep underwent a sham surgery procedure and eight sheep were subjected to an OVX operation. All were sacrificed humanely 58 weeks after surgery.

Following necropsy, one hind tibia from each animal was fresh frozen. The other tibiae were fixed in 10% neutral-buffered formalin for seven days, then transferred to 70% ETOH.

Contact radiographs were taken of all tibiae. Dimensions were measured from antero-posterior films. Data were collected for overall length and inner/outer diameters of each bone. Measurements of the diameter were taken at a distance of approximately one-third the length of the bone from the distal end. Characteristically, the tibia's weakest section (and smallest geometry) lies near the junction of the middle and distal thirds (Burstein et al., 1994).

The formalin-fixed tibial specimens remained in 70% ETOH at room temperature for four weeks. The contralateral tibiae were kept frozen at -20°C for the same period and thawed to room temperature prior to testing. Both ends of each tibia were potted in bone cement to facilitate fixturing. Mechanical testing was performed utilizing an MTS Bionix 858 test machine. Each potted tibia was fixtured such that the distal portion of the tibia was subjected to an internal rotation. An axial load of 20 N was applied to the specimens; axial displacement was then fixed. While holding the axial displacement constant, an angular displacement of 15° per minute was applied. This slow rate of loading was intended to minimize viscoelastic effects. The maximum torque prior to failure was obtained, along with the corresponding angular displacement. Additionally, torsional stiffness was calculated by linear regression. The energy of absorption was determined from the torque versus angular displacement curve using the trapezoidal rule.

RESULTS

All failures occurred in the diaphysis of the ovine tibiae. Kolmogorov-Smirnov tests showed normal distributions for all variables. Thus, frozen specimens were compared to analogous formalin-fixed specimens using a paired Student's t-test. Sham and OVX groups were compared using an unpaired t-test.

There was no significant difference in maximum torque, angular displacement, torsional stiffness, or amount of energy absorbed before failure between formalin-fixed, ETOH-stored tibial bones from OVX ewes and their fresh-frozen controls (Table 1). This was also true for tibiae from sham-operated sheep with normal hormonal status. The OVX group was significantly higher than the sham group (frozen and 70% ETOH data combined) for maximum torque ($p = 0.006$), angle at maximum torque ($p = 0.017$), and absorption energy ($p = 0.005$). There was no significant difference in any of the geometric measurements between frozen specimens and formalin-fixed specimens for either group (Table 2). Furthermore, size-related properties were not significantly different between OVX and sham groups.

	Frozen OVX	ETOH OVX	Frozen Sham	ETOH Sham
Torque (N-m)	82.04 ± 8.94	76.92 ± 6.29	71.54 ± 7.37	71.15 ± 8.14
Angle (degrees)	13.53 ± 1.51	12.52 ± 0.92	11.78 ± 0.92	11.89 ± 1.74
Stiffness (N-m/rad)	373.1 ± 25.5	360.3 ± 33.9	361.0 ± 23.4	357.2 ± 23.5
Absorbed Energy (J)	10.26 ± 2.33	8.53 ± 1.19	7.76 ± 1.31	7.35 ± 1.44

Table 1: Mean Torsional Properties.

	Frozen OVX	ETOH OVX	Frozen Sham	ETOH Sham
Cortical wall (mm)	3.94 ± 0.52	4.36 ± 0.45	4.30 ± 0.36	3.69 ± 0.44
Radius^3 (mm^3)	898 ± 157.6	914 ± 160.6	886 ± 162.0	815 ± 151.8
Length (mm)	249.7 ± 8.4	250.7 ± 7.3	244.6 ± 5.2	245.8 ± 6.6

Table 2: Mean Geometric Measurements.

DISCUSSION

Biological variation can confound results in animal studies. By using contralateral pairs, each animal serves as its own control, adding reliability to the results of fixation effect. In ANOVA tests comparing the OVX group to the sham group (where contralateral controls cannot be employed), biological factors (weight of ewe, length/radius of bone) played a more significant role than the experimental factors. This agrees with a study by Stromsoe (1995), who found that structural strength of diaphyseal cortical bone is determined more by its geometry than by its mineral density. Weight may have been crucial because it was positively correlated to geometry (length and radius). In other words, the heavier ewes had larger bones.

It was expected that bones from OVX sheep would have a larger radius than those from sham sheep. The maximum torque is proportional not only to the maximum shear stress, but also to the cube of the radius. If a bone loses shear strength due to osteoporosis, it can continue to carry the same torsional load by increasing in diameter during remodeling and bone turnover (Cordey et al., 1992). Perhaps more accurate cross-sectional measurements would have shown significant differences.

Results indicated that torsional properties in ovine tibiae are not significantly affected by storage in 70% ETOH following formalin fixation to any greater degree than they are by freezing. This holds true for tibiae from both sham-operated ewes and ewes that were ovariectomized 13.5 months earlier. Sedlin (1966) found that frozen samples of bone had mechanical properties that were similar to fresh bone samples. Most tests of fixation effects on bone tissue have been performed using healthy (non-osteoporotic) bone tissue and have involved specimens that were pieces cut from bones, in contrast to whole bones. Failure analysis of intact tibiae reveals changes in the structural properties. While structural properties are undeniably related to material properties, they are also dependent on specimen geometry.

REFERENCES

Burstein, A. et al., *Fundamentals of Orthopaedic Biomechanics*, Williams & Wilkins, 1994.

Cordey, J. et al., *J Bone Miner Res*, 7, S437-S444, 1992.

Marcus, R. et al. (editors), *Osteoporosis*, 419-434, Academic Press, 1996.

Hodgskinson, R. et al., *Clin Biomech*, 8, 262-268, 1993.

Sedlin, E. et al., *Acta Orthop Scand*, 37, 29-48, 1966.

Stromsoe, K. et al., *J Biomech*, 28, 857-861, 1995.

Biomechanical Evaluation of Fracture Healing in Normal and Diabetic Rats

J. Funk[‡], J. Hale[‡†], D. Carmines[†], H.L. Gooch[†], S.R. Hurwitz[†]

[‡] Department of Biomedical Engineering, University of Virginia, Charlottesville, VA 22908
[†] Department of Orthopaedic Surgery, University of Virginia Health Sciences Center, Charlottesville, VA 22908

Introduction

Diabetes mellitus has been shown to change the properties of bone and impair fracture healing (Macey et al., 1989). This study makes use of an established animal model using streptozotocin to induce diabetes in rats (Topping et al., 1994). The right femurs of control and diabetic animals were rodded and fractured in a standardized procedure. After sacrifice, intact and fracture-healed femurs were tested to failure in torsion. Structural data were normalized for geometry to obtain material properties using a modified version of a public domain finite element program. Fracture-healed femurs were also analyzed histologically using hematoxylin and eosin and Alcian blue staining.

Review and Theory

Fracture healing occurs through a complex series of cellular events that ultimately results in the reforming of bone tissue and the recovery of mechanical strength in the bone. The cartilaginous callus that develops around the fracture site of a bone acts both as a site for various collagens and growth factors necessary for repair of the bone and as a temporary structural support while the bone heals. Previous studies have quantified changes in the expression of extracellular matrix molecules as well as inferior tensile strength in fracture-healed bones of streptozotocin-induced diabetic rats (Macey et al., 1989). However, the temporal effects of diabetes on the recovery of mechanical strength in fracture-healed bones have not been adequately studied. The objective of this study was to document the progression of cellular events in fracture healing and the associated changes in the structural and material bone properties of streptozotocin-induced diabetic rats compared to controls after three and four weeks of healing.

Procedures

Induction of Diabetes. Twelve randomly selected male Sprague-Dawley rats (>275 g) were given an injection of streptozotocin (65 mg/kg) to induce diabetes one week prior to undergoing surgery. Fourteen normal rats received no injections and served as a control. On the day of surgery, all animals were weighed and the blood sugar level in those animals previously injected with streptozotocin was checked to verify a serum glucose concentration greater than 300 ml/dl.

Fracture Model. During the surgery, a standard closed femoral fracture was created in the right leg of each animal after intramedullary stabilization. The fracture was created using a blunt guillotine device driven by a dropped weight and was verified radiographically (Bonnarens and Einhorn, 1984). Control and diabetic groups were then randomly subdivided into three week and four week time points of healing before the animals were euthanized. All animals were weighed and the blood glucose levels were checked prior to sacrifice.

Histology. Standard hematoxylin and eosin and Alcian blue staining methods were utilized on 7μm paraffin sections prepared from the fracture sites of additional animals from the same experimental population not used for mechanical testing.

Mechanical Testing. All femurs destined for mechanical testing were cleaned of soft tissue and potted in bone cups using bismuth metal. Each specimen was then torqued to failure at a rate of 1°/sec in internal rotation. After failure, the femurs were allowed to dry and then reconstructed using a cyanoacrylate adhesive. The specimens were sliced with a diamond edge bone saw into approximately 1 mm thick sections at 30, 40, 50, 60 and 70 percent of their total bone length. The sections were optically scanned and the endosteal and periosteal surfaces of the cortical bone were manually digitized into discrete points for each section. The data were entered into a public domain program, "VA-Twist," which calculated the cortical area, maximum normalized shear stress, polar moment of inertia (J), and torsional moment of inertia (K) for each section (Levenston et al., 1994). The program was modified to output values for the major and minor outer diameters at the principle axes of each section. The maximum normalized shear stress and K values were used to normalize the structural data (torque vs. angle) into material data (stress vs. strain). For the sake of comparison, material data were also obtained

by modeling each femur as a hollow elliptical cylinder having the same major and minor outer diameters and polar moment of inertia J as the mid-diaphyseal section of the actual bone.

Maximum values for torque, angle, stress and strain were recorded. Structural and material stiffness values were also calculated. Mechanical data were normalized for each rat by dividing the value for the fracture-healed femur by the value for the intact contralateral femur, and the ratios were expressed in the form of an index (e.g., torque index, stress index, etc.). Each group had a sample size of at least six (n=6) matched pairs of femurs. All index data were statistically analyzed using a two-factor analysis of variance (ANOVA) design.

Results

Histological examination of tissue sections revealed evidence of cartilage production in both control and diabetic fracture calluses. However, after two weeks of healing, the control group exhibited much larger hypertrophic chondrocytes than the diabetic group. After three weeks of healing, many more nests of hypertrophic chondrocytes remained in the diabetic specimens compared to the controls.

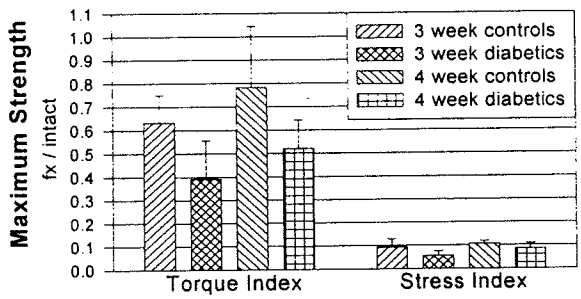

Figure 1: The average torque index and average stress index for each group.

Mechanical testing indicated superior mechanical strength in the intact femurs compared to the fracture-healed femurs for all groups. The recovered whole bone structural strength, given by the torque index, was greater for all groups than the recovered material strength of the fracture callus, given by the stress index (Figure 1). Improved structural and material strength was noted in both groups after four weeks of healing compared to three weeks of healing, and in control animals compared to diabetic animals at both time points (Figure 1). Statistical analysis revealed that the diabetic rats had significantly lower average values for the torque index, stress index, structural stiffness index and material stiffness index, and significantly greater values for the angle index and strain index compared to control rats ($p<.05$).

There was little difference in the mechanical properties of the intact femurs between groups, except that the intact femurs from diabetic animals were significantly stiffer, both structurally and materially, and failed at significantly lower angles and strains ($p<.05$). Elliptical modeling underestimated the maximum stresses in all femurs by an average of 28% (± 13%) compared to the finite element procedure.

Discussion

Diabetes mellitus has long been associated with complications in fracture healing, such as malunions and non-unions. Histological evidence from this study demonstrates that diabetes produces changes in the cellular events that occur during fracture healing. The appearance and maturation of hypertrophic chondrocytes in the fracture callus of diabetic rats during the process of endochondral ossification is delayed. Our results suggest that the changes in the cellular events of fracture healing are associated with a delay of at least one week in the recovery of mechanical strength for fracture-healed femurs in diabetic rats when compared to controls.

Additionally, we demonstrated that elliptical modeling consistently and substantially under-predicts the maximum stress in a complex structure like a rat bone compared to using the finite element method proposed by Levenston et al. (1994). The relatively modest additional effort required to section and digitize the bones with this finite element procedure results in greatly improved accuracy in the determination of bone material properties.

References

Bonnarens F and Einhorn TA. *J Orthop Res*, **2**, 97-101, 1984.
Levenston ME et al. *J Bone Min Res*, **9**, 1459-65, 1994.
Macey LR et al. *JBJS*, **71A**, 722-33, 1989.
Topping RE et al. *CORR*, **308**, 220-8, 1994.

Acknowledgments

We would like to thank Dr. H. Fujioka and R. T. Thakur for their contributions to the histological section of this study.

ANCHORAGE AND STABILITY PROVIDED BY FIVE DIFFERENT ANTERIOR LUMBAR INTERBODY FUSION IMPLANTS-A CADAVERIC STUDY

A. Tsantrizos, A. Andreou, M.Aebi, T. Steffen

Orthopaedic Research Laboratory, McGill University, Montreal, Canada H3A 1A1

INTRODUCTION

Three-Dimensional initial stability and endplate anchorage of five anterior interbody fusion system (one threaded and four ring shaped implants) were tested using cadaveric (L1-L5) human lumbar spines (n=42). Neutral zone (NZ) and ranges of motion (ROM) were compared for the intact and L3/4 instrumented segmental level. The anterior implant pull-out force was recorded. Total ROM was significantly reduced by all implants in lateral bending alone. Significant differences were also observed between implants in the same movement. Contrary, no implants managed to decrease NZ but instead some showed significant increases in flexion/extension and lateral bending. Anchoring teeth increased the pull-out strength. Implant contact surface area , disc space fit, and teeth geometry are suggested to be important for stability.

REVIEW AND THEORY

Anterior lumbar interbody fusion is an appealing procedure suitable for both open and minimal invasive surgery. The goal of inserting an implant is to reduce segmental mobility, hence providing the initial stability needed to allow formation of a biological fusion between the adjacent vertebrae. Current implants have quite different designs, suggesting differences in the initial stability provided. To our knowledge , there has been no complete study comparing the different implant designs. This study quantifies the three-dimensional initial stability (NZ and ROM) provided by five different implants.

PROCEDURES

Forty-two cadaveric lumbar spines (L1-L5) were block randomized (n=42) according to age, sex , and bone density into six groups: (i) Brantigan (Acromed) ALIF carbon fiber implant, (ii) BAK (Spine-Tech) paired threaded titanium implants, (iii) TIS (Synthes) prototype titanium ring with serrated teeth, (iv) SynCage (Synthes) prototype with convex endplate-contact surfaces (v) Screw-In-Cage (Synthes) prototype combining a ring with a threaded cylinder within the frame (vi) control group (no implant). Specimens were first tested intact and then with an implant inserted into the L3/4 disc space. The BAK cage was placed according to the manufacturers instructions, all other implants were placed using a standardized endplate preparation technique (anterior window leaving the lateral annulus intact and removing all cartilage with a ring curette). Moments of axial rotation (+/-8Nm), flexion/extension (+/-4Nm), and lateral bending (+/-4Nm) were independently applied while maintaining 200N axial preload. Three cycles were performed for each movement, with the third cycle used for data analysis. The three-dimensional segmental displacements were measured using an electromagnetic tracking device. An anterior implant pull-out test under a 600N axial preload concluded the experiment.

The range of motion (ROM) and the neutral zone (NZ) were extracted from the load-displacement curves of each specimen in each load direction. Analysis of Variance (ANOVA) along with Fisher's post-hoc comparison tests were used to evaluate segmental displacement changes and pull-out force differences within and between implants respectively.

RESULTS

(1) Neutral Zone (NZ)

IMPLANTS	MOVEMENTS		
	Ax. Rot.	Flex. Ext‡	Lat Bend‡
Brantigan	126%	40%	25%
BAK	136%	337%*	107%
TIS	322%*	53%	489%*
SynCage	130%	164%	135%
Screw-In-Cage	200%	158%*	31%
Control	4%	-2%	-51%

(2) Total Range of Motion (ROM)

IMPLANTS	MOVEMENTS		
	Ax. Rot.	Flex./ Ext	Lat. Bend‡
Brantigan	-29%	-8%	-38%*
BAK	-13%	-32%	-80%*
TIS	29%	-27%	-40%*
SynCage	-27%*	-35%*	-80%*
Screw-In-Cage	-5%	-44%*	-75%*
Control	4%	-9%	0%

Tables 1&2: Percentage changes for instrumented compared to non-instrumented specimens. A double cross (‡) indicates significant changes between implants while an asterisk (*) shows significant changes between intact and instrumented. Positive values reflect an increase of mobility while negative values indicate a decrease in mobility.

(3) Pull-Out Force

IMPLANT	FORCE (N)‡
Brantigan	653
BAK	642
TIS	957
SynCage	1033
Screw-In-Cage	938

Table 3: Mean pull-out force of each of the implants. A double cross (‡) indicates significant changes between implants.

The statistical analyses showed that the BAK implant demonstrated the largest NZ flexion/extension increase, while the TIS prototype showed the largest NZ increase in lateral bending. Furthermore, changes were found in the lateral bending ROM: Although all implants decreased significantly, post-hoc comparisons demonstrated that the Brantigan and TIS prototype decreased the least. Finally, the three Synthes prototypes showed a significantly higher pull-out force than both the Brantigan and BAK implants. The control group showed no significant changes.

DISCUSSION

According to Panjabi (Panjabi, 1992) initial stability may best be described as a decrease the NZ. None of the tested implants managed to achieve a decrease compared to the intact spine, suggesting that interbody implants alone may not be enough to limit micromotion at the bone-graft interface. In our experiment we showed consistent NZ increases, although not all showed significance. The Brantigan implant had the least NZ increase in flexion/extension and lateral bending. This cage has the largest surface contact area of all implants tested. Our data suggest that a size of the implant-endplate contact area may play a role in reducing micromotion.

Contrary to this finding, ROM did decrease on average, however only significantly in lateral bending. The Synthes prototype implants managed to reduce the ROM quite well, implying that a serrated teeth construct may contribute in reducing ROM. The teeth may need higher preloads than what were applied in our tests (200N) before they sink into the endplate and are able to reduce NZ. In the pull-out test performed with a 600N axial preload, the Synthes implants performed the best.

More emphasis needs to be placed on implant design features such as surface contact area and teeth constructs because all may improve anchorage of the device in the endplate.

REFERENCES

Panjabi M.M., J.of Spinal Disord,5, 390-396, 1992

Cement Line Quantity and Porosity Variation in Human Cadaveric Tibiae and their Relationship to Bone Strength

A. Egerer[1], B. Abraham[2], P. McMillan[1], S. Saha[3]

[1]Department of Pathology and Human Anatomy, Loma Linda University, Loma Linda, CA 92350
[2]University of California at Riverside, Riverside, CA 92521
[3]Bioengineering Alliance of South Carolina, Clemson University, Clemson, SC 29634

INTRODUCTION

The osteonal cement line is a structure found primarily within compact bone at the periphery of osteons. They have been implicated in a variety of areas concerning bone strength, namely, 1) energy absorption, 2) fracture processes, 3) fatigue processes, and 4) elastic function. In this study, we quantified cement lines and porosity in human cadaveric tibiae and investigated the relationship between these microstructural parameters and bone strength.

REVIEW AND THEORY

The composition of bone includes many structural and molecular components which provide both its inherent flexibility, strength, and overall dynamic nature. Two such components which have been implicated in overall bone strength within long bones include 1) the osteonal cement line, a 1-5μm-thick structure formed during the initial stages of bone remodeling and thus found on the outermost boundary of an osteon, and 2) the degree of porosity in both compact and cancellous regions of bone tissue. Previous research has suggested that cement lines play an important role in the fatigue and fracture properties of bone by allowing fatigue microdamage to often occur along these lines. Furthermore, it has been well established that the incidence of fractures is significantly increased with an increase in porosity. Although some information on cement lines is available in the literature, the relationship between cement line quantity, porosity, Haversian canal number, and canal size to overall bone mechanical properties, age, and gender have not yet been investigated. In the present study, we quantified the cement line, porosity, and osteonal dimensions, and investigated the relationship between these microstructural parameters and the load carrying capacity of human tibiae.

PROCEDURE

Part I: Mechanical Testing

- Twenty-one human tibiae from 12 cadavers (4 male, 8 female)
- Ages between 61 and 99 years at death
- Tibiae statically loaded in 4-point bending
- Load (kN) and energy (J) at yield, and energy (J) at break were measured

Part II: Histologic Quantification

- Two-hundred-micron-thick slices were removed from the middle 1/3 of each tibia using a circular diamond saw (Buehler)
- Slices adhered to a plexiglass slide using cyanoacrylate glue
- Bone surface processed with fine sanding (320-600 grit)
- Surface decalcification (10% HCl, 2 minutes)
- Staining (1% Coomassie Brilliant Blue R, 2 minutes) to produce unique and selective non-staining of cement lines

Each cross-section was taken to a computer workstation, and the four anatomical quadrants (anterior, posterior, medial, lateral) were analyzed under an Olympus CH-2 light microscope (10X objective) with an attached PULNiX TMC-7 video camera. Between 4 to 12 fields (images) from each of the four quadrants of each of the twenty-one tibiae were digitized, providing 582 total images. The length of cement lines per unit area (L_A) of bone was estimated using the stereologic relationship in (1):

$$L_A = (3.14 / 2)\, I_L \quad (1)$$

where I_L is the number of intersections per unit length that test lines make with cement lines. Commercially available software (Image-Pro Plus, Media Cybernetics) was used for determining the cement line unit length ($\mu m/\mu m^2$), porosity (%), mean canal number per unit area, and mean canal diameter (μm).

RESULTS

The results indicate that the mean maximum load necessary to completely fracture the bone in females (4.17 kN) was significantly less than that for males (7.92kN) (Table 1). Upon histological examination, the quantity of cement lines (males and females combined) in the anterior quadrant was found to be significantly greater ($p<0.05$) than the posterior, medial, and lateral quadrants (Figure 1). There was no significant difference in the amount of cement lines between the posterior, medial, and lateral

	Mean Maximum Load (kN)	Cement Line Quantity ($\mu m/\mu m^2$)
Males	7.92	0.0099
Females	4.17	0.0091

Table 1: *Differences in the mean maximum load carrying capacity of human tibiae and total cement line quantity between gender.*

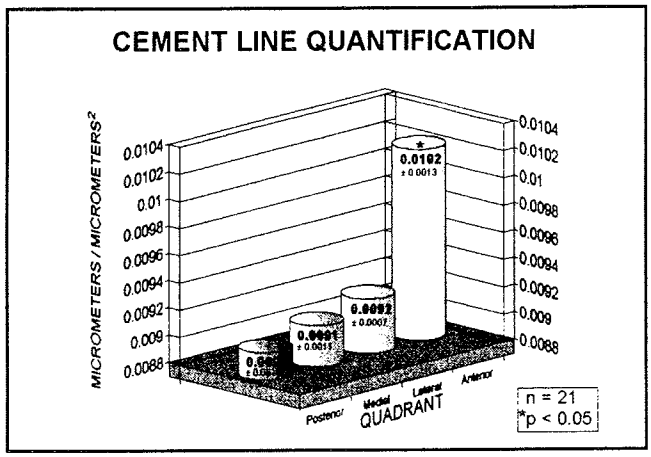

Figure 1: *Quadrant differences in cement line quantity for combined males and females.*

quadrants. Furthermore, although no significant difference in cement line quantity was found between the ages of individuals, gender did reveal a significant difference ($p<0.05$), with the mean cement line quantity in males being greater than that found in females (Table 1). Correlation analysis revealed a positive relationship between the cement line quantity ($\mu m/\mu m^2$) and the maximum load (kN) necessary to completely fracture the bone (Figure 2). When the porosity was examined for

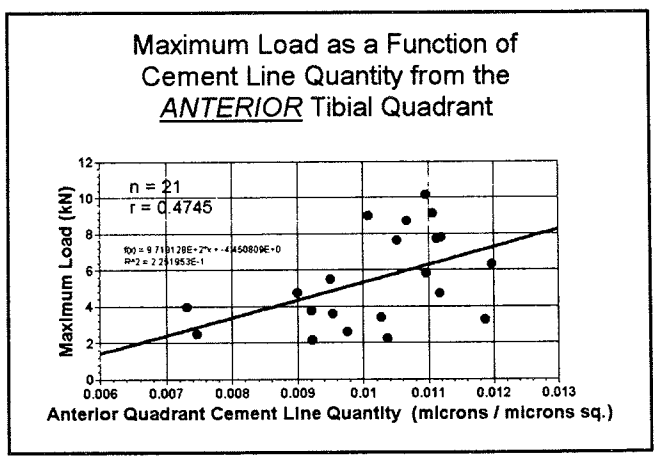

Figure 2: *Maximum load as a function of total cement line quantity from the anterior tibial quadrant.*

each quadrant in both genders, the anterior quadrant in females had approximately 40% greater porosity than the posterior, medial, and lateral quadrants. In males, there was no significant difference between each quadrant. Taking into account all quadrants combined, our results reveal mean tibiae porosity in females to be 12.24%, and in males 7.10%. Although the mean number of Haversian canals per unit area in each of the quadrants in females was *significantly less* than in males, females showed an *increased* mean canal diameter than males (Table 2).

	Mean # Canals/Area Area=$55.3x10^4$ μm^2	Mean Canal Diameter (μm)
Males	17.1	38.8
Females	13.3	53.6

Table 2: *Differences in the mean Haversian canal number per unit area and mean canal diameter between gender.*

DISCUSSION

Our results suggest that both the cement line quantity as well as porosity are important factors affecting bone strength. We hypothesize that the human anterior tibia may be accustomed to 1) a greater amount of stress over many years, 2) subject to a greater amount of fatigue microdamage, 3) increased osteon formation due to repair, and 4) a subsequent increase in the quantity of cement lines. Furthermore, our observations regarding gender differences in cement line quantity suggest that male tibiae may be subject to a greater degree of stress — and thus a greater degree of fatigue microdamage — than in females. Finally, our results suggest that although porosity is inversely correlated with bone strength, males and females have a rather different ratio between mean canal number per area to mean canal diameter (i.e. *females* showed *fewer canals with larger canal diameters* than males, whereas *males* conversely showed a *greater canal quantity with smaller canal diameters*. Although further study is needed on the osteonal cement line as well as other microstructural and molecular features within bone tissue, our data will be extremely helpful in a variety of orthopaedic sub-disciplines by 1) helping in the development of future mathematical bone models, 2) furthering our present knowledge on bone mechanical properties, and 3) understanding Normal vs. Diseased vs. Post-surgical adapted bone tissue. Proximal and distal tibiae diaphyses are presently under analysis.

REFERENCES

1. Burr, D.B. et al., Biomechanics, 21(11): 939-945, 1988.
2. Carter, D.R. et al., Clin. Orthop. Rel. Res., 127:265-274, 1977 .
3. Schaffler, M.B. et al., The Anatomical Record, 217: 223-228, 1987.

EFFECT OF ACTIVE RESPONSES ON PEAK IMPACT FORCE IN FALLS TO THE SIDE

M. Sabick[1], J. Hay[2], V. Goel[1], and S. Banks[3]

[1]Department of Biomedical Engineering, University of Iowa, Iowa City, IA 52242
[2]Department of Exercise Science, University of Iowa, Iowa City, IA 52242
[3]Orthopaedic Research Laboratory, Good Samaritan Medical Center, West Palm Beach, FL 33402

INTRODUCTION

Falls cause more injuries than any other kind of accident. However, it is not known whether active responses, such as using the arm to "break" the fall, are an effective means of decreasing fall severity. The effectiveness of using the outstretched arm to break a fall to the side was quantified using athletes trained to perform special breakfall techniques. The peak force for simulated falls when subjects fell in a relaxed manner was compared to cases in which the subjects used their right arm to actively slap the ground prior to impact.

REVIEW AND THEORY

Falls cause more injuries than any other type of accident, are the leading cause of accidental injury to children, and account for almost half of the injuries sustained in the elderly (Iskrant and Joliet, 1968). However, the biomechanics of falling has received little attention. Studies have investigated passive responses to falling, such as relaxing the body (Sabick et al., 1996) or wearing hip pads (Robinovitch et al., 1995). However, only one study has investigated the use of the arm as an active response to an impending fall (Robinovitch et al., 1996). The effectiveness of using the arm to break a fall has not been quantified in terms of the decreasing force at impact.

In the defensive martial arts, a series of techniques are taught to athletes to prevent injuries when the athletes are thrown. These techniques, called breakfall techniques, consist of a forceful slapping of the ground with the arm and leg prior to the impact of the trunk. This slapping action is meant to protect the body by using the shoulder and hip muscles to absorb fall energy. If breakfall techniques are effective in preventing injuries, as anecdotal evidence suggests, then they may have applications in other situations where falls are common but individuals are not taught how to prevent injuries from falls, such as elderly persons at risk of hip fracture, or athletes in contact sports. The purpose of this study was to quantify the effectiveness of the arm slap motion in decreasing peak impact force in side falls.

PROCEDURES

Nine athletes trained in the martial art of aikido ranging in age from 25 to 55 performed simulated falls from a kneeling position onto a 4'x4' force platform covered with 1" of foam padding. Subjects initiated falls to the side by moving their hips laterally when given a verbal command (Fig. 1). Each subject was asked to fall with the body completely relaxed, unless an audio cue was heard. A buzzer was sounded in random trials after fall initiation, signaling the subject to break the fall by using a slapping motion similar to a breakfall technique.

Each subject performed 6-9 trials of both fall conditions, relaxed and slap. EMG of the leg and trunk muscles were evaluated qualitatively to verify that subjects were relaxed at impact for relaxed trials. Force plate data were normalized to the athlete's body weight (BW). Time of impact was defined as the first time the vertical reaction force exceeded 0.10 BW. Three indices of impact severity were computed: (1) peak force, (2) time-to-peak (TTP), and (3) impulse. Time-to-peak was the difference between the peak force time and the impact time. Impulse was calculated from the instant the vertical force first exceeded BW, to the first time after the impact peak that the force fell below BW. For slap trials, the time interval between the slap and the body impact was also calculated. The peak force acting on the body at impact was considered to be the peak non-slap force.

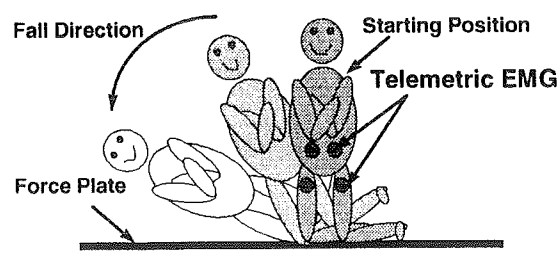

Figure 1: Diagram of a simulated relaxed fall

RESULTS

A total of 66 relaxed and 58 slap falls were performed by 9 subjects. Mean values (± SD) for three impact variables are located in Table 1. The peak force acting on the body was less for slap falls than for relaxed falls, even though the impulse was approximately equal. TTP values were slightly less for relaxed trials then for slap trials. EMG data verified that subjects were much more relaxed in relaxed falls then in slap falls. The mean slap force was 3.84±0.91 BW, much greater than the peak force acting on the body in slap falls. For 34 of the slap falls, the slap occurred after the body had impacted the ground. When the slap occurred prior to the impact of the trunk, the peak body force decreased as the interval between the slap and body impact increased (r=-0.73, p<0.01, Fig. 2).

	Relaxed (n=66)	Slap (n=58)
Peak Force (BW)	3.28±0.74	2.94±0.78
TTP (s)	0.148±0.144	0.160±0.090
Impulse (BWs)	31.97±11.64	32.30±10.49

Table 1: Comparison of variables for relaxed and slap falls.

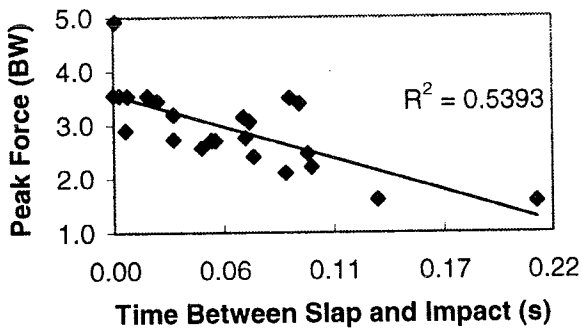

Figure 2: As the interval between the slap and body impact increased, peak force decreased.

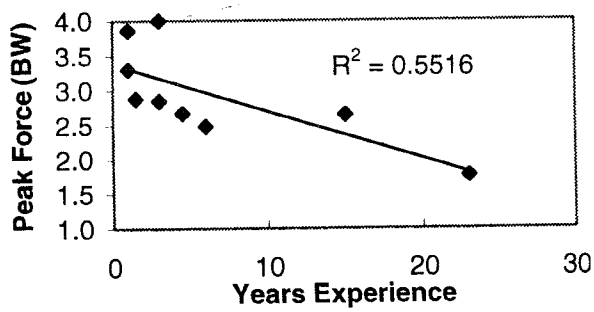

Figure 3: Relationship between experience in aikido and mean peak body force in slap falls.

The force acting on the body decreased with increasing experience in aikido (r=-0.74, p<0.01, Fig. 3). Therefore, the effectiveness of the arm slap improved with training.

DISCUSSION

Using the arm to break the fall was an effective means of decreasing peak impact force acting on the body. Even though the impulse was approximately the same for both fall types, the peak force decreased an average of 34% by using the arm to break the fall. However, this decrease in peak force was achieved in trained athletes. It is not yet known if untrained individuals can perform similarly. Therefore, the data presented here represent a "best case" scenario. Even within this trained group, almost 68% of the active responses occurred after the trunk had impacted the force platform. A larger study needs to be conducted to determine the importance of slap timing in decreasing impact force. As the time interval between the arm slap and body impact increased, peak force acting on the body decreased, suggesting that proper timing is very important.

The falls studied here were expected falls which were self-initiated and were onto a soft surface. Therefore, the responses studied may not represent those which would occur in unexpected falls onto hard surfaces. However, by comparing relaxed and slap falls in the same individuals, we have shown that using the arm to break the fall can be an effective means of decreasing the severity of impact in a fall. Obviously, the use of the arm to break the fall could lead to an increased incidence of wrist fractures, therefore the relative benefits of using the arm need to be determined. In many sports, using a type of breakfall technique may be a valid way of decreasing injuries due to falls.

REFERENCES

Iskrant A.P., and Joliet P.V., "Accidents and Homicide", Harvard Univ. Press, 1968.
Sabick M.B. et al., Proc. 43rd Annual ORS, Feb. 1997. Robinovitch, S.N. et al., Proc. 20th Annual Meeting, ASB, 1996
Robinovitch, S.N. et al., J. Biomech.Eng. 117:409-413, 1995

ACKNOWLEDGMENTS

Supported by NIA grant AG00214 and grant #R49/CCR703640 07 from the NCIPC.

POSTURAL SWAY AND LIMITS OF STABILITY ARE NOT PREDICTORS OF FALL RECOVERY IN HEALTHY OLDER ADULTS

T.M. Owings*, M.J. Pavol*, K.T. Foley†, and M.D. Grabiner*

*Department of Biomedical Engineering, †Department of Geriatric Medicine
The Cleveland Clinic Foundation, Cleveland, OH 44195

INTRODUCTION

Increased postural sway during quiet stance has been suggested as a risk factor for falling in older adults [1-3]. It also has been suggested that these increases in sway are meaningless unless referenced to the postural stability limits of an individual, raising the issue of whether these limits and the risk of falling are related. There have, however, been few or no prospective approaches to this issue. We therefore induced trips during gait in a population of older adults in a laboratory setting. The purpose was to investigate the influence of postural sway and limits of stability on the ability to recover from a trip.

PROCEDURES

Postural sway, limits of stability, and the ability to recover from an induced trip were tested in 79 older adults (mean age 72 ± 5 years). Subjects were screened by a geriatrician, tested for a femoral neck bone mineral density of at least 0.65 g/cm², and gave informed consent before participating.

Balance testing. Barefoot subjects stood upright on a force plate with their feet as close as possible together, arms at their side, and eyes directed ahead. Instructions for determining stability limits included keeping their body "rigid" and maintaining the full plantar surface of their feet in contact with the force plate. Ground reactions were recorded at 100 Hz and the associated center of pressure (COP) locations computed. Three trials were performed for each experimental condition with the feet in the same position throughout. All anterior-posterior (AP) variables were normalized to foot length, while the medial-lateral (ML) variables were normalized to the total width between the lateral borders of the feet.

Postural sway. Subjects stood quietly for 20 seconds as ground reactions were recorded. The AP and ML speeds of the COP during postural sway were computed as the average speed over the duration of the trial. AP and ML postural sway amplitudes were computed as the middle 90th percentile excursion distance of the COP in the corresponding direction. The values were averaged across trials.

Static limits of stability. Subjects leaned as far as possible in each of four directions (forward, backward, left, right) and maintained that position for 3 seconds as ground reactions were recorded. The AP (ML) static limit of stability was computed for each subject as the difference between the maximum 95th percentile COP position for the forward (right) lean trials and the minimum 5th percentile COP position for the backward (left) leans.

Dynamic limits of stability. Subjects swayed continuously as far as possible in the AP or ML direction as 20 seconds of ground reactions were recorded. For one set of trials (dynamic limit 1), subjects were instructed to sway as fast as possible. The speed of sway was self selected for the other set of trials (dynamic limits 2). The AP and ML dynamic limits of stability were computed as the maximum, across trials, of the middle 90th percentile excursion distance of the COP in the corresponding direction.

Mechanically induced trips. Trips were induced by a concealed mechanical obstacle which rose from the floor when manually triggered. A trip resulted when the toes of the shoe of the swing foot encountered the obstacle during mid-to-late swing. To ensure subject safety, subjects were secured in a harness attached by a pair of ropes to a ceiling-mounted track. A load cell, connected in series with the safety ropes, was used to determine whether a recovery was rope-assisted.

Subjects walked at a self-selected speed and were informed of an impending trip during one of the upcoming trials. They were told to recover

and continue walking if tripped. A decoy "tripping rope" was laid 1.5 m before the obstacle. Only one attempt was made to trip each subject. Each trip outcome was graded as either a recovery, a fall, a rope-assist, or a miss. Misses resulted when the foot impact with the obstacle did not meet the aforementioned criteria for a trip. A fall was classified as the subject being fully and continuously supported by the safety ropes. Recoveries and rope-assists were differentiated based on whether the integrated rope force over the second following the triggering of the obstacle was less than or greater than 5.0% body weight·second, respectively. The rope force signal from the load cell was low-pass filtered at 16 Hz prior to integration.

Statistical analysis. Group t-tests were used to compare the balance variables for the subjects whose trips were classified as a recovery or as a fall. Differences were considered significant at a p-value of less than 0.05.

Results

Of the outcomes of the 79 subjects tripped, 39 were recoveries, 10 were falls, 12 were rope-assists, and 18 were misses. The rope-assisted group comprised: (1) those who would have recovered, but were restricted by the length of the ropes, and (2) those who would have fallen without the support from the ropes. Because no distinction can be made between these subgroups, only balance data from the recovery group and the fall group was compared (Table 1). Only the ML speed of postural sway showed a statistically significant between-group difference.

Discussion

This investigation compared the postural sway, and the static and dynamic limits of stability of older adults who either recovered or fell following an induced trip. There were no significant differences between the two groups except for the ML speed of postural sway. We ascribe no functional impact to this difference, given that the recovery from a trip takes place primarily in the sagittal plane and that in no case was there a notable ML component to the direction in which the subject fell.

Because of the all-or-nothing nature of a fall following a trip, membership in either the falling or recovery group may not reflect a subject's statistical risk of falling. Results of this study must be interpreted from the viewpoint of the trips as discrete, independent events. Given this, the results suggest that the ability to recover from a trip is not influenced by postural sway or limits of stability.

Table 1: Comparison of postural sway and stability limits between the recovery and fall groups. AP (ML) speed variables are given in percent foot length (feet width) per second. Remaining AP (ML) variables are in percent foot length (feet width). Values are shown as mean ± standard deviation.

	Recovery	Falls	p-val
AP Sway	7.0±1.9	6.1±1.7	0.20
ML Sway	7.8±2.3	6.5±1.8	0.07
AP Speed	3.8±1.2	3.2±0.9	0.06
ML Speed	5.4±2.2	4.4±1.0	0.04
AP Static Lim	50.1±8.8	50.2±12.0	0.98
ML Static Lim	52.1±10.5	47.1±12.4	0.27
AP Dyn Lim 1	53.8±7.4	55.7±7.3	0.47
ML Dyn Lim 1	57.7±9.9	59.9±10.0	0.55
AP Dyn Lim 2	51.0±8.6	54.0±8.8	0.35
ML Dyn Lim 2	55.1±9.6	54.4±11.0	0.86

References

1. Fernie, G.R. et al. *Age Ageing*, 11, 11-16, 1982.
2. Overstall, P.W. et al. *Br Med J*, 1, 261-264, 1977.
3. Ring, C. et al. *Arch Phys Med Rehabil*, 69, 261-264, 1988.

Acknowledgments

This work was supported by NIH-R01AG10557 (MDG).

EFFECTS OF AGE AND BASE OF SUPPORT ON MAXIMUM FORWARD REACH

K. Kozak[1], J.A. Ashton-Miller[1-3], and L. Nyquist[3].
[1]Department of Biomedical Engineering, University of Michigan, Ann Arbor, MI 48109
[2]Department of Mechanical Engineering and [3]Institute of Gerontology, Ann Arbor, MI 48109

INTRODUCTION

Older adults experience an increased difficulty with the performance of activities of daily living (ADL), a decreased ability to maintain postural balance, and an increased rate of falls (Tinetti, 1986; Schultz, 1992). With age, elderly first experience difficulty with the more challenging activities of daily living, rather than the easier tasks. One of the ADL tasks they view as most challenging is standing on a stool or step ladder to reach for something (Powell 1995). This study was undertaken to examine how age and biomechanical factors interact to affect performance when healthy adults are confronted with having to reach forward as far as possible while standing on a base of support of different heights and sizes.

REVIEW AND THEORY

The maximal distance a person can reach forward while maintaining a fixed base of support in the standing position is a recognized clinical measure of balance. For example, Duncan et al. (1990) showed that forward reach correlates with the center of pressure excursion in a precise and repeatable manner. In addition, they reported that forward reach decreased with age and hypothesized that this decrease might serve as a protective mechanism to minimize the displacement of the center of gravity in order to prevent falling. The challenging nature of reaching is supported by the fact that falls resulting in injuries most commonly occur during daily activities requiring reaching (Nevitt et al., 1991).

In its simplest terms the maintenance of balance involves maintaining the center of gravity within the existing base of support (BOS), usually defined by the area and position of the feet. If the center of gravity moves outside the BOS, a rapid motor response must be initiated to restore balance and prevent a fall. King et al. (1994) have found that the functional base of support, defined in their study as the proportion of the anterior-posterior dimension of the base of support utilized during sustained maximal forward and backward leaning, is decreased in older persons. Their results confirmed those of Lee and Deming (1988) who also found that the effective standing BOS decreased with age for maximal forward, backward, right and left leans. This decrease in BOS may make a person more likely to lose their balance and fall during activities such as reaching, which can potentially require full BOS usage in certain directions.

The purpose of this study was to examine the functional BOS used by both young and older subjects during the performance of a maximal reach and to examine the effects of experimentally manipulating the physical BOS (PBOS) available. We tested the hypothesis that experimentally manipulating the PBOS will neither affect reach distance nor center of reaction (COR) parameters.

PROCEDURES

Ten young females (YA) (mean age 22 years) and ten community-dwelling healthy older females (OA) (mean age 72 years) were tested while wearing a ceiling-suspended full body safety harness. The OA were examined by a physician-geriatrician and cleared for participation in this experiment. After 30s of quiet stance, subjects were instructed to reach towards, and touch, a target with a finger from each hand. Maximum reach achieved in 10 trials, normalized by outstretched arm length, was recorded. Subjects performed the reaching protocol standing both on a 10 cm "low" platform and on a 60 cm "high" rigid platform. To study the effect of manipulating PBOS, the protocol was repeated using three different foot positions: 100% of the length of each foot supported by a horizontal platform, the rear 75% of each foot supported (toes off), and the rear 65% of each foot supported on the platform, much as could be the case on a step ladder. Each foot was supported by an AMTI force platform which was used to record at 100 Hz the ground reaction forces under their feet with 12 bit resolution. COR data were then calculated. Data were analyzed using a 2 (Platform Height) x 2 (Age) x 3 (PBOS) repeated measures analysis of variance.

RESULTS

The results showed that OA reached 22% less far than the YA. The reach of the YA and OA was significantly decreased by 8% and 14% respectively ($p<.001$) when the subjects stood on the high platform. However, there were no significant

interactions between height of platform and age. Decreasing PBOS from 100% to 65% foot length decreased maximum reach distance by approximately 20% ($p < .0001$) in both groups of subjects. However, YA reach was decreased by a greater absolute distance (8cm) from their larger initial reach than the OA reach (5.6 cm) ($p < .018$). The measurement of maximum reach was found to be reliable, with a high correlation ($r > .9$) between two successive maximum reaches.

The physical 'safety margin' may be defined as the distance between the edge of the force platform and the greatest anterior displacement of the COR during forward reach. For both the 100% PBOS and 65% PBOS conditions the OA had a safety margin approximately twice that of the YA ($p < .05$). Decreasing PBOS by 35% from 100% to 65% resulted in approximately a 70% decrease in safety margin in both YA and OA ($p < .0001$). The interaction between age group and PBOS manipulation was significant ($p < .016$).

The maximum anterior displacement of the COR measured from the ankle, a measure of the anterior boundary of the functional BOS (F-BOS), was about 15% larger for the YA than for the OA ($p < .05$). Decreasing PBOS from 100% to 65% decreased the maximum COR displacement by approximately 40% in both YA and OA ($p < .0001$). For the 100% PBOS condition the OA F-BOS extended 13.2 cm anteriorly from the ankle while that of YA extended 15.8 cm. Similarly, for the 65% PBOS condition, the F-BOS extended 8.0 and 9.3 cm anterior to the ankle joint, respectively. The interaction between age group and PBOS manipulation was significant ($p < .021$). Neither the maximum displacement of the COR nor the safety margin were significantly affected by platform height.

The mean initial position of the COR for a period of quiet stance showed that the OA maintained their COR significantly more posterior to that of the YA ($p < .05$). When foot position was changed from 100% PBOS to 65% PBOS, subjects in both groups moved their COR from a mean location anterior to the ankle to a mean location posterior to the ankle ($p > .05$).

DISCUSSION

This study indicates that increasing platform height decreased maximum reach distance. The significant increase in perceived task difficulty measured on the high platform (quantified by a Likert scale questionnaire, but not reported here for brevity) correlated with that reduced maximum reach distance, even though the biomechanical task demands were identical on the low and high platforms. Because platform height neither affected the safety margin nor the F-BOS used, our results show that reach on the high platform was not limited due to a change in how foot reaction forces were controlled in either young or old subjects. In fact it is interesting that, despite their perceptions of the challenging nature of this task, these healthy OA responded no differently than the YA in terms of how much they elected to increase their safety margin on the high platform.

The significant age x PBOS interaction suggests that, unlike their reach distance, the OA safety margin was more affected by the PBOS manipulation than the YA safety margin.

Decreasing the PBOS and increasing the platform height increased the perceived challenge of the maximum forward reach. This perception of increased challenge led to the observed reduction in maximum reach distance. Because the OA did not respond differently to the platform height manipulation in terms of their COR behavior, kinematic analyses of body segment control will be required to explain the age differences in reach distance.

REFERENCES

Duncan PW et al. *J. Gerontol.* **45**, M192-197, 1990.
King MB et al. *J. Gerontol.* **49**, M258-263, 1994.
Lee WA et al. *Phys. Ther.* **68**, 859, 1988.
Nevitt MC et al. *J. Gerontol.* **46**, M164-170, 1991.
Powell LE et al. , *J. Gerontol.* **50A**:M28-34, 1995.
Schultz, AB *J. Biomech.* **25**, 519-528, 1992.
Tinetti ME *JAGS* **34**, 119-126, 1986.

ACKNOWLEDGMENTS: PHS Grant P01 AG 08808.

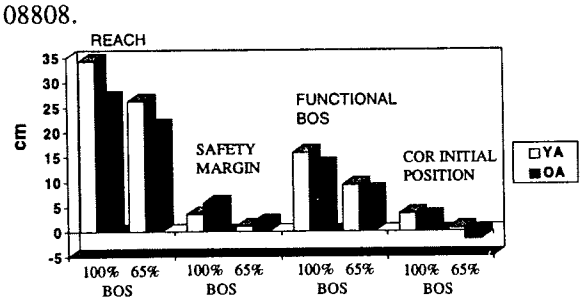

Fig. 1. Changes in reach distance and COR parameters with BOS manipulations and age.

PATTERNED CONTROL OF SHANK ORIENTATION IN SPACE DURING HUMAN UPRIGHT STANCE

G. Wu

Department of Physical Therapy
University of Vermont, Burlington VT 05405

INTRODUCTION AND BACKGROUND

Maintenance of spatial body orientation one of the main functions in postural control system [Massion, 1994]. Researches on pattern generators in control of locomotion have suggested that there exists an elaborate neural circuitry in the spinal cord (at least in animals) that is responsible for automatic execution of basic locomotion patterns [Marsden, 1982].

The purpose of this study was to establish evidence to further support the hypothesis that the control of human upright balance is by motor patterns via feedforward control mechanism during unexpected external perturbation of a balanced posture. In this study, the peak to peak magnitude spatial orientations of the foot and shank were measured when subjects' postural balance was unexpectedly disturbed. Their variations with respect to the surfaces and other conditions were examined.

METHODOLOGY

Postural perturbation was applied to the subject through an unexpected platform movement in the anterior-posterior direction of the subject. The maximum acceleration was $8m/s^2$, speed $40cm/s$ and total displacement $8cm$. The spatial orientation (or angular displacement) of the shank and foot in the sagittal plane was determined based on the measurements of Kinematometers [Wu and Ladin, 1993]. An accelerometer was attached to the movable platform to measure its acceleration in the moving direction. The output from the accelerometer was synchronized with the video data and collected at $120Hz$.

A total of 9 healthy subjects (mean age of 23.8 years) participated in this experiment. Each subject was tested for a total of 12 conditions, 4 times each, provided in a random, but blocked order. They included: vision/no vision, moving forward/backward, and standing on hard/soft/reduced surfaces.

Before each trial, the subject was asked to stand quietly on the movable platform. In response to the platform movement, s/he was instructed to try to maintain the upright balance by moving any part of the body except for the arms.

The maximum peak to peak magnitudes (P_{max}) of both foot and shank were determined and then compared using Analysis of Variance (ANOVA) to identify differences among the three surface conditions. Least Squares Means analysis was made to detect which differences among the surfaces were significant ($p < 0.05$).

RESULTS

The means of P_{max} of foot and shank on 3 surfaces are shown in Fig. 1. The results showed that there was no significant difference in shank P_{max} among three surfaces and between eyes open and closed conditions when the platform moved in either directions, except for one condition. The means of the foot P_{max}, however, were significantly larger when standing on soft and reduced surfaces. These increases were independent of vision and movement directions.

The time trajectories of foot and shank movement are shown in Fig. 2. Clearly, the shank movement patterns were independent of the surfaces. Regardless of the movement direction of the platform, the shank always rotated anteriorly to maintain balance. However, not only did the foot moved over a larger range as standing on the soft and reduced surfaces, it movement direction was determined by the platform movement.

DISCUSSION AND CONCLUSIONS

It is observed in this study that the foot and shank moved independently during the perturbed stance. Specifically, the movement pattern of the shank was not affected by any of the 12 test conditions, i.e., surfaces, visual condition and movement direction. This finding supports the hypothesis that the shank movement is controlled by a single motor pattern that is undisturbed by the changes in peripheral sensory information . Thus, it is likely that this control is initiated by a feedforward mechanism, rather than a feedback mechanism.

On the other hand, the foot movement was changing with respect to the surfaces. Even though all the subjects did not use stepping strategy to maintain their balance during the perturbed stance, their feet were not kept stationary in place. In fact, a previous study demonstrated that the foot movement was used to counter balance the shift of the center of gravity of the whole body, suggesting that the foot played a major role in postural control [Wu, 1997].

The independent relation between the foot and shank movement further suggests that the activation of ankle muscles, termed as ankle strategy [Horak and Nashner, 1986], does not necessarily mean that the two adjacent body segments (i.e., foot and shank) will act mutually to provide a single function. Similarly, the observation of the movement of the ankle joint does not necessarily provide direct information about the movement of each of the individual body segments involved.

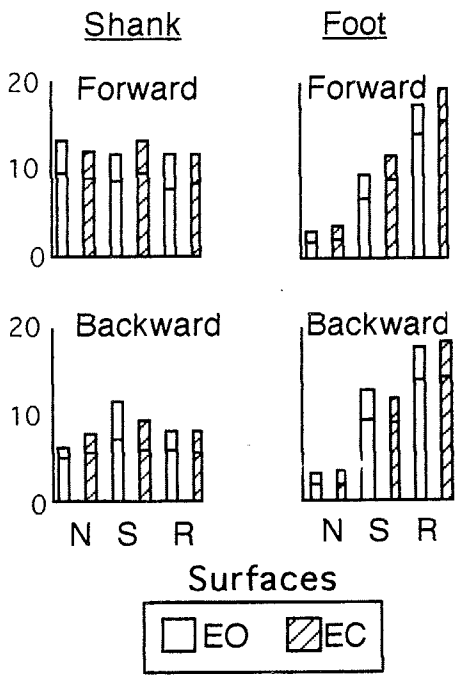

Fig. 1. Mean+std of shank and foot P_{max} [in deg] on normal (N), soft (S) and reduced (R) surfaces.

REFERENCES

Horak FB, Nashner LM. Central programming of postural movements: adaptation to altered support-surface configurations. J Neurophysiol 1986, 55: 1369-1381.

Marsden CD. The mysterious motor function of the basal ganglia. Neurology. 1982, 32:514-39,

Massion J. Postural control system. Curr Opin Neurobiol 1994, 4: 877-887

Wu G, Ladin Z. The kinematometer - an integrated kinematic segment for kinesiological measurements. ASME Trans Biomech Eng 1993, 115(1): 53-62

Wu G. Regulation of Spatial Body Orientation During Perturbed Stance in Young Adults. Exp. Brain Res. submitted, 1997

ACKNOWLEDGMENT

This work was supported by a grant from the Whitaker Foundation and by a National Institute of Health grant No. 1R29AG11602-01A2.

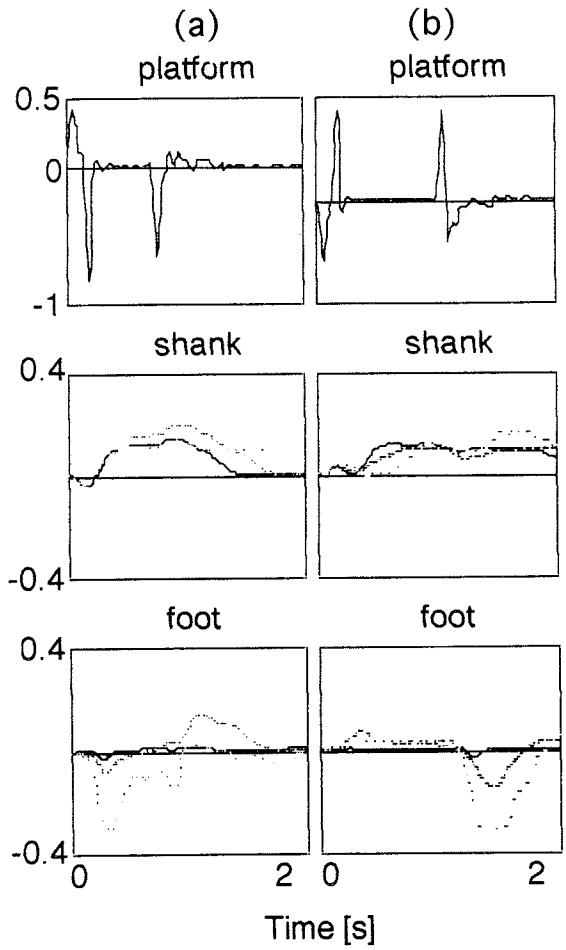

Fig. 2. Time trajectories of shank and foot movement [in rad] when standing on normal (solid), soft (dashed) and reduced (dotted) surfaces, with the platform moving in (a) forward and (b) backward directions, and eyes closed.

ANTICIPATORY ACTION FOR CHANGING DIRECTION DURING WALKING

D. Xu, K. Rosengren, J. Chow and L. Carlton
Department of Kinesiology, University of Illinois, Urbana, IL 61801

INTRODUCTION

Postural activities prior to a voluntary movement have been studied commonly for both standing postures (Belenkii, Gurfinkel, and Raltsev, 1967; Cordo and Nashner, 1982) and locomotion (Nashner and Forssberg, 1986; Patla, 1986). by examining perturbations of the upper limb. The present study examined how individuals adapt their gait and regulate their body configuration before altering direction during the prior step. The investigation examined the impulse of the ground reaction force (GRF), joint moments at the lower extremities, and the relationship between the center of mass (CM) of the whole body and center of pressure in order to understand the control strategy of the anticipatory action and how individuals adapt their gait.

REVIEW AND THEORY

The results of previous studies have showed that activity occurs in the postural muscles 40-60 msec prior to activity in the arm muscles when the subjects were asked to lift their arms (Belenkii, Gurfinkel, and Raltsev, 1967); Cordo and Nashner (1982) found that postural adjustments occur in the opposite direction of intended movement and postural adjustments are found with a variety of destabilizing body motions. In the investigation of the perturbation for locomotion by using the arm push and pull movement, the leg muscle responses associated with arm pulls and pushes, referred to as "postural activations," were directionally specific and preceded arm muscle activity (Nashner and Forssberg, 1986). Their results suggested that arm actions are preceded by posture responses in muscles of the legs and trunk. At present little is known about how and when preparations appear for locomotion , especially, for changing direction during walking. Patla (1991) found that the subjects could not change direction during an ongoing step, they must plan their altering direction on the prior step. In this study, two issues were examined included: 1) how and when do individuals generate a moment and thrust force for changing direction; and, 2) does the pivot foot, altering angle, and walking speed, affect the preparation for changing direction?

PROCEDURES

Subjects. There were eight young adults (six males and two females) who participated in this study. The age ranged was from 18 to 23 years. The height was from 1.65 to 1.80 m and the mass ranges from 56 to 79 kg. They all had no history of lower extremity injury.

Task. The subjects were asked to walk on two force platforms while walking straight forward and while changing direction. Two elementary turning movements were defined to represent walking while changing direction. They were turning to the right at 45 degrees and 90 degrees respectively. Two walking speeds of natural speed (1.35 ±0.15 m/sec.) and fast speed (1.85 ±0.15 m/sec.) were evaluated. Both right foot and left foot were used as the pivot foot for changing direction, respectively. Each subject performed 30 trials for these different pivot feet, walking speeds, and turn directions. The testing conditions were conducted in random order.

Instrumentation and Data Collection. Two AMTI force platforms and two Peak Performance video cameras were used to collect kinetic and kinematic data. The data were collected for one stride at 200 Hz and 60 Hz, respectively. A Peak Synchronization Event Unit was employed for synchronizing the force platform and video camera systems.

Data Reduction and Analysis. A mixed design (2 x 2 x 3) analysis of variance with repeated measurement for the impulses was used to determine the significant difference between a) the pivot foot, b) the walking speed, and c) altering angle conditions at the 0.01 alpha level. The moments of force at the lower extremity joints were computed in terms of the anatomic joint axes. The data, which were used for analysis of the joint moments of force were normalized by dividing the body mass before being averaged and plotted. The plotting data were ensemble averaged in these graphics.

RESULTS

The GRF of the prior step was examined in the statistic analysis. The dependent variables included

impulse for each force component during both striking phase and propelling phase. The results, shown in Table 1, indicate that 15 out of 18 variables were significantly different between walking in the different directions across the pivoting foot, walking speed, and altering angle conditions.

The results show that the moment patterns at the lower extremities were changed for altering different angles, especially the moments about the anterior posterior axis $\mathbf{M}_y$. There were considerable differences about the $\mathbf{M}_y$ component at the ankle, knee and hip joints for the prior step. The moment patterns were changed earlier for the fast walking speed than the natural walking speed. The trajectories of the CM were kept between the CP on the two feet during walking straight forward for both walking speeds. While changing direction, the trajectories of the CM were revealed differently during the prior step. Figure 1 presents an example of an individual trial while changing direction at 45^0. Trajectories of the CM shifted to the right of the CP for the ongoing step. There were significant changes for the fast walking speed while changing direction at 45^0 and 90^0.

Variables	FOOT	SPEED	ANGL
	F (1, 95	F (1, 95	F (2, 95
St.-Imp-x	199.09	39.636	54.017
St.-Imp-y	.008	10.478	46.779
St.-Imp-z	8.151*	50.001	31.517
Pr.-Imp-x	75.867	2.684	14.21*
Pr.-Imp-y	14.108	160.19	213.86
Pr.-Imp-z	1.103	360.53	97.657

Table 1: Summary of F Values from the 3 (turning angle) ×2 (pivot foot) × 2 (walking speed) ANOVA for Impulse of the GRF during the Prior Step. St.-Imp.-x, St.-Imp-y, and St.-Imp-z were impulse for the striking phase, and Pr.-Imp.-x, Pr.-Imp-y, and Pr.-Imp-z were impulse for the propelling phase.

DISCUSSION

All results suggest that changing direction during walking was prepared during the prior step. These anticipatory actions are reflected from the impulses, joint moments and body configuration. The results indicate that the muscular actions were regulated during this period of time. This type of adjustment and control strategy seem related to the turning angles and walking speeds. Individuals might even regulate the body configuration earlier during fast walking speed since some changes occurred at the beginning of the prior step. The results suggested that the anticipatory action was focused on the body lean since the significant changes were revealed of the moments $\mathbf{M}_y$. The foot location was limited on the force platform during walking, therefore, the body lean might be a better choice for regulating the body configuration. The results also indicated that walking and posture control appear to be interrelated activities. The profiles for the normal people in this study can be used to evaluate people with movement disorders. These results can also help understand the control strategy, posture, and muscle responses involved in the control of walking.

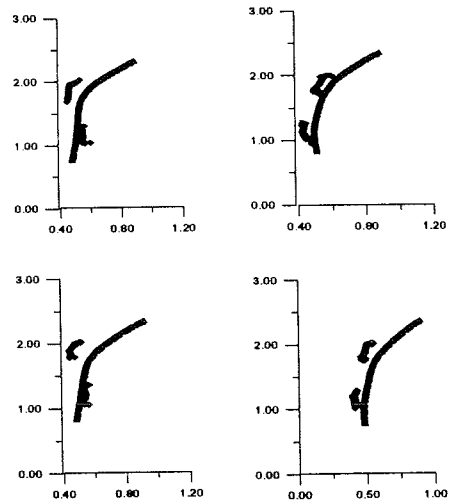

Figure 1: Trajectories of the CM and CP in the stride of changing direction at 45^0 with the different pivot feet and walking speeds. The top two plots show changing direction with the left pivot foot, the condition for fast walking speed is on the right. The bottom two plots were for changing direction with the right pivot foot and the condition for fast walking speed was plotted on the right.

REFERENCES

Bekenkii, V.Y., Gurfinkel, V.S. & Pal'sev, Y.I. Biophysics, 12, 154-160, 1967

Cordo, P.J. & Nashner, L.M. J of Neurophy. 47, 287-302, 1982

Nashner, L.M. & Forssberg, H. J of Neurophy. 55, 1382-1394, 1986.

Patla, A.E. Neuroscience Letters, 68,334-338,1986

Patla, A.E. & Stephen, D. P., Robinson, C. & Neufeld, J. JEP: HP&P 17, 3, 603-634, 1991

Xu, D. (1996). Unpublished Dissertation.

STABILITY IN NORMAL, ACL DEFICIENT AND ACL RECONSTRUCTED SUBJECTS

S.M. Colby[1], R.A. Hintermeister[2], M.R. Torry[2], J.R. Steadman[2]
[1]Division of Orthopaedics and Sports Medicine, Duke University, Durham, NC 27710
[2]Rehabilitation and Human Performance Lab, Steadman Hawkins Sports Medicine Foundation, Vail, CO 81657

INTRODUCTION

Functional testing of the ACL reconstructed (ACLr) and ACL deficient (ACLd) knee is important for evaluating the stability of the knee joint. Unfortunately, a limited number of functional tests have been reported in the literature (Barber et al, 1990, Harrison et al, 1994, Noyes et al, 1991, Risberg and Ekeland, 1994, Wilk et al, 1994). The goal of this study was to develop a functional test that could be used to differentiate between the injured and uninjured knee in ACLd and ACLr populations, and to establish the reliability of such measurement parameters.

REVIEW AND THEORY

Previous studies evaluating knee function after ACL injury have examined several types of tests including a one-legged hop for distance, a one-legged hop for time (Barber et al, 1990, Noyes et al, 1991, Wilk et al, 1994), and a single limb stance test (Goldie et al, 1989). However, it has been suggested that these tasks may not be sensitive enough to detect differences between the injured and uninjured limb (Barber et al, 1990, Noyes et al, 1991, Risberg and Ekeland, 1994, Wilk et al, 1994), or that they are testing an individual's ability to generate force, rather than the stability of the knee (Wilk et al, 1994). Additionally, the reliability and validity of many of these tests has not been established.

Stability has been defined as the ability to transfer the vertical projection of the center of gravity to the supporting base, and keep the knee as still as possible (Goldie et al, 1989). Subluxation in an ACLd or ACLr knee is most likely to occur at foot strike during running and jumping activities (McNair and Marshall, 1994). Since many activities involve landing on one leg, it is important to determine if an individual with an ACLd or ACLr knee has any type of instability when landing from a step down or a hop. Therefore the purpose of this study was threefold: 1) to establish normal variation for the step and hop tests, 2) to determine the reliability of criterion force plate measures of functional stability, and 3) to determine if criterion measures of functional stability could differentiate between injured and uninjured knees.

METHODOLOGY

Twenty-five healthy (Group 1), eleven ACLr (Group 2), and thirteen ACLd (Group 3) subjects were tested. The mean time since surgery was 158 (± 31) days for the ACLr subjects and 1213 (± 596) days for the ACLd subjects. Twelve healthy subjects participated in three testing sessions to determine reliability of the force plate measures. Force and moment data were collected for 3 seconds (200 Hz) while the subjects performed one-legged hop and step down tests onto a force plate (Bertec). The step test consisted of a single-limb step down from a height of 19 cm onto the force plate. The hop test consisted of a single limb hop with the distance relative to each subject's leg length (greater trochanter to lateral malleolus). The subjects practiced the movements before testing began, being instructed to look straight ahead, keep their hands on their waist, and to stabilize as quickly as possible at impact. Ten trials on each leg for each functional test were collected (Group 1 - dominant vs. non-dominant; Groups 2 and 3 - injured vs. uninjured). In addition, the ACLr group performed ten trials while wearing a brace.

The force and center of pressure signals (Fap,Fml,Fv,CoPap,CoPml) were analyzed to determine when they stabilized. A sequential estimation algorithm determined stabilization time when the sequential moving average fell within ± ¼ of a standard deviation of the overall mean (Clarkson et al, 1980). The standard deviations of the force and CoP signals were calculated as well. Another measure of vertical force stability (Fv%) was calculated as the time for the vertical force component to reach and stay within 5% of the subject's body weight after landing (McKinley and Pedotti, 1992). Intraclass correlations were computed to determine reliable parameters. Means and 95% confidence intervals were calculated for stabilization times and standard deviations of the force and CoP parameters for the percent difference in dominant vs non-dominant legs of normal subjects. Repeated measures ANOVA was used to determine differences in functional stability between injured and uninjured limbs.

RESULTS

The test-retest reliability results are shown in Table 1. Parameters with a correlation coefficient of 0.8 or higher on at least one limb were used for further analysis. The means and 95% confidence intervals for stabilization times and standard deviations for the normal subjects are listed in Table 2. A positive number represents a percent difference in favor of the dominant limb. Figure 1 shows the mean differences in stabilization times between the injured and uninjured limbs during the step down test for the

ACLr group. Stabilization times based on Fv took significantly longer for the injured limb with the brace ($p<0.001$) and without the brace ($p<0.001$) than for the uninjured limb. For the hop test, the standard deviation of Fv was significantly greater for the injured limb in the ACLd and less for the injured limb in the ACLr populations ($p < 0.05$).

DISCUSSION

This study demonstrated that the stabilization times produced from Fap, Fml, Fv, and Fv%, as well as the standard deviation of the Fap, Fml, and Fv signals were the most reliable measures during the hop test. These results are similar to the findings of Goldie et al (1989) who concluded that force measures were more reliable than center of pressure measures for quantifying postural steadiness during single limb stance. For the step down test, the stabilization times produced from Fap, Fml, Fv, CoPap, CoPml, and Fv% as well as the standard deviation of the Fv, CoPap, and CoPml signals were the most reliable parameters. The vertical force parameter did differentiate between injured and uninjured limbs for the ACLr population during the step down test, and for the ACLd and ACLr populations during the hop test.

The changed performance during the step down on the injured limb might be the result of an altered pattern of motion in compensation for increased knee instability (Gauffin and Tropp, 1992). In this study, there was a significant decrease in peak vertical force at foot strike during the step down for the injured limb for the ACLr population ($p < 0.01$). Differences in stabilization times between the injured and uninjured limb may be explained by kinematic and/or joint stiffness regulations made by the injured limb during the impact phase when absorbing body weight (Gauffin and Tropp, 1992) and/or during the support phase when transferring body weight. Either of these strategies could have altered the stabilization time between limbs. Future studies involving kinematics would help clarify this issue.

In conclusion, force plate stabilization times were reliable and did differentiate between ACLd, ACLr and uninjured limbs.

REFERENCES

1. Barber SD, et al., *Clin Orthop & Rel. Res.*, 255, 204-214, 1990.
2. Clarkson PM, et al., *Am J Clin Nutr.*, 33, 2245-2252, 1980
3. Gauffin H and Tropp H, *Am J Sports Med*, 20(2), 182-192, 1992
4. Goldie PA, et al., *Arch Phys Med Rehabil*, 70, 510-517, 1989
5. Harrison EL, et al., *Phys Ther*, 74(3), 245-252, 1994
6. McNair PJ and Marshall RN, *Arch Phys Med Rehabil*, 75, 584-589, 1994
7. McKinley P and Pedotti A, *Exper Brain Res*, 90, 427-440, 1992
8. Noyes FR, et al., *Am J Sports Med*, 19(5), 513-518, 1991
9. Risberg MA and Ekeland, *J Orthop Sports Phys Ther*, 19(4), 212-217, 1994
10. Wilk KE, et al., *J Orthop Sports Phys Ther*20(2), 60-73, 1994

	STEP TEST		HOP TEST	
Parameter	Dom	NonDom	Dom	NonDom
Fap	0.739	0.822	0.925	0.958
Fml	0.872	0.557	0.875	0.872
Fv	0.896	0.933	0.971	0.899
COPap	0.828	0.866	0.752	0.682
COPml	0.889	0.911	0.715	0.53
Fv%	0.933	0.942	0.768	0.885
SDFap	0.743	0.764	0.988	0.988
SDFml	0.538	0.744	0.966	0.951
SDFv	0.939	0.947	0.984	0.983
SDCOPap	0.791	0.959	0.754	0.062
SDCOPml	0.856	0.85	0.202	0.366

Table 1. The intraclass reliability coefficients for the stabilization times and standard deviations calculated from the forces (F) and centers of pressure (CoP) parameters.

	STEP TEST			HOP TEST		
Parameter	+ 95% CI	mean	- 95% CI	+ 95% CI	mean	- 95% CI
Fap	-1.2	-6.1	-10.9	1.8	0.0	-1.8
Fml	-13.1	-32.3	-51.4	28.2	8.5	-11.1
Fv	10.2	-8.0	-26.1	5.9	1.1	-3.7
COPap	34.0	8.2	-17.6	-		-
COPml	25.2	-2.7	-30.5	-		-
Fv%	40.5	-2.3	-45.1	-		-
SDFap	-		-	6.0	0.9	-4.2
SDFml	-		-	8.6	-8.8	-26.3
SDFv	26.2	1.5	-23.2	4.3	-3.1	-10.5

Table 2. Means and 95% confidence intervals for the normal subjects. Expressed as a percent difference between the dominant and non-dominant limb.

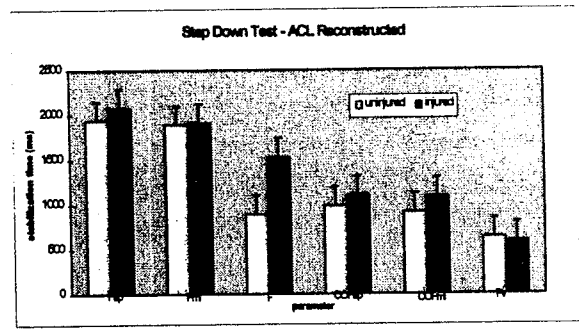

Figure 1. Stabilization times for the injured and uninjured limbs during the step down test for the ACL reconstructed group.

The Effect of Flexion Angle and Muscle Load on ACL Strain Under Applied Internal/External Tibial Rotation

Richard M. Greenwald

Orthopedic Biomechanics Institute, Salt Lake City, UT 84107

INTRODUCTION

The goal of this study was to study the role of knee flexion angle and quadriceps/hamstring loading on anterior cruciate ligament (ACL) strain and tibiofemoral kinematics under applied internal external rotation in an attempt to characterize joint positions which might be more likely to lead to ACL injury during non-contact twisting situations

REVIEW AND THEORY

The increasing incidence of anterior cruciate ligament (ACL) rupture in many sports has raised the level of concern about this particular injury among players, coaches, and the medical community. Non-contact injuries to the ACL occur frequently in sports, and often involve twisting of the leg near the extremes of the range of motion of the knee. In alpine skiing, for example, forward twisting falls occur, and may be representative of this torsional mechanism of ACL injury. Torsional laxity of the knee is a function of flexion angle, joint compression, muscular contraction, and time since exercise (Wang and Walker, 1974;Quinn et al., 1991). The ACL is considered to be a secondary restraint against tibial rotation and varus-valgus rotation, primarily near full knee extension. The purpose of this study was to simulate non-contact rotational loading on the knee joint in the laboratory and to determine ACL strain as a function of flexion angle and quadriceps and hamstring involvement. The null hypothesis tested was that there is no effect of flexion angle or muscle loading on ACL strain under applied internal or external femoral rotation.

PROCEDURES

A total of eight human cadaver knee joints (mean age 42, range 35-50) were carefully dissected leaving the joint capsule, knee ligaments, extensor mechanism, and flexor mechanisms intact. Two muscle actuators were constructed to provide closed-loop controlled force generation in both the quadriceps and hamstring (medial and lateral) tendon groups. The femur was fixed in an aluminum pot with low melt alloy and secured to the displacement and rotation actuator of an MTS 858 Bionix test system (MTS, Minneapolis, MN). The custom test jig allowed adjustment of the anterior/posterior orientation of the bone with respect to the actuator (flexion/extension), freedom of motion in the medial/lateral direction (varus/valgus), constrained rotation (internal/external), and all three translations. The tibia was attached directly to the base of the MTS through a jig that allowed adjustment of the anterior/posterior orientation of the bone with respect to the base, and constrained the other five degrees of freedom. These constraints were implemented so that the testing performed would more closely simulate loading conditions that might occur during a fall in alpine skiing. A six DOF kinematic linkage (ISL, Minneapolis, MN) was attached to the lateral aspect of the femur and tibia to measure tibiofemoral kinematics. A schematic of the test system is given below in Figure 1.

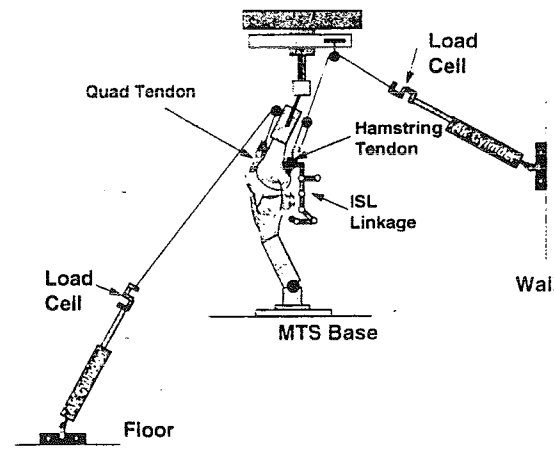

Figure 1 - Schematic of cadaveric test system showing ISL linkage, muscle actuators, and attachment configuration

A medial parapatellar incision was made to expose the joint capsule and the ACL. A differential variable reluctance transducer (DVRT, Microstrain, Burlington, VT) was attached to the anteriomedial bundle of the ACL, and preconditioning and reference positioning was performed (Fleming et al., 1994). A compressive load of 100 N was applied

and maintained through the simulated hip joint using the MTS actuator in load control. The cadaver knee was randomly fixed at either 0, 20 or 45° of flexion and neutral rotation. Muscle tension for both the quadriceps muscle group and hamstring muscle group was set randomly at 10 N, 100 N or 200 N of co-contraction. Using the rotation actuator of the MTS system, the femur was cyclically rotated through a 20 degree range for both internal and external rotation. The resulting torque at the simulated ankle joint and ACL strain were measured throughout the range of femoral rotation. A complete sequence included all three flexion angles and three muscle conditions. Separate two-way analyses of variance were performed to compare the ACL strain values at either maximum internal or external rotation between the three flexion angles and between the three muscle conditions. A p-value of .05 was used to determine statistical significance. Appropriate post-hoc analyses were done where necessary using the Student-Neuman-Kuels method.

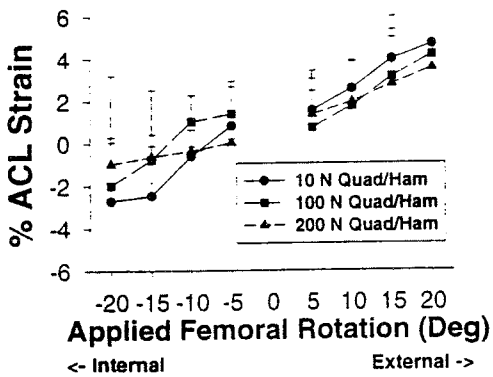

Figure 2 - Average ACL strain vs. applied femoral rotation at 0° knee flexion for three muscle load combination

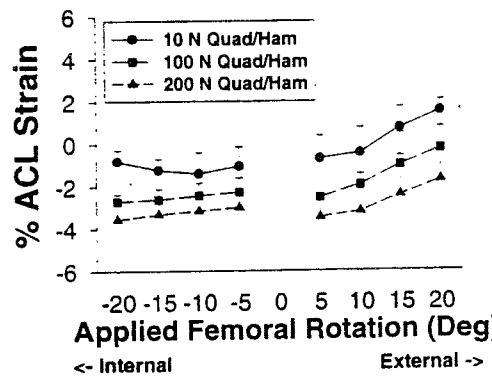

Figure 3 - Average ACL strain vs. applied femoral rotation at 45° knee flexion for three muscle load combination

RESULTS

Average ACL strains for applied internal and external femoral rotation at 0° and 45° of knee flexion for the three levels of quadriceps and hamstring co-contractions are shown in Figures 1 and 2. Data for 20° of knee flexion were similar but of lower strain magnitude than at 0°. ACL strain was significantly affected by knee flexion angle ($p<.01$) for internal tibial rotation only but not by muscle load ($p>.05$).

DISCUSSION

ACL strain with applied femoral rotation was highly dependent on knee flexion angle, with increasing strain as the knee approached full extension. At 45° of knee flexion, there was negligble ACL strain at all internal and external rotations tested. While not statistically significant, increased levels of quad/ham co-contraction resulted in decreased ACL strain at all flexion angles tested, with a 23% decrease in strain at 0° of knee flexion for 200 N vs 10 N muscle loads. ACL strain increased with internal tibial rotation, while external rotation had no effect. These results parallel those of Markolf et al (1990), who found that ACL load was maximum during internal tibial rotation and was negligible during external tibial rotation. ACL load at 0° was the highest compared to other knee flexion angles, and addition of a 200 N quadriceps force did not significantly alter ACL load. The role of dynamic muscle stabilization in preventing excessive ACL strain during a twisting episode has not been well documented. These data imply that the risk of ACL injury increases when the muscles are less active and when the knee is near full extension. Limitations of the study include a lack of applied varus/valgus rotation and 1-D measurement of ACL strain in one bundle of the ligament. The potential exists to incorporate these data into equipment designs and education strategies intended to reduce the incidence of ACL rupture.

REFERENCES

Fleming, BC, et. al., *JOR.* **12**, 789-795, 1994.
Markolf, KL, et al *JBJS.* **72A**, 557-567, 1990.
Quinn, TP, et al. *J. Biomechanics* **24**, 511-525, 1991.
Wang, C. J. and Walker, P. S. *JBJS.* **56A**, 161, 1974.

ACKNOWLEDGMENTS

This work was supported in part by a research grant from Smith and Nephew. Many thanks to Scott Harris and Ben Kaplan for their technical assistance.

IMPACT MECHANICS OF THE RABBIT MCL

J.J. Crisco[1,2], D.C. Moore[1], R.D. McGovern[1]

[1]Department of Orthopaedics, Rhode Island Hospital, Providence, RI
[2]Division of Engineering, Brown University, Providence, RI

INTRODUCTION

An impact loading protocol was used to study the dynamic mechanical behavior of ligamentous tissue at loading rates higher than those attainable with the use of standard materials testing systems. The results of these studies, coupled with results obtained via quasi-static ligament testing, were used to explore the effect of loading rate on the viscoelastic response and failure strength of rabbit medial collateral ligaments.

REVIEW AND THEORY

Loading rate has a profound effect on the behavior of viscoelastic biological materials such as ligaments and tendons (Noyes et al., 1974). In these materials, increases in the rate of extension lead to increases in stiffness, failure load, and energy to failure, but little if any change in failure displacement (Woo et al., 1990). However, these relationships have been developed with the use of standard materials testing systems and protocols that result in quasi-static loading (i.e. the rate of loading is much less than the rate of stress wave propagation).

In contrast, *in vivo* ligamentous injury is generally the result of an impact load or a high-speed dynamic event, with rates easily exceeding 1 m/s (Crowninshield et al., 1976). In these cases, the rate of loading is similar to the rate of stress wave propagation through the ligament (Crisco et al., 1996). It was our hypothesis that high loading rates would exaggerate the viscoelastic behavior of the tissue, leading to large deviations from the behavior determined with simple quasi-static testing.

The purpose of this study, therefore, was to explore the mechanical behavior of ligamentous tissue under impact loading.

PROCEDURES

Both hind limbs from ten skeletally mature (age > 18 mos., epiphyses closed on X-ray) New Zealand white rabbits were used. At sacrifice, the femur and tibia of each hind limb were removed *en bloc* from the surrounding soft tissues, and all of the structures at the knee joint were cut except the medial collateral ligament (MCL).

One MCL from each pair was randomly selected for quasi-static testing. The femurs of these limbs were mounted to the actuator of a servohydraulic materials testing system. The tibias were attached to a 1 kN load cell (661.16A01, MTS Systems Corporation, Eden Prairie, MN) through a mounting stud attached to the tibia with a PMMA casting. Tensile testing was continued to failure under displacement control at a rate of 0.167 mm/s. Load and displacement data were recorded at 100 Hz and post-processed to yield values for ligament stiffness, failure load, and energy to failure.

After the quasi-static testing was performed, the contralateral MCLs were impact tested using a drop-weight device. The femurs of these limbs were mounted to a piezoelectric load cell (208 B03, PCB Piezotronics, Inc., Depew, NY), and a one meter drop-weight guidewire (0.0625" dia.) was suspended from the tibia. A second piezoelectric load cell was mounted between the tibia and guidewire. Displacements were measured with an LVDT (500-MHR, Lucas Control Systems, Hampton, VA) mounted in parallel with the ligament.

The ligaments were impacted by dropping a 5 kg mass down the guidewire. Five MCLs were tested at a drop height of 10 cm (impact velocity = 1400 mm/s), and five were tested at a drop height of 70 cm (impact velocity = 3750 mm/s). A 5 kg drop mass was used to

guarantee ligament failure. With this mass, the impact energy available in a 10 cm drop was ten times larger than the average energy to failure during quasi-static testing. During impact testing, load and displacement were recorded at 250 kHz.

Force-time and displacement-time data were synchronized at the point where each signal first rose above the baseline noise. Failure load was defined as the point on the load-displacement curve where load dropped precipitously. Loading rates were determined with a least squares regression of the initial, linear portion of the load-time curve. Displacement rates were calculated by dividing displacement at failure load by time to failure load.

RESULTS

The measured displacement rate from the 10 cm drop height was 1,015 ± 103 mm/s and the displacement rate from a 70 cm drop was 3,712 ± 910 mm/s. During quasi-static testing the loading rate was 0.02 kN/s, while the loading rates in the impact tests were 86 ± 11 kN/s at the 10 cm drop height and 350 ± 34 kN/s at the 70 cm drop height.

A plot of loading rate versus displacement rate for the two series of impact tests revealed that at high loading rates, ligament stiffness was relatively constant (Figure 1). At these rates, the response to loading was not viscoelastic. (Stiffness was calculated by dividing the loading rate by the displacement rate.)

The impact failure loads were significantly greater than the quasi-static failure loads, ($p < 0.02$); however, there was no significant difference between the failure loads of the two impact tests (Figure 2). The quasi-static failure load (n=10) was 347 ± 87 N. The failure loads at 10 cm (n=5) and 70 cm (n = 5) drop heights were 446 ± 85 N and 424 ± 14 respectively.

DISCUSSION

In this study ligamentous tissue was impact tested to approximate the loading rates believed to be involved in clinical injury. Contrary to our expectation that the viscoelastic behavior of ligamentous tissue would be exaggerated at high loading rates, a comparison of the results from the three testing protocols used in the study suggests that, above a relatively low displacement rate threshold, 1) ligaments respond elastically (i.e. with constant stiffness), and 2) ligament failure strength becomes independent of loading rate.

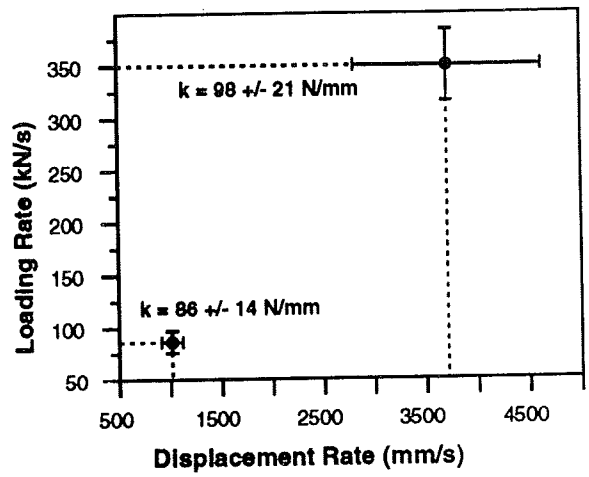

Figure 1. Ligament stiffness was constant (i.e. not viscoelastic) at high loading rates.

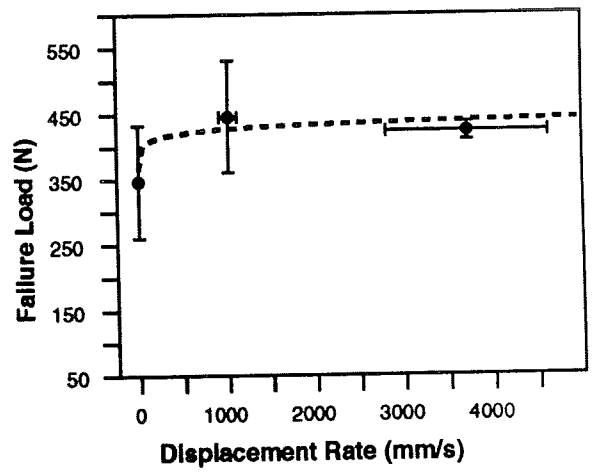

Figure 2. At high displacement rates, failure load was independent of loading rate.

REFERENCES

Crisco JJ, et al. Proc 20th ASB, 1996
Crowninshield RD. et al. J Trauma 16(2), 1976
Noyes FR, et al. JBJS 56A(2):236-253, 1974
Woo SL-Y, et al. J Ortho Res 8:712-721, 1990

"*In vivo*" DETERMINATION OF HIP JOINT SEPARATION AND THE FORCES GENERATED DUE TO IMPACT LOADING CONDITIONS

E.J. NORTHCUT[1,2], R.D. KOMISTEK[1,2], D.A. DENNIS[1,2], J.A. OCHOA[3], W.A. HOFF[2]

[1]ROSE MUSCULOSKELETAL RESEARCH LABORATORY, DENVER, CO, 80222
[2]DIVISION OF ENGINEERING, COLORADO SCHOOL OF MINES, GOLDEN, CO
[3]JOHNSON & JOHNSON P.I., RAYNHAM, MA

INTRODUCTION

Premature polyethylene failure is a major concern in the Total Hip Arthroplasty (THA). The normal hip joint prior to THA is quite commonly found disrupted or degenerated, requiring the resection of many supporting structures. During THA, resection of the femoral head within the acetabulum of the normal hip joint along with numerous supporting structures including the ligament of the head of the femur (LHF) occurs. Additionally, a portion of the remaining supporting structures are transected or resected to facilitate surgical exposure. The present study focuses on effects caused by the absence of the LHF in patients implanted with THA.

PROCEDURES

Initially, nineteen subjects were analyzed. Five subjects had a normal hip, ten subjects were implanted with an unconstrained THA and four subjects were implanted with a constrained cup THA design. A surgeon control was used, where each subject having a THA were implanted by the same surgeon. All subjects implanted with THA were judged clinically successful (Harris hip scores > 94.7). Each subject performed successive abduction/adduction leg lifts under fluoroscopic surveillance. The normal hip fluoroscopy videos were analyzed using a two-dimensional digitization technique in order to determine hip kinematics. The subjects having a THA were analyzed using a three-dimensional model fitting technique (1). Video frames at 30 frames per second of the abduction/adduction cycle were downloaded onto an SGI work station using a JPEG video compression board. A computer algorithm was utilized to select the best-fit 3D overlay of the 2D fluoroscopic silhouette images. Using AutoCAD, the components were then grouped together and rotated to a pure frontal view. Digitization was utilized to determine the distance between the femoral head and the acetabular cup. An error analysis was conducted by using fluoroscopy on an apparatus with THA components mounted. The components were separated at known distances and rotated out of plane (Figure 1). Each image was then analyzed to determine the amount of acetabular separation. The predicted values were then compared to known values to determine relative error. The average error for this analysis was less than 0.3 mm. Since the error analysis was conducted using a mechanical device and not under *in vivo* conditions, a threshold of 0.75 mm was used to define when acetabular separation occurred in the THA subjects. Using the impulse and momentum equation, a mathematical model was derived to determine the force at impact between the femoral head and the acetabular cup.

RESULTS

During the abduction/adduction cycle no separation was observed in subjects having a normal hip or subjects having constrained cup THA. However, separation of the femoral head from the acetabular component was commonly observed subjects having an unconstrained THA. The average amount of maximum separation for each subject having a THA was 3.1 mm (max=5.4 mm, min=1.9 mm). All ten subjects with the unconstrained prosthesis had at least 1.0 mm of separation, and 20% of the subjects separated at least 5.0 mm. The maximum force due to impact was 851.6 Newtons for one subject (Figures 2,3), and the minimum amount of force during impact was 23.3 Newton (Table 1). The average amount of impact force was 289.5 Newtons.

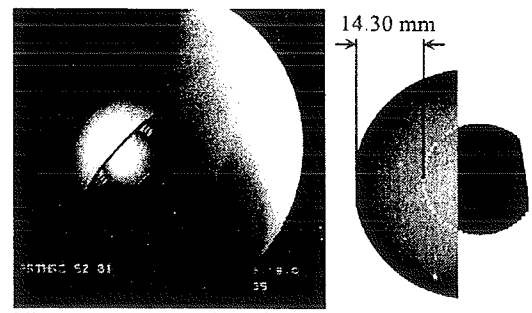

Figure 1. Example of overlay and separation of femoral component from the acetabular component.

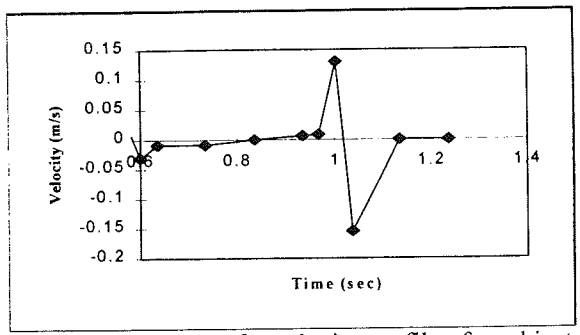

Figure 2. Segment of a velocity profile of a subject showing separation.

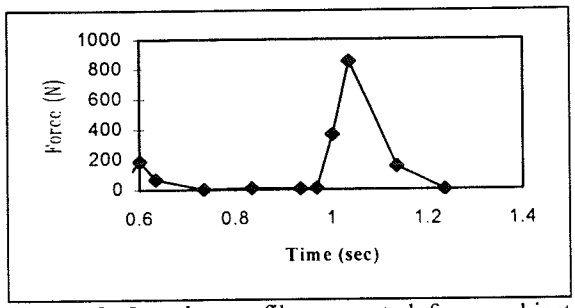

Figure 3. Impulse profile generated for a subject displaying separation

Subject	*Max Separation (mm)*	*Velocity (m/s)*	*Max Force (N)*
Not constrained			
1	2.30	0.112	23.3
2	2.49	0.060	45.9
3	4.06	0.201	259.1
4	1.86	0.035	137.2
5	2.01	0.026	112.8
6	5.38	0.129	719.8
7	3.11	0.030	456.3
8	5.22	0.143	851.6
9	1.83	0.041	140.7
10	1.91	0.036	147.9
constrained			
1	0.57	0.003	5.08
2	0.37	0.002	4.59
3	0.46	0.005	6.72
4	0.42	0.004	5.36

Table 1. Results of Maximum separation, change in velocity and maximum force occurring in the THA

DISCUSSION

This study has shown that separation of the prosthetic femoral head from the acetabular component can occur. The force due to impulse caused by two objects colliding has been shown to compromise the structural integrity of mechanical components (2). The normal hip joint has surrounding ligamentous structures and a ligament that attaches to the femoral head and the acetabulum. We hypothesize that these ligaments create a passive, resistant force at the hip joint that prevents the femoral head and the acetabulum from separating during gait. The absence of these supporting soft tissue structures following THA may generate unnaturally high joint forces that could lead to premature polyethylene wear at the hip joint. These increased loads could further effect bimaterial interfaces (such as implant/cement/bone) which are by nature susceptible to fracture and could lead to gross loosening of prosthetic components. This separation may occur during abduction/adduction leg lifts because patients do not rehabilitate their abduction/adduction muscles satisfactorily. During the abduction leg lift, it appears that the femoral head separates from the acetabular cup, but remains in contact with the most superior ridge of the cup. As the leg abducts, the femoral head pivots about a point on the polyethylene liner of the cup. Therefore, a follow-up study will be conducted to determined if this phenomenon occurs during gait exercises. It is assumed that during level walking, acetabular separation may not occur due to the fact that the flexor/extensor mechanisms are more rehabilitated.

CONCLUSION

The kinematics of the hip does change when the LHF and other supporting structures of the hip are removed during THA. The impulse loading conditions may contribute to premature polyethylene failure in THA. These conditions are hypothesized to exist within the implanted joint at a slightly faster rate than what we can measure experimentally. Mathematical models were written assuming a faster time increment which directly effects velocity, acceleration, and impulse calculations. Using this faster time increment, the maximum hip joint separation was 2844.3 Newtons. Therefore, a continuation study has been proposed to experimentally capture fluoroscopic video frames at a rate of 60 Hz or higher to determine if the loads predicted with the mathematical model are correct.

REFERENCES

[1] Dennis D.A., et. al. 1996. CORR
[2] Reinhart J.C., et al., Behavior of Metals Under Impulse Loads, Prentice Hall, 1962

RATE INDEPENDENT CHARACTERISTICS OF AN ARTHROSCOPICALLY IMPLANTABLE FORCE PROBE IN THE HUMAN ACHILLES TENDON

G. Hall[1], G. Klopp[1], J. Crandall[1], D. Carmines[2], J. Hale[2]

[1]University of Virginia Automobile Safety Laboratory, Charlottesville, VA 22902
[2]Department of Orthopaedics, University of Virginia, Charlottesville, VA, 22908

INTRODUCTION

Recent advancements in implantable sensors for cadaveric applications have enabled researchers to examine the internal loads within soft tissue structures. Previous studies have shown that implantable force transducers may be affected by the rate of loading of the tissue under test (Herzog et al., 1996). The effect of loading rate on implantable force probe calibration was investigated in the Achilles tendon of four cadaveric specimens.

REVIEW AND THEORY

Forces applied to the plantar surface of the foot are transmitted to the tibia, fibula, and surrounding musculature. By measuring the Achilles tendon tension and tibia force with implantable force sensors, and measuring all the external and inertial forces, the axial load in the fibula can be calculated by solving for dynamic equilibrium. The tendon/force probe system must be calibrated after dynamic testing to calculate tendon force from the test data. In cases of dynamic tests, it is often difficult to calibrate at the same displacement rate as the test. This study investigated whether or not the loading rate of the tendon affected the slope of the force probe calibration curve, i.e. sensor sensitivity.

PROCEDURES

Transverse loading within the Achilles tendon was measured with an arthroscopically implantable force probe (AIFP) (MicroStrain, Burlington, VT). This device consists of a C-shaped piece of metal with a strain gauge on its spine (Figure 1, 1/2 bridge model shown). The strain gauge is wired in a quarter bridge configuration and delivers a signal that is linear with transverse load across the sensor. The AIFP was inserted into the midsubstance of the Achilles tendon in the AP direction. The transverse load generated by the tendon against the probe walls was measured while tensile loads were applied to the Achilles tendon. The relationship between the axial tension in the tendon and the AIFP signal was examined at rates of 0.25 cm/sec, 2.5 cm/sec, and 12.7 cm/sec to determine the importance of calibration strain rates.

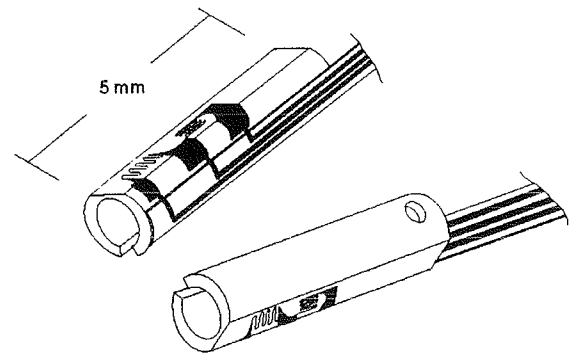

Figure 1: AIFP Sensor

Four above-knee, cadaveric lower extremities were disarticulated at the ankle joint, leaving the Achilles tendon intact (Table 1). The distal femur was fastened to the actuator of a hydraulic testing machine (MTS Bionix, Model 858) with a rope harness (Figure 2). The foot was fastened to the test machine base with a ratcheting strap over the calcaneus.

A triangular wave forcing function was applied to each specimen at the prescribed loading rate of testing for a duration of 10 cycles to precondition the tissue. Our preliminary testing with the AIFP and the

Test	Sex	Age	RMS Error	% MT
1	M	85	8.0 N	1.4
2	F	70	12.4 N	1.3
3	M	77	8.7 N	0.9
4	F	59	25.5 N	2.5

Where: RMS Error is for all three data sets about the regressed line. % MT is RMS Error divided by maximum tendon tension from the test as percent.

Table 1: Specimen Description

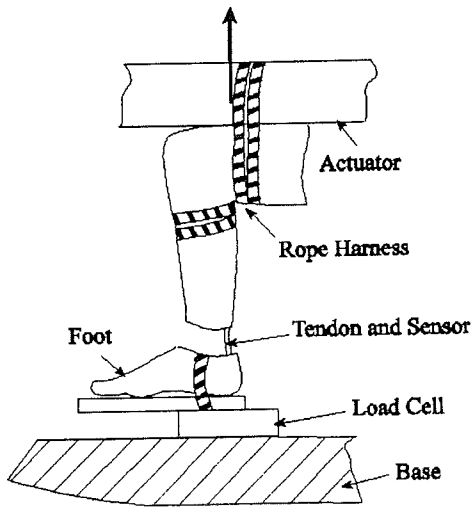

Figure 2: Test Set Up

Achilles tendon had shown that five to six cycles are enough to obtain repeatable tissue and AIFP behavior at a given loading rate. After preconditioning, the tendon was loaded at a constant displacement rate until either the AIFP reached its maximum allowable transverse force (14 N), or the tendon tension exceeded 1000 N.

RESULTS

The results indicate that the relationship between Achilles tendon tension and AIFP signal are not rate dependent (Figure 3). Data for each Achilles tendon from the slow, medium, and fast tests were regressed to one second order, polynomial curve with a mean coefficient of determination, R^2, of 99.6%. The mean RMS difference between the three loading rate data sets was 1.6 % of the full load value (Table 1).

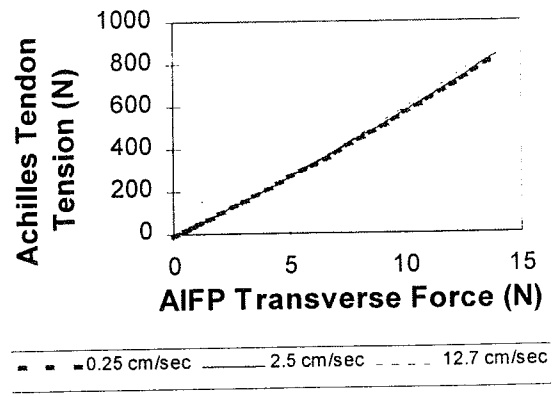

Figure 3: Sample Calibration Results at Three Strain Rates.

DISCUSSION

The results indicate that the sensitivity of the AIFP/ Achilles tendon system is primarily a function of axial force in the tendon and is not significantly affected by changes in loading rate. This contrasts the results reported by Herzog et al. (1996) who found significant changes in sensor sensitivity due to alterations in loading rate. The difference between our findings and those of Herzog may be due to either the relative size between sensor and tendon, the current study using a smaller sensor, or to a difference in sensor design. This finding validates the use of slow speed calibration tests for high speed tendon loading tests which will facilitate post-test calibration. It also demonstrates that multiple calibrations are not necessary for multi-speed tests.

REFERENCES

Herzog, W. et al., J. Biomech., 29, 103-109, 1996.

ACKNOWLEDGMENTS

MicroStrain, Inc., Burlington, VT. for technical support.

USING A TWO-STEP SEQUENCE INDEPENDENT METHOD AND A SPHERICAL ROTATION COORDINATE SYSTEM TO DESICRIBE 3D LIMB SEGMENT OR JOINT ROTATIONS

Pei Lai Cheng
Bioengineering Unit, University of Strathclyde, Glasgow, G4 ONW, UK

INTRODUCTION

Sequence dependence of the Euler/Cardan angles is an unsolved problem in the process of standardization for representation of kinematic data in the field of biomechanics. In this paper a new system, spherical rotation coordinate system, was developed to represent the 3D joint or limb-segment rotations with three sequence independent angles, longitude, latitude, and a radial rotation angle.

REVIEW

Since representation of kinematic data is under way of standardization (Wu & Cavanagh 1995, Woltring 1994, Cole et al. 1993), using which method to describe the 3D rotation of a limb segment or joint became a topic of debate in the field of biomechanics. Generally, each of the three most commonly used methods (Euler/Cardan angles, Instantaneous screw axis method, and the floating axis method) has its own advantages and disadvantages. Euler/Cardan angles is a most popular traditional method in the fields of engineering, science and biomechanics, but it gives most confusing results when it was applied in the studies of human movement due to its sequence dependence. Instantaneous screw axis method, also widely used (Woltring 1994), describes a unique rotation from one attitude to another that, however, is difficult to be interpreted in clinical terminology. Therefore it can not be easily understood by clinicians. Based on geometrical considerations, the coordinate system with a floating axis (Chao 1980, Grood and Suntay 1983) was used to describe the kinematics of the knee joint. However the geometrical characteristics of some other joints such as shoulder joint may not allow the floating axis to be properly located, which limits its application. Different opinions also existed on whether the floating axis method is sequence dependent or not (Woltring 1994). Therefore a sequence independent description for 3D joint or limb segment rotation is urgently required.

THEORY

From direct observation it was found that 3D joint or limb segment rotations can be described by a two-step rotation (Cheng, 1996, Cheng et al., 1996), a long axis rotation and a pure axial rotation (Figure.1). Where the pure axial rotation ϕ is about the long axis of the limb segment, while the long axis rotation θ is

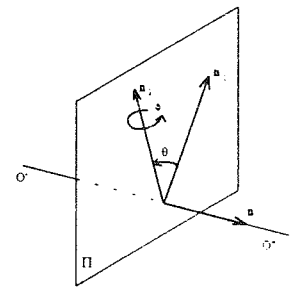

Figure 1. 3D limb segment or joint rotation is described as a two-step rotation

about an rotation axis O'O" with a unit vector **n** that passing through the proximal joint of the limb segment and perpendicular to the long axis. In Figure 1 $\mathbf{n}_1$ and $\mathbf{n}_2$ are two unit vectors representing the initial and final positions of the long axis in the reference frame, θ and ϕ are the long axis rotation angle and axial rotation angle respectively. Known any two attitudes of the limb segment in a reference frame from measurement of a human motion analysis system, the two rotation angles can be uniquely

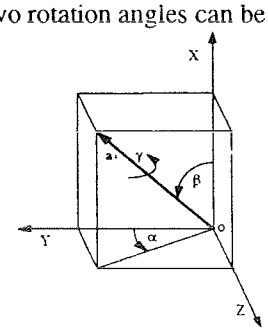

Figure 2. A spherical rotation coordinate system

determined mathematically (Cheng 1996; Cheng et al., 1996). Since the axial rotation angle is always about the long axis, and considering the long axis position in the reference coordinate system, a new coordinate system is constructed (Fig. 2). Where longitude α and latitude β in the classical spherical

coordinate system are used to represent the rotation angle of the long axis, a radial rotation angle γ is used to describe the pure axial rotation angle. There are two differences between this coordinate system and the classical spherical coordinate system. First the new system is used for describing the 3D rotations of a rigid body rather than displacements of a particle. The second difference is the use of radial rotation angle instead of radial displacement. Therefore this system is called as a spherical rotation coordinate system (SRCS).

ROTATION MATRIX

Assuming the long axis of the limb segment with a unit vector $\mathbf{a}_0$ coincided with the X-axis of the reference coordinate system initially (Fig. 3). From the initial position the long axis of the limb segment rotate an angle β about an axis with unit vector $\mathbf{n}$ to position $\mathbf{a}_1$. The position of $\mathbf{a}_1$ is determined by the longitude α and latitude β of the spherical rotation coordinate system. The rotation from $\mathbf{a}_0$ to $\mathbf{a}_1$ can be described by a rotation matrix $\mathbf{R}_l(\alpha, \beta)$. The pure axial rotation γ can be either about $\mathbf{a}_0$ which can be described by a rotation matrix $\mathbf{R}_a(\gamma, \mathbf{a}_0)$ or about $\mathbf{a}_1$ which can be described by a rotation matrix $\mathbf{R}_a(\gamma, \mathbf{a}_1)$. Therefor there are two sequence rotations for the two-step rotation. One is the axial rotation followed by the long axis rotation. The other is the long axis rotation followed by the axial rotation. It has been mathematically proved that the two sequences are equivalent (in the full paper submitted to the same meeting). A unique integrated rotation matrix has been found as:

$$\mathbf{R}(\alpha,\beta,\gamma) = \mathbf{R}_l(\alpha,\beta)\mathbf{R}_a(\gamma,\mathbf{a}_0) = \mathbf{R}_a(\gamma,\mathbf{a}_1)\mathbf{R}_l(\alpha,\beta) =$$

$$\begin{vmatrix} c\beta & -s\beta c\alpha c\gamma - s\beta s\alpha s\gamma & s\beta c\alpha s\gamma - s\beta s\alpha c\gamma \\ s\beta c\alpha & c\beta c\alpha c\gamma + (1-c\beta)(s^2\alpha c\gamma - s\alpha c\alpha s\gamma) & -c\beta c\alpha s\gamma - (1-c\beta)(s^2\alpha s\gamma + s\alpha c\alpha c\gamma) \\ s\beta s\alpha & c\beta s\alpha c\gamma + (1-c\beta)(c\alpha s\alpha c\gamma - s\alpha c\alpha s\gamma) & -c\beta s\alpha s\gamma + (1-c\beta)(c^2\alpha c\gamma + s\alpha c\alpha s\gamma) \end{vmatrix}$$

where s=sine, c=cosine. In above equation rotation matrix $\mathbf{R}_l(\alpha, \beta)$, $\mathbf{R}_a(\gamma, \mathbf{a}_0)$ and $\mathbf{R}_a(\gamma, \mathbf{a}_1)$ has similar form as:

$$\mathbf{R}(\psi, \mathbf{n}') = \cos\psi \mathbf{I} + (1-\cos\psi)[\mathbf{n}'][\mathbf{n}']^T + \sin\psi[\tilde{\mathbf{n}}']$$

where ψ is a rotation angle about a rotation axis $\mathbf{n}'$.

DISSCUSSION AND CONCLUSION

A spherical rotation coordinate system (SRCS) is developed in the paper based on the two-step rotation method. The full range of 3D rotations of limb segments or joints can be described with the three angles (longitude, latitude and radial rotation angle) in the SRCS. It has been mathematically proved that the long axis rotation and pure axial rotation are sequence independent. More importantly, the long axis rotation angle β (latitude) can occur at any angle α (longitude). Given an initial attitude, except for the long axis at neutral position when β=0, each of the three angles can change individually when other two angles were fixed. Therefor the three rotation angles in the SRCS are sequence independent. This

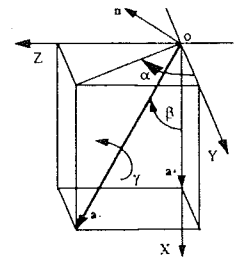

Figure 3. Long axis rotation from $\mathbf{a}_0$ to $\mathbf{a}_1$ about the axis $\mathbf{n}$

important property is the lack of previous conventions especially for the Euler/Cardan angles. All sequenced Euler/Cardan angles can be described in the SRCS. With the clear definitions of the three angles, it is believed that the SRCS can be easily understood by clinicians. As a conclusion, the SRCS provides a sequence independent, reliable and easy understandable method for the description and representation of 3D limb segment or joint rotations in nearly the same way as real movements that we observed in daily activities. It is hoped that the confusion over the standardization issue has been cleared since the disadvantages of previous methods have been overcome. It is expected that this method can be used in the investigations of any limb segment or joint rotations during various activities.

REFERENCES

Chao, E. Y. S., J. Biomechanics, **13**, 989-1006, 1980.

Cheng, P. L., Biomechanical Study of Upper Limb activities of Daily Living. Ph.D. Thesis. University of Strathclyde, Glasgow, UK. 1996.

Cheng, P. L., et al. J. Biomechanics, submitted, 1996.

Cole, G. K., et al., J. Biomech. Eng., **115**, 334-349, 1993.

Grood, E. S., et al., J. Biomech. Eng., **105**, 136-144, 1993.

Woltring, H. J. Biomechanics, **27**, 1399-1414, 1994.

Wu, G. et al, J. Biomechancis, **28**, 1257-1261, 1995.

EXPERIMENTAL VALIDATION OF A COMPUTATIONAL SIMULATION OF DISLOCATION IN THA

C F Scifert, T D Brown, D R Pedersen, J J Callaghan

Departments of Orthopaedic Surgery and Biomedical Engineering, University of Iowa, Iowa City, IA 52242

INTRODUCTION

Finite element (FE) simulations provide an opportunity to study the mechanics of total hip dislocation without the drawbacks of patient trials, but carry a burden of proof with regards to demonstrating the validity of the results. We report the development and operation of an experimental apparatus to validate the results of a finite element model simulation of a total hip dislocation

REVIEW AND THEORY

Next to aseptic loosening, recurrent dislocation is the second leading cause of failure in total hip arthroplasty [1]. Impingement of the femoral component neck on the acetabular cup is a frequent mechanism. Dislocation rates range from 2-11% in primary THA surgeries, up to 25% or more in revisions [2]. Despite this high incidence, little research has been performed to learn about contributory component design factors and how they effect the dislocation resistance and range of motion. Establishing an FE model used to study dislocation will provide systematic information about the mechanics of dislocation without the need for long term implantation studies or expensive physical testing.

PROCEDURES

A three-dimensional FE model of a total hip implant (Figure 1) was developed using PATRAN meshing software (MSC/NASTRAN). A non-linear, large displacement, sliding contact analysis was performed using ABAQUS V5.6 finite element software (Hibbit, Karlsson, & Sorensen, Inc). The FE mesh was refined in regions of anticipated high stresses in the expected impingement zone, to achieve more accurate stress results. The nonlinear material properties of ultra high molecular weight polyethylene (UHMWPE) were modeled using a fourth order finite deformation constitutive relationship [3]. The FE simulation modeled contact using an experimentally determined Coulomb friction coefficient of 0.038. Constant rate angular rotation was input to the acetabular component until impingement and dislocation occurred.

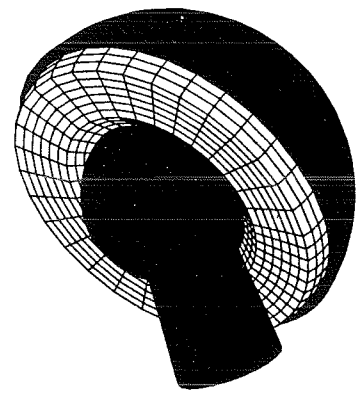

Figure 1: Finite Element Model

The experimental apparatus (Figures 2 and 3) was designed to run in an MTS Bionix dual actuator materials testing machine. The axial channel provided a constant compressive force (200 N) to the hip implant. The torsional channel provided the cup rotation in the system. The MTS ram rotated at a constant angular velocity of 1 deg/sec and pulled a cable which was fitted to the cup cradle through a set of two pulleys. This resulted in a constant angular velocity rotation of the acetabular cup for impingement and dislocation. The femoral component was attached to a radial bearing to prevent it from rotating with the MTS ram. Linear bearings were also used to allow the head to move out of the socket during the dislocation (Figure 3). Since the MTS torsional load cell only reported moments around the vertical axis, it was necessary to convert the moment around the vertical axis read from the MTS to a moment around the horizontal axis about which the cup rotates. This conversion was

accomplished by multiplying the torque from the MTS by the ratio of the horizontal distance from the center of rotation to the cable ,Rh, to the vertical distance, Rv (Figure 3). Once the conversion was made, the resulting moment values were compared to the moments reported by the finite element model.

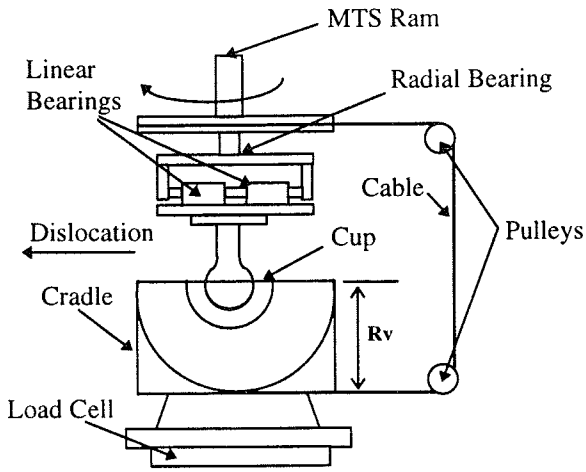

Figure 2: Experimental test setup , front view

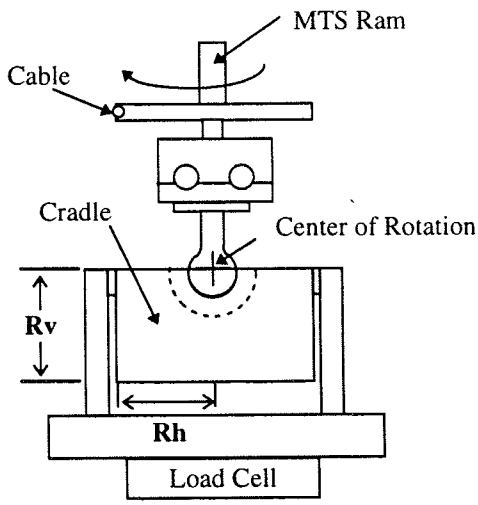

Figure 3: Experimental test setup , side view (Pulleys and cable left out for clarity)

RESULTS AND DISCUSSION

Because the FE model became unstable soon after the resultant force moved from the cup's articulating surface onto its chamfer lip, this point was defined as dislocation. Experimentally, the exact time when the force moved onto the chamfer in the experiment was difficult to determine from the physical data (Figure 4), but dislocation was easy to judge because the head visibly slid out of the cup. The results obtained from this experiment agreed reasonably with those values obtained from the FE simulation. The angular displacement until impingement was found to be 57.5° computationally and 58° experimentally, a difference of 1%. The maximum moment value reported was 1844 N-mm computationally and 1570 N-mm experimentally, a difference of 17%. The dislocation point was 68° experimentally and 67° computationally, a difference of 1.5%. Tracking of the dislocation event both experimentally and computationally showed good similarity of the range of subluxation (from impingement to dislocation).

CONCLUSION

The finite element simulation broadly modeled the experimental test. This experimental validation provides evidence that the finite element model reasonably mimics the process of dislocation in THA.

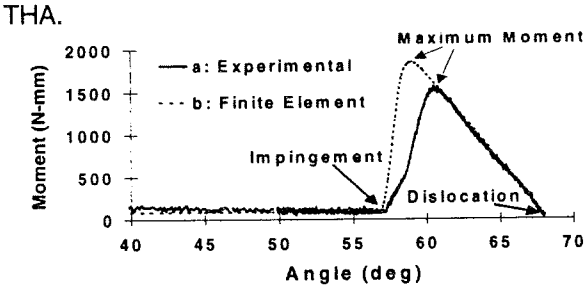

Figure 4: Moment vs. angular displacement for the a) experimental and b) finite element simulations. Values truncated before 40° because graphs are similar.

ACKNOWLEDGEMENTS

The authors would like to acknowledge the valuable assistance of Dr. Anneliese Heiner, Dr. Jim Rudert, and Tina A. Maxian. Financial Support was provided by DePuy, Inc., and by NIH AR 42845.

REFERENCES

1. Woo R *et al.*, *J Bone Joint Surg* 64-A (9)
2. Grigoris P *et al.*, *Clin Orth Rel Res* 304
3. Cripton P *et al.*, *J Biomech Eng*, in review

MECHANICS OF FIXATION OF SCREW TYPE DENTAL IMPLANTS

S. Pal[1], A. Chakraborty[2], T.K. Pal[2]
[1]School of BioSc. & Engg., Jadavpur University Calcutta - 700 032
[2]Dr. R. Ahmed Dental College & Hospital, Calcutta -700 014

INTRODUCTION

Dental implants have been emerging out as one of the most fascinating & challenging treatment modalities in lost tooth rehabilitation. Various materials with ongoing changes of designs have been constantly innovated in present-day dental implantology. The success of dental implants depend on biologic profile of host, material biocompatibility, design of the implant system and its immediate long term fixation.

The implants in orthopaedic field are fixed with the use of cements which is gradually being replaced by newer modification of design in uncemented condition. The same is also being used in the field of dentistry by adopting various mode of designs so as to achieve a very firm initial fixation. This in term facilitates the bone healing in order to get the goal of osseointegration. However, the modification of implant surface by coating of bioactive Ca-phosphate compound may give rise to chemically bonded interface satisfying literally the meaning of fixation.

Though dental implants of various designs are available, but the biomechanical aspect of the torque required to cut thread and insert screws in jaws has not been properly addressed. In this perspective attempt has been made to quantify the torque required to fix the uncoated and hydroxyapatite coated Ti-screw type dental implants in animal mandibles. These implants used were developed in the School over the past several years(1).

MATERIAL & METHODS

Special type deep parabolic threads were cut on 5 mm. nominal dia. titan-12 blank to nominal dia. 4.0 mm. and 3.5 mm screws with square heads to facilitate insertion using small box-wrench suitable for mainpulation in oral cavity. A cylindrical unthreaded part of length 4 mm was left for biological sealing. Surgical drill of parabolic flute of dia 3.13 mm were used for drilling core holes in goat mandible using hand drill at 30 r.p.m. A tap of 3.3 mm. was used after drilling the core hole. A box wrench was fabricated suitably for proper insertion of tap and dental implants. A square head was provided on the tap and the implant as well. A torque measuring manual wrench was fabricated similar to the hand operated wrench and straingaged(BLH-make 350 ohm) to measure torque during insertion of tap and screw. Ten freshly removed goat mandibles were collected from the slaughter house and kept in a fridge at -10° C until used. Each mandible was fixed in a vice and hole of 3.13 mm was drilled followed by the introduction of the tap into the drilled hole. The insertion of the tap was initiated with the instrumented wrench and torques were recorded. Five reading were taken during insertion of tap. Then the implants were inserted into the tapped hole and five readings were recorded. Edentulous area were chosen in posterior aspect of the goat mandible. Average value for the torque was calculated in each mandible and the results are tabulated in Table 1.

Table no. 1. Torqe comparison for screw insersion in Mandible

Screw Dia mm	Mean Torque, N.mm		
	Tap	Uncoated screw	Coated screw
3.5	12.00	11.00	16.02
4.0	14.50	14.25	20.07

RESULT & DISCUSSION

From Table No. 1 it is seen that the torque required to insert the tap was always higher than the torque for implant insertion as expected for uncoated screw. However, the difference of torques required for tapping as well as the insertion of uncoated implant is significantly less. It is also understood from the above observations that the extra torque required for the tapping is due to removal of spongy bone to make a threaded profile in the bone hole. Here it can be postulated that HA Coating may experience friction during its insertion and this may jeopardize the surface. Thus HA Coating of dental implant may need careful insertion in order to preserve coating characteristics and therefore need a tapped hole profile for ease of its insertion. Tapping of holes smoothen the insertion of HA - coated implants.

It is quite interesting to note that the HA-Coated(50 micron thick) screw required nearly 46% higher torque for its insertion in a tapped hole over uncoated screw for fresh goat mandibles(in vitro).

Experiments were also performed on a human subjects during surgical implantation of a HA-Coated titanium implant with conscious consent and bioethical clearence. It was found that the tapping torque was 9.29 Nmm while it was 13.36 Nmm for HA-Coated screw. It was 43.8% higher. Therefore, it is always advisable to use appropriate tap before insertion of coated screw implant during such surgery.

ACKNOWLEDGEMENT

A part of this study was funded by All India Council for Technical Education, New Delhi.

REFERENCE

1. Pal, S, Pal,T.K., et al. (1993): Proc. NCBAO held at Calcutt 202-211

A NEW INSOLE PRESSURE MEASUREMENT SYSTEM: REPEATABILITY OF POSTURAL SWAY DATA

J. Bauer, J. Cauraugh, M. Tillman

Department of Exercise and Sport Sciences, University of Florida, Gainesville, FL 32611

INTRODUCTION

This study analyzed the reliability of a new in-shoe plantar pressure measuring system (Parotec-System®). A device capable of collecting stable, reproducible values could be clinically important when diagnosing or treating individuals at risk for falling.

REVIEW AND THEORY

The quantitative measure of sway could be an important clinical tool for identifying people at risk for falling (Baloh et al., 1994). The main interactions that control postural sway occur at the interface between the plantar surface of the foot and the shoe. Therefore, plantar pressure insole systems should be well suited for this purpose, but it has been difficult to find the most ideal type of sensor for use inside a shoe. A hydrocell technology has now been developed for pressure measurement and has been independently rated to perform with less than 2% measurement error across the expected pressure, temperature and humidity ranges of normal use (Schumacher, 1995). These tests to evaluate the hydrocell sensors were all conducted using controlled mechanical loading. No data were cited using pressures generated by a human foot. While it appears that the sensor technology used by the Parotec-System® is fundamentally capable of providing accurate readings, the question we explored was: how reproducible are multiple measurements taken from individuals during a single test session as well as from the same individual on multiple days? We hypothesized that the Parotec-System® would provide repeatable postural sway data for normal adults. An additional question addressed a clinical concern: Would test data from a clinical population such as postpolio people provide high reproducibility during a multiple single session testing or would the disease state cause high variation of reported values? We hypothesized that the Parotec-System® would provide reliable postural sway data for postpolio individuals.

PROCEDURES

Seven normal adults and three postpolio survivors participated. The three postpolio individuals had polio approximately 25 years earlier and were using some type of gait assistive device regularly. Testing took place in the Biomechanics and Physical Therapy laboratories at the University of Florida. Five response variables related to the center of pressure were measured to assess the postural stability of all participants. Additionally, impulse values, maximal pressure readings for the lateral heel, fifth metatarsal, and first metatarsal were also collected. A total of nine measures were read from the software and calculated by the experimenters from raw data. Six values were directly available from the analysis software while 3 were calculated indirectly from raw data. Intra-subject measures were evaluated using the Kerlinger (1973) reliability correlation ($\underline{r}$) procedure.

$$\underline{r} = [\text{MS Individual Effect} - \text{MS residual}] / \text{MS Individual Effect}$$

Each test group completed three trials in each session. Healthy participants were tested on three consecutive days while clinical participants were tested on one day. Prior to participation, participants received a verbal overview of the procedures, after which they read and signed an informed consent form approved by the Institutional Review Board of the University of Florida.

RESULTS

Calculations were made for all 10 participants across 3 trials and for the 7 normal individuals across 3 days. For the 6 Parotec supplied dependent measures collected from all 10 individuals the range of values was from 0.93 to 0.99. For the left foot, the mean of the correlation values was 0.97 whereas the mean value for the right insole was 0.98. The same 6 direct measures were analyzed across 3 days for the normal individuals. The mean for the left insole was 0.98 and for the right insole was 0.98. The values across the three days ranged from 0.97 to 0.99. The

3 indirect measures were examined in a similar fashion. For all 10 participants across 3 trials, the range of values was from 0.63 to 0.88. For the left foot, the mean of the correlation values was 0.83 whereas the mean value for the right insole was 0.72. The reliability scores for the normal participants across 3 days ranged from 0.60 to 0.93. The mean for the left insole was 0.79 and for the right insole was 0.73.

DISCUSSION

The repeatability of the measurement values provided by the Parotec-System® was stable and consistent. Of the 24 coefficients produced by the system only a single value (0.93) was below 0.96. Of the 12 reliability coefficients calculated across the three experimenter produced measures, 8 were high coefficients (≥0.77). The four values that were between 0.60 and 0.66 do not adversely affect the interpretation that the Parotec-System® is capable of providing repeatable data (Winer, 1991). The mean values across the three different sites were 0.80, 0.72, and 0.78, respectively. Thus, the coefficients of determination range from 0.52 to 0.64. When these values are taken with the other high coefficients of determination, we concluded that the Parotec is consistent in recording pressures of the feet during quiet stance.

Podiatric physicians and other clinicians can not compromise regarding reproducibility concerning plantar pressure data (Schaff, 1993). We believe that our data show that the Parotec-System® is an effective tool in monitoring a wide range of pertinent biomechanical variables used in static postural balance assessment. The results suggest that healthy individuals show only slight variation in their postural balance strategies and that clinical populations provide highly reproducible values during multiple trials attempted during a single day.

One of the major concerns of those using any technology to evaluate performance measures of individuals is how reproducible measures are given the physical characteristics of the individual have not changed. This study evaluated the ability of a new insole pressure measurement system to provide highly consistent data for normal and gait deficient individuals who were repeatedly tested during the same test session and to determine if repeated measures over several days using normal individuals would provide sufficiently reproducible values that the system could be considered acceptable for use in tracking various postural parameters over time. The reliability results suggests that the Parotec-System® provides highly consistent data across a range of the six postural variables produced by the software and that additional measures may be calculated from raw data.

By being able to confidently view the reported data from such a device as accurate, the clinician or researcher may conclude that observed variations in postural variables are due to changes in the individual and not merely errors caused by a measurement device. This ability to rely on the reported measurements will allow for some accurate assessment of the effectiveness of prescribed gait aids, therapies and the rehabilitative or degenerative progress of the patient. Special clinical populations, such as postpolio individuals, may be evaluated in an effort to prevent falls and maintain quality of life.

REFERENCES

Baloh R.W. et al. J. Am. Geriatr. Soc., 42, 405-419, 1994.
Schumacher F. TÜV Product Service, Project No. 0895-0308; 1995.
Kerlinger F.N. Foundations of Behavioral Research, Holt, Rinehart, and Winston, 1973.
Winer B.J. et al. Statistical principles in experimental design, McGraw-Hill, 1991.
Schaff P.S. Clin. Podiatr. Med. Surg., 10(3), 403-415, 1993.

AN *IN VIVO* METHOD TO STUDY THE PROPERTIES OF THE HUMAN HEEL PAD

E. Morag, D.R. Lemmon, P.R. Cavanagh

Center for Locomotion Studies, Penn State University, University Park, PA, 16802

INTRODUCTION

This paper introduces a method to study thickness and stiffness of the plantar soft tissue during *in vivo* loading. Changes in these properties with aging and their relation to load distribution are discussed. The technique and reliability of this new method are also presented.

REVIEW AND THEORY

There has been a number of studies of the characteristics of the plantar soft tissue over the last 15 years. These studies have focused on development of assessment tools for the non-weight bearing heel pad thickness (Gooding et al., 1985) and weight bearing soft tissue thickness under different regions (Bygrave and Betts, 1992), as well as heel pad deformation (De Clercq et al., 1994) and second metatarsal pad deformation (Cavanagh, 1997). However, little is known about the stiffness of the plantar soft tissue. It would be of interest, for example, to know how such properties change with aging, and how they might affect the load distribution under the sole of the foot during walking.

PROCEDURES

In order to study the mechanical characteristics of the soft tissue *in vivo*, an ultrasound based system was developed (Figure 1). The system allows the simultaneous monitoring of the force applied to the tissue and ultrasonic images of the heel pad during computer controlled quasi-static compression. This was achieved by fitting a cylindrical Plexiglas rod (1.9 cm diameter) to the end of a 7.5 MHz ultrasound probe. A force transducer was mounted in series with the probe, and the Plexiglas rod was slowly advanced (at 15 mm/s) into the tissue using a computer controlled actuator until the applied force reached 105N (370 kPa pressure). The ultrasonic images of the right foot and the magnitude of the applied force were recorded on a S-VHS video recorder via a split screen mixer throughout the experiment (Figure 2). Subjects were in a prone position with the knees fully extended. The unloaded thickness of the plantar soft tissue under the calcaneal tuberosity was first measured at zero force level, then, multiple frames were recorded for further analysis during compression (0 to 105N force = 0 to 370 kPa pressure). The video data were manually digitized using a PEAK5 motion analysis system at a frequency of 15Hz, providing x,y coordinates for force and soft tissue data for each frame, that were used to construct a force-displacement curve for each compression. Data from fifty-five subjects (20-69 years of age, equally divided to five age groups) were collected. Plantar pressure distribution during walking were also subsequently collected. The reliability for each of the measurements was assessed by intraclass correlation coefficients (ICC). One way ANOVA was used to test for differences between groups in soft tissue thickness, stiffness, and total displacement.

RESULTS AND DISCUSSION

A typical force - displacement curve was well described by a negative exponential function of the form (Figure 3):

$$D = b_0 \cdot (1 - e^{-b_1 \cdot F}) \qquad (1)$$

where D is displacement (i.e., tissue thickness at frame i minus the unloaded tissue thickness), F is force, and b_0 and b_1 are the curve coefficients. In this quasi-static setting the heel pad can be considered to be a non-linear spring. The constant b_0 is the total tissue displacement, and for the purposes of this study, $(1/b_1)$ was defined as stiffness although it is realized that the result is actually dependent upon both probe dimensions and tissue characteristics.
The form of the curves indicates that large displacement occurs during early compression. The reliability of tissue thickness at 5N compression was greater than that of 0N compression and tissue thickness at 5N was therefore selected as a baseline for the displacement curve. Day-to-day reliability of the unloaded heel pad thickness was 0.70. Both day-to day and trial-to-trial reliability of b_0 were high (0.86 and 0.88). The ICC for b_1 was lower due to a high asymptotic correlation between b_0 and b_1, which negatively biased the

reliability of b_0 and b_1. To confirm this assumption, the reliability of selected points on the curve (displacement at 50N and at 75N) was assessed yielding high ICCs (0.79 - 0.90).

A non-significant trend of differences in heel pad stiffness (b_1) was found between the five age groups (elderly > young, p=0.14), suggesting that the heel pad may become stiffer with age. This could be due in part to the process of non enzymatic glycosylation which has been associated with age, and could stiffen soft tissue. No differences were found in either the amount of soft tissue or the total tissue displacement (b_0). Previous findings (Morag et al., 1997) have indicated that stiffer tissue and a greater amount of soft tissue under the heel are associated with lower pressure under the heel.

In summary, this study has introduced a reliable method of studying heel soft tissue properties *in vivo*. It was demonstrated that there were no significant differences in the amount of soft tissue between the young and elderly, but there were trends towards differences in tissue stiffness. The plantar soft tissue is believed to provide both protection and cushioning, and atrophy of the fat pad has been implicated in a number of pathologies. It is reasonable that changes in stiffness accompany atrophy of the soft tissue. Thus, future efforts should focus on studying soft tissue properties in patients with such pathologies.

REFERENCES

1. Gooding, GAW et al. J. Ultrasound Med, 4, 173-174, 1985.
2. Bygrave, CJ et al. The Foot, 2, 71-78, 1992.
3. De Clercq, D et al. J. Biomech., 27, 1213-1222, 1994.
4. Cavanagh PR. J. Biomech. (in press).
5. Morag et al. Proceedings NASGCMA, 1997.

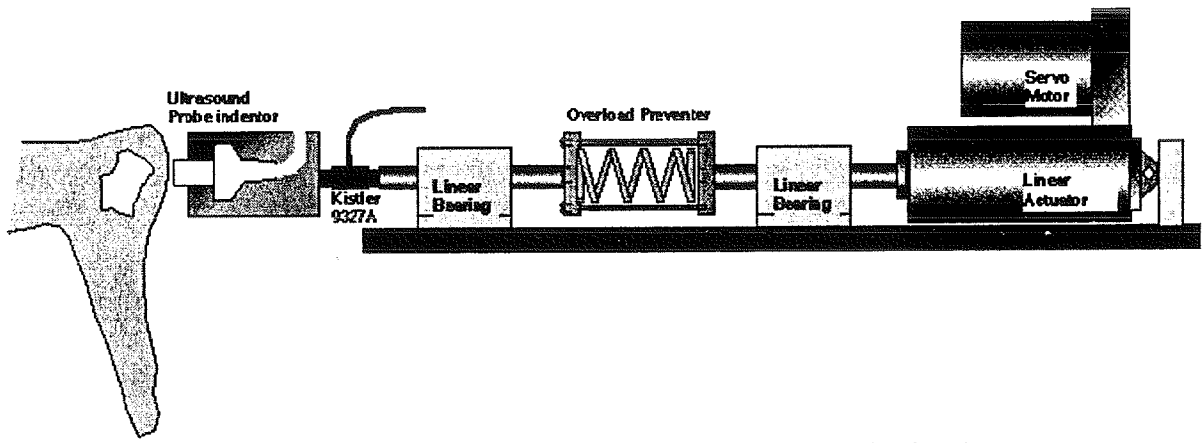

Figure 1. A computer-controlled apparatus used for compression of the heel pad.

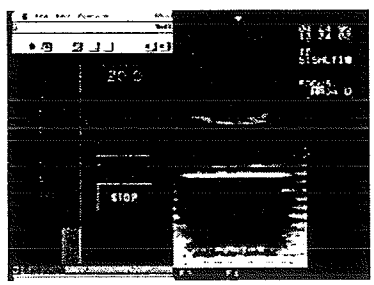

Figure 2. A sample frame of an ultrasonic image of the calcaneal tuberosity (right) and force level (left)

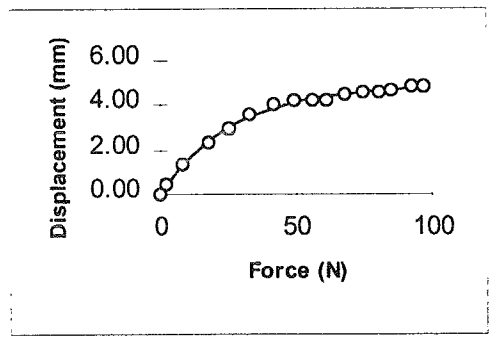

Figure 3. A sample force-displacement curve during heel compression. Fitted curve is presented as a solid line

IMPROVING ESTIMATES OF TIBIAL ROTATION THROUGH MARKER CONFIGURATION AND ATTACHMENT METHODS

K.Manal[1], I.McClay[1], S. Stanhope[2], J.Richards[1], B. Galinat[3]

[1]Biomechanics and Movement Sciences, University of Delaware, Newark, DE 19711

[2]Biomechanics Laboratory, National Institutes of Health, Bethesda, MD 20892

[3]Delaware Orthopaedic Center, Wilmington, DE 19808

INTRODUCTION

Estimates of tibial rotation for several surface marker conditions were compared to true tibial rotation calculated from markers attached to a bone anchored percutaneous skeletal tracker (PST). Helical methods were used to characterize the three dimensional error in estimating tibial rotation during the stance phase for each marker condition. The data are preliminary results of an ongoing study designed to investigate how factors such as location, attachment method and the physical characteristics (constrained vs. unconstrained) of a marker set affect estimates of tibial rotation. Identifying factors that limit the error introduced by soft tissue movement on estimates of tibial rotation could be used to improve clinical and research applications of gait analysis.

REVIEW AND THEORY

Estimates of bone motion are often inferred from tracking markers attached to the surface of the anatomical segments of interest. The tracking markers and underlying bone are separated by muscle, connective tissue, fat and skin collectively referred to as soft tissue. Soft tissue moves relative to the bone, and consequently so do the tracking markers. This relative motion is the greatest source of error in gait analyses (Cappozzo, 1991). Holden et al., (1996) reported errors of up to 8 degrees about the long axis of the shank in one of three subjects tested. This error is alarming considering the tibia undergoes approximately 10 degrees of internal rotation relative to the femur during walking (Lafortune, 1992).

A number of factors likely affect estimates of tibial rotation. Three such factors include: the location of the markers on the segment, attachment of the markers to the segment and the physical characteristics of the tracking markers. Studies have examined differences in rotational estimates calculated from constrained and unconstrained marker sets (Karlsson et al., 1990; Reinschmidt, 1996). The literature is unclear as to which method yields better results. No study has addressed the method by which the markers are attached to the segment, nor has any study attempted to improve estimates of tibial rotation by examining marker sets attached over different locations on the shank (proximal/distal and lateral/medial tibial flare). Therefore, the purpose of the ongoing study is to examine these questions and determine if better estimates of tibial rotation can be realized through marker placement and attachment method. A subset of these data are presented in this abstract.

PROCEDURES

A six camera, 60 Hz video based motion analysis system (Vicon 370, Oxford Metrics) was used to collect the motion data. The PST device was attached to the distal shank as described by Holden et al., 1996. Move3D (NIH, Bethesda, MD) was used to calculate rotational kinematics from filtered marker coordinates. Data for markers attached over three different locations are presented in this abstract. The three locations include (1) four markers taped to the proximal lateral shank, (2) four markers taped to the distal lateral shank, and (3) three markers attached over the distal tibial flare. One of the tibial flare markers was projected anteriorly using a 75 mm. wand. Three walking trials were collected for each marker location. The finite helical angle was used to compare differences in estimates of tibial rotation for the surface marker locations relative to the true rotation of the tibia calculated from the bone anchored PST markers. This angle is referred to as the relative helical angle (RHA). The RHA is a 3-dimensional measure of error in estimating tibial rotation from markers attached to the shank. In addition, the RHA was decomposed about the anatomical axes of the shank so that errors could be examined about each axis. A root mean square (RMS) error for the RHA across the normalized stance phase was used to compare the 3 marker locations ($RMS=\sqrt{\frac{(\sum_{i=1}^{100} RHA_i^2)}{100}}$).

RESULTS

The RMS error was used to compare the three marker locations. A smaller RMS value represents less rotational error during stance. These data are reported in table 1.

Subject	Prox Skin	Dist Skin	Dist Tib
KR2	2.04 (0.10)	1.65 (0.37)	1.44 (0.05)
BM3	2.67 (0.20)	2.05 (0.22)	1.70 (0.11)
BC4	2.02 (0.02)	1.41 (0.10)	1.44 (0.40)

Table 1: Mean RMS (std. dev.) for the RHA's.

The mean RHA for one subject (BM3) is presented in the top left panel of figure 1. Errors about the anatomical axes were obtained by decomposing the RHA. Peak rotational errors for all 3 subjects are reported in table 2.

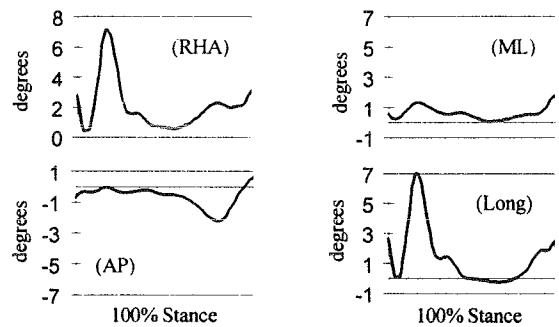

Figure 1: Mean RHA for the proximal lateral skin location. Average rotational errors about the anatomical axes: ML=medio-lateral, AP=antero-posterior, Long=longitudinal. 0° = no error.

	Prox Skin			Dist Skin			Dist Tib		
Sub	ML	AP	L	ML	AP	L	ML	AP	L
KR2	1.7	1.5	3.5	0.9	0.6	3.4	0.9	-1.5	2.7
BM3	1.5	-2.2	7.1	0.9	-1.7	5.4	-1.7	-1.0	3.2
BC4	2.0	-2.4	-3.2	-1.4	-1.0	-2.2	1.5	1.4	-2.4

Table 2: Mean peak rotational errors. ML=medio-lateral, AP=antero-posterior, L=longitudinal axis.

The bold lines in figure 2 represent the mean knee joint internal rotation angle calculated from the bone anchored PST markers relative to markers attached to the surface of the thigh. This rotation was re-calculated using the proximal lateral skin markers collected at the same time as the PST markers and referenced to the same thigh data (left panel). A similar process was repeated for the distal tibial flare markers (right panel). The distal tibial flare location was collected in a different set of trials than the proximal skin location.

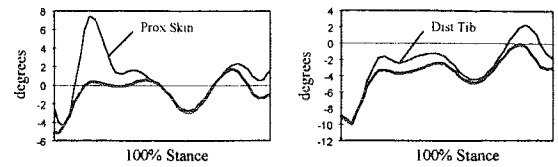

Figure 2: Mean knee internal/external (IR/ER) rotation calculated from proximal skin and distal tibial flare markers relative to surface markers attached to the thigh. The bold line represents IR/ER for the bone anchored markers relative the thigh.

DISCUSSION

The RMS comparison revealed less rotational error for the distal lateral skin markers than for the proximal lateral skin markers. This was likely due to the distal markers being positioned over less soft tissue as a result of the distal tapering of the shank. The majority of the rotational error occurred in the secondary planes of motion. This was apparent when the RHA was decomposed about the anatomical axes (figure 1). Large to moderate errors were noted at the beginning and at the end of the stance phase. The error shortly after initial contact may be due to impact vibration during footstrike, while the error noted in the later part of stance may be due to strong muscular contraction of the plantarflexors and invertors in preparation for push off. Markers attached over the distal tibial flare resulted in better estimates of tibial rotation than the distal lateral skin markers. In one case, the reduction in peak error from proximal lateral to distal tibial was nearly 4 degrees about the long axis of the shank (a 100% decrease, shaded cells table 2). Another favorable finding was the good agreement with the bone data in both magnitude and pattern of rotation as shown in (figure 2, right panel). These data suggest that target location may have a minimizing affect on soft tissue error. With the addition of 4-5 subjects and further analysis of the other factors being studied, we hope to provide additional insight into improving estimates of tibial rotation from markers attached to the shank.

REFERENCES

Cappozzo A. *Hum Mvmt Sci*, **10**, 589-602, 1991.

Holden J. et al. *Gait and Posture*, in press 1996.

Lafortune M. et al. *J. Biom*, **25**, 347-357, 1992.

Karlsson J. et al. *Issues in modeling and control of biomechanical systems*, 39-43, Ashton-Miller and Pandy, 1990.

Reinschmidt C. Doctoral dissertation, University of Calgary, Alberta, Canada 1996.

A Device for the Application of Equibiaxial Strain to Cultured Fetal Bovine Bladder Smooth Muscle Cells

N. P. Davis & R. S. Cargill II
George W. Woodruff School of Mechanical Engineering, Georgia Institute of Technology, Atlanta, GA, 30332

INTRODUCTION

Large mechanical strain is one of the major features of normal urinary bladder function. Pathologies such as outlet obstruction change the strain field within the bladder, and profound changes in bladder morphology result at both the tissue and cellular levels. We believe that mechanical environment significantly affects the growth, development, and differentiation of the different cell types in the body, and the bladder presents an excellent opportunity to study these effects. We present here a device developed to study the effects of mechanical strain on fetal bovine bladder smooth muscle cells (BBSM) *in vitro*. Our purpose in this abstract is to describe the system, characterize the elastic membranes used to impose the strains on the cultured cells, and provide preliminary cellular adhesion results illustrating the efficacy of the device for its intended purpose.

REVIEW AND THEORY

Baskin *et al.* (1), have previously demonstrated that straining cultured BBSM on a pneumatically deformed membrane alters cellular secretion levels of collagen types I and III as well as fibronectin in the absence of neurological input. Our device will provide much greater freedom to explore the specific effects of strain history on BBSM function since vertical deflection, and therefore mechanical strain, is programmable and not limited to a sinusoidal input.

Our system is based on designs by Hung and Williams (2), and Schaffer *et al.* (3) . Both of those devices generate a 2-D equibiaxial strain field, i.e., a field in which strain along any planar reference direction is equivalent. The advantage of this type of field is that cellular strain is dependent neither on cell orientation nor on cell location within the field. Our system produces an equibiaxial strain field, but has the added capabilities of simultaneously straining 16 cell wells and being programmable. Each cell well is composed of a polysulfone chamber sealed on the bottom by a circular Sylgard® membrane (Dow Corning). Vertical deflection of a well pushes the membrane over a stationary cylindrical form, producing an equibiaxial strain field. Vertical deflection of the wells is controlled by a programmable stepper motor coupled to a lead screw assembly.

This experimental setup facilitates multiple factor testing within a given strain regime and provides the capability to switch easily between different strain regimes. Our task is to verify that this device generates an equibiaxial strain field and that the membranes are a suitable culture surface.

PROCEDURES

Between ten and twenty ink dots were drawn in a uniformly distributed pattern on a membrane using a black uniball® pen (Sanford). A CCD camera was used to capture video images of the membrane during deflection. Deflection was programmed to take place at a speed of 0.089 mm/s, and eleven images were captured at uniform intervals over the course of the deflection, with the first frame being the initial position. Relative point positions were tracked by hand using NIH Image software, and the results were stored in text file format.

A Matlab m-file was written to calculate the strain field of the membrane based on a finite approximation to the 2-D Greens strain tensor using triads of point positions. Every possible triad was screened for minimum angle between sides, and normal strains and shear strain were calculated at centroids of acceptable triangles. The difference in mean normal strain along the two video axis directions was determined using a two-tailed student's t-test.

BBSM were seeded onto membranes held in the cell wells. Prior to seeding, the membranes were washed, soaked with 1-N HCl for 3 to 4 hours, then autoclaved. Three attachment factors, calf serum (Hyclone Laboratories), gelatin (Sigma), and poly-L-lysine (Sigma), were each sterilely adsorbed onto one membrane surface for 3 to 4 hours before cells were seeded. Observations over the course of several days in static culture determined the cells' ability to attach to a static membrane treated with the various attachment factors. The wells were then placed in the stretcher device and deflected with single cycles of

constant speed loading and unloading. Strength of adherence was based qualitatively on the initiation of peeling of the adherent cell layer with increasing peak strain.

RESULTS AND DISCUSSION

Analysis of 2 different membranes in 3 different wells revealed that strain in the membrane is a slightly nonlinear function of deflection, as anticipated from membrane geometry during deflection. Results are shown in Figure 1.

The difference in mean normal strain was zero for 2 wells tested with the same membrane ($p < 0.05$), indicating equibiaxial strain. Different trials on the same well with the same membrane were inconsistent, however, showing significant difference in one trial and no significant difference in two other trials. In addition, the difference between mean strains became less significant as strain levels increased for those membranes and wells which showed significant differences in mean strain. We feel that the lack of consistency in these results is due to two factors: non-uniform membrane pretension and static friction between membrane and form. Both are thought to significantly affect the strain field of a deflected membrane. Future efforts will need to examine uniform vs. non-uniform pretension in the membrane as well as quality of lubrication between the deformed membrane and the form.

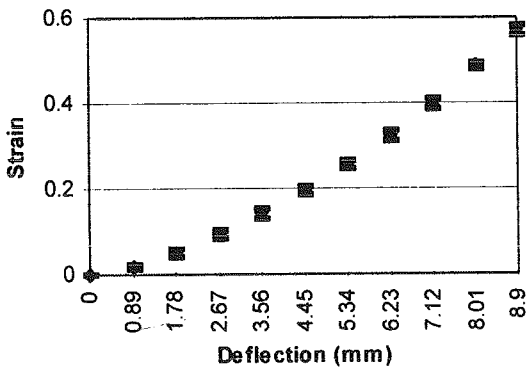

Figure 1: Average membrane strain in the loading direction based on six trials (mean ± SD).

As shown in Table 1, BBSM successfully attached to the membranes except in the case where there was no adhesion treatment. Cultures remained attached for both the static test and for the dynamic test. No detachment was observed at a maximum strain level of 57%, indicating that the most simple treatment should be sufficient for cell adherence.

Membrane Treatment	Static Attach-ment	Dynamic Attachment
None	few cells attached	no peeling
HCl only	good	no peeling
HCl + Calf Serum	good	no peeling
HCl + Gelatin	good	no peeling
HCl + Poly-1-Lysine	good	no peeling

Table 1: Adherence Test for Membrane Treatments in Static Culture and Single Cycle Dynamic Loading.

CONCLUSIONS

We have demonstrated the efficacy of this device for the culture of BBSM in a mechanically active environment. Though it will require further work to validate the capability of this device for generating equibiaxial strain fields, we feel that it has definite advantages over current designs. This device is capable of operating at strain levels up to 57% normal strain as compared with 0.4% for the design by Hung and Williams (2) and 9.4% for the design by Schaffer *et al* (3). In addition, 16 wells provide greater flexibility in experimental design, and the programmable stepper motor furnishes the means to explore the effects of a variety of strain regimes on BBSM function.

REFERENCES

Baskin L. *et al. J. Urol.*, 150, 601-607, 1993.

Hung C.T. & Williams J.L. *J. Biomechanics*, 27, 227-232, 1994.

Schaffer J.L. *et al. J. Orthop. Res.*, 12, 709-719, 1994.

ACKNOWLEDGMENTS

Sincere thanks to Dror Seliktar for help with the CCD camera and to Doug Wright for his expertise on NIH Image.

A WEBSITE FOR TEACHING FUNDAMENTAL 3D KINEMATIC ANALYSIS

J. K. Startzell, H. J. Sommer[1], D. R. Lemmor., and P. R. Cavanagh

Center for Locomotion Studies, Penn State University, University Park, PA 16802

[1]Department of Mechanical Engineering, Penn State University, University Park, PA 16802

INTRODUCTION

A website is described which provides the student of biomechanics with a progressive understanding of three dimensional rigid body kinematics. Starting with global positions of targets on two rigid bodies, the user is shown the stages necessary for anatomical calibration and calculation of the angles of a joint coordinate system (JCS). Following the initial presentation, data files from a variety of movements are available to the user who can then progress from an understanding of the calculations to an interpretation of the movement being studied.

REVIEW AND THEORY

Basic linear algebra can be used to define relative translation and rotation between two rigid bodies in 2D and 3D space. A 4x4 transformation matrix contains a location vector, which gives the location of a local body relative to a global coordinate frame, and a rotation submatrix, which gives the attitude of the local axes relative to the global axes. This matrix can be decomposed to determine the orientation of the local axes with respect to the global axes and the angles of rotation about each axis.

The joint coordinate system (JCS) proposed by Grood and Suntay (1983) defines relative rotation of two bodies about two segment-fixed axes and a floating axis. The temporal sequence dependency of Euler angle techniques is eliminated provided that the body-fixed axes are selected wisely.

The terminology and nomenclature recommended by the International Society of Biomechanics are used throughout the website (//www.kin.ucalgary.ca/isb/standards/). The recommendations of Cole et al. (1993) regarding identification of the three JCS axes have also been followed.

MATLAB is a user-friendly software package designed for matrix manipulation. It is an ideal environment in which to perform geometric transformations and angle decomposition for configuration of specified input data.

PROCEDURES

Basic Linear Algebra
A review of vector algebra and matrix algebra is first presented with simple examples where a physical process (translation or rotation) is related to the mathematics. A transformation matrix is constructed which represents the relative position and orientation of two bodies.

Anatomical Calibration
A calibration procedure is described which facilitates anatomical landmark identification. Through the use of a calibrated wand containing markers at known distances from the tip placed at an anatomical landmark, the global coordinates of this landmark can immediately be identified. This method eliminates the need for additional anatomical markers to be affixed to the skin.

Motion Analysis and Joint Coordinate Systems
The global positions of targets on a single rigid segment are used in conjunction with anatomical calibrations to determine the body-fixed axes about which segment rotation is described. The relative position of two bodies in motion can be defined by a joint coordinate system including two segment-fixed axes and a mutually orthogonal floating axis.

Integration and Application
Both graphical and analytical presentations are accessible on the website. Simple

MATLAB routines for such vector operations as unit vector calculation, dot and cross products, and matrix transformations are provided. In addition, data files from a variety of movements provide the user with a transition from theory to application of kinematic analysis.

Interactive Aspects
A JAVA applet has been implemented to provide a user interface for demonstration purposes. The student can identify angles of rotation and view the resulting rigid body movement and the corresponding transformation matrix.

The following pages are available on the site:

- Basic vector algebra - with examples
- Basic matrix algebra - with examples
- 2D transformations
- 3D transformations
- 4x4 matrices
- 3D global positions of markers from a motion analysis system
- Anatomical Calibration using a wand
- Local and Anatomical systems
- Relative position of two anatomical coordinate systems
- Joint coordinate systems and their decomposition matrices
- Example data configurations
- Examples of JCS angles for entire movements

The site can be accessed at:
//www.celos.psu.edu/kinematics/

DISCUSSION

Coverage of this material is thought to be important to students of biomechanics because the calculation of rigid body kinematics is rapidly becoming transparent to the user in many of the automated motion analysis systems. The site is not intended to provide software for routine analysis of data but rather to offer a user-friendly environment in which the basic concepts of 3D kinematic analysis can be mastered. The advantage of using the Internet rather than a textbook for such education is that interactive simulations can be performed by the student who can then see both graphical and numerical feedback of specified input.

REFERENCES

Buczek F. Three-Dimensional Kinematics and Kinetics of the Ankle and Knee Joints During Uphill, Level, and Downhill Walking, PhD Dissertation, Penn State University 1990.

Cole G., et al. *Trans. ASME* , 115: 344-349, 1993.

Craig. Introduction to Robotics, Addison Wesley, 1986.

Grood E., Suntay W. *J Biomech Eng.* 105:136-144, 1983.

Nigg B., Herzog W. Biomechanics of the Musculo-skeletal System, 264-277. John Wiley & Sons, 1994.

Sommer HJ. ASB Tutorial: Primer on 3-D Kinematics, 1991.

PRECISION OF HUMAN BODY SEGMENT INERTIAL PARAMETERS

John H. Challis

Biomechanics Laboratory, The Pennsylvania State University, PA 16802

INTRODUCTION

The mechanical analysis of human movement often requires knowledge of the inertial properties of body segments. The precision and accuracy of these inertial parameters will have an influence on any mechanical parameters computed using them (Andrews and Mish, 1996). Whilst accuracy of estimated body segmental parameters is difficult to assess precision is relatively easy yet has not been the focus of studies examining the estimation of body segment inertial parameters. It was the purpose of this study to examine the inter- and intra-operator precision with which human limb inertial parameters could be estimated.

REVIEW AND THEORY

Body segment inertial parameters can be estimated in a number of different ways including the use of statistical models (e.g. Hinrichs, 1985), medical imaging techniques (e.g. Mungiole and Martin, 1990), and modeling the body segments as series of geometric solids (e.g. Hatze, 1980). The geometric modeling techniques represent the segments of the body using geometric shapes. The dimensions of these shapes are obtained by taking anthropometric measurements on the experimental subject (e.g. segment length and perimeter). From these data it is possible to obtain an approximation of segment volume, then by providing an estimate of the segment density it is possible to estimate the inertial parameters. The density values are normally obtained from cadaver data.

In this study the precision of body segment inertial parameters determined when modeling the body segments as series of geometric solids was examined.

PROCEDURES

A group of fifty physically active subjects, equally divided into males and females, gave informed consent to participate in the study (height 1.730 m ± 0.073; mass 72.38 kg ± 9.90; age 20.7 years ± 1.8). Each subject was measured three times, twice by measurer A (data sets A1 and A2), and once by measurer B (data set B1), all sets of measurement were conducted in the same session. The measurers had no record of any previous measurements so the sets of measurements were considered to be independent. The measurers were experienced measurers who were familiar, from frequent practice, with the measurement protocols required. In a pilot study prior to the main study reported here, the precisions of the two measurers were assessed and found to be virtually identical. The subjects were measured using anthropometric measuring tapes and calipers, all measurements were made to the nearest millimeter.

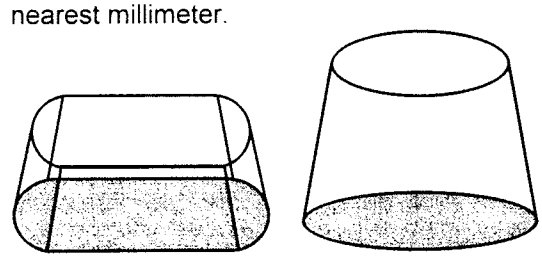

Figure 1: the stadium solid and truncated cone used to model the body segments.

The inertial parameters were determined for the limbs by modeling them as series of geometric solids. The thigh, shank, upper arm, and forearm were modeled as a series of truncated cones, the feet and hands were modeled as a series of stadium solids; figure 1 shows these shapes. The dimensions of these shapes were obtained by taking measurements on the subjects; for truncated cones length and perimeters, for the stadium solids lengths, perimeters, and widths. For each segment a system of axes were defined with its origin at the center of mass of the segment. These axes were aligned with approximate body axes: saggital (x), frontal (y), and longitudinal (z); moment of inertia values were referenced to these axes (I_{xx}, I_{yy}, and I_{zz}). Density values for these solids were taken from the data of Dempster (1955) and were assumed to be uniform throughout a given segment. All segments were measured so that each solid was 3.5 cm in length except for the terminal length

which was adjusted to accommodate the remaining portion of the segment.

In addition to modeling each segment as a series of geometric solids (*Full Geometric*), a reduced model was also employed in which each segment was modeled as two solids only (*Reduced Geometric*). The segment was divided longitudinally into two equal halves, and a different sized solid used for each half.

There were two measures of precision made, one between data sets A1 and A2 (intra-operator precision), and one between the data sets A1 and B1 (inter-operator precision). Precision was quantified using the percentage root mean square difference (%RMSD) between the data sets, and by computing the intra-class correlation (Fleiss, 1986).

RESULTS

Table 1 shows the inter- and intra-operator precisions for the inertial parameters for the lower limb, similar results were obtained for the upper limb.

Table 1: precisions of inertial parameters for the lower limb.

Segment	Full Geometric		Reduced Geometric	
THIGH	***Inter***	***Intra***	***Inter***	***Intra***
Mass	0.97	0.97	0.96	0.96
C. of M.	0.94	0.95	0.93	0.94
I_{xx}/I_{yy}	0.96	0.97	0.95	0.97
I_{zz}	0.98	0.96	0.96	0.94
SHANK				
Mass	0.96	0.96	0.97	0.95
C. of M.	0.91	0.91	0.92	0.90
I_{xx}/I_{yy}	0.95	0.94	0.96	0.94
I_{zz}	0.96	0.97	0.97	0.95
FOOT				
Mass	0.88	0.89	0.89	0.85
C. of M.	0.77	0.75	0.70	0.72
I_{xx}	0.83	0.81	0.86	0.84
I_{yy}	0.86	0.84	0.86	0.85
I_{zz}	0.82	0.72	0.80	0.67

DISCUSSION

The mass and center of mass locations estimated using the geometric solid model were compared with the data of Dempster (1955). These data compared favorably, although the *Reduced Geometric* tended to provide a higher estimate of segment mass than the *Full Geometric* suggesting that the former did not adequately account for variations in segment shape and therefore overestimated segment volume.

The results from this study indicate that human limb segment inertial parameters can be estimated with high precision when modeling the body segments as series of geometric solids. The inertial parameters for the foot and hand segments had the lowest precisions; for these segments if measurement precision is considered to be an important factor then precision can be increased by summing repeat measures. There was little difference between inter- and intra-operator precisions, therefore comparison of inertial parameters determined using the same protocol but obtained by different operators is entirely justified, as is having two measurers taking measurements on the same subject to speed the data collection process.

Comparison of the reported accuracies in Cappozzo and Berme (1990) with the precisions from the present study indicate measurement imprecision is a much smaller source of error than error due to lack of accuracy. The present study was not able to assess accuracy, but assessed and reported the precision with which the inertial parameters of human limb segments are estimated, such data has not been reported before.

REFERENCES

Andrews, J.G., and Mish, S.P. *J. Biom.* 29, 651-654, 1996.

Cappozzo, A. and Berme, N. In *Biomechanics of Human Movement*, Bertec, 1990.

Dempster, W. *WADC Technical Report 55-159*, Wright Patterson Air Force Base, Ohio, 1955.

Fleiss, J.L. *The Design and Analysis of Clinical Experiments*. John Wiley and Sons, 1986

Hatze, H. *J. Biom.* 13, 833-843, 1980.

Hinrichs, R.N. *J. Biom.* 18, 621-624, 1985.

Mungiole, M. and Martin, P.E. *J. Biom.*, 23, 1039-1046, 1990.

MECHANICAL TESTING OF TRABECULAR BONE FROM THE PROXIMAL TIBIA OF RATS

S. P. Ruhmann[1], H. A. Hogan[1], and H. W. Sampson[2]

[1] Department of Mechanical Engineering, College of Engineering
[2] Department of Medical Anatomy and Neurobiology, College of Medicine
Texas A&M University, College Station, TX 77843

INTRODUCTION

Estimating the mechanical properties of bone tissue in rats has long been a subject of interest because of the prevalence and usefulness of the rat as an animal model for studying musculoskeletal disease and function. A method has been developed and demonstrated in the present study for testing trabecular bone from the proximal tibia of rats. Sections of the proximal tibia were tested in compression in two ways: loading the whole bone slice comprised of both cortical and trabecular bone tissue, and loading only the trabecular bone portion. For the latter case, special loading platens were constructed with a loading surface area smaller than the endocortical perimeter of the specimens. This test method provides a way to estimate the properties of trabecular bone from a major load bearing bone of the hind limb.

REVIEW AND THEORY

The mechanical properties of rat bone tissue are most commonly determined from tests on whole bones such as the femur and tibia, with the loading mode being either bending or torsion (Bagi et al., 1993; Guy et al., 1993). Such tests generally focus on the midshaft region of the bones, which is primarily composed of cortical bone. In attempts to measure trabecular bone properties as well, methods have also been developed for mechanical testing of vertebrae and the femoral neck (Hou et al., 1991; Lauritzen et al., 1993). For vertebrae, compression is applied to whole vertebral bodies or to sections from the middle of the vertebra cut to have flat parallel surfaces. For the femoral neck, compression is applied to the femoral head to produce bending loads in the femoral neck. In either case, the specimen tested is actually a composite of trabecular bone and cortical bone. A notable exception to this is the work by Demetropoulos, et al. (1993). They reported a method for coring samples from vertebrae to form isolated trabecular bone specimens for compression testing. The objective of the present study was to develop and investigate methods for testing isolated trabecular bone from the rat, but we have targeted the proximal tibia as the site since this is a weight-bearing bone and may respond uniquely to treatments or diseases.

PROCEDURES

Thirteen nine-week-old rats were used in the study. The rats were housed two per cage with 12 hour light and 12 hour darkness cycles. They were fed standard MSE/RAT lab chow from Harlan Tekland and water ad libitum throughout the study. The femur and tibia from both hind limbs were collected at necropsy. All bones were cleaned of adhering soft tissue, wrapped separately in gauze wetted with Ringer's solution, sealed in plastic bags, and frozen at -10C.

To plan the cutting of test specimen slices from the proximal tibia region, contact radiographs were made. The developed x-rays were scanned into a PC for image analysis using SigmaScan/Image software. The desired location of each specimen was determined by visually identifying a section 2 mm long lying below the epiphyseal growth plate and containing a maximum amount of trabecular bone. In order to standardize the locations, the total length of each tibia was measured, and the length from the distal end of the bone to the distal extent of the specimen target region was measured as well. The ratio of these lengths was formed for each specimen and averaged. This average value was then used to locate each specimen. Slice specimens 2 mm long were cut using a low speed diamond blade wafering saw (Buehler Isomet). Additional x-rays were then made of each slice to give an image of the cross-section (see Fig. 1) from which the separate areas of cortical and trabecular bone were measured by image analysis.

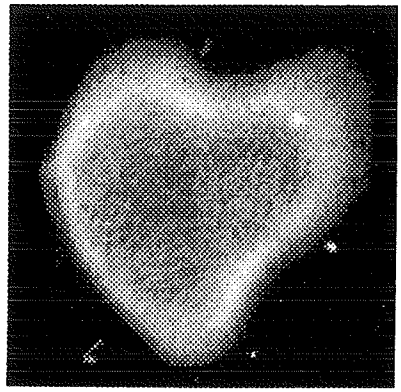

Figure 1: X-ray of specimen cross-section.

Each of these slice specimens was tested in quasi-static compression on a servo-hydraulic testing machine with a displacement rate of 0.0085 mm/sec. Two different types of platens were used. For all specimens from the left tibia, the load was applied through two plano-parallel surfaces that completely supported and loaded the anterior and posterior surfaces of the entire slice That is, the loads were applied to the whole cross-section of both cortical and trabecular bone. For specimens from the right tibia, smaller platens were used to load only the trabecular bone in the central portion of the specimen. A platen diameter of 3 mm was chose to provide a loaded area well within the endocortical perimeter of all specimens. The cortical shell remained attached to the specimen but was not loaded directly, although it likely contributed some degree of lateral constraint. Displacements were determined in both cases via an LVDT attached to the side of the loading platens. Load-displacement data were recorded using LABView software and analyzed on a PC.

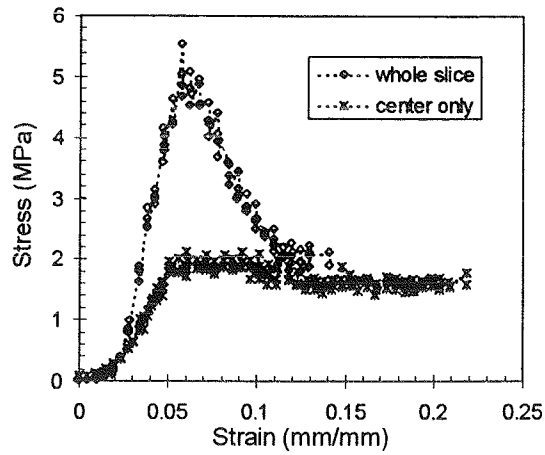

Figure 2: Typical stress-strain plots.

RESULTS AND DISCUSSION

The best-fit linear region during the loading portion of each test was determined using linear regression and the slope taken as the stiffness. Stiffnesses were converted to elastic moduli using specimen dimensions and assuming uniform stress. The ultimate stress was calculated by dividing the maximum load by the cross-sectional area (loaded). The ultimate strain was defined to be the strain (displacement per unit specimen height) at the ultimate load point. Sample stress-strain curves are given in Fig. 2, with results summarized in Table I.

Table I

	Whole Slices	Centers Only
Ult. Stress (MPa) mean (±s.d.)	5.10 (±1.94)	1.82 (±1.24)
Ult. Strain (%) mean (±s.d.)	7.2 (±1.8)	12.9 (±10.0)
Modulus (MPa) mean (±s.d.)	155.7 (±91.0)	63.6 (±55.1)

The results show clear differences for the two types of testing with the weaker and more compliant behavior for the tests on the center region of trabecular bone. This is consistent with expectations since the cortical shell would naturally stiffen the response. The results quantify this effect: loading only the trabecular bone gives an ultimate stress 64% lower, ultimate strain 70% higher, and modulus 59% lower. This method of testing is currently being used to compare the response of tibial trabecular bone in ovariectomized rats to that of cortical bone from the tibia and femur, as well as vertebra specimens.

REFERENCES

Bagi C.M. et al. Bone, 14, 877-883, 1993.
Demetropoulos C.K. et al. 39th Meeting - Ortho. Research Society, 1993.
Guy J.A. et al. Calc. Tis. Int., 53, 283-288, 1993.
Hou J. et al. J. Appl. Phys., 69, 1309-1314, 1991.
Lauritzen D.B. et al. J. Bone Miner. Res., 8, 871-879, 1993.

ACKNOWLEDGEMENTS

This work was supported by the Interdisciplinary Research Initiatives program of Texas A&M.

CONTACT FINITE ELEMENT MODEL OF AN ARTIFICIAL INTERVERTEBRAL DISC

Dwight T. Todd, Vijay K. Goel, Nicole M. Grosland, David G. Wilder, Malcolm H. Pope

Iowa Spine Research Center, Department of Biomedical Engineering
The University of Iowa, Iowa City, IA 52242

INTRODUCTION

A three-dimensional contact finite element model of an artificial intervertebral disc was constructed to study its effect on the biomechanics of one motion segment. Reaction moments and loads, stresses, and ligament strains were compiled for flexion, extension, and pure axial compression. The model predicts increased flexion-extension motion for a given moment with the artificial disc when compared to the intact case. Facet contact forces increased in extension with the artificial disc.

REVIEW AND THEORY

Past successes in total hip and knee arthroplasty have encouraged the development of artificial intervertebral discs as an alternative to interbody fusion of the spine. The proposed advantages of an artificial disc are restoration of disc height and normal biomechanics without a bone graft. Numerous artificial discs are currently under study although clinical results are limited (Cinotti et al. 1996, Enker et al. 1993). This study focuses on one experimental artificial disc consisting of two porous coated plates made of titanium alloy with a ceramic (alumina) ball and socket articulation. The primary goal of this study is to evaluate the biomechanics of one motion segment with and without the artificial disc using an experimentally validated model.

PROCEDURES

A half model of the osteoligamentous L3-L4 motion segment in the sagittal plane was used to compare the load-displacement behavior and stresses before and after implantation of the artificial disc (Kong 1995). An anterior surgical approach to the spine was simulated by removal of the anterior and anterolateral portion of the annulus and the entire anterior longitudinal ligament. Complete fixation of the prosthesis

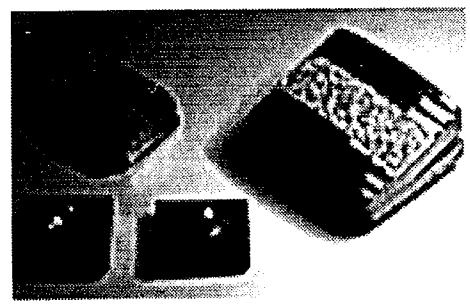

Figure 1: Artificial intervertebral disc

through bony ingrowth was simulated by 'tying' the prosthesis to the L3 and L4 endplates. The disc height before and after implantation of the artificial disc remained constant, and the axis of rotation was located 2/3 of the distance from the anterior edge of the disc space.

The socket component is comprised of solid, deformable 6 and 8-node elements with the material properties of alumina (E = 380 Gpa, v = 0.26). The ball is modeled as a rigid surface to allow three-dimensional, finite sliding contact with the socket. Reaction moments, forces, strains, and stresses were compiled for all structures of the spine during flexion (1, 5, 10, 15°), extension (1, 3, 5°), and axial compression (200, 430, 600 N). A compressive pre-load of 430 N was applied during flexion and extension.

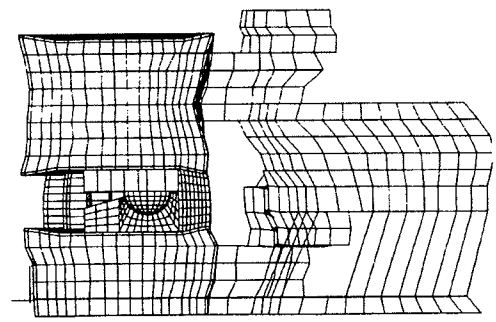

Figure 2: FE model of L3-L4 with artificial disc

RESULTS AND DISCUSSION

The reaction moment as a function of applied extension-flexion rotation with the artificial disc was 38% less at 15° flexion and 17% less at 5° extension. This may be attributed to the very low coefficient of friction ($\mu = 0.09$) between the ceramic articulating surfaces as well as the absence of the anterior longitudinal ligament and anterior annulus.

An anterior shift in loading occurred during pure axial compression with the artificial disc. Annular stress and strain decreased significantly in all loading conditions particularly in axial compression. Additionally, the facets did not come in contact during axial compression. Facet contact forces did however increase 17% at 5° extension with the artificial disc.

The results of the finite element model indicate that the artificial disc facilitates flexion and extension compared to the intact case. Fibrous tissue infiltration of the disc space may restrict this motion over time. The load-displacement behavior of the model in extension is within one standard deviation of in-vitro cadaver test data of the same disc (Gilbertson et al. 1995). In flexion the model predicts an increase in motion with the artificial disc while the in-vitro study found the opposite was true. The size of the prosthesis required excessive distraction of the endplates during insertion in-vitro. This may have induced a pre-strain in the posterior ligaments, which resist flexion.

The increased facet loads during extension underscores the significance of healthy facets in restraining excessive motion with the artificial disc. A similar finiding was made during the in-vitro study when bilateral facetectomy caused hypermobility of the affected level in extension and axial rotation. Some stress shielding is likely to occur particularly in the annulus as more load is borne by the artificial disc.

Future goals for the finite element model include a parametric study to assess the effect of ball size, material selection, and location within the disc space. An experimental wear simulation of the artificial disc is running concurrently. Collected wear rates may be used to validate an adaptive wear simulation of the artificial disc

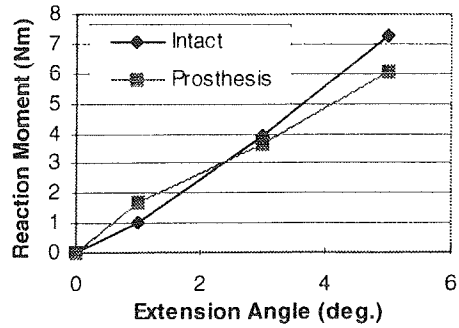

Figure 3: Reaction moment vs. extension

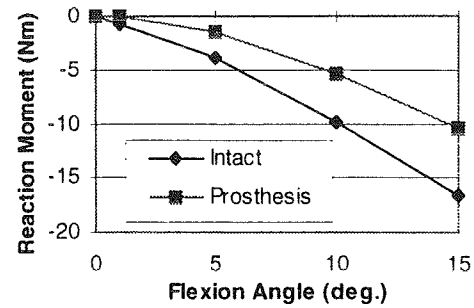

Figure 4: Reaction moment vs. flexion

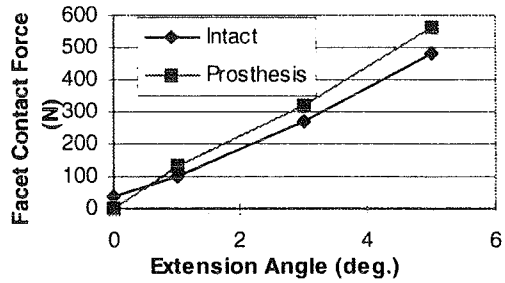

Figure 5: Facet loads in extension

using the finite element model as previously reported for polyethylene wear in total hip arthroplasty (Maxian et al. 1996).

REFERENCES

Cinotti, G. et al. *Spine*, 21(8), 995-1000, 1996.
Enker, P. et al. *Spine*, 18(8), 1061-1070, 1993.
Gilbertson, L. et al. 35TH Proc. ISSLS, 1996.
Kong, W. Doctoral Dissertation, U. of Iowa,1995.
Maxian, T. et al. *J. Orthop. Res.*, 14(4), 1996.

ACKNOWLEDGMENTS

The authors wish to acknowledge the support of Sofamor Danek Group, Inc.

COMPUTER SIMULATION STUDIES OF ACL LOADING MECHANICS

Steven J. Charlebois and Denis J. DiAngelo
Department of Biomedical Engineering, University of Tennessee, Memphis, TN 38163

INTRODUCTION

The mechanics of the anterior cruciate ligament (ACL) were studied for increasing anterior tibial drawer. A previously developed computational four-bar model of the knee joint was used. Links representing specific fiber bundles in the ACL and PCL remained isometric over the full range of motion. Ligament fiber attachment sites on the tibia were moved in unison to achieve the desired amount of anterior tibial translation in the model.

REVIEW AND THEORY

The ACL is a geometrically complex and mechanically nonhomogenous structure (Mommersteeg, 1997). In the knee, the ACL serves as a primary restraint to excessive anterior tibial displacement, a clinical condition commonly referred to as positive tibial drawer.

The load carrying capacity of the ACL has been shown to vary with flexion angle (Markolf et al, 1990; O'Connor and Zavatsky, 1992; Blomstrom et al, 1993). In addition, the mechanical contribution of different regions of the ACL change to help maintain knee joint stability over the full range of motion (O'Connor and Zavatsky, 1992). The anteromedial bundle of the ACL carries the majority of the load during knee flexion, whereas the posterolateral bundle provides restraining force during extension (O'Connor and Zavatsky, 1992).

Although evidence of the ACL's role as a primary restraint to anterior translation of the tibia exists, the associated forces generated within the ligament itself are not well understood (Blomstrom et al, 1993). Knowing the forces in the ACL is useful for elucidating mechanisms of ligament injury and in formulating rehabilitation programs for knees where ligaments have been repaired or replaced. A better understanding of the loading pattern of the ACL may lead to improved ligament replacement designs.

The main objective of this study was to employ a previously developed computational four-bar model of the knee joint to study ACL mechanics (Charlebois et al, 1997). Length changes of different ACL fiber bundle regions and total force developed in the ACL were determined for increasing amounts of anterior tibial translation.

PROCEDURES

A computational four-bar model was used to prescribe flexion-extension of the knee joint. Model development was carried out in Working Model (Knowledge Revolution Inc.) as described in Charlebois, et al, 1997. The location of the tibial attachment of each ACL fiber was moved in 2 mm increments, thus reproducing anterior (positive) tibial translation in the sagittal plane.

The ACL ligament was modeled as a series of equally spaced, parallel fiber bundles extending between the femoral and tibial attachment sites. The fiber bundles were represented by line segments and divided into three zones: anterior, central, and posterior. All of the fibers had a constant width of 3 mm.

The change in length of each fiber bundle from an original position of full extension (0° flexion) up to 140° flexion was determined. Strain in the fiber bundles relative to the original length was determined. An estimate of the ligament elasticity taken from the literature was used to calculate fiber force and stress levels. With the stress and strain in each of the fibers of the ACL known, the magnitude and direction of the corresponding force vector could be obtained. Force values were obtained by integrating along the ACL tibial attachment line.

DISCUSSION OF RESULTS

Relative length changes of the anterior, central, and posterior fiber regions of the ACL are shown in Figure 1 for several values of anterior tibial displacement. The computational results are comparable to other published data (O'Connor and Zavatsky, 1992). The anterior region of the ligament stretched with anterior tibial drawer throughout flexion. A reduction in length was

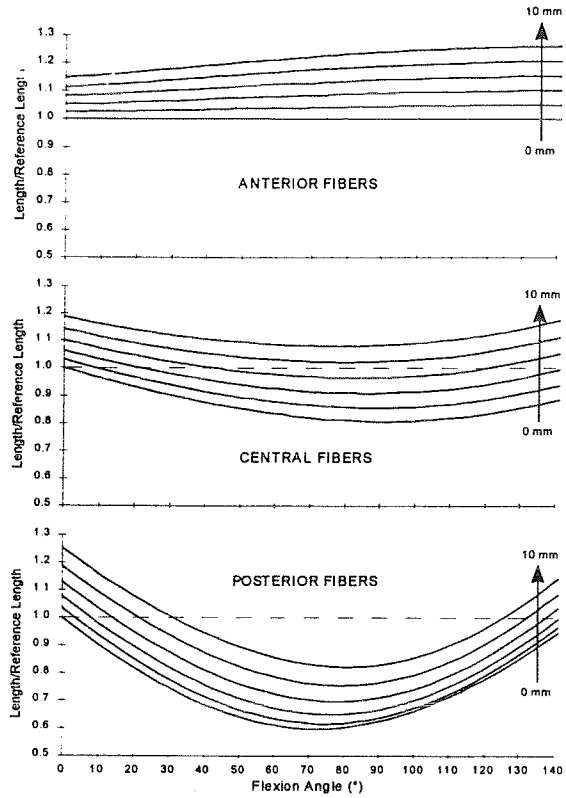

Figure 1. Relative length changes of the ACL fibers with increasing anterior drawer.

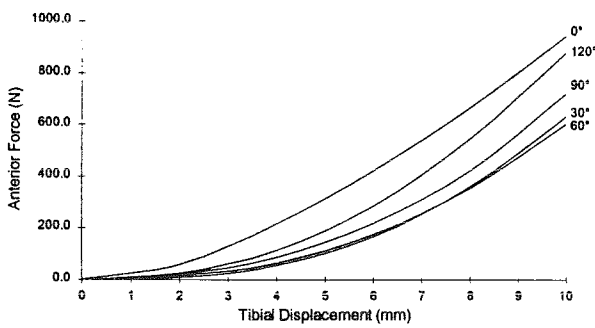

Figure 2 Applied anterior force versus tibial displacement at various flexion angles for ACL.

observed in the central and posterior regions of the ligament throughout flexion.

The AP force developed in the ACL due to increases in anterior tibial displacement is shown in Figure 2 for different levels of knee flexion. The anterior force in the ACL increased with anterior tibial displacement. A reduction in anterior force was observed though 60° flexion, where after it increased to a maximum at 120° flexion.

Figure 3 shows the ACL ligament force vector positioned along the tibial attachment line for increasing amounts of anterior tibial displacement at 30° of knee flexion. Force in the ligament increased in a posterior direction with increases in tibial displacement.

Using the computational four-bar knee joint model, we have demonstrated that mechanics of different regions of the ACL changes with knee flexion angle. The magnitude and direction of the force in the whole ACL at 30° flexion was shown to agree fairly well with results from previous investigators (Livesay et al, 1996). Ongoing research with the computation model includes the addition of patella (third body), quadricep forces, non-rigid ligaments, and contact forces to investigate how contact surface geometry affects resultant motion and loading mechanics.

REFERENCES

Blomstrom G. et al. Adv. Bioeng., 24, 359-362, 1993.
Charlebois S, DiAngelo DJ, Development of linkage Model, (Submitted to this conference).
Fujie H. et al. Adv. Bioeng., 22, 91-94, 1992.
Livesay G. et al. Adv Bioeng., 20, 443-445, 1991.
Mommersteeg T. et al. J. Biomech., 30, 139-146, 1997.
O'Connor JJ et al. Proc. Instn. Mech. Engrs., 206, 125-145, 1992.

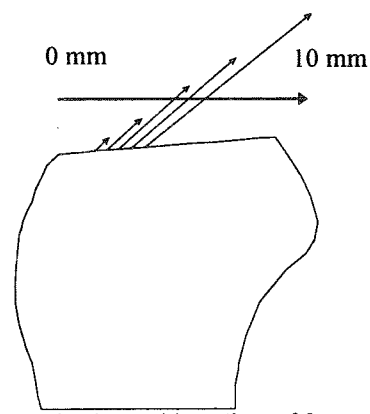

Figure 3 Magnitude and location of force vector in ACL at 30° flexion.

DEVELOPMENT OF A LINKAGE MODEL TO STUDY THE ROLE OF THE CRUCIATE AND COLLATERAL LIGAMENTS OF THE KNEE

Steven J. Charlebois and Denis J. DiAngelo
School of Biomedical Engineering, University of Tennessee, Memphis, TN

ABSTRACT

A computer linkage model of the knee was developed to study the role of the cruciate and collateral ligaments. Biomechanical data of the ligament attachment sites on the tibial plateau and femoral condyle were used to determine the kinematic and strain properties of the constituent fiber bundles and whole ligaments. The model was used to demonstrate changes in ligament length for passive knee flexion.

INTRODUCTION

Ligaments of the knee have complementary mechanical roles that contribute to the overall stability and motion of the knee joint (O'Connor and Zavatsky, 1992; Mommersteeg et al., 1997). Butler (1989) estimated that the anterior cruciate ligament (ACL) contributed 86% of the resistive force to anterior translation in the knee. Compared to ACL, relatively less biomechanical data is available for the posterior cruciate ligament (PCL). The primary role of the medial (MCL) and lateral (LCL) collateral ligaments is to maintain knee stability in the coronal plane.

The 2-D computer package Working Model (Knowledge Revolution Inc.) was used to develop a computational linkage model of the knee. Linkage theory and mathematical techniques described by O'Connor and Zavatsky (1992) were incorporated in the model to determine the displacement and strain properties of the collateral and cruciate ligaments.

MODEL DESCRIPTION

A four-bar linkage system was used to replicate the polycentric motion of the knee that occurs during passive knee flexion-extension. A four-bar linkage design was selected that reproduced the full range of motion of the knee joint and replicated the complex gliding and sliding behavior between the tibia and femur (O'Connor and Zavatsky, 1992). The knee-ligament linkage model is shown in Figure 3. Link 1 represented the most anterior fibers of the ACL, and link 2 joined the central portion of the PCL femoral attachment with the most posterior PCL tibial attachment. The anterior point of tibial attachment of the ACL was the origin of the global coordinate system. Data of the ligament attachment sites on the tibia and femur were taken from the literature (Zavatsky and O'Connor, 1992). As the knee joint flexed from a fully extended position, the change in distance between the respective knee ligament fiber attachment sites was monitored. The instant axis of rotation (IAR) of the knee model was defined by the intersection of the two "cruciate links". To track the moving IAR path, a "virtual link" was established between the cruciate links.

RESULTS

While not explicitly shown, the moving path of ligament attachment sites during knee flexion-extension ultimately changed the ligament shape. Figures 1 and 2 show the calculated relative length changes of anterior, central, and posterior fibers of the model ligaments plotted against knee flexion. The most anterior fibers of the ACL (link 1) remained isometric throughout the full range of motion. The central and posterior fibers of the ACL loosened through 70° of flexion, where after they became progressively tighter. The length of the central PCL fibers (link 2) also remained isometric. Anterior fibers of the PCL lengthened with flexion, while posterior fibers loosened until 120° of flexion and then re-tightened. The anterior portion of the MCL stretched slightly through 70° of flexion, but then became lax. The remaining MCL and LCL fibers loosened with flexion.

DISCUSSION

Results from our computer model were identical to that given by O'Connor and Zavatsky (1992). The relative length changes of ligament fibers were comparable to those observed for human specimens (Butler, 1989). The effects of complex motions of the knee on ligament mechanics were studied using a simple four-bar linkage model. Integration of linkage theory and computer programs like Working Model is an ideal teaching tool for biomedical engineering students to apply engineering principles to study musculoskeletal systems.

REFERENCES

Blomstrom G, et al: ASME Adv Bioeng, **BED-24**:359-362, 1993.

Butler DL: J. Orthop. Res., **7**:910-921, 1989.

Mommersteeg TJA, et al: J. Biomech., **30**:139-146, 1997.

O'Connor JJ and Zavatsky AB: Proc Instn Mech Engrs, **206**, 125-145, 1992.

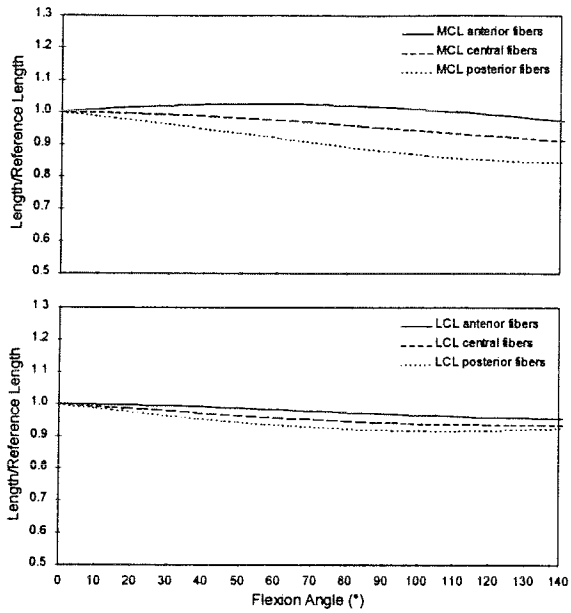

Figure 1: Relative length changes of MCL and LCL ligaments during passive knee flexion.

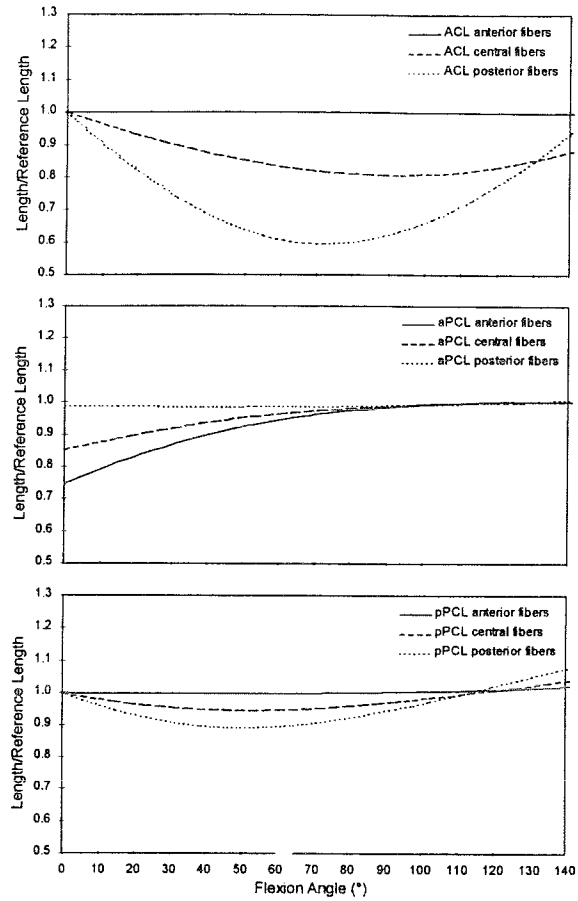

Figure 2: Relative length changes of ACL and PCL ligaments during passive knee flexion.

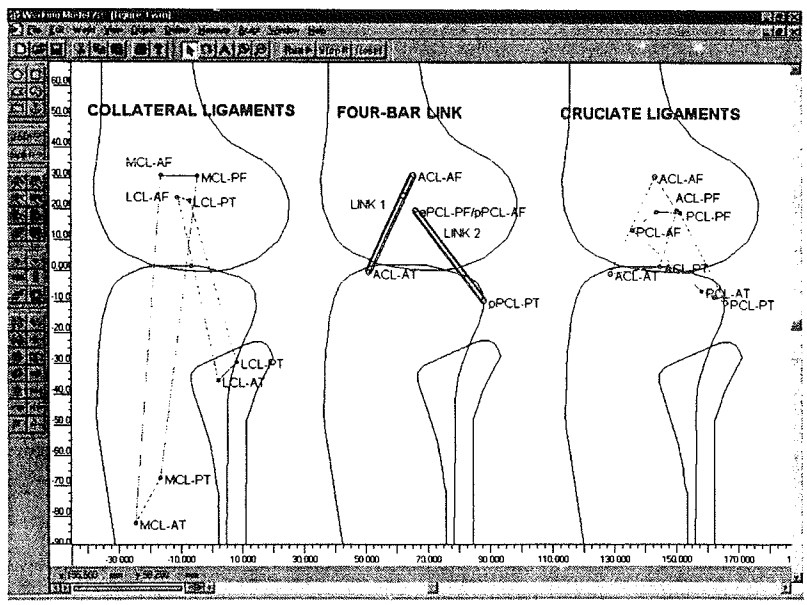

Figure 3: Schematic of the knee-ligament linkage model at full extension.

CAN QUIET STANDING BE MODELLED AS A SINGLE PENDULUM?

W. Accles, V. Fortney, V. Zatsiorsky

Biomechanics Laboratory, The Pennsylvania State University, University Park, PA 169802

INTRODUCTION

Body motions occurring during quiet standing are extremely small. Because these motions are so difficult to register body sway during quiet standing has been studied mainly by quantifying the center of pressure and hip migration (Prieto et al., 1993).

The present study measured several kinematic variables in order to determine whether the motion of the body during quiet stance occurs mainly around the ankle joint (single pendulum).

REVIEW AND THEORY

If motion occurs only around the ankle joint during quiet stance then other kinematic measures of body sway, such as the thigh, gravity line (GL), center of pressure (COP) and back displacement should all be highly correlated with the ankle angular displacement. If motions of significant magnitude occur at the knee and hip joints then these measures will not be highly correlated.

- STATEMENT OF PURPOSE: A kinematic analysis of the small motions occuring during quiet stance was performed in order to determine whether this activity can be modeled as a single pendulum.

- HYPOTHESIS: Movements occur at the ankle, knee, and hip joint during quiet stance. These movements are large enough to make modeling of quiet stance as the movement of a single pendulum unfeasible.

PROCEDURE

Ten healthy male college aged subjects participated in the study. Human Subjects Approval was received by the Institutional Review Board and after the study was explained subjects signed an informed consent form.

The following devices were used to register the motions of the body during quiet standing:

1. Bertec Force Platform: Center of Pressure and Gravity Line Migration (Calculated from the horizontal ground reaction force by method of King and Zatsiorsky (1997)).
2. Science Accessories Corporation Sonic Digitizing Device: Mid Thigh Displacement (Measured at mid point of Femur) and Back Displacement (Measured at L2 vertebra), Accuracy ± 0.5 millimeters.
3. Penny and Giles Goniometers: Ankle and Knee angular displacement, Accuracy ± .005 radians.

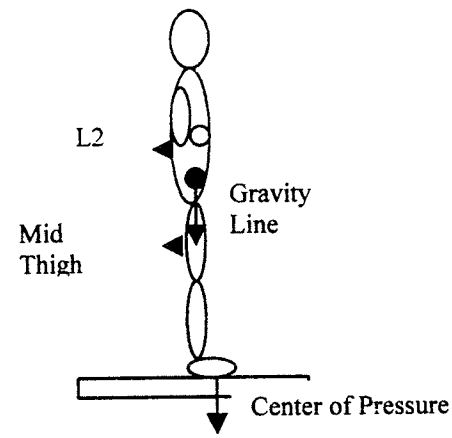

Figure 1: Schematic of Experimental Set Up

Subjects stood for 90 seconds under eyes closed or eyes open condition. Instructions were to stand with the arms folded across the chest in a relaxed comfortable manner. Subjects were informed verbally when 30 and 60 seconds of the trial had passed. Ten trials for each of the conditions were completed.

Data was collected at 12 Hz and treated with an 8^{th} order Low Pass Butterworth filter with a cutoff frequency of 4 Hz.

Normalized Cross Correlations at zero phase lag were calculated between the ankle angular displacement and Mid Thigh, L2, COP and GL displacements.

The Mid Thigh Displacement was used to make a prediction of the L2 Displacement (PL2) in order to ascertain the type of movement occurring at the hip joint. Correlations were then calculated.

RESULTS

Table 1 shows that under the eyes open condition three of the ten subjects (2, 9 and 10) behave largely like a single pendulum. This result is indicated by the high correlations between each of the measures of body sway and the ankle angular displacement. The remaining 7 subjects showed poor (3, 8) or no correlations (1, 4, 5, 6, 7) between each of the measures and the ankle angular displacement.

The results shown in the last column (L2 and PL2) suggest that for 8 of the 10 subjects there is little movement occurring at the hip. (High correlations between the measured displacement and a predicted displacement based upon the motion of the thigh.)

Subject	Mid Thigh	L2	COP	GL	L2 and PL2
1	.74	.14	.18	.12	.68
2	.84	.81	.78	.77	.99
3	.65	.78	.72	.66	.92
4	.48	.83	.73	.63	.71
5	.77	.60	.48	.49	.94
6	.18	.15	.21	.12	.95
7	-.06	-.22	-.16	-.23	.98
8	.68	.75	.80	.75	.96
9	.96	.91	.85	.84	.96
10	.95	.89	.82	.83	.98

Table 1: Eyes open condition. Correlations between ankle angular displacement and Mid Thigh, L2, COP and GL. Also includes correlations between L2 and predicted L2 (PL2)

Table 2 shows that under the eyes closed condition only two of the ten subjects (2, 10) behave largely like a single pendulum. This result is indicated by the high correlations between each of the measures of body sway and the ankle angular displacement. The remaining 8 subjects showed poor (5, 8) or low correlations (1, 3, 4, 6, 7, 9) between each of the measures and the ankle angular displacement.

The results shown in the last column (L2 and PL2) suggest that for 8 of the 10 subjects there is movement occurring at the hip. (Low correlations between the measured displacement and a predicted displacement based upon the motion of the thigh.)

Subject	Mid Thigh	L2	COP	GL	L2 and PL2
1	.85	-.09	.22	.26	-.09
2	.88	.86	.83	.84	.86
3	.44	.50	.48	.45	.50
4	.49	.42	.44	.28	.42
5	.77	.74	.71	.66	.74
6	.62	.64	.61	.40	.64
7	.82	.31	.32	.28	.31
8	.81	.73	.68	.56	.73
9	.67	.58	.40	.39	.58
10	.93	.89	.86	.77	.89

Table 2: Eyes closed condition. Correlations between ankle angular displacement and Mid Thigh, L2, COP and GL. Also includes correlations between L2 and predicted L2 (PL2)

Additionally, the magnitude of the ankle and knee angular displacements were similar in magnitude (Approximate range of ± .02 radians). This direct measurement further suggests that single pendulum modeling of quiet stance would be incorrect.

DISCUSSION

Several measures of body sway were registered in order to examine the kinematics of motion during quiet stance. Under both the eyes open and eyes closed condition only two or three subjects demonstrated motions which would resemble the motions of a single pendulum.

An additional observation is that under the eyes closed condition the number of subjects demonstrating movement at the hip jumped from two under the eyes open condition to eight.

These results suggest that it is inappropriate to model quiet standing as a single pendulum.

REFERENCES

King, D. L., and Zatsiorsky, V. M. Gait and Posture, Extracting gravity line displacement from stabilographic recordings, 1997.

Prieto, T. E., Myklebust, J. B. IEEE Trans. Rehab. Eng., 1, 26-34, 1993.

EFFECTS OF PALMAZ™ STENT CROSS SECTIONS ON RECIRCULATION AND REATTACHMENT OF BLOOD FLOW: A 2D COMPUTATIONAL MODEL

Stephen D. Ainsworth†, Jay M. Ochterbeck*, Eugene M. Langan III**, and Martine LaBerge†

Laboratory of Vascular Research
Greenville Hospital System/Clemson University Biomedical Cooperative, Clemson, South Carolina
†Department of Bioengineering and *Department of Mechanical Engineering
Clemson University, Clemson, South Carolina
**Department of Surgery, Greenville Hospital System, Greenville, South Carolina

INTRODUCTION

Knowledge of the distinct fluid dynamic factors created by an intravascular stent, placed in an atherosclerotic artery and subjected to pulsatile flow, is limited. A computational fluid dynamics modeling approach was used in this research to analyze and measure the effect of single stent struts on the flow separation, reattachment points, and re-circulation regions.

REVIEW AND THEORY

The clinical repair of atherosclerotic peripheral arteries commonly includes the use of intravascular (IV) stents in conjunction with balloon angioplasty. Introduced percutaneously, IV stents adequately expand the vessel lumen until fibrosis and natural re-intimalization occur. Animal studies have shown a rapid endothelialization following the implantation of IV stents hence discouraging a myointimal hyperplastic response [1]. However, a 20-30% restenosis rate subsequent to myointimal hyperplasia has been observed with the clinical use of IV stents [2]. Authors have proposed different models to explain vascular restenosis with a major emphasis on the contribution of hemodynamic factors. In fact, myointimal thickening has been associated with the presence of areas of re-circulation and separation, and wall shear stress gradients [3]. These factors are directly related to the design configuration of the stent. After deployment, the geometrical design of the currently FDA approved balloon expandable stent (Palmaz 154M, Johnson & Johnson Interventional Systems, Warren, NJ) involves a repeating diamond-like configuration of struts (Fig.1). The struts forming the repeating unit of the stent can be represented as backward and forward facing steps at angles inclined to the flow of blood through the vessel. This geometry creates areas of flow separation and recirculation. The point of flow reattachment behind the step is considered an area of increased shear stress gradients. Its distance from the step has been shown to be a function of both Reynolds number and height of the step.

Figure 1: a) Solid computational model of balloon expandable intravascular stent. b) SEM of strut cross section.

In order to effectively model the effect of stent geometry on the characteristics of blood flow, the geometry of the stent, the properties of the blood, and the properties of the blood vessel, must be taken into consideration both experimentally and computationally. This study is a first step toward this comprehensive approach to IV modeling and analyzes the effect of stent geometry, focusing on various cross sections of the Palmaz stent, on areas of recirculation and reattachment points in a two dimensional computational model.

PROCEDURES

A two dimensional computational model was designed using a well-validated finite volume code. The geometry of each case studied was based on the longitudinal cross section of the Palmaz 154 Balloon expandable stent as shown in Figure 2.

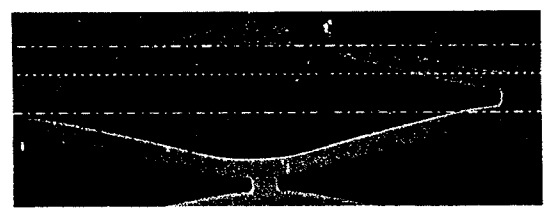

Figure 2: Picture of stent strut with lines indicating location of cross-sectional cuts.

Case 1 represents the centerline of the repeating unit (diamond). This case presents a straightforward analysis in that the steps are far apart and relatively short in length. Cases 2 and 3 are unique in that the length of the struts are varied as well as the distance between the struts. The arterial walls are assumed to be rigid, due to the combination of atherosclerotic disease and the support offered by the stent to the walls of the vessel. The three cases specified above were subjected to steady flow of a Newtonian fluid at a Reynolds number equal to 560.

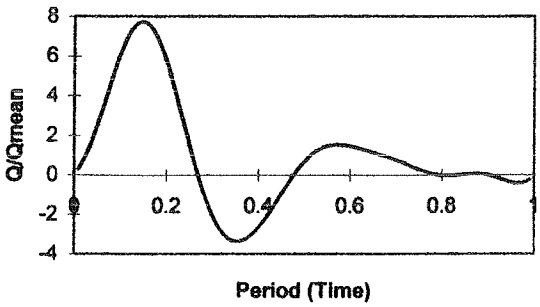

Figure 3: Input wave form for femoral artery.

In order to evaluate the variation of the reattachment point under *in vivo* conditions, the geometry for case 2 was also subjected to unsteady pulsatile flow. For this case, an input wave form for the femoral artery seen in Fig. 3 was used with a mean velocity of 6.73 cm/sec [4].

RESULTS AND DISCUSSION

Results show that the reattachment point is a function of the longitudinal cross sectional geometry of the stent. The three cases for steady flow investigated show that the reattachment point, normalized by the step height (s), changes location depending on the width of the strut and the distance between the struts. Case 1, which has the smallest cross section (t=.3 mm), has a reattachment length (x/s) equal to 4.45. Case 2 has thicker struts (t=1.08mm), but the distances between the struts is less than case 1 which effects the flow as well. Specific results for the steady flow cases are provided with contour plots of velocity in the x-direction in Figures 4,5, and 6. Reattachment point B in Case 2 is extremely close to the next strut, potentially creating a well-defined stagnation region. Figure 6 shows the results from Case 3, which has longer struts due to the location of the cross-sectional cut. The normalized reattachment point of 7.54 is the longest for steady state cases.

Figure 4: Case 1-Reattach. Length (x/s) = 4.45

Figure 5: Case 2-Reattach. Length A (x/s) = 3.99
Reattach. Length B (x/s) = 5.34

Figure 6: Case 3 - Reattach. Length (x/s) = 7.54

The unsteady pulsatile results show that under a physiological-like waveform, the reattachment point varies with time as well as with geometry. Fig. 7 is a plot of the normalized reattachment length as a function of time, corresponding to the input wave form from Fig. 3. Therefore, overall results demonstrate that it may be possible to specifically design a stent to create optimal blood flow characteristics, and consequently influence the cellular reaction.

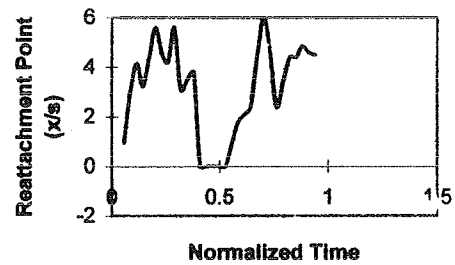

Figure 7: Reattach. plot for unsteady case 3.

REFERENCES

1. Rogers, C., *Circulation*, June, v 91 n 12,1995.
2. Serruys, P.W., *The New Eng. J. of Med.*, August,331:489-95,1994.
3. Davies, P.F., *Phys. Rev.*, v 75 n 3:519-560,1995
4. Ballyk, P.D., et al., *Biorheol.*, v 31 n 5, 1994.

ACKNOWLEDGEMENTS

Funding provided by Greenville Hospital System/Clemson University Biomedical C ›operative, Clemson, SC

Automated 3D Reconstruction of 2D Medical Images: Application to Biomedical Modeling

J. Wang, V. M. Gharpuray , R. L. Dooley
Department of Bioengineering
Clemson University
Clemson, SC 29634-0905 USA

INTRODUCTION

It is difficult to visualize the correct three dimensional (3D) geometry of an anatomical structure from medical images (CT or MRI) which are usually 2D representation of the 3D objects. In this study, an interactive software tool was developed to automatically create 3D images from 2D medical data. An interface to import the 3D images into finite element software for further analysis was also developed.

REVIEW AND THEORY

Over the last decade, considerable efforts have gone into both biomedical image processing and computation biomechanical modeling. Computer imaging techniques have become an important diagnostic tool in the practice of modern medicine. These techniques include Computed Tomography (CT) or Magnetic Resonance Imaging (MRI), which use a sampling or data acquisition process to capture information about the internal anatomy of a living patient [1]. This information is in the form of slice-plane or cross-sectional images of a patient. Since the amount of data is too large to be understood in its raw form, we wanted to extend these techniques into three-dimensions, in which image slices can be gathered into volumes and the volumes can be processed to reveal complete anatomical structures. Therefore, 3D visualization has become increasingly useful for the interpretation of medical volume data, as obtained from CT or MRI.

Also, Computer Aided Engineering (CAE) is changing rapidly with advances in computer hardware and software and rapid prototyping technologies. Solid modeling has been considered as a fundamental vehicle for communicating geometric information [2]. Among these improvements, the finite element (FE) method has become a widely used tool in biomechanical studies, especially because of its powerful capabilities of modeling irregular geometries and non linear material behaviors.

The purpose of this study was to use the techniques developed in image processing to advance the accuracy of biomechanical modeling. In particular, we wanted to be able to import the 3D reconstruction of CT or MRI scans into FE modeling software. The 3D images reconstructed this way provide a much higher resolution and take much less time than those done manually. And once the 3D data were imported into FE, biomechanical analysis can be done without much effort.

PROCEDURES

In this study, the software we chose to do the visualization is the Visualization Toolkit 1.2, which is a C++ class library with a built-in Tcl/Tk interpreter for visualization and 3D graphics. Our work was done once with the following configuration:
2 150 MHZ IP19 Processors
CPU: MIPS R4400 Processor Chip Revision: 5.0
FPU: MIPS R4000 Floating Point Coprocessor Revision: 0.0
Secondary unified instruction/data cache size: 1 Mbyte
Data Cache size: 16 Kbytes
Instruction cache size: 16 bytes
Main memory size: 128 Mbytes, 2-way interleaved

The software was evaluated using a set of CT scans of anatomically corrected human knees obtained from the Visible Human Project of the National Library of Medicine. The original medical imaging slice data is structured point data, for which the topology and geometry of the data is implicitly known, requiring only dimensions, an origin, and an aspect ratio [1]. The steps to reconstruct and then display the 3D model are as following:

1. Read the input.
2. For each anatomical feature of interest, create an iso-surface with a chosen density value.
3. Transform the models from patient space to world space.
4. Render the model

Following the steps above, we developed an interactive tool called ***Feather***, based on the Visualization Toolkit. The tool consists of three parts. The first part of ***Feather***, deals with how to create 3D models, including the generation of triangle or polydata files from the original cross-section CT data using Marching Cubes algorithm, which provides a high resolution surface construction. Different density value corresponds to different iso-surface extraction. The second part of this tool displays 3D models created from the first part. To make the tool more user-friendly, we wrote a script in Tcl/Tk to develop a flexible interface, from which the user can choose

the desired iso-surface, rotate the 3D model on display or change the opacity value of the iso-surface. The third part of *Feather*, is the interface with FE packages, especially I-DEAS ™.

RESULTS

Fig. 1 is the reconstruction of the skin around the knees. Fig. 2 demonstrates the extraction of the hard tissue around the knees. As one of the improvement in the visualization process, more than one iso-surface can be extracted and displayed at the same time, as demonstrated in Fig. 3, in which the skin and bones are shown together. The opacity value of the skin was chosen to make the skin translucent, so that the bones inside are visible.

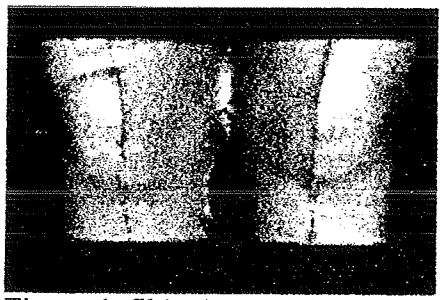

Figure 1. Skin Around the Knees

Figure 2. Bone Around the Knees

Figure 3. Skin and Bone

DISCUSSION

The 3D models reconstructed from *Feather* have a much higher resolution and require much less processing time than those done manually. The inter-slice connectivity is also preserved. In the real working environment, the surgeon can rotate the 3D models, zoom in/out or change the opacity of any tissue. This will help the surgeon to make pre- and intra-surgery plans. Further, the reconstructed models can be imported into FE analysis software for biomechanical analyses.

REFERENCES

[1]. W. Schroeder, K. Martin, and B. Lorensen, *The Visualization Toolkit*, Prentice Hall PTR, NJ, 1996.

[2]. M. H. Lawry, *I-DEAS Master Series* ™ *2.0, Student Guide*, 1994.

[3]. W. Schroeder, B. Lorensen, "3D Surface Contours", *Dr. Dobb's Journal*, vol. 21 (No. 7), pp. 26-32. July, 1996.

[4]. A. Pommert, U. Tiede, G. Wiebecke, K. H. Höhne, "Surface Shading in Tomographic Volume Visualization: A Comparative Study", *First Conference on Visualization in Biomedical Computing*, pp. 19-26. Atlanta, GA, 1990.

ACKNOWLEDGMENT

The authors acknowledges the Visible Human Project of the National Library of Medicine for the original human knee CT data.

MODELLING UNICOMPARTMENTAL MENISCAL BEARING KNEE REPLACEMENT

A Imran and JJ O'Connor
University of Oxford, Department of Engineering Science
and Orthopaedic Engineering Centre, Oxford, England.

INTRODUCTION

The successful outcome of unicompartmental knee replacement with unconstrained and congruous surfaces requires careful patient selection and precise surgical technique (1). To reproduce the normal kinematics and muscle lever arms of the knee, such prostheses require the restoration of normal patterns of length and tension to the ligamentous structures which span the joint. Surgical malplacement of the prosthesis components can result in stretched ligaments or in increased joint laxity. The purpose of this study is to develop a computer-graphics based planar model of a knee prosthesis with fully congruous and unconstrained meniscal bearing. The model is used to analyse the effects on joint mechanics of surgical malplacement of the prosthesis components. A computer-based graphics interface is being developed for visual analysis of the behaviour of the knee after joint replacement.

METHODS

The model knee is shown in figure 1. The model femoral surface was part of a circle and the tibial surface was flat. A fully congruous mobile bearing was trapped between the femoral and tibial components and held in place by the ligaments. The cruciate (ACL and PCL) and collateral (LCL and MCL) ligaments were represented by arrays of elastic fibres, which buckled when slack (2,3). Straight line representation was used for forces transmitted by the model muscles except where they wrapped around the bones. A bi-articulating model of the patello-femoral joint was used (4). A *neutral position* of the components was defined at 0° as that which allowed near isometric behaviour of selected fibres of the cruciate ligaments during flexion. The ligament forces were estimated during a simulated antero-posterior (A/P) laxity test, such as the Lachman test. The effects on joint laxity of malplacement of the tibial and the femoral components, and the effects of tibial component tilt were analysed. Also, the effects of using incorrect bearing thickness were studied.

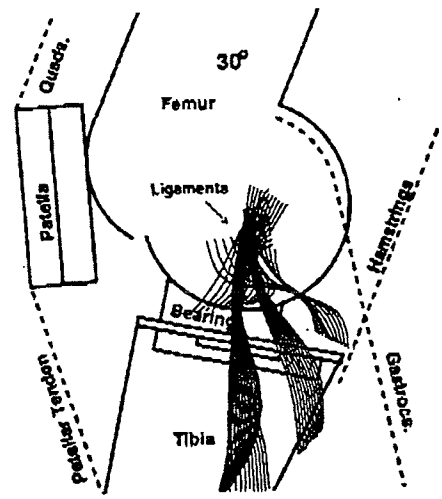

Figure 1: The model knee at 30° flexion.

RESULTS AND ANALYSIS

The neutral fibres of the cruciate ligaments remained almost isometric throughout flexion, becoming slightly slack during the mid-range. Maximum slackening was at 60°: 0.9% for the ACL neutral fibre and 1.1% for the PCL neutral fibre. This slackness accounted for about 0.5 mm A/P laxity at 60°.

From 0 to 90° flexion, the model bearing moved posteriorly by 10.2 mm, which is in reasonable agreement with the *in vitro* measurements (5) in this flexion range of 13.5 mm in the medial and 14.25 mm in the lateral compartments (average of 4 knees). Also, model calculations compared well with experimental observations available in the literature for the orientation of patellar tendon, patellar tendon to quadriceps force ratio and quadriceps force in flexed knee stance (5,6).

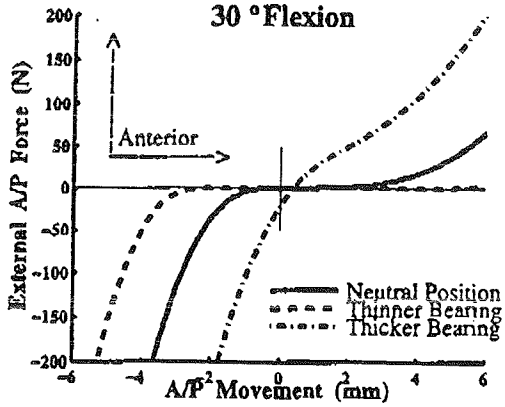

Figure 2: Force-Displacement curve for neutral position of components, and for using incorrect bearing thickness.

With reference to figure 2 during A/P laxity test, the force-displacement behaviour at the *neutral position* of the components was typical of that reported from experiments (6). Compared to the neutral position, malplacement of the components either increased joint laxity or stretched the ligaments. Joint laxity is increased by distal placement of the tibial component, by choosing too thin a meniscal. Ligament forces are increased and resistance to A/P displacement is greatly increased by proximal placement of the tibial component, by choosing too thick a meniscal bearing.

CONCLUSIONS

The results show that in an unconstrained knee prosthesis with retained cruciate and collateral ligaments, a single radius femoral component, a mobile bearing, and a flat tibial component, if positioned correctly, can accurately restore the mechanics of the joint.

CLINICAL SIGNIFICANCE

This analysis demonstrates that one mm differences in the thickness of the bearing can alter significantly joint laxity or joint stiffness after replacement.

The model developed for this study can be used for quantitative and visual analysis of the interaction between component placement and the resulting joint laxity or ligament forces over flexion.

The analysis shows that appropriate mathematical models can be useful tools for developing prosthesis designs, analysing their effects after implantation, and understanding the role of surgical technique.

REFERENCES

1. Goodfellow J and O'Connor J. *Clin Orthop Rel Res*; 276: 245-52, 1992.
2. Lu TW and O'Connor JJ. *J Eng Med*; 210(H): 71-9, 1996.
3. Zavatsky AB and O'Connor J. *J Eng Med*,; 206(H3): 125-34, 1992.
4. Gill HS, O'Connor JJ. *Clinical Biomechanics*; 2(2): 81-9, 1996.
5. O'Connor J *et al. J Eng Med*; 203(H): 223-33, 1989.
6. Buff H *et al.* J Biomech, 21: 17-23, 1988.
7. Markolf KL *et al. J Bone Jt Surg [Am]*; 58 (5): 583-94, 1976.

ACKNOWLEDGEMENTS

The authors would like to thank Mr John Goodfellow and Mr David Murray for their advice. This work was supported by Felix Scholarship for research at the University of Oxford.

RELATIONSHIPS BETWEEN BALL RELEASE VELOCITY AND 3D JOINT KINEMATICS AND IN BASEBALL THROWING

C. P. Sherwood[1], R. N. Hinrichs[1], and G. T. Yamaguchi[2]

[1]Department of Exercise Science and Arizona State University, Tempe, AZ 85287
[2]Department of Chemical, Bio, and Materials Engineering, Arizona State University, Tempe, AZ 85287

INTRODUCTION

The purpose of this study was to determine the three-dimensional (3D) angular velocities most related to release velocity in baseball throwing using subjects with a wide range of throwing abilities. The between-subject analysis showed ball release velocity (BRV) was significantly and *positively* correlated with elbow extension *angle*, and shoulder internal rotation *angular velocity*, at release. In addition, BRV was significantly and *negatively* correlated with shoulder abduction and horizontal abduction *angles*, and with elbow extension *angular velocity*, at release. The fastest subjects released the ball with their elbows closer to full extension and in so doing sacrificed elbow extension angular velocity at release in order to increase shoulder internal rotation angular velocity for an overall increase in ball velocity.

REVIEW AND THEORY

In the past, 3D analyses of throwing have been limited to reporting mean data obtained from elite throwers (e.g., Feltner and Dapena, 1986). Many of these studies have implicated rapid shoulder internal rotation (SIR) of the throwing arm near release as one of the most important body movements in throwing (Dillman et al., 1993; Feltner and Dapena, 1986; Pappas et al, 1985). SIR angular velocities in these studies were reported to be greater than 100 rad/s at ball release in elite throwers. However, these studies calculated internal rotation angle using only the joint centers to represent a stick figure of the arm. Typically the cross product of the upper arm vector (shoulder joint to elbow joint) and the forearm vector (elbow joint to wrist joint) is used to get an elbow flexion/extension axis. This axis vector is then compared with the trunk's reference frame to determine the shoulder int/ext rotation angle. The major problem with this model (hereinafter referred to as the "stick figure model") is that the cross product becomes unstable as the elbow approaches full extension near release leading to erroneous values of SIR angle and angular velocity. Contributing to this instability are the "carrying angle" of the forearm relative to the upper arm at full elbow extension and how it changes with supination/pronation of the forearm. Therefore, a secondary purpose of this study was to compare the accuracy of the stick figure model for measuring SIR angles with a complete rigid body model using three markers per body segment to determine Cardan angles. This rigid body model did not use the forearm points at all to determine SIR and hence avoided the problems associated with carrying angle and elbow extension near release.

PROCEDURES

Twenty-one right-handed college-aged males were recruited as subjects. After appropriate warm-up, subjects performed three maximal baseball throws while being filmed with two 120 Hz video cameras (Peak Performance Technologies, Inc.). A third camera (60 Hz) was placed 29 m away perpendicular to the throwing direction to select the one trial per subject with the highest ball velocity for full analysis. 3D coordinates of the ball and 11 points on the body (joint centers as well as two additional markers attached each to the forearm and upper arm) were computed using the DLT algorithm. Raw position data were padded prior to being smoothed using a Butterworth digital filter with cutoff frequencies ranging from 9-15 Hz depending on the point and coordinate. Cardan rotations were used to compute joint angles relative to a predefined neutral position. These included left/right rotation, lateral flexion, and flexion/extension for the trunk; ab/adduction, horizontal ab/adduction, and internal/external rotation for the shoulder; and flexion/extension, valgus/varus, and supination/pronation for the elbow/radioulnar joint. For comparison, SIR angles were also computed with the stick figure model as described above. Velocities were computed using finite difference differentiation.

RESULTS

Ball velocities at release ranged from 21.9 to 37.7 m/s. The external markers attached to the upper arm and forearm were found to have negligible effect on ball velocity; the average ball release velocity (BRV) for all subjects was 29.2 m/s with markers in place and 30.1 m/s with markers removed.

Of all the joint angles measured only three were significantly correlated with BVR ($p<0.01$). These were elbow extension angle and shoulder abduction and horizontal abduction angles. EE angle was positively correlated with BVR ($r=0.714$). The fastest throwers tended to release the ball with their elbows more fully extended. Shoulder abduction (SA) and horizontal abduction (SHA) angles were *negatively* correlated with BVR ($r=-0.559$ and $r=-0.579$, respectively). Hence, as throwing velocity increased, the shoulder became *less* abducted (approaching a 90 degrees) and *less* horizontally adducted (the upper arm lagged behind the shoulder more).

Only two angular velocities (measured at ball release) were found to be significantly correlated with BVR ($p<0.01$). These were SIR angular velocity and elbow extension (EE) angular velocity. As expected SIR angular velocity was positively correlated with BVR ($r=0.751$), but EE angular velocity was found to be *negatively* correlated with BVR ($r=-0.675$). In other words, the fastest throwers had the lowest EE angular velocities at release. In addition, all subjects had EE angular velocities that peaked at or prior to release. Although the magnitude of this peak value was not correlated with BVR ($r=-0.098$), the timing of this peak was significantly correlated with BVR ($r=0.738$) such that the fastest throwers had their EE angular velocities peak *earlier* with respect to ball release.

For the fastest seven subjects (with an average BRV of 34.7 m/s, comparable to BRVs measured on elite throwers in past research) the rigid body model calculated an average SIR angular velocity at release of 48.3 rad/s, while the stick figure model calculated an average value of 79.1 rad/s. Hence, the stick figure model overestimated the "true" SIR angular velocity (as measured with the rigid body model) by more than 60%.

DISCUSSION

The generation of large SIR angular velocities at release appears to be important for throwing a baseball at fast speeds. In addition, there seems to be a link between elbow extension and shoulder internal rotation such that the fastest subjects sacrifice elbow extension angular velocity at release in order to increase shoulder internal rotation angular velocity for an overall increase in ball velocity. The faster throwers also release the ball with their elbows more fully extended and their shoulders less abducted and horizontally abducted than their slower counterparts. This is consistent with Atwater (1979) who found the faster the throw the more the upper arm lags behind the shoulder line. Finally, the stick figure model appears to overestimate SIR angular velocity in throwing. Therefore it is likely that the large SIR angular velocities reported in previous studies are inaccurate. More research is needed using the rigid body model to analyze throwing performance.

REFERENCES

Atwater, A.E. *Exercise and Sport Sciences Reviews*, **7**, 43-85, 1979.

Dillman, C.J. et al. *J. Orthop. Sports Phys. Ther.*, **18**, 402-408, 1993.

Feltner, M. and Dapena, J. *Int. J. Sport Biomech.*, **2**, 235-259, 1986.

Pappas, A.M. et al. *Am. J. Sports Med.*, **13**, 216-222, 1985.

JOINT KINETIC DIFFERENCES DURING THE PROPULSIVE PHASE OF HIGH AND LOW VERTICAL JUMPS

Barry A. Munkasy and Jill L. McNitt-Gray
USC Biomechanics Research Laboratory, Department of Exercise Sciences
University of Southern California, Los Angeles, CA 90089-0652

INTRODUCTION

Improved performance of complex human movements requires an understanding of the relationship between the objective of the movement and multi-joint control. Achieving maximum vertical displacement of the total body center of mass in a jump requires the maximization of the vertical impulse while in contact with the ground. In the literature researchers have begun both experimentally (e.g. [Gregoire, 1984 #60; Bobbert, 1988 #49].) and through modeling (e.g. [Pandy, 1990 #202; Prilutsky, 1994 #209]. to understand the multi-joint control of jumping. However, this research has often addressed a simplified system by restricting arm movement.

To help improve performance, knowledge of how better performance is produced may be helpful. The scientific literature is replete with jump training studies indicating that training leads to improved performance [Bobbert, 1990 #95]. At the total body level examination of ground reaction force patterns has revealed no distinguishing characteristics of better performance. However, the magnitude of the peak force was thought to be less important than the pattern of force application [Dowling, 1993 #134]. Absent from the literature is an understanding of what changes in multi-joint control produce improved vertical jumping performance. Without such information the influence of control on jumping performance and the value of particular training protocols cannot be understood.

In this study the joint kinetic changes associated with improved jumping performance are addressed. In particular the propulsive phase of the jump movement was examined. It was hypothesized that changes in both the magnitude and timing of net joint moments would accompany improved performance.

PROCEDURES

Ten healthy physically active college age females volunteered to participate (mean (SD) mass 53.95 (9.45) kg., height 1.61 (0.08) m, age 20.3 (1.57) yr.). Participants accommodated to the testing and training protocols, were tested, and then trained twice per week for a four week period with 2 and 5 days rest between sessions. The frequency of training was designed to discourage physiological adaptations. The intensity of each jumping session was designed to encourage a maximum effort on every jump and to lessen the effects of fatigue. For each session, after monitored warm-up and stretching, participants performed 20 maximum counter movement vertical jumps with arms, with at least 30 s rest after each jump. During the sessions, participants were encouraged to experiment with their jumping mechanics however, no information was provided as to how to improve their jumping.

The jumps were performed on two Kistler force plates, one under each foot. Two trials per participant were selected for analysis based on the jump height calculated from the ground reaction force. The highest jump was selected from any training session while the low jump was selected from a pre-training session and was approximately 3.7 (0.3) cm lower. None of the selected lower jumps was thought to be atypical as each participant had other jumps at this level or lower.

Segment endpoints were marked prior to each session with reflective material and movement was recorded in the sagittal plane at 60 Hz using standard video technology. Consistency of marking was maintained with a full body template and checked by measuring the length between markers and correcting as necessary. The reflective material was automatically digitized using a video based data acquisition system (Peak Performance, Inc.). Due to the difficulty of marking the shoulder, its location was manually digitized. Each coordinate of the digitized body landmarks were digitally filtered using a fourth order Butterworth filter with a cut-off frequency derived by the method of Jackson (1979). Segment centers of mass were computed using the data of De Leva et al. (1996). Kinematic and kinetic data were synchronized and net joint moments at the ankle, knee, hip, and shoulder from the initiation of propulsion until takeoff of the vertical jump were calculated in a manner consistent with descriptions found in Winter (1990).

RESULTS AND DISCUSSION

Exemplar results for the net joint moments at the ankle, knee, hip, shoulder, and support are shown in Figure 1. A positive net joint moment indicates net muscle activity in the direction of extension for the ankle, knee, and hip and flexion at the shoulder. For the higher jump while the time of propulsion was smaller, the magnitude of the force applied was greater. The support moment indicates that the difference in force may be due to a greater application of moments early in the propulsive phase. In general the net joint moments of the knee and hip attain higher amplitude and are sustained longer during the early portion of the higher jump than in the lower jump. Later in propulsion the peak moment associated with the knee was greater in the lower jump than in the higher one. The net joint moment at the ankle was similar for both jumps. Examination of the shoulder moment reveals an extensor moment (negative) during most of the propulsive phase. For this subject the interplay between knee and hip moments appear to play a major role in differences in jumping performance, whereas the contribution of the ankle and shoulder do not.

Results of the net joint moment analysis support Dowling et al's contention that it is not just the magnitude of force generated, but also the pattern of application that is important. [Dowling, 1993 #134].

Before evaluating the effect of various plyometric and strength training programs on vertical jumping an understanding of the range of changes of which a person is capable due to changes in multi-joint control should be considered.

REFERENCES

Bobbert et. al. (1988). *J Biomech* 21: 249-262.

Bobbert, (1990). Sports Medicine 9(1): 7-22.

Dowling, et. al. (1993). *J. Ap. Biomech* 9: 95-110.

Gregoire,. et al. (1984). IJSM 5: 301-305.

Jackson. *IEEE Trans. Bio. Eng.*, 26, 122-124, 1979.

Pandy, et al. (1990). *J Biomech* 23(12): 1185-1198.

Prilutsky et al. (1994) J. Biomech. 27:25-34

Winter. (1990).*Biomechanics and Motor Control of Human Movement, 2nd ed.* (1990).

Winter. (1980). *J. Biomech.* 13:923-927.

ACKNOWLEDGMENTS

The authors wish to acknowledge the work of the members of the USC Biomechanics Laboratory.

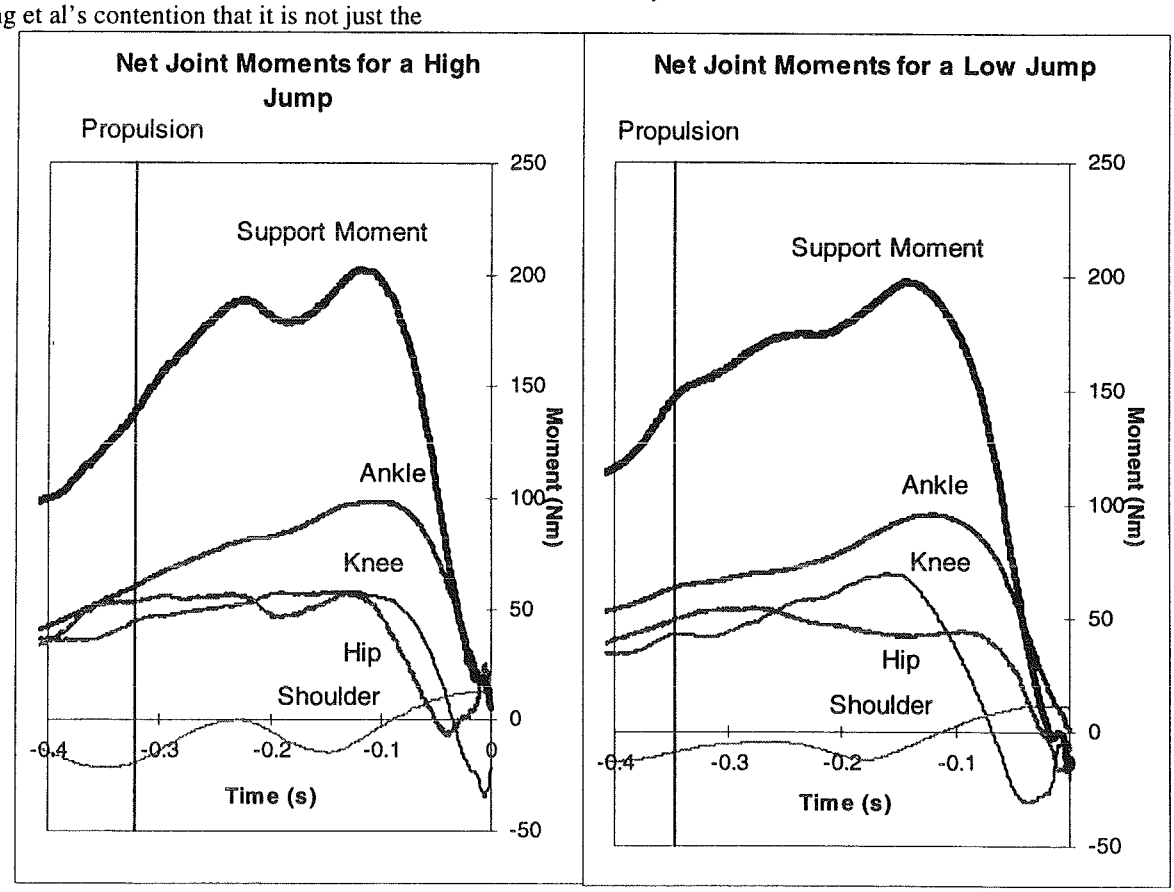

A CONTINUOUS FLEXING LOWER EXTREMITY SPORTS PROSTHESIS

Denis J DiAngelo, Charles E. Evans
School of Biomedical Engineering, University of Tennessee - Memphis

INTRODUCTION

A computer modeling technique was used to design a multi-link above-knee (A/K) prosthesis that provided continuous, controlled knee flexion during weight bearing and free knee rotation during swing. Aspects of the design were improved energy expenditure, symmetrical gait, and reduced impact loading. Biomechanical data for the computation model was obtained from a gait study of an A/K amputee jogger. The design of a Continuous Flexing Knee (CFK) prosthesis is presented. The prototype should enable A/K amputees to participate in sporting activities involving jogging or running.

REVIEW AND THOERY

Typical walking prostheses maintain stability during stance with a knee locking mechanism; i.e., a frictional device (mechanical brake) or free rotating knee joint (single pinned or multi-link system) held in a hyper-extended orientation (de Vries, 1995). Attempts to jog with a walking prosthesis are difficult and unsafe. A previous gait study of a "pogo-stick" A/K jogging prosthesis found that the device provided alternating periods of support and non-support between the amputated and non-amputated sides, but required greater energy expenditure from the intact limb and induced larger impact loads (DiAngelo et al., 1989). The objective of the study was to develop prosthetic knee that provided continuous knee flexion throughout weight bearing and free rotation during swing.

PROCEDURES

The study consisted of two phases: A) an analysis of the jogging mechanics of an A/K amputee wearing a conventional walking prosthesis and B) computer simulation modeling of a multi-link prosthetic knee. The prototype was designed to replicate the jogging mechanics of the non-amputated knee.

A) Gait Study. A gait lab study was performed on an A/K jogger wearing a conventional walking prosthesis. Measurements included rotations, moments, and muscle power at the hip, knee and ankle joints of the amputated and non-amputated sides. Knee angle and moment data of the non-amputated limb were used in the computational model.

B) Computational Design of CFK. The CFK prosthesis is shown in Fig. 1; the device consisted of a six-link knee for swing events that toggled into an eight-link device during weight bearing. A compression spring, located between the drive link (L2) and the fixed link (L1), regulated stance knee flexion.

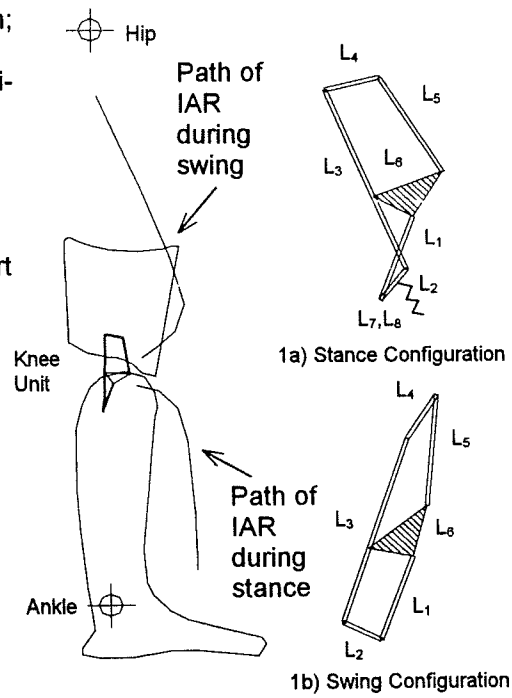

Figure 1: Schematic of Continuous Flexing Knee Prosthesis. The device toggles between an 8-link stance-phase mechanism (Fig. A) and 6-link swing-phase mechanism (Fig. B).

Working Model (Knowledge Revolution Inc.), a dynamic computer simulation program, was used to analyze the linkage kinematics and to determine the mechanical properties of the compression spring. Kennedy's Theorem (Martin, 1982) was used within Working Model to determine the Instant Axis of Rotation (IAR) of the CFK prosthesis (i.e., to characterize motion between the socket, link 4, and the shank/foot member, link 1).

Knee moment (Mk) and knee angle(θk) data from the gait study were input into the model to determine the moment arm lengths (d) between the line of action of the compression spring and the IAR of the CFK (see Fig. 2). Calculations of the spring force (Fs = Mk/d) and spring deflection (Δx) were determined at various increments of stance flexion and used to estimate the spring stiffness (Ks = Fs/Δx).

RESULTS AND DISCUSSION

The knee moment (Mk) and knee angle (θk) curves of the A/K jogger are shown in Figure 3. The prosthesis was locked in a hyper-extended configuration during stance as characterized by no knee flexion and a simulated flexor knee moment. Data of the non-amputated side was used in the computational model.

The IAR path of the CFK prosthesis is shown in Fig. 1A) for the stance operation and Fig. 1B) for the swing operation. The prototype was limited to 35° of stance knee flexion and 100° of swing rotation.

During early swing, the IAR of the CFK was near the residual hip joint, thus reducing the muscle activity required to initiate swing. As knee flexion continued, the IAR moved towards the center of the linkage system.

A typical stiffness (force-deflection) curve for the compression spring is shown in Figure 4. By varying the placement and orientation of the spring, the moment arm values could be adjusted in an attempt to linearize the spring stiffness.

The feature of a flexing knee during weight bearing should enable A/K amputees to participate in sporting activities involving jogging. Key aspects of the prototype were stable, safe knee flexion during weight bearing, improved energy expenditure of the residual hip muscles, and a natural swinging motion.

REFERENCES

deVries J. Conventional 4-bar linkage mechanisms. J Rehab Res and Dev, 32, 1995.

DiAngelo DJ, et al. Performance assessment of the TFJ prosthesis, J Biomech, 22, 1989.

Martin GH. Kinematics and dynamics of machines, 2nd ed., McGraw-Hill, NY, 1982.

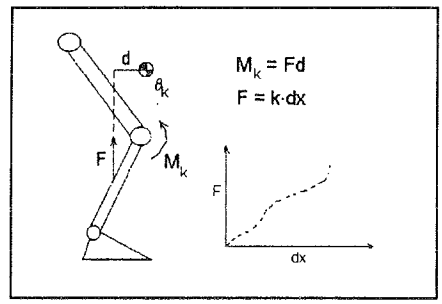

Figure 2: Calculation of spring force.

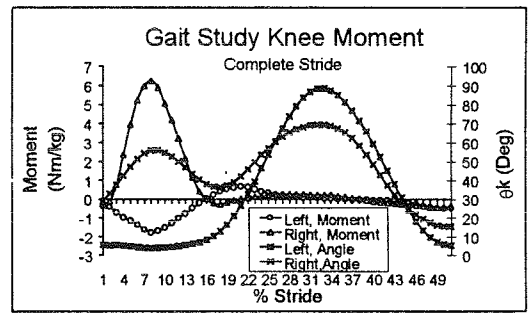

Figure 3: Biomechanical data from gait study.

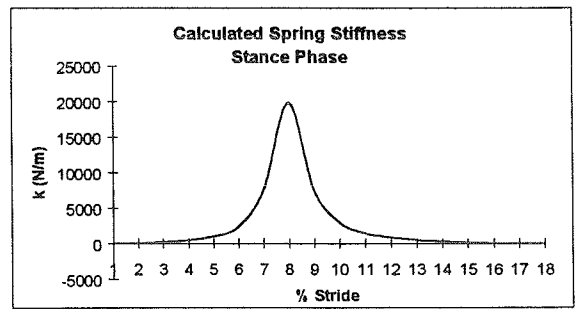

Figure 4: Theoretical spring stiffness.

RACKET ARM MUSCLE ACTIVATION PATTERNS IN HEALTHY AND INJURED TENNIS PLAYERS

J. Bauer

Department of Exercise and Sport Sciences, University of Florida, Gainesville, FL 32611

INTRODUCTION

Lateral Epicondyle Tendonosis, or common tennis elbow, afflicts many tennis players. Work in the past has examined many biomechanical and electrophysiological parameters associated with playing tennis (Bernhang et al. 1974) Some recent work by Kelly et al. (1994) has even evaluated EMG for players suffering from tennis elbow. This study was conducted to determine if the muscle firing patterns of the racket arm extensors, flexors and triceps muscles were similar between matched groups of healthy and tennis elbow suffering players.

REVIEW AND THEORY

Tennis elbow afflicts between 30% and 50% of all tennis players (Priest et al., 1980). The injury is usually the painful result of microtrauma to the Extensor Carpi Radialis Brevis caused by the excessive eccentric loading experienced while hitting backhand shots. The microtrauma eventually presents itself as pain in the lateral aspect of the elbow and persists as long as the person continues to play. With rest the condition usually disappears, however, in extreme cases surgery may be required to relieve the pain. It is our theory that the pain of this injury induces a shift in normal muscle activation patterns which is detrimental to the healing process. The muscles need to rest for healing to occur, while our observations indicate that muscle activation actually increases while playing tennis when suffering from tennis elbow. This change in the activation patterns increases the severity of the injury and prevents healing.

This study was conducted to quantify the amount of racket arm EMG activity by providing a profile of the temporal characteristics of muscle firing with respect to ball/racket impact. The hypothesis tested was that injured players would display longer muscle activation duration for the selected muscle groups for the same impact conditions when compared to their healthy counterparts.

PROCEDURES

Eight male tennis players were selected for this study. Four of the players had been clinically diagnosed as suffering from tennis elbow at the time of their participation in the study. Each of the subjects signed an informed consent form prior to testing. A one-handed backhand block volley was the tennis shot evaluated. Nine impact conditions were randomly presented to the subjects during testing. The impact conditions were selected to simulate the variety of impacts experienced during normal tennis play. The nine conditions consisted of all possible combinations of three racket face impact locations and three impact velocities. The impact locations were: 1. Center (C), the geometric center of the racket face, 2. Long Axis (L), location found at 8 cm from the end of the racket and 3. Torsional, (T), located 7 cm from the top side of the racket when held oriented with the face perpendicular to the floor and the grip parallel to the floor. The three impact velocities were: 1. Slow (S) 12m/s, Medium (M) 17m/s, and High (H) 23m/s. The tennis balls were projected by a ball machine at the stationary hand-held racket at a distance of 2m. EMG surface electrodes were placed over the Extensor (E), Flexor (F) and Triceps (T) of the subject's racket arm. EMG data were collected at 1000Hz. An accelerometer attached to the racket throat provided a signal synchronized with the EMG recordings which was used to determine the instant of impact. All trials were video taped and this information provided a visual method of selecting which impact data would be analyzed. Data were collected in nine 30 second trials during which the subject typically struck eight shots. None of the first two shots per condition were used for analysis purposes. For this study three good impacts for each condition were selected for analysis. A good impact was defined as one which struck the selected racket face location while the racket was oriented properly. Muscles were considered active if the magnitude of EMG reached 20% or greater of that recorded during

maximum voluntary muscular contractions conducted prior to the start of the experimental trials.

Data were analyzed by determining the on/off conditions of the muscles within a 2000ms window bounding impact. This allowed study of which muscles were active during the 1000ms prior to impact and 1000ms following ball/racket impact.

Single factor ANOVA's with $p = 0.05$ were performed to determine significant differences for subject health status (Injured or Healthy) vs. muscle activation times for the all impact conditions.

RESULTS

Analysis of the data indicate that the Extensor muscles were activated significantly earlier ($p < 0.05$) for the Injured subjects than for the Healthy subject group. Additionally, the Extensors were active longer after impact in the Injured group than in the Healthy subjects ($p<0.05$). The other muscle groups tested, Flexors and Triceps, showed no statistically significant differences in activation between the two subject groups either before or after impact ($p >0.05$). Figure 1 illustrates the average time of muscle activation prior to impact for the subjects tested.

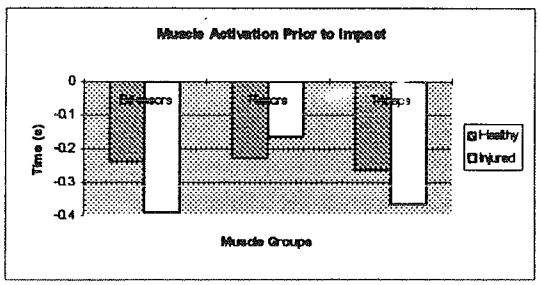

Figure 1: Illustration of muscle activation duration prior to all impact conditions.

The muscle activation patterns following impacts are shown in Figure 2.

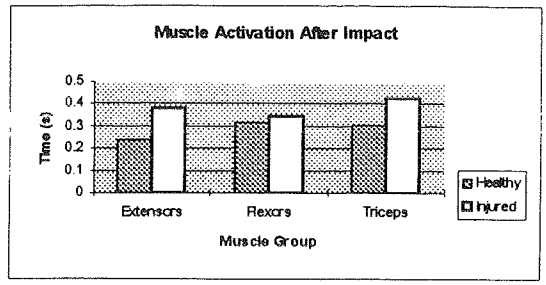

Figure 2 Illustration of muscle activation duration following all impact conditions.

The analysis indicates that the injured and healthy groups do not use identical activation patterns of racket arm musculature with respect to similar ball/racket impacts.

DISCUSSION

While other groups have used EMG to study tennis strokes, none have directly compared the muscle activation sequencing and activation duration of both healthy and injured players under various impact conditions. Results indicate a need to educate players suffering from tennis elbow about the injurious muscle activation strategies which develop once pain is present and the need to develop therapeutic or motor learning strategies which will help the players speed the healing process instead of promoting the duration and severity of the injury.

REFERENCES

Bernhang, H.B. et al., J. Sport Med., 2, 235-260, 1974.
Kelly, J.D. et al., Am. J. Sport Med., 22(3), 359-363, 1994.
Priest, J.D. et al., Phys. Sport Med. 8(4), 80-91, 1980.

ACKNOWLEDGEMENTS

I would like to thank the following people and companies for their support: Robert Murray, the Penn State Biomechanics Laboratory , Paromed Medzintecknik, Germany.

CORRELATIONS BETWEEN STATIC AND DYNAMIC PROPERTIES OF VARIOUS BASEBALLS

S. P. Hendee[1], R. M. Greenwald[1], J. J. Crisco[2]

[1]Orthopedic Biomechanics Institute, Salt Lake City, UT 84107

[2]Department of Orthopaedics, Rhode Island Hospital and Division of Engineering, Brown University, Providence, RI 02903

INTRODUCTION

This study was designed to determine if quasi-static mechanical parameters are useful in predicting dynamic impact variables of baseballs. Such correlations would facilitate testing and analysis of traditional baseballs and baseballs that have been modified for "safer" youth play. Mechanical testing may provide a useful and cost effective alternative to field studies for evaluating the injury-reducing potential of modified baseballs.

REVIEW AND THEORY

A leading cause of injury in youth baseball is impact with the ball. Manufacturers have produced modified baseballs for youth play that are more compliant than traditional balls in an effort to reduce the risk of injury. Determination of the efficacy of these modified baseballs in reducing injury risk requires an understanding of the injury mechanisms and information about the impact properties of the ball. Viano et al. (1993) impacted anthropometric dummies with traditional and "soft" baseballs and found that the modified balls reduced peak impact force and peak head acceleration. Heald and Pass (1994) used cadavers and dummies to determine that ball stiffness was strongly related to head injury risk. In this study, we performed quasi-static compression tests and dynamic impact tests on commercially available traditional and modified baseballs. The hypothesis was that static and dynamic impact properties of baseballs are correlated. Since current injury predictors are based on the acceleration-time profile of the head during impact (a dynamic event), a correlation between static and dynamic parameters would indicate that static parameters (which are relatively simple to measure) might be useful in predicting the injury-reducing potential of modified baseballs.

PROCEDURES

Nineteen commercially available baseball models (11 traditional, 8 modified) were tested. Three balls of each model were used in static tests, and five balls of each model were used in dynamic tests. In the static tests, ball stiffness and percent energy loss were computed from load-displacement curves obtained while compressing each ball by 1 cm between parallel steel plates at a rate of 1 mm/sec and then unloading the ball at the same rate. Stiffness was calculated as the average slope of the load-displacement curve, and percent energy loss was the energy lost during the loading-unloading cycle divided by the loading energy.

Dynamic impact testing was accomplished by firing baseballs from an air cannon (Movan, Inc, Toronto, Ontario) into a load cell mounted on a rigid steel plate. Each ball was tested at five impact velocities ranging from 13 to 40 m/s (30 to 90 mph). Force-time profiles were sampled at 20 kHz. A pair of photodetectors (Oehler Research, Austin, TX) was used to measure inbound and outbound ball velocities. Dynamic variables measured or calculated were peak impact force, impact duration, impulse of impact, and coefficient of restitution (COR, the ratio of rebound velocity to incident velocity). Linear least squares regression was used to evaluate correlations among static and dynamic variables for the various ball models.

RESULTS

Ball stiffness was significantly lower for the modified balls (338.3 ± 348.7 N/cm) than for traditional balls (2430.6 ± 443.1 N/cm). Modified balls showed no correlation between ball mass and ball stiffness, while the stiffness of traditional balls increased linearly with increasing ball mass (r^2=0.775) (Figure 1).

Dynamic impact data indicated that traditional baseballs had higher peak forces and shorter impact durations than did the modified baseballs. Peak impact force increased linearly with increasing ball stiffness for all impact velocities (Figure 2). Impulse of impact was more strongly correlated with ball mass (r^2=0.804) than ball stiffness. The COR of all ball models decreased linearly with increasing impact velocity (Figure 3). COR and ball stiffness were not linearly correlated. Percent energy loss (static) was not useful in predicting dynamic energy loss (COR^2).

DISCUSSION

The results of this study indicate that static mechanical properties are useful in predicting certain impact characteristics of baseballs. In particular, peak force of impact was linearly correlated with ball stiffness, and impulse of impact increased linearly with ball mass. Elastic theory suggests that differences among impact variables will decrease as target stiffness decreases (Crisco et al., 1997), implying that large differences observed among different ball models in this study might diminish for impacts with more compliant target materials (e.g., helmet, muscle or bone). Despite this limitation, correlations between static and dynamic characteristics of baseballs suggest that static testing may provide useful information about the injury-reducing potential of baseballs.

REFERENCES

Viano D.C. et al., Clin J Sports Med 3, 217-228, 1993.

Heald, J.H. and Pass, D.H. Head and Neck Injuries in Sports 223-238, ASTM, 1994.

Crisco, J.J. et al., Med Sci Sport Exer 8, 26-36 1997.

ACKNOWLEDGMENTS

This project was funded by the National Operating Committee on Standards for Athletic Equipment (NOCSAE). The ideas and opinions presented are those of the authors and do not necessarily represent the views of NOCSAE. We thank the manufacturers who donated baseballs for testing.

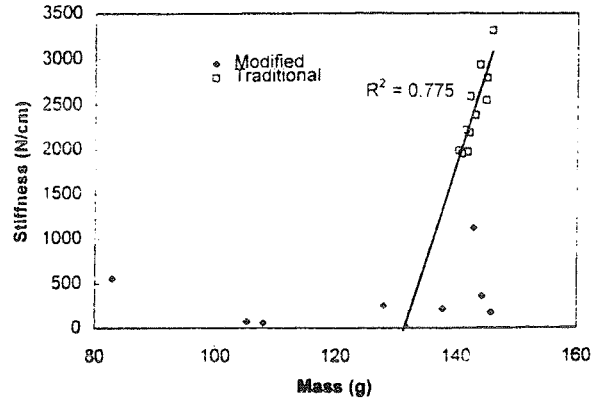

Figure 1: Ball stiffness vs. ball mass for traditional and modified baseballs.

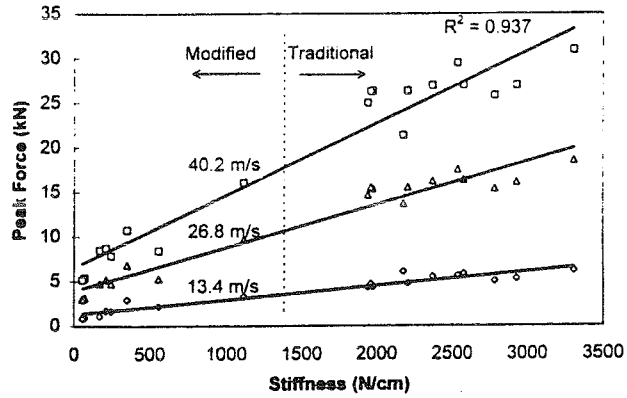

Figure 2: Peak impact force vs. ball stiffness.

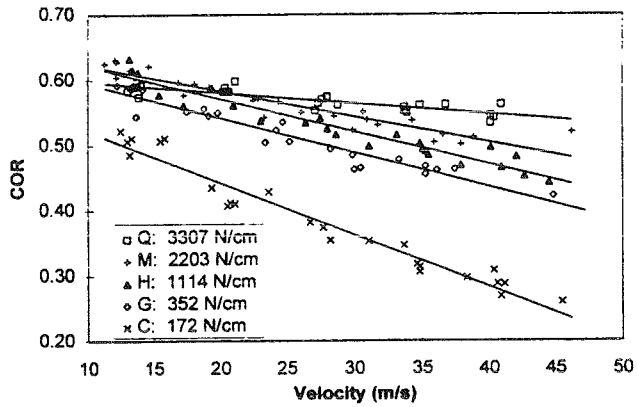

Figure 3: COR vs. impact velocity for five ball models. Q and M are traditional balls; C, G, and H are modified baseballs.

MEDIAL BALL IN SOCKET MENISCAL BEARING TOTAL KNEE ARTHROPLASTY LIMITS PARADOXICAL MOTION WHEN MEASURED USING THE SCREW AXIS

D. Wilson[1], J. D. Blaha[1], C. Mancinelli[1], W. Simons [1 2]

[1] Department of Orthopedics, West Virginia University, Morgantown, WV 26506
[2] Department of Mathematics, West Virginia University, Morgantown, WV 26506

INTRODUCTION

This study examined three dimensional kinematics of cadaver knees implanted with fixed and mobile bearing total knee arthroplasties. The VICON motion analysis system was used in order to collect kinematic data before and after total knee arthroplasty. This information has important implications for total knee arthroplasty design and function.

REVIEW AND THEORY

Knee joint kinematics have been described through the use of the screw axis. [1 2 3 4] Recently, investigators have studied the differences in fixed versus mobile bearing arthroplasties in terms of tibiofemoral translation and rotation. [5 6] Stiehl et al. reported an anterior motion of the femur on the tibia during flexion also known as "paradoxical condylar translation" in meniscal bearing designs using video fluoroscopy. [7 8] However, there have been no reports in the literature describing total knee arthroplasty kinematics in terms of the screw axis. The purpose of this study was to examine the screw axis location in an intact knee compared to the same knee implanted with a fixed bearing design and an intact knee compared to a medial ball in socket mobile meniscal bearing design.

PROCEDURES

Two right-sided knee joint specimens were dissected to leave capsule and musculotendinous attachments. Marker carrying blocks were attached to the cortical bone of the femur and tibia. The knees were then scanned using computerized tomography (CT) in order to define marker and femoral contour geometry. The femur of each knee specimen was secured into a metal testing frame (0.75m x 0.75m x 0.88m) onto which three high speed VICON cameras were attached: one lateral, one anteriosuperior, and one anterioinferior to the specimen. A motor was attached to the quadriceps tendon to generate extension and flexion of the knee joint, and the medial and lateral hamstrings were loaded with symmetric and asymmetric loads during motion. Kinematic data were collected for 2 flexion and 2 extension trials under symmetric hamstring load, lateral hamstring load, and medial hamstring load.

Total knee arthroplasties were then implanted in each specimen using the measured resection technique. The first total knee was a cemented posterior cruciate ligament (PCL) substitute fixed bearing design, and the second a cemented PCL substitute medial ball in socket mobile bearing design. The femurs were then remounted into the testing frame and the collection process repeated for the gathering of kinematic data.

Using programs internal to the VICON system, the three-dimensional positions of each of the markers were calculated. VICON coordinates were transformed to CT coordinates by an orthogonal matrix obtained by nonlinear optimization in order to prevent distortion of CT rigid body shape. A method combining least squares and cubic splines created differentiable paths for each marker which allowed the calculation of velocity vectors. [9] The marker position vectors and velocity vectors in each frame were used to calculate the screw axes throughout the range of knee motion.

An outline of each intact distal femur was constructed by digitizing CT images. Piercing points of the screw axes were plotted across three sagittal femoral contours evenly spaced between the most lateral and most medial femur. A mean reference axis (MRA) was calculated by taking an average of all screw axes for each knee under each loading condition. Differences in the location of the MRA in the intact

case compared to the total knee case were determined for each knee by calculating the distances between the MRAs across all planes. These results were then compared for each knee design. Paired t-tests were used to determine whether there was a significant difference in the MRA locations in the fixed versus mobile bearing knee (two-tailed t-test; $p \leq .05$).

RESULTS

The MRA showed a significantly greater displacement from the intact knee with the fixed bearing design compared to the mobile bearing design on the medial side of the joint under symmetric hamstring loading conditions ($p = .033$). The MRA showed a significantly greater displacement from the intact knee with the mobile bearing knee compared to the fixed design on the lateral side of the joint with medial hamstring loading conditions ($p = .031$). In the first case, the mean MRA displacement in the fixed design at the medial condyle was 2.01 cm, compared to 1.41 cm for the mobile bearing knee. In the second case, the MRA displacement in the mobile bearing design at the lateral condyle was 1.54 cm, compared to 1.08 cm for the fixed bearing knee. No significant differences in mean MRA displacements were found in either knee with lateral hamstring loading.

DISCUSSION

Analysis of the mean reference axis revealed a significant difference in displacement from the intact knee when a fixed knee design is used compared to a mobile meniscal bearing design in response to hamstring loading. With symmetric hamstring loading conditions, there was a greater change in the MRA displacement of the fixed design trials compared to the intact trials on the medial side of the joint. With medial hamstring loading, the greater change in the MRA occurred with the mobile bearing design. Unlike the fixed design, this change occurred on the lateral side of the joint. These findings suggest that a total knee fixed bearing design changes the kinematics of the medial knee under symmetric hamstring loading, whereas the mobile bearing design changes the kinematics of the lateral knee under medial hamstring loading. The mobile bearing knee used in this study was designed in an attempt to mirror "ball in socket" kinematics of the intact medial knee with a single axis of rotation. Thus the lesser displacement of the MRA on the medial side with the mobile bearing knee would be expected as the results of this study have demonstrated. The medial ball in socket mobile bearing design limits the "paradoxical translation" on the medial side of total knee arthroplasties as described by Stiehl, Markovich et al.[7,8]

REFERENCES

(1) Blacharski, P. et al. J. Biomech, 8, 375-384, 1975.
(2) Blankevoort, L. et al. J. Biomech, 21, 705-720, 1968.
(3) Van Dijk, R. et al. J. Biomech, 12, 727-731, 1979
(4) Mancinelli, C. Doctoral Dissertation, WVU, 1994.
(5) Nahass, B. et al. J. Biomech, 24, 1107-1117, 1991.
(6) Nilsson, K. et al. Ortho. Research Soc. 1997.
(7) Stiehl, J. et al. Ortho. Research Soc. 1997.
(8) Markovich, G. et al. Ortho. Research Soc. 1997.
(9) Simons, W. et al. J.Biomech. Eng,113, 348-351, 1991.

AN ANALYTICAL INVESTIGATION OF THE RESIDUAL STRENGTH OF HUMAN CORTICAL BONE AFTER FLEXURAL FATIGUE

L.V. Griffin[1], J.C. Gibeling[1], R.B. Martin[2], V.A. Gibson[2], S.M. Stover[3]
[1]Department of Chemical Engineering and Materials Science, University of California, Davis, CA 95616
[2]Orthopaedic Research Laboratory, University of California, Sacramento, CA 95817
[3]Veteranary Orthopedic Research Laboratory, University of California, Davis, CA 95616

INTRODUCTION

An analytical flexural fatigue model for cortical bone was developed for three and four point bending of cortical bone beams. This model also has the capability of calculating the monotonic bone strength in flexure as a function of the number of loading cycles. The model predicts that fatigue loading of cortical bone does not greatly affect the bone strength through much of the fatigue life, even though the damage does affect stiffness. Furthermore, the model predictions indicate that osteons contribute to cortical bone damage tolerance.

REVIEW AND THEORY

Fatigue in bone is manifest as a stiffness and strength loss that may ultimately produce stress fractures, particularly in athletes, military recruits, or elderly persons suffering from osteoporosis. Recent investigations have demonstrated that fatigue loading of bone produces observable damage to the microstructure, such as microcracks, which is hypothesized to be a dominate failure mechanism (Shaffler, *et al.*, 1989, Zioupos *et al.* 1996, Carter & Hayes, 1977).

Martin, *et al.* (1997) recently found that *ex vivo* three-point bending fatigue loading of equine cortical bone produces no significant loss in strength. Recently, a flexural model has been developed which incorporates a damage-dependent elastic model of cortical bone behavior. This model partitions damage into entities which affect the osteons and the matrix of cortical bone. The model predictions of stiffness loss and failure show excellent agreement with four-point bending data of human femoral bone obtained in our labs (Griffin, *et al.*, 1996). The flexural model is also able to predict the functional dependence of strength on the number of cycles. Therefore, the flexural model was used to study the relationship between stiffness, strength and damage. Our hypotheses for this study were 1) that matrix damage does not greatly affect the strength of human cortical bone, although the stiffness is decreased, and 2) that the osteon is the primary strengthening constituent at the microstructural level.

PROCEDURES

A laminated beam theory is used to implement the damage dependent material model of fatigue (Griffin, *et al.*, 1996). Damage in bending is assumed to result from tensile and compressive loads. The material model uses the experimental data of Pattin *et al.* (1996) as the basis of the uniaxial tensile and compressive fatigue behavior for human femoral bone.

In the present investigation, flexural strength is defined as the maximum flexural stress in a monotonic load ramp to failure as calculated using Mc/I, where M is the peak moment, c is the distance from the beam centerline to the outer surface, and I is the cross-sectional moment of inertia. Damage is defined using a modulus-based formulation: $D = 1-E/E_o$. To determine the residual strength dependence on damage, the model is loaded cyclically and the strength is calculated at regular intervals until failure occurs.

Three and four-point bending configurations were examined in load control from 5000 microstrain ($\mu\varepsilon$) to 7500 $\mu\varepsilon$.

RESULTS AND DISCUSSION

For four-point bending fatigue, the model predicts no apparent loss of flexural strength early in the fatigue life, even though there is a noticeable loss in stiffness (Figure 1). The initial stiffness loss has been experimentally verified (Griffin, *et al.*, 1996). As damage accumulates, the strength gradually decreases until a rapid loss of strength occurs near failure (Figure 1).

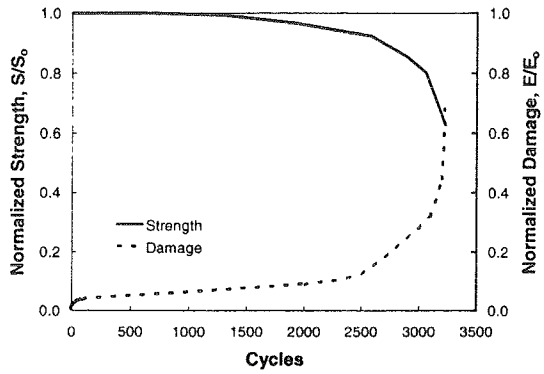

Figure 1: A comparison of strength and damage predictions for four-point flexural fatigue of human femoral bone at 6500 με which exhibits typical strength and damage characteristics.

The trends exhibited in Figure 1 were consistent for all of the bending configurations and loading modes at all levels tested. In three-point bending, the stiffness reduction is less than that of four-point bending for the same flexural load.

The model predicts a rapid initial drop in stiffness, which is associated with matrix damage; however, the strength is not affected. This suggests that that matrix damage does not significantly affect the flexural strength of cortical bone. This also reveals that cortical bone can tolerate a modest amount of damage with little effect on strength and allow remodeling to occur with only a slight decrease in fracture strength.

Martin *et al.* found that the monotonic flexural strength of equine cortical bone is not affected by 100000 loading cycles at 5000 με. For equine bone, this may be only about 25 percent of the fatigue life. For human cortical bone, the model predicts that flexural strength is not reduced any detectable amount until about 50 percent of the fatigue life (Figure 1). These predictions are therefore consistent with the observations of Martin, *et al.* (1997) for equine cortical bone. However, Martin, *et al.* reported that there was no significant loss in stiffness for equine cortical bone. The model predictions for a stiffness loss are most likely related to the fact that human cortical bone is not exactly like that of the equine metacarpus.

For bovine cortical bone in a rotating bending fatigue configuration, Carter and Hayes noted that there was a noticable loss is stiffness early in the fatigue life, but that the strength loss was only about 8 percent (1977). These data show good agreement with the model predictions (Figure 1).

The model predicts that the largest drop in strength is associated with osteon failure, supporting the hypothesis that the osteon is a strengthening component of the microstructure.

The model predicts that human cortical bone is quite resistant to fatigue damage and that a modest amount of microdamage can be tolerated without significantly affecting the strength of the bone. While the microdamage may not produce a substantial strength loss *ex vivo*, the fact remains that fatigue injuries can occur very rapidly under certain conditions. Ths suggests that physiologic processes initiated to accommodate this damage may provide a positive feedback and ultimately result in fatigue related injuries.

REFERENCES

Carter & Hayes, *J Biomech*, 10:325-337, 1977
Griffin *et al.*, *J Orthop Res,* Submitted, 1996
Martin *et al.*, *J Biomech,* 30:109-114, 1997
Pattin *et al. J Biomech* 29:63-68, 1996
Schaffler *et al.*, *Bone*, 19:207-214, 1989
Zioupos *et al.*, *J Biomech*, 29:989-1002, 1996

ACKNOWLEGEMENTS

This work was supported by NIH Grant AR41644, California Center for Equine Heath and Performance; UC Davis; Mr. and Mrs. Amory J. Cooke; and the Hearst Foundation.

Lanny V. Griffin, Ph.D.
Department of Mechanical Engineering
University of California
Riverside, CA 92521
909-787-2299 (TEL)
909-787-3188 (FAX)
lgriffin@engr.ucr.edu (E-mail)

HELICAL AXIS PATTERNS FOR INTACT AND DESTABILIZED CERVICAL SPINE SEGMENTS

J.D. Peles[1], N.R. Crawford[1,2], V.K.H. Sonntag[2], C.A. Dickman[2], G.T. Yamaguchi[1]

[1]Department of Chemical, Bio & Materials Engineering, Arizona State University, Tempe, AZ
[2]Barrow Neurological Institute, Spinal Biomechanics Research Laboratory, Phoenix, AZ

INTRODUCTION

Knowledge of uninjured spinal motion quality and variations in motion quality due to injury is an important tool for assessing spinal stability and treatment protocols. Motion quality can be defined as the path the superior vertebra of a functional spinal unit (FSU) transverses through its range of motion. Alterations in the motion quality due to injury can result in stress distribution variations within the spinal passive constraints and/or encroachment of the spinal cord or nerve roots. This research measured the motion quality of an intact cadaver C5-C6 FSU population during flexion, extension, axial rotation and lateral bending moment applications. The motion quality was depicted using finite helical axis (FHA) patterns over 0.5° increments. After collection of the intact motion quality data, the ligaments of the FSUs were dissected in various sequences and the FHAs were again collected. A statistical analysis was performed to determine the effect of FSU destabilization on the motion quality.

REVIEW AND THEORY

The FHA is defined as the directed line in space that a rigid body rotates about and possibly translates along given a finite angular displacement with the instantaneous axis being the case of vanishing displacement. With reference to FSU testing, the FHA is determined for the superior vertebra relative to the fixed inferior vertebra. During vertebral loading, different passive constraints provide resistance as the motion proceeds through its range which results in FHA variations. Thus, a sequence or pattern of FHAs can be used to characterize motion quality. It has been postulated that in an unstable FSU, the FHA will shift to the area of functional tissues (Goodwin *et al.*, 1994). Van Mameren *et al.* (1992) described how caudal/cranial shifts in the FHA provide information regarding vertebral translation versus rotation. Furthermore, the FHA direction presents the amount of rotational coupling that occurs during the movement.

Previous cervical FHA research has typically provided planar data for large angular steps. Analysis of planar FHA data precludes the rotational coupling effects while FHAs calculated over large angles reduces the resolution of the motion quality measure. The purpose of this research was to characterize three-dimensional cervical FHA patterns during small, 0.5°, angular steps and to assess FHA pattern variation caused by ligament dissection. The hypothesis is that an intact cervical FSU population possesses a consistent FHA pattern for a certain loading condition and that this FHA pattern will change upon destabilization of the spine.

PROCEDURES

Six C5-C6 cadaver FSU specimens were obtained for use in this study. Three of the specimens were male and three female. The specimen ages ranged from 41 to 77 years with the average age being 63 years. The specimens were cleaned of muscular tissue to yield an intact FSU defined as the C5-C6 vertebrae, intervertebral disc and the connecting ligaments. The FSUs were potted and three infrared emitting diodes were affixed non-collinearly to each vertebra. Non-constrained flexion, extension, axial rotation and lateral bending moments were applied to the superior vertebra using the technique of Dickman *et al.* (1993). During the motion, the three-dimensional coordinates of the diodes were measured using an Optotrak 3020 motion analysis system (Northern Digital, Waterloo, Canada). The FHA parameters, including the unit direction vector and the point where the FHA crosses a plane defined by the vertebral geometry (e.g., mid-sagittal plane for flexion/extension), were calculated through the technique of Woltring *et al.* (1985). FHA data were collected for the intact FSU and after dissection of each of the following ligaments: i) anterior longitudinal, ii) right capsular, iii) left capsular, and iv) interspinous and ligamentum flavum. The ligament dissection sequence was varied between specimens so that two FSUs underwent the same dissection protocol. The FHA data were normalized to an average FSU size and the averages and standard deviations of the data were calculated to determine

subject-to-subject consistency. Variations in FHA patterns upon dissection of a particular ligament were then documented. A paired Student's t-test was then performed to determine any significant FHA variations between the intact and destabilized FSUs.

RESULTS

The intact data exhibited relatively consistent patterns and/or locations among the specimens. General trends included the flexion/extension FHAs being clustered in the posterior half of the C6 vertebra with no discernible pattern. During axial rotation, the FHA originated in the anterior portion of the vertebral bodies. The FHAs were angled in the sagittal plane reflecting the coupling with lateral bending. In specimens with large ranges of motion, the FHAs migrated posteriorly during the movement (see Figure 1). The lateral bending FHAs started in the C5 body and were angled in the sagittal plane due to the axial rotation coupling. During the motion, the FHAs migrated caudally approaching the C6 body.

The ligament dissections resulted in variations in FHA directions, locations and patterns. The most striking variation was seen during extension motion after anterior longitudinal ligament dissection. Figure 2 shows a transverse (xz) view (cranial to caudal) of the FHA locations during extension for a typical intact FSU (solid lines). The dotted lines on Figure 2 illustrate the FHA cluster location after anterior longitudinal ligament dissection. Posterior translation and/or increased angulation of the extension FHAs was the typical response to destabilization.

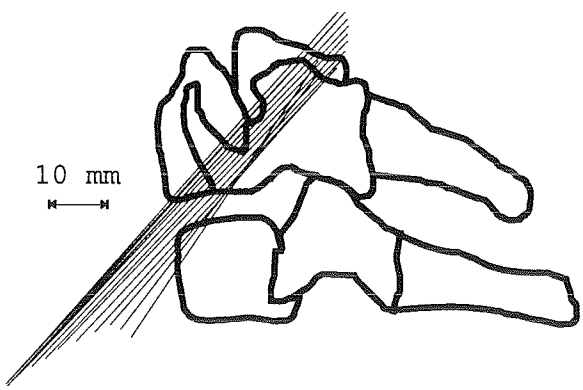

Figure 1: FHA pattern (sagittal plane view) during axial rotation for a typical specimen.

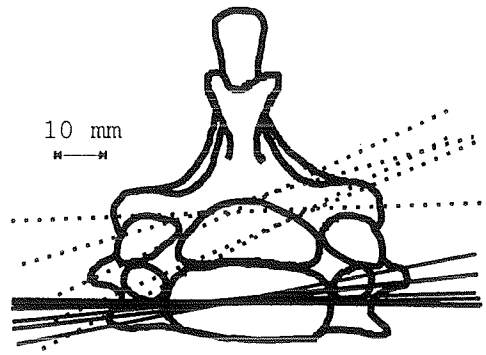

Figure 2: Extension FHAs for a typical specimen.

DISCUSSION

This research has found a C5-C6 cadaver population to exhibit consistent FHA patterns during various motions. Furthermore, variations in FHA patterns were documented after ligament dissection. The FHA results are in relatively good agreement with the limited previous work in this area. Van Mameren *et al.* (1992) located the flexion/extension FHA in the cranial end-plate of the inferior vertebra. Furthermore, Dvorak *et al.* (1993) found FHA variations (measured via radiographs) between normal and neck injured living subjects. The variations in FHA patterns upon ligament dissection documented by this research illustrates the potential for FHA analysis as a measure of spinal stability.

REFERENECES

Dickman C.A. et al. BNI Quarterly. *In vitro* cervical spine testing, 9, 17-26, 1993.

Dvorak J. et al. Spine. Clinical validation of functional flexion/extension radiographs of the cervical spine, 18, 120-127, 1993.

Goodwin R.R. et al. J. Biomechanics. Distraction and compression loads enhance spinal torsional stiffness, 27, 1049-1057, 1994.

Van Mameren H.V. et al. Spine. Cervical spine motion in the sagittal plane II, Position of segmental averaged instantaneous axis of rotation - a cineradigraphic study, 17, 467-474, 1992.

Woltring H.J. et al. J. Biomechanics. Finite centroid and helical axis estimation from noisy landmark measurement in the study of human joint kinematics, 18, 379-389, 1985.

ACKNOWLEDGEMENTS

This research was funded by the NSF (#BCS-9257395-01) and the Barrow Neurological Institute.

Finite Element Analysis of the Effects of Localized Regions of Roughness on UHMWPE Wear in THA

J. Nieman, T. Brown and J. Callaghan

Departments of Orthopaedic Surgery and Biomedical Engineering
The University of Iowa, Iowa City, IA 52242

INTRODUCTION

Radiographic and post-retrieval observations of the wear of ultrahigh molecular weight polyethylene (UHMWPE) in total hip arthroplasty (THA) show high directional variability (Shaver et al., 1997; Sychterz et al., 1996), despite the general similarity of relevant kinetic parameters such as gait pattern and prosthesis orientation. The objective of this study was to investigate whether or not localized regions of femoral head roughening could plausibly alter the global pattern of UHMWPE wear in a manner consistent with the large directional variability observed clinically.

PROCEDURES

A previous developed sliding-distance-coupled finite element computational wear formulation (Maxian et al., 1996) was modified to incorporate regions of localized femoral head roughening. This model implements a relationship of the form:

$$w(\phi,\theta) = \int k\sigma(\phi,\theta,t)v(\phi,\theta,t)dt,$$

where w is the local per-gait-cycle wear depth, σ is the contact stress, v is the sliding velocity, ϕ and θ are local (spherical) coordinates, t is time, and the integration limits are from heel strike to toe off. Simulation of local roughening was achieved by designating specific femoral head surface facets to have elevated wear coefficients (Figure 1). Unlike previous applications of the sliding-distance-coupled model having spatially uniform wear coefficients, this necessitated the usage of on-the-fly computational look-up tables to assign the appropriate (instantaneous) wear coefficient to acetabular surface nodes, based upon the state of roughening of the instantaneously opposing femoral head facet.

Seven cases were evaluated using this simulation: a femoral head with a "normal" spatially uniform wear coefficient (k= 1.0656×10^{-6} mm^3/Nm), three otherwise similar femoral heads with "roughened" regions (k=1.0656×10^{-5} mm^3/Nm) whose ranges of acetabular contact remained localized within the normal wear tract (Regions 1,3,5 Figure 1.), and three femoral heads with similarly "roughened" regions whose ranges of contact remained largely located outside of the typical wear tract (Region 2,4,6). A 10-fold increase of the wear coefficient in the "roughened" regions was inferred from the data of Dowson et al., 1987.

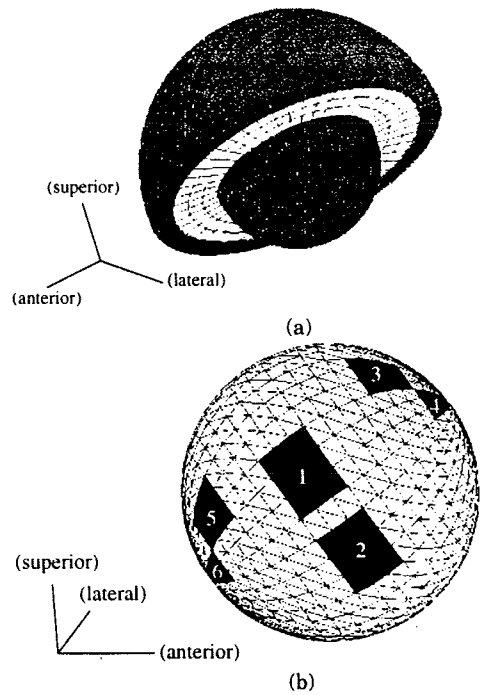

Figure 1: (a) Finite element mesh of a cobalt-chrome alloy (E=210GPa) backed polyethylene (E=1400 MPa) lined acetabular component and 28 mm prosthetic femoral head (1800 continuum elements, 439 contact nodes, 3864 DOF). The entire femoral component is a rigid (Bezier) surface, and the metal backing is rigidly fixed. (b) Localized regions of roughness assumed for the prosthetic head.

RESULTS AND DISCUSSION

Volumetric and linear wear rates for the seven cases, over a three-year period (Table 1), showed that small localized regions of roughness resulted in appreciably increases in volumetric and linear wear rates.

Case	Volumetric Wear (mm^3/yr)	Linear Wear (mm/yr)
Normal	21.39	0.123
Region 1	23.83	0.140
Region 2	25.27	0.196
Region 3	24.88	0.170
Region 4	25.37	0.172
Region 5	24.67	0.164
Region 6	27.56	0.200

Table 1: Calculated volumetric and linear wear rates.

Contour plots of wear depth (Figure 2 a,b) show that the local roughenings produced only modest perturbations of the morphology of the "normal" wear tract.

Ellipsoids fitted to each wear cavity (Table 2) showed that the general morphology of the wear front was relatively insensitive to local roughening. However, the direction of wear, as indexed by the orientation of the major axis of the fitted ellipse, changed much more appreciably than did the shape of the wear cavity (Figure 2c)

Case	Ellipsoid Axes (mm)		
	Minor 1	Minor 2	Major
Normal	28.14	28.23	28.87
Region 1	28.14	28.22	28.90
Region 2	28.13	28.21	28.92
Region 3	28.13	28.21	28.91
Region 4	28.13	28.21	28.90
Region 5	28.13	28.21	28.90
Region 6	28.12	28.21	28.92

Table 2: Axes of best-fit ellipsoids

The present results strongly suggest that femoral head roughening (presumably due to third-body debris) may be responsible for some of the variability of individual patient experience of UHMWPE wear. The specific local roughenings considered in this study (location and severity) were chosen somewhat arbitrarily, and by no means reflect the full spectrum of stochastic variability likely to be present in actual clinical series. This suggests that the present perturbations of the "normal" wear process are likely conservative.

CONCLUSIONS

Simulation of regions of local femoral head roughening in a sliding-distance-coupled finite element model of THA wear document a plausible role of third-body debris damage in the variability of wear rates and wear directions observed clinically.

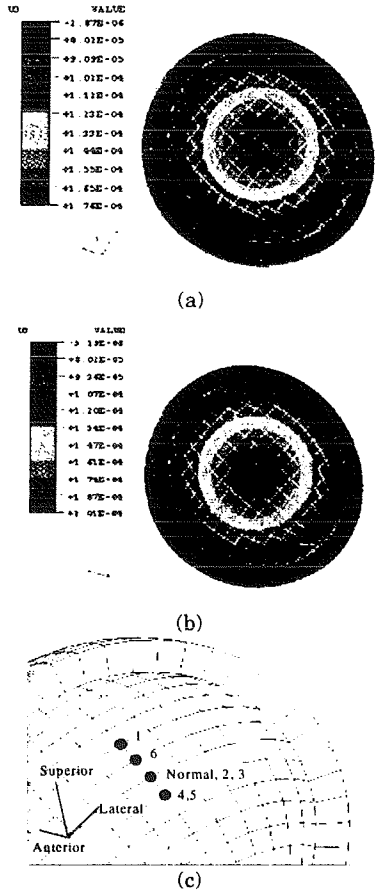

Figure 2: (a) Normal wear contour. (b) Region 2 perturbed wear contour. (c) Wear directions for the seven cases studied.

REFERENCES

Shaver et al. *JBJS*, in press, March,1997.
Sychterz et al. *42nd ORS*, 474, 1996.
Maxian et al. *Clin Orthop*, **333**, 41-50, 1996.
Dowson et al. *Wear*, **119**, 277-293, 1987.

ACKNOWLEDGEMENTS

The authors appreciate the valuable technical assistance provided by D.R. Pederson, T.A. Maxian and J.B. Winston. Financial assistance was provided by grants from the NIH (AR-43314) and DePuy, Inc.

A Cell Strain System for Small Homogeneous Strain Applications

M. Bottlang*, M. Simnacher+, H. Schmitt+, R. Brand*, and L. Claes+

Department of Orthopaedic Surgery*, The University of Iowa, Iowa City, IA 52240
Institute for Trauma Surgery Research and Biomechanics, University of Ulm, Germany

INTRODUCTION

We developed and tested a cell culture system allowing uniform strains in the range of 0.0% to 0.3%, and 0.1-30 Hz, ranges physiologic for bone as a tissue. Optically clear culture dishes allow confocal imaging and quantification of biological markers.

REVIEW AND THEORY

The mechanisms by which connective tissues adapt to their load history cannot be readily ascertained *in vivo* owing in part to a lack of appropriate assays. Molecular mechanisms of adaptation can be more readily ascertained *in vitro* using cell cultures, presuming the mechanisms *in vivo* are the same as those *in vitro*. With this presumption, one requires cell culture systems providing uniform, carefully controlled deformations simulating those occurring *in vivo*. Bone as a tissue experiences strains in the range of 0.01% to 0.3%, and from about 0.5-25 Hz (Rubin and Lanyon, 1984; McLeod et al., 1990). To explore mechanisms one would further need a system allowing quantification of various biological response markers, including those arising from contemporary confocal imaging techniques.

PROCEDURES

We designed and manufactured optically clear silicon culture dishes which sit atop Plexiglas® base plates (Fig. 1). The base plates are deformed by four-point bending in user-specified strain cycle patterns using computer controlled (LabView®, National Instruments, Austin, TX) electromagnetic linear actuators deforming the ends of the base plates (**F**, Fig. 2). Cyclic culture dish surface deformation can be induced in amplitudes of 0 to 0.3%, in frequencies of 0.1 to 30 Hz, and in any specified cyclic pattern. The cell culture system, which contains six simultaneously driven base plate and culture wells, was mechanically characterized by laser displacement sensor recordings of the dish surfaces (A_c), strain gauge monitoring of the base plates (ε_b), laser holographic interferometry of the culture dish surfaces (A_c), and axisymmetric finite element modeling (ABAQUS) of the dishes on the base plates.

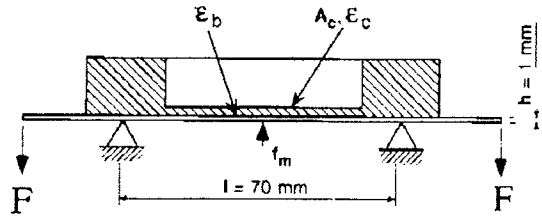

Figure 1: Four-point bending of culture dish

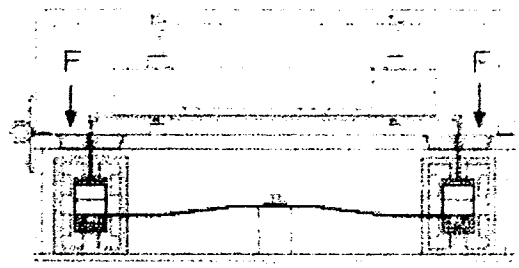

Figure 2: Cross-section of cell strain unit

RESULTS

With the laser displacement sensor, the single station reproducibility test showed standard deviations of vertical displacements of 1.73%, 1.49% and 1.61% for selected dish surface strain amplitudes of 0.03%, 0.05%, and 0.15% respectively. The station-to-station test revealed a vertical displacement standard deviation of 4.84% (corresponding to 0.007% surface strain) for a dish surface strain amplitude of 0.1% strain. The dish surface vertical deformations closely replicated the patterns of input signals (Fig. 3). At higher frequencies (up to 30 Hz), we observed modestly reduced signal magnitudes and a modest but consistent phase shift between

input signal and dish surface deformation; we accounted for these changes through calibration curves input into the computer program.

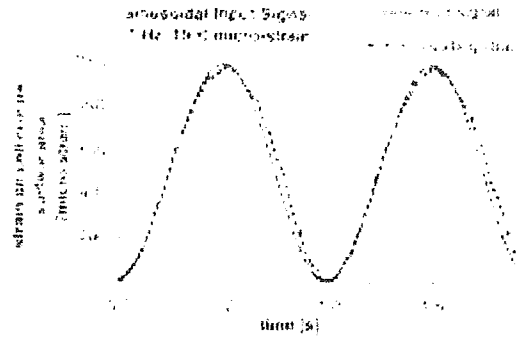

Figure 3: Input signal and generated strain

Laser holography confirmed uniform culture dish surface strains (Fig. 4).

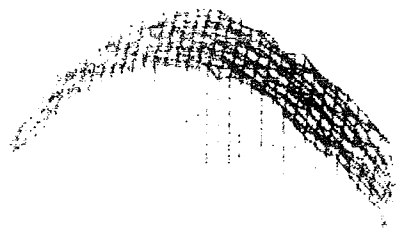

Figure 4: 3-D deformation of surface A_c (exaggerated for illustrative purposes)

The FEM (Fig. 5) demonstrated uniform strains, and provided the required base plate deformation (**F**, Fig. 1) for a desired dish surface strain.

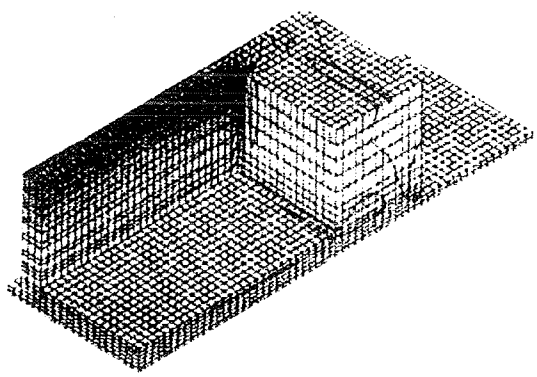

Figure 5: ¼ view of axisymmetric finite element model of culture dish

DISCUSSION

This cell culture system allows accurate generation of small magnitudes of well-characterized, homogeneous strain patterns. LabView allows flexible choice of cyclic strain patterns or duty cycles. The culture wells are easy to handle in a sterile fashion and afford light and fluorescent confocal microscopic observation of the cell cultures and markers.

REFERENCES

Rubin C.T. and Lanyon L.E. J Theor Biol 107:321, 1984.

McLeod K.J., et al. Trans Orthop Res Soc 15:103, 1990.

ACKNOWLEDGEMENTS

Study supported in part from the Deutsche-forschungsgemeinschaft (Claes) and the Deutsche Akademisher austauschdienst (Brand)

DISPLACEMENT RESPONSE OF JUVENILE ARTHRITIC WRISTS DURING GRASP

M.K. Nieuwenhuis[1], J. van der Net[2], W. Kuis[3], P.P.G. Kramer[4], T.S. Buchanan[1], P.J.M. Helders[2]

[1]Department of Mechanical Engineering, University of Delaware, Newark, 19716

[2]Department of Pediatric Physiotherapy, [3]Department of Pediatric Rheumatology and [4]Department of Pediatric Radiology, University Hospital for Children and Youth, Utrecht, The Netherlands

INTRODUCTION

Loss of ligamentous constraint is understood to be the *sine qua non* for the occurrence of malalignment of the wrist. Consequently, in theory, the displacement response of the wrist to increased compressive force could be indicative for the state of the ligaments. More importantly, this would provide a means to aid early diagnosis and intervention. To find out the practicality of this line of reasoning, this study analyzed the displacement response of juvenile arthritic wrists during grasp.

REVIEW AND THEORY

In children with juvenile chronic arthritis (JCA), the wrist joint is affected in approximately 60% of cases (Findley et al., 1983). As a result of chronic inflammation of this joint, displacement of the carpus, i.e. malalignment, occurs. In adult rheumatoid arthritis (RA), the development of ulnar carpal displacement is understood as the result of loss of radiocarpal ligamentous constraint in combination with the compressive forces of the forearm muscles acting across the wrist, and the inclination angle of the distal radial articular surface (Linscheid, 1986). Consequently, given loss of ligamentous constraint, increasing the compressive force (i.e. the tangential force vector) could provoke ulnar displacement of the carpus.

A way to increase the compressive force *in vivo* is by grasping. Schuind et al. (1992) described the changes in wrist and forearm configuration during grasp in a study involving 15 healthy adults. During grasp they found proximal migration of the radius, buckling of the carpal bones with capitate angulation and decrease in carpal height. Most interestingly, ulnar translation of the carpus was also found.

If JCA wrists act in accordance with the pathokinesiological concept for adult RA wrists, ulnar displacement should be found during grasp, and the loss of ligamentous constraints would result in a more pronounced displacement of the carpus. However, wrist involvement *per se* does not necessarily lead to the same extent of loss of ligamentous constraint (Viegas et al., 1995; Melvin, 1989). Consequently, it would be interesting to know if all JCA wrists displace to the same extent during grasp. If not, the effect of increased loading on the carpus could be indicative for the state of the ligaments, and thus aid early diagnosis and intervention.

PROCEDURE

Of 30 consecutive children with a clinical diagnosis of JCA according to EULAR criteria, x-rays of the wrist were made on clinical indication only. Visual comparisons were made regarding similarity in wrist position (deviation) of the two x-rays per child. From this it was determined that 12 wrists of 11 children were suitable for assessment (mean age: 10.4 years, sd 3.3, range 4.5-16.9; mean age at onset 5.8 years, sd 3.7; range 1.5-12.8: mean age at onset of wrist involvement 7.0 years, sd 3.2, range 2.0-12.8).

For each child, a set of two PA x-rays was made, including the metacarpals, the wrist and ± 7 cm of the distal radius, using a standardized technique. The first x-ray was taken with the wrist resting in neutral position, the second with the child grasping the rolled armcuff of a sphygmomanometer with maximum strength. A rigid dorsal splint was used to ensure that the wrist did not extend during grasp.

On the digitized x-rays osseous landmarks were identified, angles measured and lengths calculated from x- and y-coordinates. The displacement response of the carpus was obtained as the uncovered portion of the lunate (UPL) and the carpal-ulnar distance (CUD) (Youm et al. 1978). Because the position of the lunate changes with deviation, the wrist position on both x-rays was verified to be equal regarding the third metacarpal-ulna angle. Ratios were calculated for the CUD to the intermetacarpal width. Buckling of the capitate was assessed by visual observation. If the shape of the capitate had changed during grasp,

CUD was not measured. Carpal narrowing (CN) and ulnar variance (UV) were assessed to analyze if grasping had produced the expected effects of loss of carpal height (Schuind et al., 1992) and proximal migration of the radius (Schuind et al., 1992; Linscheid, 1992), respectively. The standard t-test and analysis of variance techniques were used to analyze the results. The level of significance was at $p < 0.05$.

RESULTS

Because of probable extension during grasp, despite the splint, two wrists were further excluded from the results. Change in shape of the capitate was observed in seven of the remaining ten wrists. Therefore, CUD measurements were not included in the results. The change in the third metacarpal-ulna angle ranged from 8.9° radial deviation to 4.0° ulnar deviation and was not statistically significant ($p = 0.4$). The shape of the lunate did not change during grasp, as shown by a statistical insignificant difference ($p = 0.5$) between lunate width in resting position and during grasp. During grasp a statistically significant increase in UPL ($p = 0.004$), as well as in CN ($p = 0.05$) was found, and a decrease in UV ($p = 0.05$). The mean change in UPL was an increase of 10.0% (sd: 8.4%; range: -1.2%-22.5%). The displacement responses of individual wrists are shown in figure 1, including change in CN and UV. In two cases a slight radial displacement of the lunate was found. In the other eight, ulnar lunate displacement was found, ranging from 3.1% to 22.5%.

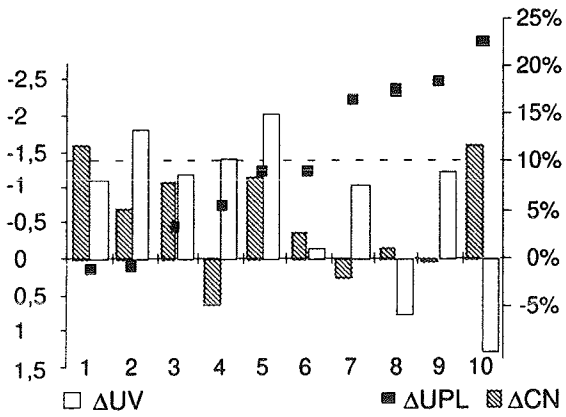

Figure 1: Change in uncovered portion of the lunate (ΔUPL), carpal narrowing (ΔCN), and ulnar variance (ΔUV), in mm, from resting position to grasp in 10 juvenile arthritic wrists.

DISCUSSION

It is the general understanding that the pattern of wrist malalignment in JCA is different from RA. How and to what extent the underlying pathokinesiology of these patterns is different and/or similar, is still unclear. In this study, ulnar displacement of the lunate, loss of carpal height (increase in UPL and CN, respectively) and proximal migration of the radius (decrease in UV) were found during grasp. These changes are similar to those found in healthy wrists (Schuind et al., 1992). Furthermore, they suggest that on the whole the juvenile arthritic wrists act in accordance with the explanation for the development of malalignment of the wrist in adult RA wrists. However, not all wrists responded the same. Radial displacement of the lunate and varying amounts of ulnar displacement were found. The amount of ulnar displacement varied substantially (3.1% to 22.5%).

The development and course of malalignment is a complex interaction of, changes in, bone geometry and configuration, ligamentous constraint and muscle performance. In view of treatment it is imperative to understand why the carpus may respond differently in terms of displacement mode and direction. This means analyzing the different factors and their influence and interaction. Analyzing the displacement response during grasp in juvenile arthritic wrists has proved not to be easy. However, further research along this line is warranted, using biomechanical modeling along with in vivo studies.

REFERENCES

Findley T.W. et al. Arch Phys Med Rehabil, 64, 69-74, 1983.

Linscheid R.L. Clin Orthop, 202, 27-38, 1986.

Linscheid R.L. Clin Orthop, 275, 46-55, 1992.

Melvin J.L. Rheumatic disease in the adult and child: occupational therapy and rehabilitation, 135-87, FA Davis Company, 1989.

Schuind F.A. et al. J Hand Surg, 17A, 698-703, 1992.

Viegas S.F. et al. J Hand Surg, 20A, 312-8, 1995.

Youm Y. et al. J Bone Joint Surg, 60A, 423-31, 1978.

ACKNOWLEDGEMENTS

This work is supported, in part, by the Royal Dutch Association of Physiotherapy and the University Hospital Utrecht.

CONSTRAINED TESTING CONDITIONS AFFECT THE AXIAL ROTATION RESPONSE OF LUMBAR FSU's

S. Grassmann[1], U. Gerich[2], T. Oxland[3]

[1] Department of Civil Engineering, Division of Biomechanics, University of Calgary, Calgary, Canada
[2] Department of Orthopedic Surgery, Inselspital, University of Bern, Bern, Switzerland
[3] M.E. Müller Institute for Biomechanics, University of Bern, Bern, Switzerland

INTRODUCTION

Rotational testing of the spine has been performed *in vitro*, by some groups under constrained conditions, by others under unconstrained test conditions (Goel 1995). Rotational testing under constrained conditions fixes the spine so that a vertebra or vertebrae are only allowed to rotate about a fixed axis. Physiologically, the spine rotates about a helical axis whose position changes with the loading applied. Groups using a fixed axis of rotation claim that using a fixed axis of rotation does not significantly affect the rotational results obtained. This study examines this claim by axially rotating a series of spine segments.

METHODS

A total of ten human cadaveric lumbar spinal units (FSU's) with five L3/L4 FSUs and five L5/S1 FSUs were axially rotated about a fixed axis under the constrained conditions of the MTS (Mini-Bionix, MTS, Minneapolis, MN). Each spine segment was axially rotated at five fixed axis locations: (a) center of the vertebral body, (b) 1.5 cm anterior from center, (c) 1.5 cm posterior from center, (d) 1.5 cm left from center, and (e) 1.5 cm right from center. The spine segments were taken from a fairly young age group of specimens (31 years to 55 years) in which no significant osteophyte formation or disc degeneration was present. All FSU's in preparation for mechanical testing were dissected of all nonligamentous tissue. Prior to axial rotation, the FSU was vertically aligned with the chosen fixed axis location. During mechanical testing, the lower vertebra remained stationary while the top vertebra with a prior applied minimal compressive load (< 25 N) rotated axially under the prescribed loading sequence. Each FSU rotated through two cycles of right axial rotation followed by two cycles of left axial rotation.

The specimens were loaded to a maximum of 10 Nm in loading steps of 2.5 Nm. Each load level was reached in 20 seconds and then the specimen remained at this load level for 30 seconds of creep prior to loading to the next load level. During axial rotation, the MTS data acquisition system recorded the compressive force and the rotational angle of the spine segment.

RESULTS

The mean rotations at each of the five fixed axis locations are summarized in Figure 1.

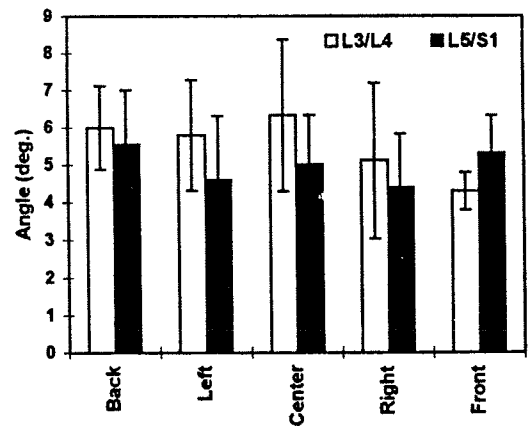

Figure 1. Means (±s.d.) for Complete Range of Motion for Different Axis Positions

A repeated measures of variance was performed and demonstrated that the mean rotations at each location are not statistically significant for either spine level (L3/L4, $p=0.22$; L5/S1 $p=0.17$). Nevertheless, the

maximum and minimum rotations of each segment are shown to be different (Figure 2).

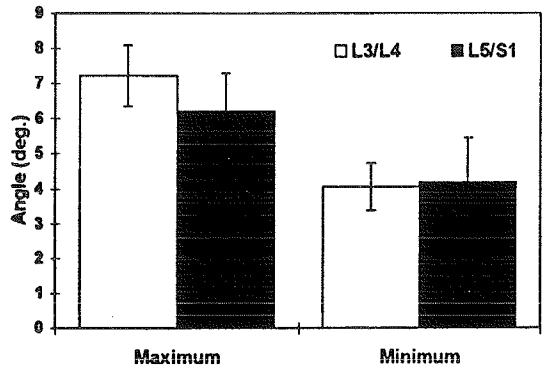

Figure 2. Average (±s.d.) Maximum and Minimum Rotations of L3/L4 and L5/S1

The percentage difference between the maximum and minimum rotations is 44% for L3/L4 and 33% for L5/S1. A simple paired t-test demonstrates that the difference between the maximum and minimum rotation of each specimen are statistically significant: L3/L4 with $p=0.001$ and L5/S1 with $p=0.007$. The maximum rotation of two of five spine segments of the L3/L4 and of the L5/S1 was measured when the fixed axis was located 1.5 cm posterior to center. For all other spine segments, the axis location for maximum rotation was equally distributed between the locations: center, right and left for L3/L4 FSUs and center, right and front for L5/S1 FSUs.

DISCUSSION

Controversy has surrounded the validation of using a constrained or a fixed axis in spine rotational mechanical testing. However, to our knowledge no study has investigated the effect of a constrained axis of rotation. We have shown that even though the average rotations at each location are not statistically different, the maximum rotation did not occur in the same location for each sample. The maximum rotations were statistically different from the minimum rotations, demonstrating that measured rotations are highly sensitive to the location of the fixed axis. Despite not having a larger number of spine segments to display certain trends, we believe that the impact of using a fixed axis in the experimental setup has been shown. This fixed axis rotation study has given further support to performing mechanical rotation studies with an unconstrained axis, allowing the spine segment to freely move under applied loading about its own instantaneous axis of rotation.

REFERENCES

Goel V.K. et al. Spine, 20(21), 2354-2357, 1995.

ACKNOWLEDGEMENTS

University of Bern, M.E. Mueller Institute of Biomechanics, Switzerland.
Department of Orthopedic Surgery, Inselspital, University of Bern, Switzerland.

QUANTIFICATION OF FEMORAL SURFACE STRAIN AFTER CEMENTLESS STEM IMPLANTATION BY COMPUTER ANALYSIS OF THE PHOTOELASTIC METHOD

R. P. Morris, M. J. Grecula, W. L. Buford, Jr., R. M. Patterson

Department of Orthopaedics and Rehabilitation, The University of Texas Medical Branch
301 University Blvd., Galveston, TX 77555-0892

INTRODUCTION

The purpose of this research is to determine to what affect different cementless stem designs have on the surface strains of the femur. This protocol follows a technique developed in a pilot study that uses the photoelastic method to resolve the fringe patterns on the femur, commercially available computer software to image these patterns, and original software programs to analyze the surface strains and provide comparative data.

REVIEW AND THEORY

Cementless femoral stems have been associated with surface strain changes and stress shielding after total hip arthroplasty. The changes may lead to post-operative bone resorption, implant micromotion, microfracture or implant failure. Therefore, detailed analysis of femoral surface strain before and after implantation can be useful in determining the features of implant designs that promote strain changes.

PROCEDURES

Four identical composite femurs (1) are used to reduce variability between specimens. The composites are coated with type PL-1 photoelastic material (2) and loaded in a MTS 858 Mini Bionix (3) from 0 to 2000 Newtons, in 500N increments. The bones are photographed from four orthogonal views at each increment. This procedure is repeated three times for the normal condition. Each femur is then fitted with one of four cementless femoral hip stem designs: proximal fit, distal fit, proximal-distal fit (4), wedge-taper fit (5), and tested again with the above procedure three times, as well. The photographs are scanned into a computer as bitmap images and the fringes converted to monochromatic areas of respective color using CorelDRAW! (6). The strain level of each fringe is determined by a calibration protocol detailed by the Measurements Group. Two Visual Basic 2.0 (7) programs are to be used to quantify the total area of individual strain patterns, and the strain plotted along the centroidal axis of the femur.

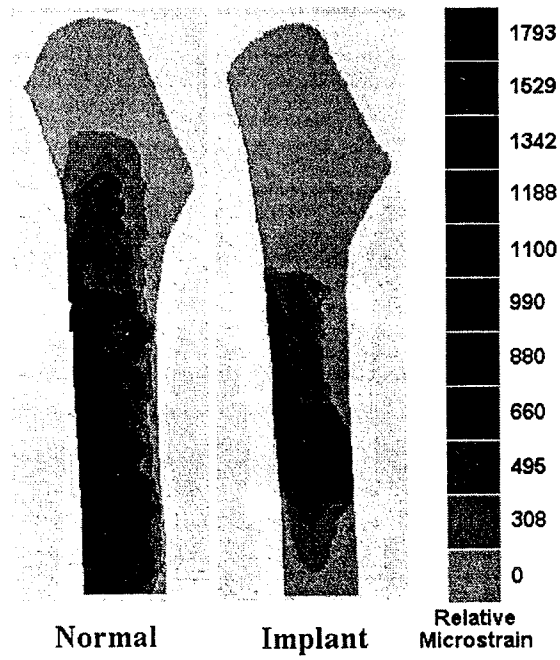

Figure 1: Processed images of femoral strain

RESULTS

The images in **Figure 1.**, from the pilot study, present the lateral views of a femur pair after image processing. The normal (left) and implanted (right) strain patterns are shown for each femur at maximum loading of 2000N. The difference in strain patterns between the normal and implanted femurs can immediately be seen in the topographical data. Stress shielding is evident by the reduced strain intensities seen in the implanted case.

The graph in **Figure 2.** is an example of strain analysis possible using Visual Basic programming tools. The normal and implanted strain values for the lateral views of a specimen are plotted along the surface of the femur with zero representing most proximal. An immediate description of stress

shielding due to stem implantation is apparent by the overall reduction in strain values along the surface of the femur. The movement of the high strain center is noteworthy since the entire strain distribution is effected. This information can be important in predicting problematic high stress areas in stem design, or poor fit.

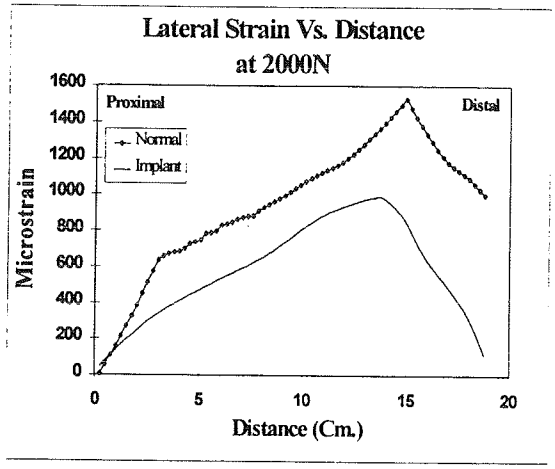

Figure 2: Strain Vs. Distance Data

The graph in **Figure 3.** is a result of plotting the femoral strain values as differences from the normal condition along the centroidal axis of the femur for the four implant designs tested. A large departure in strain distribution from the normal strain distribution of a bone may be unfavorable for an implant design. In this preliminary data, it is obvious that the proximal/distal fit exhibits the greatest difference in overall distribution from the normal bone after implantation.

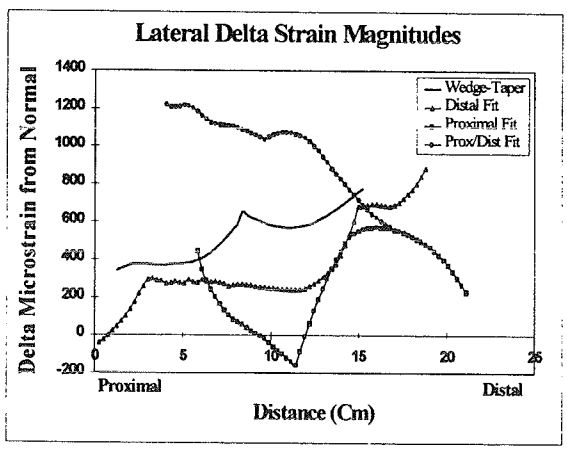

Figure 3: Strain Comparison of Four Implant Designs

With this type of strain distribution analysis, comparisons between different implant designs can be investigated over the entire surface of the bone. However, the results from the pilot study have not been scrutinized with any formal statistical analysis or verification, therefore, no statements can be made at this time as to the performance of one particular stem design over another.

DISCUSSION

The current experiment will attempt to identify differences in implant design based on strain information obtained. Verification of the consistency and repeatability of the coating, implanting, and loading procedures is necessary to validate the method. This will be accomplished through the repetition of the testing protocols and statistical analysis of the program data. A correlative follow-up testing procedure for cadaver specimens is expected in future directions, as well as comparisons of this data with clinical data and radiographic documentation of specific stem designs.

REFERENCES

1. Pacific Research Laboratories, Inc., Vashon Island, WA.
2. Measurements Group Vishay, Photoelastics Division Raleigh, NC.
3. MTS Systems Corporation, Eden Prairie, MN.
4. Richards Modular Hip System, Smith & Nephew Richards, Memphis, TN.
5. Natural Hip System, Intermedics Orthopedics, Austin, TX.
6. Corel Corporation, Ontario Canada.
7. Microsoft Corporation, Seattle, WA.

ACKNOWLEDGMENTS

Primary Funding: University of Texas Medical Branch Small Grants Program.

Prostheses Donated By:
Smith & Nephew Richards of Memphis, TN.
Sulzer Orthopedics of Austin, TX.

FALL SIMULATION RESULTING IN *IN SITU* CADAVERIC FEMUR FRACTURE

Joseph Casalena, Michael Horvath, Erez Morag, Michelle Barr, Christopher Jacobs, Peter Cavanagh, Donald Streit

The Pennsylvania State University, University Park, PA 16802

INTRODUCTION

This study demonstrates that it is possible, by an appropriately delivered external impact to an intact cadaver, to produce a fracture in the proximal femur without fracturing the pelvis.

REVIEW AND THEORY

When the trochanter of an extended cadaveric limb is impacted, the load transmitted through the femoral neck will be very small for any reasonable impact velocity. The simple (though subtle) explanation for this claim is that the femoral head is a ball joint and cannot, by itself (i.e. in the absence of muscle activity), provide any resisting moment to impacting loads. In contrast, 90 degrees of knee flexion results in a mass moment of inertia of the entire leg about the femoral shaft that is approximately 17 times greater than that in the fully extended posture. Thus, with knee flexion, lateral motion of the knee and torsional rotation of the femur are expected to be very small for the duration of short (100 ms) impacts. Various studies have observed flexed knee configurations during falls (e.g. van Kroonenberg et al. 1993). However, cadaveric hip impact studies in which the knee was flexed during impact have not been found in the literature.

The impact forces in lateral hip impact experiments are typically directed through the proximal femur, into the central portion of the acetabulum. It is reasonable to expect that both automotive crashes and falls can result in such a force application. These types of impacts present a higher probability of acetabular fracture than femoral fracture because the direction of the applied load is toward a region of the acetabulum that often receives little loading during daily weight-bearing activities and therefore is poorly mineralized.

However, it is also reasonable to expect that fall related impacts can result in a force directed into the upper third of the acetabulum - a region which generally has the highest bone mineral density. This can occur in a collapsing fall or a fall from a sitting position in which the hip joint is often flexed and adducted. A Penn State University nursing home falls survey (Streit et al., in preparation) provides valuable insight in this regard since more than seventy percent of the fractures reported over a two year period resulted from falls which began from a chair or from bed - situations in which the hip was, most likely, flexed. Such a fall loading condition probably results in a drastically different pelvic loading configuration from those which have been studied in automotive research. For example, Viano (1991) hung cadavers vertically and directed impacts laterally onto the greater trochanter. Because these forces were directed laterally, the pubic ramus was particularly at risk and did, in fact, fracture in two cases. In addition, because femoral rotation was not restrained (the knee was straight) it is possible that minimal loads were transmitted through the femoral neck.

PROCEDURES

An elderly unembalmed female cadaveric specimen was secured for this preliminary study. The specimen was 85 years old, approximately 4 days post mortem, 150 lb in weight, and Caucasian. Plain radiographs of the pelvis and both proximal femora were obtained prior to the impact testing, at which time it was found that the right femur had, some years earlier, been fractured and repaired. Although it had originally been intended to subject the two hips to different loading conditions, the prior surgery reduced our available test cases to a single hip. The left proximal femur was moderately osteopenic, the thickness of the diaphyseal cortical bone was reduced, and the primary trabeculae coarsened with thinning of the secondary and tensile trabeculae resulting in widening of Ward's triangle. The pelvis was intact but significant bone mineral loss was apparent in the pubic ramus and in the middle third of the

acetabulum. The load bearing area in the upper third was, however, well mineralized.

For this pilot study, we chose a configuration which best simulated a postero-lateral impact direction, similar to that described by Courtney et al. (1994). The cadaver was strapped in place on the table as shown in figure 1 and the location and direction of impact on the greater trochanter was verified. The hip and knee were flexed as shown in figure 1. The first impact was delivered with a velocity of 1.77 m/s - after which plain radiographs confirmed that no fracture had occurred. The cadaver was then repositioned and a second impact was delivered with an impact velocity of 2.9 m/s. Radiographs after this impact indicated that a fracture had been obtained.

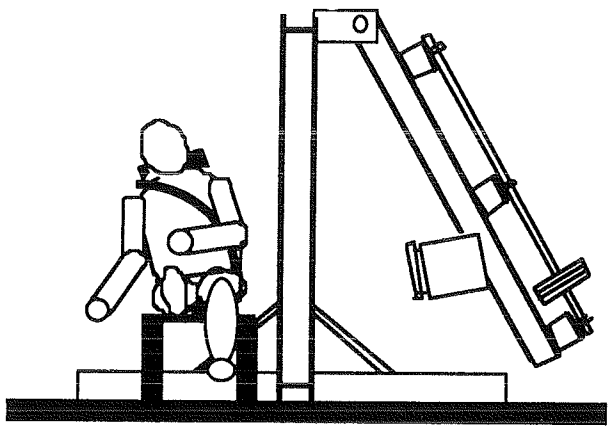

Figure 1. Impact pendulum instrumented with accelerometer, angular rate sensor, and a force plate on the impacting surface.

RESULTS

The force-time and linear velocity-time curves from the second impact are shown in figure 2. Note that the force to fracture was approximately 2150 N - a value which is toward the lower extreme of the values that have been reported for isolated femora. No doubt the osteopenic nature of the hip involved and the careful direction of the impact (there was, for example, minimal force by-pass to the gluteal region) were responsible for this comparatively low force to fracture.

The fracture itself was a comminuted sub-trochanteric fracture with two distinct fracture paths. The first extended from an intertrochanteric line down to the medial diaphyseal shaft - where slight displacement of the cortex occurred. The second path, extended from the upper third of the first fracture line into the greater trochanter.

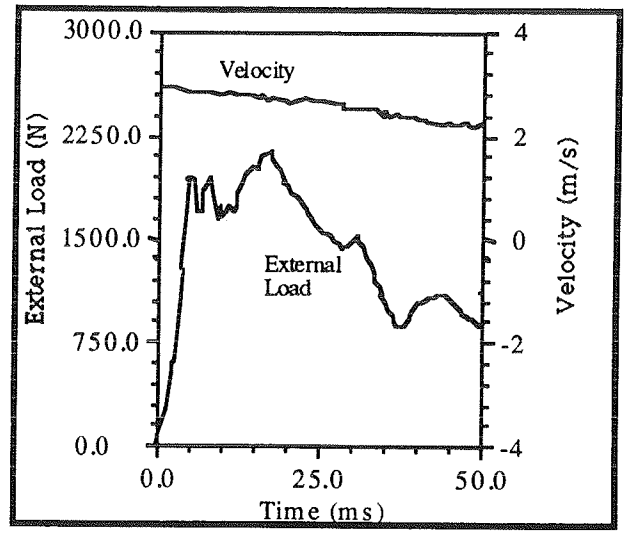

Figure 2: Force and linear velocity vs. time from the impact that resulted in fracture

DISCUSSION

This preliminary study has shown for the first time that it is possible, by an appropriately delivered external impact to an intact cadaver, to produce a fracture in the proximal femur without fracturing the pelvis. Although the fracture pattern is not the most typical one seen as a result of falls, the importance of the experiment is that a fracture was generated with a relatively small - but appropriately directed - impact force. We interpret this to mean that further refinement of the techniques presented here can be expected to allow the investigators to eventually specify the type of fracture that can be generated.

REFERENCES

Courtney AC et al. *ORS*, 2, 527, 1994.

van den Kroonenberg et al., *ORS*, 24, 1993.

Viano D.C. *STAPP*, 113-142, SAE, 1991.

ACKNOWLEDGMENTS

Support for this study was provided by the Centers for Disease Control under Grant number R49-CCR-307341-04.

COMPUTER SIMULATION STUDIES OF CERVICAL SPINE EXTENSION MECHANICS: COMPARISON OF DIFFERENT IN VITRO TESTING PROTOCOLS

Denis J. DiAngelo and Thomas H. Jansen
School of Biomedical Engineering, University of Tennessee, Memphis

INTRODUCTION

Computer simulation techniques integrated with engineering mechanics and linkage theory can be used to study the complex *in vivo* motions and loads of the cervical spine. Validation of computational models of human joints typically uses *in vitro* biomechanical data obtained from tests on human cadaver tissue. For *in vitro* studies of cervical spine mechanics, the external motions and loads applied to the end bodies of the specimen are controlled by a testing apparatus. Motions of the interior spinal bodies are measured and are affected by the testing conditions, i.e., mounting and alignment configuration.

Minimal muscle activity is needed to maintain the head in an erect neutral orientation *in vivo*. When muscles are ignored (as in *in-vitro* testing), head weight is the typical physiologic force that acts on the cervical spine. During extension of the head from an upright position, a bending moment is induced throughout the spine that increases caudally and acts in combination with the compressive (head weight) force (see Fig. 1). The distribution of the bending moment is affected by the spine's curvature and increases in the caudal direction at each vertebral level with extensional rotation. Based on this analysis, the *in vivo* characteristics of cervical spine motion and mechanics were: rotations at each vertebral level were continuous with like polarity, combined loading state of axial compression and extensional bending moment, and caudally increasing bending moment distribution.

A computer model of the cervical spine was developed that included the capacity to simulate different mounting configurations. The objective of the study was to compare different biomechanical testing configurations and to identify a mounting arrangement that closely replicated the *in vivo* extensional motion and loading behavior of the cervical spine. The four simulated experimental set-ups were: upper and lower pots pinned (P-P), upper pot pinned with lower pot fixed (P-F), upper pot connected to a translating, rotating joint offset from a fixed lower pot (TP-F), and upper pot unconstrained and subjected to pure moment with lower pot fixed (M-F).

METHODS

The simulation software package Working Model 2D™ (Knowledge Revolution, San Mateo, CA) was used to model the cervical spine (C2-T1) and to simulate the four different mounting configurations. The spine was modeled as a mechanically-equivalent system with each vertebral body modeled as a link. The vertebral geometry was approximated as trapezoidal polygons with dimensions taken from anthropometric studies [2]. The mechanical properties of the intervertebral discs were modeled as rotational springs having a linear stiffness value and were located at the center of the subjacent vertebra.

The spine model was initially placed in the TP-F configuration and motion was induced as per a previous experimental protocol [1]. Since the load vector passed closer to the lower pot with increasing spine extension, inverting the spine induced a bending moment that increased in the caudal direction (see Figure 2).

The rotational spring constants were set to the same value and iteratively changed until the loading vector in the simulation correlated to that found in our experimental studies. After successive iterations, a stiffness value of 2.0 N-m/deg for each vertebral level was determined and was comparable to values given in the literature [3].

The model was adapted to simulate the other three mounting configurations. Rotational and moment data at each spinal level and the resultant loading vector were calculated. In all cases except M-F arrangement, motion was initiated by a vertically oriented actuator set to

a constant velocity of 3.2 mm/sec. The simulations were stopped when either a force limit (>100 N) or rotation limit (> 30 deg) exceeded the nominal physiologic range. For the M-F case, the simulation was stopped when the bodies reached the maximum rotational limit.

RESULTS

The simulation results of actuator displacement, force in the actuator, total spine rotation, and execution time are listed in Table 1. Figure 3 shows the rotation or moment distribution at each vertebral level. Because the rotation spring constants were linear, the moment values are proportional to the rotation values, i.e. the moment was equal to the vertebral rotation times the spring stiffness.

DISCUSSION

In the P-F simulation, the upper limit of the actuator force was quickly exceeded. Minimal rotation occurred at each vertebral level and the polarities were negative for levels C2/C3 and C3/C4. A limited range of motion also occurred in the P-P simulation. More important, was the lack of a bending moment at the end vertebral bodies, (i.e., pinned connections can not transfer a moment). For the M-F configuration, the overall spine rotation was less than 12 degrees. Lastly, the TP-F configuration produced physiologic levels of motion (30.10 deg) and load (49.31 N).

REFERENCES

1. DiAngelo et al., ASME 1997 Adv in Bioeng, Development of an in vitro experimental protocol to study the extensional mechanics of the cervical spine, (in press).
2. Gilad et al. *Brit. J. Rad.*, 58.695:1031-1034, 1985.
3. Moroney et al., *J Biomech.*, 21.9:769-79, 1988.

	End Configuration			
	TP-F	P-F	P-P	M-F
Simulated time (sec)	32.00	0.08	0.85	0.33
Force at actuator (N)	49.31	109.30	102.63	------
Actuator travel (mm)	100.00	0.24	2.72	------
Total rotation (deg)	30.10	0.84	7.05	11.59

Table 1: Computation results for the different end-mounting configurations.

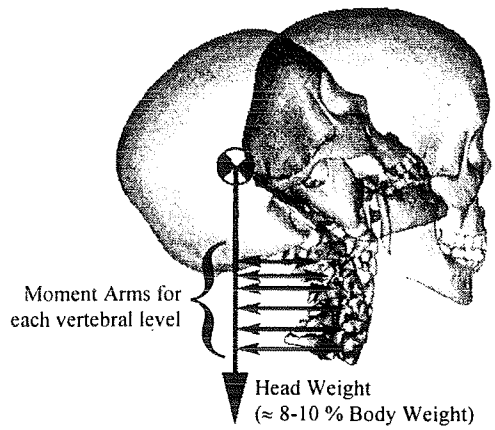

Figure 1: *In vivo* spine mechanics. Passive head weight induced a caudally increasing moment.

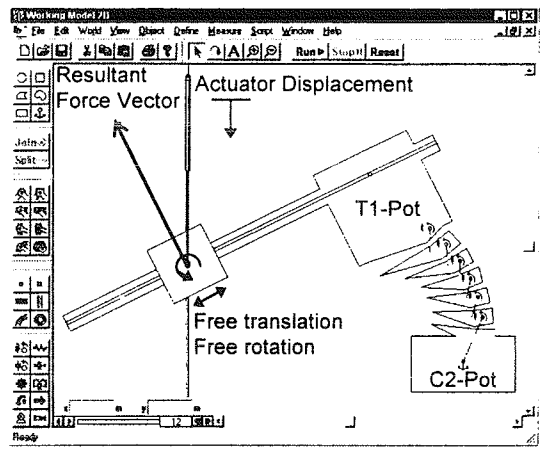

Figure 2: TF-P Simulation at 100mm actuator displacement. The actual loading vector was not in-line with the vertically oriented actuator, but was normal to the connecting arm.

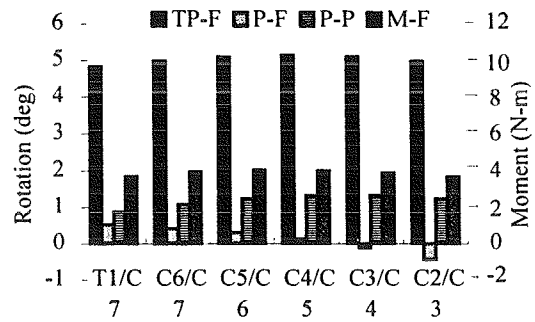

Figure 3: Rotations and moments for the cervical spine simulation at each vertebral level for each of the loading configurations

REDUCTIONS IN HIP CONTACT FORCES DUE TO GAIT ADAPTATIONS IN PREOPERATIVE TOTAL HIP REPLACEMENT PATIENTS PERSIST EVEN IF ANTAGONISTIC MUSCLE ACTIVITY IS INCREASED

K.C. Foucher[1], D.E. Hurwitz[2], T.P. Andriacchi[2], A.G. Rosenberg[2], J.O. Galante[2]

[1]University of Illinois at Chicago, Department of Bioengineering, Chicago, Illinois
[2]Rush-Presbyterian-St. Luke's Medical Center, Department of Orthopedic Surgery, Chicago, Illinois

INTRODUCTION

Studies have shown that bone loss occurs around the greater trochanter in preoperative total hip replacement (THR) patients (1) and more recently that this bone loss is related to reductions in the adduction moment (2). While it is obvious that a decreased adduction moment results in decreased abductor muscle forces and hip contact forces in the absence of increased antagonistic muscle activity, it is less clear what happens in the presence of increased antagonistic muscle activity. This study examined whether the reduction in the adduction moment in preoperative THR patients is sufficient to reduce the abductor muscle forces even in the presence of increased antagonistic muscle activity. The hypothesis tested was that even in the presence of increased antagonistic activity, the reduced adduction moment frequently found in preoperative THR patients would still result in decreased hip contact forces and decreased abductor muscle forces.

REVIEW AND THEORY

The effect of gait adaptations on the hip contact force has been previously investigated in post-operative THR patients using a parametric model to determine potential muscle force distributions based on the external kinetics during gait (3). Moments at the hip joint during gait were measured in the sagittal, frontal and transverse planes. An analytical Hill based muscle model of the lower extremity with a graphical interface was used to simulate the forces generated by muscles crossing the hip joint (4). At each point of interest in the stance phase of the gait cycle, a range of agonist muscle forces, associated with a preselected level of antagonist activity, needed to produce a net internal moment to maintain mechanical equilibrium in the sagittal and frontal planes was calculated. Recently the model has been updated so that mechanical equilibrium is maintained in all three planes. This entailed grouping agonist muscles into three subgroups rather than two. A similar parametric method was used.

PROCEDURES

The hip joint kinematics and kinetics of a group of 36 preoperative THR patients and a group of 27 normal subjects were previously collected. A three dimensional optoelectronic camera system with a multi-component force plate was used to determine the angular joint motion and external local moments as subjects walked at three self selected speeds (5). To test the hypothesis that a decreased adduction moment substantially altered the predicted forces even in the presence of increased antagonistic muscle activity, a preoperative THR patient was selected for whom this was the primary gait adaptation. A normal subject with similar sagittal plane moments as the preoperative patient was selected for comparison. The model was used to predict the range of muscle forces and contact forces at four points during the gait cycle, peak flexion and extension moments, and the first and second peak adduction moments during stance phase.

RESULTS

The preoperative subject had a substantial reduction in the contact forces and abductor muscle forces during both the first and second peak adduction moments (Figure 1-4). The contact force is reduced by 29 to 38% and the abductor muscle force is reduced by 71 to 76% during the first peak adduction moment. During the second peak adduction moment the contact force is decreased by 24 to 31% and the abductor muscle force by 41 to 51%. Even if the antagonistic activity level of the preoperative patient is increased and that of the normal subject is not increased, the results indicated that the preoperative patient still had substantially lower contact forces and abductor muscle forces.

DISCUSSION

This study indicated that the reduction in the adduction moment of the preoperative patient resulted in a substantial reduction in the hip contact force as well as the hip abductor muscle forces. Even if the antagonistic muscle activity of the patient were increased and that of the normal subject not increased, the predicted muscle forces and contact forces of the preoperative patient were still much less than that of the normal subject. Thus the reductions in the muscle and contact forces due to the reduced adduction moment in this preoperative patient was greater than the increase in forces that might result from increased levels of antagonistic muscle activity.

REFERENCES

1) Sauer et al.:ORS 21:517, 1996.
2) Hurwitz et al. ASME 29:387-8, 1995.
3) Hurwitz et al. ASME BED-28: 183, 1994.
4) Delp et al. IEEE Biomed. Eng. 757-67, 1990.
5) Andriacchi et al. NATO ASI E: 83-102, 1985.

ACKNOWLEDGEMENTS

Whitaker Foundation

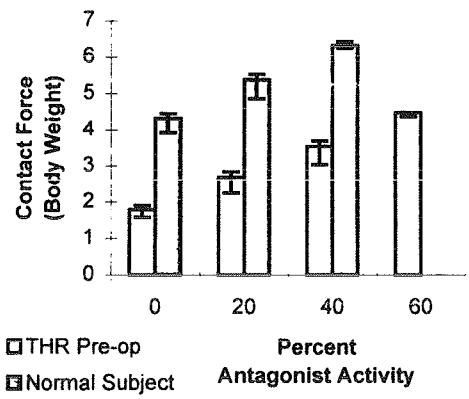

Figure 1. The range of contact forces at each level of antagonistic muscle activity during the first peak adduction moment of gait.

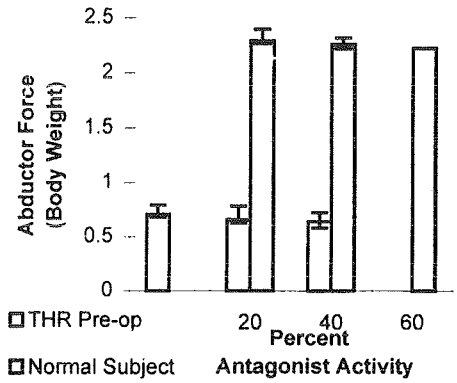

Figure 2. The range of abductor muscle force (gluteus medius and minimus) at each level of antagonistic muscle activity during the first peak adduction moment.

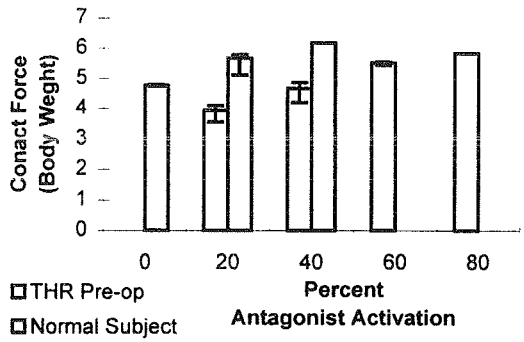

Figure 3. The range of contact forces at each level of antagonistic activity at the second peak adduction moment during gait.

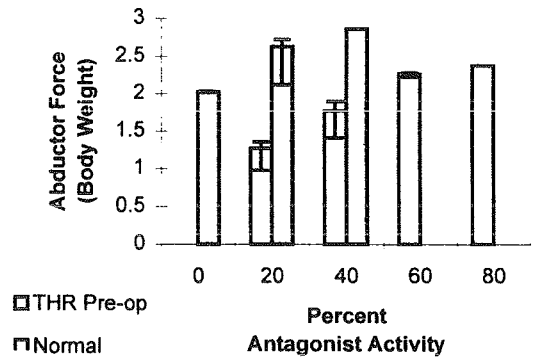

Figure 4. The range of abductor muscle force (gluteus minimus and medius) at each level of antagonistic muscle activity during the second peak adduction moment of gait.

DECOUPLING THE BILATERAL DEFICIT: THE EFFECT OF TASK INITIATION TIME ON THE EXPRESSION OF MAXIMUM MUSCULAR FORCE

PETER F. VINT[1] AND RICHARD N. HINRICHS[2]

[1]Department of Exercise Science, University of North Carolina at Greensboro, Greensboro, NC 27412
[2]Department of Exercise Science and Physical Education, Arizona State University, Tempe, AZ 85287

INTRODUCTION

The purpose of this study was to determine if the magnitude of maximum voluntary muscular force would be affected by temporal parameters related to the initiation of unilateral and bilateral tasks. The results suggested that tasks that were initiated simultaneously appeared to be coupled or constrained by a mechanism which inhibited the expression of maximum voluntary muscular force. Tasks that were initiated asynchronously, however, were apparently not subject to this inhibition and resulted in greater muscular forces. Consequently, it would appear that the traditional manifestation of the bilateral deficit phenomenon has less to do with the absolute quantity of active musculature and more to do with how unilateral and bilateral tasks are initiated. It was suggested that asynchronous task initiation strategies might have facilitated a temporary dissolution of the coordinative structure or interlimb coupling mechanism.

REVIEW AND THEORY

It has been suggested that prior to the initiation of a complex, multi-segment motor task, the CNS may attempt to impose a tight spatiotemporal coupling of the involved limbs. Theoretically, this coupling serves to minimize the computational volume required to control the increasingly complex equations of motion (Kelso et al., 1979a). In doing so, the CNS provides an elegant and effective solution to the degrees of freedom problem (Bernstein, 1967). This concept, hereinafter referred to as "coordinative structures", is an important organizational principle because it allows the human control system to enable coordinated movement without the need for excessive computation (Swinnen & Walter, 1988). When controlling a simultaneous bilateral task, for example, the CNS may attempt to provide an optimal solution by eliminating the redundant commands needed to control each limb independently and issuing one general command for the control of a single, functional unit.

By coupling the limbs to perform as one functional unit, less "attention" or "neural energy" would be required for the initiation and execution of a complex motor task. However, by reducing the neural drive that is allocated for the initiation of a given task, less would be available for its subsequent execution. Therefore, while interlimb coupling may lead to an optimal solution to the degrees of freedom problem, it may also lead to unwanted decrements in motor performance. Support for this argument has been garnered from studies involving unilateral and bilateral reaction time and movement speed, and from studies involving dissimilar bilateral activities. Unfortunately, there is no direct evidence that suggests that maximum voluntary muscular force may be similarly influenced by such a mechanism.

In their studies of bimanual coordination, Swinnen et al. (1988), and Walter and Swinnen (1990) reported that subjects were more successful in "decoupling" the limbs when bilateral reaching tasks were initiated asynchronously. This decoupling lead to improvements in the required motor performances because each limb was able to function more independently. If the results of this study can be extended and applied to tasks requiring maximal muscular force, it would seem plausible, for example, to suggest that asynchronous initiation of simultaneous bilateral leg extensions would allow for each limb to be controlled more independently. As a result, more neural energy would be available to each limb and the potential for developing greater muscular tensions would increase.

PROCEDURES

Twenty-seven recreationally active adults completed a series of maximal effort isometric knee extension tests during independent unilateral, simultaneous bilateral, decoupled bilateral, and precoupled unilateral conditions. Decoupled bilateral efforts were defined as bilateral exertions that were initiated asynchronously. Precoupled unilateral efforts were defined as unilateral exertions that were completed following a brief (0.5 to 1.0 s) simultaneous bilateral exertion. Three maximal exertions were completed for each condition.

Maximum isometric force and average integrated EMG (AEMG) of the representative knee extensor musculature were measured over the 500 ms interval of the force-time record which yielded the greatest integrated force value. AEMG of representative knee flexor musculature was also measured to account for

the possibility that any observed changes in force could have been attributable to changes in antagonist muscle co-activation.

RESULTS

Repeated measures ANOVA revealed that independent unilateral exertions elicited significantly greater forces than simultaneous bilateral exertions. Bilateral exertions that were initiated at slightly different times also generated significantly greater forces than simultaneous bilateral exertions. In fact, forces developed during these "decoupled" bilateral exertions were similar to those that had been generated unilaterally. The smallest forces were observed during the "precoupled" unilateral condition where subjects were required to initiate the trial simultaneously, but were then prompted to lower one leg and continue to exert maximum effort unilaterally (Figure 1). Average integrated EMG failed to demonstrate significant differences across either leg or condition.

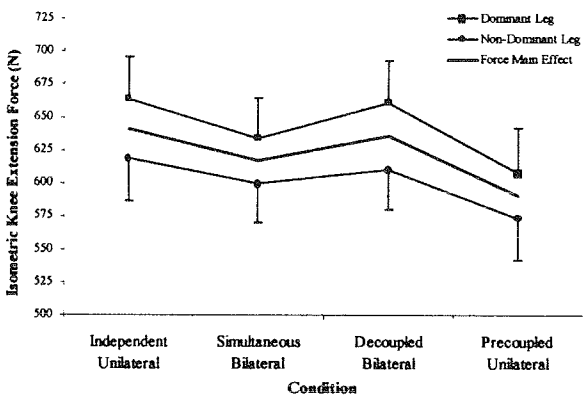

Figure 1: Maximum isometric knee extension force (± SE, n = 27). Main effect reflects the main effect for condition collapsed across leg.

DISCUSSION

It had been hypothesized that the commonly observed decrements in simultaneous bilateral force could have been attributable to an interlimb coupling mechanism or coordinative structure. By coupling the limbs to perform as one functional unit, the central nervous system could have minimized its computational volume by allocating less attention or energy for the initiation and execution of simultaneous bilateral exertions. However, by reducing the neural drive which is allocated for the initiation of such a task, less would be available for its subsequent execution and thus, in accord with Henneman's size principle, the magnitude of muscular force would be diminished. The results of this study were generally in agreement with this hypothesis. Isometric exertions that were initiated simultaneously appeared to be coupled or constrained by a mechanism which inhibited the expression of maximum voluntary muscular force. Tasks that were initiated asynchronously, however, were apparently not subject to this inhibition and resulted in greater muscular forces.

A Bernsteinian interpretation of the results might promote the idea that decoupled bilateral exertions achieved greater muscular forces because the limbs were able to function more independently. It is conceivable, for example, that the asynchronous initiation of decoupled bilateral exertions may have facilitated a temporary dissolution of the coordinative structure or interlimb coupling mechanism. This task initiation strategy may have cued the CNS to allocate more attention or "energy" for the initiation and execution of decoupled bilateral exertions.

However, if the bilateral deficit phenomenon were truly consistent with the coordinative structure hypothesis, exertions constrained by the same task initiation strategies should have resulted in similar levels of muscular force. The equivalence between decoupled bilateral and independent unilateral forces was entirely consistent with this interpretation. On the contrary, the difference between simultaneous bilateral and precoupled unilateral forces was not.

While others have demonstrated the utility of the coordinative structure hypothesis (Kelso et al., 1979a, Swinnen et al., 1988; Walter & Swinnen, 1990), the present study would suggest that this explanation is not entirely correct. It should be stated, however, that the coordinative structure is a hypothetical construct and is therefore devoid of any physical entity. It seems likely that Bernstein's original conceptualization of the coordinative structure was an elegant, if not ingenious, explanation to the infinitely complex degrees of freedom problem. Future efforts should attempt to identify the anatomical and neurophysiolgical structures that contribute to the interlimb coupling effects which are observed during simultaneous bilateral motor tasks.

REFERENCES

Bernstein, N.A. (1967). *The Co-ordination and Regulation of Movements*. Pergamon Press.

Kelso, J.A.S., et al. (1979a). *J. Exp. Psych.*, **5**, 229-238.

Swinnen, S. et al. (1988). *Brain and Cognition*, **8**, 326-347.

Walter, C.B. et al. (1990). *J. Motor Behavior*, **22** (4), 451-473.

KNEE MUSCLE STRENGTH IN ABDUCTION-ADDUCTION AND FLEXION-EXTENSION

INTRODUCTION

Human knee muscle strength in abduction-adduction and flexion-extension was studied as a function of knee abduction and knee and hip flexion angles, respectively. Study of knee muscle strength about multiple axes helps us understand the important roles of knee muscles in performing various functional tasks and in compensating for knee injuries.

REVIEW AND THEORY

The knee joint has three rotational degrees of freedom: flexion-extension, abduction-adduction, and internal-external rotation. There have been a number of studies on knee muscle strength in flexion-extension (Houtz et al. 1957, Kulig et al. 1984). However, much less work has been done on muscle strength about other axes. Knee rotational muscle strength was studied as a function of the knee flexion, tibial rotation, and hip flexion angles (Shoemaker et al. 1982). There seems a lack of information on the abduction-adduction muscle strength (Kulig et al. 1984). The objective of this study was to investigate the knee muscle strength in abduction-adduction and flexion-extension and their dependence on knee and hip positions.

PROCEDURES

Apparatus: To characterize knee muscle strength in abduction-adduction, the subject was seated upright on a custom-designed joint driving device with the knee at full extension and hip flexed to 85°. The seat could be adjusted in four degrees of freedom (DOF) so that knee abduction axis was aligned with the Z-axis of a six-axis force sensor located underneath the posterior capsule. The seat was then locked tightly to form a solid base. The femoral condyles are clamped tightly from medial, lateral and anterior sides. Two threaded rods connect the medial and lateral pieces of the knee clamp and wing nuts at both ends are tightened to squeeze the femoral condyles from the medial and lateral sides. The ankle (at the neutral position), rear part of the foot, and distal leg were cast with fiberglass tape and coupled tightly to two aluminum half-rings. The rings were mounted onto one end of an aluminum beam located beneath the leg. The other end of the beam was mounted onto the six-axis force sensor. The relative position between the rings and beam was adjusted in four DOF so that the leg was aligned with the beam and no strong compressive load was exerted onto the knee joint due to the mounting. Knee abduction angle was adjusted by rotating the beam to an appropriate position. For knee flexion-extension muscle strength, the joint driving device was repositioned so that the aluminum beam and force sensor were on the lateral side of the leg. Knee and hip flexion was adjusted by rotating the beam and folding the backrest to appropriate angles, respectively.

Anatomical axes: The knee flexion-extension axis was defined as passing through the lateral and medial epicondyles (Pennock and Clark 1990). Internal-external rotation axis was assumed to coincide with the tibial long axis. The abduction-adduction axis was determined by the right-hand rule with the ankle at the neutral position. Their positive directions were flexion, abduction and internal rotation, respectively.

Protocol: Five knee joints from three subjects were used in the study. During each trial, the subject was asked to generate maximum voluntary contraction (MVC) in abduction, adduction, flexion, or extension. Force and moment signals were measured by the six-axis force sensor, transformed to the knee joint coordinate system, and displayed in real-time on a computer monitor. The subject used the displayed torque signals to learn to generate the desired MVC several times at each position. EMG signals from the biceps femoris (BF), semitendinosus (ST), vastus lateralis (VL), vastus medialis (VM), and lateral and medial gastrocnemius (LG & MG), gracilis (GR) and tensor fascia lata (TFL) muscles were sampled at 500 Hz after low-pass filtering (8th order Butterworth filters with 230Hz cutoff).

To minimize hip contribution to knee abduction-adduction at full knee extension, the subject was instructed to adduct his hip against the medial part of the knee clamp while doing knee abduction MVC. Similarly, the hip was abducted for the knee adduction MVC task.

RESULTS AND DISCUSSION

Although producing maximum flexion or extension moment is a simple task, generating abduction-adduction MVC was more difficult and considerable torque may be produced in other directions as well. When the subject was asked to generate adduction MVC at 5° knee abduction, strong flexion and a little internal rotation moments were also produced. The ST and MG muscles contracted strongly, while the VL and BF were inactive. There were also a little activities in the VM, TFL and GR muscles. The LG muscle contracted quite a bit, indicating the subject might not contract his muscles optimally.

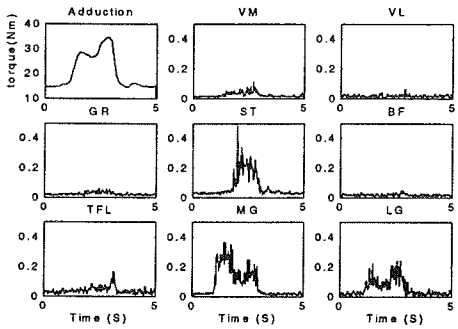

Figure 1: The adduction moment and EMG signals produced when the subject attempted to generate a maximum adduction moment. The knee was at full extension and abducted to 5°. The passive adduction torque was 15Nm. The EMG signals were normalized to their corresponding maximum values at maximum activation.

Passive resistance in abduction-adduction increased significantly and linearly with abduction-adduction angle (Fig. 2). It reached ~20Nm at 7° abduction/adduction. On top of the passive resistance, active muscle strength in abduction-adduction increased substantially with abduction angle. Abductor muscles were especially strong when the knee was adducted, and adductor generated more torque as the knee was abducted. The significant abduction-adduction muscle strength may play an important role in controlling joint movement and maintaining joint stability.

The MVC torque in flexion-extension varied with flexion angle systematically (Fig. 3). At 85° hip flexion, the knee flexion MVC peaked at 30° and decreased on both sides. In contrast, the knee flexion MVC decreased monotonically with knee flexion angle when the hip was extended to 30°. The knee extension MVC peaked at about 70° and was affected little by hip flexion.

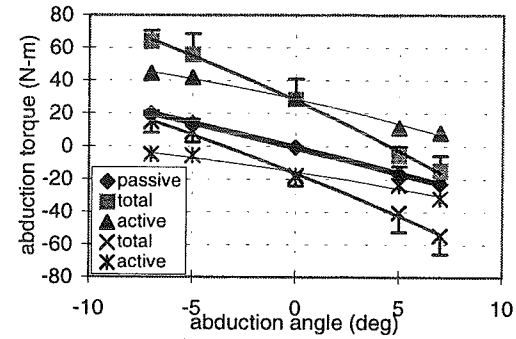

Figure 2: Abduction-adduction torque shown as a function of knee abduction angle. The thick, thin and medium lines give the passive, active and total abduction-adduction torques, respectively. Standard deviation was shown in one direction.

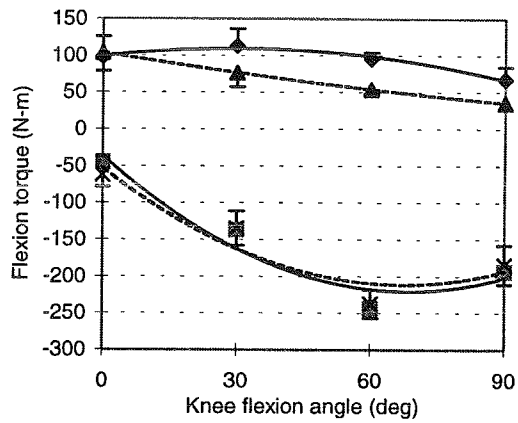

Figure 3: MVC torques in flexion-extension, shown as a function of knee and hip flexion angle. The solid and dashed curves correspond to hip flexion angle of 85° and 30°, respectively.

REFERENCES

Houtz, SM, *J. Appl. Physiol.* **11**, 475-480, 1957.

Kulig, K. et al. *Exerc. Sport Sci. Rev.*, **12**, 417-466, 1984.

Pennock GR and Clark KJ, *J. Biomech.*, **23**, 1209-1218, 1990.

Shoemaker SC, *J. Bone & Joint Surg.*, **64A**, 208-216, 1982.

A PORTABLE, CLINICAL GAIT ANALYSIS SYSTEM FOR THE REAL-TIME EVALUATION OF GAIT PATHOLOGIES

Richard F. *ff.* Weir, Ph.D., and Dudley S. Childress, Ph.D.

Rehabilitation Engineering Research Center, Northwestern University, Chicago, Illinois.

INTRODUCTION

We have developed a portable, low cost, real-time, direct ultrasound ranging system (D.U.R.S.) for the quantitative clinical evaluation of gait. We saw a need for a low-cost easy to use device that could provide valid gait data in real-time, allowing ideas to be implemented and tested immediately. To our knowledge no such device currently exists. The D.U.R.S. estimates the instantaneous forward velocity of the body center of mass from which parameters such as: gait speed; cadence; step time; step length; peak-to-peak variation; and time to achieve steady state walking are calculated.

THEORY AND METHODOLOGY

The D.U.R.S. consists of three main components: a transponder worn by the subject; a base unit infrared emitter/ ultrasound receiver; and a laptop computer. The D.U.R.S. operates by emitting high intensity infrared pulses from the base unit at a frequency of 22 Hz. Each infrared pulse triggers the transponder to emit an ultrasound pulse back to the base unit. The base unit measures the time difference between emission of an infrared pulse and the arrival at the base unit of an ultrasound pulse. The ultrasound pulse travels at the speed of sound in air. The speed of sound in air is dependent on the temperature and can be computed using:

$$Speed\ (m/s) = 331 + 0.6 * Temp.(^{\circ}C) \qquad (1)$$

The speed of sound at room temperature (22°C) ≈ 344m/s. By calibrating for the speed of sound in air, the time difference can then be converted into a measurement of the distance between the base and transponder units. Since distance measurements are taken at a rate of 22Hz, a measure of the how distance changes over time (i.e. velocity) is obtained. The general principles of the measurement have been demonstrated by Karcnik et al. (1992). For static distance measurements the principle has been exploited in inexpensive commercial distance ranging devices.

The accuracy of the D.U.R.S. was tested against that of the CODA 3 motion analysis system. The velocity profiles obtained from the D.U.R.S. and the CODA 3 system are very similar. Both devices accurately measure the periodic fluctuation in the forward velocity of the body trunk that results from the rising and falling of the centre of mass during normal gait. The gait speed determined with the D.U.R.S. was consistently within 3% of the gait speed determined from the CODA 3 system. The current system can accurately measure distance out to 15m

GAIT ANALYSIS PROCEDURE

During the clinical analysis of gait the transponder is worn by the subject posteriorly in the midline of the body at approximately sacral level two (S-2 level) (Fig. 1).

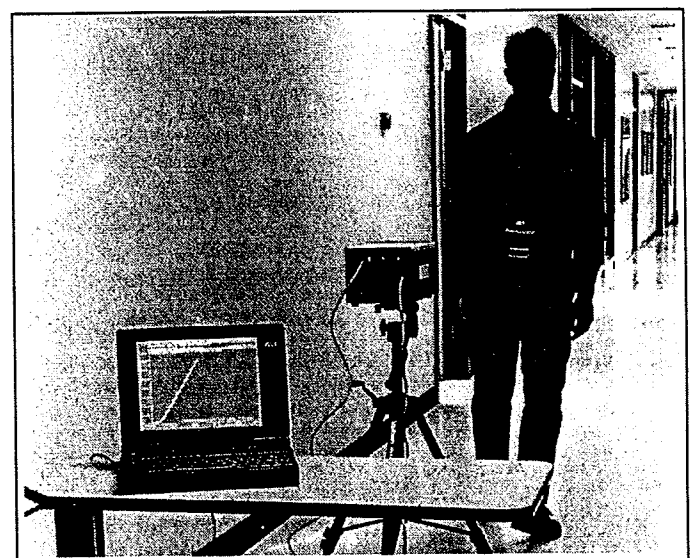

Fig 1: System in use. It is very portable and can be easily set up in a matter of minutes

The subject stands in front of the base unit such that the transponder faces the it. When instructed to do so the subject walks away from the base unit. As the subject walks away his/her forward progression is displayed in real-time on the computer. In essence the transponder acts as a single active marker at the approximate level of the body centre of mass. A trial ends when the subject walks beyond the range of the device (set at 14m). At this point the instantaneous walking velocity for that trial is processed and immediately displayed on the computer screen (Fig. 2).

The instantaneous velocity is obtained through filtering and differentiation of the forward progression data. We use software algorithms developed our laboratory for single marker gait analysis [Chan and Childress (1995)]. From this profile, gait parameters such as gait speed, cadence, stride length, step time, and time to achieve steady state walking can be calculated.

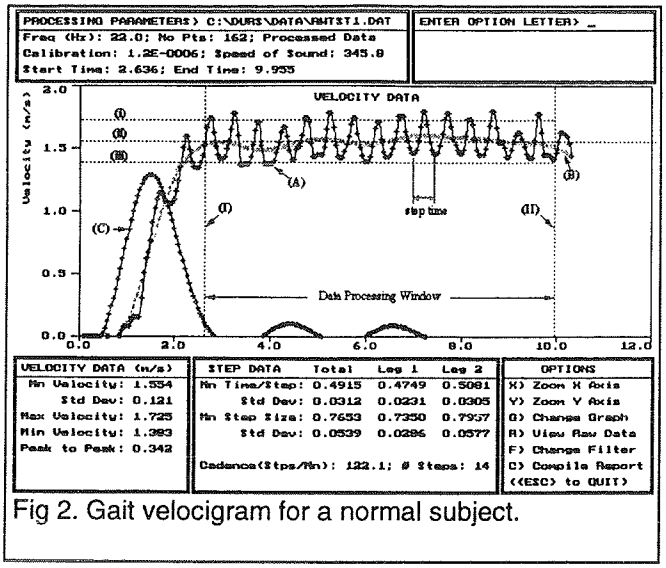

Fig 2. Gait velocigram for a normal subject.

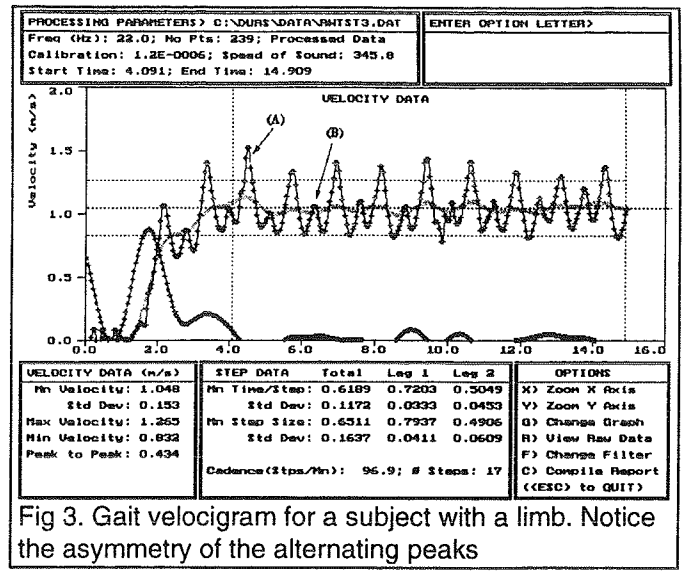

Fig 3. Gait velocigram for a subject with a limb. Notice the asymmetry of the alternating peaks

The mean velocity trace (trace B in Fig. 2) reveals when velocity transients associated with gait initiation have died out and steady state walking has been achieved (pt I in Fig. 2). It also shows up any underlying trends in the data. Steady state velocity is defined to have been reached when the acceleration (trace C in Fig. 2) declines to 10% of the maximum mean acceleration encountered during gait initiation. The duration of steady state velocity was arbitrarily defined to last as long as the mean acceleration remains within ±10% of the maximum mean acceleration (pt II marks the end of the steady state walking in Fig. 2).

DISCUSSION

The D.U.R.S. was originally conceived as a means of providing prosthetists with a low cost means of quantitatively measuring gait parameters when fitting and adjusting the alignment of lower limb prostheses. But it has application in areas outside of prosthetics. We foresee a situation where a surgeon can monitor post-operative recuperation of joint implant or musculo-tendon corrective surgery using the D.U.R.S. in conjunction with a video camera. A full analysis would be performed prior to, and following, the surgery. Further visits would be required only if the D.U.R.S. indicated something out of the ordinary.

The instantaneous forward velocity profile is a graphical representation of how a particular person walks, much like an ECG is a graphical image of a person's heart activity. Different gait pathologies have distinct instantaneous velocity profiles or gait velocigrams (GVG). Fig. 3 shows the GVG obtained for a person with a limp.

The first thing that is immediately apparent in the pathologic GVG (Fig. 3) is the asymmetry in the alternating steps, along with decreased walking speed and cadence. If this asymmetry was due to prosthesis misalignment, changes could be implemented and the subject would be asked to walk again. Thus the GVG allows immediate evaluation of changes at the time of implementation.

CONCLUSION

A new low cost, portable, real-time, clinical gait analysis system, D.U.R.S. was described. It can be set up in a matter of minutes and data is available in more or less real time, allowing changes to be implemented and tested immediately. The device outputs a profile of the instantaneous forward velocity, or a gait velocigram (GVG). In addition to this graphical representation of a particular person's gait, a number of gait parameters such as: walking speed; cadence; step length; step time; and time to steady state walking can be readily computed from the GVG.

REFERENCES

Chan R.B., Childress D.S., Gait & Posture, 4(2): 175-176, 1995.

Karcnik T. et al., Proc. 4th Vienna Mt. Workshop in FES, Sept. 23-27, 48-51, 1995.

ACKNOWLEDGEMENTS

Supported by NIDRR grants H133P20016 and H133E30007.

INTERNAL EXTERNAL KNEE ROTATION AS A FUNCTION OF KNEE FLEXION FOR ACTIVITIES OF DAILY LIVING

C.O. Dyrby and T.P. Andriacchi
Department of Orthopaedic Surgery
Rush-Presbyterian-St. Luke's Medical Center, Chicago, IL 60612

INTRODUCTION

The normal function of the knee involves a complex set of coupled motions. Knee flexion has been related to internal/external rotation as well as anterior/posterior displacement of the femur on the tibia. For passive motion, the relation between flexion and rotation has been described in terms of the "screw home" movement of the knee. However, it has not been well established as to how muscle contraction may influence this kinematic coupling.

REVIEW AND THEORY

Measurement of the true three dimensional knee motion in cadaver studies (1) and in vivo studies (2,3) have demonstrated a kinematic coupling between knee flexion and rotation. However, there is a paucity of information on the activity dependence of this kinematic coupling, since cadaver studies cannot represent physiologic muscle contraction and in vivo data is limited. An understanding of how kinematic coupling between flexion and rotation varies with activity is an important for understanding normal and pathological knee function. The purpose of the study was to test the hypothesis that coupling between knee flexion and rotation are dynamically dependent on the activity.

PROCEDURES

Seventeen adults (8 female, 9 male) with no significant musculoskeletal involvement were studied. The subjects (age: 36±13 years, height: 150±10 cm., and weight: 627±134 N) performed three activities: walking at approximately 1.2 m/s, 20 cm. step-up test, and a deep squat to a resting position. A new method for in vivo studies uses a cluster of points (4,5) placed on the lower limb segments. Kinematics were measured using a previously described Point Cluster Technique. The Point Cluster Technique (PCT) is based on a cluster of light reflective markers distributed on the two lower limb segments. One cluster of ten markers was placed on the femur and a second cluster of seven was placed on the tibia to track the respective bones motion. Motion is tracked with a video based optoelectronic digitizer. Six degree-of-freedom motion of the knee was analyzed by relating a coordinate system fixed in the femoral cluster to the coordinate system fixed in the tibial cluster. Measurement were obtained bilaterally and a representative left of right trial was selected for each subject. The ranges of internal rotation were obtained and related to amount of knee flexion. Differences in range of motion were compared using a paired T-tests with a significance level of $\alpha < 0.01$.

RESULTS

There was a range of knee flexion (0 to 60°) common to each of the three activities (Figure 1). A portion of each curve between points A and B were analyzed for rotational coupling (Figure 2). The squat test shows the femur externally rotating on the tibia throughout the flexion cycle. Walking produced a general trend of the femur being more externally rotated at full extension and being more internally rotated at maximum flexion. The first few degrees of flexion show quick external rotation, then, as the knee is flexing, the femur externally rotates. Step-up shows the knee more internally rotated at the start, approximately 60° knee flexion. There were differences in the knee rotation at the same angle of flexion for each of the activities, Table 1. Significant differences were seen at a flexion angle of sixty-five between the squat and step-up and walking. No significant differences were seen between step-up and walking at the same angle.

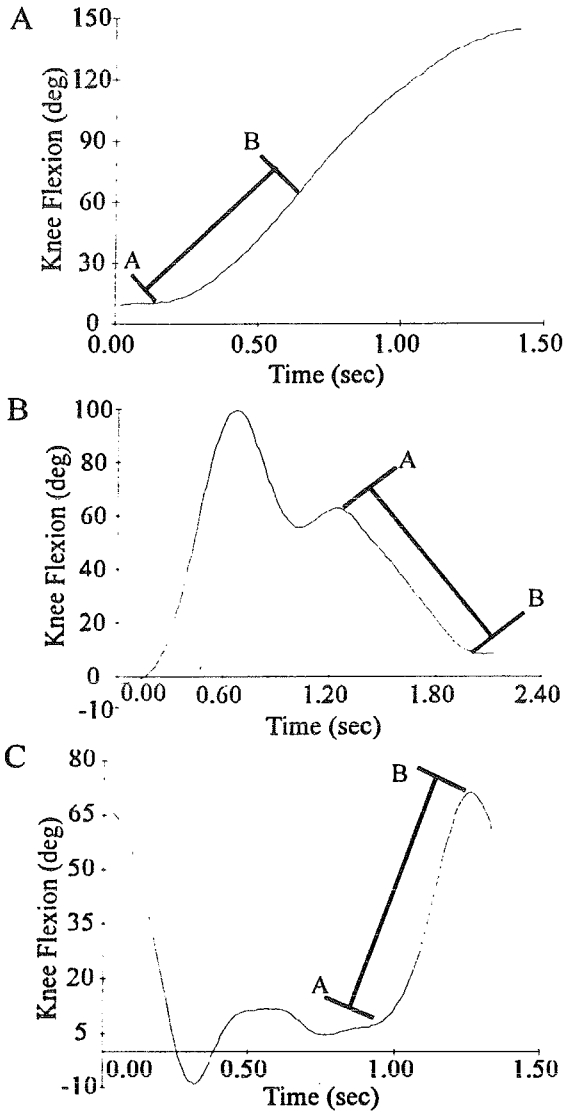

Figure 1: Graphs ofKneeFlexion. (A) Deep Squat (B) 20cm. Step-up (C) Walking. Portions A to B indicate ranges of motion under study.

DISCUSSION

The results of this study show that the coupling between internal/external knee rotation and flexion is activity dependent. Over a common range of knee flexion the femur is rotating in the opposite directions. At identical angles of knee flexion the knee is in substantially different rotational positions depending on the activity. The difference in the kinematic coupling is likely influenced by muscle contraction and the external forces acting on the leg during the different activity. Muscle activity is dominated by the concentric quadriceps contraction for the step-up test and eccentric quadriceps contraction during the squat. The final phase of walking has the hamstrings as the dominant muscle force. The influence these dynamic activity dependent factors should be considered when evaluating the functional role of the various structure of the knee.

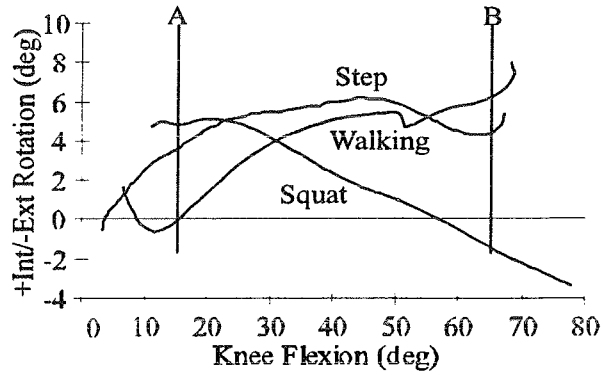

Figure 2: Internal/External Rotation versus KneeFlexion Angle

	Knee Flex Point A	Rotation Point A	Knee Flex Point B	Rotation Point B
Squat	15 (0.5)	0.0 (4.3)	65 (0.7)	-2 (6)
Step-up	15 (0.3)	4 (6)	64 (2)	5 (5)
Walking	15 (0.8)	0.6 (6)	64.5 (1)	6 (4)

Table 1: Summary of Knee Rotation at Similar Angles Note: All angles are in degrees. Standard Deviation in parenthesis.

REFERENCES

(1) More, R.C., et al. Am J of Sports Med. 21(2):231-7, 1993. **(2)** Lafortune, M.A. et al J Biomech. 25(4):347-57, 1992. **(3)** Jonsson, H. et al. J Orthop. Res. 12(6): 769-79, 1994. **(4)** Andriacchi, T.P. et al. Trans ASME 33:485-6, 1996. **(5)** Andriacchi, T.P. et al. Trans ASME 28:185-6, 1994

ACKNOWLEDGMENTS

NIH Grant # AR20702, Zimmer, Japan

QUANTIFYING TEN-HOUR LOAD BEARING ACTIVITIES IN A GROUP OF ADOLESCENT WOMEN

Jonathan B. Dingwell[1], Thomas Lloyd[2], and Peter R. Cavanagh[1]

[1] Center for Locomotion Studies, Penn State University, University Park, PA 16803
[2] Department of Obstetrics and Gynecology, Hershey Medical Center, Hershey, PA 17033

INTRODUCTION

Many applications of gait analysis require an examination of more than the single foot-ground contact that is often sampled. For example, load bearing activities (LBA's) play an important role in the development and maintenance of bone strength (Smith et al., 1989, and Chilibeck et al., 1995) but typical laboratory analysis gives no indication of cumulative loading, or of patterns of loading over the course of one or many days. This is due in large part to the lack of a convenient, accurate, and reproducible means of measuring LBA's during daily activities. A load monitoring device originally described by Breit and Whalen (1994) offers many new possibilities for long term monitoring during unrestricted activities of daily living. The first aim of the present study was to replicate this device and use it to collect continuous ground reaction force data from both feet for a ten hour period for a group of adolescent women. The second aim of this study was to use this data to quantify the daily loading patterns in these women and estimate their "daily stress stimulus" as defined by Beaupre et al. (1990).

REVIEW AND THEORY

It has been shown that decreased physical activity levels are associated with decreases in bone mineral content, and likewise that increased physical activity levels are associated with increases in bone mineral content (Smith et al., 1989, and Chilibeck et al., 1995). However, the exact nature of the relationship between long term lower extremity loading and bone remodeling is still poorly understood. Beaupre et al. (1990) defined a relationship for relative changes in ground reaction forces and "daily stress stimulus" (1) under two different conditions.

$$\frac{\Psi_2}{\Psi_1} = \left[\frac{\sum n_2 (GRF_2)^M}{\sum n_1 (GRF_1)^M} \right]^{1/M} \qquad (1)$$

Where Ψ_1 and Ψ_2 are the two daily stress stimulus values, M is an experimentally determined exponent, and n is the number of loading cycles at a given load level, GRF. It has been hypothesized that values of M between 4 and 6 represent "normal active baselines" (Whalen et al., 1988).

PROCEDURES

The Personal Force Monitoring Device (PFMD) consists of a pair of capacitative force monitoring shoe insoles and signal amplifier (Electronic Quantification, Inc.), a Tattletale microprocessor (Onset Computer, Inc.) with a four megabyte PCMCIA card for data storage, and an elastic waist belt to which these electronics are attached. The entire system is powered by four 9-volt batteries, weighs just 1.5 kg, and can be worn comfortably throughout the course of a full day's activities.

Ten hours of continuous ground reaction force data were sampled at 25 Hz from both feet of two subjects during unrestricted activities. Subject 1 was a sedentary subject, and Subject 2 was an athletic subject who ran cross-country in the afternoons. Data were downloaded from the PFMD and analyzed on a Pentium PC. To quantify the loading history for each subject, raw voltage data were converted to percent body weight (%BW), and peak force values above 15 %BW were extracted and plotted in a histogram distribution. Histograms were generated by dividing the external loads into equally spaced categories (or "bins") from 15 %BW to 300 %BW, and counting the number of peak forces that occurred within each bin. A ten hour "Stress Stimulus" measure (Ψ) was calculated for each subject according to the following equation adapted from Beaupre et al. (1990):

$$\Psi = \left[\sum_{i=1}^{k} n_i (GRF_i)^M \right]^{1/M} \qquad (2)$$

Where k was the number of histogram bins, n was the number of above threshold force peaks within each bin, and the value of M was varied from 4 to 6.

RESULTS

Each subject demonstrated distinctly different patterns of activity and distributions of peak loads over the course of the ten hour day (Figures 1 and 2). Distinct periods of activity and inactivity can be seen in the Load-Time History plots of both subjects. The increased level of forces encountered by the athletic Subject 2 compared to the sedentary Subject 1 are evident from both the Load-Time History and Peak Histogram plots.

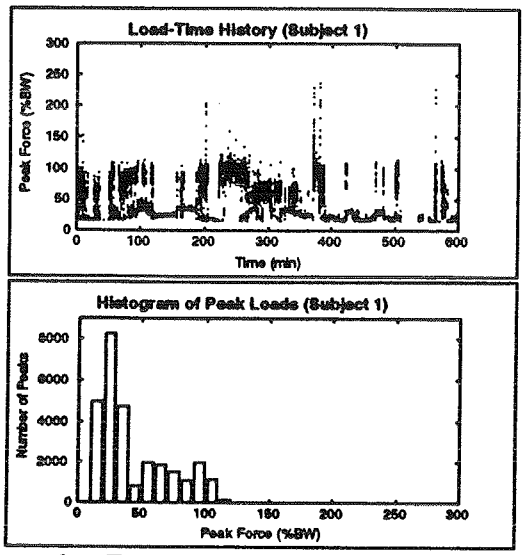

Figure 1 - Force Peaks and Peak Histogram from a 10 Hr Trial for an "Inactive" Subject.

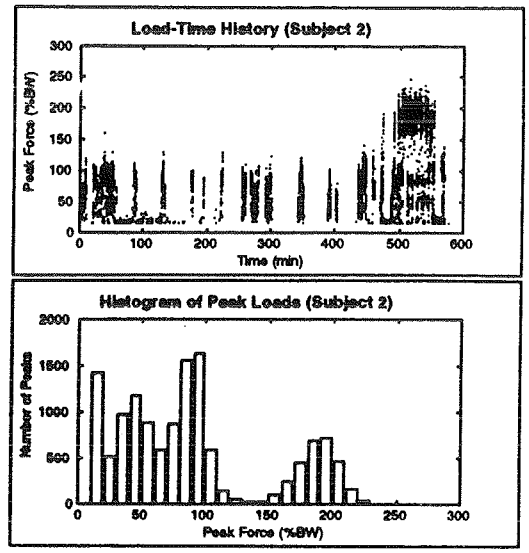

Figure 2 - Force Peaks and Peak Histogram from a 10 Hr Trial for an "Active" Subject.

While the total number of above threshold peaks was much greater for Subject 1 (33,216) than for Subject 2 (19,411), the number of force peaks greater than 125 %BW experienced by Subject 1 was only 64, compared to 2980 such peaks for Subject 2. This increase in the number of peaks at high stress levels is reflected in the 10 hr. Stress Stimulus (Ψ) values for each subject (Figure 3), where Ψ was greater for Subject 2 across all values of the exponent M despite the lower number of total force peaks.

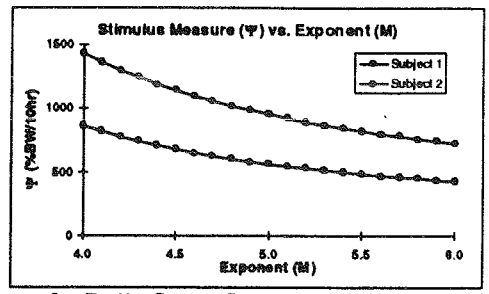

Figure 3 - Daily Stress Stimulus (Ψ) computed for exponent values (M) ranging from 4 to 6.

DISCUSSIONS

Although the PFMD is less accurate than in-ground force platforms, it can collect data during extended real life activities. Thus, data collected using this device have the potential to provide considerable insight into the mechanisms of bone remodeling. It has been hypothesized (Whalen et al., 1988, and Beaupre et al., 1990) that the response of bone to mechanical load is more a function of the magnitude than the number of peak loads. Recent evidence suggests that this theory may not be sufficient to distinguishing the daily stimulus required for bone maintenance from that required for bone remodeling (Adams et al., 1997). The large difference in higher magnitude peaks seen between these two subjects, and the subsequent differences in Ψ values would allow these hypotheses to be tested in groups of subjects with diverse profiles of physical activity. This would represent an important step in gaining a better understanding of the relationship between lower extremity loading and bone remodeling.

This information is important for understanding the role of daily activity in the acquisition of bone early in life, which is believed to be important for preventing osteoporosis later in life (Johnston et al., 1992). It is also important for understanding the relationship between daily loading patterns and bone loss that occurs in the weightless environment of space (Whalen et al., 1988, Beaupre et al., 1990), or the development of stress fractures in at risk populations such as athletes of military recruits (Grimston et al., 1991). The exploration of these and other conditions appears to be within the realm of the PFMD.

REFERENCES

Adams et al., *J. of Biomech.*., In Press, 1997.
Beaupre GS et al., *J. of Orthop. Res.*, 8: 651 - 661, 1990.
Breit GA and Whalen RT, *Proc. of the 18th Ann. Meeting of the Amer. Soc. of Biomech.*, Ohio State U., pp. 231 - 232, 1994.
Chilibeck PD et al., *Sports Medicine*, 19: 103 - 122, 1995.
Grimston S et al., *Intl. J. of Sports Biomech.*, 7: 293 - 309, 1991.
Johnston CC et al., *Osteoporosis Intl.*, Suppl. 1: S54-S55, 1992.
Smith EL et al., *Bone and Mineral Res.*, 6: 139 - 173, 1989.
Whalen RT et al., *J. of Biomech.*, 21 (10): 825 - 837, 1988.

EFFECTS OF GLOVES ON MAXIMUM FORCE AND THE RATE OF FORCE DEVELOPMENT IN WRIST FLEXION AND GRIP

Nikitas Tsaousidis[1] and Andris Freivalds[2]
[1]Biomechanics Laboratory, and [2]Dept. of Industrial & Management Systems Engineering,
The Pennsylvania State University, University Park, PA 16802, USA

INTRODUCTION

Gloves are widely used in industry and affect the mechanics of force and torque production. Among the most common industrial tasks are grip, and torque production with wrist flexion. Understanding the mechanics of gripping and wrist flexion is necessary in order to reduce the incidence of cumulative trauma disorders (CTD). The objective of this study was to investigate these tasks by creating force development profiles and by finding the effect of gloves on maximum force and the rate of force development.

REVIEW AND THEORY

Studies on the use of gloves (Hertzberg, 1955; Cochran et al., 1986) have showed that they may lead to significant reductions (15-20%) in the maximum force that can be exerted. The reasons for the drop in grip strength when gloves are worn are not clear. Cochran et al. (1986) suggested that the reasons are "interference of the glove in closing the hand around objects, the possible decreased friction between the glove and object, and the interference of the glove in tactile feedback".

The accumulated evidence that use of gloves reduces maximum grasp force raises the question of whether similar reductions occur in twisting. Two studies that looked into wrist torque production found that gloves have a positive effect on maximum torque (Riley et al., 1985; Mital et al., 1994).

A second question that has not been addressed at all is how wearing gloves affects the rate of force development. A reduced rate of force development would mean either that the response time of the workers is reduced (slower performance), or that in order to avoid the performance deterioration the workers resort to increased levels of muscle activation (higher risk of injury).

PROCEDURES

Subjects: Fifteen healthy college students (twelve male and three female) volunteered for this study. All participants were right-handed.

Procedure: The subjects were asked to perform —with their self-reported dominant hand— three maximum effort trials for every task (grip, wrist flexion, and the 'dual' task which was a combination of wrist flexion and grip) with and without glove, in random order. Subjects were asked to start from an initial state of relaxation, develop their maximum force as fast as possible and maintain it. However, reaction time was not to be minimized, the emphasis was solely on maximum force and the rate of force development. In the 'dual' task the instructions were to try to produce both maximum grip and wrist torque.

Apparatus: A leather glove without lining was used in the experiments.

(a) Grasp force: The apparatus for the grasping task consisted of a handle wrapped around by tubing. The diameter of the cylindrical handle —with the tubing— was 4.5 cm. The liquid-filled was closed on one end, on the other it was connected to a pressure transducer.

(b) Wrist flexion (twisting): The apparatus was the same handle that was used for the grasp force measurements, connected to a torque transducer.

Data collection and analysis: The sampling rate was 200 Hz and the data were low-pass filtered at a 20 Hz. The following variables were examined: (a) maximum value, and (b) rate of force or torque development for the following parts of the data - time curve: 0 to 30%, 0 to 50%, 0 to 90%, 30 to 70%, and 50 to 90% of maximum force or torque. For instance to calculate the rate of force development in the '0 to 50%' period the maximum force of the particular trial was multiplied by 0.5 and divided by the time it took to reach 50% of the maximum force.

RESULTS

The data suggest that in all tasks and conditions the time to reach the maximum strength was approximately double the time to reach 90% and three to five times the time to reach 70%.

Grip: The results of the t-tests for the grip task reveal a strong negative effect of glove wearing for all variables. Maximum force dropped by 15% while the reductions in the rate of force development ranged from 24% to 38%. The p-values show a statistical significance (a=0.05) except the rate of grip force development in the intervals 0 to 30%, 0 to 50% and 0 to 70% of the peak value.

Wrist flexion: The main focus of that task was torque production but since grip pressure was also produced in the process, both variables were examined in an effort to see how their combination relates to performance.

(a) Torque: None of the results was statistically significant. The data show there was no change in performance when gloves were worn.

(b) Grip pressure during wrist flexion: Interestingly these results are very similar to those obtained in the grip task. Once again, the effect of wearing gloves is negative, both for maximal grip force and many aspects of the rate of its development (particularly in the late stages of development).

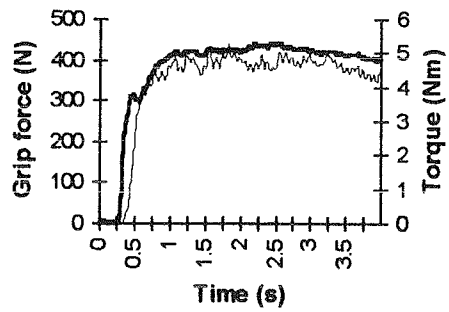

Fig. 1: Grip force (thick line) and torque (thin line) in sample 'dual' task trial.

'Dual' task (wrist torque and grip combination): Figure 1 shows a sample trial of the 'dual' task. The effect of gloves was negative and concentrated primarily in the grip components of the task. In contrast, wrist flexion torque results in the 'dual' task showed no significant change.

DISCUSSION

The maximum grip force results, that showed a decrease in the gloved condition, are in agreement with the published literature (Cochran et al., 1986; Sudhakar et al., 1988). The highest rate of force development appeared in 30 to 70% period. It was interesting to record that wearing gloves leads to significant deterioration in the rate of grip force development. This deterioration could contribute to loss of performance and/or increased risk of injury. The drop in the rate seems to be concentrated in the late phases of exertion. In essence the only period unaffected by gloves is the first one (0 to 30%) and after that, the rate of grip force development starts to suffer. It is possible as compression forces on the glove increase, more and more of the work done by the hand is stored as elastic energy in the glove material and its creases.

Torque production was unaffected by gloves. As far as peak torque is concerned, this contradicts the findings of Riley et al. (1985) and Mital et al. (1994) who recorded improvements in peak magnitude as a result of wearing gloves. However, the differences can be attributed to slippery handles used by Riley et al., or to calibration differences in Mital et al. Grip force during torque production followed a very similar pattern to grip force in the dedicated grip task. This seems to imply that, although grip is a prerequisite for torque, the two variables, torque production and grip, are controlled independently by the central nervous system, at least in the task under examination in this study. For instance, even in the 'dual' task where equal emphasis was placed on the two tasks, torque development was much faster than grip force development especially in the periods up to 70% of maximum.

REFERENCES

Cochran, D.J., et al. Proc. of Human Factors Soc., 30th meeting, 1986.
Hertzberg, T. Annals of NY Acad. of Sc., 63, 621-23, 1955.
Mital A., et al. Ergon., 37, 333-43, 1994.
Riley, M.W., et al. Ergon., 28, 441-47, 1985.
Sudhakar, L.R., et al. Proc. of the Human Factors Soc., 32nd meeting, 1988.

EFFECTS OF TRAINING ON JOINT AND HANDRIM KINETICS IN WHEELCHAIR USERS

MM Rodgers, PJ Russell, RE Keyser, JA Parker, PH Gorman
University of Maryland, School of Medicine, Departments of Physical Therapy and Neurology, and VA Maryland Health Care System, Physical Medicine and Rehabilitation Service, Research & Development Services, Baltimore, MD

INTRODUCTION

Overuse injuries are an impediment to basic function for manual wheelchair users and may be facilitated by adaptations in muscle strength that result from longterm manual wheelchair use. The purpose of this study was to determine if wheelchair propulsion mechanics can be changed by an exercise intervention designed to reduce the risk of overuse injuries.

REVIEW AND THEORY

The reliance of wheelchair users on their upper-body musculoskeletal system and the repetitiveness of the stroke pattern predisposes them to overuse injuries at the shoulder, elbow, and wrist. Wrist and hand overuse injuries often result in inflammation of the tendons. Most shoulder injuries stem from muscle imbalance, inflexibility, poor technique, and/or overuse (Olenik, et al., 1995). Such injuries often involve stretch weakness, resulting from the prolonged elongation of the inadequately developed opposing muscles. Kibler, et al. (1992) advocated a preventive exercise program to stretch the muscles most likely to be overdeveloped and strengthen the muscles most likely to show stretch weakness. In wheelchair users, the anterior upper body musculature is most likely to need stretching and the posterior upper body musculature is most likely to need strengthening. Results from our earlier work (Rodgers, et al., 1994) suggested that a therapeutic exercise intervention specifically designed to stretch and strengthen these muscle groups may possibly reduce the risk of overuse injuries.

PROCEDURES

After medical screening, the propulsion mechanics of 15 wheelchair users were measured at a standard velocity of 3 km/hr during a submaximal exercise test. A prototype wheelchair ergometer with instrumented handrims for three dimensional (3-D) handrim force and moment measurement was used to collect these data. The wheelchair measurement system included three Peak 3D CCD cameras (Peak Performance Technologies, Colorado Springs, CO), a VCR/monitor assembly, an image processing unit, a 3D force/torque transducer, a potentiometer, an amplifier, an analog-to-digital unit, and a PC. The wheelchair ergometer was instrumented with a PY6-4 six-component force/torque transducer (Bertec Corp., Worthington, OH) in its wheel hub to detect handrim forces and moments. The Bertec force/torque transducer uses bonded strain gages to measure forces and moments in three dimensions (six channels). This transducer has a maximum torque (Mz) capacity of 150 Nm and a maximum plane-of-wheel force (Fx and Fy) capacity of 3500 N. Those capacities correspond to a gain setting of unity, and the maximum usable range can be set by user selected gains. The full scale output of the transducer is $\pm$ 10 V. A potentiometer monitors the angular position of the wheel, transducer, and handrim assembly.

A three-dimensional linked segment model was used to study wheelchair propulsion. This model assumed the arm to be three rigid segments (hand, forearm and upper arm) connected by the wrist, elbow and shoulder joints. Three dimensional motion analysis data (collected at 60 Hz) and 3-D handrim contact forces and moments (collected at 360 Hz) were collected using the 3-D motion analysis system, that included an instrumented wheelchair, video cameras and a data acquisition system. The linear displacements of markers placed on joints were measured and differentiated to obtain movement kinematics. Joint kinetics were calculated by using an inverse dynamics approach that employed the Newton-Euler method based on body coordinate systems (Rodgers, et al., in press).

Motion analysis and force data were collected during submaximal exercise tests to fatigue which were performed before and after six weeks of training. Training was conducted three times a week and included stretching for anterior shoulder and trunk muscles, strengthening with free weights for posterior shoulder and trunk muscles, and aerobic exercise using a rowing machine adapted for wheelchairs. Kinetic data were averaged over three cycles (contact to contact) and compared before and after training using paired t-tests. The 0.05 level was used for significant findings.

RESULTS

Handrim kinetic changes with training were reflected in a 17.4% (-18.26 ± 4.09 Nm to -22.11 ± 6.21 Nm) increase in the peak propulsive moment (Mz). There were also significant increases in peak joint moments at the wrist, elbow, and shoulder following training (Figure 1). At the wrist joint there was a 14.4% increase in the ulnar deviation moment. The extensor moment at the elbow increased by 16.9% and the flexor moment at the shoulder increased by 13.6%. Peak joint reaction force changes at the wrist included a 14.5% decrease in the shear force in the radioulnar direction and a 7.6% increase in the compressive force (Figure 2). The anteroposterior shear forces increased 15.8% at the elbow and 14.3% at the shoulder (Figure 3).

DISCUSSION

Comparison of results with others is complicated by differences in instrumentation, wheelchair velocity, resistance levels, kinetic models, and sample composition (e.g., wheelchair dependent users or able-bodied individuals). However, the range of handrim and joint force and moment magnitudes are generally comparable to results from Robertson et al. (1996) and Veeger et al. (1991).

The increase in handrim propulsive moment (Mz) indicated a positive training effect. More torque was applied towards turning the wheel. The increase in joint moments showed an improved ability to generate effective torque on the wheel. The joint reaction force changes at the wrist indicated improved ability in transmitting forces. The increased shear forces at the elbow and shoulder may have resulted from increased joint moments. Initial findings suggested that specific training for wheelchair users improved wheelchair propulsion mechanics and decreased the probability of overuse injuries. Further investigation of joint kinetic changes is continuing.

REFERENCES

Kibler WB, et al., *Ex Sport Sci Rev.* 20:99-126, 1992.

Olenik, et al., *Paraplegia.* 33:148-152, 1995

Robertson R. et al., *Arch Phys Med Rehabil,* 77:856-64, 1996.

Rodgers M. et al., *Arch Phys Med Rehabil,* 75:85-93, 1994.

Rodgers M. et al., *J Appl Biom,* in press.

Veeger, H. et al., *J Electromyogr Kinesiol,* 1:270-80, 1991.

ACKNOWLEDGMENTS

Supported by the Office of Research and Development, Rehabilitation Research and Development Service, Department of Veterans Affairs, Washington, DC 20420 (B92-465A).

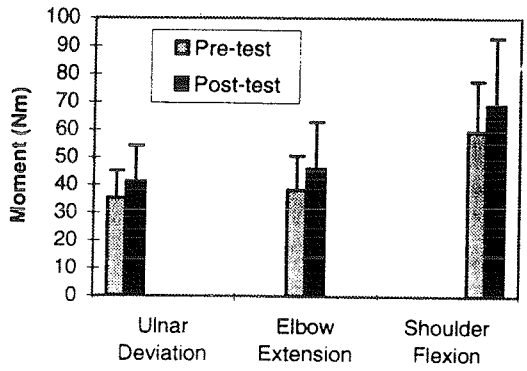

Figure 1. Joint moment changes with training.

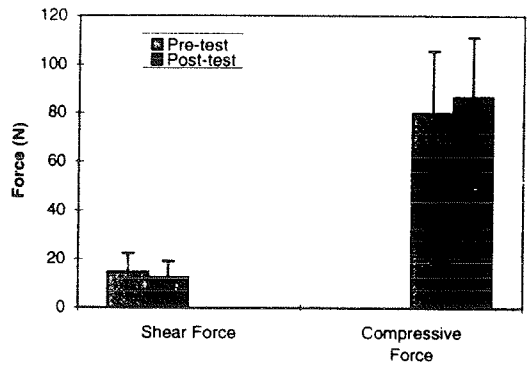

Figure 2. Wrist joint reaction force changes with training.

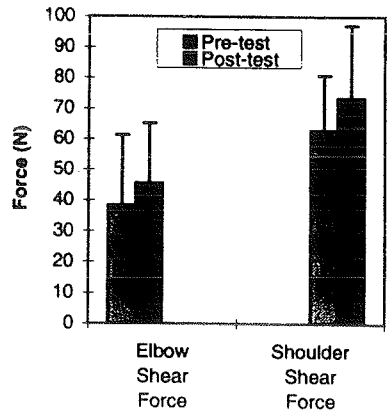

Figure 3. Elbow and shoulder anterior-posterior joint reaction force changes with training.

A KINEMATIC ANALYSIS OF OBSTACLE CLEARANCF STRATEGIES IN NORMAL GAIT

T. Thomas, M. Tillman

Department of Exercise and Sport Sciences, University of Florida, Gainesville, FL 32611

INTRODUCTION

Two distinct strategies have been identified for clearing obstacles in the path of gait. The purpose of this study was to determine which strategy is used by normal individuals while stepping over obstacles.

REVIEW AND THEORY

Walking is a familiar cyclic activity. Despite its apparent simplicity, walking has been scientifically studied for years. Most studies have been concerned with studying normal gait and identifying pathological gait. However, one's gait constantly changes (Grieve, 1969) because it must accommodate for the demands of various environments. The surfaces we normally walk on are not the same flat surfaces present in a gait lab. They are filled with obstacles that alter our gait. When faced with an obstacle in our path, we have one of two options: go around it by changing direction or go over it by modifying limb trajectory (Patla et al., 1991). Both techniques are effective for avoiding obstacles, but the present work focuses on strategies used for going over obstacles.

Little is known about how humans avoid tripping or stepping on obstacles (Chen et al., 1991). Tripping occurs when the toes of the swing leg contact some object during gait. This disturbs the gait pattern and if severe enough will cause a fall. Falls are potentially dangerous for people of all ages. Patla et al. (1991) has identified a pair of strategies for stepping over obstacles: upward bias to the swing-limb trajectory and elevation of the swing limb. The first strategy is characterized by an unchanged limb trajectory accompanied by an elevation of the body. The second strategy is characterized by an alteration of the swing limb trajectory. The purpose of this study was undertaken to determine if, based on Patla's suggestions, normal healthy adults change their strategies according to the height of the obstacle that must be stepped over.

PROCEDURES

Eighteen healthy individuals (2 females, 16 males) participated in the obstacle clearance study. The average age of the participants was 25.4±7.1 years and their average mass was 74.9±11.0 kg.
To assess obstacle clearance quantitatively, a reflective marker was placed on the lateral side of the right shoe, at the location of the 5th toe. An RCA video camera was used for data collection. The video data were collected at 30 Hz and were analyzed using the PEAK Video Illustrator™. The three obstacles were constructed from ordinary plywood. Each obstacle was 1.6cm in width and 56cm in length. They were prepared in three different heights: 2cm, 8cm, and 16cm. The heights were selected to correspond to the approximate heights of a door threshold, a small toy, and a sidewalk curb respectively. The obstacles were color contrasted to the floor and therefore were easily seen. A video camera was placed perpendicular to the line of motion and parallel to the line of the obstacle providing a sagittal view of the movement. A high intensity lamp was positioned next to the camera to illuminate the reflective shoe marker (see Figure 1). The camera and lamp were 7.3m from the line of motion. The obstacles were placed in the middle of a flat level 5.5m runway.

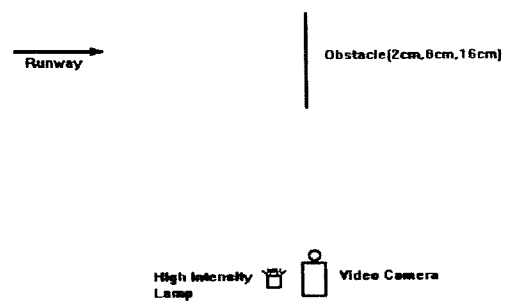

Figure 1: Experimental setup.

Three trials were performed by each subject at each of the three heights. The order that the obstacles appeared in was randomized using a Latin Square design.

The PEAK Video Illustrator™ was used to determine obstacle clearance height and the angle of

ascent during clearance. To measure angle of right foot ascent, the path of the 5th toe was traced from right foot contact before clearance to right foot contact after clearance. The path was divided into 16 distinct points and the slope was measured at the steepest part of the ascending portion of the curve. The toe was chosen for digitizing because tripping over an obstacle usually begins with an unexpected toe strike (Chen et al., 1991).

RESULTS

All participants successfully cleared all obstacles during testing without contacting or tripping on the obstacles. The trajectory of the 5th toe of each participant was manually digitized using the Peak Video Illustrator™. Average trajectories for the 3 obstacle heights appear in Figure 2. Two values were calculated from the trajectory of the toe: slope of the path and clearance height over the obstacle. Both values were collected for the swing leg during obstacle clearance. The second trial for each subject performing each condition was analyzed. The slope was analyzed to determine whether the swing limb trajectory was altered for the different obstacles. The steepest slope during the ascent phase of the trajectory was selected for analysis. The portion of the curve with the highest slope value occurred immediately after the foot left the ground for most trials. A one-way analysis of variance was used to detect any possible differences among the slopes for the 3 obstacle heights. No significant difference was detected ($p>0.05$).

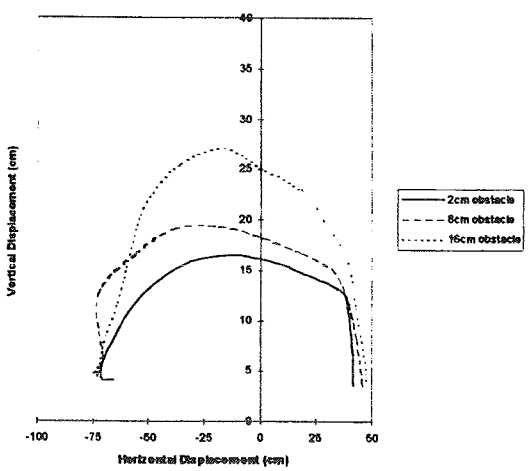

Figure 2: Toe trajectories.

Clearance height above the obstacle was also calculated. A one-way analysis of variance was used to detect any possible differences among the clearance heights for the 3 obstacle conditions. A significant difference was detected ($p<0.05$). Post hoc analysis was performed using a Student Newman-Keuls test. Clearance heights were significantly different ($p<0.05$) between the 16cm obstacle and the 8cm obstacle as well as the 16cm and 2cm obstacles. There was no significant difference ($p>0.05$) between the 8cm and 2cm clearance heights.

DISCUSSION

It appears that the subjects tended toward the first strategy of higher swing limb elevation in response to an obstacle in the path of gait (Patla et al., 1991). This idea is supported by the lack of a significant difference in initial 5th toe trajectory slope. Differences in slope were not detected thereby suggesting that test participants did not change their swing limb trajectories, but merely elevated the same basic trajectory higher with increases in obstacle height. However, it should be noted that the mean initial slopes showed an increasing trend with increasing obstacle height.

The significant difference among clearance heights for the three obstacle heights is another interesting result. The largest clearance is demonstrated for the 16cm obstacle while the smallest clearance is demonstrated for the 2cm obstacle. This seems to be in agreement with the work of Chen et al. (1991). This result suggests obstacle clearance strategies become more conservative with increased obstacle height.

The choice of the first strategy could not have been easily predicted. People will tend to choose a more economical strategy for clearing obstacles when they are fully aware of planning and execution time available for gait adjustments. This infers that participants in this study should have chosen the second strategy for the conservation of energy. The laboratory setting and knowledge of video taping could have encouraged the participants to choose a more conservative strategy at some increased physiological cost.

REFERENCES

Grieve D.W. Physiotherapy, 56, 452-460, 1969.
Patla A.E. et al. J Exp Psych, 17(3), 603-634, 1991.
Chen H.C. et al. J Geron, 46(6), 196-203, 1991.

MECHANISMS BY WHICH PATIENTS WITH ANTERIOR CRUCIATE LIGAMENT DEFICIENCY GENERATE THE "QUADRICEPS AVOIDANCE GAIT"

R.R. Patel*, D.E. Hurwitz, T.P. Andriacchi, C.A. Bush-Joseph and B.R. Bach, Jr.

Department of Orthopedic Surgery, Rush-Presbyterian St.Luke's Medical Center, Chicago, IL 60612
* Department of Bioengineering ,University of Illinois, Chicago, IL 60612

INTRODUCTION AND THEORY

Past studies have shown that subjects with anterior cruciate ligament deficiencies (ACLD) alter the manner in which they walk. Normal subjects have an external knee flexion moment during midstance (biphasic gait) while ACLD patients often have a decrease in the external knee flexion moment at midstance (1). In addition, some ACLD patients never achieve an external knee flexion moment during midstance. This type of gait has been referred to as the "Quadriceps Avoidance Gait". It is thought that this adaptation may provide a means for stabilizing the knee. A decreased external knee flexion moment during midstance would be reflective of decreased quadriceps forces or increased hamstring forces. If the quadriceps forces were decreased, this would minimize the anterior pull of the tibia near full extension and may therefore stabilize the knee. While the "Quadriceps Avoidance Gait" has been identified, it remains unclear how subjects generate this type of gait. The purpose of this study was to identify mechanisms used when walking with a "Quadriceps Avoidance Gait".

PROCEDURES

First, a group of 19 ACLD patients (15M, 4F; 29±7 years) who all had a "Quadriceps Avoidance Gait" on their affected side were identified from a much larger group of previously tested ACLD patients. Second, a group of ACLD patients (14M, 5F; 31±7 years) with a biphasic gait were identified such that their age, gender and time since injury were similar to the ACLD group with the "Quadriceps Avoidance Gait". The average time since injury for the two ACLD groups was (66 ±81) months. A group of 19 normal subjects (age and gender matched) with a biphasic gait were also identified.

Lower extremity joint positions and ground reaction forces were measured with an optoelectronic system and force plate as subjects walked at 3 self selected speeds of slow, normal and fast (2). Inverse dynamics was used to calculate the lower extremity kinetics. All external moments were normalized to percent body weight multiplied by height (%Bw*Ht). To minimize the effect of walking speed on the associated kinetics, a representative trial at about 1.0 m/sec was chosen for analysis. The average walking speed for the three groups was 1.0 ± 0.1 m/sec ($p > 0.32$). Differences between the three groups were identified using an ANOVA with a bonferroni correction for multiple comparisons. A significance level of $\alpha < 0.05$ was used.

RESULTS

Those patients with a "Quadriceps Avoidance Gait" walked with a significantly decreased midstance knee flexion angle and a significantly increased peak external hip flexion moment as compared to both the ACLD group with a biphasic gait ($p < 0.001$, $p < 0.001$) and the normal group ($p < 0.001$, $p < 0.01$) (Figure 1). The external hip flexion moment is the peak that occurs after that of heelstrike. In the ACLD group with a "Quadriceps Avoidance Gait" the midstance knee flexion angle was significantly correlated with this peak external hip flexion moment ($p < 0.001$) (Figure 2).

The external knee flexion moments during midstance for the ACLD group and normal group with a biphasic gait were not significantly different (2.0±1.0 %Bw*Ht) ($p > 0.53$).

Similarly, the midstance knee flexion angles and external hip flexion moments for the two groups were not significantly different ($p > 0.77$, $p > 0.92$).

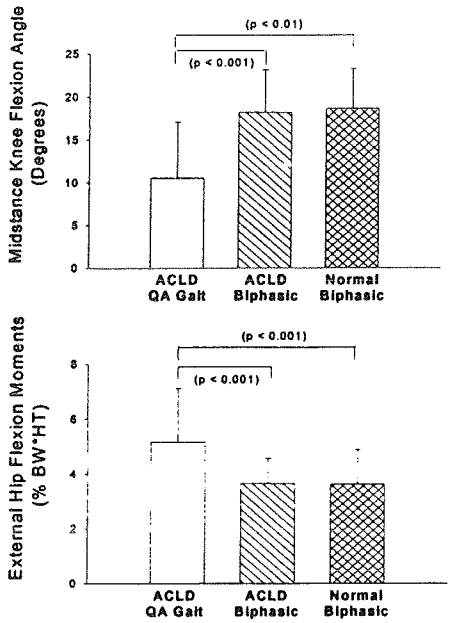

Figure 1: The midstance knee flexion angle and external hip flexion moment were significantly different in the ACLD group with the "Quadriceps Avoidance Gait" (QA Gait) as compared to the other two groups with a biphasic gait.

DISCUSSION

This study demonstrated that there are two mechanisms for generating a "Quadriceps Avoidance Gait". The first mechanism was to reduce the midstance knee flexion angle. The second mechanism may have been to lean forward during midstance. The increased external hip flexion moment was interpreted to be reflective of a forward lean.

The correlation between the midstance knee flexion angle and external hip flexion moment seems to indicate that the two mechanisms were related to each other. Hence, some patients achieved their "Quadriceps Avoidance Gait" by greatly decreasing their midstance knee flexion angle and did not need to increase their external hip flexion moment. The converse was also true. However, many patients employed a combination of both mechanisms. By decreasing the amount of knee flexion or by leaning forward during midstance, the net demand on the quadriceps is reduced. This decreased net demand on the quadriceps would help maintain knee stability.

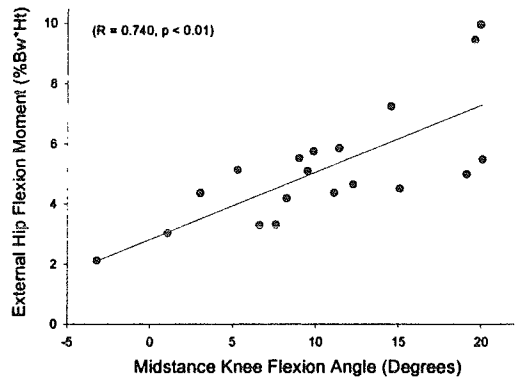

Figure 2: The midstance knee flexion angle and external hip flexion moment were significantly correlated for the ACLD group with the "Quadriceps Avoidance Gait"

REFERENCES

(1) Berchuck M et al.: *Journal of Bone and Joint Surgery*, 72A: 871-877, 1990.
(2) Andriacchi et al.: NATO ASI E:83-102, 1985.

ACKNOWLEDGMENTS

National Institutes of Health Grant AR39432

MODEL FOR PRODUCING TRIPPING OF THE TRAILING FOOT ON AN OBSTACLE

Louis F. Draganich and Li-Shan Chou

Section of Orthopaedic Surgery and Rehabilitation Medicine, Department of Surgery
The University of Chicago, Chicago, Illinois

INTRODUCTION

Falls are a serious problem in the elderly. A model was developed for producing tripping of the trailing limb on an obstacle. The differences in motion of the "tripping" limb between successful and failed attempts was investigated using this model.

REVIEW AND THEORY

The costs for acute care associated with fractures resulting from falls are estimated to be $10 billion annually (Satin, 1992). Most falls by elderly persons occur during activities such as walking or changing position (Ashley et al, 1977) and tripping or tripping over an obstacle is among the most reported causes of falls (Blake et al, 1988; Campbell et al, 1990; Tinetti and Speechley, 1989). Incidences of tripping in the laboratory during studies of obstacle crossing have been reported (Chen et al, 1994; Patla et al, 1991). However, tripping was not consistently produced in these studies. The purposes of the present study were to develop a model for producing tripping of the trailing limb consistently but unintentionally on an obstacle and to investigate the differences in motion of the "tripping" limb between successful and failed attempts.

PROCEDURES

Gait analysis was performed on fourteen healthy young adults (7 males, 7 females) having a mean age of 23 years (range, 19 to 32 years). Subjects wore their own low-heel shoes. Three sets of experiments were performed. For each experiment subjects walked along a 9.5 m walkway at their comfortable, self-selected speeds. In the *first* experiment, each subject's average step length over several strides was measured. In the *second* experiment, the subject was instructed to walk along the walkway and step over an obstacle (white elastic band 1 mm thick and 6 mm wide) of 51, 102, 153, or 204 mm height (2, 4, 6, or 8 inch height) in his/her usual self-selected manner. To do this, the obstacle was placed at a fixed location. The subject's beginning position was adjusted until with practice the subject had established a comfortable gait and the toe of the trailing foot landed within ±5 cm of a marker before lifting to step over the obstacle. This beginning position was used in the third experiment. For the *third* experiment the average step length for the subject found in the first experiment was used to compute lengths of 10, 20, 30, and 40% of step length. The obstacle of each height was selected randomly and placed randomly at these distances from (and beyond) the marker. The subject was instructed to maintain the stride attained in the second experiment until heel-strike of the trailing foot just prior to stepping over the obstacle and then to step over the obstacle as usual. Thus, the distance from the toe of the trailing foot (during stance of the trailing foot just before stepping over the obstacle) to the obstacle was controlled. Three trials were accepted for each combination of obstacle height and distance when the trailing foot was $< \pm 5$ cm from the marker. Tripping was defined as contact with the obstacle. Motion data were collected with a two camera Watsmart digitizing system at a rate of 100 Hz. The average RMS accuracy of the system was better than 5 mm. Clusters of six or eight infrared light-emitting diodes were attached to the foot, shank, thigh, and pelvis of the left lower limb with elastic straps. Foot switches indicated heel contact. Temporodistance data were analyzed for the crossing stride of the trailing limb, from heel-contact just before crossing the obstacle to the next heel-contact just after crossing the obstacle. Hip, knee, and ankle flexion of the trailing limb were analyzed for the 204 mm high obstacle at the various distances when the toe was directly over or under the obstacle. Paired t-tests were applied at the $\alpha \leq 0.01$ level to compare angles at 10%, 20%, and 30% of step length.

RESULTS

Twelve of the 14 subjects (86%) tripped on the 8 inch high obstacle with the trailing limb at a distance of 10% of step length (Figure 1). Only 1 subject (7%) tripped on the 6 inch high obstacle at 20% or 30% of step length. Obstacle contact with the leading limb did not occur. Flexion of the knee was greater for the successful than for the failed

crossings, ranging from 5° at the 20% distance to 10° at the 10% distance (Figure 2). The difference for the 10% distance was significant ($p = 0.01$). Trends towards significance were found for the 20% and 30% distances ($p = 0.06$ to $p = .2$). Flexion of the hip was up to 5° greater for the successful than for the failed crossings (Figure 3). Trends towards significance were found for the 10% and 30% distances ($p = 0.04$ to $p = 0.1$). The ankle was dorsiflexed at the 10% and 20% distances and plantarflexed at the 30% and 40% distances (Figure 4). Ankle Flexion was 10° greater for the successful than for the failed crossing at the 10% distance. The difference was significant ($p = 0.004$). The crossing speeds for the successful and failed crossings were nearly identical, ranging from 1.07 to 1.17 m/s, depending on the distance.

DISCUSSION

We developed a physical model for producing a high rate of contact of the trailing foot with an obstacle, representing tripping, when attempting to step over the obstacle. The rate of tripping was dependent upon both the distance between the obstacle and the trailing foot during stance as well as the height of the obstacle. As might be expected, the closer and higher the obstacle the greater the rate of tripping. The results of this pilot study demonstrate that the knee and ankle and probably the hip are all challenged at the 10% distance. The knee is also likely challenged at the other distances investigated as suggested by the trends. The requirements for hip flexion are less clear at the other distances. The ankle appears not to be challenged as the distance from the stance position of the trailing foot to the obstacle increases beyond the 10% to 20% distance. We are currently increasing our sample size and also testing elderly subjects to better address the effects of these and other factors on tripping.

REFERENCES

Ashley et al: Age Ageing 6:211-220, 1977
Blake et al: Age Ageing 17:365-372, 1988
Campbell et al: Age Ageing 19:136-141, 1990
Chen et al.: J Gerontol 49: M227-233, 1994
Patla et al.: J Exp Psych 17: 603-634, 1991
Satin: Annu Rev Public Health 13:489-508, 1992
Tinetti, Speechley: N Engl J Med 320:1055-1059, 1989

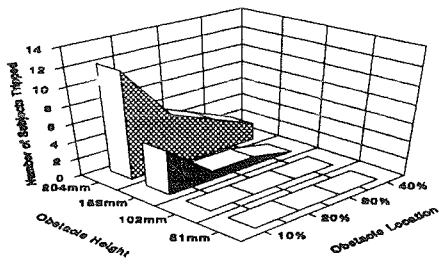

Figure 1: Number tripping among 14 healthy young subjects.

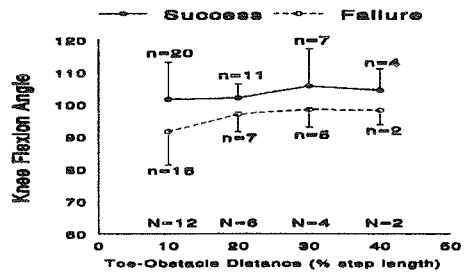

Figure 2: Knee flexion for successful and failed crossings. In this and the following figures, the means (+ or -1 SD) are reported. N = total # of subjects tripping and n = total # of tripping occurrences. For each subject who tripped, the results for two successful or failed trials were averaged and the average was used in computing the mean.

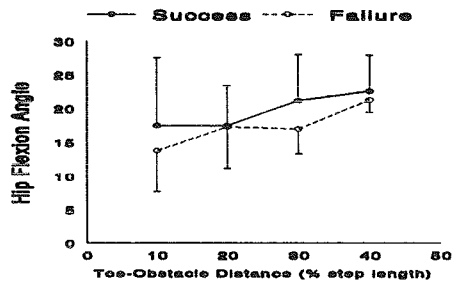

Figure 3: Hip flexion for successful and failed crossings.

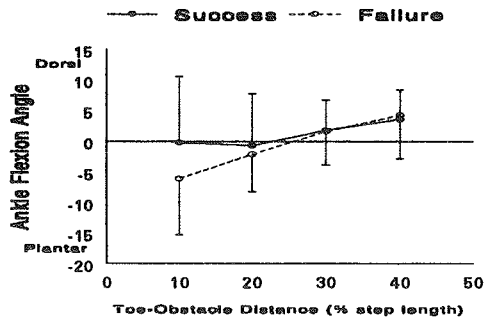

Figure 4: Ankle flexion for successful and failed crossings.

KINEMATIC AND KINETIC STRATEGIES AFTER LIMB SALVAGE PROCEDURE

T. Dang[1], M. Brown[1], J. Carter[1], M. Malawar[2]
[1]Rehabilitation Engineering. Dept., National Rehabilitation Hospital, Washington, DC 20010
[2]Orthopaedic Oncology, Cancer Inst. at Washington Hospital Center, Washington, DC 20010

INTRODUCTION

Limb sparing surgery for distal femoral osteosarcomas is a surgical procedure that provides an alternative to above knee amputation and involves resection of the bony tumor and surrounding soft tissue. The bone is subsequently replaced by a endoprosthesis and radical muscle transfers are performed to restore function and provide soft tissue coverage for the prosthesis.

The procedure results in alterations in muscular anatomy which may be associated with functional limitation and disability. A functional limitation is an unexpected restriction in the effective use of an organ or an organ system, while a disability is an unexpected restriction in the performance of a functional task (National Center for Rehabilitation Research, 1993). A common functional limitation associated with limb sparing procedures is the loss of strength in one or more muscle groups.

There is evidence that suggests individuals can compensate for muscular weakness through the use of adaptive biomechanical strategies (Pedotti, 1977; Siegel, 1993). If the parts of the body are defined as segments (e.g. foot, shank, thigh, pelvis, trunk, etc.), then a biomechanical strategy is the series of segment positions and intersegmental moments (rotational forces) that is coordinated by the central nervous system in order to allow an individual to perform a functional task. Each biomechanical strategy has a kinematic component (segment positions) and a kinetic component (intersegmental moments).

THEORY

The purpose of this investigation was to identify the adaptive biomechanical strategies that best correlate to functional outcome measures as defined by the MSTS evaluation protocol for limb sparing procedures.

PROCEDURES

A group of fifteen subjects with good functional outcomes (MSTS >20) were studied two to five years postoperatively, after the rehabilitation process was complete and gait patterns and function appeared to be consistent over time. Biomechanical gait evaluations were performed on each subject using a four camera VICON motion analysis system, two AMTI force platforms, an eight channel EMG telemetry system, and a PC workstation. All of the biomechanical data was collected using a unilateral laboratory setup. A minimum of three trials was collected for each side of the lower extremity. The data was processed using a PC workstation which uses PC-AMASS (ADTECH, Inc.) for the 3-D reconstruction and MOVE3D (a software package developed at the National Institutes of Health, Bethesda, MD) for inverse dynamics calculations. A one way ANOVA was used to compare the average

intersegmental angles and moments generated by the affected limbs during level over ground ambulation to those generated by the unaffected limbs.

RESULTS

The average intersegmental ankle (dorsiflexion +), knee (extension +), and hip (flexion +) angles generated by the affected limbs during the stance phase of gait were +0.08, -9.35, and +0.88 degrees, respectively; while those generated by the unaffected limbs were +0.24, -21.02, and +5.61 degrees, respectively. Intersegmental angle differences were significant at the knee and hip ($p = .0007$ and .0129, respectively). The average intersegmental ankle (dorsiflexion +), knee (extension +), and hip (flexion +) moments generated by the affected limbs during the stance phase of gait were -0.36, -0.15, and -0.18 Nm•Sec/kg, respectively; while those generated by the unaffected limbs were -0.55, +0.13, -0.16 Nm•Sec/kg, respectively (See Figure 1). Intersegmental moment differences were significant at the ankle and knee ($p = .0087$ and .0001, respectively).

DISCUSSIONS

The successful biomechanical strategy used by individuals with good functional outcomes after limb sparing procedures involves full extension or "locking" of the affected knee during the stance phase of gait which results in a flexion moment. Although this strategy allows for knee stability while ankle and knee moments provide forward propulsion, it also places extreme stresses on the endoprosthesis which may eventually result in fracture.

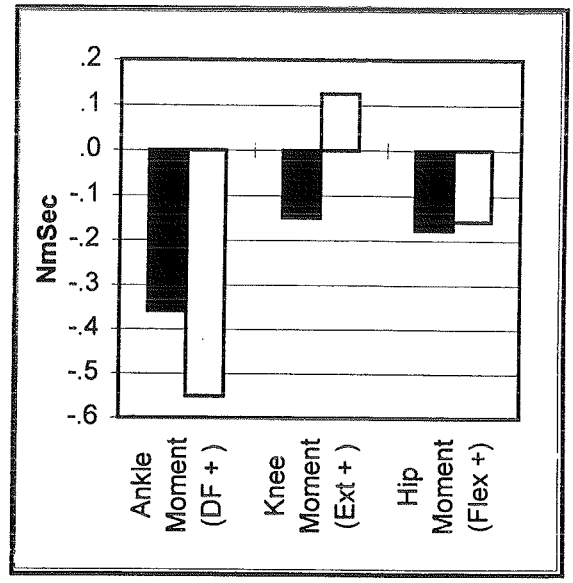

Figure 1. Level Overground Ambulation Stance Phase. *Black bar is affected limb & White bar is normal limb.*

REFERENCES

1. Frieden L: *Research plan for the National Center for Rehabilitation Research.*, **NIH Pub. No. 93-3509**, 31-38, US Government Printing Office, 1993.

2. Pedotti A. *Biological Cybernetics.* 1977, **26**, 53-62, 1977.

3. Siegel KL et al. *Clinical Biomechanics*, **8**, 147-156, 1993.

ACKNOWLEDMENTS

This study was funded by the Medlantic Research Institute (Project # 96-173).

IN VIVO FINGER FLEXOR TENDON FORCE DURING ISOMETRIC PINCH

JACK TIGH DENNERLEIN [1,2], EDWARD DIAO [3], C.D. MOTE, JR. [2] AND DAVID M. REMPEL [1]

[1] Ergonomics Program, Department. of Medicine, University of California, San Francisco
[2] Department of Mechanical Engineering, University of California, Berkeley
[3] Department of Orthopaedic Surgery, University of California, San Francisco

INTRODUCTION

Force may be a risk factor for musculoskeletal disorders of the upper extremity associated with repetitive fingertip loading. Understanding how force is transmitted from the site of external application (fingertip) to the internal tissue (finger flexor tendons) is critical to understanding the mechanics of repetitive motion disorders. Knowledge of *in vivo* tendon tension also guides techniques of tendon repair, procedures for rehabilitation (Schuind et al, 1992) and the design of joint replacements (Weightman and Amis, 1982). The goal of this study is to measure and characterize the *in vivo* tendon tension in the flexor digitorum superficialis (FDS) of the long finger during isometric pinch.

METHODS

Eight subjects(43 ± 17 years), undergoing open carpal tunnel release surgery participated in the study. Subjects retained motor control of the forearm musculature throughout the procedure. After dividing the transverse carpal ligament, the surgeon (E.D.) mounted a tendon force transducer (Dennerlein, 1997) on the flexor digitorum superficialis (FDS) tendon of the long finger. The subject gradually (> 10 seconds) increased the force applied by the fingertip to a load cell from 0 to 10 N and then decreased it monotonically to zero while observing a measure of the force on a visual monitor. A video camera recorded finger joint angles. The surgeon removed all transducers once the tasks were completed.

Data from the load cell and the tendon force transducer were recorded on a computer data acquisition system at 50 Hz. A tendon force model, modified from Chao (1989) predicted tendon force for each subject based on observed posture during fingertip contact. The solution of the set of indeterminate equilibrium equations for the muscle-tendon forces minimized the square of the muscle stresses.

RESULTS

The tension in the FDS tendon was proportional to the force applied at fingertip (Fig. 1). The slopes of the linear regression of the tendon and tip force data were approximately equal for the loading and unloading data. Therefore the slopes of the loading and unloading regions were averaged to represent the tendon-to-tip force ratio for each posture. Correlation coefficients of the linear regression ranged from 0.9 to 1.0 across all subjects. Subject mean tendon-to-fingertip force ratios ranged from 1.7 to 5.8 (mean = 3.3, s.d. = 1.4).

Subjects self-selected either a tip pinch posture (DIP joint flexed, N=4)) or a pulp pinch posture (DIP joint fully extended or hyper-extended, DIP angle 0° N=4)) during the isometric tasks. The tendon-to-tip force ratios measured for subjects using pulp pinch postures were significantly higher ($p = 0.022$) than the ratios observed during tip pinch postures (Fig. 2).

DISCUSSION

The tendon force was proportional to force applied by the fingertip as expected because the mechanical advantage of the tendon to the tip remains constant during an isometric task. Because the posture is assumed to be constant, tendon and fingertip force moment arms do not change. The linearity also suggests that recruitment of synergist muscles, like the flexor digitorum profundus (FDP), follows the flexor digitorum superficialis.

The FDS tendon-to-tip force ratios were larger than the ratios reported by Schuind (1992). Schuind (1992) studies limited the DIP posture to tip pinch with flexion of the DIP. However, Schuind observed a larger

range of forces than predicted by Chao (1989) and speculated that the unreported difference in joint posture explained the larger range. It follows that the range of tendon force measured here was larger than the estimated range reported by both Chao (1989) and Harding (1993). Furthermore, the measured ratios were larger than that estimated by the tendon force model for all subjects.

Reasons for the larger range of FDS tendon-to-tip force ratios include the difference observed between pulp and tip pinch postures. This difference results from the different mechanics of the DIP joint in these postures and the assumptions made in the model structure. Chao (1989) defines and models the DIP joint as an unrestrained hinge joint. As a result, the mechanical advantage of the FDP decreases in the pulp pinch posture and its estimated tension increases in order to balance the moment at the DIP joint. This larger FDP tension exists proximally at the PIP joint, and therefore less FDS tension is required to balance the moment at the PIP. Both Chao (1989) and this model predict such behavior, yet it is not observed *in vivo*. The fact that the DIP joint hyper extends and the FDS tension is larger during pulp pinch suggest a mechanism other than the FDP balances the moments at the DIP. A good candidates are the connective tissue and or the ligaments of the DIP joint. The assumption of an unrestrained hinge joint breaks down for the extended postures. The result is that the FDP force is smaller than needed to balance the DIP moments and, the smaller FDP force at the PIP joint requires a larger FDS force.

Other reasons for the larger tendon tension may be due to limitations in the experimental procedure, muscle co-contraction or errors in predicting the tendon moment arms. The invasive nature of the procedure, the inability of the subject to view the hand, and the effects of local anesthesia may alter muscle recruitment creating the pulp pinch posture; however, hyper extension of the DIP joint can occur during tasks such as touch typing or hand writing. The model assumes co-contraction does not occur, providing the lowest tendon tension estimate necessary to balance the moments at the finger joints. Sensitivity analysis indicates the tendon force model is most sensitive to errors in the moment arms by as much as 1 N/N per 1 mm error.

In conclusion, the isometric, *in vivo*, tendon force measurements indicate a large variation of FDS tendon-to-tip force ratios across individuals for a pinch task. Previous isometric tendon force models do not predict this range. The findings indicate the importance of validating models predicting tendon force.

ACKNOWLEDGMENTS:

UCSF Ambulatory Care Surgery Center. UCSF School of Medicine REAC Cason Fund.

REFERENCES

Chao et al., *Biomech. Hand*, Wld Sci, Sing. 1989.
Dennerlein et al., *J. Biomech*, **30**(4): 395-7 1997.
Harding et al., *J. Biomech*, **26**(12): 1403-12, 1993.
Schuind et al., *J. Hand Surg*, **17A**(2), 291-8, 1992.
Weightman et al,*J. Biomed. Eng.* **4**:197-205, 1982.

Table 1: Ratios of Tendon to Tip Force. Subject Mean Values and (standard deviations).

Subject	1[t]	3[t]	4[t]	8[t]	Mean
Ratio	3.3	1.7	2.3	2.8	2.5
	(0.9)	(0.1)	(0.3)	(0.8)	(0.3)
Predicted	1.7	1.3	0.7	1.9	1.4
Subject	2[p]	5[p]	6[p]	7[p]	Mean
Ratio	2.5	4.6	5.8	4.5	4.4
	(0.2)	(0.9)	(1.9)	(0.4)	(0.7)
Predicted	0.8	1.1	1.0	0.9	0.9

[t] Subjects which selected tip pinch posture.
[p] Subjects which selected pulp pinch posture.

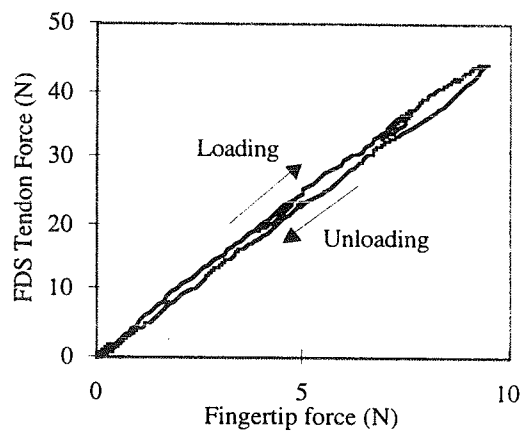

Figure 1: Flexor Digitorum Superficialis tendon and fingertip force during an isometric pinch.

METACARPOPHALANGEAL JOINT KINEMATICS OF THE INDEX FINGER DURING PHYSIOLOGIC LEVEL OF MUSCLE LOADING: STABILIZING ROLES OF THE RADIAL CAPSULOLIGAMENTOUS STRUCTURES

Yeou-Fang Hsieh, Louis F. Draganich, Daniel P. Mass, and Gary A. Piotrowski

Section of Orthopaedic Surgery and Rehabilitation Medicine, Department of Surgery
The University of Chicago, Chicago, Illinois 60637

INTRODUCTION

The importance of the stabilizing role of the radial collateral ligament (RCL) to the metacarpophalangeal (MCP) joint of the finger coupled with the functional instability and pain as a result of the untreated RCL rupture is the motivation for the present study. We investigated the effects of the transection of the radial capsuloligamentous structures on the kinematics of the MCP joint of the index finger during physiologic levels of muscle loading in nineteen cadaveric hands. The three-dimensional kinematics of the MCP joint were determined for passive loading of the intact MCP joint and active muscle loading of the joint produced by applying constant loads, based on one-third of the maximum voluntary isometric force previously reported, to the extrinsic flexor tendons to represent MCP joint loading during pinch. Active muscle loading tests were performed for three experimental states on each specimen: first on the intact MCP joint, second following transection of the RCL and accessory RCL (RCL complex), and finally following transection of the dorsal capsule (DC) and volar plate (VP) in order to test the joint without any radial-aspect stabilizing structures.

REVIEW AND THEORY

Flexion and extension of the MCP joint by the extrinsic muscles is the most commonly produced motion of the finger. Tests of muscle loading to simulate more physiologic loading of the joint have not been performed. Such tests are likely important because instability during pinch or grasp is a clinical problem. Clinical studies (Dray et al., 1979; Schubiner and Mass, 1989) had reported that following rupture of the RCL, patients have complained of pain, swelling, and instability of the MCP joint when grasping objects. These findings suggest that disruptions of the collateral ligaments lead to abnormal changes in the kinematics of the MCP joint during flexion induced by the active contraction of the extrinsic muscles. Thus, the objective of this study was to investigate the effects of the transection of the radial capsuloligamentous structures on the kinematics of the MCP joint during physiologic levels of muscle loading. The following hypotheses were tested: 1) the kinematics of the MCP joint of the index finger resulting from transection of the RCL complex are significantly different from those of the intact joint during active muscle loading and 2) transection of both the DC and VP increases the laxity of the MCP joint in which the RCL complex has been transected.

PROCEDURES

Nineteen unembalmed adult human cadaver hands (9 left and 10 right) were amputated at the level of the distal radius and studied. The flexor digitorum profundus (FDP), flexor digitorum superficialis (FDS), and extensor digitorum communis (EDC) of the index finger were isolated proximally at the wrist level and tagged. The distal interphalangeal and proximal interphalangeal joints were fixed in 10° and 30° of flexion, respectively, so that all motion would take place at the MCP joint. These angles were chosen to mimic the pinch configuration. The spatial positions of the metacarpal bone and proximal phalanx and anatomic geometry of the MCP joint were measured with the Fastrak system (Polhemus Navigation Sciences, Colchester, Vt), a six-degree-of-freedom measuring device. Two sets of static loads were applied for MCP flexion angles ranging from 0° to 90° in 15° increments: 1) passive loading of the MCP joint and 2) simulated active muscle loading produced by applying constant loads to the extrinsic flexor tendons to represent MCP joint loading during pinch. Active muscle loading tests were performed for three experimental states on each specimen: first on the intact MCP joint, second following transection of the RCL complex, and finally following transection of the DC and VP in order to test the MCP joint without any radial-aspect stabilizing structures. Testing of active muscle loading consisted of prepositioning the MCP joint at a desired flexion angle with a force of 1 N applied to the tendon of the EDC, simultaneously applying external loads to the tendons of the FDP and FDS, based on 1/3 of maximum voluntary isometric force previously reported (Brand et al., 1981), and measuring the spatial positions of the metacarpal bone and proximal phalanx. After the position data for all states were collected, the MCP joint was disarticulated and bony landmarks of the metacarpal bone and proximal phalanx were digitized for construction of the anatomic coordinate systems. Those bony landmarks were used in conjunction with the position data to determine the kinematics of the MCP joint. MCP kinematics were represented by three clinical

rotations and three clinical translations of the proximal phalanx with respect to the metacarpal bone using a joint coordinate system previously reported (Grood and Suntay, 1983; Hsieh et al., 1997). The MCP kinematics were normalized according to $Q_m^E = q_m^E - (q_m^I)_P$, where Q_m^E represents the normalized kinematics at the mth joint position, q_m^E represents the kinematics for each of the three experimental states during active muscle loading, and $(q_m^I)_P$ represents the kinematics of the intact MCP joint during passive loading. We performed one-way ANOVAs with repeated measures and Tukey's 'honestly significant difference' tests to determine the flexion angles for which significant differences between test states would be found. Statistical significance was defined as $p<0.01$ to correct for multiple comparison.

RESULTS

For active muscle loading of the intact MCP joint, the proximal phalanx rotated radially (abducted) from -14.8° of ulnar position at 0° of flexion to a maximum of -7.3° at 90° with respect to the metacarpal bone (Figure 1), supinated from 6.2° of pronation at 0° to a maximum of -14.9° at 60° (Figure 2), and translated volarly from -1.1 mm at 0° to a maximum of -3.3 mm at 90° (Figure 3). Transection of the RCL complex resulted in significant increases in ulnar deviation ($p<0.01$) ranging from 4.4° to 4.8° between 0° and 30° and at 75° and in volar translation ($p<0.005$) ranging from 1.0 to 1.3 mm between 60° and 90° compared to those found for the intact MCP joint. Additional transection of both the DC and VP caused significant increases in ulnar deviation ($p<0.007$) ranging from 4.0° to 10.4° between 0° and 90°, in pronation ($p<0.002$) ranging from 6.2° to 33.6° between 0° and 90°, and in volar translation ($p<0.001$) ranging from 1.5 mm to 4.2 mm between 15° and 90° when compared to those found for the MCP joint in which the RCL complex has been transected. These increases were also found significant ($p<0.001$) when compared to those found for the intact MCP joint.

DISCUSSION

Unlike previous studies, we applied loads through the musculotendinous structures to simulate more physiologic loading of the MCP joint. Our results indicate that the RCL complex is a restraint to ulnar deviation of the MCP joint when flexed by the extrinsic flexor tendons. Ulnar deviation of the joint increased significantly when the RCL complex was transected suggesting that abnormal ulnar deviation would also occur during pinch. Our results also demonstrate that together the DC and VP play a significant stabilizing role in resisting ulnar deviation, pronation, and volar translation of the proximal phalanx on the metacarpal head when the RCL complex has been transected. Our findings for transection of the RCL complex, DC, and VP correlate with our clinical experience of grossly abnormal kinematics of the MCP joint.

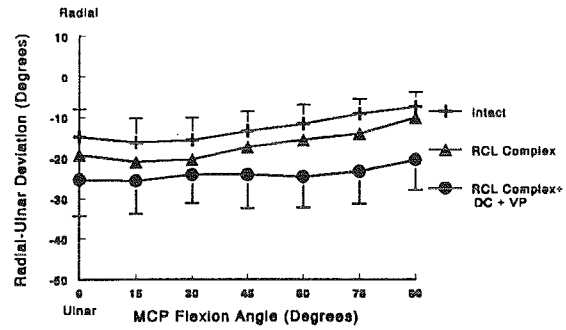

Figure 1. Radial-ulnar deviation of the MCP joint

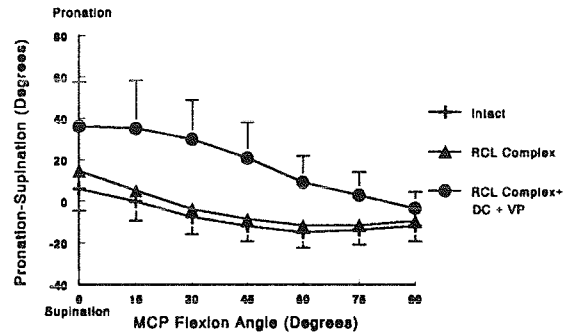

Figure 2. Pronation-supination of the MCP joint

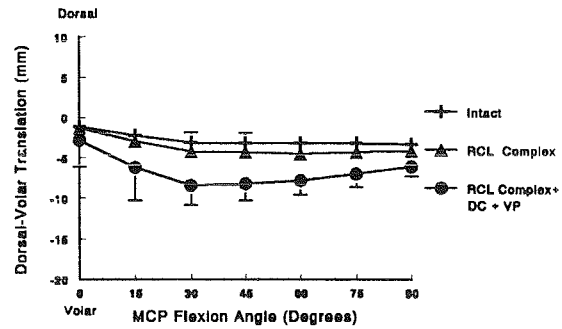

Figure 3. Dorsal-volar translation of the MCP joint

REFERENCES

1. Brand et al: J Hand Surg 6: 209-219, 1981.
2. Dray et al: J Hand Surg 4: 346-350, 1979.
3. Grood and Suntay: J Biomech Eng 105: 136-144, 1983.
4. Hsieh et al: Trans ORS 22: 279, 1997.
5. Schubiner and Mass: JBJS 71B: 388-389, 1989.

TENDON FORCE DURING A KEYSTRIKE

JACK TIGH DENNERLEIN [1,2], EDWARD DIAO [3], C.D. MOTE, JR. [2] AND DAVID M. REMPEL [1]

[1] Ergonomics Program, Department. of Medicine, University of California, San Francisco
[2] Department of Mechanical Engineering, University of California, Berkeley
[3] Department of Orthopaedic Surgery, University of California, San Francisco

INTRODUCTION

Force may be a risk factor for musculoskeletal disorders of the upper extremity associated with typing and keying. However, the internal finger flexor tendon forces during a keystrike are unknown. Models predicting tendon force (e.g. Harding, 1993) have not been validated with experimental data. Experiments by Schuind (1992) were limited to isometric pinch tasks and unloaded finger movements. Our goals are to measure and characterize the *in vivo* force in the finger flexor tendon during a keystrike.

METHODS

Five subjects(38 ± 8 years), undergoing open carpal tunnel release surgery participated in the study. Subjects retained motor control of the forearm musculature throughout the procedure. After the carpal tunnel release, a tendon force transducer (Dennerlein, 1997), was mounted on the flexor digitorum superficialis (FDS) tendon of the long finger. The subjects tapped on a keycap and keyswitch assembly containing a load cell (Rempel, 1994). A buzzer connected to the switch provided audible feedback. The forearm and wrist were manually stabilized during the tapping tasks. The transducer was then removed and surgery continued.

Data from the fingertip load cell and tendon force transducers were recorded on a computer at 2 kHz and then digitally low pass filtered with 300 Hz cut-off. Seventeen to thirty-five keystrokes were collected per subject.

A static tendon force model, modified from Chao (1989) predicted tendon force for each subject based on the observed posture during fingertip contact. Optimization techniques minimizing the square of the muscle stresses solved the indeterminate set of equilibrium equations for the muscle-tendon forces.

RESULTS

Fingertip force patterns (Fig. 1) contained the three phases observed by Rempel (1994): (I) key switch compression; (II) high frequency finger impact; and (III) fingertip pulp compression and release. The average fingertip maximum force ranged from 1.6 N to 3.4 N across subjects. The duration of contact ranged from 136 ms to 277 ms and the average key switch compression velocity ranged from 0.08 m/s to 0.23 m/s.

The tendon tension increased with fingertip force and then decreased more slowly, remaining elevated after fingertip force vanished (Fig. 2). The average tendon maximum force ranged from 8.3 N to 16.6 N (mean = 12.9 N, s. d. = 3.3 N) and the average tendon mean force during contact ranged from 5.0 N to 8.6 N (mean = 7.2 N, s. d. = 1.4 N). As the force at the fingertip decreased, tendon force remain elevated twice as long as the tip force. The average half relaxation times were 71 ms (s. d. = 13 ms) for the tip and 151 ms (s. d. = 23 ms) for the tendon force.

Maximum tendon force was 3.5 to 7 times larger than maximum tip force during a keystroke (Table 1) while the model (Chao 1989) predicted tendon forces some 1 to 2 times larger than the tip force.

DISCUSSION

The tendon tension did not contain the high frequency impact forces observed at the fingertip (Phase II) (Fig. 1). Other *in vivo* studies of force report that impact forces during locomotion are not observed in the tendons (Komi, 1987). Thus the impact force dissipates into tissues distal to the tendons at the wrist.

The longer half-relaxation time of the tendon force may be the result of residual eccentric muscle contraction and/or passive muscle forces. These forces overlap with increasing extensor activity, co-contraction. The speed associated with the keystroke movement requires that the finger flexion

force be removed quickly; however, the relatively slow relaxation of the FDS muscle force is set by muscle physiology. EMG studies of typing indicate that the beginning of extensor activity overlaps with the end of the flexor activity (Weiss, 1996). As the fingertip releases the keycap, the flexor muscle lengthens and its passive muscle force increases.

The ratios of FDS tendon-to-tip maximum and mean forces (Table 1) were higher than the ratios and slopes estimated previously by isometric tendon force models. Harding's (1993) quasi static model predicted ratios that ranged from 0.8 to 2.7. The estimates from isometric tendon models implemented from the literature (Chao et al., 1989) fail to predict the observed range of force ratios (Table 1). Causes for this under prediction include the assumption that there is no co-contraction in the system. The models therefore provide a lower bound for the possible tendon force. Chao (1989) describes a lower bound with there graphical solution methods.

This *in vivo* study provides a unique opportunity to characterize tendon force during a keystrike. The data relates the external force exposure at the fingertip to the internal force dosage at the tendon tissues. The next step is to determine how the tissues respond to these repetitive loads.

CONCLUSIONS

The FDS tendon force histories are a complex function of fingertip loading. After peak force, the tendon force relaxes at a slower rate than the tip force. The maximum forces in the FDS tendon were 4 to 7 times larger than the maximum forces at the fingertip during a keystroke. This is greater than the levels predicted using existing models. This study suggests the need to understand the role of co-contraction on tendon tension during rapid finger movements.

ACKNOWLEDGMENTS:

UCSF Ambulatory Care Surgery Center. UCSF School of Medicine REAC Cason Fund.

REFERENCES

Chao et al., *Biomech. Hand*, Wld Sci, Sing 1989.
Dennerlein et al., *J. Biomech*, **30**(4):395-7, 1997.
Harding et al. *J. Biomech*, **26**(12): 1403-12, 1993.
Komi *Intern'l J. Sports Med*, **8**: 3-8, 1987.
Rempel et al., *J. Biomech*, **27**(8), 1101-4, 1994.
Schuind et al., *J.Hand Surg*, **17A**(2), 291-8, 1992.
Weiss et al., Occup Ergo & Saf I **2**: 508-10, 1996.

Table 1: Parameters relating the Ratio of flexor digitorum superficialis (FDS) tendon tension to fingertip force. Mean (st. dev.)

Subject	1	2	3	4	5
Ratio of Max.	3.5	4.4	6.6	5.5	6.8
	(1.0)	(0.3)	(1.0)	(1.7)	(1.5)
Ratio of Means	3.4	4.5	6.5	6.2	5.6
	(1.2)	(1.2)	(1.0)	(1.8)	(1.3)
Predict Ratio	1.9	1.4	0.9	0.8	1.0
	(0.6)	(0.1)	(0.3)	(0.1)	(0.2)

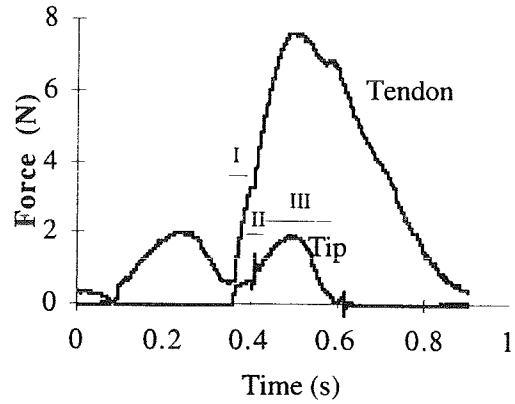

Figure 1: Flexor Digitorum Superficialis tendon and fingertip force histories during keystrike.

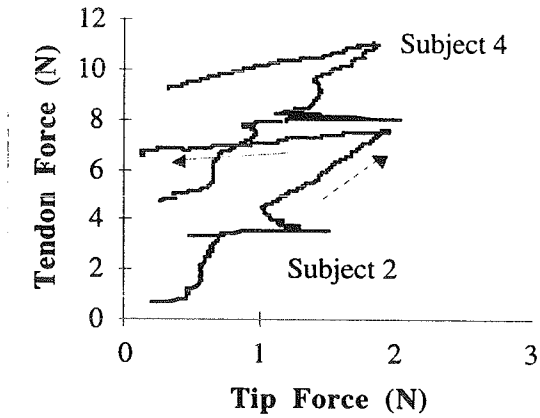

Figure 2. FDS tendon and fingertip force for keystrikes of two subjects.

COORDINATION OF GRIPPING FINGERS: THE ROLE OF THUMB POSITION IN MAXIMAL EXERTION

Zong-Ming Li, Mark L. Latash, Vladimir M. Zatsiorsky
Department of Kinesiology, The Pennsylvania State University, University Park, PA 16802

This study was motivated by two considerations. First, to gain a deeper insight into the strategies utilized by the CNS to resolve the problem of motor redundancy, in particular the task of sharing force among several effectors/fingers acting in parallel. Secondly, to clarify the cause of the large dissimilarity in published data on the force sharing among the individual digits during grip strength exertion (Amis, 1987; Kinoshita et al. 1995; Ohtsuki, 1981; Radwin et al., 1992).

METHODS

Maximal normal force as well as the force-time curves produced by individual fingers (See Figure 1 for the experiment setup.) were measured in 10 young male subjects in the three tasks: (A) Holding an instrumented handle with the finger pads in opposition to the thumb, with the thumb at seven different locations—from the thumb opposing the index finger, L_0, to the thumb opposing the little finger, L_6 (See Figure 2); (B) Holding the handle with the finger pads in opposition to the thumb, with the thumb at an individually selected comfortable location; and (C) Pressing with the four fingers against a secured handle. In tasks (A) and (B) the subjects were asked to lift the handle slowly and then gripped maximally. In all three tasks the fingers were in the same positions.

In addition, the maximal forces from individual fingers in single-finger tasks were measured, the pinch force and the press force. In position L_6 some subjects were not able to perform the grip; for this position exemplary data are only presented.

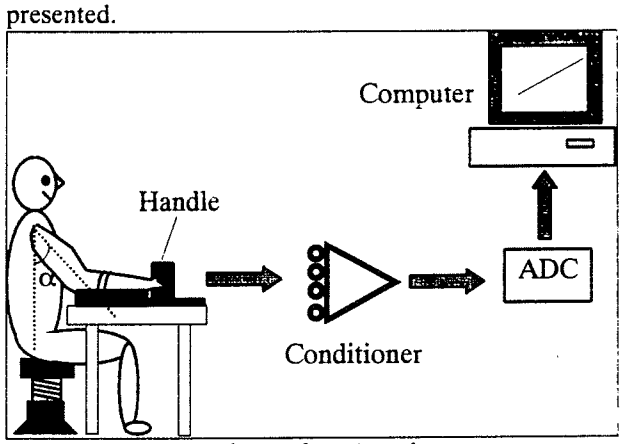

Figure 1 Experimental setup for grip tasks

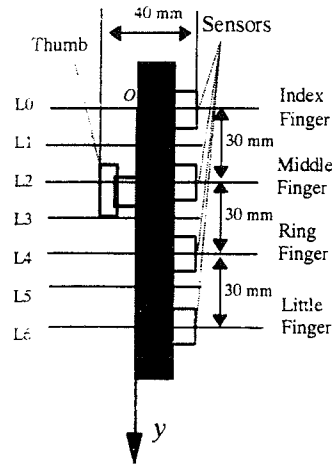

Figure 2 Grip handle with moveable thumb locations

RESULTS

(1) The moment due to the normal finger forces changed systematically when the thumb position varied from L_0 to L_5/L_6 and it was equal to zero at a certain middle position of the thumb, the *neutral position*. At this position, the shear force produced by the fingers was also zero (Figure 3).

(2) The total normal force changed in an ascending-descending manner when the thumb position varied from L_0 to L_5/L_6. The highest value of the maximal total normal force was produced at a neutral position of the thumb. (See Figure 3.)

(3) The neutral thumb position was preferred as the most comfortable position in the grip task.

(4) In the press task, the neutral line—the line with respect to which the moment generated by the four fingers equals zero—was at the same location as the neutral thumb position in the grip tasks.

(5) The larger the total normal force produced by the fingers the smaller the total shear force produced by them. The dependence was curvilinear (r^2= 0.962).

(6) In individual attempts with the thumb in a comfortable position as well as in the 'central' positions L_1-L_4 , the force-force relationships in the beginning phase of the force development were linear. Hence, in these thumb positions the force sharing pattern was established by the

CNS at the beginning of the trial. The stable sharing pattern was not, however, maintained at the level of maximal force exertion. In position L_5 with the thumb in a pad opposition to the small finger, irregular patterns of the force-force relationships were found.

(7) Among trials, a large correlation was found between the maximal force displayed by the index and small fingers. These fingers, due to their large moment arms with respect to the neutral line, make the largest contribution to the total torque and counterbalance each other.

(8) Peak forces exerted by individual fingers in the multi-finger tasks were much smaller than the maximal force displayed by the same fingers in the single-finger tasks. The peak force depended on the thumb position and varied from 11.3% to 65.2% of the maximal force exerted by the same finger in the single-finger task. With the thumb in the comfortable position, the relative peak forces for all fingers were approximately at the same level, 50-55%.

SUMMARY

(1) To stabilize an object in space at various thumb positions, the CNS changes: (a) a force sharing among the fingers, in % of the total force; and (b) the contribution of the normal and shear force into the total force.

(2) There exists a functional neutral line of the hand with respect to which the moment of force in a four-finger press task is zero. In the gripping tasks, when the thumb was along this line: (a) the moment of force and the shear force were zero; (b) the total normal force and the total resultant force were maximal; (c) the relative peak force—in % of the maximal force exerted by the digit in the single-finger test—was alike in all the fingers; and (d) this position was preferred by the subjects as the most comfortable.

(3) The disagreement between the previously published data on the force sharing during grip strength exertion may be due to different—but not specified by the researchers—thumb positions.

(4) Except for the extreme thumb positions, L_0 and L_5/L_6, the force sharing among fingers is established at the beginning of a trial.

(5) Existence of the force deficit in the multi-finger tasks was confirmed. The amount of the force deficit in individual fingers—the difference between the peak force produced by the same finger in the four-finger task and the single-finger task—depended on the thumb position.

(6) In general, the data are in agreement with the 'secondary moments' hypothesis: the CNS tends to selects a pattern of muscle activation that reduces unnecessary, additional moments acting with respect to the degrees of freedom which are not immediately involved in the motor task.

REFERENCES

Amis AA, J Biomed Engin 9: 313-320, 1987

Kinoshita H et al., Ergonomics 38(6): 1212-1230, 1995

Ohtsuki T, Ergonomics 24(1): 21-36, 1981

Radwin R et al., Ergonomics 35(3):275-288, 1992

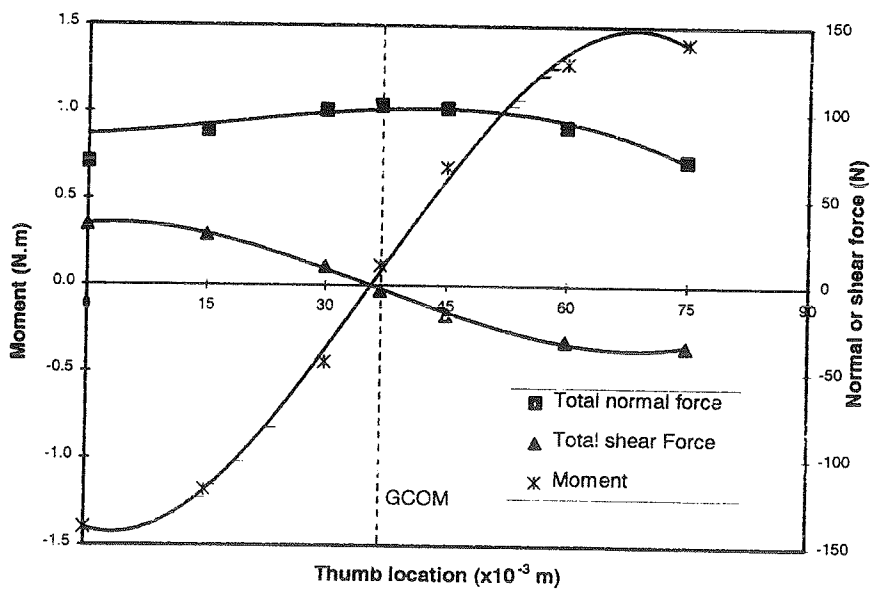

Figure 3 The moment, total normal force and shear force as a function of thumb location. The lines are the corresponding polynomial approximation of the third power. "GCOM" indicates the comfortable location of the thumb.

THE INTERACTION AND ENSLAVING OF FINGER FLEXORS IN MULTI-FINGER TASKS — A NEURAL NETWORK MODEL

Vladimir M. Zatsiorsky, Zong-Ming Li, Mark L. Latash
Department of Kinesiology, The Pennsylvania State University, University Park, PA 16802

Humans have freedom to move their fingers selectively. However, anatomical and neural connections among finger flexors 'enslave' fingers in fine movement — when some fingers/muscles are voluntarily activated, other fingers/muscles are also activated (Leijnse et al., 1993; Kilbreath et al., 1994). The experiment was designed to study the enslaving effect among finger flexors. A neural network model was constructed to model the interaction among fingers.

METHODS

Four force transducers (Model 208A03, Pizeotronic, Inc.) were used to measure the press finger forces (Figure 1). Subjects were told to press maximally with various combinations of the fingers— the index (I), middle (M), ring (R) and little (L) fingers. All 15 combinations were utilized, they are I, M, R, L, IM, IR, IL, MR, ML, RL, IMR, IML, IRL, MRL and IMRL, respectively. For each combination, subjects were instructed to keep the uninvolved fingers on the sensors, but to pay no attention to these fingers when pressing. The sequence of the 15 combinations was randomized. Two consecutive trials were performed for each combination. The forces of individual fingers at the moment of the maximal total force were extracted for later analysis. Ten right-handed university students participated in the experiment.

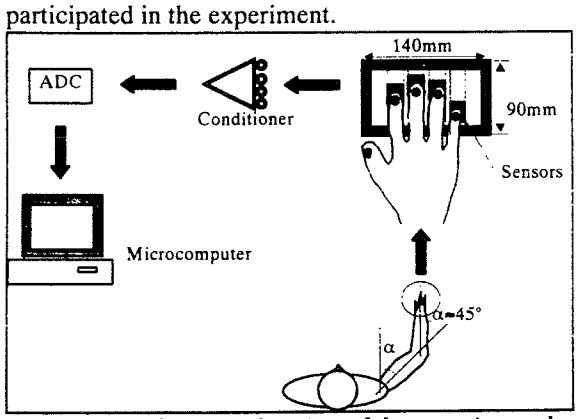

Figure 1 Schematic drawing of the experimental setup

EXPERIMENTAL RESULTS

Figure 2 (on the next page) shows the experimental results of the forces of individual fingers in various finger combinations. It shows significant enslaving forces of the uninvolved fingers in the tasks.

NEURAL NETWORKS MODELING

A neural network model (Figure 3) was constructed to simulate the interaction among fingers. The model consists of three layers: (a) the input layer that models a central neural drive, (b) the hidden layer modeling extrinsic finger flexors serving several fingers simultaneously, and (c) the output layer representing finger force output. Note the existence of direct input-output connections that model intrinsic hand muscles serving individual fingers. The mathematical expressions are as follows:

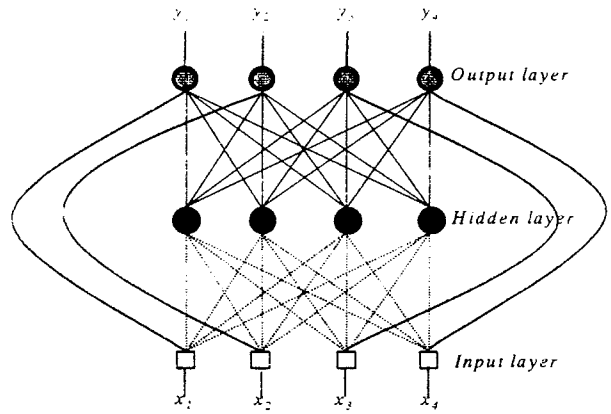

Figure 3 The neural networks consisting of three layers and their connections.

$$s_j^{(1)} = \sum_{i=1}^{4} w_{ij}^{(1)} x_i \qquad j = 1, 2, 3, 4$$

$$z_j = f_1(s_j^{(1)}) = \frac{x_j}{s_j^{(1)}} \qquad j = 1, 2, 3, 4$$

$$s_k^{(2)} = \sum_{j=1}^{4} w_{jk}^{(2)} z_j + v_k x_k \qquad k = 1, 2, 3, 4$$

$$y_k = f_2(s_k^{(2)}) = s_k^{(2)} \qquad k = 1, 2, 3, 4$$

where $s_j^{(1)}$ are the net input to the j^{th} unit of the hidden layer from the input layer. $w_{ij}^{(1)}$ are connection weights from i^{th} unit in the input layer to the j^{th} unit in the hidden layer. f_1 is the transfer characteristics of input/output of the hidden layer unit. z_j is the output from the hidden layer. $s_k^{(2)}$ is the net input to the k^{th} unit in the output layer from

the hidden layer. $w_{jk}^{(2)}$ are connection weights from j^{th} unit in the hidden layer to the k^{th} unit in the output layer. v_k are the connection weights directly from k^{th} unit in the input layer to the k^{th} unit in the output layer. f_1 is an identity transfer function in the output layer.

The inputs to the network were set as x_i=1, if finger i was involved in the task, or $x_i = 0$ otherwise. The weights from the input layer to the hidden layer were set as unit constant ($w_{ij}^{(1)} = 1$).

Let the training exemplar set be $\{\vec{x}(l), \vec{d}(l)\}_{l=1}^{15}$, where $\vec{x}(l)$ is the input pattern vector to the network and $\vec{d}(l)$ is the desired output vector for the input patter $\vec{x}(l)$. Herein, $\vec{d}(l)$ is the finger force output from experiment for a given finger combination l. The sum of squares of the error over all input units of all exemplars was defined as

$$E = \sum_{l=1}^{15} \left\{ \frac{1}{2} \sum_{k=1}^{4} [y_k(l) - d_k(l)]^2 \right\}$$

The objective was to adjust the network weights to minimize the error function. On application of the backpropagation algorithm with a set of initial weights, a satisfactory result for this problem was obtained after 500 epochs with a learning rate of 0.01. The final network values yielded a root mean square difference of 1.14 N between the experimental results and the network output.

The results for the connecting weights are written below as a matrix and a vector

$$[w^{(2)}] = \begin{bmatrix} 32.7 & 9.1 & 3.8 & 3.7 \\ 14.2 & 29.0 & 13.6 & 3.5 \\ 9.0 & 20.2 & 22.4 & 10.9 \\ 8.8 & 7.6 & 16.0 & 17.2 \end{bmatrix} \quad [v] = \begin{bmatrix} 16.9 \\ 10.1 \\ 8.3 \\ 7.2 \end{bmatrix}$$

SUMMARY

In the experiments, it was found that activation of one finger is accompanied by the activation of other fingers (the enslaving effect).

The modeling results confirm that there are two neural pools which control the finger flexors. The first pool, represented by the connections from the input layer directly to the output layer, is the direct control of each individual finger without any interaction among fingers. Such an independent control of fingers can be realized by the intrinsic muscles of the hand. The second pool explains the enslaving effect. A certain amount of neural drive is divided among the involved fingers, as reflected by the connections from the input layer to the hidden layer. The divided neural drives further interact with each other. This procedure corresponds to the co-activation of the extrinsic muscles of the hand, which have common muscle bellies.

REFERENCES

1. Kilbreath SL and Gandevia SC, J Physiol 479(3): 487-497, 1994
2. Leijnse JNAL et al., J Biomech 26(10): 1169-1179, 1993

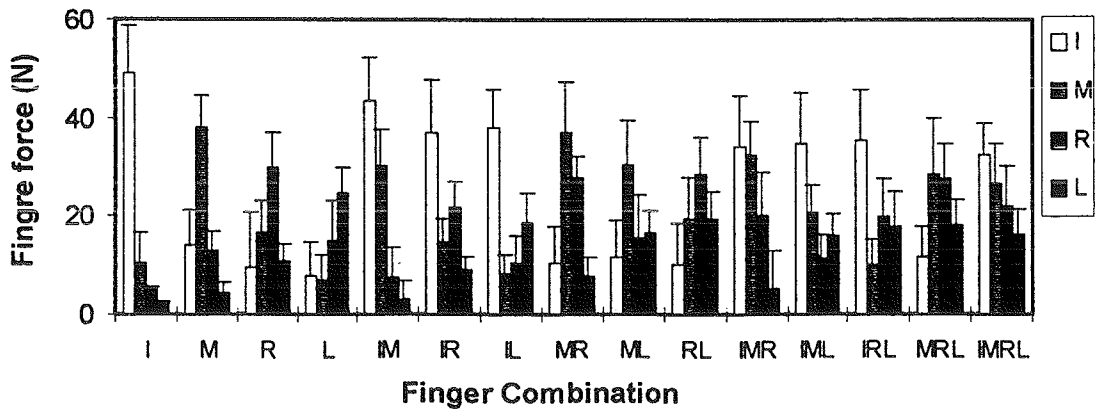

Figure 2 Enslaving effect: The force produced by involved and uninvolved fingers in various finger combinations.

JOINT MOMENTS AT THE LOWER EXTREMITIES FOR CHANGING DIRECTION DURING WALKING

D. Xu, J. Chow, K. Rosengren and L. Carlton
Department of Kinesiology, University of Illinois, Urbana, IL 61801

INTRODUCTION

Kinetic analysis of the lower extremities has been considered as a useful tool in understanding the mechanisms of locomotion, helping clinical diagnosis in movement disorders, and designing surgical procedures and implants to reconstruct diseased joints. The sagittal view provides the kinetic characteristics for the plane of progression forward, however, there are few studies providing three dimensional analysis of the joint moments at all three lower extremity joints (Bresler & Frankel, 1950, Eng & Winter, 1995). The purpose of this study was to investigate the joint moments of force at the lower extremities for changing direction during walking. The functional role of each component of the moments and the effect of altering turn angle and pivot foot were investigated.

REVIEW AND THEORY

The results of sagittal plane kinetic analysis have provided very useful profiles for examining motor patterns of normal and pathological gait (Winter, 1987). However, planar kinetic analysis does not provide enough information for movement stability, particularly at the hip joint where hip abductors are critical for balance control of the trunk in the frontal plane (MacKinnon & Winter, 1993). The forward leg swing and the torsional twist also affect the joint moments in the transverse plane at the lower extremities. Examining the three-dimensional characteristics of the moment patterns at the lower extremities will provide insight for the study of muscle activities and movement control, diagnosing gait motion with movement disorders, and walking under different conditions, such as changing direction during walking. Individuals not only need to translate their body forward, but also need to rotate their body to a new orientation while altering direction. During this period of time, abduction/adduction and rotation occur at the hip and knee, and inversion/eversion appears at the ankle (Xu, 1996). This is different from walking straight forward. Bresler, et al. (1950) pointed out that before attempting to correct any mechanical deficiencies in the human body, the surgeon, limb and bracemaker, and physiotherapist must be well-acquainted with the mechanical functions of the affected parts of the body.

What are the unique characteristics of the moment patterns while changing direction during walking? Previous work has shown that there are significant changes in the angular momenta of the body segments while changing direction (Xu, 1996). In the present study, different motor patterns appeared for altering turn angle and pivot foot. Individuals with movement disorders at the lower extremity joints might not be able to change direction. Due to this investigation, the functional motion of the lower extremity joints and control strategy during walking will be better understood.

PROCEDURES

Subjects. Six males and two females university students participated in this study. They all had no history of injury at the lower extremities. The age range was from 18 to 23 years. The height was from 1.65 to 1.80 m and the mass ranged from 56 to 79 kg.

Task. The subjects were asked to walk on force platforms while walking straight forward and while changing direction. Two elementary turning movements were defined to represent walking while changing direction. They were turning to the right at 45^0 and 90^0. It was assumed that the result of turning to the right direction was the same as the turning to the left direction. The natural walking speed (1.35 ±0.15 m/sec) was evaluated. Both the right foot and left foot were used as the pivot foot for changing direction, respectively. Each subject performed 18 trials for these different walking directions and pivot feet. The testing conditions were conducted in random order.

Instrumentation and Data Collection. Two AMTI force platforms (200Hz sampling rate) and two Peak Performance video cameras (60Hz) were used to collect the kinetic and kinematic data, respectively. The Peak Synchronization Events was employed for synchronizing the force platform and video camera systems.

Data Reduction and Analysis. The three-dimensional coordinate data were computed with the DLT technique. The kinematic data were smoothed using a quintic spline before computing the joint moments. The moments of force at the lower extremity joints were computed in terms of the anatomic joint axes. The data, which were used for analysis of the joint moments of force, were normalized by dividing the body mass before being averaged and plotted. The plotting data were ensemble averages in these graphics.

RESULTS

The joint moments at the lower extremities were examined by comparing the moment patterns during the stance phase for different pivot feet and turning angles. Figure 1 presents the results for altering direction at 0^0, 45^0, and 90^0 with the right pivot foot and natural walking speed. The lines in each plot are representative of the ensemble averages of the joint moments for inter- and intra- subjects' trials. The solid line with a square indicates walking straight forward; the dashed line with a triangle indicates altering direction at 45^0, and the dotted line with a across marker indicates the turning angle of 90^0. The plots titled **Mx-a**, **Mx-k**, and **Mx-h** are the joint moments at the ankle, knee, and hip with respect to the sagittal plane; **My-a**, **My-k**, and **My-h** are the moments at the ankle, knee, and hip with respect to the frontal plane; and **Mz-a**, **Mz-k**, and **Mz-h** are the moments at the ankle, knee, and hip with respect to the transverse plane. The results showed that there were significant changes for the moments in the frontal and transverse planes, especially the moments at the hip and knee joints. There were also large plantarflexor moments at the heel contact before the propelling phase at the ankle joint for changing direction during walking. Changes for the moments at the lower extremities also appeared for the different pivot feet.

DISCUSSION

The results of this study showed that changes of moments at the sagittal plane for altering direction appeared at the ankle joint during the heel strike before propelling forward. This suggests that during this period of time, the subjects tried to decrease the forward speed by increasing the plantarflexor moment to translate the entire body to the new direction. It is obvious that during the propelling phase while changing direction, the moments for abduction/adduction at the knee and hip joints, and rotation at the ankle, knee and hip joints were increased significantly. The magnitudes of the peak moments for the frontal plane and transverse plane at the knee and hip joints were twice larger for changing direction than that for walking straight forward during the propelling phase. Increases in moments may cause control and stability problems for individuals with the lower extremity joint disorders. Turning to the right with the left pivot foot seems to demand smaller joint moments when compared to the right pivot foot condition. Therefore, the results suggest that less stress is placed on the joints of the supporting leg if the contralateral left foot is used as the pivot foot when making a turn during walking. The moment patterns found in this study can be used as the profile for clinical diagnosis in gait disorder.

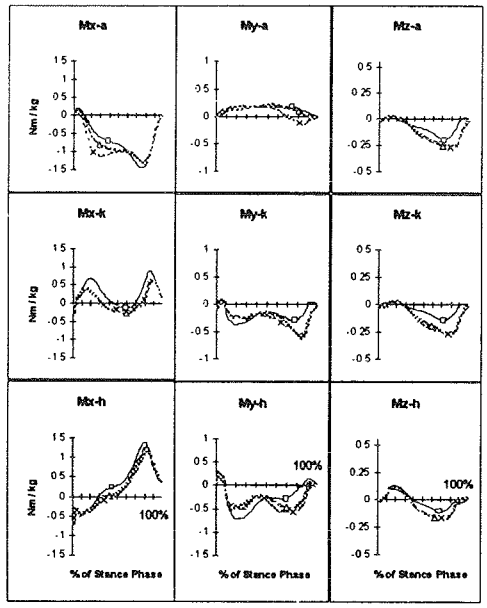

Figure 1. Moments at the lower extremities for changing different directions with the right pivot foot and natural walking speed.

REFERENCES

Bresler, B. and Frankel, J. P. (1950). Trans. ASME, 72, 27-36.

Eng, J. and Winter, D. (1995). J of B. 28, 635-646

MacKinnon, C. D. & Winter, D. (1993).J of B. 26, 633-644.

Xu, D. (1996). Unpublished dissertation.

BIOMECHANICAL ALTERATIONS IN GAIT DURING PREGNANCY

T. Foti, A. Bagley, J. Davids

Motion Analysis Laboratory, Shriners Hospital for Children, Greenville, SC 29605

INTRODUCTION

This study involved a measurement of biomechanical deviations in gait during pregnancy. This information will increase the understanding of how gait is altered during pregnancy. In addition, this information will be useful to increase the understanding of factors which contribute to various musculoskeletal disorders during pregnancy (such as low back pain, hip pain, and other painful conditions).

REVIEW AND THEORY

Significant hormonal and anatomical changes occur during pregnancy which dramatically alter body mass, body mass distribution, joint laxity, and tendon and muscle strength. The effects of these changes on standing posture have been fairly well documented, however, little has been reported about the effects of these changes on walking gait. The walking gait of pregnant women has been characterized as a "waddling gait" (Heckman and Sassard, 1994). Characteristics of a waddling gait include: wide base of support, external foot progression angle ("toeing out"), and large pelvic obliquity (tilt of the pelvis side to side in the coronal plane) range of motion. However, a review of literature revealed no studies documenting overground walking kinematics and kinetics of pregnant women. The purpose of this study was to assess the gait of women during pregnancy and compare it to their non-pregnant gait.

PROCEDURES

Ten women were studied in the 2nd half of the last trimester of pregnancy and again one year postpartum. Lower extremity joint kinematic and kinetic data were collected using a Vicon 370 3-D Motion Analysis system (60 Hz) and an AMTI force platform (600 Hz). The subjects performed repeated walks at a self selected pace across the room (about 10m) until 6-8 strides of kinematic and kinetic data were obtained. Pelvic angles; hip, knee, and ankle joint angles, moments and powers; and dynamic base of support width were compared for the pregnant and non-pregnant conditions. Selected maximum, minimum and range of motion values for the pelvic and joint angles; selected maxima and minima for the joint moments and powers; and dynamic base of support width (measured as the average width of the ankle joint centers during double support) were analyzed using a one-way ANOVA with repeated measures at a 95% significance level.

RESULTS

Statistically significant findings ($p<0.05$) for selected kinematic and kinetic variables analyzed for the pregnant and non-pregnant conditions are presented in Table 1 below. Significant increases in anterior pelvic tilt, hip adduction during stance, double support time, and hip abduction/adduction power (H3-F); and decreases in maximum hip extension, and single support were found during walking during pregnancy ($p<0.05$).

Variable	Pregnant	1 Year Post	p-value
Maximum Pelvic Tilt	18.7 °	14.3 °	0.0109
Max. Hip Extension	2.5 ° (flex.)	5.3° (ext.)	0.0429
Average. Hip Adduction (during stance)	5.6 °	3.6 °	0.0158
Double Support Time	27.9 % cycle	25.5 % cycle	0.0342
Single Support Time	36.1 % cycle	37.4 % cycle	0.0305
Hip Ab/Add. Power (H3-F)	0.76 Nm/kg-s	0.59 Nm/kg-s	0.0490

Table 1: Significant ($p<0.05$) deviations in gait due to pregnancy. Means for each condition and p-values from statistical analysis are presented.

Selected findings which were not statistically significant are presented in Table 2. Mean dynamic base of support was slightly larger during pregnancy than 1 year post, however this difference was not

significant ($p > 0.05$). Pelvic obliquity range of motion and foot progression angle during stance were also not significantly different ($p>0.05$) for the two experimental conditions.

Variable	Pregnant	1 Year Post	p-value
Dynamic Base of Support	0.207 m	0.192m	0.4585
Pelvic Obliquity ROM	9.5 °	10.3 °	0.3731
Foot Progression Angle	8.2 ° (external)	8.3 ° (external)	0.8721

Table 2: Selected variables which were not significantly different ($p>0.05$) for the pregnant and non-pregnant conditions. Means for each condition and p-values from statistical analysis are presented.

DISCUSSION

Little evidence was found to support the popular contention that the gait of pregnant women can be described as a "waddling gait". The results of this study show that the dynamic base of support is not significantly wider, pelvic obliquity range of motion is not greater, and the foot progression angle is not significantly more externally rotated which are characteristics of a 'waddling' gait. The changes in gait during pregnancy quantified by this study are mild and can be explained by the increase in body mass and width, and the change in mass distribution about the trunk.

Increases in hip abduction/adduction power during late stance (H3-F) with pregnancy are apparently a result of an increase in body mass. Hip abduction/adduction power generation at this time period has been identified as a measure of the muscular power of the stance side hip abductor muscles used to raise the unsupported side of the pelvis (Eng and Winter, 1995). With the increased body mass during pregnancy, an increased load must be lifted by the hip abductor muscle group. Significant increases in double support time and decreases in single support time during pregnancy appear to be compensations to minimize the time spent in single limb support when this increased muscular effort is required to support an increased body mass with only one foot.

The increase in width of the pelvis during pregnancy apparently was compensated for by an increase in maximum hip adduction during stance. Evidently the hip adduction angle was increased during the single support phase of gait in order to keep the foot centered under the body to avoid a wide base of support. Walking with a wide base of support necessitates large side to side excursions of the center of mass and is energy inefficient.

The significant increase in anterior tilt of the pelvis (top of the pelvis tipped forward) during pregnancy that was observed can be explained by the increase in the amount of body mass located in a low anterior position on the trunk during pregnancy. An increased anterior load on the lower trunk causes a forward rotating moment tending to rotate the pelvis forward. Unfortunately, trunk position was not measured in order to identify how trunk posture was altered to compensate for the increased anterior pelvic tilt. Typically, increased lumbar lordosis is necessary to bring the upper body backwards into a stable position when anterior pelvic tilt is increased.

The results of this study indicate that women alter their gait in order to compensate for the increase in body mass and change in body mass distribution during pregnancy. It should be noted that these deviations, although statistically significant, were mild and a surprising normal kinematic and kinetic profile was generally appreciated.

REFERENCES

Eng J.J., and Winter D.A., J. Biom., 28, 753-758, 1995.

Heckman J.D., Sassard R., J. Bone Joint Surgery, 76-A, 1994.

THE EFFECT OF STANCE-PHASE KNEE FLEXION ON THE VERTICAL DISPLACEMENT OF THE TRUNK DURING NORMAL WALKING

S. Gard, D. Childress

Rehabilitation Engineering Research Program
Department of Orthopaedic Surgery & Biomedical Engineering
Northwestern University, Chicago, IL 60611

INTRODUCTION

Clinical decisions regarding specific treatments for pathologic gaits often involve a differential approach with respect to normal walking. That is, the treatment attempts to minimize observed and measured differences in the gait of the patient to make the walking movements more normal in appearance. Therefore, effective clinical treatment requires a good understanding of how and why the body moves the way that it does in normal gait.

We measured stance-phase knee flexion and the vertical displacement of the trunk in normal adult male ambulators. From the kinematic data we calculated the effect of stance-phase knee flexion on the trunk's vertical displacement. The data that we present challenges a long-held theory in gait analysis that stance-phase knee flexion reduces the vertical excursion of the trunk in normal walking.

REVIEW AND THEORY

Stance-phase knee flexion was identified as one of six so-called "determinants" of normal walking in a theory originally proposed by Saunders, Inman and Eberhart (Saunders et al, 1953). These six determinants are simply kinematic descriptions of the movements that the legs and pelvis make during the normal gait cycle. These determinants are claimed to reduce and smooth the excursions of the body's center of mass during normal gait, thereby reducing the energy expenditure of walking. Stance-phase knee flexion has been claimed to reduce the peak-to-peak vertical displacement of the trunk by about 7/16" (~11 mm) during normal gait (Bowker and Hall, 1975; Bowker, 1981).

The theory of the six determinants of gait has never been rigorously tested or evaluated, though many researchers and clinicians today regard it as proven fact. Previously, we showed that pelvic obliquity, the second determinant of gait, doesn't reduce the vertical excursion of the trunk (Gard and Childress, In press) as claimed by the theory, but appears to play a crucial role in shock absorption.

The purpose of our research was to investigate the third determinant of gait, stance-phase knee flexion. We believe that stance-phase knee flexion, like pelvic obliquity, doesn't reduce the vertical excursion of the trunk.

PROCEDURES

Data was acquired from three, adult male subjects, of approximately the same age, height, and weight, and who were considered to be normal ambulators. Kinematic measurements were made using a Vicon (Oxford Metrics Ltd) six-camera system using a standard clinical marker arrangement, and the data was subsequently process with Vicon Clinical Manager software. The subjects walked at five speeds (approximately 0.8 m/sec, 1.0 m/sec, 1.4 m/sec, 1.7 m/sec, 2.0 m/sec). Kinematic gait data was acquired for three walking trials per speed for each subject.

We assumed that the vertical displacement of the trunk, $y_{TRUNK}(t)$, was equal to the sum of two vertical displacement variables:

$$y_{TRUNK}(t) = y_{KF}(t) + y_{NO\text{-}KF}(t)$$

where $y_{KF}(t)$ is the vertical displacement of the trunk due to stance-phase knee flexion, and $y_{NO\text{-}KF}(t)$ is the vertical displacement of the trunk in the absence of stance-phase knee flexion.

The vertical displacement of the trunk, $y_{TRUNK}(t)$, was measured from a virtual anterior marker lying at the midpoint between the two anterior superior iliac spine (ASIS) markers. The knee flexion angle was measured over a single gait cycle in each of the data trials. The vertical displacement of the trunk due to the stance-phase knee flexion wave, $y_{KF}(t)$, was determined by finding the vertical distance between the measured position of the hip joint center and the calculated position if the knee was assumed to be extended during the cycle. We assumed that stance-phase knee flexion would have the same vertical effect on the ipsilateral hip joint center

as it would on the trunk. The variable $y_{NO-KF}(t)$ was found by subtracting $y_{KF}(t)$ from $y_{TRUNK}(t)$.

RESULTS and DISCUSSION

A typical knee flexion record for one of the subjects walking at about 1.4 m/sec is shown in Figure 1. In this record, the stance phase knee flexion reaches its peak at about 12% of the gait cycle, and decreases to a local minimum at about 42% of the gait cycle. We assumed that the lead limb would be dominant in affecting the trunk's vertical displacement, and would have sole influence from the time of initial contact to contralateral limb initial contact. Because the data that we collected was unilateral for a particular gait cycle, we assumed symmetry between the two legs and artificially extended the stance-phase knee flexion wave into the latter half of the gait cycle to simulate the opposite limb's stance-phase knee flexion wave. Therefore, the effect of stance-phase knee flexion could be calculated over an entire gait cycle. The effect of knee flexion in the trailing limb on the trunk during double support was not considered in our calculations.

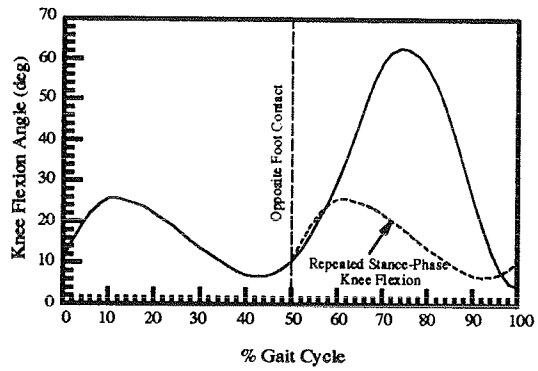

Figure 1: Sample Knee Flexion Record

The repeated stance-phase knee flexion curve enabled $y_{KF}(t)$ to be calculated (Figure 2), which was found to have peak-to-peak values from about -10 mm to -45 mm across the range of walking speeds. These values are quite significant compared to the measured peak-to-peak values of $y_{TRUNK}(t)$, which varied from about 25-85 mm across the range of walking speeds. However, the phase relationship between these two waveforms determines the ability of $y_{KF}(t)$ to affect the magnitude of $y_{TRUNK}(t)$. Stance-phase knee flexion is maximum at around the time of contralateral toe off, and is approaching its minimum when the trunk reaches its peak vertical displacement.

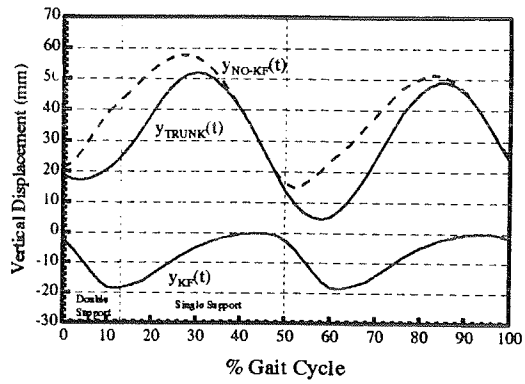

Figure 2: Sample Vertical Displacement Waveforms

When $y_{KF}(t)$ is subtracted from $y_{TRUNK}(t)$, yielding $y_{NO-KF}(t)$, the magnitudes of $y_{NO-KF}(t)$ and $y_{TRUNK}(t)$ are observed to be nearly equal (Figure 2). In fact, across the range of walking speeds from 1.0-1.8 m/sec, $y_{KF}(t)$ was found to reduce the vertical excursion of the trunk by a mean value of only 0.5 mm, which is significantly less than Bowker and Hall's claim of 11 mm (Bowker and Hall, 1975; Bowker, 1981). At speeds above 1.8 m/sec, stance-phase knee flexion consistently increased the trunk's vertical excursion.

Our results show that stance-phase knee flexion does not significantly reduce the vertical excursion of the trunk, contrary to the theory of the six determinants of gait (Saunders et al., 1953). Instead, we believe that, like pelvic obliquity, stance-phase knee flexion plays a critical role in shock absorption as load is rapidly transferred from the trailing to the leading limb during normal gait.

REFERENCES

Bowker J.H., Hall C.B. *Atlas of Orthotics*, 133-143, C.V. Mosby Co., 1975.

Bowker J.H. *Atlas of Limb Prosthetics*, 261-271, C.V. Mosby Co., 1981.

Gard S.A., Childress D.S. *Gait & Posture*, (In press).

Saunders J.B. et al. *JBJS*, 35-A(3), 543-558, 1953.

ACKNOWLEDGMENTS

Supported by NIDRR grant H133P20016. We wish to extend our sincere appreciation to Children's Memorial Hospital Gait Analysis Laboratory for use of their facilities.

INTERSEGMENTAL DYNAMICS OF THE SWING PHASE OF NONPREFERRED WALKING AND PREFERRED RUNNING

Mary M. Ryan[1] and Robert J. Gregor
Georgia Tech Research Institute[1],Department of Health and Performance Sciences, Georgia Institute of Technology, Atlanta, USA

INTRODUCTION

The purpose of this study was to examine the changes in the intersegmental dynamics of the swing phase of walking and running at a speed where running is preferred to walking. High speed video data was collected for three subjects as they locomoted overground at 3.2 m/s. Motion dependent torques were calculated for the thigh, shank and foot. The knee and hip generalized muscle moments and summed motion dependent torques were greater for the walk than the run at the end of swing. The increased summed motion dependent torque was due to a change in the interaction of the individual motion dependent torques. These large increases may indicate why walking is considered a nonpreferred gait compared to running at a speed of 3.2 m/s.

REVIEW AND THEORY

Comparisons between the segmental interactions in the swing phase of human walking and running have previously been reported (Zernicke et al., 1991 and Putnam, 1991). While there are distinct differences in walking and running intersegmental dynamics, a comparison of the segmental interactions at speeds at which one is capable of walking and running may provide additional information about the kinetic changes that make fast walking a nonpreferred gait. Various hypotheses have been proposed about the reason for gait transition (Farley and Taylor, 1991, and Hreljac, 1993), however no clear answer has emerged. While much of the information about gait transition has focused on kinematic and physiological changes, more information about the changes in kinetics is needed to highlight possible differences in lower extremity mechanics which may lead to gait transition. Therefore, the purpose of this study, was to examine the intersegmental mechanics of the lower extremity during the swing phase of walking and running at a speed where running is preferred to walking.

METHODS

A linked segment rigid body model of the lower extremity was used for a 2-dimensional analysis of the swing phase of walking and running. Data were collected at an outdoor track for three subjects locomoting overground at 3.2 m/s. Lower extremity movement was captured at 200 Hz using two high speed video cameras (NAC, Inc.). Motion dependent torques (MDTs) at the foot, shank and thigh were calculated using intersegmental dynamics equations as described by Feltner (1989).

RESULTS AND DISCUSSION

All data presented are the average of 10 trials for each condition and expressed as a percent of swing. While the generalized muscle moments during the swing phase are not shown, these moments are approximately equal in magnitude and opposite in sign to the summed motion dependent torque.

The primary changes in the motion dependent torques at the shank and thigh were observed during the last 30% of swing. The knee and hip GMM both displayed greater peak moments in the nonpreferred walk compared to the run (Table 1).

Condition	Knee GMM	Hip GMM
Walk	50 Nm	80 Nm
Run	35 Nm	45 Nm

Table1. Peak Knee & Hip GMM for the last 30% of swing

These differences were also reflected in a 10 - 15 Nm increase in the summed MDT acting on the shank (Figure 1) and 25 Nm increase in the summed thigh MDT, for the walk compared to the run. The increase in thigh and shank summed MDTs at the end of swing were attributed to differences in the relative contribution of the individual MDTs.

The torque due to the linear acceleration of the hip (AHIP) displayed a knee extensor torque

for both the walk and run for the last 20% of swing. In contrast, the torque due to the angular acceleration of the thigh (AAT) acting on the shank, was near zero or slightly extensor in the walk, but displayed a flexor torque in the run (5 to 10 Nm). The combination of an extensor AHIP torque and flexor AAT torque acting on the shank, aided in reducing the magnitude of the summed MDT in the run condition (Figure 2). In the walk however, none of the individual motion dependent torques contributed to reducing the effect of the extensor AHIP torque, resulting in an increased summed MDT acting on the shank. These interactions were reflected as an increase in the knee GMM in the nonpreferred walk.

The thigh GMM magnitude was also larger for the walk, due to the combination of the AHIP torque and the torque due to the angular acceleration of the shank. Similar to the shank, the AAT torque acting on the thigh acted to decrease the summed MDT in the run but not the walk.

Increases in GMM magnitude would be expected with increased walking or running speed, as the demand on the lower extremity became greater. The larger hip and knee GMM magnitudes for the walk condition suggest that a greater demand was placed on the musculature for this condition than for running at the same speed. The increased muscular demand could also be reflected in increases in EMG activity. Nilsson et al. (1985) reported increases in lower extremity EMG magnitude as speed increased for both walking and running. Therefore, increased GMM magnitudes at the knee and hip would likely be accompanied by increases in EMG activity. The change in the AHIP torque acting on the shank would therefore contribute to an increase in the demand on the musculature, as reflected by the increased GMM and summed MDT magnitudes.

Kinetic analysis of the swing phase of nonpreferred walking and preferred running indicate changes in segmental interactions at a speed of 3.2 m/s. The increased GMMs at the knee and hip, for the walk compared to the run, were attributed to changes in the individual contribution of the MDTs. In the run, the MDT interactions tended to reduce the summed MDT thereby decreasing the GMM. This resulted in a decreased demand on the lower extremity in running at 3.2 m/s compared to walking at this speed. The increased muscular demand at the end of swing may contribute to the inability to maintain a walking gait at this speed, thus making running the preferred gait at this speed.

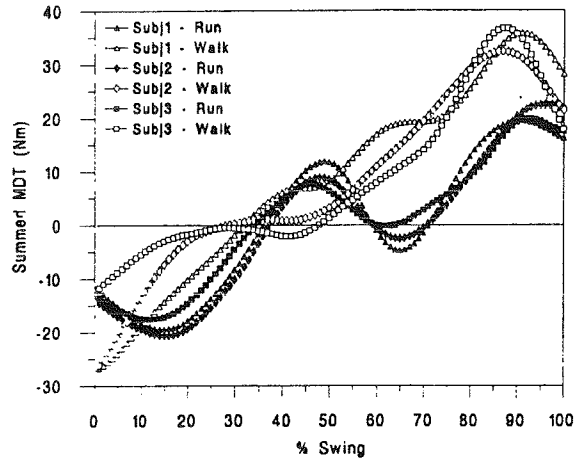

Figure 1. Summed Motion Dependent Torques acting on the Shank for 3 Subjects

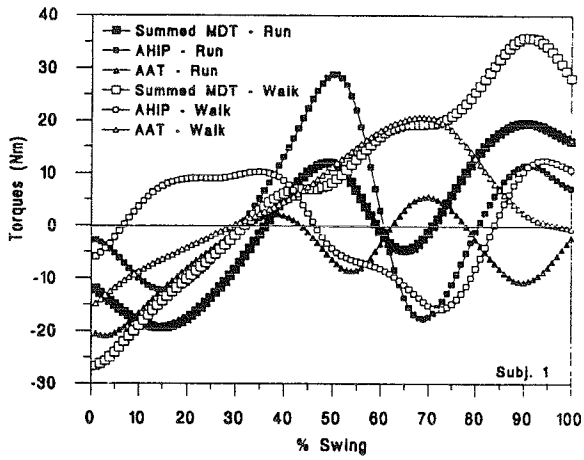

Figure 2. Motion Dependent Torques acting on the Shank (Subj. 1)

REFERENCES

Farley and Taylor. Science, 253, 1991.
Feltner, M. Int J. Sport Biomech, 5, 1989.
Hreljac, A. Med. Sci. Sports Ex. 25(10), 1993.
Nilsson et al., Acta Physiol. Scand. 123, 1985.
Putnam, C. Med Sci Sports Exer, 23 1991.
Zernicke et al., In *Adaptability of Human Gait*, edited by A.E. Patla, 187-202, 1991.

GROUND REACTION FORCES IN 1G AND SIMULATED ZERO-GRAVITY RUNNING

Jean L. McCrory, Janice Derr*, and Peter R. Cavanagh
Center for Locomotion Studies , Department of Kinesiology and *Statistical Consulting Center
Penn State University, University Park, PA 16802

INTRODUCTION

This research compared ground reaction forces during overground (1G) running and zero-gravity (0G) simulated treadmill running at a full body weight load in two restraint harness designs.

REVIEW AND THEORY

Exercise will almost certainly play an integral part in minimizing the bone mineral loss and muscular atrophy that occur during spaceflight. It is hypothesized that an effective exercise regimen would elicit loads on the lower extremities that resemble those on Earth (Convertino and Sandler, 1995). No on-orbit testing has yet quantified the forces to which the lower extremity has been exposed, but it is believed that, to date, these forces have been much less than the forces experienced in 1-G (Cavanagh, 1987).

The Penn State Zero-Gravity Simulator (PSZS Davis et al. 1996) is a device which suspends subjects horizontally from multiple latex cords, with each cord negating the weight of a limb segment. A treadmill mounted on the wall under the PSZS enables subjects to run in simulated 0G. Subjects wear a harness to which a number of springs, which provide a gravity replacement load, are connected. The opposite end of each spring is connected to the side of the treadmill. During exercise, astronauts currently wear a similar harness in which the spring tethering load pulls at both the waist and shoulders (Greenisen and Edgerton, 1994).

The purpose of this study was to compare ground reaction forces from subjects wearing one of two harness designs under a 100% BW load in the PSZS with data from the same subject running across the laboratory floor. The objective was to gain insight into the effectiveness of the present exercise countermeasures for bone mineral loss and muscular atrophy in space.

PROCEDURES

Sixteen subjects (age 22.9±6.9 yrs, height 178.1±6.68 cm, and mass 72.8±5.8 kg) participated in this study. Subjects ran at 2.68 m/s. One Kistler force plate recorded normal force data as subjects ran across the laboratory floor and another, mounted within the treadmill belt, measured normal ground reaction forces of subjects in the PSZS. Two PSZS subject load configurations were assessed: a "shoulder only" design (SSO), in which 4 springs were attached to shoulder pads worn by the subject, and "waist and shoulder " design (WSS), in which 4 springs were attached to the shoulder pads and 4 to a waist harness. Load cells measured tension in the springs. Data were collected at 500 Hz.

RESULTS

All subjects could tolerate a 100% body weight load applied through the harness. The maximum active force was significantly greater in the 1G condition, although the timing of this event was the same in all conditions (Figure 1, Table 1). The magnitude of the passive peak was similar in all conditions, but this peak occurred earlier in the PSZS conditions, resulting in a significantly greater loading rate. The impulse was greater in the 1G condition.

Table 1: Ground Reaction Force results

	1G	SSO	WSS
Max. Active GRF (%BW)	*240.61 ±7.04	180.04 ±3.77	159.75 ±3.97
% stance Max Active GRF	43.57 ±2.89	43.80 ±1.60	43.99 ±1.64
Max. Passive GRF (%BW)	159.29 ±7.34	161.84 ±3.90	150.08 ±4.01
% stance Max Passive GRF	*15.01 ±1.11	10.64 ±0.59	10.07 ±0.60
Load Rate (BW/sec)	40.60 ±2.85	*51.97 ±1.52	*51.81 ±1.57
Impulse (BW sec)	*0.41 ±0.14	0.33 ±0.01	0.30 ±0.01

* indicates that $p<0.01$

The tension in the tethering springs fluctuated by 17.89±1.25%BW in the SSO condition and 36.83±1.30%BW in the WSS condition as the subject's COM oscillated toward and away from the treadmill surface. The average subject load was 96.36±1.59 %BW in SSO and 88.95±1.66%BW in the WSS condition. The flight phase impulse in the 1G was only approximately 87% of the flight phase impulse in the PSZS conditions.

DISCUSSION

The maximum force occurred at approximately the time of the minimum subject load (Figures 1 and 2), which was less that body weight at this time. The subject was pushing off less because a smaller force was needed to overcome the "gravitational" load. If the force curves are normalized to the gravity in 1G or the instantaneous subject load in the PSZS instead of body weight, the curves look similar in all conditions, as shown in Figure 3.

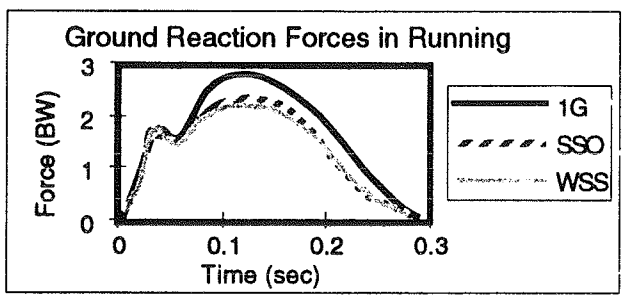

Figure 1: Representative ground reaction force curves from the running conditions.

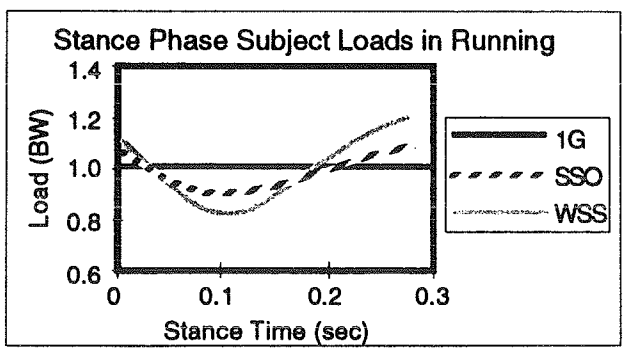

Figure 2: Representative subject load curves during the stance phase of running.

Because the flight impulse was greater in the PSZS conditions, the subject had a higher impact velocity - resulting in a greater loading rate.

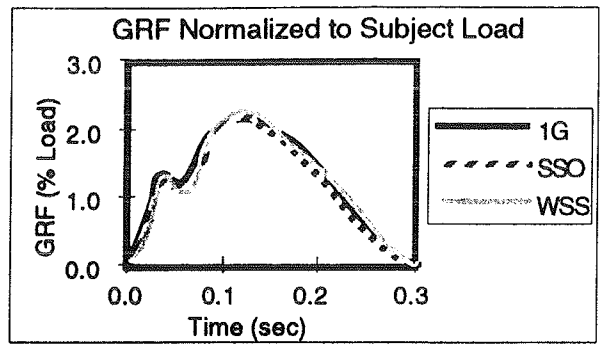

Figure 3: Maximum ground reaction force, for one subject, normalized to subject load instead of body weight.

The conclusions of this study are entirely dependent upon what aspects of the 1G forces are important for maintaining bone and muscle. If the aim is to equal 1G peak forces (Whalen et al., 1988), the fluctuation of subject load should be minimized since this appears to be responsible for requced normal GRFs during mid-stance. If it is greater loading rates that result in increased bone density (Lanyon and Rubin, 1984), then fully loaded 0G treadmill exercise will be effective as long as it is of the necessary duration.

ACKNOWLEDGMENTS

This research was supported by NASA grant NAGW-4421.

REFERENCES

Cavanagh, P.R. et al. A Final Report to Krug International, 1-126, 1987.

Convertino, V.A., and Sandler, H. Acta Astro., 35, 253-270, 1995.

Davis, B.L. et al. Av. Space Env. Med. 67, 235-242, 1996.

Greenisen, M.C. and Edgerton, V.R. In: Space Physiology and Medicine, (pp. 194- 210), Lea & Febiger, 1994.

Lanyon, L.E. and Rubin, C.T. J Biom. 17, 897-905, 1984.

Whalen, R.T. et al. J Biom. 21, 825-837, 1988.

EXPLORING MINIMAL NORM OPTIMIZATION FOR SOLVING THE REDUNDANCY PROBLEM IN MULTI-FINGER TASKS

Zong-Ming Li, Mark L. Latash, Vladimir M. Zatsiorsky
Department of Kinesiology, The Pennsylvania State University, University Park, PA 16802

Various optimization techniques and cost functions have been used to examine how individual muscles contribute to the resultant moment at a joint (Crowninshield and Brand, 1981; Challis and Kerwin, 1993; Dul et al., 1994). However, because individual muscle forces cannot be immediately measured, the optimization results cannot be directly validated. The purpose of this paper is to explore how a total force is shared among individual fingers in maximal voluntary press tasks. This approach allows validating directly the optimization results.

METHODS

Experimental procedures

Maximal normal forces (F_i) produced by individual fingers were measured in 10 young subjects in press tasks (See Figure 1 for the setup of force sensors.). Three multi-finger tasks (IM, IMR, IMRL) were performed to measure the maximal individual finger forces (F_i). I, M, R and L stand for the index, middle, ring and little fingers, respectively. The maximal forces from individual fingers in single-finger (F_{mi}) tasks were also measured. During testing, the subjects received visual feedback information about the total force they produced.

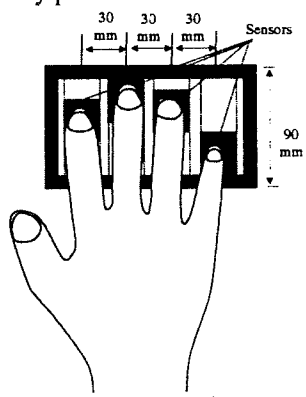

Figure 1 Force sensor setup for press tasks

Optimization model

We hypothesize that the CNS is trying to minimize a certain norm of the relative force values (% of F_{mi}). This approach is not new in motor control and biomechanics. It has been broadly used to explore the sharing/motor redundancy problem at the level of individual muscles and their contribution to a total joint torque. It seems natural to employ this approach for the finger force sharing problem where all the finger forces can be directly measured. More formally the problem can be formulated as follows:

Minimize
$$g(F_i)=\left(\sum_{i}^{N}\left(\frac{F_i}{F_{mi}}\right)^{n}\right)^{\frac{1}{n}} \quad (1)$$

Subject to:
$$h(F_i)=\sum_{i=1}^{N}F_i = C \quad (2)$$

where i stands for a finger involved in a task, N is the number fingers involved in the tasks (N = 2, 3, 4). C is a total force level achieved by the involved fingers. The model can be stated as follows: find the force sharing pattern by minimizing a certain norm of relative force.

Theoretical solution to the optimization

The problem can be reformulated by using a Lagrangian function (note that the n^{th} root is removed without change in the solution to the problem.)

$$L=\sum_{i}\left(\frac{F_i}{F_{mi}}\right)^{n}+\lambda\sum_{i}F_i \quad (3)$$

where λ is a Lagrangian multiplier. Differentiating Eq (3) with respect to F_i to find a minimum, we have

$$\frac{\partial L}{\partial F_i}=n\left(\frac{F_i}{F_{mi}}\right)^{n-1}\left(\frac{1}{F_{mi}}\right)+\lambda=0 \quad (4)$$

After appropriate rearrangement of Eq (4), we have the following force ratios among fingers,

$$\frac{F_i}{F_j}=\left(\frac{F_{mi}}{F_{mj}}\right)^{\frac{n}{n-1}} \quad (5)$$

and

$$F_i=\frac{C}{\sum_{j=1}^{N}\left(\frac{F_{mj}}{F_{mi}}\right)^{\frac{n}{n-1}}} \quad (6)$$

Eq (5) and (6) are expressions for force sharing among fingers. It can be seen that force sharing among fingers is dependent on their single-finger maximum force and the power (n) of the cost function. If the power of the cost function is known, the force sharing among fingers can be predicted accurately.

RESULTS AND DISCUSSION

The maximal finger forces in single- and multi-finger tasks are shown in Table 1.

Task	I	M	R	L
Single-Finger	52.6 (13.9)	54.1 (15.0)	40.5 (10.1)	24.6 (7.9)
IM	32.8 (11.7)	33.0 (10.2)	— —	— —
IMR	26.9 (10.0)	31.4 (9.9)	18.3 (7.0)	— —
IMRL	24.8 (8.9)	26.2 (8.6)	18.4 (7.7)	9.5 (5.7)

Table 1 Experimental results: Maximal finger forces (N) in single- and multi-finger tasks. Mean (SD), n=10.

Figure 2 reflects the accuracy of finger force prediction by optimizing the cost function—the norm of relative force—with changing values of the power ($1.1 < n < 1000$). In the figure the x axis was scaled by $log_2(n)$. y axis is the root mean square error, the difference between the experimental data and the results predicted by the model. Generally when an appropriate power value of the cost function was chosen the model predicted the force sharing among fingers quite well. For IM task, the larger the n, the less the error. The error was only 0.36 N at n =1000. The best prediction for the IMR task corresponded to n = 2.3, with an error of 1.26 N. The least error for the IMRL task was 0.25 N at n = 4.9.

Note that as the value of n increases, the ratio of the two finger forces in Eq (5) tends to approach the ratio of their single-finger maximal forces. With n approaching infinity, the force sharing among fingers could be accurately predicted by making all the relative forces equal, i.e.,

$$\frac{F_i}{F_{mi}} = K = constant, \quad i = involved\ finger \qquad (7)$$

This tendency was observed in the IM task where the force sharing between the two fingers is relatively simple. In the IM task, the fingers share the total force proportionally to their own maximal capabilities. However, in the IMR and IMRL tasks, the optimal values of power in the cost function were n = 2.3 and n = 4.9, which indicated that the involved fingers did not share the total force proportionally to their single-finger maximal forces.

CONCLUSIONS

Using a norm of relative force as a cost function allows to predict the force sharing among fingers. The power is dependent on the complexity of the task.

The multi-finger model provides an opportunity to validate optimization methods: how well they are imitating/mimicking what the central nervous system (CNS) is doing. The similarity of the experimental and predicted results does not imply, however, that the ways of solving the problem are also similar. The CNS is evidently using other ways—not the cost function minimization—to solve the redundancy problem.

REFERENCES

Challis JH, Kerwin DG, Proc Instn Mech Engrs, 207:139-148, 1993

Crowninshield RD, Brand RA, J Biomech, 14(11):793-801, 1981

Dul J et al., J Biomech, 17:675-684, 1994

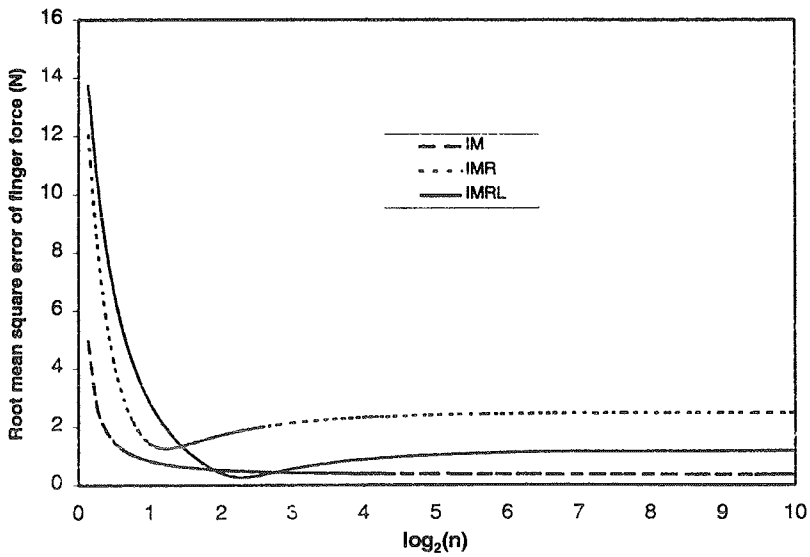

Figure 2 The root mean square error of finger force as a function of the power of the minimal norm cost function.

THE EFFECT OF ASYMMETRIC LOADING ON TARGETED REACHING

Christopher C. Pagano
Department of Psychology, Clemson University, Clemson, SC, 29634-1511

INTRODUCTION

Previous research has demonstrated that reaching entails the use of kinesthetic information available during the reach (e.g., Ghez et al., 1995). Further work has indicated that perceived limb orientation corresponds to the orientation of the limb's mass distribution (e.g., Pagano & Turvey, 1995). Accordingly, the mass distribution of the limb may provide a quantification of kinesthetically perceived limb configuration during reaching. Results are presented indicating that the perceived spatial configuration of the limb can be perturbed during blind reaching by the application of an asymmetrical load.

REVIEW AND THEORY

For targeted reaching to be most accurate, vision of both the target and the hand is required (e.g., Carlton, 1992; Jeannerod & Prablanc, 1983). However, continued vision of the target and hand during the reach are not required to bring the hand within the ballpark of a target (Goodale et al., 1986; Pélisson et al., 1986). Relatedly, it has been demonstrated that in bringing the hand to a target, information obtained visually regarding target location must be coupled with kinesthetic information regarding the configuration of the limb both before (Pélisson et al., 1986) and during (Ghez et al., 1995) the reach. Thus accurate reaching entails the use of visual and kinesthetic information obtained before reach initiation, as well as visual and kinesthetic information available during the reach. What sort of information regarding a limb's configuration and movement is available kinesthetically? Evidence suggests that sensitivity to limb position and movement originates in muscle and tendon receptors rather than in the joints themselves (e.g., Gilhodes et al., 1993; Goodwin et al., 1972; Kelso, 1978). Further research indicates that perceived limb orientation corresponds to the orientation of the limb's mass distribution, which can be manipulated independently of the joint angles (Pagano et al., 1996; Pagano & Turvey, 1995). Accordingly, the mass distribution may provide a quantification of kinesthetically perceived limb segment orientations during reaching. Thus it may be expected that reach trajectories can be perturbed by asymmetrical loading.

PROCEDURES

Each trial began with the right hand holding a cross-shaped object in a launchpad located at the participant's hip. The object was held with the 'stem' oriented horizontally and the 'cross piece' oriented vertically. The participant was instructed to remove the object from the launchpad and bring the front of the stem as rapidly and accurately as possible to the target, while keeping the cross piece oriented vertically. The target was positioned at eye level at a distance reachable by fully extending the arm forward without moving the shoulder or trunk. Participants closed their eyes before each reach so as to receive no visual feedback concerning their performance during the reach. Participants were asked to bring the distal tip of the hand-held stylus as close as possible to the target without making contact. This procedure rules out kinesthetic feedback regarding the endpoint of the trajectory, provides a target whose effect on the limb trajectory is through vision only, and ensures that the experimental effect reflects perceived limb position. Reaches were measured using a two-camera WATSMART system sampling an infrared diode (IRED) at 100 Hz. The IRED was placed on the metacarpophalangeal joint of the index finger.

Participants completed a block reaches with a 4 g wood cross piece attached symmetrically (WS1), followed by a block with a 296 g metal cross piece attached symmetrically (MS), a block with the metal cross piece attached above the hand (MA), a block with the metal cross piece below the hand (MB), and a second block of reaches with the wood cross piece (WS2). The metal cross piece conditions are illustrated in Figure 1. Each block consisted of ten reaches separated by several seconds of rest.

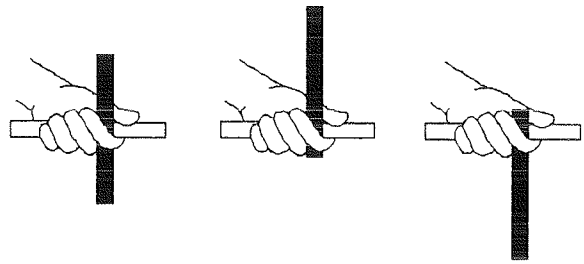

Figure 1: In some trials participants reached with a metal cross piece attached symmetrically, above the hand, or below the hand.

RESULTS

The mean vertical component (z) of the hand trajectory at the end of the fast phase of movement is presented in Table 1 as a function of mass condition. The target corresponded to a vertical coordinate of zero. The participants tended to reach lower when the mass of the hand-held object was distributed higher, and tended to reach higher when the mass of the hand-held object was distributed lower. The trend was for z to remain constant when the mass remained evenly distributed about the hand (compare Conditions WS1, MS and WS2 in Table 1), for z to drop when the mass was moved to above the hand (compare Conditions MS and MU), and for z to rise when the mass was moved from above the hand to below the hand (compare Conditions 3 and 4). A 4 x 5 ANOVA on z with subjects and mass condition as factors resulted in a significant main effect for mass condition [$F(4, 36) = 5.7$, $p < .001$]. Post hoc t-tests confirmed that z for Block 4 was significantly higher than that of each of the other Blocks, and that Block 3 was significantly lower than Block 2 (all $p < .05$).

Table 1: Mean vertical coordinate z (mm) of the hand trajectory at the end of the fast phase of movement for each of the participants (P).

	Mass Condition				
P	WS1	MS	MU	MD	WS2
1	11.5	11.7	8.2	20.9	11.8
2	5.5	4.1	0.3	15.2	-2.7
3	-11.3	-13.2	-18.6	-7.8	-8.2
4	21.1	26.3	15.6	26.0	14.0
Mean	6.7	7.2	1.4	13.6	3.7

DISCUSSION

These results indicate that in the absence of vision, the location that the hand is brought to during a reach is affected by manipulations of the limb's mass distribution. A reliable perturbation in the trajectory of the limb was produced as a function of the altered mass distribution. The procedure employed ensured that this perturbation was in fact perceptual. What was perturbed was the perceived spatial configuration of the limb during the reach.

The effect reported is small. This is due in part to the measurement limitations caused by recording only a single IRED placed on the hand. The perturbation caused by the asymmetrical mass is likely involved a rotation about the wrist. In future experiments, multiple IREDs will be placed on the object and hand in order to accurately detect and measure rotations of the object and hand.

REFERENCES

Carlton L.G. in Proteau L. & Elliott D. (eds.) Vision and Motor Control, North-Holland, 1992.

Ghez, C. et al. in Gazzaniga M.S. (ed.) The Cognitive Neurosciences, MIT Press, 1995

Gilhodes J.C. et al. Biol. Cybern., 68, 509-517, 1993

Goodale M.A. et al. Nature, 24, 748-320, 1986.

Goodwin G.M. et al. Brain, 95, 705-748, 1972.

Jeannerod M. & Prablanc, C. in Desmedt J. (ed.) Motor control mechanisms in man, Raven Press, 1983.

Kelso J.A.S. Psychol. Rev., 85, 474-481, 1978.

Pagano C.C. & Turvey M.T. J. Exp. Psychol. Hum. Percept. Perf., 21, 1070-1087, 1995.

Pagano C.C. et al. Ecol. Psychol., 8, 43-69, 1996.

Pélisson D. et al. Exp. Brain. Res., 62, 303-311, 1986.

ACKNOWLEDGEMENTS

This work was supported by U.S. PHS NRSA 1FS32NS09575-01. The author gratefully acknowledges the assistance of Geoffrey Bingham and Michael Stassen.

EFFECTS OF AGE AND TARGET DIRECTION ON FAST REACH-REVERSAL MOVEMENTS

H. Chai and M.Gross
Deaprtment of Movement Science, University of Michigan, Ann Arbor, MI 48109-2214

INTRODUCTION

Reaching movements have been widely studied to investigate movement patterns and neuromotor control mechanisms for the past two decades (Georgopoulos, 1995). Many of those studies have focused on reaching movements while seated that require less postural control than during standing (Moore et al, 1992). Other studies have investigated reaching towards a target, but not returning from it (Duren et al, 1990). Few studies have investigated the more natural movement of quickly reaching towards and returning from a target while standing. These reach-reversal movements may be particularly challenging for the elderly since they have less dynamic balance control.

The purpose of this study was to investigate the ability of young and elderly subjects to perform fast reach-reversal movements to targets in different directions. Reach-reversal movements are defined as the motion towards a target and return to the start position. Results indicated that both age and target direction affected the reach biomechanics.

REVIEW AND THEORY

Decreased postural stability is associated with an increased risk for falling in the elderly. The maximum excursion of the center of pressure (MCOPE) decreases with age (Duren et al, 1990). Recently Blaszczyk et al. (1994) reported that the decrease in MCOPE with age depends on movement direction. In that study, the elderly had significantly smaller MCOPE than young subjects while leaning backwards or to the left side but not while leaning to the front or to the right side. However, they examined static leaning movements only, however, rather than the disturbance of balance associated with functional tasks such as reaching movements. In this study, we examined both age and target direction effects in order to have a more clear understanding of the factors affecting control of reaching movements in the elderly.

PROCEDURES

Eight healthy, right-handed elderly subjects (74.1±5.4 yrs, 4 male and 4 female;) and eight young subjects (23.2±4.1 yrs; 4 males and 4 females) volunteered to participate in the study. They all reported no history of neurologic or muscular abnomalities.

Each subject performed reach-reversal movements in 4 directions (0, 45, 90, and 120 deg from body midline) and at 2 distances (arm-length and maximum reach) while standing on the force platform. Markers were placed on the hand, wrist, elbow, shoulder, hip, knee, ankle and metatarsophalangeal joints, and kinematic data were recorded with a 3D video-based motion analysis system. An accelerometer was placed on the wrist to determine movement onset. Subjects reached to the target as fast as possible and then brought their arm back to the starting position immediately. The order of reach direction was randomized. Each dependent variable was analyzed separately in a $2 \times 2 \times 4$ ANOVA with repeated measures for age, gender,and target direction. The significance level was set at $\alpha = .05$.

RESULTS

Subjects were similar in body weight and body height. The base of support (BOS) was significantly greater in the elderly than in the young subjects ($p<.01$).

Reach distance (difference between maximum reach and arm-length reach distance) decreased with increase in target direction for both young and elderly subjects. Although young subjects reached farther than the elderly subjects in all directions, the difference was significantly only for the 0 deg direction ($p<.001$).

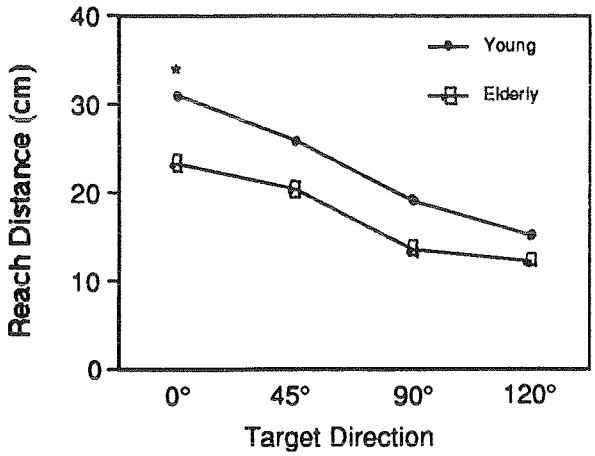

Fig. 1: Reach distance in different target directions.

Movement time depended on age and reach distance. Movement time was similar for both age groups and all directions in the arm-length reaches. For the maximum distance reaches, however, movement time was significantly longer for the elderly than for the young subjects ($p<.01$). Thus, the elderly took longer to move the same distance as the young. In contrast, the movement reversal time showed age and gender effects during arm-length reaches but no differences occurred during maximum reaches. Reversal time increased with age ($p<.01$) and was greater for female than for male subjects ($p<.05$). No target direction effect occurred.

Shoulder joint angular velocity depended on age and target direction. Both age and target direction affected the peak shoulder flexion angular velocity (SFAV) ($p<.05$ and $p<.01$), but not the peak shoulder extension angular velocity. SFAV decreased with age ($p<.05$) and target direction ($p<.01$).

Maximum excursion of the center of pressure (MCOPE) showed no gender or age effects during arm-length reaches. In maximum reaches, however, MCOPE was significantly greater in the young subjects (0 and 45 deg targets) ($p<.05$) (Fig. 2). MCOPE depended on target direction in both young and elderly subjects ($p<.001$). To determine relative stability between age groups, MCOPE was normalized by both BOS and reach distance (RD). MCOPE/BOS was greatest for the 45 deg target for both elderly (2.06%) and young subjects (3.46%). MCOPE/BOS was significantly greater in the 45 deg target direction than for the other directions ($p<.0005$). When normalized by reach distance, however, MCOPE/RD increased with direction ($p<.05$).

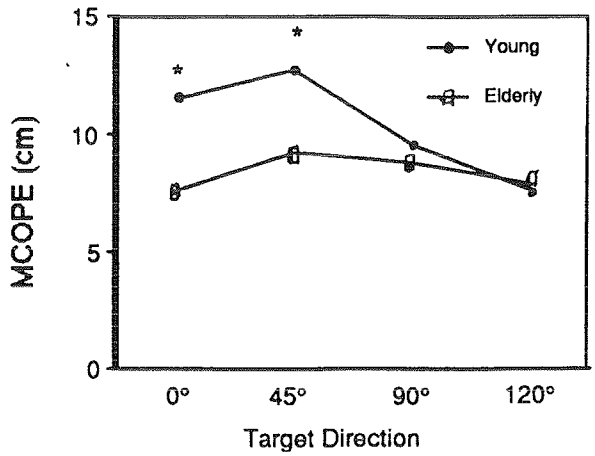

Fig. 2: Maximum center of pressure.

DISCUSSION

The results of this study supported the hypothesis that elderly subjects generated reach-reversal movements differently than young subjects, especially in the maximum reaches. Elderly subjects moved relatively more slowly, and spent more time near the target during the reversal portion of the movement. Shoulder flexion velocity was also slower in the elderly subjects.

There was no difference, however, in how elderly and young subjects reached to the different target directions. When normalized by reach distance, MCOPE/RD changed in the same way with target direction for both age groups, suggesting that subjects used the same strategy to modify their MCOPE as a function of reach distance. When normalized by base of support area, MCOPE/BOS was greatest at the 45 deg target direction, indicating that all subjects were statically most stable when reaching to the 45 deg target, regardless of age.

REFERENCES

Blaszczyk, J.W., Lowe, D.L. Hansen P.D. Gait Posture 2, 11-17, 1994.
Duran, P.W. et al. J Gerontol. Med. Sci. 45, M192-197, 1990.
Georgopoulos, A.P. Trend Neurosci, 18, 506-510, 1995
Moore, S., et al. Phys. Ther. 72, 335-343, 1992

THE EFFECTS OF LOAD AND UNEXPECTED DELAYS, ON LONG-LATENCY STRETCH RESPONSES OF HUMAN ELBOW MUSCLES

Nikitas Tsaousidis[1] and Pierre Gervais[2]

[1]Biomechanics Laboratory, Pennsylvania State University, University Park, PA 16802, USA
[2]Dept. of Phys. Ed. and Sport Studies, University of Alberta, Edmonton, AB, Canada T6G 2H9

INTRODUCTION

Skillful execution of a motor task relies heavily on the anticipation of an upcoming event and on accurately timed patterns of muscle activation. This study tried to find whether modifications in long latency (M2-M3) stretch responses in arm muscles, can be caused the ability to predict the time and the magnitude of a stretch perturbation. The long latency components are preprogrammed but their exact mechanism is still unclear. The findings of our study suggest that timing information affects the magnitude of the M2-M3 EMG of the agonist muscles. The magnitude of the perturbation (load) also influenced EMG responses on agonists and antagonists.

REVIEW AND THEORY

In order to understand how the reflex EMG is affected by different load intensities and levels of anticipation, one should go back to the concept of preparatory set. Evarts et al. (1984) defined it as a state of readiness to receive a stimulus that has not yet arrived or a state of readiness to make a movement. In tasks of catching falling light loads, Lacquaniti and Maioli (1987, 1989) argued that anticipatory and reflex EMG responses were centrally preset and showed that catching tasks involve coactivation rather than the usual reciprocal inhibition. Yamamoto and Ohtsuki (1989) applied heavy loads (without momentum) of up to 50% of MVC, to extend the elbow joint and found that the M2 and M3 components of the biceps reflex EMG were strongly affected by vision and instruction.

The purpose of this study was to examine the role of load and unexpected delays of the stretch stimulus onset during braking-and-accelerating forearm movements. The investigation focused on the effects of these factors on mechanical performance and the reflex responses of the biceps brachii and triceps brachii.

PROCEDURES

A stretch stimulus, caused by the 20 cm free fall of a weight, was applied to the elbow flexors of the dominant arm of thirty male subjects. Initially the arm was relaxed –no anticipatory activation was allowed– with the elbow joint at a right angle. The subjects were warned of the imminent fall of the weight and were instructed to brake the movement of the load and try to move it backward as fast as possible. No visual or auditory cues were provided. The participants were told that the exact time of the perturbation might vary randomly and for the first forty trials the weights were released two seconds after the warning. To test the effect of unexpected delay, the weights in the last two trials performed by each subject were released four seconds after the warning instead of the usual two seconds expected in the previous trials. The subjects were divided into three groups and each group was tested with a different load intensity (11, 19 or 27% of maximum isometric strength).

Angular displacement data of the elbow joint were acquired using a Penny & Giles electrogoniometer and low-pass filtered at 12 Hz. Surface EMG recordings from biceps brachii and triceps brachii were full wave rectified and low-pass filtered at 100 Hz. The data were averaged for the last five 'regular' and the two 'delayed' trials of each subject. In this study, the reflex bursts of EMG (M1, M2, M3) could not be clearly distinguished in the averaged data and therefore the analysis defined as long latency the normalized integrated EMG in the period 50-100 ms after the stretch stimulus. Subsequently, 2x2 repeated measures MANOVAs were conducted.

RESULTS

The findings suggested that mechanical performance (reflected in the maximum angular displacement during the

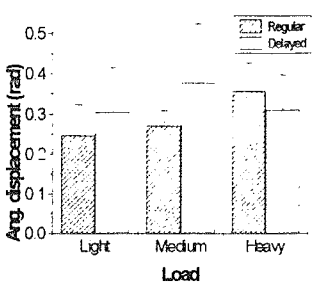

Fig. 1: Max. displacement

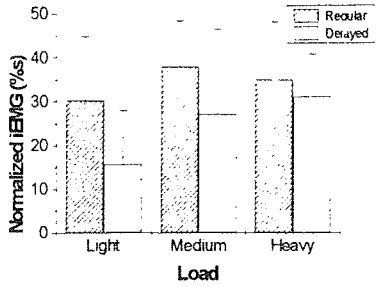

Fig. 2: Biceps M2-M3

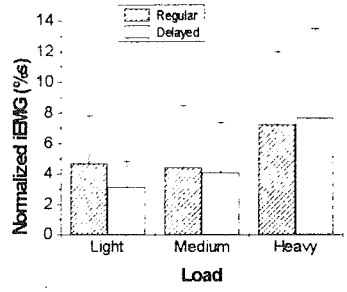

Fig. 3: Triceps M2-M3

braking phase of the movement) deteriorated when the load increased and when the stretch stimulus was delayed. The analysis revealed a significant interaction of Load by Type of stimuus onset (expected/delayed). It appears that the increase in angular displacement in the 'delayed' trials, was more pronounced in the medium load (angle in 'delayed' trials 40% larger than in regular) and it existed in the light load (23%) but not in significant levels. On the heavy load condition there was actually a 19% reduction in the angular displacement in the 'delayed' trials.

The long latency EMG response of the biceps was enhanced when the load increased from light to medium but didn't show any significant changes from medium to heavy. Unexpected delays led to a 48% reduction under light load, 28% under medium load and 11% under heavy load.

The reflex EMG responses of the triceps were not affected by the type (expected or unexpectedly delayed) of stimulus, and light and medium loads, but increased sharply when heavy loads were applied.

DISCUSSION

In the particular experimental task, the data provided support for the notion of a preparatory set of limited duration in the flexors. To better comprehend that, one should bear in mind two important features of the experimental procedures: a) No anticipatory action or muscle activation was allowed prior to the stimulus onset. Thus, the gain of the reflex responses was not influenced by any anticipatory activity. b) In the 'delayed' trials, the subjects were still under the instructions to wait for the falling of the weights. If the state of readiness could be maintained for as long as the subjects wanted, no differences would have been observed when the stretch stimulus was delayed.

In the present study, the preparatory set is considered to apply to the action of the two muscle groups investigated. As the speed, novelty and difficulty of a movement increases, so does the preset gain of the stretch reflex responses (see Prochazka, 1989). This provides a possible explanation for the effects of load on biceps EMG reflex responses: the increased loading presents additional difficulty to the task and the gain is set higher. Yamamoto and Ohtsuki (1989) postulated that the preparatory set which was based on temporal anticipation due to the visual information could not be maintained for even a few seconds but did not specifically test the effects of delaying the stimulus onset. This study however, focused on these effects and it seems that indeed, the preparatory set –in the particular experimental task– begins to lose its effectiveness after just a two second delay.

The observed reflex coactivation patterns suggest the existence of two different preparatory sets, one with limited duration for the flexors and a second –not affected by delays– for the extensors.

REFERENCES

Lacquaniti, F. & Maioli, C. J. Neuroscience, 9(1), 134-148, 1989.

Lacquaniti, F. & Maioli, C. Brain Res., 406, 373-378, 1987.

Evarts, E.V, et al. Neurophysiological Approaches to Higher Brain Functions, John Wiley, 1984.

Prochazka, A. Progress in Neurobiology, 33, 281-307, 1989.

Yamamoto, C. & Ohtsuki, T. Exp. Brain Res., 77, 12-22, 1989.

OVERSHOOTING ERRORS IN HYPERGRAVITY ARE NOT EXPLAINED BY THE REINTERPRETATION HYPOTHESIS

R. D. Seidler-Dobrin[1], G. T. Yamaguchi[2], G. E. Stelmach[1]
[1]Motor Control Laboratory, Arizona State University, Tempe, AZ 85287-0404
[2]Bioengineering Program, Arizona State University, Tempe, AZ 85287-6006

INTRODUCTION

We used a biomechanical simulation to investigate whether the overshooting errors seen in hypergravity are due to the reinterpretation hypothesis (proposed by Bock, 1992). This hypothesis suggests that increased gravity is actually interpreted as an increase in limb mass. Movements are then correctly programmed for the weight of the limbs, but their inertia is overestimated and therefore the endpoint target is overshot.

REVIEW AND THEORY

It is important to understand the effects of altered gravity on the control of aiming movements because these movements are crucial for Shuttle control and during any potential emergency egress that astronauts need to perform. Hypergravity exposure, such as occurs during parabolic jet flight or in centrifuge apparatuses, can be used to mimic the mechanical effects of return to a 1G environment after adaptation to microgravity. Several investigations have demonstrated that subjects vertically overshoot when initially pointing to targets in hypergravity (Bock et al., 1992; Bock et al., 1996a, 1996b). This is quite surprising; if the subjects had executed their movement plan for a normal G environment without modifying it, they would vertically undershoot the target due to the increased weight of the arm. The reinterpretation hypothesis suggests that the increase in G is interpreted as an increase in limb mass. Movements are then planned for the correct weight of the arm, but the inertia is overestimated, causing subjects to overshoot the target. The purpose of the current investigation was to simulate arm movements in a hypergravity environment with typical parameters for the human limb and task conditions set to match the reinterpretation hypothesis. We hypothesized that the endpoint error in the hypergravity simulation would match that obtained experimentally by previous investigators, thus supporting the reinterpretation hypothesis.

PROCEDURES

The experimental setup of Bock and colleagues (1992) was replicated. A subject pointed to a visual target placed at eye level 33 cm in front of him. The movement started with the hand in the subject's lap. The subject was instructed to view the target, close his eyes, and point to the remembered target location. Five trials were performed. Movements were recorded with an OPTOTRAK movement recording system. Joint angles were calculated at each instant in time such that positive angles represented shoulder adduction, shoulder flexion, shoulder internal rotation, elbow flexion, wrist flexion, ulnar deviation, and finger flexion.

A seven degree of freedom model of the arm was derived with the shoulder joint as the origin of the system. De Leva's adjustments to Zatsiorsky-Seluyanov's segment inertia parameters (1996) were scaled to the subject to provide the mass, center of mass location, and moment of inertia for each principal axis for all of the arm and hand segments. Kane's method for formulating the dynamic equations of motion (Kane and Levinson, 1985) and AUTOLEV, a dynamic symbol manipulator, were used to produce code that would take as its input the starting position for each degree of freedom and driving torques and would integrate forward in time to predict angular accelerations. The code was validated by providing initial system configuration and allowing the arm to drop under the force of gravity; the total energy of the system remained constant. Velocity and position dependent damping coefficients were added for each degree of freedom. The code was again validated by comparing the joint angle profiles obtained from running the experimentally-derived torques through it with the joint angles calculated from the experimental data. Damping coefficients were adjusted to provide the best match (see endpoint trajectories in Figure 1), which resulted in the simulated endpoint position being 3 cm further forward, 5 cm to the left, and 0.1 cm lower than the actual endpoint.

The hypergravity simulation was performed using a G value of 1.6, which was within the range of those reported by Bock and colleagues (1992). The same torque values were used as in the normal g simulation with the limb mass values scaled down. Thus the torques were appropriate for the limb weights in hypergravity but were too large for the inertia values.

RESULTS

Figure 1 displays the simulated and acutal endpoint trajectories. It can be seen from the time scale that the movement time to the target board was much shorter for the hypergravity simulation than for the normal G one (380 ms vs. 650 ms). In contrast, Bock and colleagues demonstrated that movement times are virtually the same in normal G and hypergravity. The hypergravity simulation resulted in 17.0 cm of vertical overshoot, while the subjects in Bock and colleagues' investigation (1992) had vertical overshoot errors of 3.7 cm in hypergravity.

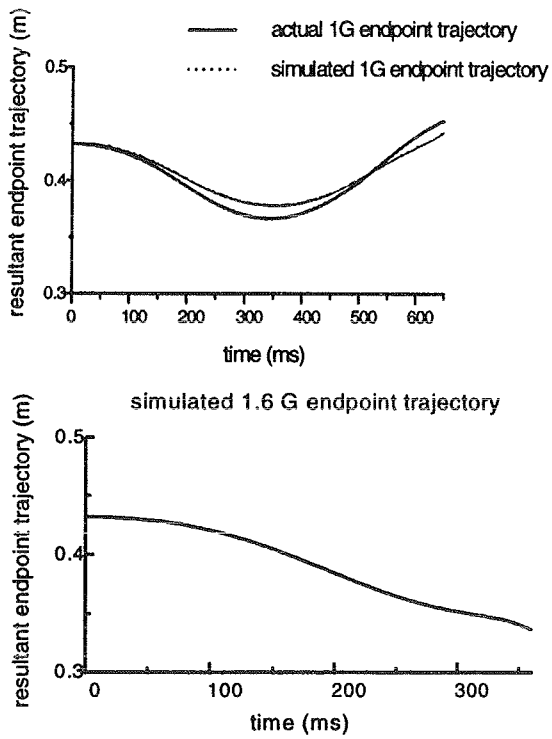

Figure 1. The top panel displays the actual and simulated 1G endpoint (fingertip) trajectories. The lower panel displays the simulated 1.6 G endpoint trajectory; note the difference in time scales.

DISCUSSION

The large difference in movement times between the simulated normal and hypergravity movements is at first striking, especially since the experimental data suggests that movement times are equal for varying gravitational environments. However, this discrepancy may be because the simulation does not allow for feedback corrections, which could have prolonged subjects' movement times in hypergravity to the point where they were equivalent to those in normal G. The simulation also suggests that if subjects were reinterpreting the increase in G force as an increase in the mass of the limb, they would have overshot the target by 17 cm rather than approximately 4 cm. Bock and his colleagues do speculate that subjects realize their error of reinterpretation somewhere en route to the target and attempt to correct the error, as evidenced by skewed velocity profiles in hypergravity such that the deceleration phase constitutes a greater portion of the movement (1996a). However, there are no obvious corrective submovements evident in the velocity profiles presented, and it seems unlikely that subjects could correct a 17 cm vertical overshoot down to 4 cm in a 650 ms movement. Thus the simulation suggests that movements in hypergravity are not planned with a simple reinterpretation of increased G force as an increase in the mass of the limb, as proposed by the reinterpretation hypothesis.

REFERENCES

Bock, O, Arnold, KE, Cheung, BSK (1996a). Performance of a simple aiming task in hypergravity: I. Overall accuracy. *Aviat Space Environ Med,* 67, 127-132.

Bock, O, Arnold, KE, Cheung, BSK (1996b). Performance of a simple aiming task in hypergravity: II. Detailed response characteristics. *Aviat Space Environ Med,* 67, 133-138.

Bock, O, Howard, IP, Money, KE, Arnold, KE (1992). Accuracy of aimed arm movements in changed gravity. *Aviat Space Environ Med,* 63, 994-998.

Kane, TR, Levinson, DA (1985). *Dynamics: Theory and Applications.* McGraw-Hill: NY.

De Leva, P (1996). Adjustments to Zatsiorsky-Seluyanov's segment inertia parameters. *JOB,* 9, 1223-1230.

ACKNOWLEDGMENTS

NINDS17421

STRIDE LENGTH CHANGES FOLLOWING SURGICAL HAMSTRING LENGTHENINGS IN INDIVIDUALS WITH CEREBRAL PALSY

M. Orendurff, R. Pierce, R. Dorociak, M. Aiona

Gait Laboratory, Shriners Hospital for Children, Portland Unit, Portland, Oregon 97210

INTRODUCTION

Individuals with cerebral palsy (CP) may develop muscular contractures which can limit joint motion. For example, tight hamstrings can lead to flexed-knee gait, making ambulation difficult. If a contracture of the hamstrings is sufficient to warrant intervention, a surgical lengthening may be performed with the goal of increasing knee extension and correcting the patient's crouch gait. Since crouch gait is claimed to be associated with decreased stride length (Root, 1992), a collateral goal of this surgery is often to improve stride length.

REVIEW AND THEORY

Previous work in our laboratory (Orendurff, et al., 1997) led to the development of a regression equation to predict stride length in individuals with CP. An equation was developed with 54 consecutive individuals (54 sides chosen randomly) with CP (mean age 11.8 ± 4.2 years, range 20.5 to 4.7 years) who under went computerized gait study as part of their ongoing care. From this group the following equation was derived:

Stride length (cm) = -0.130 + 1.165(leg length) + 0.637(hip arc) - 2.082(first double support) + 1.267(contralateral ankle push-off energy) + 0.647(ankle push-off energy)

$p < .0454$, $R^2 = .739$

This equation suggests that stride length is not associated with restricted knee motion, or that other strategies may be used to compensate for restricted knee motion. The goal of the present study was to determine which variables improved following hamstring lengthenings, and how these changes were associated with increased stride length.

PROCEDURES

In this experiment, we retrospectively evaluated 15 consecutive individuals with crouch gait (15 sides chosen randomly) to examine knee kinematics prior to and one year post hamstring lengthenings. These patients received computerized gait analysis as part of their ongoing care at a regional children's hospital. In addition to hamstring lengthenings, 4 individuals also had tendo achilles lengthenings, 3 had rectus femoris transfers, 6 had adductor lengthenings, and 2 had iliopsoas lengthenings. Barefoot, appliance-free gait data were collected 4.2 ± 1.4 months prior to surgery and 14.0 ± 4.3 months following surgery, for a total of 18.1 ± 5.0 months between gait studies. A six camera VICON 370 system with two AMTI force plates was used to collect gait data, which was processed using Vicon Clinical Manager (Oxford Metrics, Oxford, England). Variables of interest were extracted and analyzed using StatView (Abacus Concepts). Analysis of variance was used to determine which variables showed significant differences postop. In addition, multiple linear regression was used to predict stride length based on leg length (LL), sagittal hip arc (HA), first double support period (DS1), contralateral ankle push-off energy (A2Ecl), and ipsilateral ankle push-off energy (A2E) both preop and postop. The $p < .05$ level of significance was chosen.

RESULTS

Following hamstring lengthenings significant improvements were seen in stride length (SL) total knee arc (KA), peak knee extension (PKE) and peak knee extension in terminal swing (PKEtsw) ($p < .01$). Peak knee flexion (PKF) showed a significant decrease following intervention ($p < .01$).

None of the variables from the multiple regression model to predict stride length showed significant differences following surgery, with the exception of leg length (LL) which increased significantly ($p = .0002$) presumably due to growth.

When applying the model to the preop patient data only three variables proved significant (LL, HA and A2Ecl; $p < .02$, $R^2 = .797$). Postop, HA and A2Ecl dropped out of the model and only LL, DS1 and A2E proved significant predictors of stride length ($p < .007$, $R^2 = .917$).

	Preop	Postop	*p* value
SL	95.8 ± 17.9	103.8 ± 18.0	.0056
KA	31.6 ± 15.4	40.5 ± 12.7	.0099
PKE	24.6 ± 9.7	8.1 ± 9.4	<.0001
PKEtsw	32.5 ± 7.7	17.9 ± 6.7	<.0001
PKF	56.2 ± 12.1	48.6 ± 9.5	.0050

Table 1. Knee kinematics following hamstring lengthenings (mean ± SD).

	Preop	Postop	*p* value
LL	75.2 ± 12.1	78.7 ± 10.4	.0002
HA	41.8 ± 8.3	43.1 ± 6.4	.5368
DS1	13.7 ± 4.7	15.5 ± 2.4	.1300
A2E	6.4 ± 2.5	6.9 ± 2.1	.4442
A2Ecl	8.3 ± 4.4	7.6 ± 2.9	.5100

Table 2. Stride length prediction variables following hamstring lengthenings (mean ± SD).

DISCUSSION

This group of individuals with CP who underwent hamstring lengthenings to correct crouch gait showed significant improvements in knee kinematics, including improvements in knee extension in stance and in terminal swing. Stride length significantly improved 8 cm postop for the group, but individual results were highly variable. Six individuals showed stride length increases of between 10 and 28 cm (Improved), five showed increases between 0 and 7 cm (Unchanged) and four showed decreases in stride length of between 0 and 3 cm (Decreased) even though improvements in knee kinematics were similar. Much of the overall change in stride length for the group can be attributed to changes in leg length due to growth between the preop and postop evaluations: leg length alone can account for 40% of the stride length variance.

Similar improvements in stride length were seen in a group of 8 individuals with CP who had gait abnormalities, but did not require intervention. They increased their stride length 8 cm as well (p = .0064) in 15.8 + 2.8 months, presumably due to growth.

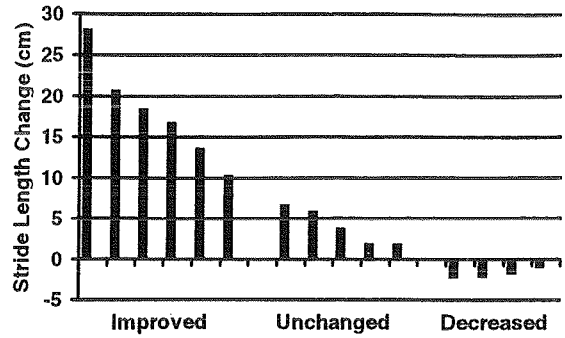

Figure 1. Improvements in stride length following surgical hamstring lengthenings.

In an effort to understand why some individuals improved their stride length following intervention and others did not, patient data was fitted to a model developed earlier. Although this method does reveal significant results, indicating that hip arc and contralateral ankle push-off energy were important in determining stride length preop and that the first double support period and ipsilateral ankle push-off energy were important postop, interpretation is complex. It seems unlikely that mechanisms to increase stride length would be so different from preop to postop without significant changes in the variables following intervention.

By evaluating the three groups (Improved, Unchanged and Decreased) using a Kruskal-Wallis test to determine which variables were associated with improved stride length it appears that improved sagittal hip motion was associated with increased stride length postop ($p < .03$).

This suggests that individuals who were able to compensate for their knee flexion preop by increasing hip motion did not show large improvements in stride length, whereas individuals who had knee flexion and were unable to compensate with sagittal hip motion showed large changes in stride length following intervention. Further study of this highly variable group is needed before the effects of improved knee extension on stride length are known.

REFERENCES

Orendurff, M.S., et al., *Dev Med Child Neurol*, in press, 1997.

Root, L., in M. Sussman, Ed., *The Diplegic Child*, 309-315, AAOS, Rosemont, IL., 1995.

INERTIAL MANIPULATIONS OF BELOW-KNEE PROSTHESES: EFFECTS ON WALKING SYMMETRY

S. Mattes, P. Martin and T. Royer

Exercise and Sport Research Institute, Arizona State University, Tempe AZ 85287-0404

INTRODUCTION

Research indicates that amputees demonstrate asymmetrical gait patterns and use more energy than able-bodied individuals (Menard et al., 1992; Torburn et al., 1990). Prosthetists have embraced the notion that prostheses should be as light as possible to minimize the muscular effort and metabolic energy required during locomotion. Consequently, commonly used prosthetic limbs are considerably lighter than the anatomical parts they replace. Modeling studies suggest that the ideal design would be one whereby inertial characteristics of the prosthesis are matched to the those of the intact limb (Tsai et al., 1986; Mena et al., 1981). This research project has attempted to match inertia characteristics (mass, center of mass and moment of inertia) of the prosthesis with the estimated inertial characteristics of the intact limb by selective positioning of the additional load to the prosthesis. It was hypothesized that the gait patterns of uni-lateral below-knee amputees are more symmetrical as inertial characteristics of the prosthesis and intact limbs become more closely matched.

PROCEDURES

Six active, uni-lateral, below-knee amputees (age=32.3, mass=84.5 kgs, height=177.7 cm) volunteered to serve as subjects for this project. All subjects used a Flex-foot prosthesis and had been amputees for 6.8 ± 4.7 years. They attended two data collection sessions. During the first session, subjects were acclimated to all testing procedures and the inertial characteristics of the prosthesis were measured (Table 1). Mass was measured using a standard laboratory scale, center of mass was determined using a reaction board method, and moment of inertia of the prosthesis was estimated using an oscillation technique (Martin et al., 1989). Calculations of mass, center of mass and moment of inertia were estimated for the intact limb using the body segment parameter estimations of DeLeva (1996). The residual limb was modeled as the frustum of a right circular cone (Hanavan, 1964) with a uniform density of 1.1 g/cm^3 (Martin et al., 1989).

Three load conditions were used: a) no load, b) 50% of the difference between the estimated mass of the intact limb and the combined mass of the prosthesis and stump, and c) 100% of the difference in limb masses. The load was placed on the prosthesis in a position that the moment of inertia about the knee was the same as the intact limb during the 100% load condition. The average location of the added mass was 40.8 cm below the knee (82% of shank length). The mass was placed in the same position for the 50% load (table 1).

During the second testing session, subjects walked on a motor driven treadmill at a speed of 1.34 meters/second for 10 minutes for accommodation for each loading condition. Subjects were then asked to walk across a walkway at 1.34 ± 0.04 m/s while being video taped. Reflective markers were placed on the following six anatomical landmarks: greater trochanter, lateral femoral condyle, lateral malleolus, lateral heel, medial heel and the head of the 5th metatarsal. Walking speed was monitored by the consecutive passing of two photocells spaced approximately 4 meters apart. Trials not meeting the speed requirement were repeated. A symmetry index (SI) was developed to assess symmetry between the prosthetic (P) and the intact (I) limbs during each condition:

$$SI = (P - I) / \tfrac{1}{2}(P + I).$$

Dependent variables included: step length, relative swing time and relative stance time, and hip and knee range of motion.

	Mean	SD
Mass of intact limb	4.91	0.40
Mass of prosthesis	1.48	0.32
Mass of stump	1.74	0.36
50% mass condition	0.85	0.31
100% mass condition	1.70	0.62

Table 1: Mass manipulations (kgs)

RESULTS

The results of this project did not support the hypotheses. No improvement in symmetry occurred as prosthetic inertial characteristics became more similar to those of the intact limb (Fig 1). Prosthetic limb step length, relative swing and stance time increased while remaining the same for the intact limb (Fig 2).

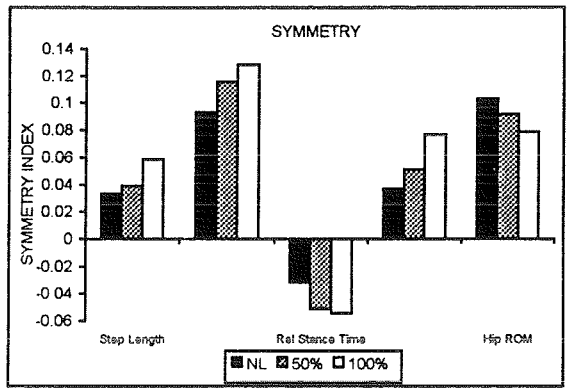

Figure 1: Symmetry: A smaller SI indicates more symmetry, positive SI indicates that the prosthetic limb value is larger. Only hip range of motion symmetry increased as load was increased.

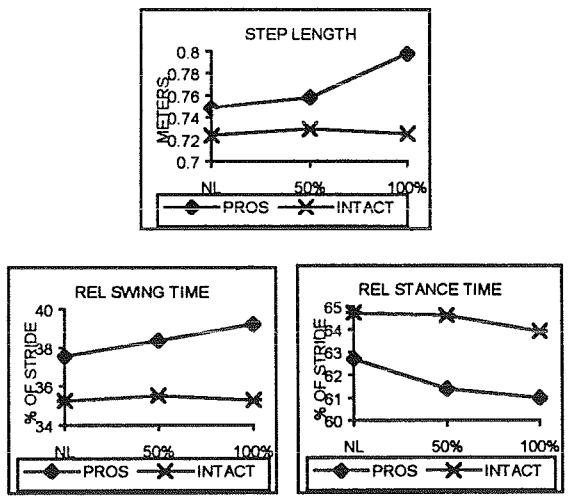

Figure 2: Leg comparisons. Relative swing and stance times for the intact limb did not change as load was added. Swing time increased and stance time decreased for the prosthetic limb.

DISCUSSION

Several modeling studies point to the importance of matching the inertial characteristics of the prosthesis to those of the intact limb (Tsai et al., 1986, Mena et al., 1981). The results of this project disagree with these models. Symmetry did not improve as the inertial characteristics of the prosthesis were more closely matched to the intact limb.

It is contended that the motion of the swing leg can be modeled like a pendulum (Mochon et al., 1980). The pendular model suggests that the addition of mass to the lower extremity will produce an increase in period of oscillation (T) if the moment of inertia (I) increases to a greater extent than the product of the mass (M) and the distance to the center of mass (d):

$$T = 2\Pi (I / Mgd)^{1/2}$$

Since the loads were placed below the center of mass of the prosthetic limb, d increased. The product of d and M increased less than the increase in I during both load conditions, causing an increase in the period of oscillation.

Swing time of the prosthetic limb is longer than that of the intact limb, and amputees spend more time in stance on the intact limb. Increasing the mass and moment of inertia of the prosthetic limb, according to the pendular model and the results of this research project, further increased the prosthetic swing time, creating greater asymmetries between the limbs during walking.

REFERENCES

DeLeva P. J Biomech, 29, 1223-1230, 1996.
Hanavan E. Wright Air Force Base, 1964.
Martin P. et al. J. Biomech, 22, 367-376, 1989.
Mena D. et al. J. Biomech, 14, 823-832, 1981.
Menard M. et al. Arch Phys Med Rehab 73, 451-458, 1992.
Mochon S. et al. J. Biomech 13, 49-57, 1980.
Torburn L. et al. J Rehab Res Dev, 27 369-384, 1986.
Tsai C. et al. J Biomech Eng, 108, 65-72, 1996.

ACKNOWLEDGMENTS

This research project was supported by the Graduate Research Support Office Grant and by the Douglas L. Conely Scholarship.

GAIT ABNORMALITIES IN PATIENTS WITH LUMBAR DISC HERNIATION

E. Morag, R. Hennessy, G.B.J. Andersson, M. Hickey, D.E. Hurwitz, T.P. Andriacchi

Department of Orthopedic Surgery, Rush-Presbyterian-St. Luke's Medical Center, Chicago, IL, 60612

INTRODUCTION

Lumbar disc herniation is commonly associated with pain in the lower extremity. Clinical signs for herniated nucleus pulposus (HNP) may include pain, sensory changes, impaired reflexes, muscle weakness, and reduced walking capacity. However, gait changes resulting from disc herniation are yet to be documented. This study determined differences in net joint moments between 21 HNP patients and 21 age-matched healthy individuals. Reduced ankle plantar and dorsi flexion moments were found in HNP patients with a lesion to the L5-S1 disc.

REVIEW AND THEORY

HNP at the L4-5 and L5-S1 lumbar levels are often associated with motor deficits of lower leg muscles. Thus, physical examination includes tests of muscle strength and evaluation of walking. For example, weakness of the gastrocnemius is a clinical neuorologic sign for involvement of the L5-S1 disc (S1 level), while weakness of the extensor hallucis longus is a positive sign for involvement of the L4-5 disc (neurologic level L5). Weakness of the hamstring may accompany both injuries. Jonsson and Stromqvist (1996) reported severe reduction in walking capacity in HNP patients, using a scale of four levels (<0.5 km, 0.5-1 km, 1-5 km, >5km). However, there is a need to identify specific functional motor deficits in order to understand the mechanisms by which HNP affect gait.

Gait analysis can provide quantitative information regarding the dynamic function of specific muscle groups, by analysis of net joint moments, and is sensitive enough to potentially identify subclinical deficits in muscle function in HNP patients (Schipplein et al., 1992).

The purpose of this study was to test the hypothesis that the external dorsi flexion moment will be reduced in patients with L5-S1 herniations, the external plantar flexion moment will be reduced in the patients with L4-L5 herniations, and the external knee extension moment will be reduced in all patients.

PROCEDURES

A total of 42 subjects participated in this study, including 21 patients (36.6 years of age) diagnosed with HNP who were candidates for surgery (7 L4-5 HNP and 14 L5-S1 HNP patients), and 21 control subjects (matched by age, mean age = 34.8 years). A complete physical examination was conducted, including history of pain symptoms, feeling of weakness, lower extremity reflexes, sensory changes, and motor function of the lower extremity muscles. MRI or myelogram with post myelogram CT scans of the lumbar spine were available for all patients. The level of pathology for each patient was determined based on these tests, and was later confirmed during surgery. Subjects performed six walking trials at a range of self selected walking speeds. A representative walking trial at approximately 1 m/s was selected for analysis (the mean walking speeds were 0.97, and 0.93 m/s for the healthy and pathological groups respectively). By allowing the patients to walk at different walking speeds, and selecting one trial, there were no constraints or potential gait alterations. Ground reaction forces and 3D kinematic data were obtained during walking. Motion and net joint moments at the hip, knee and ankle were computed (Andriacchi et al., 1985). One way analysis of variance (alpha=0.05) was used to test for differences in means in peak knee and ankle moments. A Tukey post hoc test was conducted for multiple comparison.

RESULTS

The peak knee and ankle external moments (Figure 1) were analyzed to evaluate dynamic function of the ankle dorsi-flexors and plantar-flexors, and the knee flexors. The peak net plantar flexion moment (PF1) at the ankle (sustained by the dorsi flexors) was reduced in L5-S1 HNP patients compared with the normal individuals (Table 1, $p<0.05$). Similarly, the peak net dorsi flexion moment (DF1) at the ankle (sustained by the plantar flexors) was reduced in L5-S1 HNP patients ($p<0.05$). These results were consistent with the hypothesis.

A non-significant trend (p=0.15) towards reduced knee extension moment (EX2, the moment sustained by the knee flexor muscles at the start of push off) was found for both pathological groups. No differences in the early peak net knee extension moment (EX1, sustained by the hamstring), were found.

DISCUSSION

The findings of this study support the hypothesis that joint moments are reduced in HNP patients, and that these moments are related to the level of involvement. Smaller than normal ankle plantar flexion and dorsi flexion moments, as found in the L5-S1 HNP patients, are an indication of reduced dynamic function of the dorsi flexors and plantar flexors respectively. Neurologically, herniation of the L5-S1 disc is associated primarily with weakness of the plantar flexors of the ankle (and to a lesser degree with weakness of the dorsi flexors). Therefore, we conclude that objective differences in gait are present in HNP subjects, and that the obtained abnormalities are consistent with the neurological lesion for the L5-S1 group.

Smaller than normal knee extension moment and ankle plantar flexion moment are indications of reduced function of the knee flexors and ankle dorsi flexors respectively. The trend towards reduced knee extension moment and the lower ankle plantar flexion moment, as found is this study, may be indications of reduced dynamic function of the knee flexors and ankle dorsi flexors. Neurologically, HNP of the L4-5 lumbar disc is associated with impaired function of these muscle groups.

REFERENCES

1. Jonsson B et al. *Spine, 21*, 500-5, 1996.
2. Schipplein OD et al. *NACOB II*, 403-4, 1992.
3. Andriacchi TP et al. *NATO ASI* E:83-102, 1985.

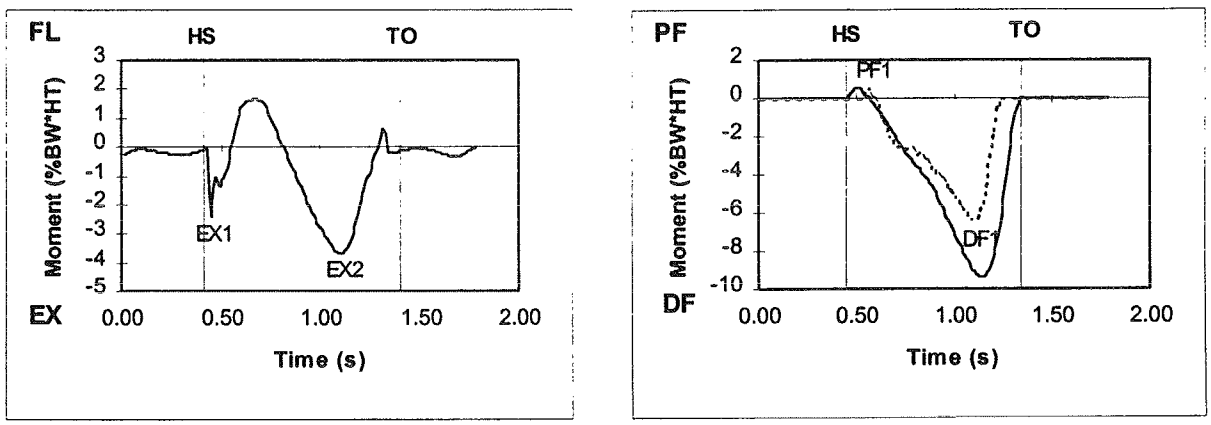

Figure 1: A typical normal moment at the knee (left) and ankle (right, solid line) during gait, with the vertical lines represent heel strike (HS) and toe-off (TO). Moments at the ankle of a patient with HNP at the L5-S1 level are also shown (dashed line)

Gait Moments	Normal (N)	L4-5	L5-S1	p value	post hoc
Ankle DF1 (%BW*HT)	8.340	8.236	6.846	< 0.05	N > L5-S1
Ankle PF1 (%BW*HT)	0.617	0.495	0.317	< 0.05	N > L5-S1
Knee EX1 (%BW*HT)	2.610	2.070	2.296	NS	NA
Knee EX2 (%BW*HT)	2.309	1.657	1.532	0.15	NA

Table 1: Mean values of peak joint moments. Results of multiple comparison are shown on the right

GREATER TROCHANTER BONE LOSS IN PREOPERATIVE TOTAL HIP REPLACEMENT PATIENTS IS RELATED TO THE HIP ADDUCTION MOMENT DURING GAIT

D.E. Hurwitz, K.C. Foucher*, R.D. Sumner, T.P. Andriacchi, J.O. Galante, A.G. Rosenberg

Rush-Presbyterian-St. Luke's Medical Center, Department of Orthopedic Surgery, Chicago Illinois
*University of Illinois, Department of Bioengineering, Chicago Illinois

INTRODUCTION AND THEORY

Preoperative bone loss, especially in the region of the greater trochanter, has been documented in candidates for total hip replacements (THR) (1). This bone loss may be attributable to the disease process as well as limb unloading during activities of daily living. Decreased external moments are reflective of decreased muscle forces and decreased forces at the hip joint and femur. Thus, the decreases in the hip joint moments during gait that have been previously reported in candidates for THRs (2) may contribute to the decreases in bone mineral density (BMD) previously reported in candidates for total hip replacements. The hypothesis tested in this study was that reductions in the greater trochanter BMD were significantly correlated with reductions in the hip adduction moment during gait.

METHODS AND MATERIAL

33 patients (22 males, 11 females; age 60 $\pm$ 10 years) scheduled for unilateral THR were evaluated with gait analysis and dual energy x-ray absorptiometry. The average Harris score was 54 $\pm$ 14 and none had any other significant joint involvement. All received a THR within a month of their evaluation.

A three dimensional optoelectronic camera system with a multi-component force plate was used to calculate the joint kinematics and kinetics as subjects walked at 3 self selected speeds of slow, normal and fast (3). A representative trial on the affected and unaffected side was chosen such that the speeds of the two sides were as similar as possible (0.88 $\pm$ 0.23 m/sec, $p > .63$). BMD of the greater trochanter was measured with a Lunar x-ray bone densitometer.

Pearson correlation coefficients were used to test for significant relationships between the greater trochanter BMD and the external hip joint moments. The influence of confounding variables (gender, age, diet, hormonal levels) was first minimized by using each subject as his/her own control (asymmetries). Secondly the multi-variate linear regression model that was used to determine if the gait kinetics on the affected side were significant predictors of the greater trochanter BMD on the affected side also tested for a significant effect of gender, height or weight. Paired *t* tests were used to test for significant differences between the two sides. A significance level of $\alpha < .05$ was used throughout.

RESULTS

There was a relationship between the reductions in the hip adduction moment and the loss of greater trochanter BMD. The asymmetry in the hip adduction moment (affected /unaffected) was a significant predictor of the asymmetry in the greater trochanter BMD ($R = 0.41$,

$p<.018$). In addition the hip adduction moment on the affected side was a significant predictor of the greater trochanter BMD on the affected side ($R=0.51$, $p<.003$) (Figure 1). The external rotation moment on the affected side was also significantly correlated with the greater trochanter BMD ($R=0.56$, $p<.001$). Using both the external rotation and adduction moments together significantly increased the ability to predict the greater trochanter BMD ($p< .0017$) (Figure 2). These two variables accounted for 49% of the variation in the greater trochanter BMD ($R=0.71$, $p<.0001$).

The greater trochanter BMD and hip adduction moment of the affected side were only 90 ± 11% and 90 ± 33 % of that of the unaffected side, respectively ($p<.001$, $p<.015$). The flexion, and external and internal rotation moments were also all significantly less on the affected side as compared to the unaffected side ($p< .001$).

DISCUSSION

The hip adduction moment during gait was a significant predictor of greater trochanter BMD. The abductors are the primary structures responsible for balancing the adduction moment. Since the abductors insert on the greater trochanter, reduced hip adduction moments may reflect reduced forces in this region and may result in bone loss.

Understanding the causes of preoperative bone loss may help improve the long term outcome of THRs. The extent of this bone loss can minimize the surgical options available for a THR and may even be related to the extent of subsequent postoperative bone loss (4).

REFERENCES

1)Sauer et al. ORS 21:517, 1996.
2)Hurwitz et al. ASME 29:387-8,1995
3)Andriacchi et al. NATO ASI E:83-102 1985.
4)Engh et al. JBJS 74:1009-20, 1992.

Acknowledgment: Whitaker Foundation

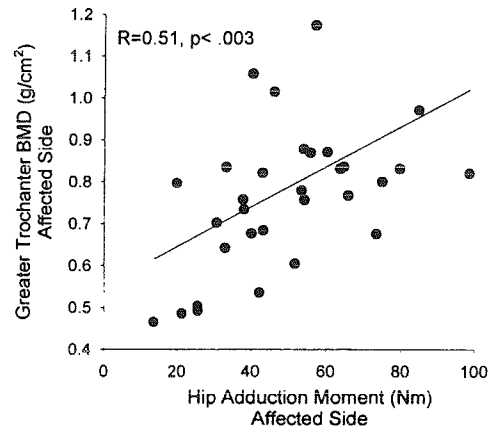

Figure 1: The adduction moment was significantly correlated with greater trochanter BMD.

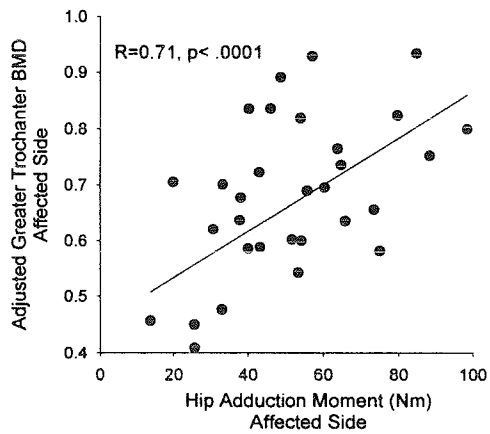

Figure 2: The adduction moment and external rotation moments accounted for 49% of the variation in the greater trochanter BMD.

VARIABILITY OF NEUROPATHIC AND NON-NEUROPATHIC SUBJECTS WALKING ON A MOTORIZED TREADMILL

Jonathan B. Dingwell[1,2], Jan S. Ulbrecht[1], Dagmar Sternad[2], Peter R. Cavanagh[1,2]

[1] Center for Locomotion Studies, Penn State University, University Park, PA 16802
[2] Department of Kinesiology, Penn State University, University Park, PA 16802

INTRODUCTION

Peripheral neuropathy (PN) affects as many as 50% of patients with Diabetes Mellitus (DM) for more than 10 years (Greene et al., 1990). Afferent input to the central nervous system is thought to play an important role in the control of posture and locomotion. It has been hypothesized that PN leads to changes in gait variability (Brand, 1988, Cavanagh et al., 1993); however, attempts at defining differences in the statistical variability of these patients' gait patterns (Cavanagh et al., 1993) have met with limited success. This abstract reexamines the data of Cavanagh et al. (1993) and presents evidence to suggest that motorized treadmill walking is inherently less variable than overground walking, and that the structure of stride-to-stride variability in walking may be a reflection of more than merely random noise.

REVIEW AND THEORY

As many as 50% of patients with DM for more than 10 years will experience peripheral neuropathy (PN) in the lower extremities (Greene et al., 1990). Patients with DM and peripheral neuropathy are at greater risk of falling, and of suffering injuries during falls (Cavanagh et al., 1992, Richardson et al., 1992). It has been alternately hypothesized that the loss of sensory input associated with PN leads to a less variable (Brand, 1988, Cavanagh et al., 1993), or a more variable (Cavanagh et al., 1993) gait pattern. However, Cavanagh et al. (1993) found no significant differences between neuropathics and matched control subjects in the standard deviation of "Leg Angle" (the angle between vertical and the line joining the hip and fifth metatarsal head markers) when subjects walked on a motorized treadmill.

One limitation of the statistical approach to examining variability is that it implicitly assumes that locomotion can be represented by a sequence of independent strides, and that stride-to-stride variability is a reflection of random noise. To test this hypothesis, it is useful to analyze the noise in the frequency domain, by examining the characteristics of the power spectral density (PSD) function plotted on a log-log scale. In many natural systems this plot is roughly linear and scales as $1/f^{\beta}$, where β is the slope of the plot (Hausdorff et al., 1995). For random white noise, $\beta = 0$. If $\beta > 0$, then the "noise" in the system contains long-range correlations, such that the motion of the system many cycles in the future is influenced by motion many cycles in the past. $1/f^{\beta}$ noise has been found in stride interval data from human locomotion (Hausdorff et al., 1995) and in center of pressure patterns during quiet standing (McClenaghan et al., 1996). The structure of these patterns has also been shown to change with age and pathology (Hausdorff et al., 1997, McClenaghan et al., 1996), suggesting that the temporal variability in these motions reflects the presence of deterministic as well as stochastic processes.

The treadmill walking results of Cavanagh et al. (1993) appear to contradict clinical evidence that subjects with PN are less dynamically stable than those without (Cavanagh et al., 1992, Richardson et al., 1992). It was hypothesized that differences in the dynamics of locomotion may have been either overshadowed by having subjects walk on a motorized treadmill (effectively "driving" the system externally) or "averaged out" by normalizing and averaging data across multiple strides of gait. Variability of movements in frontal plane may also be more important to maintaining stability during locomotion than variability in the sagittal plane. The purpose of the present study was to examine in more detail the statistical variability in the sagittal plane treadmill walking data of Cavanagh et al. (1993), and to examine the temporal structure of this variability using spectral analysis techniques.

PROCEDURES

Three matched groups of fifteen subjects participated in the study; diabetic patients with neuropathy (NP) and with out (NNP), and non-diabetic controls (Control). Subjects walked on a motorized treadmill at 1 m/s and 25 seconds of sagittal plane kinematic data from the left leg were recorded during the 15th minute of walking (Cavanagh et al., 1993). For the current study, within-subject stride-to-stride standard deviations (SD's) were computed for six kinematic variables; stride time, minimum toe clearance during swing, "leg length" (linear distance between hip and fifth metatarsal head) at heel strike, "leg angle" (angle between hip and fifth metatarsal head markers) at heel strike, and knee angle and ankle angle at heel strike. Additionally, coefficients of variation (CV's) for knee and ankle angles were calculated over the entire stride as defined by Winter (1983). To examine spectral characteristics of the kinematic data, Log-Log PSD plots were generated

and slopes (β) were calculated for the knee and ankle angle data from the full 25 second trial for each subject. Two-factor (3 x 15) ANOVA's were performed on the data for each variable and multiple pair-wise comparisons were used to distinguish significant "Group" effects differences.

RESULTS

The Control group showed the lowest variabilities for all eight variables measured, and the NP group showed the largest variabilities for 5 of the 8 variables measured. However, only "leg length" at heel strike and knee angle at heel strike produced significant differences between groups. Differences between groups were nearly significant for CV of knee angle ($p = 0.082$), but not for CV of ankle angle ($p = 0.748$). More importantly, these CV values were substantially less (from 43% to 57% less) than those reported by Winter (1983) for a group of young, healthy adults walking overground at their preferred walking speed (Figure 1).

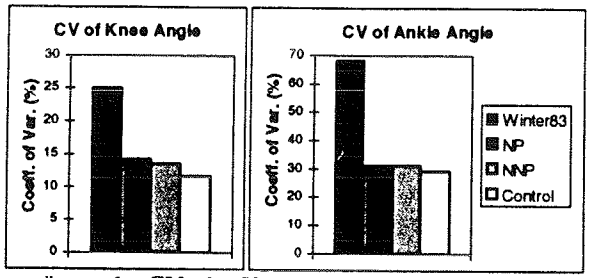

Figure 1 - CVs for Knee and Ankle Angle Data.

Linear PSD functions appeared to show periodic motion; however, the Log-Log PSD plots indicated the presence of $1/f^{\beta}$ scaling in the knee and ankle joint kinematics during locomotion (Figure 2). Although there was a trend towards increasing slopes for the diabetic subjects, these differences were not significant (Figure 3).

DISCUSSION

The substantial differences in knee and ankle CV values between this study and the data of Winter (1983) (Figure 1) suggest that these subjects' gait patterns may have been externally driven by the treadmill, which artificially reduced the overall variability, and which may have led to the lack of significant group differences in the final analysis. While the magnitudes of the Log-Log PSD slopes (Figures 2 & 3) are strongly determined by the cyclic nature of the data, the trend towards increased slopes (i.e. more structured and less random movements) for the NNP and NP groups may be a reflection of a more active feed-forward form of movement control being used by these subjects. These differences, however, are difficult to interpret given the nature of this data set and the differences in overall variability.

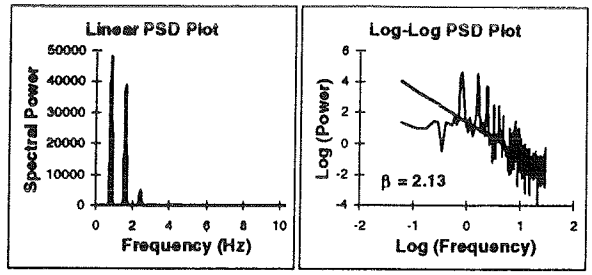

Figure 2 - Representative Linear and Log-Log PSD Plots for Knee Angle Data for One Subject.

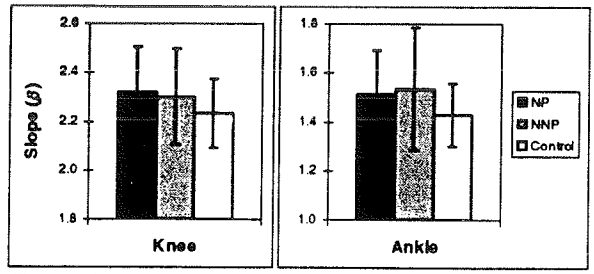

Figure 3 - Log-Log PSD Slopes for Knee and Ankle. (Means ± Standard Deviations)

It was concluded that any differences which may have been present in the variability of sagittal plane kinematics between NP, NNP, and Control subjects were likely overshadowed by having them walk on a motorized treadmill. Log-Log PSD analysis revealed the presence of possible long range correlations in the structure of these subjects' movement patterns; however, these data may also have been affected by having subjects walk on a motorized treadmill. It is anticipated that further analysis of continuous overground locomotion for three similar groups of subjects will demonstrate that peripheral neuropathy does indeed lead to increased variability of walking patterns, and that techniques from spectral analysis and nonlinear dynamics can provide further insight into the temporal structure of movement variability and motor control of locomotion.

REFERENCES

Brand, PW, in *The Diabetic Foot*, Levin, ME, et al., Eds., CV Mosby, St. Louis, 83-90., 1988.

Cavanagh, PR, et al., *Diab. Med.*, 9: 469-474, 1992.

Cavanagh PR et al., *J. of Biomech.*, 26 (Suppl. 1): 23-40, 1993.

Greene DA et al., *Ann. Rev. of Medicine*, 41: 303-317, 1990.

Hausdorff JM et al., *J. of Appl. Physiol.*, 78 (1): 349-358, 1995.

Hausdorff JM et al., *J. of Appl. Physiol.*, 82 (1): 262-269, 1997.

McClenaghan BA et al., *Gait & Posture*, 4: 112-121, 1996.

Winter, DA, *J. of Motor Behav.*, 15 (4): 302-330, 1983.

A BONE ADAPTATION SIMULATION FOR THE FEMUR BASED ON DISUSE AND DAMAGE REPAIR

S.J. Hazelwood and R.B. Martin

Orthopaedic Research Laboratories, University of California Davis, Sacramento, CA 95817

INTRODUCTION

Remodeling of bone serves both to eliminate bone in a disuse state and repair fatigue damage. These effects were investigated simultaneously in an adaptive finite element model for the human femur. This model accounted for the temporal and porosity effects caused by the fact that resorption precedes formation in remodeling by basic multicellular units (BMUs).

REVIEW AND THEORY

A modified version of the model of Martin (1995) was used. The rate at which damage was formed in the bone (D'_F) was assumed to be related to the loading rate (R_L) and the resulting strain range (s) from a mixture of loads applied over the course of a day:

$$D'_F = k_D \sum_{i=1}^{n} s_i^q R_L$$

where k_D is the damage coefficient found from the equilibrium state and q was taken to be 2.89. The damage for the equilibrium condition was determined to be 0.085mm/mm^2 from the average crack density for 50 year old females and males (Schaffler et al., 1995) and an assumed crack length of 75μm. This gave k_D=2.18, which would produce an equilibrium condition for 1800με applied for 3000 cycles per day (cpd). Minimum principal strain was used as the predictor (s) for damage formation.

The rate at which damage was repaired (D'_R) was:

$$D'_R = D f_a \pi r_c^2 F_s$$

where D is the existing damage, f_a is the BMU activation frequency, r_c is the osteonal cement line radius (assumed to be 0.095mm), and F_s is the damage repair specificity factor (set to 5 for this study).

Based on the data by Mori et al. (1993), Martin (1995) hypothesized a relationship between the BMU activation frequency and fatigue damage. Evidence also suggests that BMU activation frequency increases in disuse (Schaffler et al., 1990). The total daily activation frequency was assumed to be a function of the existing damage (Figure 1), strains below an equilibrium value (Figure 2), and the internal surface area available for the remodeling of bone in the region being investigated (Martin, 1984).

The remodeling period was assumed to be 90 days; 21 days for resorption (T_R), 9 days for reversal (T_I), and 60 days for refilling (T_F). The history of the activation frequency was used to determine how many BMUs were in the resorption and refilling stages on a given day. The total number resorbing for the current day (N_R) was found by integrating f_a from T_R days ago to the present time. The number refilling for the

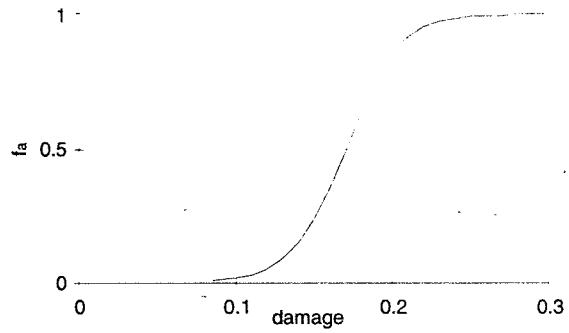

Figure 1. BMU recruitment as a function of the accumulated damage

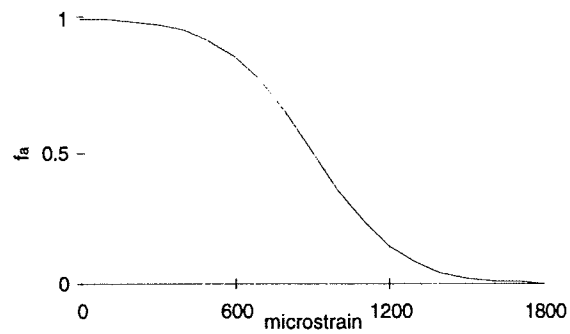

Figure 2. BMU recruitment as calculated for strains below the equilibrium value

current day (N_F) was found by integrating from (T_R+T_I+T_F) to (T_R+T_I) days ago.

The net amount of bone removed or added per day was estimated as

$$Q_C = \pi r_c^2 / T_R \quad \text{and} \quad Q_B = \pi r_c^2 / T_F$$

for each resorbing and refilling BMU, respectively. The daily change in porosity (p), expressed as a percentage, was then calculated to be

$$\Delta p = Q_C N_R - Q_B N_F.$$

A minimum cortical bone porosity of 5% was allowed in this simulation. Young's modulus was determined from the relationship

$$E = 23440(1-p)^{5.74} \text{MPa}$$ (Currey, 1988).

PROCEDURE

A two-dimensional finite element model (linearly elastic, isotropic) of the proximal femur, consisting of 1117 4-node quadrilateral elements, was created from radiographs. The structural contribution of the out-of- plane cortical bone was accounted for by the addition of a bony side plate (Weinans et al., 1992). An initial porosity of 5% and Poisson's ratio of 0.3 were assumed for all elements and the porosity of the bony side plate was kept constant throughout the simulation. Three load cases, each consisting of joint reaction and abductor muscle forces, were used to simulate the daily loading history for normal activity (Carter et al., 1989). For this simulation, the first load case was applied for 3000cpd while the second and third were applied for 1000cpd.

The simulation was run for the equivalent of 1600 days using ABAQUS 5.5 (HKS, Pawtucket, RI), with the bone adaptation algorithm integrated into the analysis through a UMAT subroutine. Daily porosity changes were calculate at the integration points for each element.

RESULTS AND DISCUSSION

Porosity distribution contour plots (Figure 3) for (a) 500, (b) 1100, and (c) 1600 days of the simulation show predictions similar to observed femoral morphology: distinct cortices surrounding a porous medullary canal, dense bone in the calcar region of the neck, and a dense region in the head aligned with the primary load case and surrounded by bone of higher porosity. Activation frequencies were found to be higher and more variable in trabecular areas than in cortical regions. Results for trabecular bone, however, appear to simulate porosities lower than those expected.

Most of the porosity and cortical thinning resulted from low strain, but damage repair also introduced significant porosity. The distribution of porosity from these two factors was similar. These preliminary results show that the internal structure of the femur can be predicted on the basis of remodeling provoked by both disuse and damage repair.

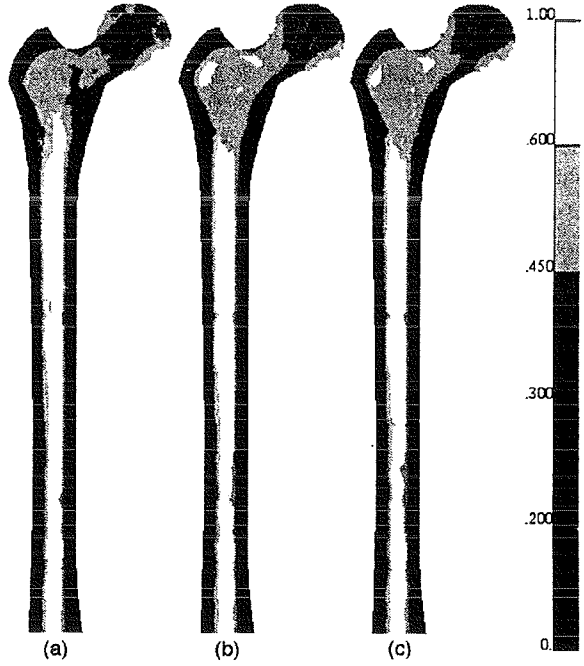

Figure 3. Predicted porosity distribution after (a) 500, (b) 1100, and (c) 1600 days

REFERENCES

Carter et al. *J Biomech*, 22:231, 1989.
Currey *J Biomech*, 21:131, 1988.
Martin *CRC Crit Rev Biomed Eng*, 10:179, 1984.
Martin *J Orthop Res*, 13:309, 1995.
Mori et al. *Bone*, 14:103, 1993.
Schaffler et al. *Trans ORS*, 15:187, 1995.
Schaffler et al. *Bone*, 17:521, 1995.
Weinans et al. *J Orthop Res*, 10:845, 1992.

THE MECHANICAL EFFICACY OF SURGICAL TREATMENT IN LCP DISEASE USING FINITE ELEMENT ANALYSIS

Zobitz, M.E., Baker, K.J., Herring, J.A.

Texas Scottish Rite Hospital for Children, Dallas, TX 75219

INTRODUCTION

It is proposed that the outcome following surgical treatment in Legg-Calve-Perthes (LCP) disease is partially attributable to the mechanical state of the proximal femur following treatment. Using the finite element method (FEM), a model of the pediatric proximal femur was developed to evaluate changes in stress patterns following a simulated surgical treatment.

REVIEW AND THEORY

LCP disease, observed clinically since the early part of the 20th century, has been described as an idiopathic pediatric form of avascular necrosis, although the exact etiology is unknown (McCarthy, 1988). It has been hypothesized that LCP initiation follows a trauma severe enough to loosen the femoral head epiphysis, but not strong enough to produce a femoral neck fracture, causing a blood supply disruption and thus, a nutritional impairment of the epiphysis (Schwarz, 1986). If left untreated, long-term flattening of the femoral head may occur. Current treatment modalities are based on containment principles which presume that femoral head sphericity will be achieved by repositioning the lateral portion of the femoral head beneath the acetabulum. However, in the more severe cases the prognosis following surgery is unpredictable. In these instances an analytical model may help predict the mechanical benefits of surgical treatment. Previous FEM investigations of LCP have addressed the role of articular cartilage swelling (Ueo et al., 1987) and necrotic lesion size (Rab et al., 1982) on stress patterns in the femoral head. This study models specific configurations of LCP involvement and age development in order to correlate the mechanical effects of surgical treatment with clinical outcomes.

PROCEDURES

Using digitized slices from a CT scan of the proximal femur, a three-dimensional FEM model was constructed. The model used 15,043 six and eight node linear elements (34,359 degrees of freedom). Age representations (4, 7, 11, and 16 years old) and lateral pillar groups (Herring et al., 1992) (Group A: Normal lateral pillar height on radiograph; Group B: >50% height; Group C: <50% height) were simulated by modifying material properties. The effects of two common surgical treatments were modeled by rotating the pre-operative applied hip joint load in the directions corresponding to a 30° varus femoral osteotomy and a 20° varus, 10° anterior rotation innominate osteotomy. A stress-to-strength ratio (SSR) (compressive principal stress/yield strength) was used to analyze the risk of bony failure. The maximum SSR (MAX SSR) and volume-weighted average SSR (VWA SSR) within the femoral head ossification center were used to assess the surgical effectiveness by calculating the ratio of the difference between post-operative and pre-operative values of the SSR indices to the difference between the normal and pre-operative levels.

RESULTS

The percent effectiveness following surgery for the MAX SSR index is displayed in Figure 1. The 4 year old group showed only nominal improvements (-41.6% to 9.06%) while the 7 year old (181% to 250%), 11 year old (86.7% to 117%), and 16 year old (122% to 163%) groups showed significantly larger improvements following surgical treatment. The VWA SSR index showed a different trend following surgery (Figure 2). For this variable the 4 year old (27.9% to 48.3%) and 7 year old (41.2% to 61.7%) groups showed much larger improvements

than the 11 year old (4.55% to 18.8%) and 16 year old (0% to 12.7%) groups, following osteotomy.

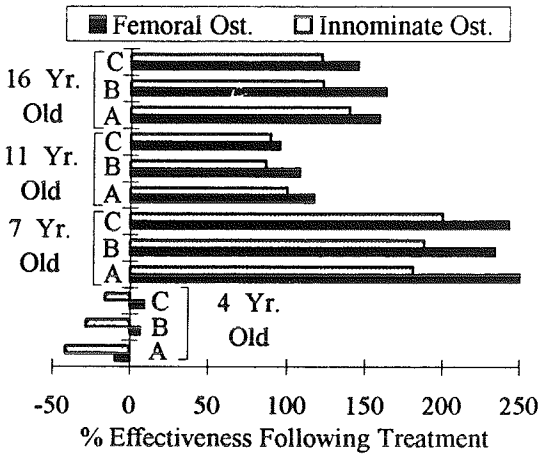

Figure 1: Percent Effectiveness for MAX SSR

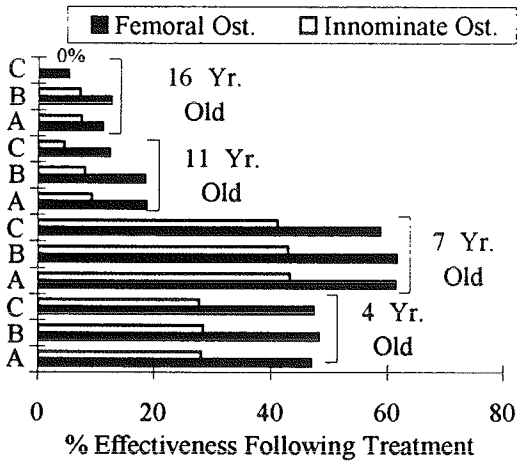

Figure 2: Percent Effectiveness for VWA SSR

DISCUSSION

The MAX SSR and VWA SSR indices complement each other in giving local and global indications, respectively, of the SSR state within the femoral head. Thus, when the percent effectiveness of the SSR indices for a particular case are inconsistent (one high, one low), surgery may not be warranted. From a multicenter study of LCP disease (Herring, 1994), it has been observed that young children (<6 years old) usually have good results without surgery. Correspondingly, the FEM results showed mixed results (low MAX SSR improvement and high VWA SSR improvement) indicating that surgery may not be mechanically beneficial. The 6, 7, and 8 year old age group typically experiences good outcomes following surgery for the more severe cases. Likewise, for this age group both SSR indices showed large improvements following surgery. Older children (>9 years old) have had mixed clinical results following surgery. Similarly, the MAX SSR improvements were high and the VWA SSR improvements low for the older age groups, again inconclusive as to the efficacy of surgical treatment. For all cases, the location of the necrotic lesion following treatment had the greatest influence on the result. When the lesion was large enough to fall outside the acetabular loading pathway, the model predicted a poor outcome. Therefore, positive clinical results following surgery may be attributed, in part, to protection of the weakened lateral pillar from high stresses, by the more stable bone adjacent to the lesion. The results of this study also give confidence in the use of the finite element method as a predictive tool, especially in cases such as age 7 Group C or age 11 Group B, where surgical outcomes are uncertain. With further development, FEM models could be used as an aid in pre-operative planning in such LCP cases.

REFERENCES

Herring J.A. et al. *J. Ped. Orthop.*, 12(2), 143-150, 1992.

Herring J.A. *JBJS*, 76-A(3), 448-458, 1994.

McCarthy R.E. *Instr. Course Lec.*, 37, 59-65, 1988.

Rab G.T. et al. *J. Ped. Orthop.*, 2(1), 39-44, 1982.

Schwarz E. *Clin. Orthop.*, 209, 5-12, 1986.

Ueo T. et al. *Arch. Orthop. Traum. Surg.*, 106, 202-208, 1987.

ACKNOWLEDGMENTS

This work was supported by the Research Fund of Texas Scottish Rite Hospital for Children, Dallas, TX.

A RHEOLOGICAL MODEL OF THE HUMAN HEEL PAD

S.E. D'Andrea[1,2], D.R. Lord[1,3], B.L. Davis[1]

[1]Department of Biomedical Engineering, The Cleveland Clinic Foundation, Cleveland, OH 44195
[2]Biomedical Engineering Center, The Ohio State University, Columbus, OH 43210
[3]Department of Aerospace and Mechanical Engineering, Case Western Reserve University, Cleveland, OH 44106

INTRODUCTION

During walking and other impact activities, the heel is most commonly the first structure to contact the ground (Cavanagh and Lafortune, 1980). Therefore, the shock absorption capabilities of the human locomotor system are strongly influenced by the properties of the fat pad in the heel of the foot. Numerous studies have attempted to characterize the mechanics of the human heel pad (Bennett and Ker, 1990; Cavanagh et al., 1984; Aerts et al., 1995). *In vivo* investigations have utilized pendulum or other impact experiments while *in vitro* tests were performed with isolated heel pads in mechanical testing machines. Differences in experimental set up and testing parameters make comparisons of the two types of tests difficult. Additionally, large discrepancies are evident in reported values of energy dissipation and stiffness.

A mathematical model would provide a more controlled method of studying the mechanical properties of the heel pad. The purpose of the current investigation, therefore, was to develop a rheological model which would predict the non-linear, viscoelastic behavior of the human heel pad.

REVIEW AND THEORY

The fat pad of the heel covers the tuber of the calcaneus and measures 13 to 21 mm in thickness (Gooding, 1985). The heel pad is composed of a system of globules of specialized fat cells separated into chambers by septa of elastin and collagen. The unique configuration of the fat and septa give the heel pad its powerful shock absorbing capabilities. The septa are oriented in an arrangement described by Blechschmidt (1982) as a "whorl pattern." As the heel pad is deformed during weight bearing, the septa twist in a spiral fashion around one another, preventing the fat globules from being displaced. This effect minimizes compression of the heel pad, increasing its ability to attenuate force.

Since the heel pad contains both viscous and elastic components, corresponding to the fat cells and septa respectively, it lends itself to rheological modeling. Rheological modeling is a means to describe the stress/strain behavior of a material mathematically. There are four fundamental rheological properties: elasticity, viscosity, plasticity and strength. Complex behaviors such as viscoelasticity can be described by combining these essential properties in a network of Hookean springs and Newtonian dampers. To date, rheological models have been developed for biological tissues such as tendon, bone and ligament, but no such model exists for the heel pad.

PROCEDURES

A model of the heel pad was developed using the ADAMS® software (Automatic Dynamic Analysis of Mechanical Systems, Mechanical Dynamics, Inc., Ann Arbor, MI). Figure 1 shows a schematic of the model. Spherical balls with negligible mass were positioned 0.5 cm apart horizontally. Connecting arms were composed of elastic springs and viscous dampers. Arms 1,4,7,8 and arms 2,3,6 and 9 were given stiffness values of 1.5×10^4 and 1.5×10^5 N/cm respectively and had unstrained lengths of 1.0 cm.

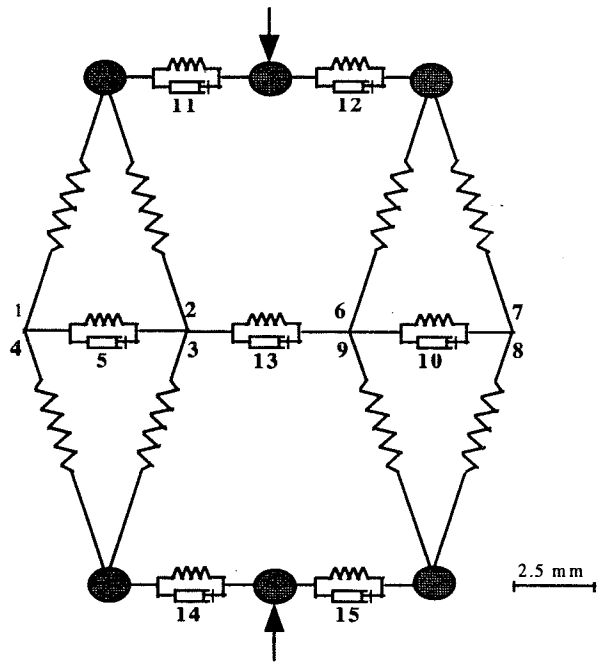

Figure 1: Rheological Model of the Heel Pad

The remaining arms consisted of Kelvin bodies - a spring and damper in parallel - with lengths of 0.5 cm in the unloaded state. The properties of these links were: arms 5,10 and 13 - stiffness, $1.5x10^4$ N/cm, damping, 3.0 N-s/cm; arms 11,12,14 and 15 - stiffness, $1.5x10^4$ N/cm, damping, 435 N-s/cm. A compressive, sinusoidal force equal to $(600*\sin(2\pi t - \pi/2) + 1.0)$ was applied to the center nodes in the model.

RESULTS

The behavior of the model of the heel pad is shown in Figure 2. The resultant curve initially exhibits a large displacement with relatively little increase in force. A distinctive "knee" in the curve follows, suggesting a change in apparent stiffness of the model at the corresponding deformation. This increase in stiffness results from the deformation of the Kelvin bodies of the upper and lower horizontal arms as they move to a more vertical orientation. With continued increases in force, deformation rises relatively linearly to maximum load (1200 Newtons) and deformation (4.2 mm). The curve exhibits a hysteresis effect as the force and deformation subsequently decrease. At the end of the cycle, with zero force applied, the deformation of the heel pad model remained at 1.44 mm. The energy absorbed by the heel pad, represented by the area between the two curves, was 20.4% in the model.

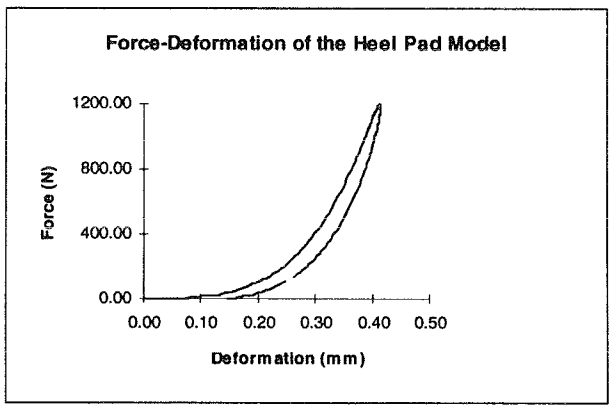

Figure 2: Force-Deformation Curve

DISCUSSION

A relatively simple rheological model has been developed which can describe the non-linear, viscoelastic behavior of the heel fat pad. Such a model provides an objective means of assessing the mechanical properties of the heel pad and eliminates problems associated with experimental design. Furthermore, the model can be used to describe the effects of disease states, such as musculoskeletal disorders, acromegaly or diabetes, which are thought to have a detrimental effect on the soft tissue of the heel.

Simulation of impact on the heel pad produced force-deformation curves comparable to those found in previous studies (Bennett and Ker, 1990; Aerts et al., 1995). A maximum deformation of 4.2 mm in the model fell well within the range reported by these investigators (1.9 to 6.3 mm). Comparisons for energy dissipation, however, are more difficult as experimental values show a wide discrepancy. Reported values were 95% during *in vivo* and *in vitro* impact tests and 30% during *in vitro* Instron tests. This large variation has been attributed to compliance in the proximal joints and soft tissues. Although the true energy absorption characteristics of the heel pad are unknown, adjustment of the parameters of the mathematical model will allow any energy absorption profile to be duplicated.

By eliminating the sources of variability between and within experiments, the rheological model is capable of analyzing the individual effects of stiffness, damping and loading rate. This ability becomes crucial when attempting to assess the role of the heel pad in the reduction of impact forces. A direct relationship between these variables (stiffness, damping and loading rate) and shock absorption can be ascertained. This model will also be useful in describing the effect of clinically observed changes in the heel pad structural properties.

REFERENCES

Aerts, P et al., *J. Biomech.*, 28(11): 1299-1308, 1995.
Bennett, M and Ker, R, *J. Anat.*, 171: 131-138, 1990.
Blechschmidt, E, *Foot and Ankle*, 2(5): 260-283, 1982.
Cavanagh, PR and Lafortune, MA. *Sports Shoes and Playing Surfaces.* Human Kinetics Publishers, 1980.
Cavanagh, PR et al., *Sports Shoes and Playing Surfaces.* Human Kinetics Publishers, 1984.
Gooding, GAW et al., *J. of US Med*, 4: 173-174, 1985.

DESIGN OPTIMIZATION OF A THICK LAMINATED COMPOSITE FEMORAL COMPONENT FOR HIP JOINT ARTHROPLASTY

W. Fu[1], S.B. Biggers Jr.[1], and R.A. Latour Jr.[2]
[1]Dept. of Mech. Engr., Fluor Daniel Building, Clemson University, Clemson, SC, 29634
[2]Dept. of Bioengr., 501 Rhodes Hall, Clemson University, Clemson, SC 29634

INTRODUCTION

A multi–level optimization process has been developed specifically to design thick laminated composite femoral components for hip joint arthroplasty[1]. The large number of design variables present in this type of structure makes such a process a necessity so that reasonable computational efficiency can be achieved. The optimization process has been applied to a conceptual finite element (FE) model of a composite femoral component for total hip joint replacement. By controlling the complexity of the models, the number of design variables, and the nonlinearity of the optimization problem at each level, the required computational efficiency is achieved to allow structural optimization to be accomplished.

REVIEW AND THEORY

Total hip arthroplasty using metallic hip prostheses has been performed successfully for over three decades. However, it has been found that stress shielding and subsequent bone resorption of the proximal femur are problems that may contribute to stem loosening and complicate revision surgeries. Low–stiffness composite implants have been shown to reduce stress shielding. However, clinical experience thus far has shown that such stems may have inadequate strength. In a laminated composite ster.., the designer has the freedom to vary the orientation of each ply to independently control component stiffnesses and strength. However, due to this increased design freedom and the heterogeneous anisotropic nature of composite materials, composite stems are much more complex to design than their homogeneous isotropic metallic counterparts. In a thick laminated composite structure for a femoral component application, the primary design parameters of interest are in–plane and out–of–plane bending stiffness and strength. Composite materials provide the advantage that in–plane and out–of–plane stiffness can be controlled independently of one another by the manner in which ply orientation and stacking sequence are arranged within the material. In addition, numerous different ply orientations and stacking sequences can be used to provide a given level of in–plane and out–of–plane stiffness, with each different layup possessing a different strength level. This allows the strength level of the laminate to be varied, and thus optimized, independently of in–plane and out–of–plane stiffness. Based upon these recognized properties inherent in the design of a thick laminated structures, a three–level hierarchical optimization procedure has been developed. This abstract summarized this procedure which enables a laminated composite femoral component to be efficiently designed and optimized for in–plane and out–of–plane bending stiffness and ply–level strength.

PROCEDURES

A three–level optimization procedure was developed for the design of thick laminated composites implants fabricated from unidirectional carbon fiber reinforced polyetherether ketone prepreg.

In the first level (in–plane optimization), the structural model to be optimized was the global model representing a simplified human femur with its lower end fixed and the upper region containing a modeled composite femoral component inserted within the femur's central canal and extending out of the top. The composite laminate structure was optimized for its global in–plane bending stiffness. The structure was treated as a homogeneous orthotropic (balanced and symmetric) laminate under in–plane loading. The objective to be maximized was the strain energy in the femur's calcar region. The design variables consisted of the 5 independent coefficients of the laminate global material stiffness matrix, i.e., C_{11}, C_{22}, C_{13}, C_{44}, C_{55}. The feasible domain for these design variables can be obtained by classical laminate theory. The interfacial shear stress between the proximal–medial stem and the femur are constrained to be below user–defined limits.

In optimization Level 2 (out–of–plane optimization), the global model used in Level 1 was modified so that the laminate structure was divided into a number of sublaminates. The feasible domain was defined for each sublaminate the same way as in Level 1. However, the additional constraint was that the combined in–plane stiffnesses of the sublaminates must equal the optimal value as obtained in Level 1. The objective in Level 2 was to minimize the maximum shear stresses along the femur and the proximal–anterior/posterior stem interface when the laminate was under out–of–plane loading. The design

variables in this level were the 5 stiffness coefficients of each sublaminate. Level 1&2 optimization was conducted by using DOT (Design Optimization Tools, VMA Engineering, Goleta, CA) and Level 3 optimization by using the genetic algorithm.

Finally, optimization at Level 3 (strength optimization) was conducted by determining the optimal ply orientations and stacking sequences which maximized the strength of the laminate composite while maintaining the stiffness of the sublaminates determined in optimization Level 2. In this level, a local FE model was generated from the maximum strain energy area in the global FE model (Fig. 1) used for Levels 1 and 2 based on a 3–D global–local method[2] for strength optimization. 3–D ply–level stress values were then accurately determined by this local FE analysis. The objective in this level was to minimize the sum of the two failure criteria values (ex. Tsai–Hill)[3] and the difference between the coefficients of the optimized sublaminate stiffness matrices in Level 2 ($^2C_{ij}$) and the stiffness coefficients of the specific laminate being determined in Level 3 ($^3C_{ij}$) determined by laminated plate theory.

RESULTS AND DISCUSSION

Global and local finite element models are shown in Fig. 1. The results of the optimization are shown in Table 1. In Table 2, the optimal results have been compared to a set of suboptimal results. Compared to the suboptimal case, the optimal design results in greater stress transfer to the calcar as indicated by calcar strain energy(U), with the Level 1 interfacial shear stress being within the user set limit of <10.0 MPa. As expected, the suboptimal stem exhibits lower Level 1 interfacial stresses (and calcar strain energy) as a result of its greater in–plane bending stiffness. Considering Level 2, the optimal stem, despite its lower in–plane bending stiffness, was able to be designed with equivalent out–of–plane stiffness as the stiffer suboptimal stem design, with resulting approximately equivalent anterior/posterior interfacial stresses. Finally, in Level 3, it was demonstrated that the optimal design has much higher strength than the suboptimal design even though it was a more flexible stem. Following the Level 3 analysis, the Level 1&2 properties of calcar strain energy and anterior/posterior stem–bone interfacial stresses were recalculated using the Level 3 defined stacking sequence to confirm that these values were approximately maintained in the Level 3 optimization. This three–level process capitalizes on the computational efficiency associated with the global–local analysis and with the use of laminate theory to condense the number of design variables to provide an efficient way to optimize a structure having three–dimensional geometry and loading, complex material properties, and multiple objectives. This technique is currently being applied for the design optimization of actual femoral components using an anatomically modeled femur and 3–D joint loading.

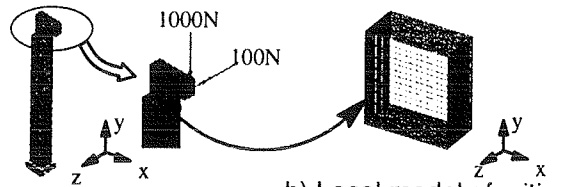

a) Global model b) Local model of critical stress area

Fig 1. Conceptual model of hip stem

Level 1 (GPa) stiffness coef.	Level 2 (GPa) stiffness coef.		Level 3 (degrees) ply lay–up
C_{11}=112.2 C_{22}=23.18 C_{13}=5.833 C_{44}=2.905 C_{55}=3.092 max strain energy = 25.03 N–mm; max shear stress < 10.0 MPa	sub1	C_{11}=106.9; C_{22}=26.14 C_{13}=5.495; C_{44}=2.412 C_{55}=2.239	$[\pm 39/\pm 47/\pm 30/\pm 18/\pm 36]_s$
	sub2	C_{11}=116.0; C_{22}=21.09 C_{13}=5.497; C_{44}=5.20 C_{55}=1.903	$[\pm 45/\pm 28/\pm 11/\pm 15/\pm 15]_s$
	sub3	C_{11}=106.9; C_{22}=26.14 C_{13}=5.495; C_{44}=2.412 C_{55}=2.239	$[\pm 39/\pm 47/\pm 30/\pm 18/\pm 36]_s$

Table 1: Results of three level optimization

	Level 1		Level 2	Level 3		
	strain energy (U)	interfacial shear stress (S)	interfacial shear stress	failure criteria value	verification Level 1	verification Level 2
optimal design	25.03 N–mm	9.0 MPa	2.307 MPa	0.6328	U=23.89 N–mm S=9.375 MPa	3.01
sub–optimal design	8.05 N–mm	5.62 MPa	2.85 MPa	0.9262		

Table 2: Comparison between the optimal and suboptimal designs

REFERENCES

1) W. Fu, S.B. Biggers Jr., and R.A. Latour Jr., Proc. Am. Soc. Compos., 11th Tech. Conf., 1996. 2) S. Srinivasan, S.B. Biggers Jr., R.A. Latour Jr., Int. J. Num. Meth. Eng., 39:805–828, 1996. 3) S.G. Zhou and C.T. Sun, J. of Comp. Tech.&Res., 12:91–97, 1990

ACKNOWLEDGEMENT

We thank the Whitaker Foundation, Roslyn, VA for funding this research.

A QUASI-LINEAR, STRUCTURAL MODEL OF THE SOFT TISSUE ON THE PLANTAR ASPECT OF THE HUMAN FOOT

W. R. Ledoux [1,2], H. J., Hillstrom [2,3,1], D. F. Meaney [1], A. Radin [4]
[1] Department of Bioengineering, University of Pennsylvania, Philadelphia, PA 19104
[2] Gait Study Center, Pennsylvania College of Podiatric Medicine, Philadelphia, PA 19107
[3] School for Biomedical Engineering, Science, and Health Systems, Drexel University, Philadelphia, PA 19104
[4] Laboratory for Research on the Structure of Matter, University of Pennsylvania, Philadelphia, PA 19104

INTRODUCTION

As the foot progresses through the stance phase of gait, there are seven primary areas on the plantar aspect through which force is transferred to the ground. These areas include the tissue beneath the heel (subcalcaneal), each of the five metatarsal heads (submetatarsal) and the big toe or hallux (subhallucal). Although many researchers have explored the structural properties of the subcalcaneal tissue [1, 3, 4, 7, 12] most of the research has concentrated on the response of the tissue to impact loads and little has been done to develop constitutive relationships. Furthermore, no work has been published on the properties of the other six areas of loading.

REVIEW AND THEORY

It has been shown that the subcalcaneal tissue changes with age [8, 11] as well as with the existence of vascular disease. [2, 6] Additionally, since fat is a major constituent of the soft tissue and it melts near body temperature, [10] it is probable that the temperature of the specimen could affect its properties. The quasi-linear viscoelastic (QLV) theory has been developed in order to obtain constitutive properties of non-linear viscoelastic tissue. [5] The theory incorporates an elastic response, $T^{(e)}(\lambda)$, which is the stress obtained from a finite strain. The stretch ratio (λ) is defined as the length divided by the original length. A reduced relaxation response, G(t), is obtained from a stress relaxation experiment. The two functions are combined in the following equation:

$$T(t) = T^{(e)}[\lambda(t)] + \int_0^t T^{(e)}[\lambda(t-\tau)]\frac{\partial G(\tau)}{\partial \tau}\,d\tau \qquad (1)$$

This theory is employed to generate material models, since stress and strain are normalized to cross sectional area and initial length respectively. For our protocol, this presented two problems. First, the stress during an indentation test is not merely the force divided by the area; it is a much more complex function. Second, equation 1 involves the assumption of a continuum, which our complex anatomy precludes. The worst example is probably beneath the first metatarsal head, where in addition to the epidermis and dermis, there are sesamoids, cartilage, fat bodies, neurovascular bundles, muscles, tendons, ligaments, and the plantar aponeurosis. Therefore the QLV theory was modified to develop structural (geometry dependent) rather than material models. Force (F) and displacement (d) were substituted for stress (T) and stretch ratio (λ).

$$F(t) = F^{(e)}[d(t)] + \int_0^t F^{(e)}[d(t-\tau)]\frac{\partial G(\tau)}{\partial \tau}\,d\tau \qquad (2)$$

The elastic response was modeled as a fourth order polynomial:

$$F^{(e)} = A_1 + A_2 d + A_3 d^2 + A_4 d^3 + A_5 d^4 \qquad (3)$$

where A_n are constants determined empirically. The reduced relaxation response was in the form of a double exponential:

$$G(t) = K_1 + K_2 e^{-K_3 t} + K_4 e^{-K_5 t} \qquad (4)$$

where K_n are constants determined empirically. We employed this modified version of the QLV to model each of the seven areas of interest.

PROCEDURE

Five young (18 - 47 years), healthy (no peripheral vascular disease) cadaveric feet were studied. Each foot was disarticulated at the subtalar joint and the dorsal aspect was dissected down to ligament and bone. The specimen was mounted plantar side superiorly in polymethylmethacrylate in an aluminum box. The box was mechanically grounded to the loading frame of an Instron series 1331 with one of the seven areas of interest centered beneath the actuator. An appropriate size punch, corresponding to the area of contact during stance, was attached to the Instron. Thermofoil™ heaters were attached to the sides of the aluminum box. The heaters were part of a closed loop proportionally controlled system that maintained the specimens at 35° C (slightly less than core body temperature).

Stress relaxation experiments, where a constant displacement was applied and held for a period of time, were conducted. These experiments were guided by the physiological force normally experienced at each area during stance phase. These data were obtained from previous work by the authors. [9] The displacement required to generate the specified force was determined. The area of interest was stimulated with single displacement pulses, beginning with small amplitudes and slowly increasing in magnitude

until the approximate physiological force was obtained. The displacement level was retained for the remainder of the testing on that area.

The specimen was then preconditioned to the appropriate displacement by sinusoidally oscillating at 1 Hz for 30 seconds. The specimen was allowed to recover for exactly 3 minutes. Finally, the stress relaxation experiment was conducted; a ramp displacement function, achieving proper magnitude in 0.2 seconds, was applied. This displacement was held for 3 minutes. The entire process was repeated for each of the 7 areas.

On one subcalcaneal test area, several ramp and hold tests of increasing displacement were performed. The tissue was allowed to recover for three minutes between tests.

Both force and displacement were collected. The force versus displacement data were fit to equation 3 (the elastic response) and the force versus time were fit to equation 4 (the reduced relaxation response), both with a least squares approach.

RESULTS

Five feet were tested, but due to procedural problems, one was discarded. Three were tested at 35° C and one at room temperature. A typical fit of the elastic function (equation 3) to the ramp data is found in figure 1, while a typical fit of the reduced relaxation response (equation 4) to the hold data is found in figure 2. The response of the specimen that was tested at several displacement ramps (not shown) demonstrated that the subcalcaneal tissue is nonlinear.

DISCUSSION

This body of work demonstrates the utility of the quasi-linear viscoelastic theory to model the mechanical properties of the plantar soft tissues. Both elastic and reduced relaxation functions have been generated successfully for each of the seven areas of interest on four feet. Preliminary work on the subcalcaneal tissue has demonstrated its nonlinear properties. Temperature dependence could not be determined in this initial analysis. Due to the fact that structural models were generated, it could not be ascertained whether variability in the response of the tissue was caused by differences in temperature or structure. Future work will include studying the linearity of the other areas and the effect of strain rate on the soft tissue properties. The effect of temperature will also be explored further by testing structurally similar feet (i.e., from the same donor) at room and body temperature. Additionally, the QLV theory will be employed to describe other functions besides the ramp and hold (e.g. ramp up and ramp down, oscillatory). Lastly, a different materials testing machine (an MTS high frequency model 810 materials testing system with the TestStar™ II digital control system and software) will be employed to conduct the ramp and hold tests immediately after the preconditioning, allowing for testing of the steady state properties of the soft tissues.

REFERENCES

1. Aerts, P., *et. al.*, (1995) *J. Biomechanics* 28, 1299-1308.
2. Buschmann, W. R., *et. al.*, (1995) *Foot & Ankle International* 16, 254-8.
3. Cavanagh, P. R., *et. al.*,. (1984) in *Biological Aspects of Modeling Shoe/Foot Interaction During Running*, ed. Fredericks, E. C. (Human Kinetics Publishers, Inc, Champaign, Illinois), pp. 24-46.
4. De Clercq, D., *et. al.*,(1994) *J. Biomechanics* 27, 1213-22.
5. Fung, Y. C. (1993) *Biomechanics: Mechanical Properties of Living Tissues* (Springer-Verlag, New York).
6. Jahss, M. H., *et. al.*,(1992) *Foot & Ankle* 13, 233-42.
7. Kinoshita, H.,*et. al.*, (1993) *Int. J. Sports. Med.* 14, 312-9.
8. Kuhns, J. G. (1949) *JBJS* 31-A, 541-547.
9. Ledoux, W. R., *et. al.*, (1997) in *Evaluation of the Distributed Plantar Vertical Force in Rectus and Pes Planus Foot Types*, N. A. Soc. Gait and Clin. Move. Society
10. Phinney, S. D.,*et. al.*, (1994) *Am. J. Clin. Nutr.* 60, 725-9.
11. Prichasuk, S., *et. al.*, (1994) *Clin. Orthop.* , 197-200.
12. Valiant, G. A.*et. al.*, (1984) *Ph.D. thesis*, Penn State

ACKNOWLEDGEMENTS

The American Podiatric Medical Association
PCPM Institutional Research Committee

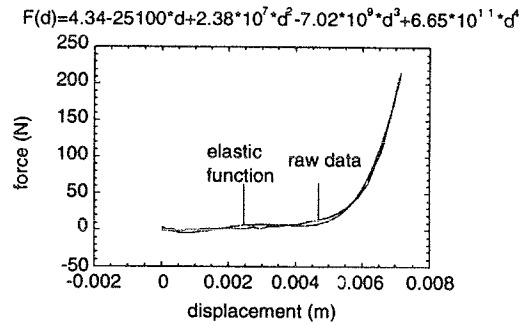

Figure 1 - The raw ramp data and the elastic function for the first metatarsal of foot #6.

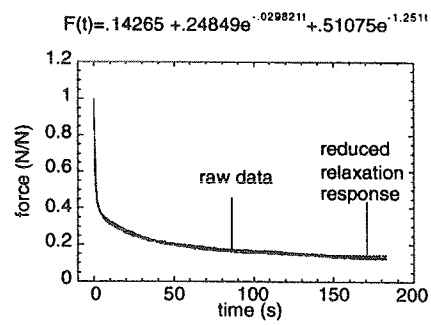

Figure 2 - The raw hold data and the reduced relaxation response for the first metatarsal of foot #6.

ACCURACY OF TRUNK ALIGNMENT TO VISUALLY SPECIFIED AXES IS SIMILAR IN GYMNASTS AND NON-GYMNASTS

J.M. Hondzinski, W.G. Darling and A.M. Bordignon

Department of Exercise Science, The University of Iowa, Iowa City, IA 52242

INTRODUCTION

Proprioceptive and visual signals are very important in maintaining proper body positions used for balance and control of movement in daily activities as well as acrobatic skills. To determine whether gymnasts are able to align their body to external axes with greater accuracy than non-gymnasts we compared their abilities to align the long trunk axis to visually identified external axes when: 1) standing (ST), suspended-upright (SU) and suspended--inverted (SI); 2) the head is aligned with the long trunk axis and tilted; and 3) allocentric cues are available or not.

REVIEW AND THEORY

It has been reported that positioning of the trunk can be used as a very good indicator of orientation ability (Hondzinski and Darling, 1993, Jakobs et al, 1985, Ross et al., 1969). These studies examined trunk alignment to either gravitational vertical or to anatomical position while horizontal. To our knowledge no studies have tested the accuracy of trunk alignment to oblique axes. In previous work it was observed that divers and non-divers were very accurate at the task of aligning their trunk to the vertical whether vision was permitted or not (Hondzinski and Darling 1993). In contrast, Ross et al. (1969) observed that inverted SCUBA diver's use of vision (underwater) resulted in more accurate indication of vertical trunk alignment. Because it has been shown that visual perception of vertical is influenced by head and body orientation (Parker et al., 1983), the first purpose of this experiment was to determine how accurately subjects could align their longitudinal trunk axis to various oblique axes in three body positions and two head positions. The second purpose was to compare gymnasts to control subjects under these conditions with and without use of allocentric cues. Gymnasts were studied because their awareness of the body position relative to the gravitational vector and visual stimuli are both needed and used while performing. We hypothesized that subjects' errors in aligning the trunk to visually specified axes would be higher: (1) in the SI condition than the SU and ST conditions; (2) when the head is misaligned to the trunk; (3) when external orientation cues were not available; and (4) in controls than in gymnasts in the SI condition.

PROCEDURES

Five college gymnasts and five control subjects participated in this experiment. Infrared emitting diodes (IREDs) were attached to goggles worn by subjects, to a device that fit firmly to the trunk and to an external rod for optoelectronic recording of their orientation.

Suspension of subjects was accomplished using a tandem skydiving harness and a stable overhead spotting system, similar to that used in gymnastics training. A simple hollow metal pole, to which the subjects' legs were attached using "anti-gravity boots", was stabilized by securing its ends to ropes of the system.

A straight visible rod was presented to the subject at varying oblique angles (in three dimensions) by the experimenter. Subjects were instructed to align their longitudinal trunk axis to the rod as accurately as possible in each trial. Trials in each of the three body positions were performed with the head position in alignment with the trunk and tilted (in three dimensions) and in both darkness and in normal room lighting. In darkness subjects could view the dimly illuminated rod, but not the surrounding area. Subjects were able to complete dark trials in each condition before dark adaptation occurred. Twenty trials were tested in each of the 12 conditions.

Errors in trunk alignment to the external axes were measured in three dimensions and computed as frontal and sagittal plane errors. Variable errors (VEs), computed as the standard deviation of the signed individual trial errors in each plane in each condition, were used as a measure of random error. These were compared across group, plane and experimental

condition using a repeated measures analysis of variance (ANOVA).

RESULTS AND DISCUSSION

Surprisingly, variable errors were similar for gymnasts and controls ($F_{1,8}$=0.769, p=0.4) even in the SI condition ($F_{2,16}$=1.38, p=0.3) and during normally lit and darkened background environments ($F_{1,8}$=1.521, p=0.25). VE data was therefore combined across groups and light/dark conditions (figure 1). Clearly, the subjects could accurately align the trunk to an external rod as indicated by the low mean VE in each condition. These low VEs show that subjects accurately transform visually specified axes into trunk orientation using kinesthetic information (proprioception, vestibular afferents and tactile senses).

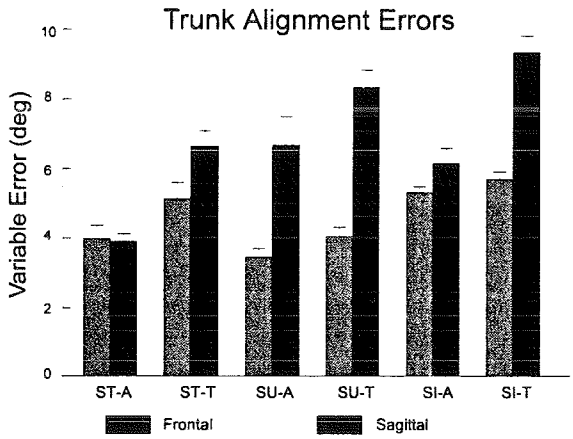

Fig. 1 Mean variable trunk alignment errors are shown in both frontal and sagittal planes. ST-standing, SU-suspended upright, SI-suspended-inverted, A-head aligned, T-head tilted.

Figure 1 also shows that subjects had higher errors in the sagittal plane than in the frontal plane ($F_{1,8}$=43.14, p<0.001), when the head was tilted ($F_{1,8}$=47.89, p<0.001) and when suspended and inverted ($F_{2,16}$=10.58, p<0.01). The errors were lower in the frontal plane probably because of the position of the eyes in humans. Left and right tilt in the frontal plane of an external object can easily be identified. It is more difficult to determine the angle of tilt in the sagittal plane because the rod projects a vertical image on the retina due to their frontal plane orientation. Differences in rod dimension must be used for determining the sagittal plane angle to align the trunk appropriately.

Greater alignment errors when suspended suggest that ground contact by the feet is important in maintaining accurate perceptions of trunk orientation. This agrees with the results of Thomas and Lyons (1966) that ground contact is important in visual awareness of the vertical in pigeons. The increased errors may also be due to the novelty of the suspended positions.

When the head and trunk are aligned, the task is presumably easier because the vestibular otoliths can be used to specify trunk orientation. Tilting the head requires incorporation of the neck angle information to determine trunk orientation, which resulted in larger perceptual errors. This is consistent with other findings that tilting the head causes greater errors in trunk alignment to either the vertical or an anatomical position when horizontal (Hondzinski and Darling, 1993, Parker et al., 1983).

REFERENCES

Hondzinski, J.M. and Darling W.G. ASB Proceedings, 17th annual meeting 113, 1993.
Jakobs, T. et al. Exp Brain Res, 90, 129-138, 1985.
Parker, D.E. et al. Percept & Psychophys, 33, 139-146, 1983.
Ross, H.E. et al. Aerospace Med, 40, 728-732, 1969.
Thomas, D.R. et al. Percept & Psychophys, 1, 93-95, 1966.

ACKNOWLEDGMENTS

A special Thanks to the Iowa Space Grant Consortium, Bill Morrissey, Jay Speckeen and Jeff Davidson.

KINEMATIC AND EMG CHANGES IN BASEBALL PITCHING DURING A SIMULATED GAME

S.W. Barrentine[1], Y. Takada[2], G.S. Fleisig[1], N. Zheng[1], J.R. Andrews[1]

[1] American Sports Medicine Institute, Birmingham, AL, 35255
[2]Kobe University, Kobe, Japan

INTRODUCTION

One of the main responsibilities of a baseball pitching coach is to determine when a pitcher has become fatigued, as a fatigued pitcher is believed to be less effective and also at higher risk of injury. Sports medicine clinicians share this concern, as the vast majority of pitching injuries are attributed to overuse (Fleisig et al., 1995).

REVIEW AND THEORY

Although most people agree that pitching while fatigued is potentially detrimental, kinematic changes associated with fatigue have not been quantified. Furthermore, the changes in muscular activity have not been studied. The purpose of this study was to measure kinematic and electromyographic changes in baseball pitching during a simulated game.

PROCEDURES

Ten collegiate pitchers served as subjects in this study. Subjects were tested in pairs in an indoor laboratory. After providing informed consent, and medical history, anatomical measurements were taken and reflective markers were attached to fourteen bony landmarks (Fleisig et al., 1995, 1996). Bipolar surface electrodes were attached to the mid deltoid, biceps brachii, triceps brachii, and flexor carpi radialis muscles of the throwing arm (Delagi and Perotto, 1980). After stretching and warming up, the pair of subjects alternated pitching for a simulated complete game (18 half innings), or until unable to continue. Each subject threw up to 7 warm-up pitches prior to each half inning and 15 game pitches during each half inning. Each subject threw from a portable pitching mound to a catcher behind home plate located 18.4 m away. As in actual games, the catcher signaled for a pitch type (fastball, curveball, etc.) and location before each pitch. After each pitch, a researcher announced a result (called strike, homerun, etc.) according to a predetermined randomized chart and the pitch location. Data were collected for three fastballs thrown from a windup position during each half-inning. Using methods described by Fleisig et al. (1996), three dimensional kinematics were calculated from digitized data collected with a four camera (200 Hz) Motion Analysis system. Electromyographic (EMG) data were collected during pitching and during maximum voluntary isometric contraction (MVIC) with a four channel (1000 Hz) telemetry system (Noraxon USA, Inc). Motion and EMG data collection were electronically synchronized.

RESULTS

Relative to the first inning, kinematic changes were observed over nine innings (Figures 1 to 4). A pitcher had greater shoulder abduction (+5°), horizontal adduction (+5°), and external rotation (+8°) at the instant of foot contact with the mound (FC).

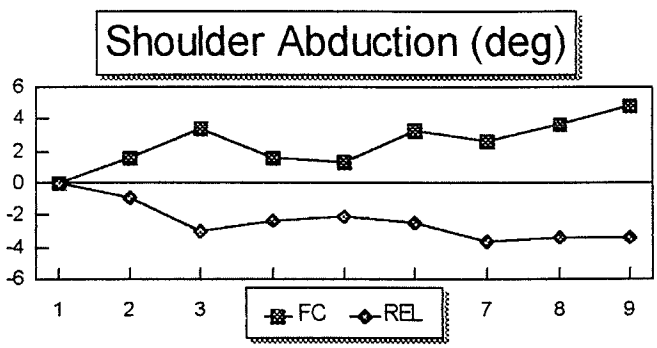

Figure 1. Shoulder abduction v. inning, relative to first inning.

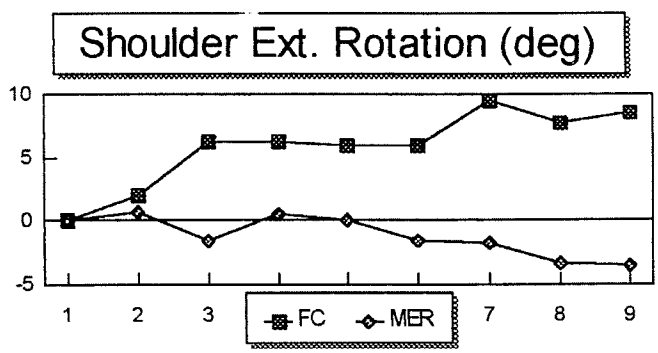

Figure 2. Shoulder external rotation v. inning, relative to first inning.

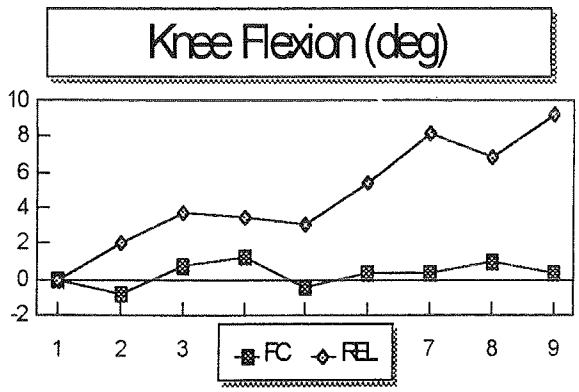

Figure 3. Knee flexion (deg) v. inning, relative to 1st inning.

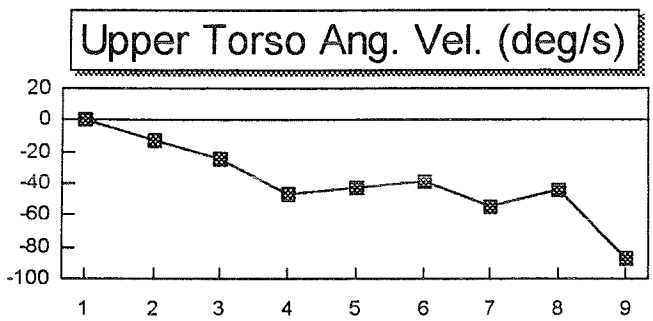

Figure 4. Upper torso angular velocity (deg/s) v. inning, relative to 1st inning.

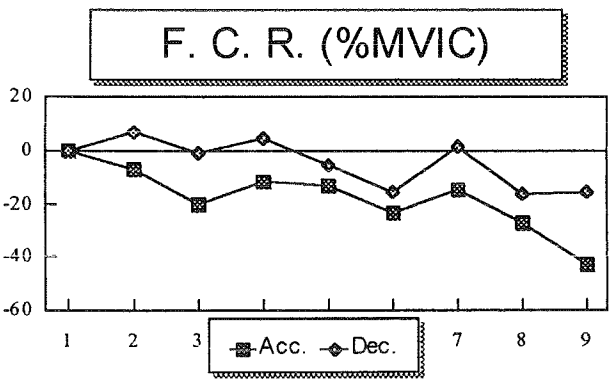

Figure 5. Flexor carpi radialis activity (%MVIC) v. inning, relative to 1st inning. (N=4)

During the arm cocking and arm acceleration phases, a pitcher had less shoulder external rotation (-4°), and upper torso angular velocity (-90°/s). At the instant of ball release (REL), a pitcher had less shoulder abduction (-4°), greater lead knee flexion (+9°, defined at 180° when leg completely straight), and decreased ball velocity (-1 m/s). EMG data from only four subjects were reliable. Gradual changes were seen for

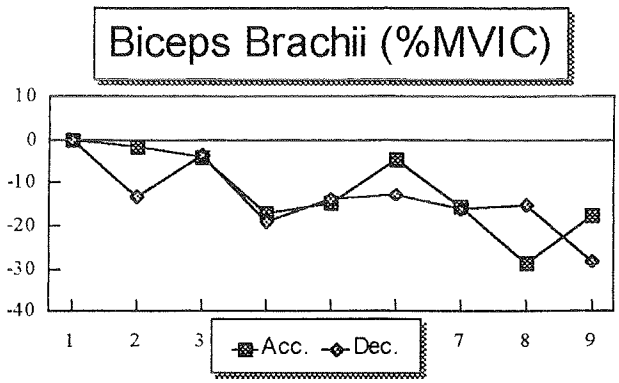

Figure 6. Biceps Brachii activity (%MVIC) v. inning, relative to 1st inning. (N=4)

the flexor carpi radialis and biceps brachii (Figure 5 and 6) during arm acceleration (Acc) and deceleration (Dec) phases, however no consistent changes were observed for other muscle groups or phases.

DISCUSSION

The decreased ball velocity as the game progressed was partially due to reduced shoulder external rotation and reduced upper torso velocity. Two kinematic changes often observed by coaches were also found: a lower elbow (reduced shoulder abduction) and a straighter lead leg at ball release. The pitcher tried unsuccessfully to prevent decreased shoulder abduction and external rotation during arm cocking by increasing these angles at foot contact. Results from this study help explain how a pitcher alters kinematics during a game. Further research on muscle activity and joint kinetics may provide more insight about the mechanisms and warning signs for overuse injury.

REFERENCES

Delagi, E.F. and Perotto, A. Anatomic Guide for the Electromyographer - The Limbs. Charles C. Thomas, 1980.

Fleisig, G.S., et al. Am J Sports Med **23**, 233-239, 1995.

Fleisig, G.S., et al. J Appl Biomech **12**, 207-224, 1996.

ACKNOWLEDGMENTS

The authors would like to thank Andy DeMonia and David Downs for their assistance with data reduction and the members of the University of Alabama at Birmingham and Samford University baseball teams for their participation in this study.

A COMPARISON OF THE EFFECTS OF TWO STYLES OF SQUATS AND THE POWER CLEAN EXERCISE ON MAXIMUM ANAEROBIC POWER IN EIGHT WEEKS OF BEGINNING WEIGHT TRAINING

J. Abendroth-Smith, J. Howard, L. Hendy
Department of HPER, Utah State University, Logan UT 84322

INTRODUCTION

Popular modes for increasing lower body strength and power are the isotonic full squat, the 3/4 squat and the power clean. The full squat technique has a notable risk of injury even when being performed properly (Chandler & Stone, 1991). Previous research has shown that athletes who train with the full squat do improve their max anaerobic power, but is this improvement any different if the training involves the 3/4 squat or the power clean rather than the full squat? This question has not been adequately addressed in the literature.

REVIEW AND THEORY

The literature demonstrates a discrepancy as to whether there is a greater improvement in anaerobic power when training for speed or training for strength (Wenzel & Perfetto, 1992). The full and 3/4 squats are noted for increasing strength, while the power clean is noted for increasing speed, but it is unclear which may provide an advantage when training to increase anaerobic power production. With the inherent risks associated with the full squat, would the 3/4 squat and power clean be effective alternative training modalities?

The purpose of this study was to determine whether eight weeks of weight training with the full squat, the 3/4 squat or power cleans resulted in greater increases in maximum anaerobic power, as measured by vertical jump performance, in 18-24 year-old female and male beginning weight trainers.

PROCEDURES

The subjects in this research were a convenience group of 18-34 year-old male and female students enrolled in beginning weight training classes at a moderately sized state university. All were screened to exclude those with previous injuries that could be aggravated by the lifts. A total of 77 participants signed informed consents and IRB approval was obtained.

Independent variables included the type of lift being performed (i.e., full squats (FS), 3/4 squats (3/4S) or power cleans(PC)) and gender. Subjects were divided into three groups and each assigned a lift. Proper form was taught and used on all lifts, under the supervision of an instructor. The remainder of the students' workout were the same, and included no other leg exercises.

For the pretest, all participants performed five vertical counter-movement jumps. Measurements included peak vertical force produced during the jump (Bertec force plate 4060A, calibrated to standard specifications, and set at 500 Hz), peak vertical velocity prior to takeoff and vertical jump, both measured by videotape analysis on a 2D Motion Measurement System (collected at 30 Hz and filtered at 12 Hz with a lowpass Butterworth type filter). Max anaerobic power was estimated via peak vertical force x peak vertical velocity. Subjects participated for eight weeks, lifting twice a week and progressing in the amount of resistance of weights via a standard weight training protocol. All were postested in the same manner as the pretest.

One-tailed paired t-tests were used to examined differences in the pre and post test data, and 3 x 2 ANOVAs were used to examine statistical significance between treatment groups and gender for the mean differences between pre and post tests, for all dependent variables. Significance was set at the .05 level for all tests.

RESULTS AND DISCUSSION

Sixty-one students completed the study (FS = 16, 3/4S = 24, PC = 21). Across all subjects, significant differences were observed between pre and post test data for the paired t-tests ($t_{Power} = 11.5$, $p < .0001$; $t_{velocity} = 17.28$, $p < .0001$; $t_{jump} = 10.29$, $p < .0001$; 60 df) indicating training twice a week for eight weeks was of benefit for beginning weight trainers for improvement in vertical jump performance, peak vertical velocity, and anaerobic power, in all the training styles. No significant differences were noted in peak force production for any of the groups ($t_{force} = .76$, $p < .223$, 60 df). This may be due to the fact that in every group, force production decreased almost as often as it increased for the post test between subjects (Figure 1).

Examining the raw mean differences between treatment groups demonstrated the variability between subjects. For example, in Figure 1, many of the participants demonstrated a lower peak force during the post test jumps (hence the negative forces graphed).

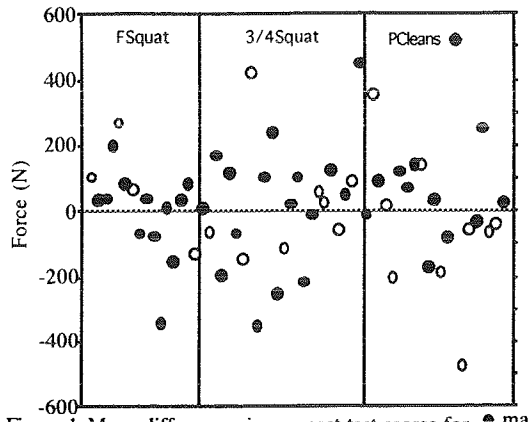

Figure 1. Mean differences in pre-post test scores for ● males force production between treament and gender groups○ females

However, most all of the subjects still demonstrated an increase in power production (Figure 2), meaning many lifters were able to increase their peak velocity at takeoff without increasing their force production. These results indicate the current study did not find differences between the exercises if indeed they did exist. It would appear that all modes of exercise are successful in improving anaerobic power production. but no one lift was more successful than another. These results may also indicate no apparent benefit exists for performing full squats over the 3/4 squat, which is the safer of the two exercises to perform.

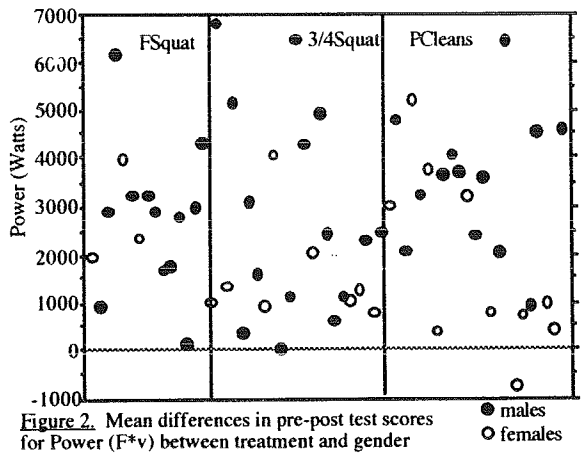

Figure 2. Mean differences in pre-post test scores for Power (F*v) between treatment and gender

The only significant factor noted for gender was for power ($F = 5.29$, $p < .02$), and no significant interactions were noted. However, some trends exist to support the power clean exercise over either squat exercise for improvement on specific variables. The women power clean group demonstrated a 2.6 cm improvement in vertical jump over all other groups, but the women full squat group demonstrated greater power gains, by an average of almost 500 J.

The male power clean group showed a greater improvement in their peak power production, by an average of 500 J. The improvement in vertical jump was similar for all males (Figure 3.).

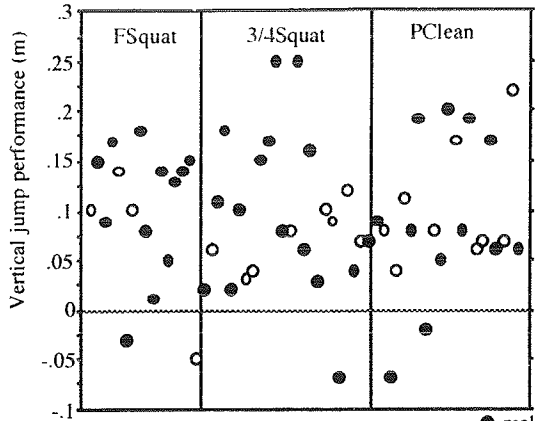

Figure 3. Mean differences in pre-post test scores for vertical jump performance and gender groups.

In previous research using athletes who performed both the power clean and full squat exercises, it was noted that the women demonstrated stronger correlations for the power clean scores and similar jump variables, while the men demonstrated similar correlations for the both the power clean and squat scores against the jump variables (Abendroth-Smith & Sword, 1996). The current study appears to follow similar trends in that the women power cleaners improved the most in vertical jump performance. The male groups were very similar with the exception of the PC group demonstrating greater power gains.

REFERENCES

Abendroth-Smith, J. & Sword, K. Maximum Anaerobic Power and Gender Differences in Relation to the Squat and Power Clean Exercises. In Fyhrie, D. & Gregor, R. (Eds.) Proceedings of the American Society of Biomechanics 20th annual meeting, Atlanta, GE. Georgia Tech University, 49-50, 1996.

Chandler,T.J. & Stone, M.H. The squat exercise in athletic conditioning: A review of the literature. National Strength and Conditioning Association Journal, 13(5), 52-29, 1991.

Wenzel, R.R. & Perfetto, E.M. The effect of speed training vervus non-speed training in power development. Journal of Applied Sport Science Research, 6(2), 82-87, 1992.

ACKNOWLEDGMENTS

The authors wish to acknowledge and thank Bertec Force Plates for their support and the students of Utah State University for their help.

A KINEMATIC AND STRENGTH COMPARISON OF SPORT ROCK CLIMBERS

J. Abendroth-Smith, R. Slaugh
Utah State University, Logan, UT 84322-7000

INTRODUCTION

The sport of rock climbing has increased in popularity in recent years, to the point of being included as an exhibition sport in the 2002 Winter Olympic games. Little research exists examining the kinematics of rock climbing, nor have gender differences been examined as to what strength and anthropometric characteristics good rock climbers possess.

REVIEW AND THEORY

The use of strength assessments and the analysis of kinematic characteristics are typical methods for analyzing athletic performance of more common sports such as freestyle swimming and boxing (Cappaert, Pease, & Troup, 1995; Whiting, Gregor, & Finerman, 1988). The recent acceptance by the International Olympic Committee for review of competition rock climbing as an Olympic sport warrants use of these methods in the analysis of elite rock climbers. The identification of gender differences such as the rapid movement kinematic and EMG control characteristics found by Ives, Krull, and Bultman (1993) lend justification to the need to assess strength and kinematic differences across gender in the sport of rock climbing.

The purpose of this study was to identify common anthropometric, strength and kinematic movement characteristics as related to performance measures, among adult sport rock climbers and to identify differences across gender.

PROCEDURES

The subjects in this study consisted of a convenience group of moderate to elite level sport rock climbers, climbing in the northern Utah area. The subjects included 8 females and 21 males. All subjects signed informed consents and IRB approval was obtained.

The women ranged in age from 18-28 years with reported redpoint performance levels ranging from 5.9 to 5.12c/d and flash performance levels ranging from 5.9 to 5.12b. The men ranged in age from 18-45 years with reported redpoint levels from 5.10a to 5.13d, and flash levels ranging from 5.10a to 5.12c/d. Redpoint and flash levels are ratings of climbing skill, and range from 5.1 to 5.14d.

Movement characteristics of the subjects performing the same simulated rock climbing movement were analyzed using a 2D Video Motion Measurement System. Data were collected at a rate of 30 Hz, and filtered at a 23 Hz cut-off rate using a low pass Butterworth type filter. The variables analyzed included velocity and acceleration of the center of gravity (COG), absolute angular trunk displacement (Figure 1), velocity of left wrist movement, and absolute angular acceleration of the left forearm.

Figure 1. Moderately (l) and highly skilled (r) climbers. The trace is angular trunk displacement.

The anthropometric measurements taken included body composition (hydrostatic), hand width and length, finger circumference, hip width, shoulder width, height, arm wingspan, flexibility (two leg sit and reach), and ape index (wingspan - height). The strength measures included grip strength, (three trial mean / body mass, using a hand dynamometer (kg)). Peak leg force production was measured using vertical counter-movement jumps off a force plate (three trial mean / body weight using a Bertec force plate 4060A, calibrated to standard specifications, set at 500 Hz). The isometric flexed arm hangs were performed hanging from a 3.8 cm pull-up bar. The subjects were asked to attempt a timed 1 arm hang in a fully flexed position with the chin over the bar. The subjects who failed to maintain this position for more than one second also performed a 2 arm hang from the same position with the palms in. The times were averaged over both arms and calculated as an impulse using the subject's mass. Isometric abdominal

flexion strength was tested on a Cybex situp machine and measured as impulse. Lat pull down strength was tested on a Cybex overhead pulley machine, performing a 3 repetition max. These measurements were also normalized with the subjects' mass. Correlations were used to examine relationships between the variables tested and the performance criterions of redpoint and flash levels for the two gender groups.

RESULTS

For the male group the variables which provided the strongest relationships with the performance measures of redpoint and flash levels were the 1 arm hang impulse, normalized lat pull-down strength, averaged normalized grip strength, ape-index measurement (negatively), the timing of maximum acceleration of COG (negatively), and angular trunk displacement (Table 1). The variable of percentage of body fat showed a trend towards a negative relationship with redpoint level.

Selected Variables	Females mean (SD)	Red point r	Males mean (SD)	Red point r
Ang Trunk Displ.(deg)	20.5 (±6.0)	0.7	23.1 (±7.7)	0.43
Max Vy C.G.(m/s)	9.23 (±2.0)	0.85	9.7 (±3.4)	**
Max Ay C.G.(m/s/s)	26.9 (±8.3)	0.44	23.8 (±9.2)	**
Grip Strength (kg/kg)	0.64 (±0.07)	0.7	0.76 (±0.04)	0.46
Leg Force (N/N)	21.08 (±2.3)	0.3	20.82 (±4.5)	**
Lat Pull-Down (kg/kg)	0.79 (±0.01)	**	1.14 (±0.19)	0.37
Flexibility (cm)	17.8 (±8.4)	0.7	9.6 (±8.3)	**
Body Fat %	17.4 (±3.4)	**	8.7 (±6.5)	**

** correlations were < .3

Table 1. Means, SD and Correlations of Selected Variables with Performance Criterion of Redpoint.

Of these variables the only two in common with the female group included averaged normalized grip strength and the kinematic variable of angular trunk displacement. The other variables in which relationships were found for the women included height (r = -.84) flexibility, normalized peak leg force, the kinematic variables of maximum velocity and acceleration of COG, and the maximum velocity of the left wrist.

DISCUSSION

Differences in angular trunk displacement are shown in Figure 1. The dark trace is of the trunk sections of a moderately skilled and a highly skilled male subject as the climbing movement is performed, showing the larger displacement which was more prevalent for both gender groups. For the women, the differences in movement found across the performance measures was attributed to the relationship with the variables of peak leg force production and flexibility, resulting in the higher angular trunk displacement, and greater velocity and acceleration of COG. The males in movement and performance differences are attributed more to the relationships between the upper body strength measures of one arm hang impulse, and normalized lat pull-down strength which resulted in higher angular trunk displacement, greater velocity and acceleration of COG. The relationship with the timing of the maximum acceleration of COG suggests that the highly skilled male subjects were attaining the greater acceleration sooner in the movement. This allowed for the slower and more precise acceleration of the left forearm which is an act of prehension of the next hold.

The noted differences in strength and kinematic characteristics are attributed to being rather unique to sport rock climbing movement, and to the subjects which performed these tests and the simulated movements which were analyzed in this study. It is recommended that the examinination of these characteristics be expanded to include other climbing movements.

REFERENCES

Cappaert, J.M., Pease, D., & Troup, J.P. J of App Biomech, 11(1), 103-112, 1995.

Ives, J.C., Kroll, W.P., & Bultman L.L. Res Q Exer Sport, 64(3), 274-283, 1993.

Whiting, W.C., Gregor, R.J., Finerman, G.A. Amer J of Sports Med, 19(2), 130-136, 1988.

ACKNOWLEDGMENTS

The authors wish to thank Martha Hyder for her assistance in this study.

A NEW 'TWIST' ON GOLF KINEMATICS AND LOW BACK INJURIES:
The Crunch Factor

D. Morgan[1], H. Sugaya[2], S. Banks[1], F. Cook[1]

[1]Orthopaedic Research Lab., Good Samaritan Medical Center, W. Palm Beach, FL 33401
[2]Dept of Orthopaedic Surgery & Sports Medicine, Kawatetsu Hospital, Chiba 260, Japan

INTRODUCTION

Golf is one of the most popular sports in the world for people of all ages and skill levels. Unfortunately, low back injuries are not uncommon in golfers, with reported incidence as high as 40-50% in amateur and professional golfers. Very few studies have focused on the mechanics of the lumbar spine during the golf swing. We hypothesize that lateral bending and high axial rotation velocities contribute to lumbar degeneration and injury. We propose a new parameter, the "crunch factor", in an attempt to objectively quantify lumbar spine mechanics which may result in injury and serve as the basis of comparison between "healthy" and "pathological" golf swings.

REVIEW AND THEORY

Hosea *et al.* reported that peak forces and torques at the L3/L4 level of the lumbar spine occur during the forward swing and follow-through, in agreement with many golfers' subjective reports of pain just after impact. Further, it is generally accepted that golfers who exhibit an exaggerated lateral bend with back extension (reverse "C") during follow through will experience higher stress and a greater incidence of injury in the low back. Sugaya et al. reported radiographic findings of distinctly asymmetric arthritic changes in golfers with back injuries, showing greater right side degeneration at the facet joints and vertebrae in right handed golfers.
Based on this empirical evidence, we hypothesize that lateral bending and axial rotation velocities in combination contribute to lumbar degeneration and injury. In this study we show the need for examining lumbar spine mechanics separate from whole trunk motions and we propose a new parameter, the "crunch factor", in an attempt to objectively quantify lumbar spine mechanics.

PROCEDURES

Ten healthy male, right handed, collegiate golfers (19.4±1.1years) were studied. The subjects' golf career averaged 7.9±4.1years, with a mean handicap of 3.2±3.4. Twenty-nine reflective markers were attached to the subject, including those at C7, T12, S1, bilateral acromions, bilaterally at the base of the ribs, anterior superior iliac spines, and the ball and club. Six 200Hz synchronized video cameras, two force platforms (1000Hz), and eight trunk EMG electrodes (1000Hz) were used to record three tee shots with a driver. Movement between the rib and pelvic marker planes defined the motions of the lumbar spine, including the axial rotational angle (ARA) and the lateral bending angle (LBA). Five events were defined: maximal shoulder rotation during the back swing ('top of shoulder', or TOP), club horizontal during the downswing (DH), ball impact (IMP), club horizontal during the follow-through (FTH), and the 130 ° shoulder rotation during the follow-through (FIN). The "crunch factor" was defined as the product of the lumbar lateral bending angle and axial rotation velocity. Lateral Bending angles and axial rotation velocities were also computed for the shoulders relative to the pelvis.

RESULTS

The event times relative to ball impact (Time=0.0ms) are shown in Table 1, along with the corresponding lumbar LBA, ARA, and ARA velocity (hereforth labeled as ARV). The maximum ARA was 25±6° occurring 219±65ms before impact. The average ARV was greatest from DH through FTH, peaking at 248±85°/s at 25±93ms after impact. Average LBA was largest from the DH through FIN, reaching a maximum of 16±4° at 174±171ms after impact. The average "crunch factor" for the group peaked at 52ms after impact. One subject had excessive ARV (460°/s) occuring at the same time (25ms after

impact) as his maximum LBA (20°), causing a peak "crunch factor" almost three times the group average.
Times for maximum lumbar ARV and crunch were dramatically different than the same parameters for the whole trunk. These are shown in Table 2. The time for maximum trunk ARV was just after FTH as opposed to shortly after impact for the lumbar spine.

Event	Time (ms)	LBA (deg)	ARA (deg)	ARV (°/sec)
TOP	-312	8 ±3	22 ±7	31±52
DH	-45	-5 ±4	15 ±5	-74±90
IMP	0	-8 ±4	11 ±5	-96±89
FTH	60	-13 ±4	3 ±6	-123±82
FIN	289	-11 ±2	-10 ±6	-28±50

Table 1: Event Times, Angles, and Velocities

Spine Segment	ARV time max (ms)	Crunch time max (ms)
Lumbar	25	52
Full Trunk	78	108
p-value (Student's t-test)	.039	.091

Table 2: Occurrence of Max. ARV & Crunch for each Back segment.

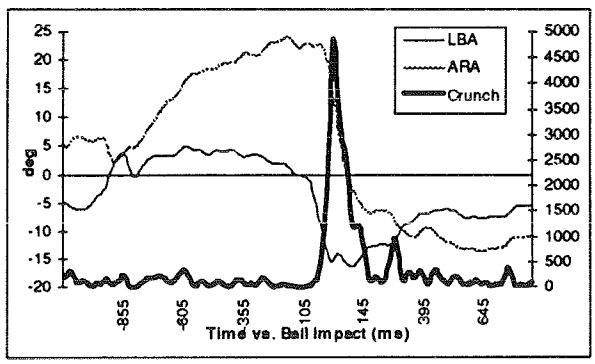

Figure 1: LBA, ARA, and the Crunch Factor

DISCUSSION

The purpose of this study was to examine the kinematics of the lower back during the golf swing and to define a parameter illustrating the influences on low back injury. The "crunch factor", which quantifies the intuitive notion that lateral bending and axial rotation velocities jointly contribute to lumbar spine injury, exhibits a peak 52ms after impact. The ARV is greatest in the lumbar spine 25ms after impact, correlating well reports that the greatest pain occurs shortly after impact. Figure 1 illustrates how the LBA and the first derivative of the ARA of one subject combine to form the crunch factor. It was also shown that looking specifically at the lower back kinematics during the forward swing helps better evaluate the loading on the lumbar spine than examining motions of the full back. Using the full back to evaluate ARV and crunch factor would estimate the point of injury and pain occurring well into the follow through, which would be inconsistent with the subjective reports and may lead to golf swing modifications during the wrong phase. Thus, we feel it is important to look specifically at the motions of the lumbar spine when evaluating healthy and pathological swings.
By understanding the factors which contribute to low back pain, we hope to help golfers at all age and skill levels continue to play safely. We believe that the "crunch factor" might be a useful measurement for assessing injury risk during the golf swing, and hope to demonstrate it's utility with further studies.

REFEERNCES

Hosea, T. M. and Gatt, C. J. Jr. Clinics Sports Med, 15, 37-53, 1996.
Sugaya H., et. al., Jpn J Ortho Sports Med, 14, 272, 1994.
Sugaya H., et. al., AOSSM 22nd Annual Meeting, June 1996.

RESPONSES OF ANKLE JOINT KINETICS TO NATURAL, SOFT AND STIFF LANDINGS

G. Jameson[1], K. Simpson[2]
[1]American Sports Medicine Institute, Birmingham, Alabama 35205
[2]Department of Exercise Science, University of Georgia, Athens, Georgia 30606

INTRODUCTION

It is well documented that an individual can reduce the amount of force that must be attenuated during an impact situation by allowing greater knee flexion (1,2). Although we know that soft landings reduce the amount of force applied to the body, we do not know if a person naturally lands softly. This study determines whether or not a subject naturally selects a landing stiffness (amount of knee flexion) during a high impact landing situation that minimizes impact force loading. Variables related to vertical ground reaction forces (Fz) and ankle joint moments (Ma) were compared for soft, stiff and natural landings from two different drop heights.

REVIEW AND THEORY

Sports involving repetitive landing often present a significant risk of chronic overuse injuries due to impact loading on the lower extremities (3, 4). These injuries have been found to account for nearly half of all injuries experienced by college athletes. Microtraumatic overuse injuries, including trabecular microfractures and articular cartilage degeneration have been linked to repeated impact situations (5, 6, 7). Findings from studies comparing soft and stiff landings demonstrate greater peak Fz and lower extremity joint moments during stiff landings (1, 2). It is not known, however, if individuals naturally attempt to optimize landing stiffness to reduce impact forces. Therefore, the purpose of this study was to compare a subject's natural landing stiffness to soft and stiff landings. It was hypothesized that a person naturally selects a landing stiffness that helps protect the lower extremities from injury. Minimum knee joint angle (Θ_{Knee}), maximum ankle joint moment (Ma_{MAX}), maximum vertical ground reaction force (Fz_{MAX}), the time to Fz_{MAX} (TFz_{MAX}) and the vertical loading rate (LR_{PEAK}) will be used to validate this hypothesis.

PROCEDURES

Kinematic and kinetic data of the right lower extremity were synchronously collected for ten male college-aged subjects (height: 1.79 ± 0.06 m, mass: 73.82 ± 13.82 kg, age: 24.5 ± 4.35 yrs). After giving informed consent and medical history, the subjects' anthropometric values were obtained. Each subject was then tested during a single session while wearing laboratory footwear. During the data collection, subjects were asked to step off of 2 drop platforms (45 and 70 cm) onto an AMTI force platform (960 Hz). For the first two conditions the subjects were asked to land naturally from each drop platform, no further instructions were given. The order of the four remaining conditions were randomized and consisted of, soft and stiff landings from both of the platform heights. To minimize horizontal motion, the subjects were instructed not to step forward from the drop platform, but to stand with the right foot over the force platform and to simply unweight the left leg and fall straight down. The knee joint angle was measured during testing using an electrogoniometer, but the actual Θ_{Knee} values were derived from digitization. The criterion for a successful soft landing was a maximum knee joint angle less than 75 degrees; and successful stiff landing criterion was maximum knee joint angle no less than 115 degrees. Five successful trials were recorded for each condition.

High speed video (120 Hz) of the descent and landing were recorded. Retroreflective markers were placed on the hip, knee, ankle, calcaneus and fifth metatarsal of each subject. Peak Performance Technologies Peak 5 software was used to digitize and calculate the two-dimensional coordinates and parameters. Fz_{MAX} and TFz_{MAX} were measured from the ground reaction force data, while an inverse dynamics approach was used to calculate Ma_{MAX}. Mean values across trials were calculated for each condition. The results of the chosen variables were subjected to a between subject and within subject multivariate analysis of variance to determine interactions between independent variables (drop height and landing stiffness). 2 x 3 (ht x stiffness) analysis of variance and Tukey post-hoc tests were performed on significant variables ($p < 0.05$).

Figure 1. Representative graphs for C-I subject. Negative values represent plantarflexor moment.

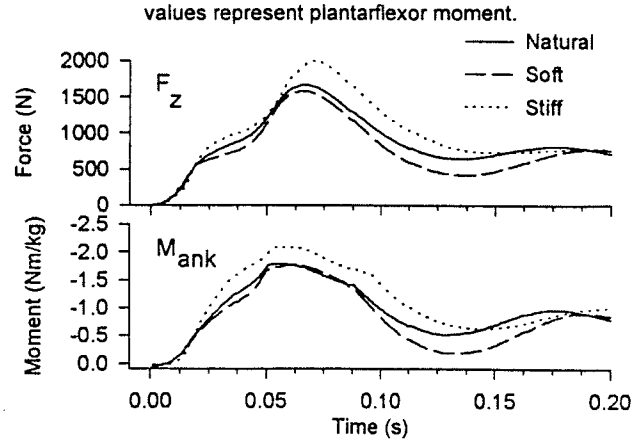

Height	Stiffness	Θ_{Knee}	Ma_{MAX}(Nm/kg)	Fz_{MAX} (BW)	TFz_{MAX} (s)	LR_{PEAK} (BW/s)
70 cm	Natural	93.8 (17.2)§‡	-1.84 (.500)§‡	2.52 (.493)§‡	.049 (.011)	53.6 (14.6)
	Soft	62.0 (12.8)*‡	-1.40 (.318)*‡	2.02 (.353)*‡	.055 (.041)	45.4 (17.5)‡
	Stiff	119.7 (7.4)*§	-2.24 (.482)*§	3.13 (.410)*§	.053 (.010)	61.8 (16.7)§
45 cm	Natural	101.0 (17.0)§‡	-1.69 (.364)§	2.16 (.455)§‡	.052 (.014)§	44.7 (15.0)§‡
	Soft	61.1 (12.4)*‡	-1.27 (.257)*‡	1.53 (.223)*‡	.082 (.081)*‡	29.9 (14.9)*‡
	Stiff	126.5 (6.2)*§	-1.89 (.561)§	2.85 (.461)*§	.053 (.015)§	58.3 (18.9)*§

Table 1. * significantly different from the natural condition at the same height.
§ significantly different from the soft condition at the same height.
‡ significantly different from the stiff condition at the same height.

HT	Variable	C-I	C-II	C-III	C-IV
70	Ma_{MAX}	1,2,3, 4	5,9,10	6,7,8	--
	Fz_{MAX}	1,2,3, 4,6,10	8,9	7	5
	LR_{PEAK}	9,10	8	1,2,3,4, 5,6,7	--
45	Ma_{MAX}	2,4	3,5,7, 9	1,3,6, 8,10	--
	Fz_{MAX}	1,2,4	3	--	5,6,7,8, 9,10
	LR_{PEAK}	1,4,5, 6,10	3,8,9	2,7	--

Table 2.

RESULTS

Table 1 includes the means, standard deviations and statistical significance for Θ_{Knee}, Ma_{MAX}, Fz_{MAX}, TFz_{MAX} and LR_{PEAK} for the total population. Natural landing values from the 70 cm height for Θ_{Knee}, Ma_{MAX} and Fz_{MAX} fell between the soft and the stiff landing values. TFz_{MAX} was not different for any of the 70 cm landings. Natural landing LR_{PEAK} did not differ from either the soft or stiff landings, although the soft was significantly less than the stiff.

From the 45 cm drop height, natural landing Θ_{Knee} and Fz_{MAX} were significantly different from the soft and stiff landings. MA_{MAX} and TFz_{MAX} for the natural and stiff landings did not differ; however, the soft landing values were different than the natural. LR_{PEAK} for the 45 cm landings showed significant differences for all stiffnesses.

The individual data were analyzed and divided into four categories (C-I, C-II, C-III, C-IV). Table 2 shows these divisions and the subject numbers of those in that category. Subjects in C-I had natural landing kinetics that were not significantly higher than the soft landing, but were significantly lower than the stiff. Figure 1 is a representative graph of Fz and Mz for a subject in C-I. C-II subjects' natural landings were not significantly different from the stiff but were different from the soft. C-III consisted of subjects whose landing kinetics were not significantly different regardless of landing stiffness. C-IV subjects were the individuals whose natural landings were different from both their soft and stiff landings.

DISCUSSION

Based on these results and consistent with other studies, conclusions can not be generalized based on the population's results as all subjects employed different landing strategies. Due to this high variability between subjects, within subject comparisons provide better insight into the specific nature of the different landing strategies.

At the 70 cm height most subjects were in the same category for Ma_{MAX} and Fz_{MAX}. This was not the case, however, when landing from the lower height. It was also interesting to see that the subjects who were in C-I ("soft landers") for Fz_{MAX} and Ma_{MAX} were not in C-I for LR_{PEAK}. Furthermore, subjects were not found to exhibit consistent landing strategies for the 70 and 45 cm heights.

In summary, because external forces as well as the rates at which they are applied have been linked to overuse injuries, people must learn to dissipate landing forces over a greater time as well as over a greater distance (i.e. knee flexion).

REFERENCES

1 McNitt-Gray, J.L. et al. *J. Biomech.*, 26 1037-1046, 1993.
2 Devita, P. and Skelly, W.A. *Med. Sci. Sports & Exer.*, 24, 108-115, 1992.
3 National Collegiate Athletic Assoc.; Injury Surveillance Survey Data, 1992.
4 Weiker, G.G. *Phys & Sports Med.*, 13, 63-66, 1985.
5 Fazzalari, N.L. *Calcif. Tissue Int.*, 53, S143-S147, 1993.
6 Robbins, S.E. & Gouw, G.J. *Sports Med.*, 9, 76-85, 1990.
7 Radin, E.L. & Paul, I.L. *Arth. & Rheum.*, 13, 139-144, 1970.

MODELING FEMALE VS MALE WHOLE-BODY VIBRATION RESPONSE

S. D. Smith
Armstrong Laboratory, Wright-Patterson Air Force Base, OH 45433-7901

INTRODUCTION

A five degree-of-freedom (5-DOF) lumped-parameter model was found to be effective in simulating the driving-point impedance and transmissibility responses of a female and male exposed to whole-body vibration. The model showed that there were differences in the distribution of the mass as well as the stiffness and damping characteristics of the major anatomical regions between the female and male. The ability to predict the effects of these differences is important for improving equipment concepts which reduce vibration transmission.

REVIEW AND THEORY

Seating system designers are challenged with developing equipment which will minimize the adverse effects of vehicle vibration on the human body. A previous study has shown that a 5-DOF mathematical model was relatively effective in simulating the vibration responses of the male body (Smith, 1994). The model elements represented the major anatomical regions contributing to the observed resonance behaviors. Significant differences in resonance behaviors have been shown to occur between the vibration responses of females and males, particularly those females falling in the 5th percentile or less of the population for body weight (Smith, 1996). The objective of this study was to evaluate the effectiveness of the 5-DOF model in simulating both the female and male responses and to identify those factors contributing to the differences in resonance behavior.

PROCEDURES

Human subjects were exposed to seated whole-body vertical vibration at sinusoidal frequencies between 3 and 21 Hz and 0.59 m/s^2 rms acceleration. The rigid seating system was mounted on top of three load cells which measured the transmitted whole-body force. Miniature accelerometers were attached to the chest, the spine (in the vicinity of the seventh cervical vertebra), and the thigh for measuring the acceleration of these body regions. An accelerometer was also placed beneath the seat for measuring the input acceleration. Driving-point impedance was calculated as the ratio between the transmitted force and input velocity at the seat. Transmissibilities were calculated as the ratios between the accelerations measured at the chest, spine, and thigh and the input acceleration at the seat. Testing details are provided in Smith (1996). The impedance and transmissibility frequency response profiles were used to determine the location and magnitude of the major peak resonance responses for the whole-body and for the measured regions. The results for a 56 kg female and 75 kg male were used in the modeling effort.

The 5-DOF model (Smith, 1994) was modified to represent the leg as a two degree-of-freedom structure uncoupled to the torso and spine. Figure 1 depicts the model. The initial distribution of mass

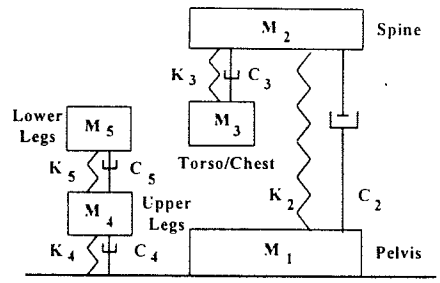

Figure 1 5-DOF Model

among the model elements was based on the previous modeling efforts and on human body mass data (Cheng et. al, 1994). The observed resonance frequencies were used to estimate the stiffness coefficients. The model coefficients were adjusted to produce the best match for the major resonance peaks observed in both the impedance and transmissibility profiles for the female and male.

RESULTS AND DISCUSSION

Figure 2 illustrates the data and model simulations for the impedance, and torso (chest) and spine transmissibilities. The figure shows that the 5-DOF model was quite effective in simulating both the impedance and transmissibility responses for the female and male. Table 1 lists the undamped natural frequencies of the modeled anatomical regions calculated from the mass and stiffness coefficients. The frequencies correspond closely to the location of the observed peaks. Both subjects showed the expected impedance and torso resonance peaks

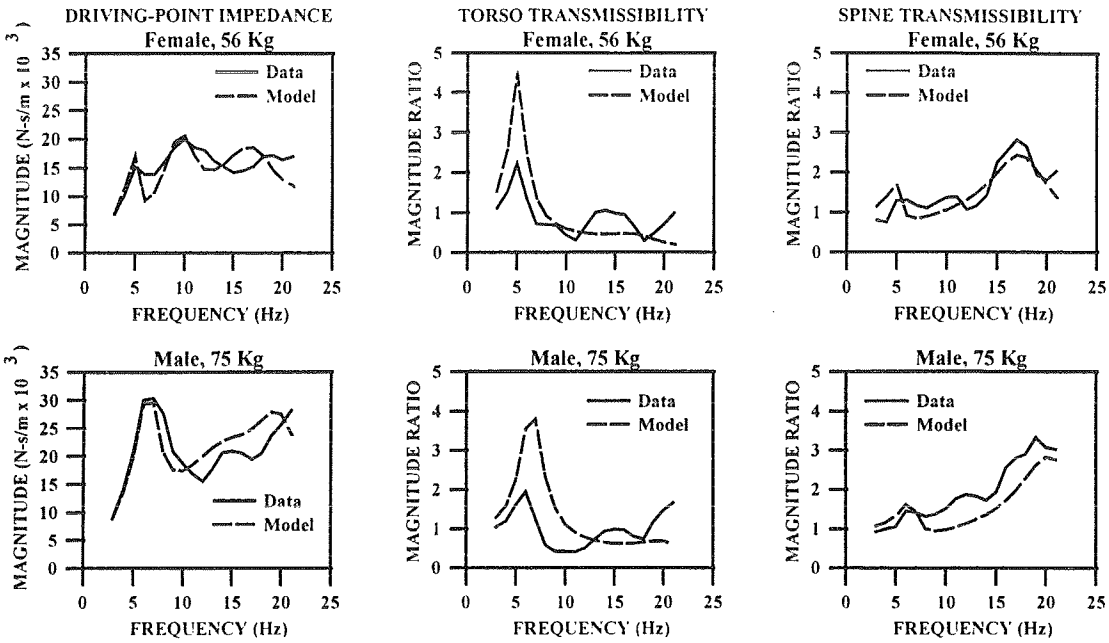

Figure 2 Impedance and Torso and Spine Transmissibility Frequency Responses - Data and Model

REGION	FEMALE (f_n)	MALE (f_n)
Spine	17.9 Hz	19.0 Hz
Torso	5.0 Hz	6.3 Hz
Upper Leg	18.1 Hz	15.9 Hz
Lower Leg	9.8 Hz	6.8 Hz

Table 1 Undamped Natural Frequencies (f_n)

located between 5 and 7 Hz. The higher predictions for the torso transmissibility were assumed to be due to the external measurement site for the acceleration of the torso. The model did simulate the lower resonance frequency (1 Hz) and higher transmissibility peak observed in the torso of the female as compared to the male, as well as the differences observed in the spine resonance frequency and magnitude peak. Although not illustrated, the first resonance peak observed for the thigh was simulated in the transmissibility response of the upper legs (M_4). The model showed that this peak, located between 9 and 10 Hz for the female and around 7 Hz for the male, was due to the coupled motion between the upper and lower legs, with the lower legs producing a single peak at these frequencies. For the female, the thigh transmissibility increased between 12 and 20 Hz with the second resonance peak not being easily identified. The model showed a lower transmissibility magnitude in this frequency range. For the males, the model was effective in simulating the second peak located at about 15 Hz. The legs showed the most dramatic differences in the distribution of mass among the anatomical regions between the female and male. The modeled mass for the upper legs in both the female and male were identical, suggesting a greater contribution of the thigh to the observed responses in the female. The significance of this contribution was observed in the impedance response where the female showed the primary, or highest, resonance peak occurring between 9 and 10 Hz. This peak coincided with the first resonance peak observed in the thigh and the single resonance peak predicted for the lower legs. In the male, a relatively smaller resonance peak was observed in the impedance at about 15 Hz. This region coincided with the second resonance peak observed in the thigh. The coupled motions between the upper and lower legs of the female, and the associated mass, stiffness, and damping characteristics, were important factors influencing the resonance behavior of the smaller female as compared to the larger male.

REFERENCES

Cheng, H., et al. AL/CF-TR-1994-0051, 1994.
Smith S. D., Shock and Vibration, 1(5), 439-450, 1994.
Smith, S. D., ADA309219, USAMRMC, 1996.

ESTIMATION OF KNEE AND HIP JOINT MOMENTS FROM KIN-COM FORCES

M.J. Pavol[1], M.D. Grabiner[2]
[1]Biomedical Engineering Center, The Ohio State University, Columbus OH 43210
[2]Dept. of Biomedical Engineering, The Cleveland Clinic Foundation, Cleveland OH 44195

INTRODUCTION

KIN-COM isokinetic dynamometers (Chattanooga Corp., Chattanooga, TN) are commonly employed to measure characteristics of the strength of an individual. Strength, as quantified by the joint moment generated, is most often estimated as the product of the KIN-COM load cell moment arm and the force recorded. However, this recorded force reflects not only the joint moment of interest, but gravitational and inertial effects as well [1,2]. Compliances in the system may also introduce oscillatory force artifacts [3]. Motion about distal joints and differing directions of the applied and measured forces further affect the relationship between the generated and estimated joint moment. We report here a method of compensating for the effects of these various factors, allowing more accurate estimation of the joint moments generated during knee or hip exertions on the KIN-COM 500H dynamometer.

MODEL

Figure 1 displays the model employed. The limb segment of concern (combined leg-and-foot for knee strength, thigh for hip strength) is a rigid rod connecting the proximal and distal joints. The KIN-COM arm and load cell are a single rigid body. The arm and limb segment rotate about a common axis. The knee/hip joint attachment is a rigid massed body in series with a viscoelastic element consisting of a Hookean spring and linear viscous element in parallel. The joint attachment is pinned to the load cell at the measured moment arm (r_k) from the axis of rotation and is connected to the limb segment through a slider joint that keeps the attachment perpendicular to the limb. The KIN-COM angle and velocity outputs specify the orientation (θ_k) and angular velocity (ω_k) of the load cell about the axis of rotation. The force (F_k) recorded by the KIN-COM is the component of force normal to the KIN-COM arm at the point of fixation between the load cell and joint attachment.

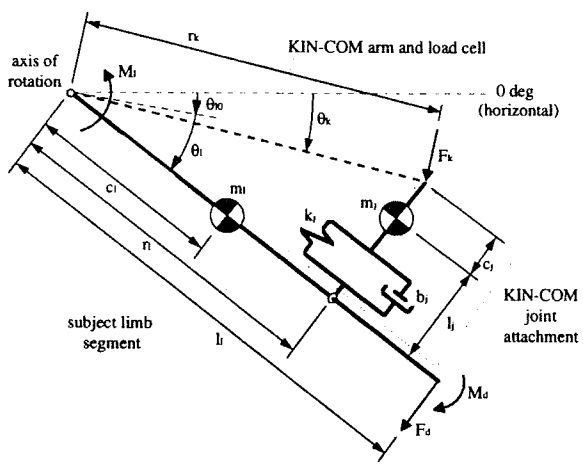

Figure 1

IMPLEMENTATION

Computed variables are the force acting through the viscoelastic element (F_j), the length of this element (l_j), the effective moment arm (r_l), the limb segment angle (θ_l) and angular velocity (ω_l), and the desired joint moment (M_l). F_j is computed from the equation of motion governing the joint attachment center of mass in the angular direction, assuming no viscoelastic element strain and that the distance (c_j) to the attachment center of mass is much smaller than r_k. l_j is found from the difference equation describing the viscoelastic element force-length behavior, initialized assuming static conditions. r_l and θ_l are computed from the model geometry. Differentiating the expression for θ_l yields that for ω_l. Finally, M_l is found from the equation of motion governing the angular acceleration of the limb segment. Included are a reaction force (F_d) and moment (M_d) at the distal joint due to any limb segments distal to that of the model. Such reactions are derived from θ_l, ω_l, and goniometer measurements at the distal joint. Accelerations are found through numerical differentiation of the corresponding velocity signals.

Filtering is required at several stages. Initially, the KIN-COM force, angle, and velocity signals are low-pass filtered with a 50 Hz cut-off to reduce quantization noise. The computed θ_l and ω_l are similarly filtered at 20 Hz prior to use. Finally, the computed joint moment is low-pass filtered to reduce model-induced noise. Respective cut-offs of 8 and 6 Hz are used for knee and hip moments. All filters are fourth-order Butterworth no-lag type.

PARAMETER ESTIMATION

The limb segment mass (m_l), center of mass distance (c_l), and moment of inertia are identified from anthropometric sources. The zero-reference orientation (θ_{l0}) of the limb segment axis is determined by the KIN-COM set-up used. The joint attachment mass (m_j) and center of mass location (c_j) are found by weighing and multiple-point suspension. The viscoelastic element unstrained length is measured from the joint attachment center of mass to the limb segment axis.

The viscoelastic element spring constant (k_j) and viscous damping (b_j) are estimated for each experimental set-up from the force oscillations observed during a rapid isokinetic exertion. The mean frequency (in rad/s) of selected cycles of oscillation in F_j defines the imaginary component of the system poles. The real component of the poles is computed from the value of F_j at the four quarter-period points of a selected cycle of oscillation (starting at a local extrema) assuming the data represent an underdamped second-order decay superimposed on a linear function. Finally, k_j and b_j are computed such that the poles of the equation: $(I_{eff} / r^2)\, s^2 + b_j\, s + k_j$ match those identified, assuming no viscoelastic element strain. I_{eff} is the moment of inertia of the entire limb distal to the joint of interest, assuming average joint positions. In practice, mean pole locations over several oscillations and exertions are used to compute k_j and b_j.

RESULTS AND DISCUSSION

Figures 2 and 3 compare the moment-angle relationships estimated directly from the KIN-COM force and moment arm to those computed with the methods presented for a representative maximum voluntary 90°/s isokinetic knee and hip extension respectively. Initial force generation was as rapid as possible, KIN-COM acceleration was at the medium rate, and the respective knee and hip movement thresholds were 18.7 and 59.2 Nm. Data was sampled at 500 Hz. 0° corresponds to full knee extension and the anatomical hip position. Hip strength was measured while supine.

The moment-angle relationships computed using the two techniques vary greatly. The offset between the displayed curves reflects the effect of gravitational forces. Inertial effects, visible in the unprocessed curves during the initial acceleration, the variations in speed early in the motion, and the

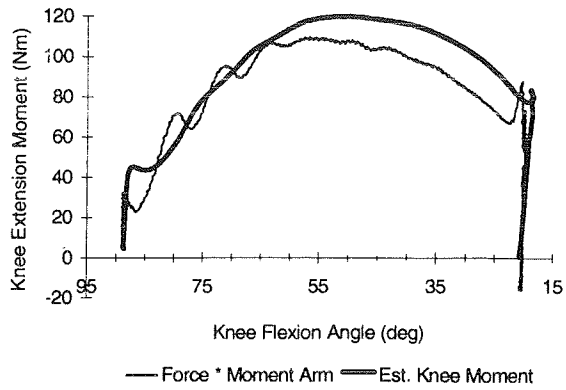

Figure 2

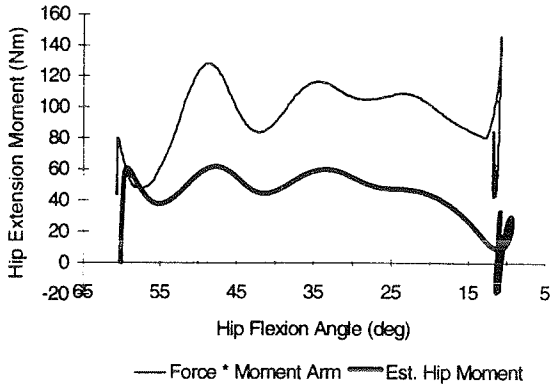

Figure 3

final deceleration, are substantially reduced by the processing. Compliances in the padded joint attachment and soft tissues of the limb magnify and multiply any oscillatory force artifacts. Use of the viscoelastic element model reduces these effects while preserving more of the system dynamics than would low-pass filtering alone. Knee motion during hip strength measurement introduces variable distal thigh loads that should be accounted for. Effects of this variation are visible as the oscillations, directly corresponding to observed knee accelerations, that remain in the processed hip moment curve. As can be seen, failure to account for these various effects can lead to non-trivial errors in predicted strength.

REFERENCES

1. Sapega, A.A. et al. Med Sci Sports Exer, 14, 368-375, 1982.
2. Herzog W. J Biomechanics, 21, 5-12, 1988.
3. Hof A.L. J Biomechanics, 30, 295-297, 1997.

ACKNOWLEDGMENTS

Funded by NIH-R01AG10557 (MDG).

Effects of Aging on Skeletal and Muscular Components of Lower Limb Quasi-Stiffness

P. DeVita, T. Hortobagyi, J. Barrier, J. Money, E. Anderson
Dept. of Exercise and Sport Science, East Carolina University, Greenville, NC 27858

INTRODUCTION

Lower limb stiffness provides resistance to floor reaction forces enabling humans to remain erect during locomotion. Stiffness is a function of skeletal and muscular components (2,5,6). Aging from 22 to 66 years has been shown to increase lower limb stiffness 2.5 fold in stair descent (9). The mechanism causing this is unknown. The purpose of the study was to identify the effects of aging on skeletal and muscular components of lower limb quasi-stiffness (an estimate of stiffness) in simulated stair descent. It was hypothesized that elderly adults had relatively greater skeletal and lower muscular components compared to young adults.

REVIEW AND THEORY

Daily movements apply forces onto a person's limb that tend to cause the limb to collapse. These forces are applied too rapidly for response through proprioceptive means (1,3) particularly in elderly who are slower in developing functional levels of joint torques (13). Stiffness of the lower limb, its intrinsic resistance to external loads, is therefore crucial for successful locomotion (4). Lower limb stiffness is a function of skeletal and muscular components either of which can be modified to change stiffness (2,5,6,7).

Elderly individuals walk slower with shorter steps and have a greater chance of falling while on stairs (12,13). Physiological changes leading to this decline in performance are lower muscle strength, joint range of motion, reaction time and proprioception (2,13). These changes suggest that lower limb stiffness is increased with aging although only one pilot study has investigated this issue (9). Shorter step lengths and reduced range of motion in the elderly during walking should increase the skeletal component and reduce the muscular component of lower limb stiffness and therefore increase total stiffness.

METHODS

Five elderly (mean age=68 yrs) and 6 young (mean age=23 yrs) males were tested in this pilot study. Subjects stepped down from boxes set at 10 & 20% of their height onto a force plate. Sagittal plane video was recorded at 60 Hz. Subjects practiced the movements until they were comfortable. Five stepping trials were then collected per subject and step height.

Video tapes were digitized and the data digitally filtered. Resultant ankle joint reaction force in the stepping limb was calculated with inverse dynamics. The lower limb was modeled as a two element spring between the ankle and hip. The two spring elements were skeletal and muscular components. Lower limb quasi-stiffness (q) was used to estimate limb stiffness. Quasi-stiffness was calculated as a ratio of the maximum force applied at the ankle joint in the direction of the hip to the amount of shortening of the ankle-hip distance occurring between initial floor contact and the time of maximum ankle-to-hip force.

Skeletal and muscular components of lower limb quasi-stiffness were calculated as a function of the angle between the maximum ankle-to-hip force vector and the leg with:

$$q \cos^2 \phi + q \sin^2 \phi = q \qquad (1)$$

where ϕ= angle between the force vector and leg, $q \cos^2\phi$ = skeletal component, $q \sin^2\phi$ = muscular component. A completely extended and vertically oriented limb impacting the floor after a vertical descent would have ϕ=0 and all quasi-stiffness due to the skeletal component. As knee flexion increases and the descent trajectory moves away from vertical, $\phi > 0$ and the muscular component is increased. The relative contribution of skeletal to muscular components was assessed by the ratio of the two

components (skeletal / muscular) in each subject group and condition.

RESULTS

Lower limb quasi-stiffness was 43% and 88% greater in elderly compared to young at 10 & 20% heights (Table 1). Elderly had 21% larger external forces applied to the limb, on average, yet had 26% less shortening of the limb. The absolute skeletal component to quasi-stiffness was 68% greater, on average, in elderly while the absolute muscular component was about equal between groups. The relative contribution of skeletal to muscular components differed greatly between ages. The ratio of skeletal to muscular components was 212% and 173% greater in elderly compared to young at 10 & 20% heights. Therefore elderly were about twice as dependent on the skeletal component for lower limb quasi-stiffness as were the young.

DISCUSSION

The greater lower limb quasi-stiffness in elderly compared to young was in agreement with our previous estimates in other samples from these populations (9). Variations in lower limb quasi-stiffness may be due to either a change in the relative contributions of its components or in the intrinsic stiffness of each component, notably the muscular element. Stiffness of muscular tissue is highly variable depending on length, contraction state and age of the muscle (7,8). Present results indicated that changes in lower limb quasi-stiffness with age are due to a shift in the relative contribution of its components. Elderly individuals increased their dependence on the skeletal system and reduced their dependence on the muscular system. This was done by reducing the angle between the external force flexing the limb and the leg (ϕ, Table 1).

The increased skeletal component of lower limb quasi-stiffness may contribute to orthopaedic problems in elderly. Stair descent applies loads of two times body weight onto the lower limb (10). As lower limb quasi-stiffness increases, impact forces are also increased and greater loads are applied to the bones and joints of the skeletal system (2). Increased quasi-stiffness with aging therefore, may be related to the increased incidence of knee osteoarthritis in the elderly which is caused by increased joint loading (11).

REFERENCES

1. Alexander et al. J. Gerontol. Med. Sci. 47:M79-M87, 1992.
2. DeVita et al. MSSE. 108-115, 1992.
3. Do et al. J. Biomech. 933-939, 1982.
4. Farley et al. J. Biomech. 181-186, 1996.
5. Farley et al. Proc. Integr. Biol. Exerc. A59,1996.
6. Greene et al. J. Biomech. 881-891, 1979.
7. Grillner, Acta Physiol. Scand. 92-108,1972.
8. Haut, J. Biomech. Eng. 196-199, 1983.
9. Hortobagyi et al. Proc. 20th Ann. Mtng. Amer. Soc. Biomech. 131-132, 1996.
10. McFadyen et al. J. Biomech. 733-744,1988.
11. Messier et al. J. Appl. Biomech. 161-172,1996.
12. Ostrovsky et al. Phys. Ther. 637-646, 1994.
13. Shultz, J. Gerontol. 60-63, 1995.

Table 1. Group Means (Standard Deviations)

	Young		Elderly	
Step heights:	10%	20%	10%	20%
Quasi-stiff. (kN/m)	89 (41)	54 (24)	128 (67)	102 (52)
Skeletal comp. (kN/m)	87 (40)	52 (24)	126 (54)	99 (52)
Muscular comp. (kN/m)	2.2 (0.8)	2.5 (0.9)	1.5 (0.7)	2.7 (1.2)
Ratio Skel./Musc. components	40	21	85	36
Ank-hip force(N)	1101 (62)	1444 (116)	1259 (439)	1827 (213)
Ank-hip displ.(m)	.012 (.007)	.026 (.010)	.010 (.008)	.018 (.009)
ϕ (°)	9.3 (1.2)	13.5 (3.5)	5.7 (4.5)	9.8 (2.3)
Max. knee flex (°)	18 (2)	26 (7)	11 (8)	19 (5)

ACKNOWLEDGMENTS

Supported by NC Institute on Aging (P.D.), NIHCD-30422 (T.H.), & Research & Creative Activity Grant, East Carolina University (T.H.)

THE RELATIVE IMPORTANCE OF JOINT FLEXIBILITY AND MUSCLE ACTIVITY PATTERNS TO THE STIFFNESS OF THE LEG SPRING DURING HOPPING

G.D. Heise, E. Bressel, S. Carroll, T. Ciapponi, and J. Smith

School of Kinesiology and Physical Education, University of Northern Colorado, Greeley, CO 80639

INTRODUCTION

The purpose of this study was to determine if static flexibility and muscle activity patterns explain inter-subject variability in normalized leg spring stiffness (K) during hopping. Subjects, 10 women and 10 men, hopped in place at their preferred frequency while vertical ground reaction force and EMG data were collected. Results showed that men and women hop at the same preferred frequency (2.2 hops/s) and exhibit the same normalized leg stiffness (K = 25.3). Several multiple regression models, with four variables as inputs, explained up to 59% of the inter-subject variance in K. However, coactivation measures during ground contact, which contribute to stiffness at individual joints, were not related to K.

REVIEW AND THEORY

When humans and animals run, hop, or trot, they literally bounce along the ground, storing and recovering energy like a bouncing ball (Cavagna, et al., 1977; McMahon & Cheng, 1990). McMahon and colleagues modeled the leg(s) in contact with the ground during hopping and running as a simple linear spring (see Fig. 1) and model predictions were validated by experimental evidence (Farley et al., 1993; He et al., 1991; McMahon & Cheng, 1990; McMahon et al., 1987).

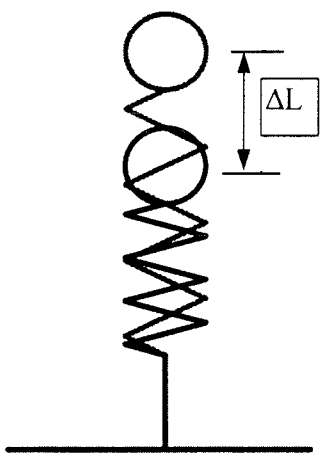

Fig. 1. Leg spring model for hopping (adapted from Farley et al., 1991).

Using this model, researchers have shown that leg spring stiffness (k_{leg}), the ratio of maximum force during ground contact to ΔL, remains constant as humans run faster (He et al., 1991) and as various species of animals, representing a wide range of sizes, trot and hop faster (Farley et al., 1993). In addition, Farley et al. (1991) reported low variability in k_{leg} between four humans hopping at their preferred frequency. Consequently, constant leg spring stiffness has been proposed as an invariant feature of bouncing-type locomotion (McMahon & Cheng, 1990; Farley et al., 1993).

Recently however, for a group of well-trained distance runners, k_{leg} exhibited a high amount of inter-individual variability (Heise & Martin, 1995) at one running speed. This finding is in disagreement with the hypothesized leg stiffness invariance proposed by McMahon and colleagues. It was suggested that this between-subject variability observed in k_{leg} is a function of musculotendinous structural differences and neuromuscular factors that are ultimately reflected in movement dynamics.

In the present study, we hypothesized that flexibility, an example of a musculotendinous structural characteristic, and muscle activity patterns, an example of a neuromuscular factor, will explain the variability observed in normalized k_{leg} (K). In addition, we examined if hopping frequency, k_{leg}, and K are different between men and women as they hop in place at their preferred frequency.

PROCEDURES

Ten healthy women and ten healthy men volunteered as subjects (Body $Mass_W$ = 56.3 ± 9.0 kg; Leg $Length_W$ = 74.5 ± 5.8 cm; Body $Mass_M$ = 79.3 ± 8.8 kg; Leg $Length_M$ = 81.6 ± 3.3 cm). Each subject attended one test session. After a 10-min warm-up walk at 1.57 m/s, a series of flexibility measures were taken. Flexibility was evaluated through passive range of motion (ROM) using the muscular end-feel technique (Norkin & White, 1985). One experimenter moved the limb to the proper end-feel and another took goniometric measurements.

Then, after appropriate skin preparation, surface EMG electrodes were positioned over the bellies of muscles rectus femoris (RF), vastus lateralis (VL), biceps femoris-long head (BF), and gastrocnemius (G). Subjects hopped on a force platform at their preferred frequency for 3 min. After 60 s and 90 s of hopping, vertical ground reaction force data and the four EMG signals were digitized at 1000 Hz for 5 s. All channels were then stored in digital format on a microcomputer.

Hopping frequency and k_{leg} were determined from force platform data (Farley et al., 1991). Normalized leg spring stiffness, K, was calculated by multiplying

k_{leg} by the ratio of leg length to body weight. EMG data were full-wave rectified and low-pass filtered (f_c = 15 Hz). Muscle onset and cessation were identified using an interactive, computer-graphics program that plotted the submaximal, linear envelope of each channel against time. Muscle on-time durations were calculated as a percent of contact time and flight time depending on when the muscles were active during the hopping cycle. Durations of coactivation were determined by calculating, as a percent of contact and flight, the common durations of muscle on-time between antagonistic muscles. Four hopping cycles were analyzed from both trials. The resulting means, taken from eight cycles, were used in statistical analyses. T-tests were used to test for differences in hopping frequency, k_{leg} ,and K between men and women. Multiple regression was used to determine if flexibility and EMG measures explain the variance in K.

RESULTS AND DISCUSSION

Preferred hopping frequency was the same between women and men with a coefficient of variability of 9% among the entire sample (Table 1). The overall mean hopping frequency was equal to the value reported by Farley et al. (1991).

	WOMEN	MEN
hop. freq. (Hz)	2.2 ± 0.2	2.2 ± 0.2
k_{leg} (kN/m)	18.9 ± 1.8	24.6 ± 7.5 (*)
K (unitless)	25.5 ± 3.4	25.3 ± 7.2

Table 1: Means and Standard Deviations of Selected Variables (* $p < .05$ between women and men).

Although no difference existed between men and women, K exhibited a high amount of variability. The lowest value of K was 17.9, the highest was 38.0, and the coefficient of variability among all subjects was 22%. This variability is in agreement with previous findings from a group of runners (Heise & Martin, 1995) and questions the notion, put forth by McMahon and colleagues, of K being an invariant feature of hopping-type movements.

This variability in K was significantly explained by several multiple regression models. Each model consisted of four independent variables combined as shown in Table 2. The variables considered, in various combinations, were: hip ROM; ankle ROM; RF-on-time (the duration that muscle RF was on during contact); COA1 (coactivation between RF and BF during contact, C, and flight, F); and COA3-F (coactivation beween VM and BF during flight).

The best regression model explained 59% of the variability in K (Table 2). Women exhibited greater hip ROM than men, which may explain why both gender and hip ROM contributed to one of the statistically significant regression models. Although some COA durations also contributed to significant regression models, most exhibited low correlations with K. COA, particularly during contact, contributes to joint stiffness and therefore was thought to influence K. Perhaps single-joint muscles, which were not monitored in the present study, play more significant roles than bi-articular muscles in this regard.

In summary, preferred hopping frequency and K were not significantly different between men and women. K exhibited considerable inter-subject variance which was significantly explained by several regression models.

REFERENCES

Cavagna, G.A., et al. Am. J. of Phys., 233, R243-R261, 1964.

Farley, C.T., et al. J.App.Phys., 71, 2127-2132, 1991.

Farley, C.T., et al. J. of Exp. Biol., 185, 71-86, 1993.

He, J., et al. J. of App. Phys., 71, 863-870, 1991.

Heise, G.D. & Martin, P.E. ASB Proceedings, Palo Alto, CA, pp. 111-112, 1995.

McMahon, T.A. & Cheng, G.C. J. of Biomech., 23(Supp), 65-78, 1990.

McMahon, T.A., et al. J. App. Phys., 62, 2326-2337, 1987.

Norkin, C.C. & White, D.J. Measurement of Joint Motion, F.A. Davis Co.: Philadelphia, 1985.

ACKNOWLEDGEMENTS

Funding provided by the Faculty Research and Publications Board of the University of Northern Colorado and the UNC Research Corporation.

	Independent Variables to Regression Model								
Intercept	Gender	Hip ROM	Ankle ROM	RF-on-time	COA1-C	COA1-F	COA3-F	R^2	Adj R^2
41.4	-5.94	.23	----	-.77	.19	----	----	.50	.37
18.84	----	.12	-.14	----	-.06	----	.34	.59	.48
13.5	----	.13	-.14	----	----	.05	.31	.58	.47

Table 2: Regression Coefficients and Intercepts for Various Regression Models that Explain the Variance in Normalized Leg Stiffness During Preferred-Frequency Hopping (see text for explanation of variables).
Note: The above regression analyses were statistically significant ($p < .05$).

DECREASED NEUROMUSCULAR EFFICIENCY DURING FATIGUE FOLLOWING LOWER LIMB IMMOBILIZATION

T. Hortobágyi[1], L. Dempsey[1], J. Lambert[2], G. Hamilton[2], P. DeVita[1]

[1]Biomechanics Laboratory and [2]Physical Therapy Department,
East Carolina University, Greenville, NC 27858

INTRODUCTION

Limb immobilization is often inevitable following an injury. Although the changes in muscle strength and size are well characterized, the mechanisms associated with fatigability and neuromuscular adaptations are poorly understood. Thus, changes in neuromuscular efficiency by surface electromyography (EMG) of the human vastus lateralis during a 4-minute sustained isometric contraction were examined before and after 3-week lower limb immobilization.

REVIEW AND THEORY

A reduction in mechanical and neural stimulation of skeletal muscle results in an apparent strength loss and atrophy. The impact of reduced use on fatigability is less clear. Against predictions, several reports have demonstrated that immobilization actually increases fatigue resistance in animal muscles (Haida et al., 1989) and at least in one muscle of the human hand (Fuglevand et al., 1995). In contrast, 5 weeks of lower limb unloading resulted in a reduced resistance to fatigue of the human quadriceps (Berg et al., 1993). Because the magnitude of strength loss is substantially greater than what can be accounted for by muscle atrophy (Berg et al., 1993), neuromuscular adaptation such as a reduced motor unit discharge rate may also contribute to the strength loss (Tang et al., 1981). Hence when a previously immobilized muscle is in the fatigued state, recruitment of a greater portion of the available motor units may be necessary to sustain a submaximal force. Such changes in the neuromuscular system would appear as an increase in surface EMG activity. The aim of the present work was to test the hypothesis that sustenance of a submaximal force is associated with a significantly greater surface EMG activity in a previously immobilized compared to non-immobilized muscle.

PROCEDURES

Healthy sedentary young men (n=13) and women (n=14) (age 21.1 years ±3.1 SD) volunteered for the study. Subjects' skin over the bellies of the vastus lateralis and medialis were alcohol washed. One box electrode with a built-in preamplifier (Motion Control, Salt Lake City, UT) powered by 9-V batteries, was placed axially, taped, and ace bandaged on each muscle belly. The two electrodes had similar electronics characteristics (a common mode rejection ratio of 370 dB, a bandwidth of 8 Hz to 28 kHz, quiescent current of 0.12 mA, and a direct current input impedance of 1 MΩ). The force and the EMG signals were digitized at 1 kHz by a 12-bit A/D board (Keithley Metrabyte 1402, Boston, MA).

The left and right quadriceps muscles of each subject were tested for maximal voluntary isometric knee extension force (MVC) using a Kin-Com dynamometer (Chattecx, Chattanooga, TN). Subjects performed six submaximal warm-up trials and after three minutes of rest, two trials of 5-second MVCs at 2.18 rads of knee joint position with one minute of rest between trials. Subjects then held 20 % of MVC for 4-minutes. Five-second samples were recorded every 30 s and the initial ($EMG_{initial}$) and final (EMG_{final}) 5-second data are presented here. This testing was repeated on both legs after 3 weeks of immobilization of the left leg. The Myosoft software package (Noraxon, Scottsdale, AZ) was used for data storage and analysis. The peak EMG activity (EMG_{max}) associated with MVC was

measured after the data were full wave rectified and smoothed (20-ms moving average). Peak values for $EMG_{initial}$ and EMG_{final} were determined from the middle 2-second portion of a 5-second epoch. Analysis of variance was used to analyze the changes in MVC, EMG_{max} (vastus lateralis reported only), and $EMG_{max}/EMG_{initial}$ and EMG_{max}/EMG_{final} ratios.

RESULTS AND DISCUSSION

Figure 1 shows that immobilization significantly (* $p = 0.0001$) reduced MVC by 44 % (±14) and the associated peak vastus lateralis EMG activity by 53% (±11, * $p = 0.0001$). The EMG/force ratio did not change. Figure 2 shows that before immobilization the peak surface EMG activity of the vastus lateralis was 29% (±32) of EMGmax at the beginning (0 s) and 39% (±13) at the end (240 s) of the fatigue bout.

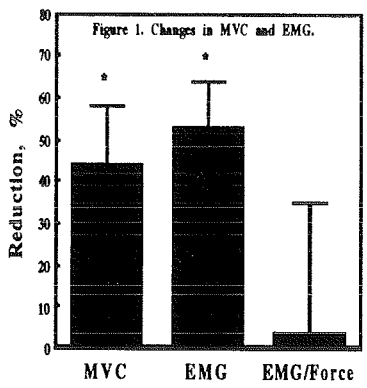

After immobilization, this activity was 26% (±8) at the beginning (0 s) and 83% (±28, * $p = 0.002$) at the end (240 s) of the fatigue test. Corresponding values for the non-immobilized leg ranged between 21% to 37% and the changes were statistically not significant. The trends in the data for the vastus medialis were similar to the ones reported for vastus lateralis. These data suggest that after immobilization the EMG associated with holding 20% of MVC for 4 minutes approached EMG_{max}. The present data confirm some earlier findings in the arm muscles (Duchateau et al., 1990) but

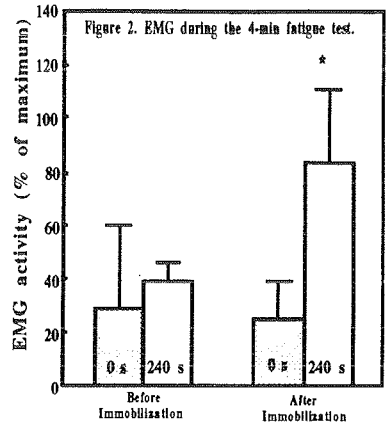

are in conflict with data reported for the human leg muscles (Dudley et al., 1989). The substantial increase in EMG activity during the fatigue test is probably related to an increase in motor unit recruitment as a compensatory mechanism for the reduced motor unit availability and discharge rate and muscle atrophy (Tang et al., 1981). Increased EMG was also noted during MVC in hemiparetic patients (Tang et al., 1981). EMG augmentation during fatigue may thus indicate the use of a larger portion of atrophied muscle, suggesting a decreased neuromuscular efficiency of skeletal muscle after immobilization.

REFERENCES

Berg H. et al. Clin. Physiol. 13, 337-347, 1993.

Duchateau J. et al. J. Physiol. 422, 55-65, 1989.

Dudley G. et al. Aviat. Space Environ. Med. 63, 678-683, 1992

Fuglevand A. et al. J. Appl. Physiol. 78, 847-855, 1995.

Haida N. et al. Exp. Neurol., 103, 68-76, 1989.

Tang et al. J. Neurol. Neurosurg. Psychiatry. 44, 690-698, 1981.

ACKNOWLEDGMENTS

Supported by NIHCD-30422 and Research Creative Activity grants from East Carolina University's Faculty Senate (to T.H.).

THE EFFECT OF FATIGUE INDUCED ASYMMETRY ON THE EXPRESSION OF MAXIMUM SIMULTANEOUS MUSCULAR FORCE

PETER F. VINT[1] AND RICHARD N. HINRICHS[2]

[1]Department of Exercise Science, University of North Carolina at Greensboro, Greensboro, NC 27412
[2]Department of Exercise Science and Physical Education, Arizona State University, Tempe, AZ 85287

INTRODUCTION

The purpose of this study was to induce an asymmetry in muscular strength, via unilateral submaximal fatigue, and observe the precipitating effects during subsequent maximal effort simultaneous bilateral exertions. The results suggested that simultaneous bilateral exertions resulted in significantly less force than independent unilateral exertions prior to and immediately following unilateral fatigue. Among the majority of subjects, the magnitude of the bilateral deficit of the non-dominant leg appeared to be unaffected by dominant leg fatigue. It was therefore suggested that the bilateral deficit phenomenon was more strongly related to central mechanisms associated with the perception or sense of bilateral symmetry than to peripheral mechanisms associated with the equilibration of the absolute magnitudes of bilateral force. However, while the centrally mediated corollary discharge may have served as the preferred locus of bilateral control, some subjects appeared to depart from this tendency and integrate afferent information from peripheral sources. And, while the criteria which are used to modulate central and peripheral influences are not yet known, it is possible that the magnitude of the interlimb difference may play a role in these response selection strategies.

REVIEW AND THEORY

One of the most remarkable examples of the bilateral deficit phenomenon was reported by Secher et al. (1988) who measured maximum effort muscular strength from a female polio patient with severe dysfunction of one leg. During a series of isometric tests, unilateral leg extensions resulted in strength measures of 86 and 457 N for the right (affected) and left leg, respectively. During simultaneous bilateral efforts, however, her total strength was only 243 N. Therefore, her total bilateral strength had diminished by approximately 50% when she had tried to use her affected and normal leg together. Although Secher et al. (1988) failed to discuss this finding in detail, it is conceivable that this patient may have grown accustomed to her leg strength imbalance and attempted to maintain or improve stability by preserving kinetic symmetry. Owing to the stability of the isometric testing apparatus, however, it is unlikely that postural effects would have played a significant role in the observed reductions in strength.

Results obtained from Secher et al.'s (1988) polio patient have never been validated. Consequently, a number of questions remain unanswered. Can interlimb coupling be implicated in such a finding? If so, is this coupling mechanism attributable to a centrally mediated representation of symmetry, a regulation of peripheral feedback, or both?

PROCEDURES

Twenty-one recreationally active adults completed a series of maximum effort isometric knee extension tests during independent unilateral and simultaneous bilateral conditions prior to and following intermittent submaximal fatigue of the dominant leg. The submaximal fatigue protocol was similar to that described by Bigland-Ritchie et al. (1986). Maximum isometric force and average integrated EMG (AEMG) of the representative knee extensor musculature were measured over the 500 ms interval of the force-time record which yielded the greatest integrated force value. AEMG of representative knee flexor musculature was also measured to account for the possibility that any observed changes in force could have been attributable to changes in antagonist muscle co-activation.

RESULTS

The results indicated that independent unilateral exertions elicited significantly greater muscular force than simultaneous bilateral exertions prior to and following unilateral fatigue (Figure 1). This result provided further support for the presence of the bilateral deficit phenomenon. Average integrated EMG did not change in parallel to the observed differences in unilateral and bilateral force.

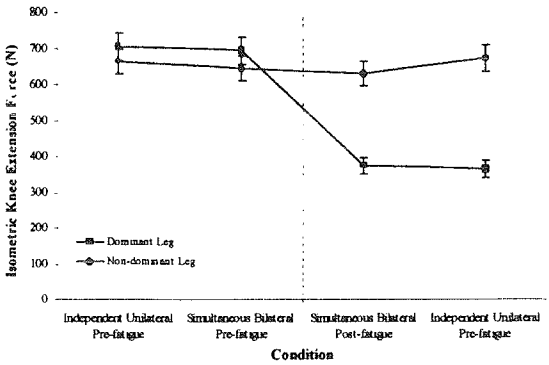

Figure 1. Average Maximum isometric knee extension force (±SE. n = 21).

DISCUSSION

The intermittent submaximal fatigue protocol that was employed to elicit a 50% reduction in dominant leg force did not appear to compromise the magnitude of the descending efferent drive. Support for this statement was garnered by the observation that the maximum isometric knee extension force and corresponding EMG activity of the non-dominant leg appeared to be unaffected by dominant leg fatigue. Therefore, it is likely that any changes in post-fatigue bilateral force were attributable to changes in the control strategies themselves rather than to fatigue-induced impairments in the central drive.

Perhaps the most intriguing observation in this experiment was that, on average, the magnitude of he bilateral deficit between pre- and post-fatigue exertions of the non-dominant leg was not statistically different. It is therefore concluded that the bilateral deficit phenomenon is more strongly related to *central mechanisms associated with the perception of bilateral symmetry* than to peripheral mechanisms associated with the equilibration of the absolute magnitudes of bilateral force. This interpretation fits well within the context of the "sense of effort" research (e.g., McCloskey et al., 1974), and, hence, implicates the centrally mediated corollary discharge as the primary or *preferred* mechanism in the governance of simultaneous bilateral motor tasks. Decrements in simultaneous bilateral reaction time and movement speed provide additional support for this argument.

However, results from the present study, Secher et al. (1988), and others related to sense of effort research do not completely exclude the possibility that peripheral factors may play a significant, although perhaps secondary, role in the performance of simultaneous bilateral motor tasks. Inspection of the individual data from the present experiment revealed that 7 of 21 subjects experienced dramatic reductions in simultaneous bilateral force of the non-dominant leg following dominant leg fatigue. Among these subjects, non-dominant forces during pre-fatigued simultaneous bilateral exertions were –3.2% of their respective unilateral values. Following fatigue, however, this difference was –14.6% (Figure 2). While these decrements were certainly not of the same magnitude as the 50% reduction of combined bilateral force observed in the polio patient described by Secher et al. (1988), it is apparent nevertheless that among *some* young and physically active subjects, *central and peripheral* mechanisms may contribute to the bilateral deficit phenomenon.

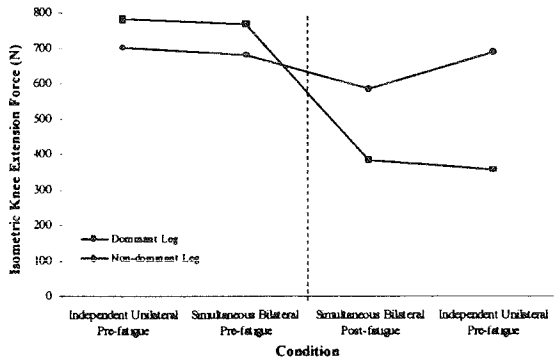

Figure 2. Average Maximum isometric knee extension force for selected subjects (n = 7).

If both central and peripheral factors can and do participate in the control of bilateral motor tasks, the question then becomes one of degree. What are the relative contributions of these mechanisms? Which parameters trigger the selection of the central, peripheral, or central *and* peripheral response? Why do some subjects appear to be bound by centrally driven perceptions of symmetry while others prefer, consciously or not, to integrate information from both central and peripheral sources? The answers to these questions are not known at this time. However, it would appear that the magnitude of the interlimb difference whether it be in terms of force, time, movement speed, or movement trajectory may have some relationship to the issue of central and peripheral scaling.

REFERENCES

Bigland-Ritchie, B. et al. (1986). *J.Appl. Phys.*, **61** (2), 421-429.

McCloskey, D.I. et al. (1974). *Exp. Neurol.*, **42**, 220-232.

Secher, N.H. et al. (1988). *Acta Phys. Scand.*, **134**, 333-339.

MUSCLE STRENGTH ABOUT KNEE FLEXION, ABDUCTION, AND AXIAL ROTATION AXES

L. Zhang, G. Wang, and G. Nuber

Sensory Motor Performance Program, Rehabilitation Institute of Chicago
Departments of Orthopaedic Surgery and Physical Medicine and Rehabilitation
Northwestern University, Chicago, IL 60611

INTRODUCTION

Human knee muscle strength about the axes of flexion-extension, abduction-adduction, and internal-external rotation was investigated as a function of knee and hip flexion angles. Study of knee muscle strength about multiple axes helps us understand the important roles of knee muscles in performing various functional tasks and in compensating for knee injuries.

REVIEW AND THEORY

The knee is the largest joint in the human body and has three rotational degrees of freedom: flexion-extension, abduction-adduction, and internal-external rotation. There have been a number of studies on knee muscle strength about the flexion-extension axis (Houtz et al. 1957, Kulig et al. 1984). Much less investigation has been done on muscle strength about other axes. Ostering et al. (1981) tested the rotational muscle strength as a function of the rotation angle. Shoemaker et al. (1982) investigated the rotational strength at several combinations of different knee flexion, tibial rotation, and hip flexion angles. They reported that there were no significant difference in the generated torque between preferred and non-preferred lower limbs, and the subjects generally produced greater internal rotation torque than external rotation one. There seems a lack of information on the abduction-adduction muscle strength (Kulig et al. 1984).

The objective of this study was to investigate the knee muscle strength about the flexion-extension, abduction-adduction, and internal-external rotation axes and its dependence on knee and hip flexion angles.

PROCEDURES

Apparatus: The subject was seated on a custom-designed seat and the thigh was strapped to the seat and the medial and lateral femoral condyles were clamped. The upper trunk was strapped to the backrest which could be fold to the appropriate hip flexion angle and also adjusted in the anterior-posterior direction. The seat could be adjusted in four degrees of freedom (DOF) so that knee flexion axis could be aligned with the Z-axis of a six-axis force sensor and locked tightly to form a solid base. The ankle, part of the foot, and distal leg were cast with fiberglass tape and coupled tightly to two aluminum half-rings. The rings were mounted onto one end of an aluminum beam located on the lateral side of the leg. The other end of the beam was mounted onto the six-axis force sensor. The relative position between the rings and beam was adjusted in four DOF so that the leg was aligned with the beam and no extra load was exerted onto the knee joint due to the mounting.

Anatomical axes: The axis of knee flexion-extension (the Z-axis) was defined as passing through the lateral and medial epicondyles (Pennock and Clark 1990). Internal-external rotation axis (X-axis) was assumed to coincides with the tibial long axis. The abduction-adduction axis (the Y-axis) was determined by the right-hand rule with the ankle at the neutral position. The positive X and Z directions were distal and medial , respectively.

Protocol: During each trial, the subject was asked to generate maximum voluntary contraction (MVC) in one of the following six directions: flexion, extension, abduction, adduction, internal rotation, and external rotation. Force and moment signals were measured by the six-axis force sensor, transformed to the knee joint coordinate system, and displayed in real-time on a computer monitor. EMG signals from the biceps femoris, semitendinosus, rectus femoris, vastus lateralis, vastus medialis, and gastrocnemius muscles were recorded. The signals were low-pass filtered with 8th order Butterworth filters (230 Hz cutoff frequency) and sampled at 500 Hz. The subject was instructed to use the feedback torque signals to help generate the desired MVC in each direction. The MVC was measured twice for each direction and each body position. Each EMG signal was

normalized to the corresponding maximum value during the experiment. Quiescent EMG and force/moment signals were recorded at the beginning and end of the experiment.

RESULTS AND DISCUSSION

Producing maximum flexion or extension moment is generally a simple task for the subjects. In contrast, generating MVC in other directions may be difficult. When a subject attempted to generate an MVC in the internal rotation direction, for example, he might not generate as much internal rotation torque as he did when he tried to generate abduction MVC. In addition, when a subject tried to generate an MVC in certain direction, substantial torque was generally produced in other directions as well, especially when the MVC was not about the flexion-extension axis. Fig. 1 shows the torques and EMG signals from six muscles crossing the knee when the subject was asked to generate external rotation MVC. Among the three moments, external rotation was the strongest. However, the substantial flexion and adduction moments were also generated. In addition to the biceps femoris muscle which produced strong external rotation moment, the rectus femoris also helped to produce external rotation moment. The gastrocnemius and semitendinosus co-contracted during the external rotation MVC.

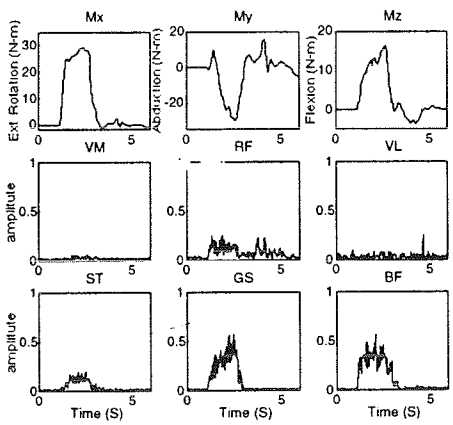

Figure 1: The M_X (external rotation), M_Y (abduction) and M_Z (flexion) moments produced when the subject attempted to generate a maximum external rotation moment. The knee flexion angle was 30°.

In summary, the MVC torques in the directions of flexion, extension, abduction, adduction, internal rotation, and external rotation as functions of knee and hip flexion angles are shown in Fig. 2. The ankle was at the neutral position. Five knee joints from three normal subjects were involved. At 85° hip flexion, the knee flexion MVC peaked at 30° and decreased on both sides. In contrast, the knee flexion MVC decreased monotonically with knee flexion angle when the hip was extended to 30°. The knee extension MVC peaked at about 70° and was affected little by hip flexion. Strong muscle strength was shown in the abduction-adduction and internal-external rotation directions. This may plays an important role in controlling joint movement and maintaining joint stability.

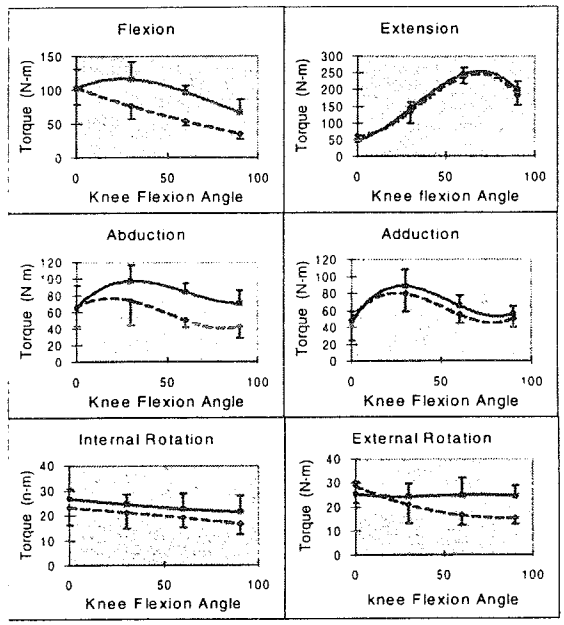

Figure 2: MVC torques in the directions of flexion, extension, abduction, adduction, internal rotation, and external rotation, respectively. The solid and dashed curves correspond to hip flexion angle of 85° and 30° (0° is full extension), respectively. The vertical bars shows the standard deviation in one direction.

REFERENCES

Houtz, SM, *J. Appl. Physiol.* **11**, 475-480, 1957.

Kulig, K. et al. *Exerc. Sport Sci. Rev.*, **12**, 417-466, 1984.

Ostering, LR, *Biomechanics VII-B,* 601-605, Univ. Park Press, 1981.

Pennock GR and Clark KJ, *J. Biomech.*, **23**, 1209-1218, 1990.

Shoemaker SC, *J. Bone & Joint Surg.*, **64A**, 208-216, 1982.

ACKNOWLEDGMENT

The authors gratefully acknowledge the supports of the Whitaker Foundation and Falk Trust Fund.

WHOLE MUSCLE LENGTH-TENSION PROPERTIES VARY WITH RECRUITMENT AND RATE MODULATION IN AREFLEXIVE CAT SOLEUS

T. G. Sandercock and C.J. Heckman
Department of Physiology, Northwestern University School of Medicine, Chicago, IL 60611

INTRODUCTION

The length-tension characteristics of cat soleus muscle were measured during activation by the crossed-extension-reflex, thus preserving the recruitment and firing rate patterns seen with voluntary activation. The resulting length-tension curves were much steeper than those measured during tetanic stimulation at 100 Hz. The steepness of the ascending limb of the length-tension curves were inversely correlated with the level of activation. Furthermore, length-tension characteristics were strongly influenced by activation history. These results suggest that the length-tension characteristics of normally activated muscle are of primary importance to whole muscle properties, and need to be incorporated in mathematical models of muscle.

REVIEW AND THEORY

During maximal tetanic stimulation, the length-tension properties of muscle are well accounted for by overlap of the sliding filaments (Gordon et al. 1966). This relationship is often used in mathematical models of muscle. However, the length-tension relationship has not previously been measured in muscle activated with normal recruitment and rate modulation. During artificial stimulation at low rates the ascending limb of the length-tension curve becomes steeper and the peak shifts to longer lengths (Rack et al. 1969), probably due to changing calcium sensitivity at different sarcomere lengths (Balnave et al. 1996). Because high motoneuron firing rates are seldom observed during voluntary contractions, the length-tension properties during normal activation may be quite different than those measured during tetanic stimulation. The purpose of this study was to measure the length-tension properties of cat soleus during activation by the crossed-extension-reflex and to test the hypothesis that the steepness of the ascending portion of the length-tension curve is correlated with the activation level.

PROCEDURES

This study presents preliminary results from 3 cats. An areflexive decerebrate preparation was used (Lin et al. 1993). A laminectomy exposed the spinal roots from S2 to L5. An ipsilateral dorsal rhizotomy eliminated reflex modulation of the soleus. The left hindleg was denervated and mounted in a rigid frame, preserving the nerve and blood supply to soleus. The calcaneus was cut and attached to a servomechanism to control muscle length and measure force from the soleus.

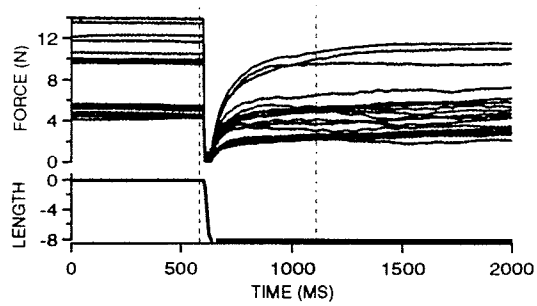

Figure 1: Superimposed step trials during crossed-extension-reflex.

Measurement of the length-tension properties during the crossed-extension-reflex required a technique different from that used during direct muscle stimulation because the same level of activation cannot be reproduced from trial to trial. Each trial began by mechanically compressing the contralateral leg which reflexively activated the soleus. Following an 8 mm release, force was allowed to redevelop. Thus, force could be measured at two lengths, the start length and end length after the step (see figure 1). There are three potential problems with this technique. 1) Activation from the crossed-extension-reflex must remain constant for about 1 s. This was not a major problem and trials where force varied before the step were discarded. 2) When an active muscle is allowed to shorten and then contract isometrically at a new length, the muscle often produces less tension than if the stimulus had begun at the new length (Abbot et al. 1952). This problem was minimized (error less than 2%) by using step changes large enough to fully unload the muscle. 3) Enough time must

be allowed for tension to redevelop after the step.

RESULTS AND DISCUSSION

A typical example of the length-tension data collected during the crossed-extension-reflex are shown in figure 1. The muscle was allowed to relax between each of the trials.

Figure 2 shows a comparison of the length-tension curves measured by direct muscle stimulation to the two point length-tension measurements made during the crossed-extension-reflex. All measurements were made from the same muscle. Note the activation levels up to 80% of maximal tetanic tension were achieved with the crossed-extension-reflex yet the length-tension properties were steeper that observed during 20 Hz direct stimulation. Most measurements fell below the 10 Hz direct stimulation curve.

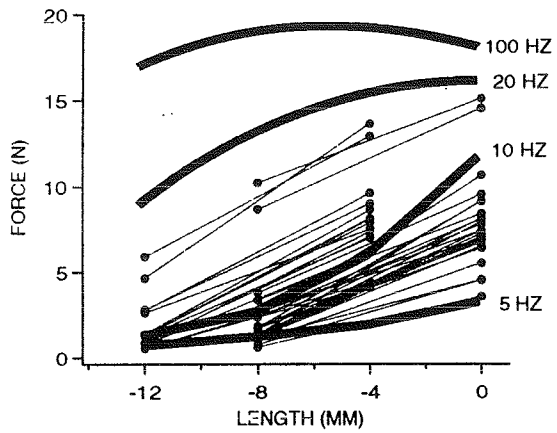

Figure 2: Length-tension during the crossed-extension-reflex (light lines) compared to direct muscle stimulation at different frequencies (heavy lines)

The hypothesis that the steepness of the ascending portion of the length-tension curve is correlated with the activation level was tested by plotting the force before to force after the step (figure 3). A Spearman Rank Order test showed significant correlation (P<.005) supporting the hypothesis. Increased motoneuron firing rate with increased activation probably explains the correlation.

Activation history also influenced the length-tension properties. Figure 4 shows repeated

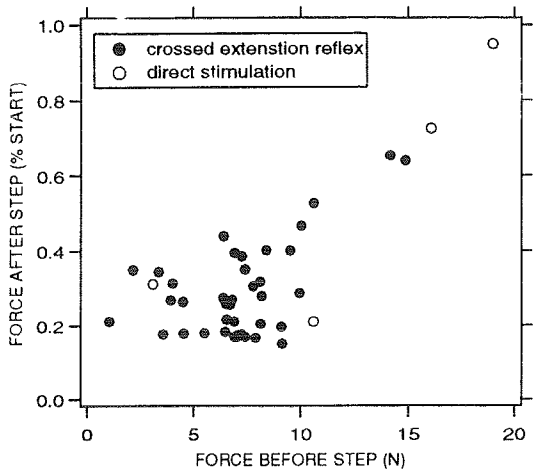

Figure 3: Correlation of force before and after a 8 mm step during the crossed-extension-reflex

step measurements during continuous crossed-extension activation. The top plot shows the history of force before the step. The lower plot shows the force waveforms from trials A and B. Note there is a substantial difference in the force following the step. The difference may be due to either decreased firing rate of the motoneurons or changes in muscle properties.

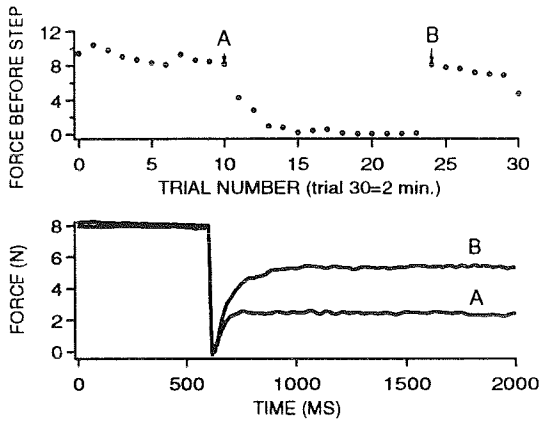

Figure 4: Effect of activation history on length-tension properties

REFERENCES

Abbot , B.C. et al. *J. Physiol.* 117:77-86, 1952.
Balnave, C.D. et al. *J. Physiol.* 492: 705-713, 1996.
Gordon, A.M., et al. *J. Physiol.* 184: 170-92, 1966.
Lin, D.C. et al. *J. Neurophysiol.* 70: 997-1008, 1993.
Rack, P.M.H. et al. *J. Physiol.* 204: 443-460, 1969.

ACKNOWLEDGMENTS

The project was supported by The National Institutes of Health grant number AR 41531.

TWO CYCLING TECHNIQUES -- ONE STRATEGY OF MUSCLE CO-ORDINATION?

B. I. Prilutsky, R. J. Gregor, A. M. Albrecht, M. M. Ryan

Department of Health and Performance Sciences, Georgia Institute of Technology, Atlanta, GA 30332

INTRODUCTION

The purpose of this study was to examine if the strategy of muscle co-ordination during cycling with two techniques: (1) pushing and (2) pulling the pedal, corresponds to the strategy that minimizes muscle fatigue. Pedal forces, kinematics, and electromyographic activity of major leg muscles were recorded in 4 subjects during pedaling. The muscle forces were calculated for each trial using a musculo-skeletal model, a static optimization, and the criterion of minimum fatigue. It appeared that muscle activation patterns of both cycling techniques corresponded to the minimum fatigue strategy.

REVIEW AND THEORY

It is not known why in skilled multi-joint tasks such as cycling, the pattern of muscle activity is rather stereotypical at similar cycling conditions (Ryan and Gregor, 1992), whereas an infinite number of activity patterns can theoretically be used by the CNS to perform the same task -- to produce the same combination of joint moments. Prilutsky and Gregor (1997) demonstrated that in a static task of exerting external forces in different directions by pushing on the ground, the muscle co-ordination seemed to correspond to the strategy that minimizes muscle fatigue (or the sum of muscle stresses cubed; Crowninshield and Brand, 1981). The simulation of pulling a strap with the same co-ordination strategy predicted features of muscle forces similar to those of the pushing task (Prilutsky and Gregor, 1997). The static task of exerting an external force in different directions is similar to that of cycling except cycling is a dynamic task. The purpose of this study was to examine if the strategy of muscle co-ordination during cycling with two techniques: (1) pushing and (2) pulling the pedal, corresponds to the co-ordination strategy that minimizes muscle fatigue.

PROCEDURES

Four subjects were instructed to pedal a bicycle mounted on a fixed-fork Velodyne trainer at a cadence of 60 r.p.m. and power of 200 W using two cycling techniques: pushing and pulling the pedal. Subjects' feet were secured to piezoelectric force pedals (Broker and Gregor, 1990) using tightly drawn rail/toe strap interfaces. The recorded pedal forces and pedal and leg kinematics were used to calculate the resultant joint moments. Surface EMG of seven leg muscles -- tibialis anterior (TA), soleus (SO), gastrocnemius medialis (GA), vastus medialis (VA), rectus femoris (RF), semimembranosus (HA), and gluteus maximus (GLM), were also recorded. The EMG was rectified and low-pass filtered (Butterworth, zero phase lag, cut-off frequency of 10 Hz) and then normalized with respect to the peak filtered EMG recorded in maximum isometric contractions. The muscle forces were calculated for each trial using a musculo-skeletal model, a standard static optimization, and the criterion of minimum fatigue (Crowninshield and Brand, 1981). The joint moments, muscle forces, and filtered EMGs were averaged over four pedaling cycles of each trial and all subjects for each cycling technique. The high coefficients of determination (0.85 to 0.98), calculated between the joint moments and filtered EMG of muscles crossing the corresponding joints, revealed that the muscle mechanical properties could explain less than 15% of variation of the joint moments. Therefore, in this study, the muscle properties were not taken into consideration, and patterns of filtered EMG, shifted in time to account for electromechanical delay between muscle activation and the joint moment, were considered qualitative estimates of muscle force patterns. The muscle forces predicted by minimizing muscle fatigue were compared with the filtered EMG.

RESULTS AND DISCUSSION

The resultant joint moments during pedaling by pushing and pulling the pedal had similar patterns and were consistent with those reported in the literature for cycling (Gregor et al., 1985). The muscle activation patterns of the two techniques (Fig. 1) were also consistent with data from the literature reported for normal cycling (Ryan & Gregor, 1992). There was a qualitative agreement between the muscle forces calculated by minimizing muscle fatigue and filtered EMG (Fig. 1). Peaks of EMGs and forces of one-joint extensor muscles (SO, VA, and GLM) were typically higher in pushing compared to pulling pedaling. The ankle, knee, and hip flexors (TA, HA, and RF) typically had higher peaks of EMGs and forces in pulling than in pushing pedaling. The strategy of minimum muscle fatigue predicted coactivation of one- and two-joint antagonists (VA vs HA and VA vs GA) and reciprocal activation of one-joint antagonists (SO vs TA) and two-joint antagonists (RF vs HA) typical for cycling (Fig. 1). The EMG and predicted forces of two-joint muscles were statistically ($p<0.05$) greater when the muscles acted as agonists at both joints they cross than when they acted as agonist at one joint and antagonist at the other (Fig. 2). Two-joint muscles had the lowest activity and predicted forces when they acted as antagonists at both joints ($p<0.05$; Fig. 2). Thus, it appears that the stereotyped patterns of muscle activity in cycling with pushing and pulling the pedal correspond to the minimum fatigue strategy.

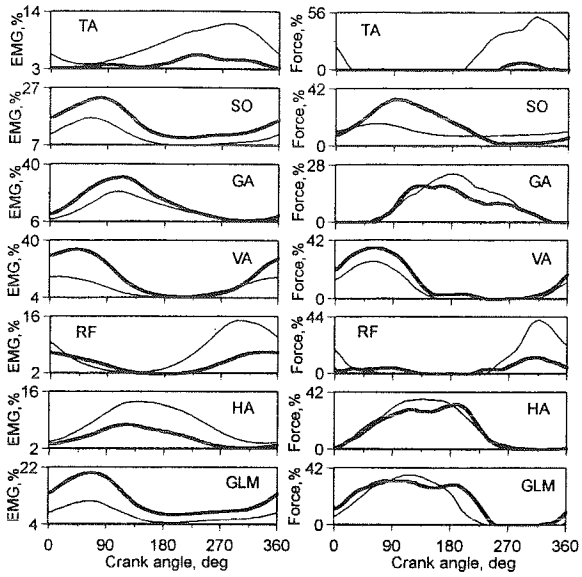

Figure 1: Averaged EMG filtered with a zero phase lag and predicted muscle forces as a function of crank angle. Thick and thin lines correspond to pushing and pulling cycling techniques, respectively.

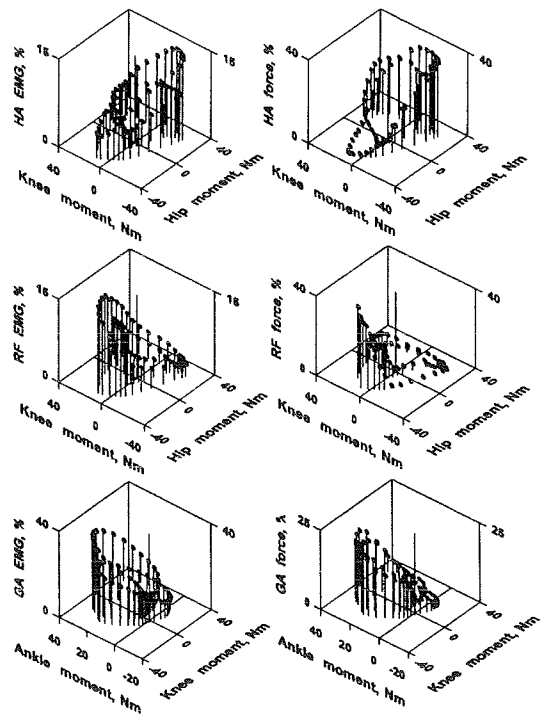

Figure 2: Averaged filtered EMG and predicted forces of two-joint muscles as a function of moments at the joints they cross during pushing and pulling cycling. Positive moments tend to extend the joints. The EMG is shifted in time to account for the electromechanical delay between muscle activity and joint moments.

REFERENCES

Crowninshield R., Brand R. J. Biomech., 14, 793-801, 1981.

Broker J., Gregor, R. Int. J. Sport Biomech., 6, 394-403, 1990.

Gregor R.J. et al. J. Biomech., 18, 307-316, 1985.

Prilutsky B., Gregor R. Motor Control, 1, 92-116, 1997.

Ryan, M. and Gregor R. J. Electromyography and Kinesiology, 2, 69-80, 1992.

DIRECT MEASUREMENT OF STRAIN RATE VARIATION IN THE VICINITY OF A ROUND HOLE IN MANDIBULAR CORTICAL BONE

Sean J. Kirkpatrick[1], David A. Covey[2], Brent W. Brooks[2]

[1]Department of Biomaterials and Biomechanics, Oregon Health Sciences University, Portland, OR 97201

[2]Department of Adult Restorative Dentistry, University of Nebraska Medical Center, Lincoln, NE 68583

INTRODUCTION

Cortical bone defects, such as surgical screw holes or osteotomies can result in post-operative complications, such as bone fracture leading to failure. An understanding of the 'effective' strain field around a circular hole in cortical bone is necessary for predicting situations in which the bone may fail, as well as for developing computational algorithms based on effective mechanical measures for predicting adaptive modeling and remodeling of bone in response to local damage. The purpose of the research described herein was, then, to experimentally describe the variations in the surface strain field surrounding a hole in a cortical bone plate using a novel laser speckle-based technique.

A non-imaging, laser speckle-based, strain-rate measurement technique that is sensitive to scale-size dependencies on strain rate was employed to measure directly the variations in the local strain field in the vicinity of a circular hole in a mandibular cortical bone plate undergoing a dynamic tensile load. Intact specimens (without a circular defect) were also examined using the same technique. Estimates of the Young's modulus of the intact samples were made based on the ratio of the imposed stress rates and the strain rates as measured via the laser speckle technique. As a means of confirming the modulus estimates (and by extension, the strain rate estimates), the intact specimens were also subjected to 3-point bending tests and the moduli of each sample was estimated by this means. Care was taken in all tests to keep the stress level well below the yield stress of cortical bone.

REVIEW AND THEORY

The effects of surgical hole defects have been studied by many authors, both experimentally (*e.g.* Brooks *et al.*, 1970; Zioupos *et al.*, 1995) and theoretically (Zioupos *et al.*, 1995). Previous work on the development of the laser speckle technique employed herein has demonstrated that it is sensitive to scale size dependencies on strain rate (Duncan *et al.*, 1994). Scale size is defined as the separation between the individual light scatterers in the bone samples. Modifications to the technique of Duncan *et al.*, (1994) have proven successful in evaluating surface strains in cortical bone taken from the mid-diaphysis of porcine femurs (Kirkpatrick *et al.*, *in press*). The present work combines the approaches of Duncan *et al.* (1994) and Kirkpatrick *et al.* (*in press*) to investigate the local mechanical effects of a round hole drilled into a cortical bone plate.

PROCEDURES

Five rectangular cortical bone samples were machined under constant irrigation from the corpus of a bovine mandible. At no time, either during the machining nor testing, were the samples allowed to dry. Each sample was subjected to dynamic tensile testing twice; once intact and once with a circular defect drilled through the center. The samples were tested in a direction parallel to the long axis of the mandible. In addition, the intact specimens

were subjected to 3-point bending tests. The tensile testing was conducted in a custom micro-tensile testing machine. Strain rates were measured directly via the laser speckle technique as described by Duncan *et al.* (1994) and Kirkpatrick *et al.* (*in press*). Briefly, this technique samples the back-scattered light from the bone samples as they are sequentially illuminated by laser light from equal, but opposite illumination angles. The back-scatter is recorded by a linear array CCD camera and the sequential exposures from each illumination angle are placed into 'stacked-speckle histories' which are spatio-temporal displays of the sequential, one-dimensional exposures stacked into a two dimensional array such that position (pixel number) is given by the abscissa and time (as set by the sample interval) is given by the ordinate (Fig. 1). The tilt of the structure of Fig. 1 is related to the strain rate. The rate of speckle pattern shift was determined by performing a 2-D frequency transform on a portion of the data of Fig. 1 (defined by the arrows). This transform results in a focused 'image' in the frequency domain, the slope of which is microns per second, or the time rate of speckle pattern shift. Any statistically significant curvature in this focused image indicates a scale-size dependence on strain rate. By differencing the rate as seen from the two illumination angles, the rigid body motion, out-of-plane, and rotational terms are eliminated. Thus the technique is sensitive only to in-plane strain rates.

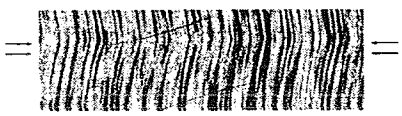

Figure 1: Stacked speckle history

RESULTS

The mean modulus for the intact specimens as determined by 3-point bending was 17.65(±0.22)GPa and that determined by the speckle technique was 17.37(±0.21)GPa. There was no statistical difference between the two means. In no cases was there determined to be a scale size dependence on strain rate for the intact specimens.

In all of the drilled samples a scale-size dependence on strain rate was found. The mean strain rate variation due to the presence of the hole was 1.75(±0.65):1. This variation in strain rate reflects the fact that the circular hole acts as a stress concentrator, locally varying the effective strain rates.

DISCUSSION

The Young's moduli determined in this study are in good agreement with published data on mandibular cortical bone (Dechow *et al.*, 1993). This indicates that the speckle technique was successful in characterizing the mechanical properties of intact bone. The strain rate variation found due to the stress concentrator is similar to that found by Brooks *et al.* (1970) on drilled whole bones in torsion. The fact that neither the present study nor that of Brooks *et al.* conforms with the predictions of linear elasticity theory reflects the fact bone is an anisotropic material with properties of an orthotropic or transversely isotropic material. The results presented here can be applied towards the development of damage-based (re)modeling algorithms.

REFERENCES

Brooks, D.B. et al. *J. Bone Jt. Surg.*, **52**, 507-514, 1970.

Duncan, D.D. et al. *Appl. Opt.*, **33**, 5177-5186, 1994.

Dechow, P.C. et al. *Am. J. Phys. Anthro.*, **90**, 291-306, 1993.

Kirkpatrick, S.J. et al. *J. Biomed. Mater. Res.* **in press.**

Zioupos, P. et al. *Phil. Trans. Roy. Soc. Lond. B*, **347**, 383-396, 1995.

A NONLINEAR MODEL TO STUDY THE INITIATION AND PROGRESSION OF DAMAGE ACCUMULATION IN A HEALTHY LUMBAR INTERVERTEBRAL DISC

R.N.Natarajan and G.B.J. Andersson
Dept. Orthop. Surg.; Rush-Pres-St.Luke's Med. Ctr, Chicago,IL 60612.

INTRODUCTION

The intervertebral disc is susceptible to degenerative processes. It is known that the formation of micro-cracks in endplate is an early feature of this process (Brickmann et al., 1983), which also includes crack development in the annulus. The effect of these degenerative process on the disc mechanical performance is difficult to study by experimental techniques. The aim of the present study was to study the initiation and progression of the damage accumulation due to different types of physiological loadings in a healthy lumbar intervertebral disc using analytical techniques. To that purpose a finite element model of a lumbar motion segment was developed.

METHOD

The geometrical shape was generated from a serial computed axial tomographic scan of an L4/L5 disc body unit. A disc height of 8.5 mm and disc cross-sectional area of 1512 mm^2 was chosen based on available literature. These dimensions represent the average of the anterior and posterior disc heights which are quite different. Validity of the finite element model was tested against an in-vitro study by Panjabi et al (1984) since results in this study were available for all types of physiological loading. A non-linear method of solution was used to identify the initiation and the progression of lesions in the motion segment. In the current study, the damage zone was identified either by breakage of an annular fiber or a crack in the endplate. The breakage of the fiber was modeled to occur with axial tensile strain exceeding the ultimate value of 16%. An average tensile strength of 2.8 MPa with corresponding failure tensile strain of 15% was used to model crack initiation in endplates. Initiation and progression of the cracks was studied for moment loads (flexion, extension and torsion) with compressive pre-load as well as for direct compression load. The compressive pre-load was 400 Newton and the magnitude of the maximum moments was 15 Nm. A direct compressive load of 5000 Newton was applied to study failure progression under compressive load. The biomechanical response of the models were studied to conclude on the effect of loading on intervertebral disc failure. The finite element analyses include non-linear behavior of annulus, ligaments and facet contacts and were conducted using ADINA 6.1.6.

RESULTS

Model Validation : Finite element model results obtained for moment as well as force loadings fell not only within the experimental range of values but also the trend of the finite element results followed those predicted by in vitro model results.
Failure initiation and progression : From the analyses of an intact motion segment, it was found that failure always initiated as cracks in the endplate and there was no failure in annular fibers for the loading conditions considered. Endplate failure always started at the junction of endplate and annulus: in the posterior quadrant of the lower endplate for compression and flexion moment loading, in the anterior quadrant of the lower endplate for extension moment loading and in the anterior quadrant of the upper endplate for torsional moment

loading. Failure initiated at a compressive load of 1250 Newton (Figure 1). Only a small extension moment (1 Nm) was required to initiate the failure in the endplate whereas large moments were required for crack initiation under flexion (7 Nm) and torsion (8 Nm) (Figure 2). As the load increased, the failure progressed to the other endplate as well. At the maximum load considered in this analysis, an almost equal number of cracks were observed both in the upper and lower endplates for all loading modes except compression. Maximum compressive load produced 67% of the cracks on the upper endplate mostly in the posterior quadrant while 33% of cracks were produced in the lower endplate once again at the posterior quadrant.

DISCUSSION

The validated finite element model showed that a failure in a motion segment starts at the endplate and not in the annulus fibers for all physiological modes of loading. This is in agreement with the current literature (Adams and Hutton, 1985). Initial failure zone was always at the junction of endplate and annulus because stress concentration occurs at these junction points under all loading conditions. In compression loading mode alone, a larger percentage of cracks were produced at the upper endplate. This may be due to the fact that the superior endplate attached to superior vertebra was free to deform under load, whereas the inferior endplate was constrained in its deformation as it was attached to inferior vertebra whose bottom surface was fixed and not allowed to deform. Extension moment not only initiated the failure at a very low moment magnitude, but the crack progression was also exponential. In all loading modes, the progression of the endplate fracture was found to accelerate with increasing load. These types of injuries therefore can be expected to more rapidly lead to mechanical failure of the disc as a composite.

REFERENCES

Adams & Hutton.Spine, 10:524-31, 1985
Brickmann P, etal., Spine, 8: 851-856, 1983
Panjabi et al., Spine, 9: 707-713, 1984

ACKNOWLEDGEMENT

PSC Grant Number BCS940010P

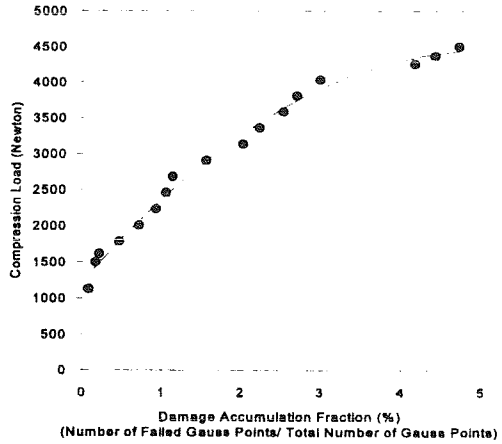

Figure 1. Damage Accumulation in An Intact Disc Due to Uniform Compressive Load

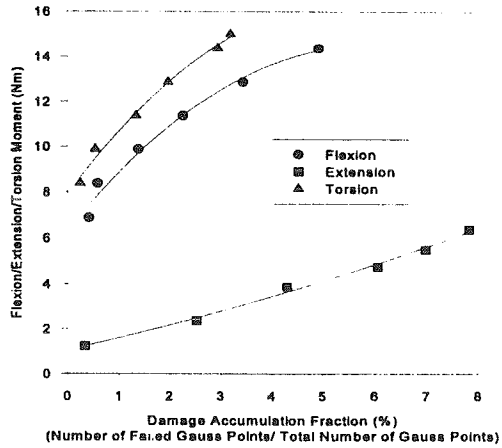

Figure 2. Damage Accumulation in An Intact Disc Due to External Moment

INTERNAL PLATING AS AN ALTERNATIVE TO EXTERNAL FIXATION OF COMPLEX DISTAL RADIUS FRACTURES - A BIOMECHANICAL EVALUATION

Abhinav B. Chhabra[1], Gregory G. Degnan[1], Todd A. Milbrandt[2], David V. Carmines[1], and Joseph E. Hale[1,3]

[1] Department of Orthopaedic Surgery, University of Virginia Health Sciences Center, [2] University of Virginia Medical School, and [3] University of Virginia Department of Biomedical Engineering

INTRODUCTION

Biomechanical evaluation of two plates and three external fixators was performed using a standardized model of wrist instability. Model design and testing protocol were based on previous investigations by Frykman et al. (1993). Each device was subjected to controlled mechanical loading in five modes (compression, tension, anterior-posterior bending, lateral bending, and torsion) and data were analyzed to compare construct stiffness.

REVIEW AND THEORY

Fractures of the distal radius account for one-sixth of all fractures seen and treated in emergency rooms (Graff & Jupiter, 1994). Treatment of these fractures is based on the neutralization of deforming muscle forces across the fracture site and Vidal's theory of ligamentotaxis by which reduction is obtained and maintained through distraction forces working on capsuloligamentous structures attached to the fracture fragments.

Despite the effectiveness of external fixation in the treatment of complex distal radius fractures (healing rates ranging from 78% - 92%), complication rates as high as 62% have been reported (Weber and Szabo, 1986). The most common complications are related to the use of percutaneous metal pins for fixation and include pin tract infections, pin loosening, osteomyelitis, and scarring of the extensor mechanism of the fingers.

An internal fixator device placed through limited incisions on the dorsal surface of the radius across the fracture site and secured by cortical screws to the radius and metacarpal eliminates the need for percutaneous pins without compromising ligamentotaxis and neutralization. In addition, these internal devices theoretically act as a mechanical dorsal buttress to prevent dorsal collapse and loss of palmar tilt in a manner analogous to volar buttress plates used for volar Barton fractures of the distal radius (Ellis, 1965). An internal fixator device may be a reasonable alternative to external fixation if it is biomechanically equivalent in maintaining distraction and withstanding applied loads.

PROCEDURES

Two commercially available metal plates, a 3.5 mm ten hole straight stainless steel pelvic reconstruction plate (Synthes; Monument, CO) and a nine hole titanium tapered limited contact wrist fusion plate (Synthes), were used as internal fixators. The three commercially available external fixators used included a unilateral dynamic EBI Distal Radius Fixator (EBI, Parsippany, NJ) and two unilateral rigid frame fixators, an original Hoffman wrist frame (Howmedica; Rutherford, NJ) and a Richards Distal Radius System (Smith and Nephew Orthopaedics; Memphis, TN). Extruded acrylic rods (2.54 cm dia. x approx. 15.24 cm lg.) were used to simulate the distal radius and third metacarpal. A two centimeter gap between the ends of two rods was used to simulate an unstable fracture.

For each of the five devices, four constructs were created for testing. Each construct was mounted between the actuator and load cell of a biaxial, servo-hydraulic test system (MTS Model 858) and stabilized with an axial preload of 1N. Loading was then applied at a constant displacement rate until a predetermined load or displacement limit was exceeded (Table 1). Stiffness of the construct was determined from the slope of the force - displacement curve using linear regression. Analysis of variance (ANOVA) and Duncan's multiple range test were performed to determine statistically significant differences between groups.

Table 1. Loading conditions. Four-point AP and lateral bending were performed with the construct rotated 90 degrees about its long axis.

Test mode	Rate	Max Load	Max Displ
Compr	1 mm/min	50 N	10 mm
Tension	1 mm/min	50 N	10 mm
AP/Lat Bend	3.5 mm/min	100 N	1.75 mm
Torque	5 deg/min	10 N-m	15 deg

RESULTS

For each testing mode, mean stiffness and standard deviation were calculated for all devices (Figure 1). In compression and tension, both internal fixator devices exhibited mean stiffness values that were significantly greater than that of the three external fixation devices. In lateral bending, the two internal fixator devices also exhibited significantly greater mean values than the external fixators. In AP bending, the three external fixators were significantly stiffer than the internal fixators. The difference in torque results, although significant, was not as impressive. The EBI and Hoffman external fixators had higher mean values than the internal fixators, but within a narrow range.

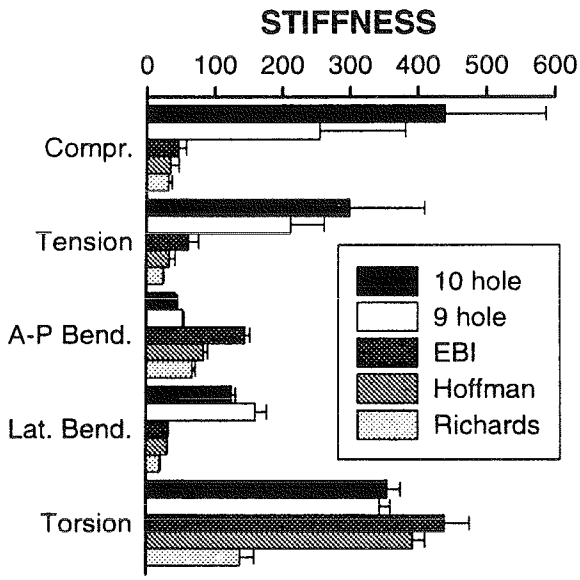

Figure 1. Mean stiffness of each construct, grouped by loading mode. All values reported in N/mm, except torsion (N-mm/degree). Error bars indicate one standard deviation.

DISCUSSION

The results of the biomechanical testing revealed that the compression and tension mean stiffness values for the two internal fixator devices were almost ten times the stiffness of the three external fixators. The internal fixators also showed the greatest standard deviation in these two modes. This variation may have resulted from screw slippage in the elongated holes of the plates when the constructs experienced axial loads perpendicular to the axis of the screws. Despite this large standard deviation, the results of compression and tension were still statistically significant.

From a clinical standpoint, a consistent loss of reduction in intraarticular radius fractures utilizing the current available treatment modalities results from collapse in the axial plane (dorsal angulation and shortening). Therefore, we believe axial loading, specifically compression, is the most significant loading parameter. In our model, internal fixator devices are superior to external fixators in this mode and theoretically may prevent the dorsal collapse of the distal radius and resultant loss of palmar tilt and anatomical reduction by acting as a rigid dorsal buttress. With regard to the other test modes, the internal fixators were stiffer in lateral bending and comparable to the external fixators in torque, although the differences were statistically significant. The internal fixators were less rigid in AP bending as expected, due to a position closer to the neutral axis and a smaller moment of inertia compared to external fixation devices. The clinical significance of these other test modes is not clear. If these modes are determined to be important for maintaining anatomical reduction, other means can be employed to compensate for weaknesses in the internal fixator device. For instance, if clinically necessary, an external splint can be used during fracture healing to compensate for decreased stiffness in AP bending.

These preliminary studies demonstrated that the internal fixator devices tested were biomechanically better than the external fixators in clinically significant testing modes. Further investigation is warranted to assess the clinical feasibility of internal fixation devices for the treatment of intraarticular distal radius fractures and their effect as a rigid dorsal buttress. Cadaveric testing will be utilized to assess the feasibility of this technique and to assess the dorsal buttress effect prior to a prospective randomized clinical study to determine the potential of this promising treatment modality.

REFERENCES

Ellis, J. *JBJS* 47B:724-7, 1965.
Frykman, G. et al. *Hand Clinics* 9:555-65, 1993.
Graff, S. & Jupiter, J. *Injury* 25(S4):14-25, 1994.
Weber, S. & Szabo, R. *J Hand Surg* 11A:157-65, 1986.

ACKNOWLEDGEMENTS

The authors acknowledge Smith & Nephew Orthopaedics, Synthes, Howmedica, and EBI for their contribution of hardware. Financial support was provided by the University of Virginia Research and Development Committee.

STRUCTURAL BEHAVIOR OF COMPOSITE FIBERGLASS SURROGATE VS. NATURAL HUMAN FEMORAL HEADS: IMPLICATIONS FOR AVASCULAR NECROSIS MODELING

A. Heiner[1], T. Brown[1,2], M. Schneiders[2]

Departments of [1]Orthopaedic Surgery and [2]Biomedical Engineering,
University of Iowa, Iowa City, IA 52242

INTRODUCTION

The stiffnesses of composite surrogate (sawbone) and cadaver femoral heads were measured when intact and with a simulated necrotic defect. Intact surrogate femoral heads were 39% stiffer than intact cadaver femoral heads. Removing cancellous bone or cancellous surrogate foam to model a necrotic defect had much more of an effect on cadaver femoral head stiffness (50% decrease) than on surrogate femoral head stiffness (8% decrease). These results indicate that these surrogate femurs, as they are now supplied, do not accurately mimic the natural femoral head in terms of mechanical load transmission.

REVIEW AND THEORY

Composite fiberglass surrogate femurs (Sawbones, Pacific Research Labs, Vashon, WA), have several well recognized advantages over cadaver femurs, namely less variability and easier availability, handling, and preservation (Cristofolini et al., 1996). The overall stiffnesses of these surrogate femurs under axial, bending, and torsional loading are within the range of human cadaver femurs, as are the dimensions (Cristofolini et al., 1996). They are in widespread use for testing implants and prostheses.

These surrogate femurs were used to study femoral head avascular necrosis (AVN) and the effect of a structural graft. The necrotic defect was simulated by removing cancellous foam from the head, from mid-hemisphere to the level of the fiberglass shell (Figure 1). This testing compared subchondral plate deflection (relative to the rest of the femur) of a necrotic femoral head, with and without a structural graft. The minimal change in femoral head deflection between these two cases led us to question whether or not these surrogate femurs were an appropriate model for studying AVN.

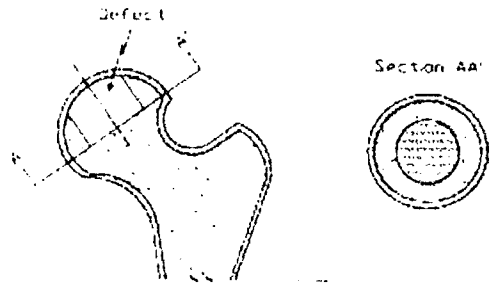

Figure 1: Necrotic defect simulation in composite surrogate femoral head

The purpose of this study was to compare the mechanical properties of surrogate and cadaver femoral heads, when intact and with a simulated necrotic defect. This was a necessary step to determine if these surrogate femurs can reasonably model AVN with the necrotic defect simulation currently in use.

PROCEDURES

Five surrogate femoral hemi-heads and five fresh-frozen human cadaver femoral hemi-heads were prepared by sawing off the "northern hemisphere" of the femoral head, then sanding the equatorial plane flat. The average height of the surrogate femoral hemi-heads was 25.0 mm (range: 24.3 - 25.5), and the average height of the cadaver femoral hemi-heads was 26.3 mm (range: 24.8 - 27.7). The femoral hemi-heads were compressed between parallel platens in an MTS 858 materials testing machine (MTS, Eden Prairie, MN) at a rate of 0.005 mm/sec, until a load of 450 N was achieved. The femoral hemi-heads were preconditioned with 3 loading cycles, then data were collected over 5 cycles by MTS software sampling at 10 N increments.

Necrotic defects were then simulated by hollowing out material from the bottom surfaces of the femoral hemi-heads. For the surrogates, a 28.6 mm diameter core of cancellous rigid foam was removed to the depth of the fiberglass shell (Figure 1). For the cadavers, an equivalent region of cancellous bone was removed. The necrotic femoral hemi-heads were then tested as before.

RESULTS

	Intact	Necrotic	Decrease
Surrogate	3.85 (0.58)	3.53 (0.57)	8%
Cadaver	2.35 (0.79)	1.18 (0.41)	50%
Decrease	39%	67%	

Table 1: Femoral head secant stiffness (N/μm), measured between 10 N and 450 N. Standard deviation given in parentheses. All decreases significant at $p < 0.005$.

DISCUSSION

The cadaver femoral heads were less stiff than the surrogate femoral heads, for both the intact and necrotic conditions. Introducing the necrotic defect decreased surrogate femoral head stiffness by only 8%, but decreased natural femoral head stiffness by 50%.

The higher stiffness of the surrogate femoral heads can be attributed to the increased thickness and relative stiffness of the fiberglass cortical shell/subchondral plate (Table 2). For the surrogate femoral heads, the fiberglass shell thickness was 3-5 mm and the cancellous foam was 600 times less stiff than the fiberglass shell; therefore, removing cancellous foam had little effect on femoral head stiffness. For the cadaver femoral heads, the cortical shell thickness was less than 1 mm and the cancellous bone was only 3 times less stiff than the cortical shell; removing cancellous bone therefore had a much greater effect on structural support, and caused a large decrease in femoral head stiffness.

Although the overall stiffness and dimensions of the composite surrogate femurs are comparable to cadaver femurs, there is emerging recognition

	Subchond plate thickness	Subchond plate modulus	Cancellous bone modulus
	mm	GPa	GPa
Surrogate	3-5	18.6[1]	0.031
Cadaver	< 1	1.4[2]	0.414

Table 2: Surrogate and cadaver femoral head material components ([1]Pacific Research Labs; [2]Brown, Vrahas, 1984)

of specific circumstances for which composite surrogate femurs may not be appropriate for biomechanical testing. Cristofolini et al. (1996) noted an abnormal strain distribution in the proximal medial region of these surrogate femurs; this could affect studies of hip stems. The same authors noted that it may not be wise to optimize a prosthetic design for only the geometry of a surrogate femur (Cristofolini et al., 1996). Otani et al. (1993) found that surrogate femurs were unreliable for measuring circumferential strains under axial loads, or any strains under torsional loads (circumferential strains were of interest because of the tendency of the upper femur to fail by longitudinal splitting). The present study demonstrated that composite surrogate femoral heads are stiffer than cadaver femoral heads, and that the same necrotic defect simulation had a much larger effect on cadaver femoral head stiffness than on surrogate femoral head stiffness. The excessive thickness and stiffness of the fiberglass shell led to minimal effect on femoral head stiffness when AVN was simulated by removing cancellous foam.

REFERENCES

Brown T, Vrahas M, *J Orthop Res*, **2(1)**,32-38, 1984.

Cristofolini L. et al. *J Biomech*, **29(4)**, 525-535, 1996.

Otani T, Whiteside L, White S, *J Biomed Mater Res*, **27**, 575-585, 1993.

Pacific Research Labs product literature.

ACKNOWLEDGMENTS

The authors wish to thank Douglas Pedersen for technical assistance, and Dr. Robert Poggie of Implex Corp., for helpful discussions. Financial support was provided by NIH AR-35788.

EXPERIMENTAL DETERMINATION OF CONSTITUTIVE EQUATIONS FOR BRAIN TISSUE

E. G. Takhounts, J. R. Crandall, B. T. Matthews

University of Virginia Automobile Safety Laboratory, Charlottesville, VA 22903

INTRODUCTION

The brain may be the most critical organ to protect from trauma, since injuries to its structures are currently nonreversible, and the consequences of injury can be devastating. A head injury occurs every 15 seconds in the United States and more than 75,000 people die each year as a result of traumatic brain injury (DHHS, 1989).

The development of analytical models of the head for the study of brain injury has been an active field of research for many years, but a lack of knowledge regarding the deformation properties of the brain tissue has been an inherent weakness of these models. With the increased sophistication of finite element computer models of the head, the need for better knowledge of the material properties of the human brain tissue has intensified.

The research presented in this paper develops constitutive relations for brain material subject to large deformations for subsequent implementation in finite element models.

REVIEW AND THEORY

Previous research on the material properties of brain tissue (Galford et al., 1970; Arbogast et al., 1995), has assumed that brain tissue behaves as an isotropic viscoelastic material. The simplest constitutive equations are obtained by modeling brain tissue as an isotropic linear viscoelastic material in which the stress $\sigma(t)$ is related to the strain $\varepsilon(t)$ by

$$\sigma(t) = \int_{-\infty}^{t} G(t-\tau)\dot{\varepsilon}(\tau)d\tau, \qquad (1)$$

where the function G is the *stress relaxation function* of the brain material. If the material is subjected to the strain

$$\varepsilon(t) = \varepsilon_0 H(t-\tau), \qquad (2)$$

where $H(t-\tau)$ is the Heaviside step function defined as

$$H(t-\tau) = \begin{cases} 1 & \text{if } t \geq \tau, \\ 0 & \text{if } t < \tau \end{cases} \qquad (3)$$

then the stress is given by

$$\sigma(t) = \varepsilon_0 G(t) \qquad (4)$$

and the stress relaxation function $G(t)$ is determined by dividing the measured stress response by the known strain amplitude ε_0.

While a linear theory of viscoelasticity is reasonable for small deformation tests, the nonlinear stress-strain characteristics of the brain tissue must be accounted for when subjected to large deformations. The Quasi-linear theory of viscoelasticity (QLV), developed by Fung (1981), is used to represent nonlinear behavior of the brain material, where the history of the stress response, called the *relaxation function*, and denoted by $K(\lambda,t)$, is assumed to be of the form

$$K(\lambda,t) = \varphi(t)T^{(e)}(\lambda), \quad \varphi(0) = 1, \qquad (5)$$

in which $\varphi(t)$, a normalized function of time, is called the *reduced relaxation function*, and $T^{(e)}(\lambda)$, a function of the stretch λ alone, is called the *elastic response*. The stress $\sigma(t)$ is linearly related to elastic response $T^{(e)}$ (Fung, 1981) as follows:

$$\sigma(t) = \int_{-\infty}^{t} \varphi(t-\tau)\dot{T}^{(e)}(\tau)d\tau. \qquad (6)$$

The function $T^{(e)}$ is analogous to the strain ε in the linear theory of viscoelasticity. For large deformations tests the instantaneous elastic function $T^{(e)}$ is assumed to be a polynomial function of strain

$$T^{(e)}(\varepsilon) = A\varepsilon + B\varepsilon^2 + C\varepsilon^3, \qquad (7)$$

where A, B and C are experimentally determined constants. The reduced relaxation function $\varphi(t)$ is represented by a sum of exponentials

$$\varphi(t) = \varphi_0 + \frac{\sum C_i e^{-\nu_i t}}{\sum C_i}, \qquad (8)$$

where ν_i are usually called the time constants and C_i are arbitrary constants determined experimentally.

The study presented in this paper applies to linear and quasi-linear theories of viscoelasticity to characterize the mechanical properties of the human and bovine brain tissue material.

PROCEDURES

Stress relaxation tests were performed on human and bovine brain samples. All the tests were performed within 30 hours post-mortem. Cylindrical samples were excised from the frontal lobs of the brain using a custom coring tool with an internal diameter of 20 mm.

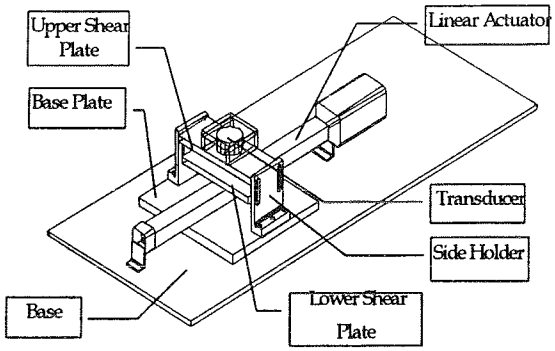

Figure 1: Parallel Plate Experimental System.

Samples were trimmed while in the coring tool to provide parallel surfaces and then placed in a jar filled with saline solution; the dimensions of the samples were measured while in saline. Samples were fixed between shear plates using cyanoacrylate glue (Super Glue Corporation). The plates were kept parallel th:oughout the testing such that both axial extension and shear were imposed on the samples. The shear strains of values 0.25, 0.35, 0.4 and 0.5 were applied to the brain samples after preconditioning the samples for at least six cycles. Figure 1 shows the experimental system while Figure 2 depicts the upper shear plate assembly with the brain sample attached to it.

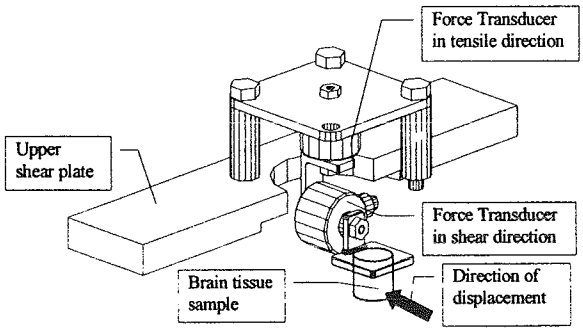

Figure 2: Upper Shear Plate Assembly.

A programmable linear actuator (NSK Technologies, Model XY-FS0060-902) was used to apply displacements to the lower shear plate (Figure 1) at the rates of 50 mm/sec, 100 mm/sec, 300 mm/sec and 400 mm/sec. The IDDAS (Robert A. Denton Inc., Rochester Hills) data acquisition system was used to collect the data at sampling rate of 10,000 samples/sec. Over 500 tests were performed on human and bovine brain tissue samples in this study.

RESULTS AND DISCUSSION

An instantaneous modulus of elasticity was calculated using quasi-linear theory of viscoelasticity (Equation 7). The time constants were found (Equation 8) and compared with the results obtained by previous research. Figure 3 shows a stress-strain relationship of the elastic function for bovine brain tissue.

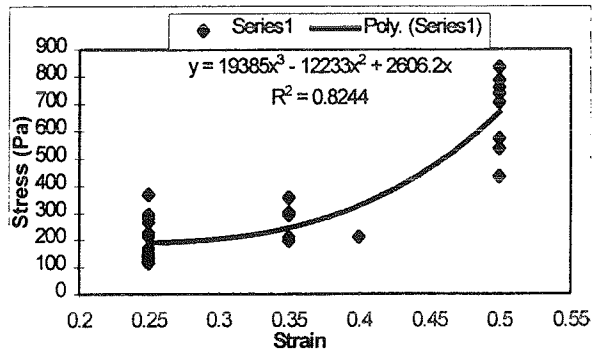

Figure 3: A sample elastic function calculated for the bovine brain tissue obtained after application of six preconditioning cycles.

The results indicate that the shear modulus of elasticity found from application of linear theory of elasticity is generally higher than the one found from QLV for large deformations. This confirms the original assumption that using the QLV is more appropriate for representing the large deformation response.

REFERENCES

Arbogast K. B. et al., *Proceedings of the 39th Stapp Car Crash Conference*, P-299, 153-159, 1995.

Fung Y. C., *Biomechanics: Mechanical Properties of Living Tissues*, 226-238, Springer-Verlag New York Inc., 1981.

Galford J. E. et al., *J. of Biomechanics*, 3, 211-221, 1970.

Department of Health and Human Services (DHHS), *Interagency Head Injury Task Force report,* National Institutes of Health, NINDS, 1-29, 1989.

ACKNOWLEDGMENTS

This work was performed under a grant from the AAMA. The authors would like to thank Mr. Guy Nusholtz for providing technical support.